Book of abstracts

Christophe Dano, Gioacchino Cinno Viggiani, Pierre Bésuelle

The International Symposium on Geomechanics from Micro to Macro

Book of Abstracts

IS-Grenoble 2024

23-27 September 2024
Grenoble • France

UGA Université Grenoble Alpes

cnrs

GRENOBLE INP UGA

3SR

Citation: Book of abstracts of the International Symposium on Geomechanics from Micro to Macro, IS-Grenoble 2024, 23-27 september 2024, Grenoble, France. https://is-grenoble2024.sciencesconf.org/page/book_abstracts/

Book of abstracts editors:
Christophe Dano, Cino Viggiani, Pierre Bésuelle.

Version September 6, 2024, Grenoble, 556 pages, ISBN 979-10-415-5139-2.

Symposium sponsors:
La Région Auvergne-Rhône-Alpes, Grenoble Alpes Métropole, Centre National de la Recherche Scientifique (CNRS), Université Grenoble Alpes (UGA), Grenoble INP, RX Solutions, Fédération 3G.

Table of contents

Advances in experimental methods

Advances in experimental methods

(TH)M experimental characterization of geomaterials behaviour

A HYDROMECHANICAL CONCEPT FOR THE TRIGGERING OF INTERNAL EROSION IN WIDELY-GRADED SOIL

G. Vinoth[1,2], and J. Fannin[1]
[1] Univ. of Brit. Columbia, 6250 Applied Science Lane, Vancouver, BC, Canada
[2] INGEO2 B.V., Papsouwselaan 119, 2624 AK, Delft, The Netherlands

1. Introduction

Dam owners are funding research to inform a micromechanics-based understanding of internal erosion in zoned embankment dams. The specific focus is on erosion of widely graded and gap graded soils by the process of internal instability, wherein finer fraction particles erode from the matrix of coarser particles. Theoretical analysis of rigid-wall permeameter test data on gap-graded soil indicates the triggering of such erosion is governed by a combination of: (i) material susceptibility, (ii) stress state, and (iii) hydraulic demand [1]. Herein we report newly acquired data using a flexible-wall permeameter (FXP) device, from research funded by BC Hydro, with the objective of establishing a triggering relation in stress-gradient space for widely graded soil obtained from the borrow source of the WAC Bennett Dam (formerly Portage Mountain Dam) in British Columbia.

2. Large Flexible-wall Permeameter (FXP) testing

The flexible-wall permeameter (see Fig. 1a) accommodates a specimen diameter D = 200 mm that mounts in a dual-wall triaxial cell. The moist-tamped test specimen is reconstituted by moist-tamping, back-percolated with water, saturated under a back-pressure, and then consolidated to the target mean effective stress (p_o'). Thereafter, a flow-controlled hydraulic demand is applied to the specimen. Instrumentation records the resulting hydraulic gradient, finer fraction mass loss in real-time, and any volume change as a consequence of internal erosion.

The widely graded BSM-12:30 soil specimen is a sandy gravel with trace of silt (see Fig. 1b), with d_{100} = 25 mm. It plots within construction records for soil of the zoned Transition material, or fine filter, to the zoned Core material of the WAC Bennett Dam [2]. The BSM-12:30 gradation is scalped-and-replaced to D/d_{100} = 8, which satisfies requirements for permeameter testing [3].

(a)

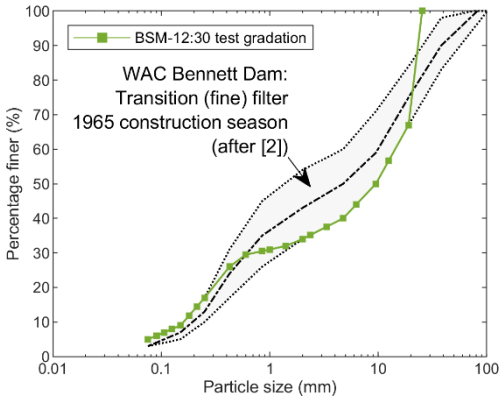

(b)

Figure 1. (a) Flexible-wall permeameter (FXP) device; (b) Widely graded BSM-12:30 test gradation

3. Results and Analysis

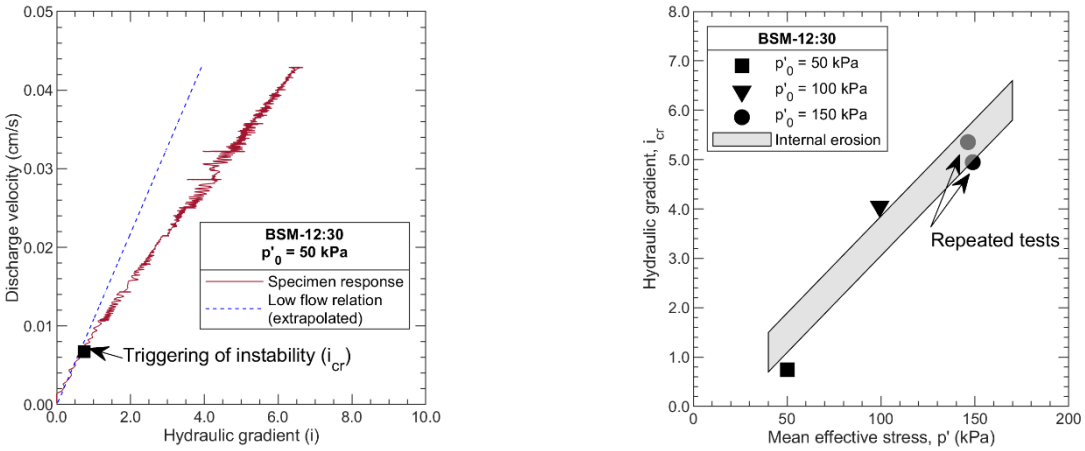

Figure 2. (a) BSM-12:30 test (p_o' = 50 kPa); (b) Triggering relation in stress-gradient space

A change in the velocity-gradient relation, and thus variation from the initial hydraulic conductivity of the specimen, defines the critical hydraulic gradient (i_{cr}) at which internal instability is triggered in the widely graded soil (see Fig. 2a). The companion measurement of real-time finer fraction mass loss informs the interpretation of the specimen response.

Results of four FXP tests at $50 \leq p_o' \leq 150$ kPa show a strong dependency of critical hydraulic gradient on the mean effective stress (Fig. 2b). Good repeatability is observed for the test at p_o' = 150 kPa. The data yield a triggering relation in stress-gradient space for seepage-induced internal instability in the BSM-12:30 gradation. The triggering relation establishes a hydromechanical envelope to the stability of the soil. We postulate the hydromechanical envelope is governed by the micro-mechanics of the grain assemblage, and thus the proportion of mean effective stress that acts upon the finer fraction content of the widely graded soil.

4. Summary remarks

Results are reported from internal erosion tests, on a widely graded sandy gravel with trace silt, using a custom-designed flexible-wall permeameter (FXP) device. The BSM-12:30 test gradation is believed representative of the zoned Transition, or fine filter, of the WAC Bennett dam. Data analysis identifies a critical hydraulic gradient to trigger internal instability in the widely graded soil. The FXP test results establish a relation in stress (p_o') - gradient (i_{cr}) space for the soil. The relation describes a hydromechanical envelope that is believed governed by the micro-mechanics of the grain assemblage.

5. References

[1] Li, M. & Fannin, R. J. (2022). Internal erosion: critical hydraulic gradient in one-dimensional vertical seepage and its relation to soil gradation. *Can. Geotech. J.*, **59(5)**:769-772.

[2] Morgan, G. C. & Harris, M. C. (1967). Portage Mountain Dam: II. Materials. *Can. Geotech. J.*, **4(2)**:142-166.

[3] Vinoth, G. & Fannin, R. J. (2022). Scalp-and-Replacement of oversize particles: laboratory permeameter testing. *Geotech. Test. J.*, **45(5)**:1030-1036.

CHARACTERISATION OF PDMS GRANULATE IN GEOTECHNICAL MODEL TESTS

J. Sławińska-Budzich[1]***, B. Świtała***[1]***, M.A. Kalwar***[1,2] ***and D. Leśniewska***[1]
[1] *Institute of Hydro-Engineering, Polish Academy of Sciences, Gdańsk, Poland*
[2] *Doctoral School at Gdańsk University of Technology, Gdańsk, Poland*

1. What is PDMS?

PDMS – polydimethylsiloxane is a silicone elastomer, a transparent material, resistant to chemical agents and heat, readily available and safe for health. Since it is in a liquid form, the material can be easily poured into the mould of an arbitrary shape. Furthermore, it is possible to produce spherical grains out of it in lab conditions. What is important, PDMS grains, when cured, are relatively elastic and free of frozen stresses, which makes them ideal material for photo-elastic experiments. Additionally, an immersion liquid with a matching refraction index is readily available and comprises a mixture of water and glycerine in appropriate proportions.

2. Production of PDMS granules

Water-based production of PDMS grains was initially introduced in the work of Frank-Richter [1] and patented. Therefore, an independent procedure has been elaborated. Since the material is slowly hardening, the portions of liquid poured from a certain height and embedded in water have to be stopped in the tank before they reach the bottom and lose the spherical shape. Therefore, fluids with two different densities can be applied to achieve that. If the density of the top fluid (pure water) is lower than the density of PDMS, whereas the bottom fluid is denser than the considered material, the drops of PDMS will float on the boundary between these two layers, and the sphericity of the granule will be preserved. After a curing time, the droplets are taken out of the water, air-dried and segregated according to their diameters. The pile of produced grains of one of the selected fractions is presented in Fig. 1.

Figure 1. Cured and segregated PDMS granules - overview

3. Experiments

The characterization of the new material and determination of its strength parameters and physical properties are essential to enable conscious use in experiments and to calibrate discrete element

models (DEM). Interestingly, PDMS granules exhibit different behaviour when dry (surface charges) and when immersed in water.

The simplest yet informative test performed on granular material is the repose test. Consequently, the repose angle of dry and water-lubricated PDMS is determined.

Furthermore, a series of triaxial tests in the true triaxial apparatus is performed to study the stress-strain relationship characteristic for PDMS granules. The tests conducted on dry and wet samples, in drained conditions. Several values of confining pressures are applied and the response of the sample is monitored. Consequently, it is possible to determine the friction angle and cohesion of the material and compare the results for dry and water-saturated conditions.

Furthermore, the stress-strain relationship and Young modulus are determined for individual grains in the axial compression test. The tests are performed for various grain sizes and compared.

The results of the above experiments may serve as a base for calibration and validation of DEM models, which can be further used to model more complex, larger problems, or to delve into micro-scale and investigate the micro-mechanics of the assembly consisting of PDMS particles. Moreover, new experimental setups e.g. for photo-elastic tests can be designed more consciously, knowing the stress level which is necessary to obtain a clear photo-elastic effect and the geometry and dimensions of the test boxes needed to be able to capture the desired mechanical response of the granular assembly.

References

[1] Frank-Richter, S. (2014). *Disordered binary granular packings in three dimensions*. Ph.D. thesis, PhD thesis, Heinrich-Heine-Universität, Düsseldorf.

EFFECT OF A POROUS LIMESTONE'S MICROSTRUCTURE ON ITS MECHANICAL BEHAVIOUR AND STRAIN LOCALISATION MODES UNDER TRIAXIAL LOAD

A. Quacquarelli[1,2], C. Dore-Ossypian[1,2], M. Bornert[2], A. Dimanov[1], J. Sulem[2], A. King[3]
[1]Laboratoire de Mécanique des Solides, École Polytechnique, CNRS UMR 7649, Palaiseau, France
[2]Laboratoire Navier, École des Ponts, Univ. Gustave Eiffel, CNRS UMR 8205, Marne-la-Vallée, France
[3]Psiché beamline, Synchrotron Soleil, Saint Aubin, France

1. Introduction

The CO_2 sequestration in depleted gas reservoirs is an encouraging solution to reduce emissions into the atmosphere. In particular, porous rocks seem to be suitable for this scope thanks to their high permeability, i.e., their capacity to allow fluids to flow through their interconnected porosity. Although these host rocks have been extensively studied in the past, their actual potential to sequestrate CO_2 still remains an unknown. The gas injection can disturb the *in situ* stress state, inducing some fractures, seismic activity and reducing the porosity of the rocks, therefore reducing its sequestration potential. Moreover, the strain accommodated in these rocks are significantly influenced by *in situ* confining pressures [1, 2]. The inherent microstructural heterogeneities influence deformation mechanisms and strain heterogeneities [3] The conditions of formation of compaction bands are of particular interest, as they may act as barriers to hydraulic flow. We investigate here the additional influence of microstructure on the overall behavior and local deformation modes.

2. Material and experimental set-up

The Saint-Maximin limestone is a high porosity (38% in average) grain-stone from the Parisian basin in France. It is composed of 80% calcite and 20% quartz, and is enriched by *Miliolidae* shells. Its porosity ranges from polydisperse inter-granular pores to smaller intra-granular pores confined within calcite grains. Large isolated pores are also observed within low porosity zones. Significant porosity fluctuations are observed at a centimetric scale and have been shown to strongly influence strain localization in standard-sized sample [4]. Calcite grains are more present in high porosity zones, here the calcite dissolutions generate new pores increasing the interconnected average porosity. These denser zones are considerably more heterogeneous than the more porous ones.

To investigate the role of mean porosity and its heterogeneity on the mechanical response of the rocks at sub-centimetric scale, dry cylindrical samples of 8 mm in diameter and 16 mm in height were cored in respectively dense and porous zones. The mean porosity varies between 30 and 37%, and between 41 and 45%, for porous and dense samples respectively. Figure 1 illustrates the two considered microstructures, which differ not only by their average porosity but also the statistical distributions of their local porosity and the typical size of its spatial variations. Local porosity is here defined over windows 250µm in width. A specifically developed *in situ* triaxial testing device compatible with synchrotron X-Ray micro computed tomography observations allows to follow the progressive development of damage and failure.

Dense and porous samples were tested at confining pressures of 1, 3, 6, 8, 10.5 and 20 MPa. Axial strain is estimated indirectly in real time from piston position corrected for setup compliance and is validated by processing the 3D images by Digital Volume Correlation technique (DVC), allowing in turn to build 3D strain maps and to identify the strain localization patterns.

3. Results

The variation of the mean stress against the axial strain is plotted in Figure 2 for porous and dense samples at different confining pressures. In both cases, a transition from brittle to plastic behaviour (i.e., quasi-perfect plastic behaviour) is observed going from low to high confining

pressure: it is expected under a confining pressure of 3 MPa for the porous sample and 6 MPa for the dense one. In spite of the modest difference in porosity, porous and dense samples behave differently under the same confining pressure, highlighting the role of the microstructure on the rock strength and strain accommodation. DVC analyses reveal diffuse deformation in porous samples due to their microstructural homogeneity, while deformation remains localised in bands in dense samples and is accommodated in the more porous areas whereas the denser ones remain almost intact.

The microstructural characteristics, as well as the confining pressure, play a key role in the localisation of deformation, with strong effects on the local mean porosity and potential implications on its interconnectivity and therefore on the rock permeability and storage capacity of CO_2.

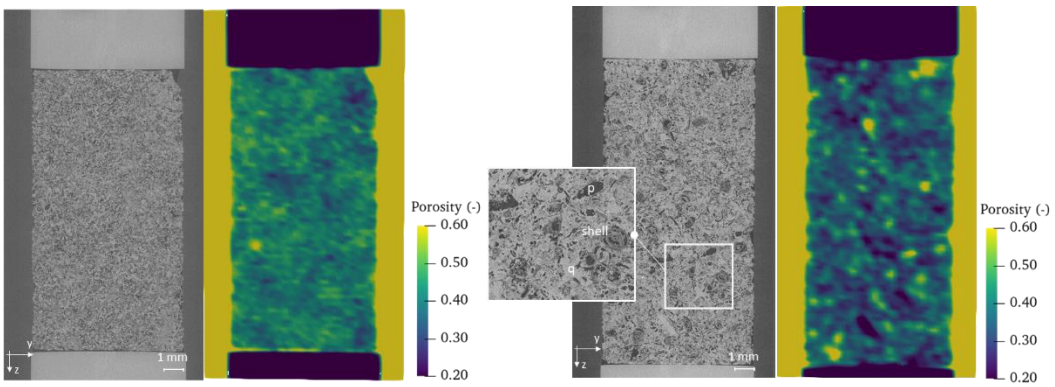

Figure 1.Vertical cross-sections of a porous (left) and dense sample (right) and respective initial porosity maps; local porosity is here defined over 250µm wide windows.

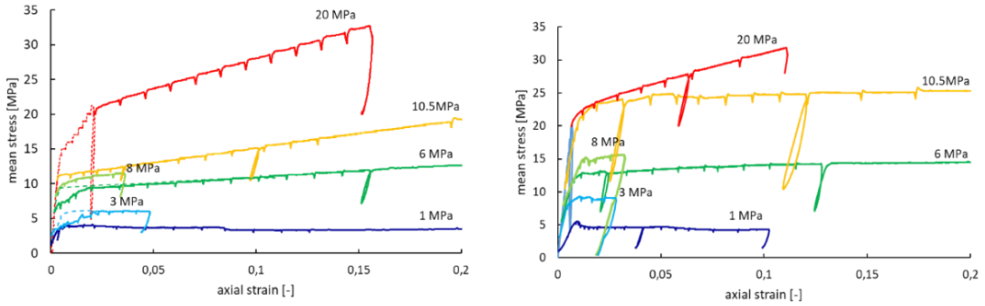

Figure 2. Overall behaviour under triaxial compression of porous (left) and dense (right) samples at different confining pressures

4. References

[1] Baud, P., Schubnel, A., Heap, M., & Rolland, A. (2017). Inelastic compaction in high-porosity limestone monitored using acoustic emissions. *Journal of Geophysical Research: Solid Earth*, *122*(12), 9989-10.

[2] Leuthold, J., Gerolymatou, E., & Triantafyllidis, T. (2021). Effect of Compaction Banding on the Hydraulic Properties of Porous Rock-Part II: Constitutive Description and Numerical Simulations. *Rock Mechanics and Rock Engineering*, *54*, 2685-2696.

[3] Dautriat, J., Bornert, M., Gland, N., Dimanov, A., & Raphanel, J. (2011). Localized deformation induced by heterogeneities in porous carbonate analysed by multi-scale digital image correlation. *Tectonophysics*, *503*(1-2), 100-116.

[4] Abdallah, Y., Sulem, J., Bornert, M., Ghabezloo, S., & Stefanou, I. (2021). Compaction banding in high-porosity carbonate rocks: 1. Experimental observations. *Journal of Geophysical Research: Solid Earth*, *126*(1), e2020JB020538.

EFFECTS OF TWO DIFFERENT TYPES OF FINES ON THE COMPRESSION BEHAVIOUR OF CLEAN BALLAST

C. Silvani[1], I. Djeran-Maigre[1], R. Dutarte[1] and E. Valles-Lopez[1]
[1] Univ. Lyon, INSA Lyon, GEOMAS Lab. Lyon, France

1. Introduction

The railways are still a highly demanded mean of transportation worldwide, thanks to their cost efficiency, ease of drainage, and capacity to withstand cyclic imposed loadings from trains. This trend is likely to continue to grow as carbon emissions are reduced and the goal of a more energy-efficient society is pursued.

The track structure, composed of ballast, frequently undergo deformations of high significance owing to recurring stresses stemming from high speed and heavy trains and with increased traffic densities. Owing to the high level of solicitations, the new ballast is progressively degraded and accumulated fouling material in voids between ballast particles will eventually cause poor track geometry performance. Ballast fouling materials have also other sources such as fouling attributed to the dust from trains carrying coal or soil intrusions from the base [1]. When fooling becomes important, ballast life expires and should be cleaned or replaced.

Degradation of ballast is a main issue for railway owners and thus studied by many researchers [2-4]. Many studies have been done on the strength of ballast and on degraded ballast with fooling produced by ballast inherent degradation, but fewer studies have been carried on the behavior on ballast contaminated by soil intrusions from the bottom of the track, or eventually particles coming from windblown processes.

To improve the understanding of ballast behavior with fooling, two different types of fines have been studied and the experimental tests carried out are presented below.

2. Materials and methods

The clean ballast used come from the Poccachard quarry located in Poleymieux-au-Mont-d'Or (France). The grain size of limestone aggregates is between 10 mm and 40 mm. The typical sample weighs around ten kilograms and it is placed into a cylindrical metal cell used for the oedometric compaction experiments. The sample has a diameter of 26 cm and its height is variable according to material used, around 26 cm. The aggregates are mixed to ensure a homogeneous sample A specific press applies the uniaxial compression on the sample.

The degraded ballast is represented by sample including fines of grain size less than 10 mm. Two experiments were carried out using fines of the same material as the clean ballast, while the other two samples were prepared using kaolinite fines. Polwhite kaolinite is a medium particle size (between 1 and 20 μm) kaolin produced from deposits in Brittany (France) with specific gravity of 2.6. The initial grain size distribution of the clean ballast and of degraded ballast are shown in Figure 1. In order to verify the influence of the types of fines on the behaviour of the material, the same mass (2.57 kg) was selected. To compare the effect of fines content, taking into account their respective dry densities, half the weight of the kaolinite (1.28 kg) and twice the weight of the limestone (5.17 kg) has been tested.

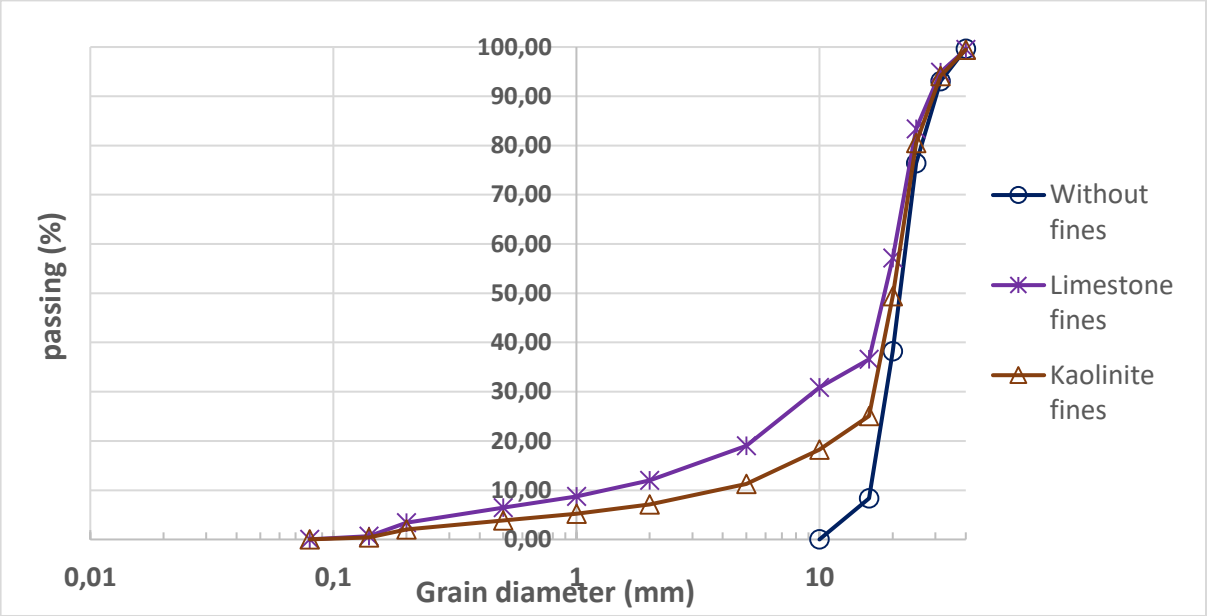

Figure 1. Grain size distribution of clean and degraded ballast with two different kinds of fines.

3. Results

The addition of fine particles to the large particles of limestone aggregate contributes to better compactness, thus reducing the total void ratio. Two different behaviours can be seen comparing the type of fines, i.e. limestone fines and kaolinite particles.

The introduction of limestone fines to limestone matrix induces less strain for the same stress level, thus, improving the mechanical properties of the sample. This stabilized behaviour is probably due to the small particles that induce more homogenized force distribution around the large particles. More the mass of fines, the more the rigidification of the sample.

The kaolinite fines have not the same effect, the sample deforms more with fines. Additionally, an increasing mass of clay particles, seems to act as a lubricant permitting the rearrangement of grains, due to the loss of contacts between large particles.

5. References

[1] Anbazhagan, P., Lijun, S., Buddhima, I., & Cholachat, R. (2011). Model track studies on fouled ballast using ground penetrating radar and multichannel analysis of surface wave. Journal of Applied Geophysics, **74(4)** : 175-184.

[2] Qian, Y., Tutumluer, E., Hashash, Y. M., & Ghaboussi, J. (2022). Triaxial testing of new and degraded ballast under dry and wet conditions. Transportation Geotechnics, **34:** 100744.

[3] Rohrman, A. K., & Ho, C. L. (2019). Effects of fouling containing plastic fines on abraded ballast strength and deformation properties. Transportation Geotechnics, **21**: 100278.

[4] Indraratna, B., Tennakoon, N., Nimbalkar, S., & Rujikiatkamjorn, C. (2013). Behaviour of clay-fouled ballast under drained triaxial testing. Géotechnique, **63(5) :** 410-419.

EXPERIMENTAL BEHAVIOUR OF FROZEN COARSE-MATRIX SOILS WITH VARIABLE FINE CONTENT

G. La Porta[1], F. Casini[2], and M. Pirulli[1]

[1] Politecnico di Torino, Department of Structural, Geotechnical and Building Engineering, Turin, Italy

[2] University of Rome Tor Vergata, Department of Civil Engineering and Computer Science Engineering, Rome, Italy

1. Introduction

Artificial Ground Freezing (AGF) is an eco-friendly consolidation technique, commonly adopted for the construction of shallow tunnels and wells below groundwater level [1]. The application consists of the insertion of freezing pipes around the excavation area. A coolant is circulated inside the pipes, thus provoking the surrounding soil to freeze. When a continuous frozen wall is formed, the area with lower permeability and higher strength allows for a safer and easier building phase.

AGF is often applied in soils characterized by intermediate or well-graded granulometry (e.g., along the new Line C of Rome Underground [2]). Consequently, the influence of heterogeneous and variegate grain size distribution on the thermo-hydro-mechanical (THM) behavior of soils must be systematically investigated. In literature different experimental studies focus on site materials. Although they are important for the effectiveness of individual projects, they are rarely generalizable. The presented research consists of an experimental campaign on gap-graded materials aimed at standardizing the behavior of intermediate soils. A sandy matrix is mixed with kaolin at percentages in mass from 0 to 15%, then the mixtures are subjected to a freezing process to investigate the influence of fine content on the THM behaviour observed. To these aims, a temperature-controlled triaxial apparatus, *FROZEN*, is used [3]. Its setup allows for the reproduction of on-site freezing conditions around a freezing pipe.

After a brief description of the materials and experimental device, the paper contains the main results of the experimental campaign aimed at understanding the THM behavior of the mixtures upon freezing. In particular, the performance of pure sand is compared with that observed when kaolin is added to the matrix. Additionally, the influence of increasing confining pressure (from 50 to 800 kPa) on freezing behavior is investigated.

2. Materials

The Fontainebleau sand, adopted for the experimental campaign, is characterized by an almost uniform grain size distribution [4]. Speswhite kaolin, a common clay of the literature, is mixed with the coarser matrix [5].

Kaolin is added to sandy soil at percentages of 0 and 15%. All mixtures are prepared with a constant theoretical initial water content and a fixed initial porosity, to be able to quantitatively compare the water movement (inlet/outlet) during freezing between mixtures.

3. Experimental setup

FROZEN [3] is a temperature-controlled triaxial device developed at the Tor Vergata University of Rome (Rome, Italy) and it is constituted by three main parts (Figure 1): 1. a triaxial cell, 2. a

mechanical press, 3. a refrigeration system. A copper tube axially crosses the centre of the specimen, and the refrigeration system circulates a coolant inside it with a mechanical pump, thus the frozen front advances radially from the center outwards.

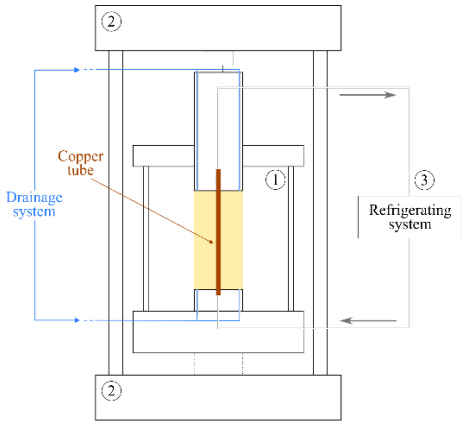

Figure 1: Scheme of the temperature-controlled triaxial device *FROZEN*.

The drainage system is designed as far away as possible from the copper tube: in this way, the sample is free to drain water until it is almost completely frozen, when the freezing front reaches the drainage tubes.

Tests follow the standard triaxial procedure, except for an additional freezing step: the sample is first saturated and then consolidated. Then freezing starts while the isotropic consolidation pressure is maintained. This stage lasts around ten hours.

4. Main results

During the experimental campaign, the pure sand showed to be not frost-susceptible, i.e., no strain was measured at freezing, as expected. Water outflow was registered, because of the water on the freezing front turning into ice, causing the drainage of the remaining liquid water out of the sample. This behaviour was confirmed in all confinements. On the contrary, the sand with 15% kaolin importantly swelled during freezing, with associated water inflow towards the freezing front, due to cryogenic suction. However, increasing confinement gradually inhibited strain and water inflow, so that at the highest confining pressure the water outflow turned to govern the behavior and the sample did not deform.

5. References

[1] Andersland, O. B. and Ladanyi, B. (2003). *Frozen Ground Engineering*. John Wiley & Sons.

[2] Viggiani, G. M. and de Sanctis, L. (2009). Geotechnical aspects of the construction of underground railways in the urban environment: The examples of Rome and Naples. *Geol. Soc. Spec. Publ.*, 22(1):215‑240.

[3] Bartoli, M., Casini, F., and Grossi, Y. (2020). Geotechnical characterisation of an artificially frozen soil with an advanced triaxial apparatus. *Tunnels and Underground Cities: Engineering and Innovation Meet Archaeology, Architecture and Art*, 646‑654. CRC Press, 2020.

[4] Vu, Q. H., Pereira, J. M., and Tang, A. M. (2022). Effect of fines content on soil freezing characteristic curve of sandy soils. *Acta Geotech.*, 17(11) :4921-4933.

[5] Boussaid, K. (2005). *Sols intermediaires pour la modelisation physique: application aux fondations superficielles*. PhD thesis, Ecole Centrale de Nantes et Universite de Nantes.

Experimental investigation of the evolution of fabric and elastic wave velocity in sand under shearing

Xiaomin Liang[1], Xiaoqiang Gu[1], Gioacchino Viggiani[2]and Alessandro Tengattini[2]
[1] Univ. Tongji, Department of Geotechnical Engineering and Key Laboratory of Geotechnical and Underground Engineering of the Ministry of Education, Shanghai, China
[2] Univ. Grenoble Alpes, CNRS, 3SR Lab., Grenoble, France

Strain-controlled drained triaxial tests were carried out on dry sand specimens to explore the correlation between the evolution of fabric and the elastic wave velocity in sand. During shearing, continuous measurements of sound waves were conducted, and X-ray tomography was employed at designated stress state to quantify the evolution of particle orientation and contact normal fabric. The experimental findings conclusively demonstrated that the measured sound wave velocity serves as evidence of structural alterations within the material during shearing.

Elastic waves serve as a unique and highly sensitive tool to probe the contact network configuration at the grain level and extract valuable information about the nonlinear dynamics of granular materials during slow shear flow[1]. Notably, wave velocities are found to be governed by sand fabric[2], presenting a compelling opportunity to extract information of microscopic fabric anisotropy in granular soils through multi-directional wave velocity measurements[3]. However, investigating the relationship between fabric evolution and macroscopic elastic wave velocity in sand during shearing remains a significant challenge. To address this challenge, this study employs piezoelectric transducers to excite and detect ultrasound waves propagating through randomly packed Hostun sand specimens subjected to drained triaxial tests. Concurrently, in-situ X-ray tomography measurements of contact fabric are conducted at designated strain levels. This research sheds some light on the underlying the intricate relationship between wave velocity and fabric evolution during shearing, offering valuable insights into the subject.

In experimental work, Hostun sand, a granular siliceous material with an angular to sub-angular shape, is used in this study. The specimen is prepared by sand pluviation method and it has a height of about 22mm and a diameter of 12 mm with relative density equal to 67%-77%. Drained triaxial tests were performed under a confining pressure of 100 kPa. The experiments were conducted in the X-ray tomography chamber at Laboratoire 3SR in Grenoble, France, which allows in-situ X-ray tomography measurements of contact fabric at designated strain levels. Before and after each X-ray scanning, the wave velocity of the specimen was measured by an ultrasound piezoelectric transducers.

About part of the results of elastic wave velocity evolution during shearing, Figure 1 illustrates the variation of deviator stress q and P-wave velocity with axial strain. Initially, both q and P-wave velocity exhibit a linear trend with increasing axial strain. The increments subsequently occur at a slower rate. Notably, the axial strain corresponding to the peak wave velocity is comparable to the deviator stress peak. After reaching the peak, the wave velocity experiences a subsequent decline.

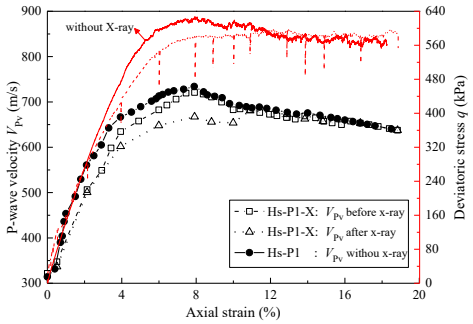

Figure 1. Variation of deviator stress and wave velocity with axial stain.

About part of the results of fabric evolution during shearing based on image analysis, Figure 2 shows the variation of both deviator stress and coordination number (*CN*) with axial stain. During the triaxial compression, the coordination number exhibits initial stability, remaining nearly constant, followed by a subsequent decrease. After surpassing the axial strain at which the peak stress and peak wave velocity are attained, the strain localization becomes prominent in the specimen, while particle arrangement undergoes minimal changes, leading to a relatively stable coordination number.

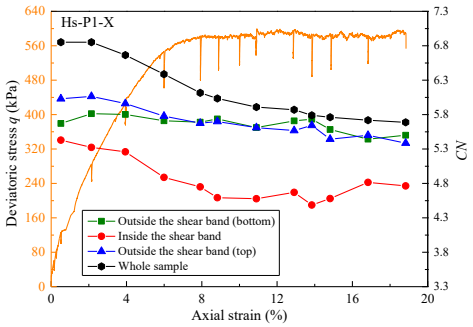

Figure 2. Variation of both the deviator stress and coordination number with the axial stain.

In conclusion, this investigation delves into the intricate interplay between the elastic wave velocity and the microstructural fabric within sand specimens subjected to triaxial compression. The findings underscore the significance of macroscopic wave velocity as a pivotal indicator for discerning and inferring the evolution of microstructure.

References

[1] Khidas, Y. & Jia, X. (2012) Probing the shear-band formation in granular media with sound waves[J]. *Physical Review E*, 85(5): 051302.

[2] Wiebicke, M., Andò, E., Viggiani, G., et al. (2020) Measuring the evolution of contact fabric in shear bands with X-ray tomography[J]. *Acta Geotechnica*, 15(1): 79-93.

[3] Gu, X. Q., Liang, X. M. & Hu, J. (2023) Quantifying fabric anisotropy of granular materials using wave velocity anisotropy: a numerical investigation[J]. *Géotechnique*, 1-13.

EXPERIMENTAL STUDY OF GRANULAR MATERIALS COMPOSED OF PLATONIC POLIPODS: EXPLORING GEOMETRIC COHESION AND SOLID FRACTION

D. Aponte[1,2], N. Estrada[1], J. Barès[2], M. Renouf[2] and E. Azéma[2,3]
[1] Universidad de los Andes, Dept. Civil and Environmental Engineering, Bogotá, Colombia
[2] Université de Montpellier, LMGC, CNRS, Montpellier, France
[3] Institut Universitaire de France, Paris, France

Granular systems generally exhibit solid-like behavior when grains are bound together by adhesive or cohesive forces. When these forces disappear, the material collapses in the form of a heap of grains. However, recent studies have shown that even in the absence of local cohesion, solid-like behavior can occur simply because of the shape of the grains, typically, using very non-convex grains. This was shown, for example, with particles such as superballs [1], U-shaped and Z-shaped grains [2 - 6], spiky particles, and polypods [7 - 10]. Despite the absence of adhesive forces, such systems can generate vertical surfaces and freestanding walls and columns or support high stresses. From a mechanical point of view, such extraordinary abilities have been attributed to the concept of "geometric cohesion", term coined for the first time by S.-V. Franklin [2]. In this investigation, we explore the emergence of this solid-like behavior in granular systems composed of strongly non-convex particles. To do so, we designed and built polypods with arms of different lengths and thicknesses, inspired by platonic solids, i.e., with 4, 6, 8, 12, and 20 arms (N_a), uniformly distributed around the particles' center. The relationship between the diameter of the particle and the thickness of the arms varies with the aim of analyzing particles with very thin arms to particles with arms so thick that they resemble a sphere (see Figure 1). This relationship corresponds to the parameter η, which we define as follows.

$$\eta = \frac{d-\delta}{d} \quad \#(1)$$

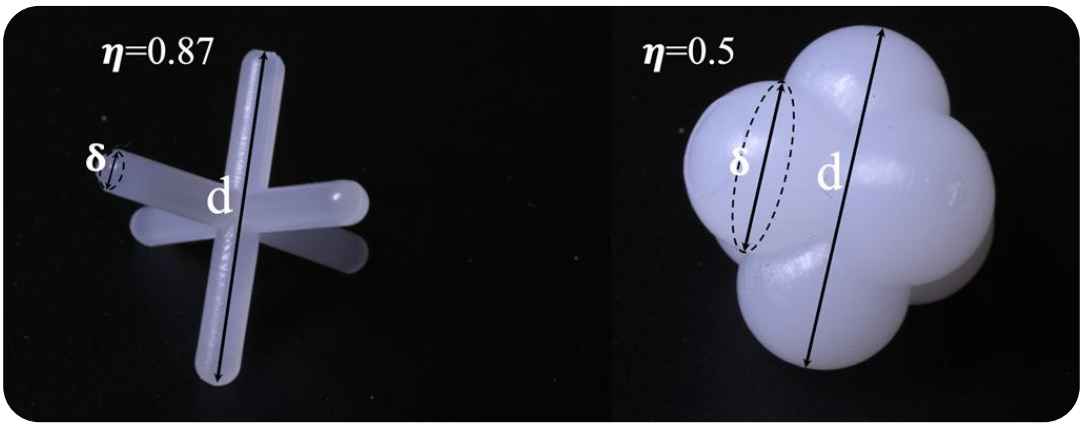

Figure 1. Geometric parameters of the particles. d = diameter of the particle. **δ**= thickness of the particle arm.

In order to study the effect of the local friction coefficient, we used three types of materials and construction techniques: (i) injected high-density polyethylene (PEHD) with a low friction coefficient; (ii) injected ethylene propylene diene monomer (EPDM), with intermediate friction; and (iii) printed polyamide 12 (PA12), which is highly frictional. Figure 2a shows the particles with the three materials used in the experiments, the geometric parameters of the analyzed systems are also presented. Monodisperse systems were built with the particles, which were poured by

pluviation into an acrylic cylinder. When the particles reached rest, the walls of the cylinder were removed, and the stability of the system was analyzed (see Figure 2b). The number of particles increases until the system reaches a state in which the constructed column always collapses. The experiment was carried out for different cylinder diameters ($\boldsymbol{D/\delta}$), i.e., with 2.75, 5.16, and 8.08.

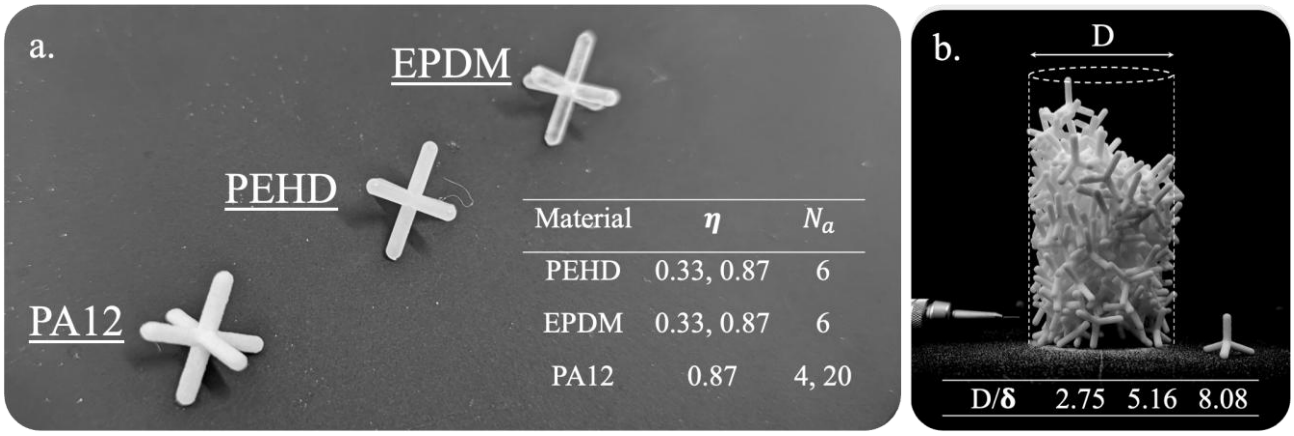

Figure 2. a. Characteristics of the different materials used in the experiments. $\boldsymbol{\eta}$ = aspect ratio (equation 1), $\boldsymbol{N_a}$= number of arms of the particles. b. The final state of stability analysis for particles with 4 arms and D/δ = 2.75. The range of diameters of the cylinder that forms the columns is also presented.

We find that geometric cohesion (i.e., solid-like behavior in the absence of adhesion between particles) emerges as an interplay between particle shape and local friction coefficient. In particular, this property is maximized when using highly frictional polypods with many thin arms. We also investigate the solid fraction of these unique materials, finding that it can reach values as low as 20%! This means that the voids occupy a volume that is four times larger than that of the grains. This delineates an exciting opportunity in the context of designing granular systems for a sustainable infrastructure.

[1] Y. Jiao, F. H. Stillinger, and S. Torquato, Phys. Rev. E **79**, 041309 (2009).
[2] S. V. Franklin, Physics Today **65**, 70 (2012), ISSN 0031-9228.
[3] N. Gravish, S. V. Franklin, D. L. Hu, and D. I. Goldman, Phys. Rev. Lett. **108**, 208001 (2012).
[4] S. V. Franklin, Europhysics Letters **106**, 58004 (2014).
[5] T. A. Marschall, S. V. Franklin, and S. Teitel, GranularMatter **17**, 121 (2015), ISSN 1434-7636.
[6] K. A. Murphy, N. Reiser, D. Choksy, C. E. Singer, and H. M. Jaeger, Granular Matter **18**, 26 (2016), ISSN 1434-7636.
[7] I. Malinouskaya, V. V. Mourzenko, J.-F. Thovert, and P. M. Adler, Phys. Rev. E **80**, 011304 (2009).
[8] J. de Graaf, R. van Roij, and M. Dijkstra, Phys. Rev.Lett. **107**, 155501 (2011).
[9] A. G. Athanassiadis, M. Z. Miskin, P. Kaplan, N. Rodenberg, S. H. Lee, J. Merritt, E. Brown, J. Amend, H. Lipson, and H. M. Jaeger, Soft Matter **10**, 48 (2014).
[10] F. Ludewig and N. Vandewalle, Phys. Rev. E **85**, 051307(2012).

Exploring Highly Deformable Mixtures of Soft and Rigid Grains: An Experimental Perspective from the Local Scale

Manuel Cárdenas-Barrantes[1], Jonathan Barés[2], Mathieu Renouf[2] and Émilien Azéma[2;3]

1 CFTC, Universidade de Lisboa, Lisbon, Portugal
2 LMGC, Université de Montpellier, CNRS, Montpellier, France
3 Institut Universitaire de France (IUF), Paris, France

Granular systems can consist of grains with vastly different mechanical properties. In our experimental study, we examine the compaction of 2D bidisperse systems made of soft and rigid particles. We analyze the evolution of their main macroscopic observables throughout the compaction process. This analysis spans from the quasi-loose state, through the jamming transition, to very high densities, considering both the local scale at each particle and the entire macroscopic system. We demonstrate the primary characteristics of such systems when each phase dominates, as well as identifying the main characteristic during the phase transition. This study marks the initial step towards a deeper understanding of the mechanical behavior of polydisperse granular materials in terms of grain rheology.

MACRO TO MICRO: RHEOLOGY AS A PROBE FOR MICROSTRUCURAL EVOLUTION IN CLAY-WATER SYSTEMS

M. Sasar[1], W. Hurdle[2] and M. Santagata[2]

[1] *Charles E. Via Jr. Department of Civil and Environmental Engineering,* Virginia Tech, Blacksburg, VA, USA

[2] *Lyles School of Civil Engineering, Purdue University, West Lafayette, IN, USA*

Abstract

Clay water dispersions exhibit complex rheological response, with significant differences observed even for a single clay mineral depending on solid concentration and geochemical parameters (ionic strength, pH and types of anions and cations). This large response function reflects the effects that these parameters have on the clay's double layer, and, as a result, on particle-to-particle interactions and microstructure.

This paper illustrates the use of rheological measurements as probes for monitoring the evolution of the microstructure of montmorillonite dispersions resulting from of changes in pore fluid salinity. The novelty of the work stems from: a) the custom experimental setup and testing protocol designed for seamless integration of pore fluid modification and rheological measurements; and b) the nature of the data extracted and the approach used to analyze them.

The experiments rely on a novel integrated setup (Figure 1) consisting of an injection system, an optical probe, and an Anton Paar MCR 301 rheometer. The first component (brine injection system) ensures controlled delivery and uniform mixing of pore fluid modifying additives (NaCl brine in the case of the experiments presented here) into a clay dispersion specimen inside the measuring cup of the laboratory rheometer. This setup enables modification of the pore fluid of the dispersion with real-time or quasi-real time (i.e. immediately following) rheological measurements. The optical probe allows detection of water solid separation in the clay-water system as well as the formation of bifurcation or complex flows inside the rheometer cup at high shear rates. The rheometer and the injection system are controlled using the same computer interface, ensuring complete automation of the process. The components of this patent-pending setup [1] are depicted in the schematic shown in Figure 1.

In the experiments described in this paper, a custom multi-stage testing protocol is used in conjunction with the above setup to perform repeat rheological measurements on a single specimen, as the pore fluid salinity of the bentonite clay-water mixture is increased in a step-wise fashion through controlled dosing of the brine. Because material non-linearities are known to be very sensitive to microstructural variations, changes in viscous and elastic non-linearities are monitored by performing large amplitude (0.01% to 1500%) oscillatory shear (LAOS) tests, with measurements of the intra-cycle instantaneous stress and strain.

The oscillatory data are first analyzed assuming linear viscoelastic behavior throughout the strain range. This approach is effective in identifying the dispersion's sol-to-gel transition, and clear trends are observed between salinity and key rheological parameters (small strain storage modulus, small strain phase angle, linear visco-elastic threshold, cross-over shear strain). Additional insight into microstructural transitions occurring as a function of salinity is provided by the large strain waveform data. Analysis of these data using the Sequence of Physical Processes' (SPP) method [2] shows how the bentonite clay-water structure deforms, undergoes failure and subsequently rebuilds

under oscillating deformations. These observations are used to develop a microscopic model of the interaction of bentonite particles with each other under various salinities.

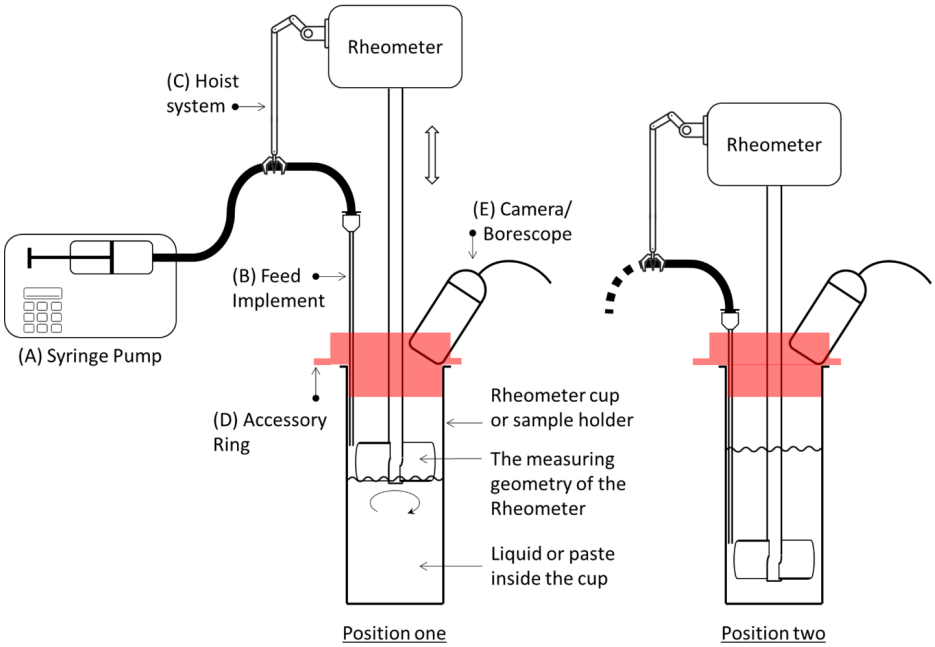

Figure 1. In-Rheometer automated additive dosing system. Positions 1 and 2 depict the beginning and the end of the brine dosing stages. Rheological measurements occur in position 2 [1].

References

[1] Purdue Research Foundation (2023) PRF. Ref.: 70391-01; Disclosure Title: Apparatus and Method for In-rheometer Automated Chemical Dosing and Reaction Monitoring of Fluid and Semi-solid Materials; US Provisional Patent App. No.: 63/612,020; Filing Date: December 19, 2023.

[2] Rogers, S. A. (2017). In search of physical meaning: Defining transient parameters for nonlinear viscoelasticity. *Rheologica Acta*, ***56***: 501-525.

MICROMECHANICAL BEHAVIOUR OF 'GRANULAR' SILT: IS IT CONTROLLED BY DLVO INTERACTIONS LIKE CLAYS?

Süleyman Demir [1], Arianna Pagano[2], and Alessandro Tarantino[3]
[1] Univ. Grenoble Alpes, CNRS, 3SR Lab., Grenoble, France
[2] University of Glasgow, James Watt School of Engineering, UK
[3] University of Strathclyde, Dept. of Civil and Environmental Engineering Glasgow, UK

1. Introduction

Experimental investigation of micromechanical behaviour of soils has focused on either sand [1] or clay [2] materials. Silt materials live in a limbo. They are often considered 'granular' [3], that is they are assumed to exhibit sand-like behaviour from a micromechanical standpoint. On the other hand, silt is often associated with clay when identifying the finer fraction of soils. The research question addressed in this work is whether silt behaves like sand materials, with inter-particle interactions dominated by mechanical contact forces, or like clay materials, with inter-particle interactions also controlled by non-contact interaction forces, namely van der Waals attraction and Coulombic repulsion (i.e., DLVO interaction).

Research hypothesis: If Columbic forces play a key role in micromechanical behaviour of silt, then a change in electrolyte concentration should produce a measurable change in macroscopic behaviour. Such a change should be interpreted within the framework of the DLVO theory.

2. Materials and specimen preparation

Silica silt was employed in the experimental study. The silt was obtained by crushing quartz sand; its mineralogical composition is silicon dioxide (SiO_2). The grain size distribution showed it to have 95% silt fraction (particle size ranging from 0.002 mm to 0.075 mm). The median grain size (D_{50}) of the silt was 0.02 mm, and the coefficients of curvature (Cc) and uniformity (Cu) were 1.29 and 7.3 respectively. According to the Unified Soil Classification System, the silt is classified as low plasticity silt (ML). To investigate the effect of electrolyte concentration, the silt was saturated with either deionised (DI) water or sodium chloride (NaCl) solutions with concentrations of 0.05M, 0.5M, 3M, and 5M respectively.

3. Experimental procedures

An oedometer ring with a diameter of 75 mm and a height of 20 mm was filled with dry silt. After applying a vertical stress of 2 kPa to ensure adequate contact between the specimen and the top cap, the sample was flooded from the bottom by letting either the deionised water or the NaCl solutions to flow into the sample from a large reservoir. The reservoir was positioned at the same elevation as the oedometer cell rim to allow for gentle ingress of fluid into the sample and avoid excessive and undesirable deformation caused by excessive hydraulic gradients.

4. Results

Figure 1 shows vertical deformation following flooding with electrolyte solutions of varying NaCl concentrations (0.05 M, 0.5 M, 3 M, and 5 M) and DI water. The progressive deformation recorded over the initial ~2min is associated with the progressive saturation of the initially dry silt specimen. The deformation levelled off at ~2min when the water front finally reached the sample top surface.

The initial volumetric collapse recorded at ~2min reduced with increasing NaCl concentration. The deformation after 2min following this initial stabilisation was also affected by the NaCl concentration, with time-dependent deformation decreasing as NaCl concentration increased. The volumetric collapse of silt saturated with DI water was approximately 60% higher than that of silt saturated with a 5M NaCl solution 2 minutes after the onset of flooding. This initial stage was followed by a full loading and unloading cycle that will be presented in the paper. The differences in void ratio generated during the first flooding persisted during the loading and unloading.

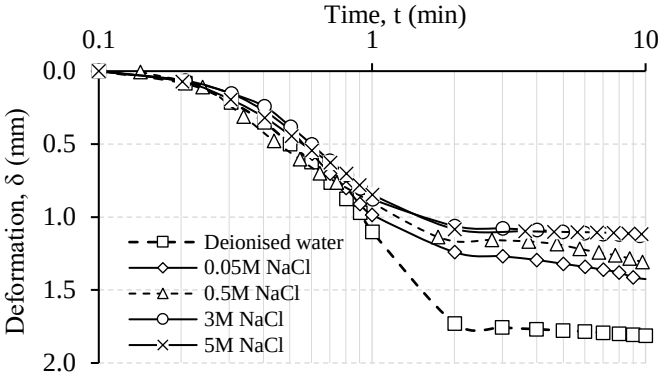

Figure 1. The creep deformation of silt saturated with varying electrolyte solution of NaCl

5. Discussion

The volumetric change can be associated with a re-arrangement of the 'granular' skeleton following sliding at the interparticle contact. The higher is the (compressive) interparticle normal force, the higher is the shearing resistance at the interparticle contact, and the lower is the susceptibility of the particles to slide and, hence, of the sample to change its volume. The normal force is generated by i) the mechanical force in turn associated with the external stress applied, ii) the van der Waals attraction, and iii) the Columbic repulsion. As a first approximation, the mechanical force does not play significant role in this process because the external stress is maintained constant before and after flooding. Volume change observed after flooding and its dependency on electrolyte concentration must therefore be associated with the van der Waals attraction and Columbic repulsion.

Under dry conditions, the surface density charge can be assumed to be equal to zero (the absence of water does not generate electrical charge associated with deprotonation of the silica interface). The interparticle normal force is therefore augmented by the van der Waals attraction. Upon flooding, the silica surface develops a negative charge due to deprotonation of the silanol group. In turn, this generates a Columbic repulsion that reduces the net normal (compressive) interparticle force compared to the case of dry silt. This explains the volumetric collapse upon flooding.

The effect of electrolyte concentration can be explained by two mechanisms, i) the decrease the of the surface density charge of the ionisable surface due to the charge regulation in the electrical double layer, and ii) the depletion of the diffuse double layer due to the far-field higher ionic concentration. Both mechanisms decrease the Coulombic repulsion and, hence, generate a higher 'stabilising' net normal compressive interparticle force. The higher is the electrolyte concentration, the higher is the normal interparticle force, and the lower is the volumetric collapse upon flooding.

References

[1] Andò E., Hall S. A., Viggiani G., Desrues J. & Bésuelle P. (2012). Grain-scale experimental investigation of localised deformation in sand: a discrete particle tracking approach. Acta Geotechnica, **7**: 1-13

[2] Pedrotti M. & Tarantino A. (2018). An experimental investigation into the micromechanics of non-active clays. Géotechnique, **68**: 1-18

[3] Paniagua P., Fonseca J., Gylland A. et al. (2018). Investigation of the change in soil fabric during cone penetration in silt using 2D measurements. Acta Geotech. **13**: 135–148.

MONOTONIC AND CYCLIC BEHAVIOR OF MALAYSIAN KAOLIN UNDER DIFFERENT SHEARING RATES

Covilla, E.[1]*, Mašín, D.[1], Duque, J.[1,2], Najser, J.[1], Roháč, J.[1]
[1] Charles University, Prague, Czech Republic
[2] Universidad de la Costa, Barranquilla, Colombia

Abstract

Several different geotechnical structures are under loading whose magnitude presents a stochastic nature in terms of amplitude and frequency [1, 2, 3, 4]. Examples of those scenarios are the loadings by the wind, waves, floods, among others. It is then relevant to evaluate the behavior of fine-grained soils under a wide range of loading conditions.

This article presents the results of an extensive experimental program conducted to evaluate the influence of the displacement rate on the monotonic and cyclic response of Malaysian kaolin samples. On the one hand, a series of undrained monotonic triaxial tests were initially performed with different displacement rates, where a clear rate-dependency was observed up to a threshold, see Figure 1. On the other hand, it was found that under cyclic loading for a given loading frequency, the variation in the deviatoric stress influences the rate of pore water pressure accumulation and strains. Additionally, a dependence of the loading frequency on the shapes of the mobilized effective stress loops was observed (Figures 2 and 3). Higher loading frequencies result in "banana" shaped effective stress loops, while lower frequencies reproduce eight-shaped effective stress loops.

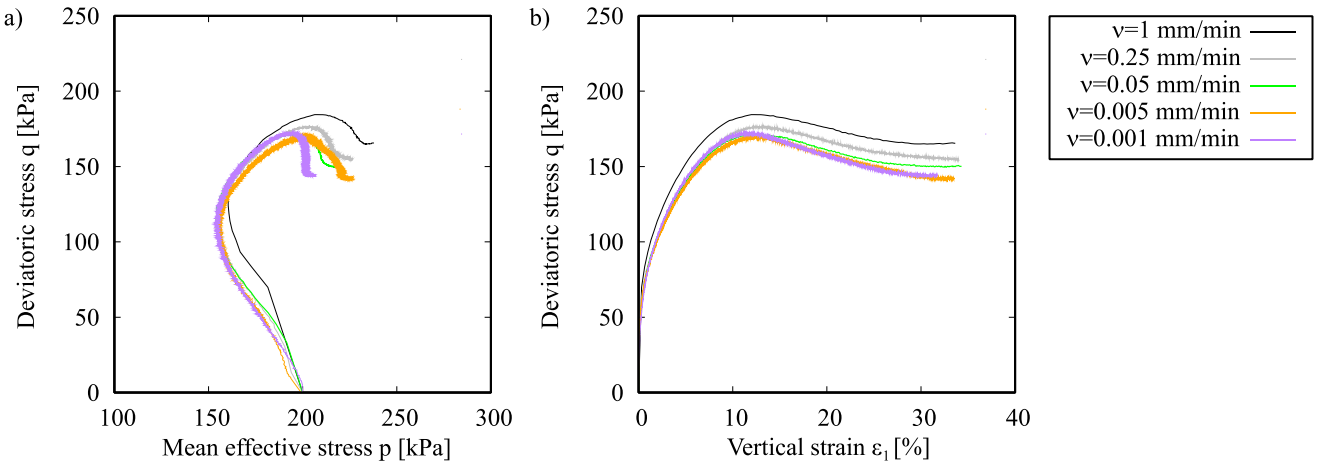

Figure 1. Undrained monotonic triaxial tests on samples with isotropic consolidation and variation of the displacement rate ν = {1.0, 0.25, 0.05, 0.005, 0.001} mm/min

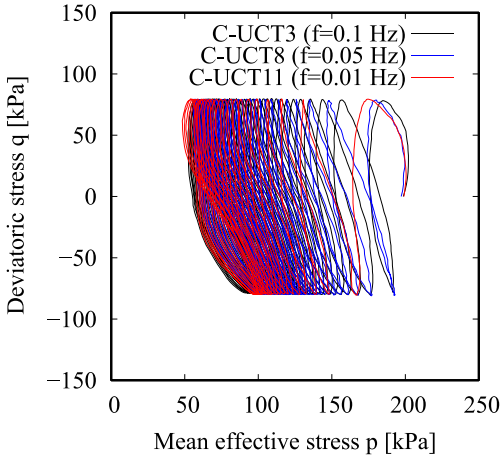

Figure 2. Typical results of undrained cyclic triaxial tests with isotropic consolidation (p_0 = 200 kPa), deviatoric stress amplitude of q^{amp} = 80 kPa and variation of the loading frequency f = {0.1, 0.05, 0.01} Hz

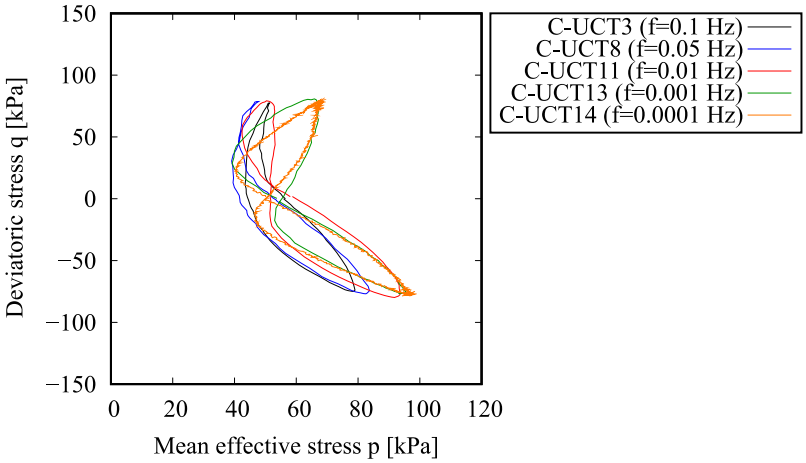

Figure 3. Mobilized effective stress loops obtained on undrained cyclic triaxial tests with isotropic consolidation (p_0 = 200 kPa), deviatoric stress amplitude q^{amp} = 80 kPa and variation of the loading frequency f = {0.1, 0.05, 0.01, 0.001, 0.0001} Hz

References

[1] K. Andersen. Bearing capacity under cyclic loading - offshore, along the coast, and on land. The 21st Bjerrum lecture presented in Oslo, 23 november 2007. Canadian Geotechnical Journal, 46(5):513–535, 2009.

[2] M. Tafili, J. Duque, M. Ochmański, D. Mašín, and T. Wichtmann. Numerical inspection of miner's rule and drained cyclic preloading effects on fine-grained soils. Computers and Geotechnics,156:105310, 2023.

[3] T. Wichtmann. Soil behaviour under cyclic loading: Experimental observations, constitutive description and applications. Habilitation, Karlsruhe Institute of Technology (KIT), 2016.

[4] T. Wichtmann, A. Niemunis, and T. Triantafyllidis. Gilt die minersche regel für sand? Bautechnik, 83(5):341–350, 2007.

NEW EXPERIMENTAL DEVICE FOR THE VISUALISATION OF FLUID-DRIVEN CRACKS IN CLAYS

J. Liaudat[1,2], P.J. Vardon[2], M.A. Hicks[2] and A.C. Dieudonné[2]

[1] Technische Universität Darmstadt, Institute of Geotechnics, Darmstadt, Germany

[2] Delft University of Technology, Department of Geoscience & Engineering, Delft, The Netherlands

1. Introduction

The generation or injection of gas into a liquid-saturated, clay-rich material can lead to the development of narrow channels or fractures, a result of the mechanical action of gas pressure. The complexity inherent in the mechanical and transport properties of clays, along with the high compressibility of gas, present significant challenges in understanding and addressing this phenomenon. Gas fracturing occurs in various engineered processes such as gas (CO_2, H_2, CH_4…) injection and storage in subsurface reservoirs, pneumatic fracturing for enhanced remediation of contaminated soils, and gas transport through natural and engineered clay barriers in geological disposal facilities for radioactive waste. Despite its wide-ranging environmental and economic implications, predicting and controlling gas fracturing remains a challenge due to a lack of fundamental scientific insight.

In this context, this paper introduces a novel experimental device currently under development at TU Delft. This device is designed to study gas-driven cracking in clays within a model system. It enables the induction and observation of 'two-dimensional' cracks in clay-rich, low-permeability materials through the injection of gas or water. The device design draws inspiration from the work of Wiseall et al. [1,2], albeit with significant enhancements.

2. Experimental setup and preliminary results

The proposed experimental device is schematically described in Figure 1. In this setup, a thin layer (~1mm) of clay paste is compressed between two transparent discs of 110 mm diameter and 50 mm height. The bottom disc has a central hole through which a steel pipe is inserted to inject the fluid at the centre of the clay sample through a tip filter. A perimeter filter contains the sample laterally while allows to control the back-pressure during the fluid injection. The transparent discs and the perimeter filter are positioned by means of three steel rings, which are guided by four precision shafts. The compression of the clay sample is achieved by tightening nuts at the threaded ends of the shafts.

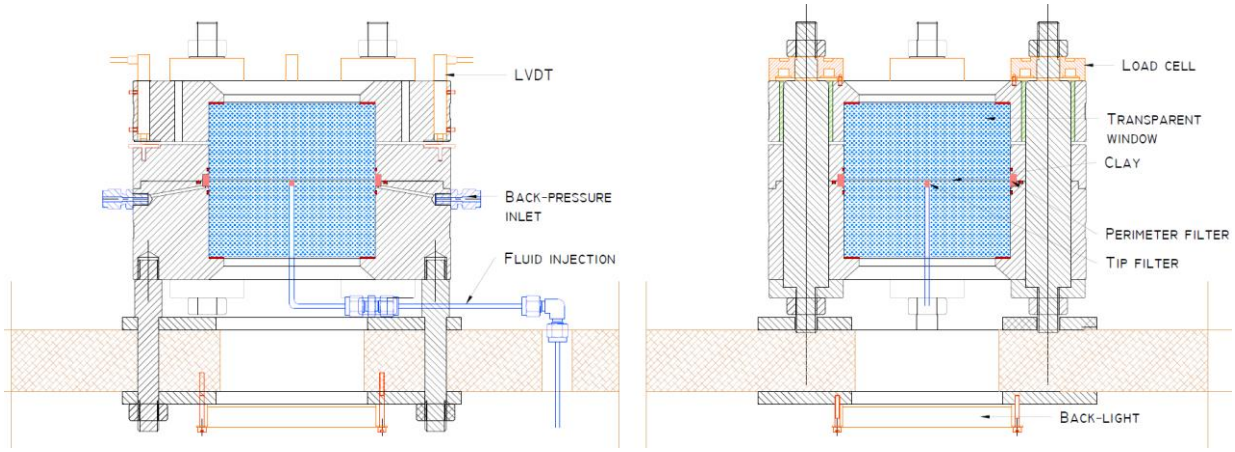

Figure 1. Two cross-sections of the new experimental device (45° rotation).

The device is instrumented with four donut load cells (one per shaft) placed in between the tightening nuts and the top ring to measure the compression forces, two displacement traducers (LVDT) to measure the relative displacement of the transparent discs, and fluid pressure transducers connected to the injection pipe and to the perimeter filter. The experimental setup is completed with two high-precision high-pressure pressure-volume controllers, that permit to control fluid injection rate and the back-pressure. In addition, pictures are taken with a high-resolution camera at a regular rate during the fluid injection, through the top transparent disc. To enable the detection of thin cracks, the device and the camera are placed in a dark box, with a collimated backlight panel placed under the bottom transparent disc.

The new experimental setup and the associated testing protocol has been evaluated in a series of preliminary tests performed on reconstituted Boom clay samples. In these tests, Helium gas was injected at a constant rate of 25 mL/h, for different compression and back-pressure levels. As the injection progress, the injection pressure first follows the gas compressibility curve, until the pressure is high enough to invade the sample creating cracks that propagate into the sample towards the back-pressure filter (Figure 2). When cracks connect the injection and back-pressure filters, a sharp drop is observed in the injection pressure. This depressurisation is followed by a partial sealing of the cracks.

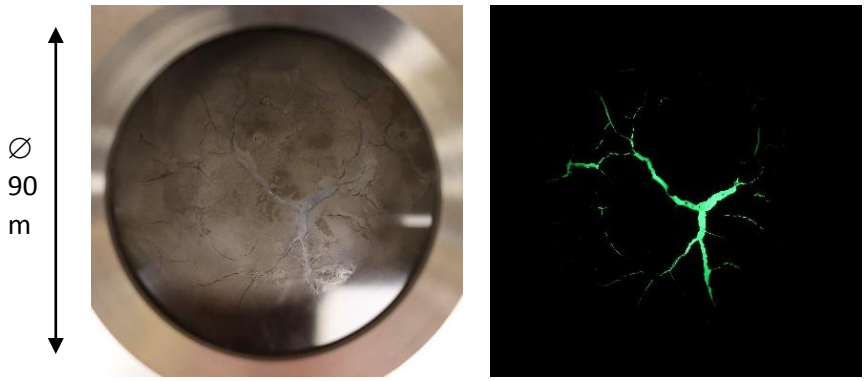

Figure 2. Boom clay sample cracked by gas injection: pictures obtained with normal room light (left) and with a dark box and collimated green back-light (right).

3. Conclusion

The new experimental device makes it possible to study in a model system the factors controlling the formation and vanishing of discrete pathways in clay-rich materials as fluids (gas or water) are injected. In particular, these experiments will allow to validate numerical models with explicit representation of fluid-driven fractures as the one recently proposed by the authors elsewhere [3].

4. References

[1] Wiseall, A. C., Cuss, R. J., Graham, C. C., & Harrington, J. F. The visualization of flow paths in experimental studies of clay-rich materials. *Mineral. Mag.*, 79(6), 1335–1342

[2] Wiseall, A. C., Cuss, R., & Hough, E. (2019). Visualising hydraulic fractures in bedded and fractured shales: A series of analogue experiments. In *Proceedings of the 5th International Conference on Fault and Top Seals*, Palermo, Italy, September 2019, EAGE Publications BV.

[3] Liaudat, J., Dieudonné, A., & Vardon, P. J. (2023). Modelling gas fracturing in saturated clay samples using triple-node zero-thickness inter-face elements. *Comput. Geotech.*, 154, 105128

STACKING AND COLLAPSE OF SEDIMENTS FORMED BY AIR-FALL DEPOSITION: AN EXAMINATION OF PARTICLE-SIZE EFFECTS

Zhonghao Sun[1], Suying Nong[1] and Ling Xu[1]

[1] Xi'an Jiaotong University, School of Human Settlements and Civil Engineering, Xi'an, China

1. Introduction

Aeolian deposition is important in the landscape formation on Earth. Particle-size effects on the structure and mechanical behavior of aeolian deposits remain less understood. Particularly, collapsible soils such as loess present abundant silt-size particles whose role in collapsibility is unclear. This study aims to examine the effect of particle size on the structure and collapsibility of sediments formed by air-fall deposition and investigate the underlying particle-scale mechanisms.

2. Methods

Materials. Six quartz samples (Q1-Q6) with different particle size distributions were tested (Figure 1a). Representative diameter d_r is the particle size at the highest point of the differential curve.

Air-fall deposition. Air-fall deposition method (Figure 1b) was used to simulate dust deposition (Assallay et al., 1997). Particles fall from a sieve controlled by an oscillator to an oedometer ring.

Compression and collapse tests. One-dimensional compression and collapse tests were conducted using oedometers to measure the mechanical properties and collapse potential.

Deposition process monitoring. The deposition process of particles on a thin flat surface (width < 1 mm) was monitored by a digital camera and the structure was examined by an optical microscope.

X-ray tomography analysis. The microstructure of deposits of samples Q4, Q5, and Q6 was examined by X-ray tomography analysis (Zeiss Xradia 610versa). A special sampling tube was designed to obtain high-resolution images.

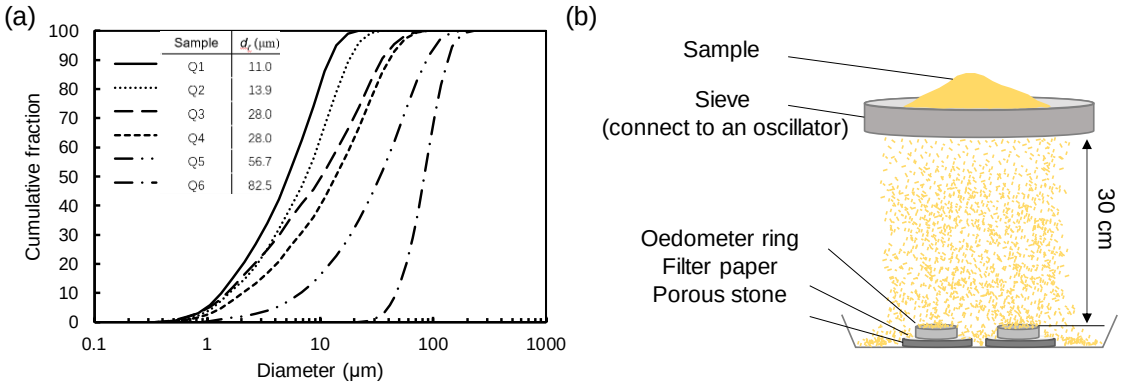

Figure 1. (a) Particle size distribution of tested materials and (b) the air-fall deposition setup.

3. Results and Discussion

Particle stacking. We observed vertical stacking of particles on the thin wall of the oedometer ring for Q1-Q5 (Figure 2a). The stacking height can be over 1 cm, hundreds of times the size of particles. The stacking height increases as particle size decreases or wall thickness increases. However, no particle stacking was observed for Q6 (d_r = 82.5 mm, fine sand).

Packing density and collapse potential. The packing density (or initial void ratio) was measured after deposition. The collapse potential was measured after compression to σ_v = 50 kPa and water

flooding. Results displayed in Figure 2b show that as particle size increases, the void ratio of sediments formed by air-fall deposition decreases and gradually stabilizes. The void ratio is 0.930 for Q6, which is close to the void ratio of a simple cubic packing. The collapse potential also decreases as particle size increases for Q1-Q5. And no collapse of the sediments was observed for Q6.

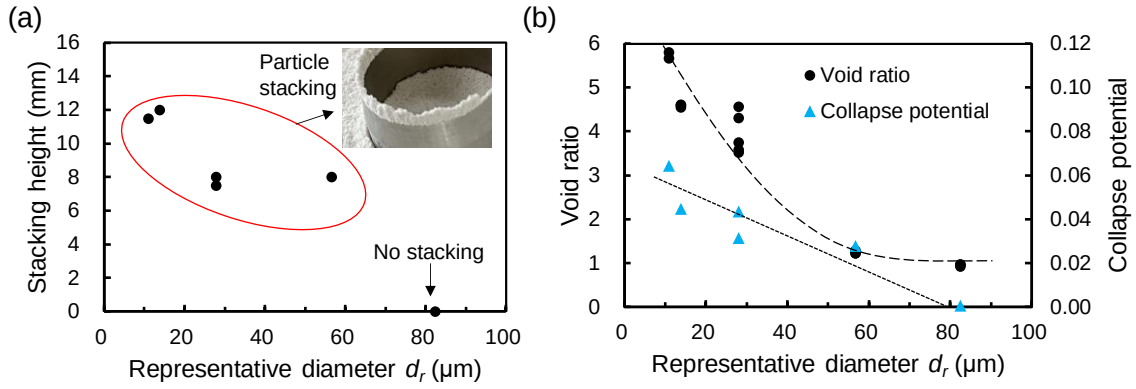

Figure 2. (a) Particle stacking on a 1.6 mm thin wall and (b) the initial void ratio and collapse potential of deposits formed by Q1-Q6 (revised from Xu et al., 2024).

Particle-scale mechanisms. We observed the falling of particle aggregates for small particles (Q1-Q5) and the falling of discrete particles for Q6 (Figure 3). The deposition process of Q1 (Figure 3a) shows that aggregates can adhere, stack, and form inter-aggregate pores. The interparticle forces outweigh gravity as particle size decreases. We identify a dimensionless granular Bond number *Bo* which is the ratio of van der Waals attraction F_{vdw} to gravity G: $Bo = A/(4z_0^2\rho_w d_s \pi g D^2)$. The granular Bond number decreases with increasing particle size. The adhesion effect between particles dominates when $Bo > 10$ and particle stacking and structure collapse are observed (Figure 3b).

The particle-size effects on mixtures, the microstructure of collapsible sediments, and implications on the properties of aeolian deposits have also been investigated. Results are relevant to understanding the formation of collapsible aeolian deposits on Earth and even other planetary bodies.

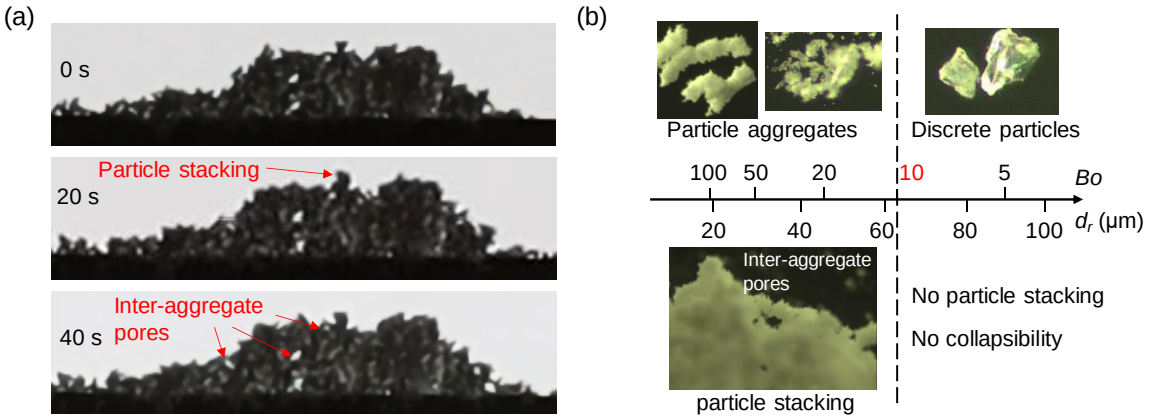

Figure 3. (a) Deposition of Q1 on the surface of a 0.1 mm thin wall and (b) particle-scale analysis.

4. References

[1] Assallay, A. M., Rogers, C. D. F., & Smalley, I. (1997). Formation and collapse of metastable particle packings and open structures in loess deposits. *Engineering Geology*, **48**: 101-115.

[2] Xu, L., Nong, S., Yu, D., & Sun, Z. (2024). Particle-size control on the structure and collapsibility of sediments formed by air-fall deposition. *Catena*, **236**: 107743.

STIFFNESS AND DAMPING OF ASSEMBLIES OF ENGINEERED PARTICLES

K. Garzon-Sabogal[1], M. Santagata[1], J. V. Sinfield[1] and M. Velay-Lizancos[1]
[1] Lyles School of Civil Engineering, Purdue University, West Lafayette, IN, USA

Abstract

Extensive research has been conducted over the past 50 years to explore the stiffness and attenuation behavior of granular soils, as these properties are critical to geotechnical engineering design. These studies have revealed that many factors affect both damping and shear modulus and their evolution with strain level. These include: packing of grains, applied stresses, stress history, bonding/cementation, aging, particle gradation, presence and quantity of fines, with more recent work highlighting the role played by the morphology and mineralogy of the grains themselves. Collectively, these factors determine the number and nature of interparticle interactions. Different mechanisms have been put forth to describe these interactions and explain the observed variation of damping and shear modulus with stress and strain level. Slippage at the grain contacts is generally considered responsible for fabric changes that lead to a reduction of the modulus, while the increase in damping with strain level has been attributed to frictional losses. More complex mechanisms including thermoelastic relaxation, interactions between asperities and grain-pore fluid viscous interactions have been hypothesized to control damping at very small strains.

This paper adds to this body of work by exploring contributions to stiffness and damping that arise from non-homogeneity in the mechanical characteristics of the grains. Specifically, the experimental program investigated the stiffness and attenuation response of a model material comprised of custom engineered particles with a rigid core (glass beads) and a softer solid shell (soft silicone). The modulus of the core and the shell differ by several orders of magnitude.

The paper describes the novel material manufacturing method conceived to enable control of the shell thickness, and presents preliminary results of tests used to characterize the particles at the microscopic scale, and to evaluate the macroscale dynamic response of granular assemblies of these particles. Results are compared to reference data from tests on the unaltered core particles (glass beads).

Characterization of the macro response focused on measurements of the shear modulus and damping in the resonant column apparatus, using frequency sweeps. This novel approach to resonant column testing relies on applying a fixed amplitude sinusoidal torque over a wide range of frequencies that encompasses the resonant frequency, and allows semi-continuous characterization of the shear modulus degradation and shear damping increase with strain level.

The results of the resonant column tests show that when the shell is sufficiently thick the damping at small strains is increased, mainly dominated by the lossy characteristics of the soft silicone. The opposite behavior is observed for the small strain shear modulus, which is reduced due the softer nature of the shell. These effects are reduced with increasing confining stress, as the rigid cores start interacting with each other. The modulus degradation curves are also altered as the frictional losses are not controlled by the rigid core, but by the softer shell.

UNDRAINED INSTABILITY RESPONSE OF GRANULAR MATERIAL IN FLEXIBLE BOUNDARY PLANE STRAIN CONDITIONS

Sukrit Sharma[1], Viswanath Parol[2] and Amit Prashant[1]

[1] Department of Civil Engineering, Indian Institute of Technology Gandhinagar, India

[2] Department of Civil Engineering, Amrita School of Engineering, Coimbatore, Amrita Vishwa Vidyapeetham, India

Instabilities in granular materials arise in the form of diffused instability, shear banding, buckling, or barrelling. In boundary value problems, these instabilities are reflected as the zones of intense shearing leading to the formation of failure mechanisms. Solid-fluid instability or static liquefaction is another kind of instability which can cause catastrophic failures in geotechnical structures. Various studies have characterised the different modes of instability in both triaxial and plane-strain conditions [1–4]. However, the boundary conditions significantly influence the observed response of granular materials. The shear bands formed under triaxial [5] and plane-strain conditions [1] were observed to reflect from the rigid end conditions in the experimental test setup. The boundary conditions can influence the instability onset and the post-instability response. The present study, therefore, uses a flexible boundary plane-strain (FB-PS) apparatus [6] to characterise the instability behaviour under undrained conditions.

The FB-PS test setup includes pressure application along the lateral (σ_3) and principal (σ_1) loading directions, as shown in Figure 1. The deformations occurring in these two directions are also measured using the LVDTs placed inside the pressure housings. The flexible membranes fabricated using butyl rubber material used along all four sides provide a distinct advantage over other plane-strain test setups. It prevents non-uniform stress distribution in the soil specimen, as observed in tests with rigid boundaries [7]. The variability in response due to boundary conditions is explored under two different boundary conditions. Firstly, a flexible boundary case involves employing flexible butyl rubber membranes along all four sides. Secondly, a mixed boundary case wherein a slightly rigid boundary is adopted along the deformation-controlled boundary (σ_1) by combining thin aluminium sheets with flexible butyl rubber membranes. Consolidated undrained tests are performed on medium-dense (RD 50%) Sabarmati sand at two confining pressures ($\sigma_3' = 25\ and\ 50\ kPa$) for the above-mentioned boundary conditions.

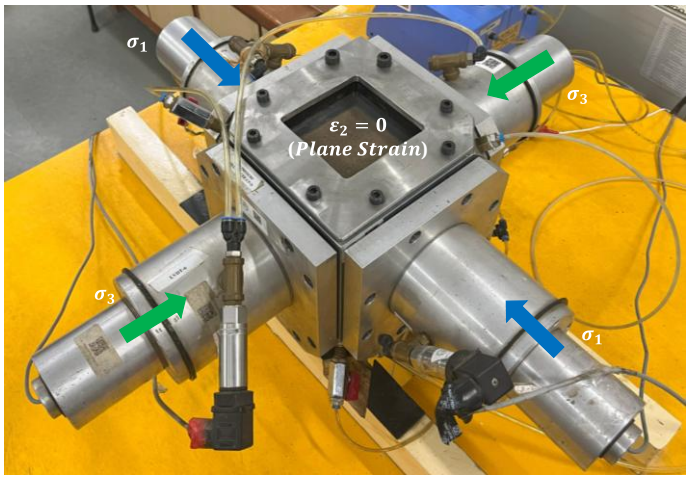

Figure 1. Flexible Boundary Plane-Strain (FB-PS) Test Setup.

The soil specimen could resist greater deviatoric stress in the flexible boundary case, as shown in Figure 2a. Moreover, the excess pore water pressure response is more dilative with a flexible boundary as compared to the mixed boundary case (Figure 2b). The onset of instability is comparatively slower in the case of flexible boundary as compared to mixed boundary case.

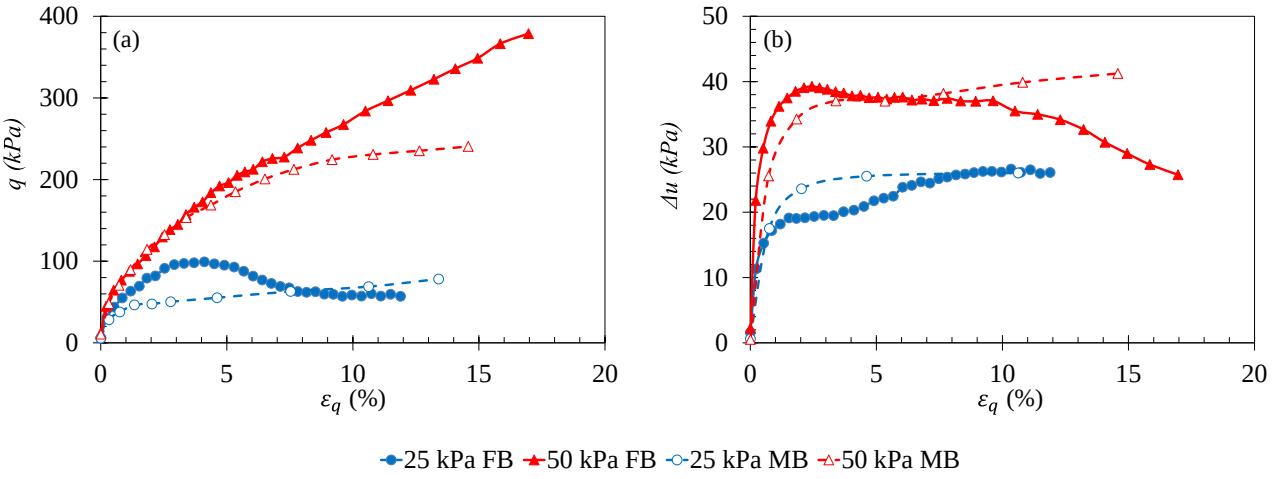

Figure 2. (a) Deviatoric stress and (b) excess pore pressure response for medium-dense Sabarmati sand under different boundary conditions.

References

[1] Desrues J, Lanier J and Stutz P 1985 Localisation of the deformation in tests on sand sample *Eng. Fract. Mech.* **21** 909–21

[2] Desrues J and Viggiani G 2004 Strain localisation in sand: an overview of the experimental results obtained in Grenoble using stereophotogrammetry *Int. J. Numer. Anal. Methods Geomech.* **28** 279–321

[3] Chu J and Wanatowski D 2008 Instability Conditions of Loose Sand in Plane Strain *J. Geotech. Geoenvironmental Eng.* **134** 136–42

[4] Bobei D C, Lo S R, Wanatowski D, Gnanendran C T and Rahman M M 2009 Modified state parameter for characterising static liquefaction of sand with fines *Can. Geotech. J.* **46** 281–95

[5] Rowe P W and Barden L 1964 Importance of Free Ends in Triaxial Testing *J. Soil Mech. Found. Div.* **90** 1–27

[6] Bhattacharya D and Prashant A 2020 Effect of Loading Boundary Conditions in Plane Strain Mechanical Response and Local Deformations in Sand Specimens *J. Geotech. Geoenvironmental Eng.* **146** 1–16

[7] Arthur J 1988 State-of-the-Art Paper: Cubical Devices: Versatility and Constraints *Advanced Triaxial Testing of Soil and Rock* vol STP 977 (100 Barr Harbor Drive, PO Box C700, West Conshohocken, PA 19428-2959: ASTM International) pp 743-743–23

Advances in experimental methods

Experimental observations of geomaterials behaviour using imaging

3D characterization of microstructure and strain localization due to large deformation in ring shear tests on sand using X-ray CT image analysis

S. Nohara[1], T. Mukunoki[2]

[1] Central Research Institute of Electric Power Industry, Chiba, Japan

[2] Kumamoto University, Faculty of Advanced Science and Technology, Kumamoto, Japan

1. Introduction

When a granular material is loaded, strains are localized within the material and eventually form a shear zone that leads to failure. Since the ground is composed of a number of particles with different properties, localization and heterogeneity have a significant influence on the formation of shear zones. Therefore, in order to achieve an accurate understanding of the mechanical properties of the ground, the correspondence between microstructure and strain that changes as shear progresses must be determined. In particular, it is significant to conduct laboratory experiments using sand materials to evaluate the microstructural evolution during the sequence of processes from peak shear stress, strain softening, and residual state.

The authors are conducting laboratory experiments using microfocus X-ray computed tomography (CT), which can visualize the inside of a sample nondestructively, in combination with CT imaging and mechanical tests, and are attempting to quantitatively evaluate the microstructure inside the shear zone by imaging analysis [1]. Especially, this study focuses on the residual strength, which is important for the stability evaluation of civil engineering structures. A ring shear experimental apparatus was developed that can reproduce long shear deformations in a laboratory [2] and is compatible with visualization using X-ray CT. In this study, ring shear experiments were conducted using sand, and the internal structure was visualized using microfocus X-ray CT.

2. Ring shear experiment

Figure 1 (a) and (b) shows a schematic figure of the ring shear experimental apparatus. The ring shear vessel had an outer diameter of 40 mm, inner diameter of 20 mm, and height of 20 mm. The size of the ring shear vessel was smaller than that of a general ring shear vessel because of the soil particle size and the size of the field of view in CT imaging. The vessels within the area filled with

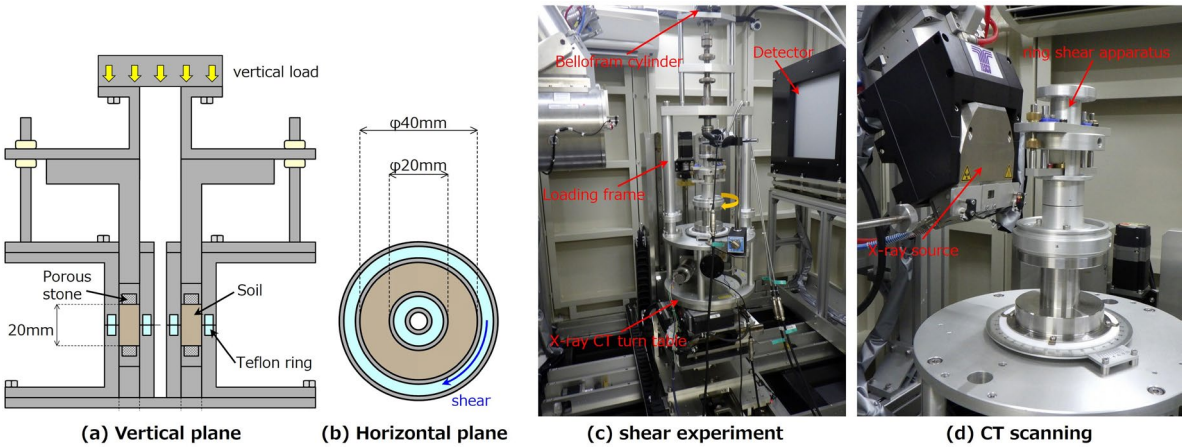

Figure 1. Ring shear experimental apparatus installed on the turntable of an X-ray CT.

sand were fabricated from aluminum to ensure the transmission of X-rays. Figure 1 (c) and (d) shows the experimental and CT imaging setup. As the specimens were not lifted off the turntable during this test, it was assumed that there was no misalignment of the specimens.

In this experiment, silica sand (D_{50} = 0.66 mm) was used as the experimental material. CT imaging was performed using a 160 kV X-ray source (minimum focal spot size: 4 μm) for the microfocus X-ray CT system (TXS-450/160) installed at CRIEPI. The vertical stress was 300 kPa, and the shear velocity was 0.2°/mm. CT imaging was performed at rotational angles (θ_r) of 0°, 2°, 6°, 12°, 20°, 40°, 90°, and 180°.

3. CT scanning results

Figure 2 shows a CT scanning results. The size of the CT image is 2100 × 2100 × 1200 voxels, and the pixel size is 0.023 mm/voxel. The CT images obtained in this study had sufficient resolution to identify the structure of the particles. As shear is applied through rotation, pixel values are obtained every 0.1° at a radius of 15 mm from the center of rotation (Fig. 2(a)), and a cross section is created along the direction of shear (hereinafter referred to as a circumferential direction image). Figure 2(b) shows a circumferential direction view at θ_r = 0°, and Figure 2(c)-(f) shows the enlarged images near the shear plane at θ_r = 0, 20, 90, 180°, respectively. In this experiment, the shear stress reaches its peak at θ_r = 15°. The CT images show that the structure of the initial particle array structure was preserved until θ_r = 20°, however, as the shear progresses, the local voids increased, and the direction of the particles changed near the shear plane.

Furthermore, the authors were conducted a quantitative evaluation of the particle array structure (porosity, direction of particle) and visualized strain localization from DIC analysis. The correspondence between the strain and the microscopic structural changes on the sand material was investigated.

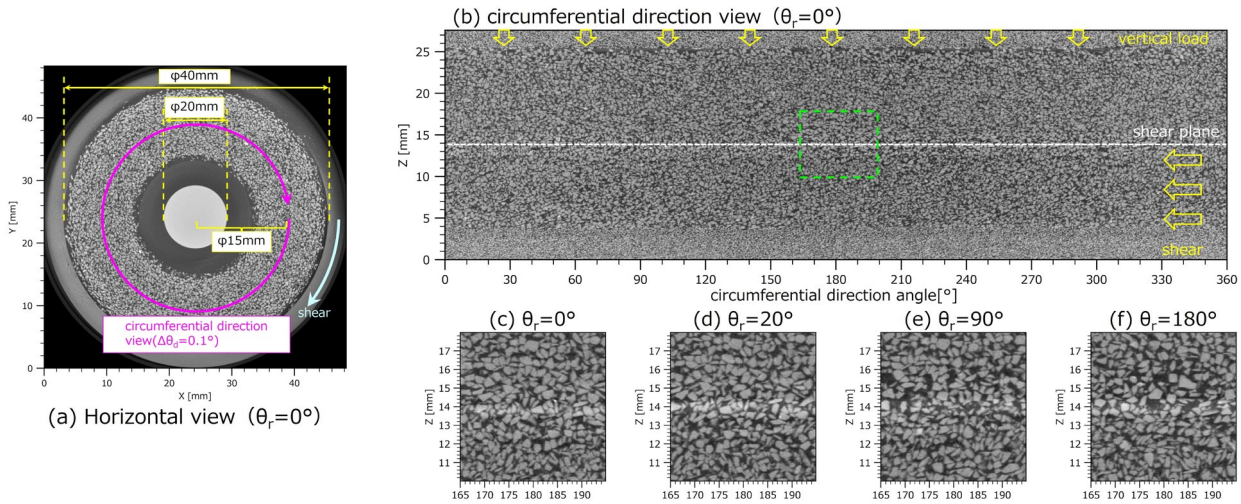

Figure 2. CT scanning result.

4. References

[1] Nohara, S., Mukunoki, T. (2021). Quantitative Evaluation of Soil Structure and Strain in Three Dimensions under Shear Using X-ray Computed Tomography Image Analysis, *J. Imaging*, 7(11), 230.

[2] Nohara, S., Mukunoki, T. (2022). Development of ring shear experiment in micro-focus X-ray CT scanner, *10th International Conference on Physical Modelling in Geotechnics 2022*, 308-311.

A glimpse over granulence in cyclic isochoric shear tests

***M. Komodromos*[1], *V. Richefeu*[1] *and G. Viggiani*[1], *G. Combe*[1]**
[1] *Univ. Grenoble Alpes, CNRS, 3SR Lab., Grenoble, France*

1. Introduction

The mechanical behavior of granular soils is a complex matter in terms of comprehension and prediction. Classic approaches founded on continuum present significant limitations on reproducing the unfolding kinematics, which are dictated by mutual exclusion at the grain scale. Despite the fact that constitutive modeling has been a strong mean of incorporating the mechanical properties of geo-materials to the material point approach, such as plasticity or loading memory, solid mechanics can not display the discrete nature of coarse soils. The divergence between continuum predicted and actual displacement fields of particle assemblies is expressed by the notion of granular fluctuations. Numerical and experimental studies have revealed evident similarities with turbulence as encountered in fluids [1]. Furthermore, granular fluctuations carry internal lengths that follow the same non-extensive up-scaling laws that apply on complex physical systems out of thermal equilibrium. In this work, an experimental campaign is performed and aims to analyze of full field kinematic evidence, derived from Digital Image Correlation, via approaches proposed by statistical mechanics [2].

2. Experimental cyclic isochoric test on 2D granular material

The experiment was performed using the shear apparatus $1\gamma 2\varepsilon$, fully described in [3]. The 2D analogue material is enclosed by a rectangular frame with initial dimensions 0.56m $\times$ 0.50m. The frame sides can be tilted, shortened or elongated to apply complex strain paths under quasi-static loading conditions. The tested material consists of an assembly of 7875 wooden circular rods that have a standard length of 0.06 meters and incorporate 12 distinct diameters ranging from 3 mm to 30 mm, Fig. 1 (a). A cyclic isochoric shear test is conducted that rotates the principal strain axes for six consecutive cycles. The experiment is displacement-driven, by imposing the following set of strain rates:

$$\dot{\varepsilon}_{xx} = \dot{\varepsilon}_0 \cos\omega t \qquad \dot{\gamma} = \dot{\gamma}_0 \sin\omega t \qquad \dot{\varepsilon}_{yy} = -\dot{\varepsilon}_{xx}$$

The mechanical response is monitored by LVDT sensors and load cells attached to the boundaries of the granular sample. The resulting strain and stress evolutions are shown in Figs. 1 (b,c). Simultaneously, the rod assembly is exposed to a digital camera which shoots high resolution images (150 MPixels). The image sequence serves as input to a Lagrangian Particle Image Tracking (PIT) technique [4], in order to capture the full kinematics (translations and rotation) of particles.

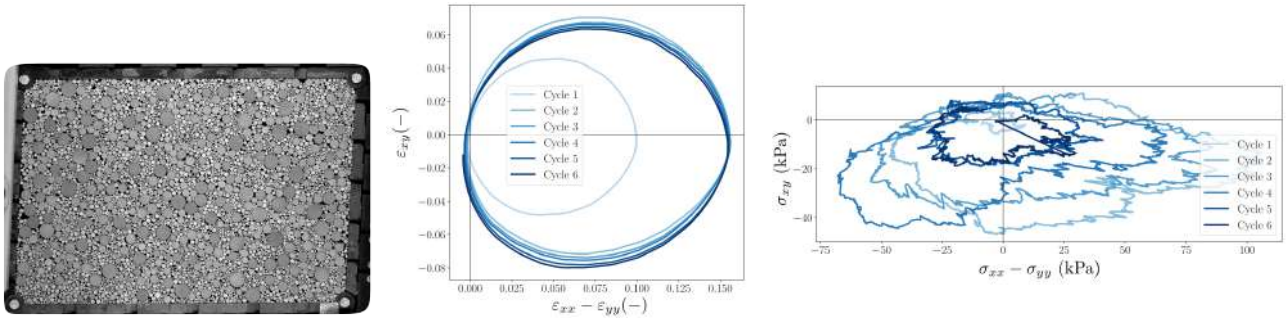

Figure 1. Cyclic isochoric test: (a) 2D granular assembly (b) strain path, (c) stress path

3. Assessment of granular fluctuations

In a granular sample, the trajectories of the grains do not necessarily follow the homogeneous displacement field imposed at the boundaries. This is the result of the geometrical constraints at the grain scale (steric exclusion); grains are not able to displace as continuum mechanics dictates that they should. The fluctuation of displacements $\boldsymbol{u}$ can be defined as the difference between the actual displacement δr, currently measured by PIT, and the displacement that the same point would have if it had followed the homogeneous strain applied to the boundaries. This magnitude is quantified by $\boldsymbol{u} = \delta r(\varepsilon, \Delta\varepsilon_d) - \delta r^*(\varepsilon, \Delta\varepsilon_d)$, where ε is the current strain state and $\Delta\varepsilon_d$ the deviatoric strain increment used to assess kinematics. The displacement fluctuation norm V is the amplitude of $\boldsymbol{u}$ normalized by the mean diameter D of the rods and the strain increment, as expressed by the formula $V = \frac{\|\boldsymbol{u}\|/D}{\Delta\varepsilon_d}$.

A visual illustration of captured granular displacement fluctuation field is provided in Fig. 2 (a). Patterns of vortex structures can be observed, which is a raw proof of the existence of internal lengths during granular re-arrangement. The characterization of these fluctuations depends on $\Delta\varepsilon_d$ and their behavior can be analyzed by means of Probability Density Functions (PDF). The right tail displayed on Fig. 2 (b) is a clue of long range spatial correlation of V [5]. Such evidence of correlation is stronger when the right slope decrease, i.e. the strain window is shortened.

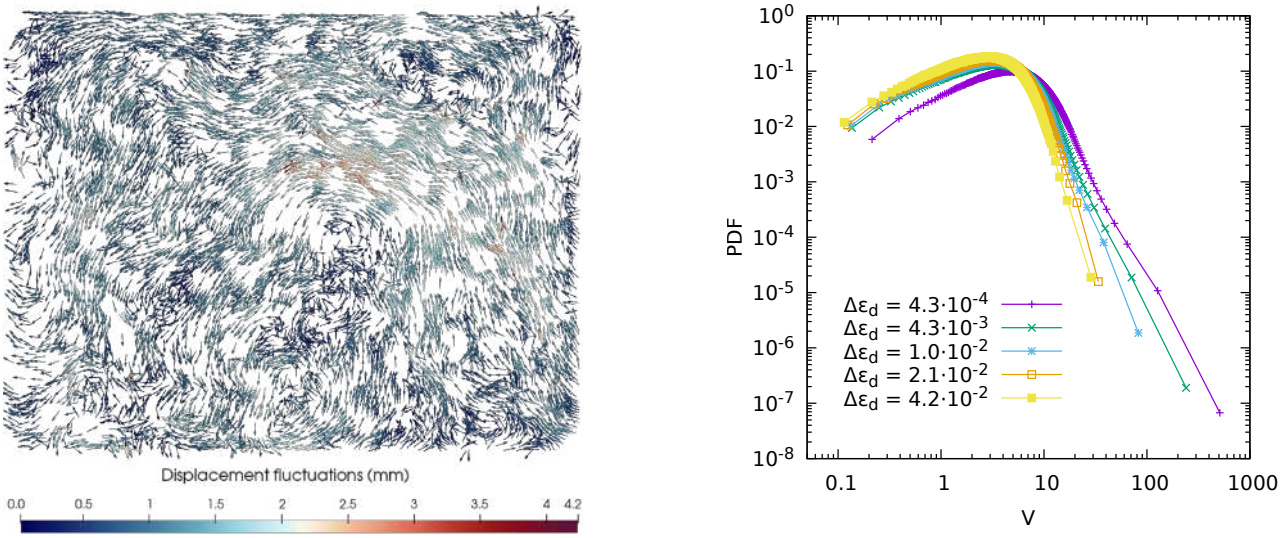

Figure 2. Granular fluctuations: (a) second cycle, (b) Probability Density Function of the normalized fluctuation V

References

[1] Radjai, F. and Roux, S. (2002). Turbulentlike fluctuations in quasistatic flow of granular media. *Phys. Rev. Lett.*, **89**, 064302.

[2] Tsallis, C. (2023). *Introduction to Nonextensive Statistical Mechanics*. Springer-Verlag, New York, USA.

[3] Calvetti, F., Combe, G., and Lanier, J. (1997). Experimental micromechanical analysis of a 2d granular material: relation between structure evolution and loading path. *Mech. Cohes.-Frict. Mater*, **2**, 121–163.

[4] Richefeu, V. and Combe, G. (2020). The particle image tracking technique: An accurate optical method for measuring individual kinematics of rigid particles. *Strain*, **56**, e12362.

[5] Combe, G., Richefeu, V., Stasiak, M., and Atman, A. P. F. (2015). Experimental validation of a nonextensive scaling law in confined granular media. *Phys. Rev. Lett.*, **115**, 238301.

Effects of particle shape and friction on the mechanics of granular media – an experimental study using x-ray tomography

***G. Pinzón*[1], *E. Andò*[1,2], *A. Tengattini*[1] *and C. Viggiani*[1]**
[1] *Univ. Grenoble Alpes, CNRS, 3SR Lab., Grenoble, France*
[2] *Center For Imaging, École Polytechnique Fédérale de Lausanne, Lausanne, Switzerland*

Particle shape plays a major role in the understanding of the mechanical behaviour of geomaterials. Previous experimental studies have shown that the morphology of the constituent particles has a direct effect on the bulk response [1, 2]. However, due to the intrinsic variability of particle shape of natural materials, the effects of their morphology are not fully isolated. This limits shape studies to perform a comparison between opposing scenarios, *e.g.*, flat against rounded particles [3, 4].

This study presents the experimental investigation of the role of particle shape and inter-particle friction under controlled and repeatable conditions. Plastic ellipsoidal particles of three aspect ratios, obtained through injection moulding, are used as proxy materials. Talc powder is used to modify the inter-particle friction coefficient, resulting in two friction scenarios of $5°$ (smooth) and $10°$ (rough) for each particle shape. The experimental conditions ensure a full isolation of the effects of particle shape and inter-particle friction, under controlled and repeatable conditions. Six cylindrical specimens of more than 20000 mono-dispersed particles, each using one of the six particle shape and friction combinations, are subjected to triaxial compression conditions, and are imaged *in-operando* each $0.5\,\%$ of axial shortening using x-ray tomography at Laboratoire 3SR (Grenoble, France). The tests are performed under dry conditions, using a confining pressure of 50 kPa, and a novel triaxial compression setup is designed, which includes a sliding base on one of the ends of the triaxial cell [5].

Each test results in more than 30 tomography volumes, which are analysed using the open-source software *spam* [6]. Individual particles are identified from the initial image, and segmentation errors are solved, resulting in a golden-standard initial segmentation for each experiment. Particles are tracked between each pair of consecutive images throughout the test, using a particle-based DVC method. The labelled images are used to evaluate the evolution of fabric-based measurement, along with particle kinematics. Additionally, for each strain increment, the particle displacements are projected onto a regular grid and used to measure deviatoric and volumetric strain fields inside the specimens.

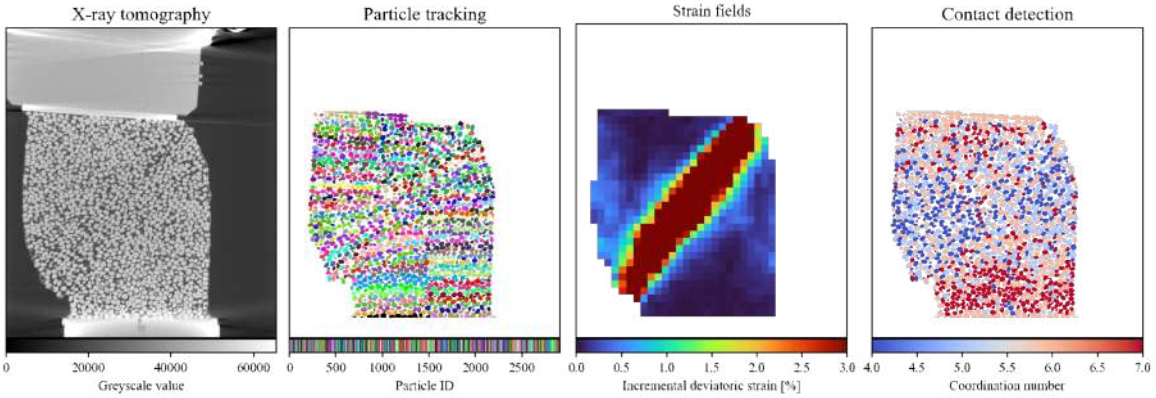

Figure 1. Example of the raw images and data. From left to right: Raw x-ray tomography, Labelled image, Maximum incremental deviatoric strain field, and particles code-coloured based on their coordination number

The macroscopic response of the specimens shows a characteristic stress evolution of dense granular assemblies, presenting well-defined strain hardening and softening regimes. The results show that the specimens composed of particles with higher aspect ratio and higher friction have a greater shear resistance, due to the interlocking between the anisometric particles. However, the inverse relation is observed for the specimens with lower friction. Regarding the volumetric strain behaviour, it is observed that all specimens show a dilatant response from the beginning of the test, reaching a constant value at the end. As the aspect ratio of the particles increases, the volumetric strain at the end of the test increases accordingly, while a decrease in inter-particle friction produces a lesser dilative response. The interplay between particle shape and friction influences how particles interact with each other, which reflects on differences at the bulk scale. To understand this, the analysis must be made at the contact scale, especially the evolution of the contact network, as well as the kinematics of the particles.

It is observed that the development of contact anisotropy is strongly related to the degree of anisometry of the particles. As their shape becomes more elongated, the average number of contacts that each particle can arrange increases proportionally, resulting in a higher range of number of contacts that can be rotated or removed without affecting the overall stability of the contact network. This higher flexibility allows the assembly to withstand greater external loads. Additionally, the initial state of the contact network has a major role in the development of shear resistance. Specimens where the initial arrangement of particles has a higher degree of anisotropy towards the direction of loading, develop a greater peak stress ratio, as a consequence of the preferential alignment of the contact network. In contrast, specimens where there is no preferential direction of contacts, require a further alteration of their contact network and thus withstand lower external loads.

Finally, the deformation processes at the bulk scale are the product of particle rotation and interlocking between the particles, which arise from their anisometry. Rounded particles show higher levels of rotation, due to their lower degree of interlocking. However, this implies that the local kinematic events have a reduced effect on the neighbouring particles. In contrast, highly anisometry particles have an enhanced interlocking due to their shape, which results in a greater impact on local kinematic events. Nonetheless, the rotation of particles is strongly constrained, limiting the amount of strain that the specimen undertakes. These results show that the macroscopic deformation must be understood as an interplay between interlocking and particle rotation. It is found that the medium particles show the highest amount of interlocking with the lowest degree of restriction to particle rotation, thus generating the highest amount of dilatancy for the specimens tested in this work.

References

[1] Santamarina, J. C. and Cho, G.-C. (2004). Soil behaviour: The role of particle shape. *Advances in geotechnical engineering: The Skempton conference*, pp. 604–617, Thomas Telford Publishing.

[2] Donev, A., Connelly, R., Stillinger, F. H., and Torquato, S. (2007). Underconstrained jammed packings of nonspherical hard particles: Ellipses and ellipsoids. *Physical Review E*, **75**, 051304.

[3] Xiao, Y., Long, L., Matthew Evans, T., Zhou, H., Liu, H., and Stuedlein, A. W. (2019). Effect of particle shape on stress-dilatancy responses of medium-dense sands. *Journal of Geotechnical and Geoenvironmental Engineering*, **145**, 04018105.

[4] Miura, K., Maeda, K., Furukawa, M., and Toki, S. (1998). Mechanical characteristics of sands with different primary properties. *Soils and foundations*, **38**, 159–172.

[5] Pinzon Forero, G. A. (2023). *Etude expérimentale des effets de la forme des particules et de la friction sur la mécanique des milieux granulaires*. Ph.D. thesis, Université Grenoble Alpes.

[6] Stamati, O., et al. (2020). Spam: software for practical analysis of materials. *Journal of Open Source Software*, **5**, 2286.

ENGINEERING ASPECTS OF AN ASH REFUSE TIP OBSERVED WITH MICROSCOPIC TECHNIQUES

***M. Thompson*[1], *V. Angelidakis*[1,2], *L. Parreiras Nogueira* [3], *and S. Nadimi*[1]**

[1] *School of Engineering, Newcastle University, Newcastle upon Tyne, NE1 7RU, UK.* [2] *School of Natural and Built Environment, Queen's University Belfast, Belfast, BT9 5AG, UK.* [3]*X-ray MicroCT platform, Institute of Clinical Dentistry, University of Oslo, Norway.*

Summary: The engineering aspects of ash made ground are unique, desirable and provide an opportunity for re-use as a stable load bearing substrate. Validation of the relative level of compaction in situ relies on laboratory testing of these soils. Ash made ground samples were obtained from a former refuse tip and dried at two different temperatures (110°C and 40°C). Samples were prepared and examined using Nano X-ray Computed Tomography (NXCT), Scanning Electron Microscopy (SEM) and X-ray Diffraction (XRD) to understand the soil microstructure. In addition, a series of laboratory tests and site tests were conducted to investigate their mechanical properties when subjected to different drying temperatures.

1. Introduction

It is more sustainable and plausible to re-develop brownfield sites by reusing the site-won made ground materials, rather than encroaching onto greenfield land. The ash samples were obtained from a site in Skipton, North Yorkshire, UK. The results from laboratory testing set the guidelines for optimal performance of the ground (*i.e.* compaction state *etc.*) which are used for relative comparisons to in-situ tests to ensure the ground is within specification guidelines. However, some studies have shown that the drying process in the lab can alter the soil structure and in turn, its engineering properties [1]. The overall aim of this study is to characterise refuse tip Ash for use as an effective engineered fill on brownfield sites and to confirm that current validation works are reliable.

2. Methodology

Microscopic techniques: Samples were dried at 110°C and 40°C, followed by sieving the soil through 20mm and 300μm sieves to obtain only fine-grained soil. These were separated into sample tubes ca. 1cm in diameter, with two loose and two compacted samples (using a 2.5kg hammer) and extruded using a small metal ring (see sample tubes in Figure 1a). The NXCT scanning was performed on the ash samples at the University of Oslo using a Bruker Skyscan 2211 Multiscale NanoCT machine and gave 8-bit final reconstructed images with a voxel size of 400nm. A total of ca. 2500 projections were collected per scan (see diagram of instrumentation in Figure 1b). The number of sample slices varied, but each slice had a size of 3000 x 3000 pixels. Slices representing loose samples dried at 110°C and 40°C are shown in Figures 1c and 1d, respectively. These images were then processed in ImageJ through thresholding, despeckling and binarization [2]. Once processed, analysis was carried out using the image intensity histograms, to calculate the void ratio.

Soil laboratory testing: samples prepared at 110 °C and 40 °C were and will be subjected to Particle Density, Atterberg Limit tests, Particle Size Distribution and 4.5kg compaction tests in the laboratory.

In-situ Sand Replacement Density (SRD) testing: in situ SRD tests using glass beads and conventional kiln dried sand (with pre-determined bulk densities) were conducted in August 2023, using the same sand cone (calibrated for volume) and completed within a metre of each other.

3. Results

NXCT and SEM imaging have revealed that loose samples prepared at 40°C gave a lower void ratio, e, than the 110°C samples (e=1.91 compared to 3.04, respectively); when subjected to compaction the 110°C sample had a significant reduction in the void ratio (from e=3.04 to 1.94), while the 40°C sample experienced slight expansion after the compaction (e=1.91 to 2.07). Initial Atterberg Limit tests gave plasticity indices of 9% and 11% for the 40°C and 110°C, respectively. In situ testing using glass beads enabled higher relative compaction than testing using conventional kiln-dried sand (dry densities of 1.54 Mg/m^3 and 1.52 Mg/m^3).

4. Conclusions and Further Work

The initial stages of this research have shown significant differences in sample void ratio for different drying temperatures and compaction states. However, more tests are yet to be completed to discover whether the void ratio differences extend significantly to the results from the laboratory tests.

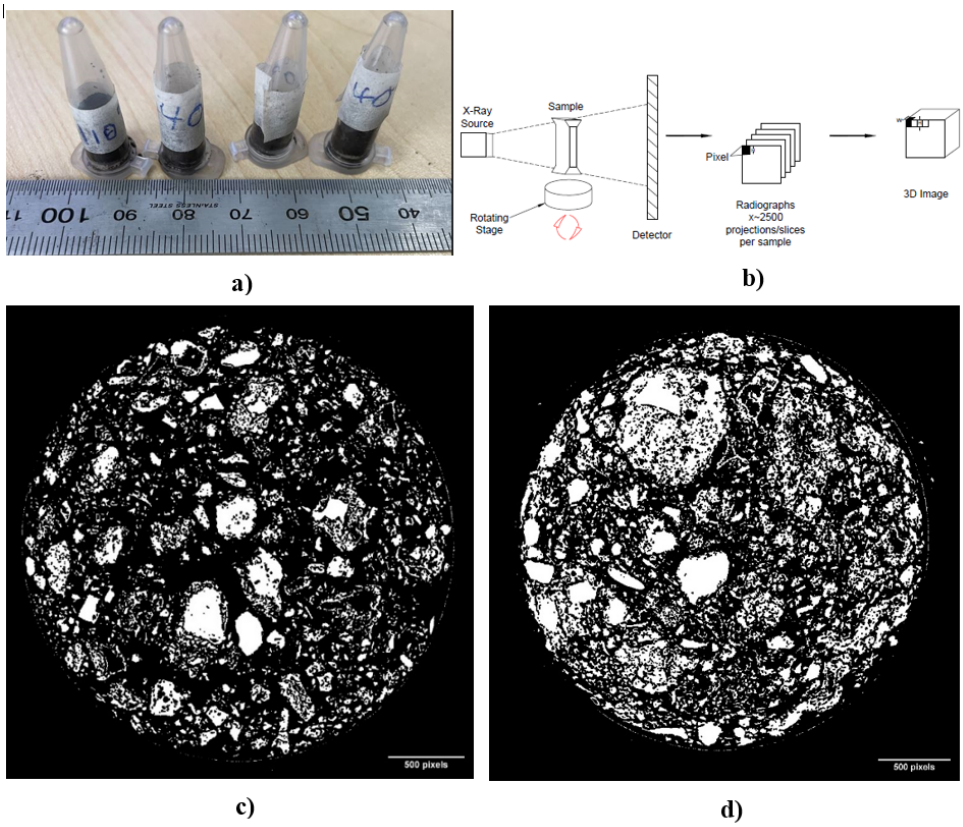

Figure 1: a) Samples prepared for imaging; b) Basic NXCT scan set-up; c) 110°C loose ash sample; and d) 40°C loose ash sample.

5. References

[1] Menendez, O., Lopes, B., Caicedo, B., and Neto., M (2022). Microscopic and mineralogical characteristics behind the engineering properties of a compacted andesitic volcanic soil. Journal of South American Earth Sciences, no. 115.

[2] Schindelin, J., Arganda-Carreras, I., Frise, E., Kaynig, V., Longair, M., Pietzsch, T., ... Cardona, A. (2012). Fiji: an open-source platform for biological-image analysis. Nature Methods, 9(7), 676–682.

EVOLVING DEFORMATION FIELDS IN SHALLOW INDENTATION OF WEAKLY CEMENTED SANDS

Bhupendra Chand[1] & Tejas G Murthy[2]

[1]Department of Civil Engineering, Indian Institute of Science Bengaluru, India
[2]Department of Civil Engineering, Indian Institute of Science Bengaluru, India

1. Abstract

Indentation is an important severe plastic deformation process encountered in infrastructure engineering. This problem of indentation has had many important implications in the design of shallow foundations and other sub structures. An understanding of the mechanics of indentation of soils/granular materials has emerged at the ensemble scale-mostly derived from the framework offered by plasticity theory and metal indentation. Solutions to this shallow indentation problem provided by the underpinning of continuum theories of plasticity and elasticity which have been the backbone of shallow foundation design [1][2]. While design of shallow foundations has focused on calculating the collapse load, the corresponding deformation in the sand underneath the indenter (or shallow footing) has been largely overlooked. A detailed mapping of the deformation in sands is important in optimising design solutions - especially those that emanate from limit theories.

The visualisation of the deformation field in 3D ensemble is not possible from the conventional geotechnical tests however the advancement brought forth with the advent of X-ray computed tomography (XRCT) in the recent past have made this possible. Integration of XRCT with model tests provides valuable insight not only on the ensemble deformation, but also gives us access to the mechanics at the particle scale. Phenomena such as particle breakage, cement disintegration, inter particle arrangement etc, have all become feasible. In effect allowing us to bridge the gap between the micro scale or particle scale response to the ensemble response [3][4]. The addition of cohesion in the granular material changes its mechanical response markedly. The presence of inter-particle cementation increases the stiffness of the ensemble and influences overall stress-strain response. In this study, a shallow indentation problem is investigated in a chamber, inside a computed tomography (CT) apparatus, and the high resolution XRCT scans are used to understand the failure mechanisms of the weakly cemented sand.

An aluminium indenter is used to model the shallow footing and is allowed to penetrate the indentation with a constant speed. Two sets of samples - uncemented and cemented sand samples are tested during the experiments. Gypsum is used to introduce the cohesion between the sand particles. The inner diameter of the acrylic chamber is 38 mm and the ratio of sample to the indenter diameter is 10. In order to acquire the progressive sand deformation, the CT scans are obtained at three different penetration depths with a resolution of 0.044 mm. The analysis of the scans is carried out by MATLAB codes and a Morse-gram tool [5] is used for

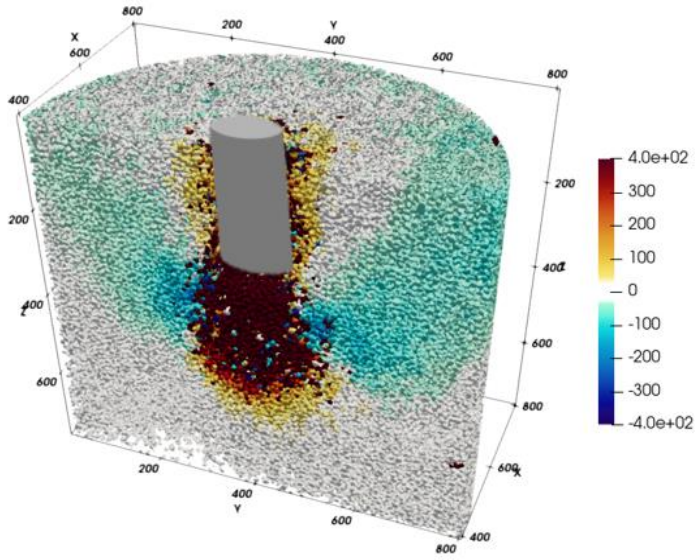

Figure 1. Contour map of vertical displacement field obtained from the uncemented sand specimen while driving the indenter by 80 voxels (3.5 mm).

the segmentation of the particles. Using the high resolution XRCT scans, the overall deformation of the sand particles assembly along with the individual particle rotations and displacements are evaluated. A digital volume correlation (DVC) technique is used to quantify the particle's movement at different levels of penetration and contour maps are generated to visualise the deformation fields (see fig.1). The experiments show the presence of a compressive zone underneath and near the indenter surface which is surrounded by a zone of negative (upward) displacement. Additionally, the kinematics of the uncemented and cemented samples, their influence zone and deformation fields are also compared to explore the effect of cohesion in the mechanical response of granular materials.

2. References

[1] Reese, L. C., Isenhower, W. M., & Wang, S. T. (2005). *Analysis and design of shallow and deep foundations* (Vol. 10). John Wiley & Sons.
[2] Scott, R. F. (1981). *Foundation analysis* (No. 04; TA775, S2.). New Jersey: Prentice-Hall.
[3] Singh, S., Miers, J. C., Saldana, C., & Murthy, T. G. (2020). Quantification of fabric in cemented granular materials. *Computers and Geotechnics*, *125*, 103644.
[4] Singh, S., & Murthy, T. G. (2022). Evolution of structure of cohesive granular ensembles in compression. *International Journal of Solids and Structures*, *238*, 111359.
[5] Pandey, K., Bin Masood, T., Singh, S., Hotz, I., Natarajan, V., & Murthy, T. G. (2022). Morse theory-based segmentation and fabric quantification of granular materials. *Granular Matter*, *24*, 1-20.

IN-SITU INVESTIGATION OF DEFORMATION AND FRACTURE COALESCENCE OF SANDSTONE

K. Taghizadeh, R.C. Hurley
Hopkins Extreme Materials Institute (HEMI), Department of Mechanical Engineering, Johns Hopkins University, Baltimore, USA

Structural discontinuities such as fracture and deformation bands are pervasive in the Earth's crust. They have profound influence on the extraction of petroleum from reservoirs, structural integrity of repositories, and potential leakage of sequestered CO2 and disposed waste. Highly porous unconsolidated sands and poorly consolidated sandstones (porosity ≥20%) constitute important reservoirs targeted for hydrocarbon extraction. It is their high porosity that makes such reservoirs suitable for fluid production due to the often-high permeability. However, changes in effective overburden stress due to fluid extraction can result in compaction at the reservoir level. Even relatively tiny amounts of compactive strain (few tenths of a percent) can lead to surface subsidence and induced seismicity, while larger strains (several percent) and strain localization can lead to geotechnical problems, such a wellbore casing collapse, or reduce reservoir permeability impacting production. Compaction is most likely caused by a direct poro-elastic response and time- or rate-independent inelastic compaction, as well as time-dependent compaction creep, which may continue long after production has ceased.

Continuum models are more desirable for field-scale applications, where the macroscopic field variables can be obtained via micro-meso-macro averaging procedures on small, representative elementary volumes. Attempts to model granular systems with a classical continuum theory, standard numerical methods, and design tools often fail, because of the discreteness and disordered nature of granular assemblies at the microscopic scale. The main challenge is that models disregard the influence of micro- and meso-scale variables and mechanisms on macroscale deformation patterns. Results from the current study provides new insights into the relationship between micro- and meso-scale processes (grain breakage, pore collapse, deformation banding) and macroscale stress-strain-porosity evolution in sandstone which are used to validate and calibrate a mechanism-based constitutive model (based on continuum breakage mechanics) currently being developed for predicting penetration of various geomaterials.

Microscale and mesoscale mechanisms contributing to macroscopic deformation of sandstone include grain breakage and pulverization, pore collapse, and the development of shear, dilatational, and compaction bands (a subset of deformation bands). At low confining pressures, sandstone exhibits a brittle response in which deviatoric loading induces cement bridge breakage, Hertzian particle fractures, and particle rearrangements that coalesce into macroscopic dilatant shear bands. As the confining pressure increases, the behavior of sandstone shifts from brittle to ductile. This transition involves deviatoric loading causing Hertzian particle fractures and pore collapse through particle comminution. These processes lead to the formation of macroscopic compaction bands or diffuse cataclastic flow, depending on grain-size distribution and porosity. In Figure 1, we illustrate microscale and mesoscale deformation mechanisms in rocks and granular materials relative to pressure (p) and deviatoric stress (q). The areas below and above the solid curve (yield envelope) signify elastic and plastic deformation, respectively. The peak of the yield envelope marks the point of transition from brittle to ductile behavior [1].

In this research, we study local and global failure mechanisms using a custom-built triaxial compression apparatus [2] (permitting confining pressure up to 50 MPa) and provide the first test

data with a revised version of the apparatus (permitting confining pressure up to 200 MPa). The apparatus allows for high-resolution in-situ x-ray computed tomography (XRCT) measurements of material structure and in-situ 3D x-ray diffraction (3DXRD) measurements of grain-resolved stresses during material deformation. Digital volume correlation (DVC) will eventually be used to calculate full-field strain from sequential XRCT images using the open-source Software for Practical Analysis of Materials (SPAM) [3].

Analysis of data for grain-resolved structure and stress measurements involves: (*i*) data-processing of XRCT and 3DXRD, (*ii*) analysis of grain-resolved stresses, and (*iii*) validation with DVC. These analyses are then used to understand the heterogeneity (using probability distributions) of stresses in each sandstone as a function of pressure, porosity, mineral content, and grain size distribution. Earlier studies [4] have shown that lowering porosity, narrowing particle size distributions, and increasing sample stress (hydrostatic or deviatoric) will promote more homogeneous grain-resolved stresses (hydrostatic or deviatoric stresses). Finally, grain-resolved stresses are used with grain-resolved strain measurements from DVC to assess coaxiality and associative plastic flow as a function of length scale. The principal directions and magnitudes of local stress and strain increments during deformation of each sandstone are calculated. Finally, we will assess associative plastic flow by comparing locally-resolved plastic stress and strain from XRCT and 3DXRD measurements, or by using the "inelastic compaction factor" (ratio of plastic porosity and plastic strain increments).

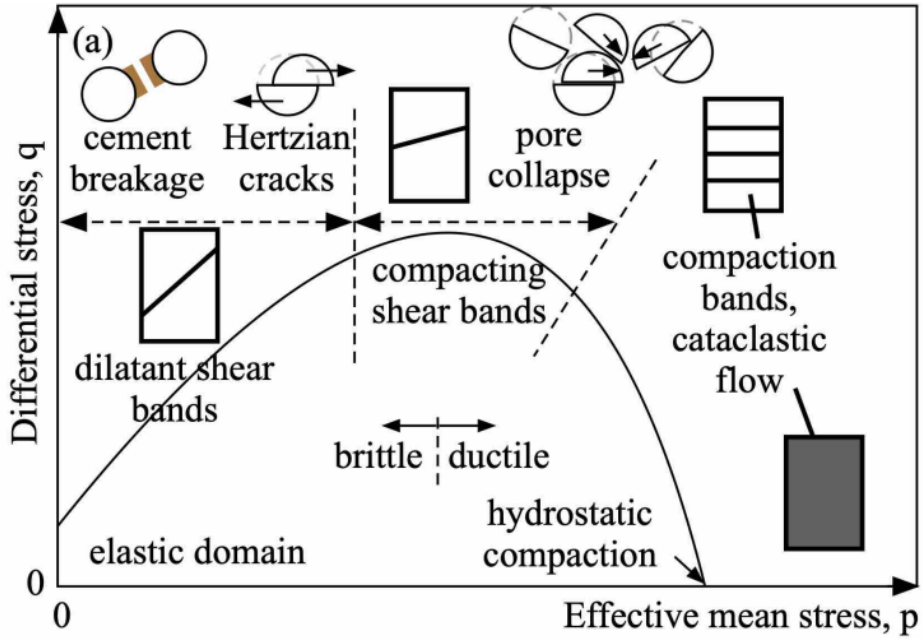

Figure 1. – Schematic of microscopic and macroscopic mechanisms during sandstone deformation.

References

[1] T. F. Wong and P. Baud, "The brittle-ductile transition in porous rock: A review." *J. of Structural Geology*, vol. 44, p.25-53, 2012.

[2] G. Shahin, and R. C. Hurley, "Micromechanics and Strain Localization in Sand in the Ductile Regime." *J. of Geophysical Research: Solid Earth*, vol.127, no. 11, 2022, e2022JB024983.

[3] O. Stamati et al., "spam: Software for Practical Analysis of Materials." *J. Open Source Softw.*, vol. 5, no. 51, p. 2286, 2020.

[4] R. C. Hurley, S. A. Hall, & J. P. Wright, "Multi-scale mechanics of granular solids from grain resolved X-ray measurements." *Proc. R. Soc. A*, vol. 473, no 2207, p20170491, 2017.

INVESTIGATION OF ACTIVE DEFORMATION MECHANISMS IN NATURAL SALT ROCK USING DIGITAL IMAGE CORRELATION

X. Li[1], A. Dimanov[1], M. Bornert[2], S. Hallais[1], and H. Gharbi[1]
[1] Solid Mechanics Lab., CNRS UMR 7649, École Polytechnique, France
[2] Navier Lab., École des Ponts, G. Eiffel University, CNRS UMR 8205, Marne-la-Vallée, France

Salt rock, recognized as promising host rock for hydrogen storage, faces the challenge of pronounced viscoplastic rheology, experiencing significant creep at small differential stresses and cumulating micro-damage [1]. The envisaged diversified usages of hydrogen imply relatively short periods of storage and withdrawal, resulting in cyclic loading to the salt cavern walls due to the short-term internal pressure variations [2]. The effects on salt rock integrity of the combination of long-term creep (cavern convergence) and short-term fast cyclic need to be thoroughly assessed, at the light of well identified salt rock deformation mechanisms [3].

Within the existing literature, numerous research endeavours have been directed towards both macro-scale and micro-scale investigations. Macro-scale studies primarily concentrate on natural salt, enabling the observation of mechanical phenomena at sample scale and the formulation of phenomenological constitutive relations [4]. However, these efforts often lack crucial micromechanical insights into the underlying physical mechanisms of deformation and microstructural characterization, which in turns determines the active mechanisms. Some recent works have clearly demonstrated the concomitance of dominant crystal plasticity and minor but necessary grain boundary sliding, with corresponding interfacial damage [5] . In particular, micro-damage development at the grain scale must be understood, because of its subsequent influences on the macroscopic mechanical behaviour and the material tightness to gas.

Conversely, most laboratory investigations at the micro-scale have predominantly utilized synthesized salt rock. This choice is driven by its relatively low cost, reproducibility and control on sample composition and microstructures. Nevertheless, the intricate and variable microstructure inherent to natural salt rock, encompassing factors such as grain size distribution, impurities, porosity, and cracks, significantly deviates from the simplified synthetic salt rock. Consequently, direct applicability of constitutive relations obtained from synthetic salt rock to natural salt rock remains questionable. Also, the micro-mechanisms identified in synthetic salt rock may differ in relative proportion from those operating in natural materials [5-6].

This research intends to bridge the existing gap between macro-scale and micro-scale paradigms, with a focused exploration into the qualitative and quantitative micro-mechanisms of natural salt. We used different natural salt rocks from different geological formations and re-synthetic salt rock produced through the cold compaction of grinded natural salt powder. Initial microstructure characterization utilizes SEM, EBSD, and CT, followed by classic uniaxial compressive tests coupled with optical microscopy monitoring. To unveil active deformation mechanisms in the different salt rocks. Digital Image Correlation (DIC) analysis is applied to high-resolution images continually captured during testing. Homogeneously distributed surface markers adapted to salt rock grain size facilitate full-field measurements of displacement fields and calculation of corresponding strain fields over representative domains.

The analysis places particular emphasis on the interaction between intra-granular crystal slip plasticity and grain boundary sliding. As illustrated in Figure 1, distributed continuous intra-granular strain is strongly associated with grain boundary discontinuities, present from the very onset on

plasticity. Microstructure effects on active mechanisms can be inferred: the relative contributions of both mechanisms seem to depend on local microstructural features, in particular grain size. Micro-cracks dominantly initiate and propagate along grain boundaries, as a direct by-product of grain boundary discontinuities; intra-crystalline damage is also observed in the form of propagating straight cracks but with a much lower density.

To quantitatively assess the respective contributions of crystal slip plasticity and grain boundary sliding to overall deformation, and to analyse the influence of salt grain size, an in-house program will be applied on segmented digital images. The objective is to derive physically grounded micromechanical constitutive relations, enabling the construction of numerical models taking into account simultaneous viscoplasticity, grain boundary sliding and damage development. These insights may be of crucial importance for the safety assessment of industrial applications involving salt rock caverns, particularly under short-term mechanical loading conditions associated with daily hydrogen filling and withdrawal operations.

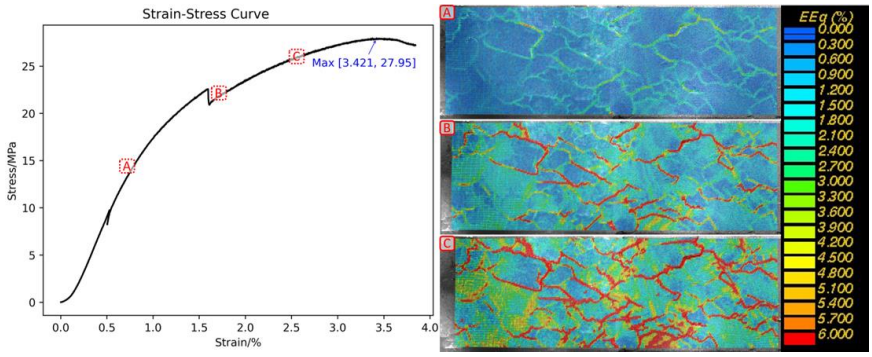

(1) (2)

Figure 1. DIC analysis on a salt rock sample: (1) Global strain-stress curve; (2) Local deviatoric strains maps (local gauge length = 192 μm) of three loading stages marked correspondingly in (1).

References

[1] Wu, F., Zhang, H., Zou, Q., Li, C., Chen, J. & Gao, R. (2020). Viscoelastic-plastic damage creep model for salt rock based on fractional derivative theory, *Mech. Mater.*, vol. 150, p. 103600.

[2] Bachu, S. & Dusseault, M. B. (2005). Underground Injection of Carbon Dioxide in Salt Beds, *Developments in Water Science*, vol. 52, C.-F. Tsang and J. A. Apps, Eds. Elsevier, pp. 637–648.

[3] Ma, L., Wang, Y., Wang, M., Xue, B. & Duan, L. (2021). Mechanical properties of rock salt under combined creep and fatigue, *Int. J. Rock Mech. Min. Sci.*, vol. 141, p. 104654.

[4] Bérest, P., Antoine Blum, P., Pierre Charpentier, J., Gharbi, H. & Valès, F. (2005). Very slow creep tests on rock samples, *Int. J. Rock Mech. Min. Sci.*, vol. 42, no. 4, pp. 569–576.

[5] Bourcier, M., Bornert, M., Dimanov, A., Héripré, E., & Raphanel, J. L. (2013). Multiscale experimental investigation of crystal plasticity and grain boundary sliding in synthetic halite using digital image correlation, *J. Geophys. Res. Solid Earth*, vol. 118, no. 2, pp. 511–526.

[6] Gaye, A., Bornert, M., Lenoir, N., Sab, K. , Dimanov, A., Bourcier, M. , Héripré, E., Raphanel, J., Gharbi, H., Picard, D. & W. Ludwig. (2014). Micromechanics of Halite Investigated by 2D and 3D Multiscale Full-Field Measurements, presented at the 48th U.S. Rock Mechanics/Geomechanics Symposium, Minneapolis, Minnesota.

INVESTIGATIONS ON PARTICLE MIGRATION DURING SUSPENSION INJECTION THROUGH POROUS MEDIUM USING X-RAY CT

Jithin S Kumar[1] ***NSSP. Kalyan***[1] ***Lijith K P***[2] ***and Ramesh Kannan Kandasami***[1]
[1]*Department of Civil Engineering, IIT Madras, India*
[2]*Department of Civil Engineering, University of Calgary, Canada*

1. Outline

Impairment of porosity while injecting suspensions in porous medium holds significant relevance in diverse fields such as the oil and gas industry, grouting, and hydraulic fracturing [1, 2]. During permeation, a complex transient filtration process segregates suspended particulates from the injecting fluid to deposit them in void spaces or constrictions because of the hydrodynamic forces [3, 4]. The fluid-solid separation originates at the fluid injection point in the porous medium through solid buildup and result in the formation of an external filter cake (mud cake). Simultaneously, the internal filter cake that is formed in the porous medium reduces the permeability as some particles are retained in the pore spaces and cause a decrease in suspension concentration away from the injection point. Permeability of the filter cakes and particulate content in the suspension control the fluid loss to the formation. The complex process involved in filtration are further influenced by additives such as viscosifier and weighting agents added to the suspension. Influence of these additives on the particle transport dynamics needs to be clearly understood in order to better engineer the fluid systems. In this study, the influence of additives on the migration mechanicsms are studied by employing computer tomography (CT) with a custom-designed flow cell, as shown in Figure 1. When fluid is injected into the saturated porous medium under a constant injection rate, a layer of filter cake is formed near the top of the porous packing, followed by the formation of filtration zones with depth. The pressure profile is linked with the particle migration during the injection process when different additives are added to the fluid.

2. Methodology

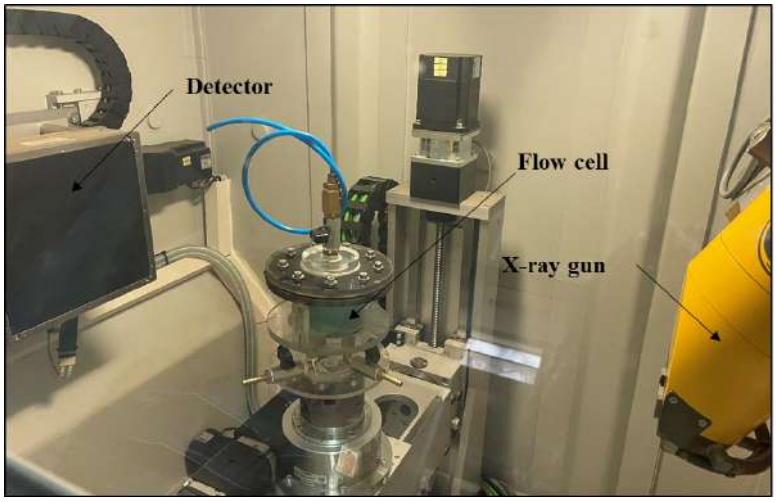

Figure 1. The custom-made flow cell inside the CT scanner between the X-ray gun (right) and the detector (left).

A carefully designed and fabricated experimental setup (injection cell) has been used for performing the stop-gap experiments within the X-ray CT equipment (depicted in Figure 1). This setup consists of an injection port and three drainage ports at the bottom. The cylindrical portion of the setup has a fixed outer diameter of 5 cm and a height of 8 cm. A moist tamping technique is employed to reconstitute a uniformly packed saturated porous bed, following a systematic protocol. Ennore sand (grade 3) with an effective size (d_{10}) of 0.3 mm is specifically chosen for preparing the porous bed.

To replicate the water-based drilling fluid systems, the injection fluid is prepared by mixing 0.4 % of xanthan gum- XG (viscosifier) and 10 to 15 % of barite (weighing agent) in water. The fluid is prepared by mixing the additives with water using a mechanical stirrer at 6000 rpm and injected into the cell using an accumulator and a syringe pump, at a constant injection rate. Notably, the experimental setup has been rigorously tested and proven leak-proof up to 1 MPa to guarantee a secure environment for the experiments within the CT equipment. A 1 cm thick coarse sand layer (with an average particle size of d_{50} = 2 mm) is placed at the top of the porous medium to evenly distribute the injected suspension. Multiple scans at specific time intervals (stop-gap method) have been carried out. Care was taken that there is no migration or creep between different scan intervals. After scanning, image processing is carried out to capture the temporal and spatial variation of particle deposition that occur during the injection process. Image processing involves usage of adaptive thresholding technique for separating three phases i.e., suspension, soil and voids based on respective X-ray attenuation number.

3. Preliminary outcomes

After a trial experiment, the three-dimensional data sets are reconstructed from the images, enabling the spatial and temporal tracking of filter cake formation. A cross-sectional view at the center of the specimen is shown in Figure 2, both before and after the injection of fluid. Figure 2b reveals the formation of filter cake at the junction between the coarse and fine granular packing. This filter cake grows during the injection process. The utilization of CT imaging in these experiments facilitates the precise quantification of filter cake growth and identification of filtration zones. The analysis of fluid permeation and particle migration within a three-dimensional domain is anticipated to offer insights into the intricacies of the particle migration process in a saturated porous medium. A discernible progression of filtration/permeation spanning the spatial domain will be observed and carefully compared with the injection pressure variation with time.

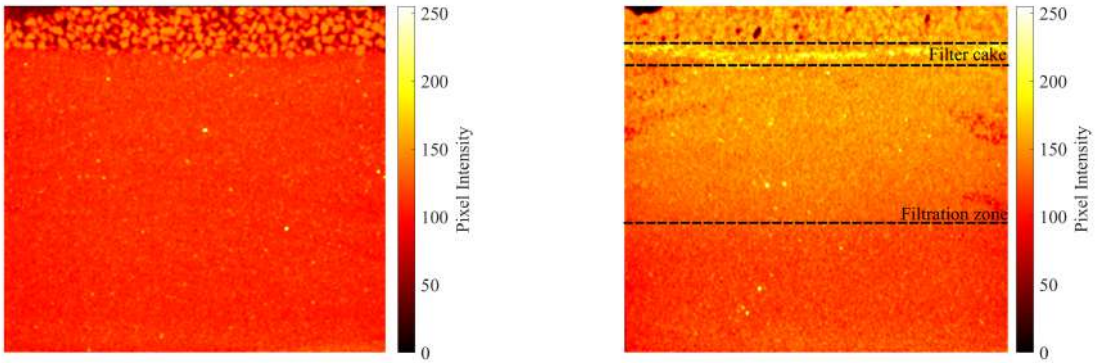

(a) Specimen before fluid injection (t = 0)

(b) Specimen at t = 22 min

Figure 2. Filter cake formation with fluid injection

References

[1] Kumar, J. S., Chaudhuri, A., Detournay, E., and Kandasami, R. K. (2023). Fluid injection-induced cavity expansion in dry porous medium. *International Journal for Numerical and Analytical Methods in Geomechanics*.

[2] Kumar, J. S. and Kandasami, R. K. (2021). Fluid induced deformation in porous media–sensitivity analysis of a poroelastic model. *IOP Conference Series: Earth and Environmental Science*, vol. 861, p. 072147, IOP Publishing.

[3] Nguyen, C. D., Benahmed, N., Andò, E., Sibille, L., and Philippe, P. (2019). Experimental investigation of microstructural changes in soils eroded by suffusion using x-ray tomography. *Acta Geotechnica*, **14**, 749–765.

[4] Aérens, P., Torres-Verdín, C., and Espinoza, N. (2023). Experimental time-lapse visualization of mud-filtrate invasion and mudcake deposition using x-ray radiography. *Petrophysics-The SPWLA Journal of Formation Evaluation and Reservoir Description*, **64**, 448–461.

Influence of sand fabric on pore water pressure build-up

B. Bacic[1]***, I. Herle***[1]
[1] *TU Dresden, Institute of Geotechnical Engineering, 01062 Dresden, Germany*

1. Introduction

It is generally accepted that sands have the highest tendency to generate pore water pressure (PWP) and, thus, to liquefy. Besides granulometric properties (grain size distribution, grain shape) that are the most important, but not the only influencing factors, the influence of the stress-dependent relative density and the soil fabric on the PWP build-up and tendency of soil to liquefy needs to be considered. After specimen preparation of different sands using a defined procedure (e.g., pluviation under water), a comparable soil fabric is created, which, however, is reflected by differences in the relative density after installation due to different granulometry. Despite these differences, the loosest state for the specified installation method is achieved for each sand.

2. Experimental testing

Within this research, a simplified undrained cyclic shear test (PWP-Tester) [1] enabling a fast and systematic comparison of the excess PWP build-up in coarse-grained soils has been developed. The principle of this experimental procedure is based on the evolution of the PWP during the cyclic shearing of a water-saturated sand sample. The procedure can be divided into three phases. At the beginning of the test, a de-aired sand-water mixture is installed via a funnel in a supported rubber membrane (underwater funnel pluviation, UWFP). As a result, a highly saturated soil sample is obtained (D/H = 50/100 mm). The effective stress is increased by applying suction (negative PWP) to the soil sample. The total stress results from the relative air pressure and remains equal to zero during the entire test. Cyclic sinusoidal loading is applied to the top cap of the consolidated soil sample in the horizontal direction, which results in a simple shear deformation of the soil sample. Undrained conditions during the experiment allow for the PWP build-up. The duration of a single shear test, including sample preparation, is approximately 30 minutes. During the test, the evolution of the PWP in the sample and the relative air pressure are measured. Also, the top cap displacement and its settlement are measured contactless via two laser distance sensors.

Four differently graded sands (Karlsruhe fine sand, KFS; Toyoura sand, TS; Karlsruhe sand, KS; silica sand, SiS) with $C_U < 3$ and d_{50} ranging from 0.1 mm to 1 mm were used within this experimental study. All specimens, after their preparation, were consolidated to 60 kPa and subsequently loaded with displacement amplitude A = 2.4 mm and frequency f = 1 Hz. The relative densities D_r of these sands after their preparation via the UWFP method range from a loose state in the case of silica sand (D_r = 0.29) to a middle-dense state for Karlsruhe fine sand (D_r = 0.586). These differences in relative density reflect the differences in the granulometric properties of these sands. Despite these large differences in D_r, the number of loading cycles N necessary for complete reduction of effective stress (state of liquefaction) is very similar for all sands and ranges from N = 10 to N = 14 (Figure 1). It seems that the same soil fabric prescribed by the same specimen preparation method has a stronger impact on the excess PWP build-up than different relative densities.

3. Sand fabric

In order to further analyse the observations from Figure 1, µCT scans of silica sand SiS and Karlsruhe sand KS specimens after their preparation via the UWFP method were acquired, and contact fabric was evaluated using spam [2].

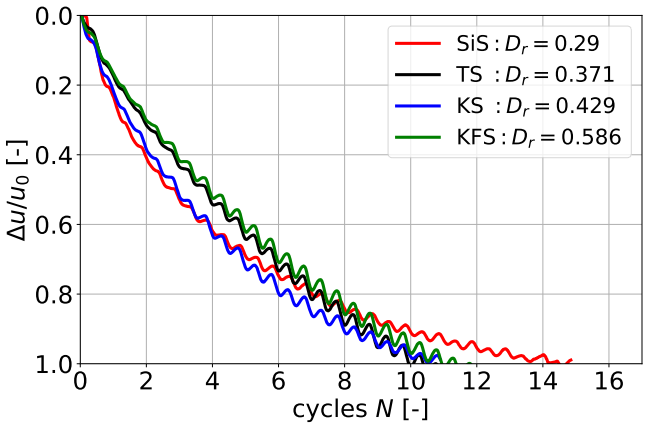

Figure 1. Evolution of normalized excess PWP build-up $\Delta u/u_0$ with the number of cycles N for four different sands.

The contact fabric tensors of these two sands (Figure 2), indicate a similar anisotropic contact fabric of these sands. It can be recognised that SiS has a slightly more anisotropic fabric than KS since its contact fabric tensor is peanut-shaped while the contact fabric tensor of KS resembles a capsule. The dark colour denotes a high density of contact normal orientations, which are obviously oriented vertically due to the sand pluviation during specimen preparation. These observations confirm the similarity of the contact fabric in sands prepared with the UWFP method. Therefore, it can be concluded that similar fabrics of different sands, obtained by the same preparation method, lead to similar resistance to the excess PWP build-up, regardless of their relative density.

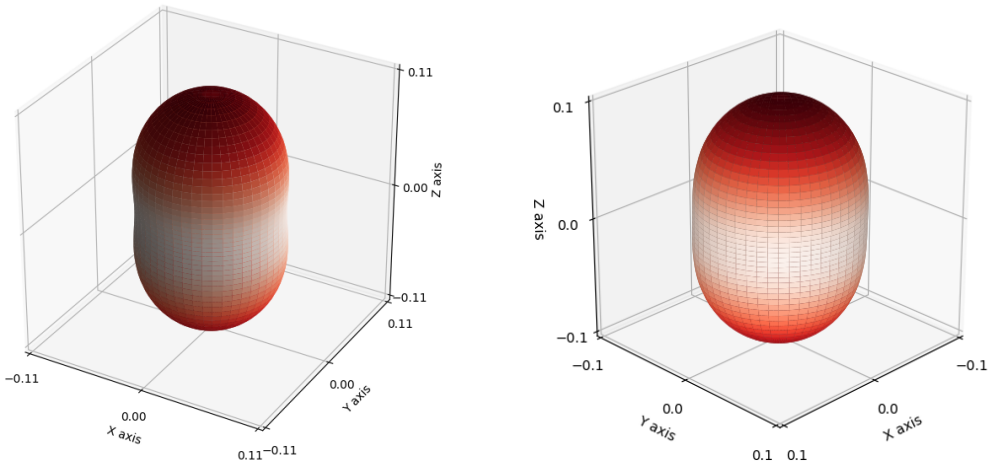

a) b)

Figure 2. Contact fabric tensor of a) silica sand SiS and b) Karlsruhe sand.

References

[1] Baćić, B. and Herle, I. (2023). Density-dependent pore water pressure evolution in a simplified cyclic shear test. *International Journal of Geosynthetics and Ground Engineering*, **9**.

[2] Stamati, O., et al. (2020). spam: Software for practical analysis of materials. *Journal of Open Source Software*, **5**, 2286.

Lessons learned in micro-imaging in two years out of geomechanics

E. Andò[1]
[1] *EPFL Center for Imaging, École Polytechnique Fédérale de Lausanne, Lausanne 1015, Switzerland*

1. Intro

This abstract pertains only to a possible oral presentation in IS-Grenoble 2024: it is a communication I think will be of interest to the community but cannot be written in the form of a conventional research paper.

I have accompanied and in some moments lead the developments in 3D micro-scale imaging of granular geo-materials that underpin the experimental branch of the micro-to-macro concept.

At the beginning of 2022 I was recruited by the EPFL Center for Imaging and "upscaled" to doing imaging at all different scales and across communities. I have learned a tremendous amount of things about how imaging is organised, communicated and shared in different communities (esp. the bio-imaging), as well as different and up-coming imaging techniques that are not necessarily in the experimental-geomechanics toolbox. I propose therefore to share the following thoughts with the community:

- The interest in having an institution-wide imaging centre
- How imaging is organised in different academic communities
- Imaging techniques not usually used in geomechanics

2. A Centre for Imaging

The EPFL Center for Imaging (see: https://imaging.epfl.ch), created in 2021 by Michael Unser and Laurène Donati is rather a unique object in the academic landscape. Our objective is to support research in imaging and using imaging, as well as provide coordination and education on the topic of imaging.

This particular discipline is an excellent choice for organisation at the institutional level for several reasons:

- It is transdisciplinary *par excellence*, with cameras being used far and wide from electron microscopy, x-ray tomography, in microscopes, in direct monitoring, on satellites...
- The quantitative image analysis that is performed on these direct or indirect measurements generalises surprisingly well between different fields (where many questions fall under common "segmentation" and "tracking" categories)
- It is a field that is developing very fast with use of machine learning and deep learning tools, and so there is significant benefit to share recent developments between communities

My position is that such centres greatly benefit the local community, and I would be glad to see more of being created and supported in academia.

3. Organising imaging within a community

Bio-imaging is the most significant example of a well-structured community around common imaging problems (bio-imaging is typically on different types of microscopes looking at cell-level information). This community is structured around a number of key points:

- Associations: communities have created associations at different scales (SwissBIAS, NEUBIAS, soon: GloBIAS – where BIAS "Bio-Image Analysts"). This facilitates communication about events, jobs and techniques. Furthermore, this informally reinforces the actual *concept* of a "Bio-Image Analysts" allowing people to recognise and organise themselves.
- Discussion forums: There are a number of venues, but a key example is https://forum.image.sc where many members of the above-mentioned communities discuss imaging techniques and problems. This is a very valuable historical resource and a resounding way to feel the pulse of a vibrant community.
- Developments driven by community needs: since there are many users of bio-imaging microscopy facilities with varying levels of technical skill, this community has spent significant effort making tools that are easy to use. The very well used ImageJ/Fiji finds its origins in this community (as does "napari"), but recent efforts to make Deep Learning tools available to everyone have yielded DeepImageJ and the "Zero-Cost Deep Learning for Microscopy" efforts.

The imaging-micro-scale-mechanics world would significantly benefit from such organisation. A personal anecdote: in 2023 I tried to organise a workshop along with my other co-developers around a software that's now well used to analyse time-evolving images of deformation experiments in geomechanics. We realised that there is not real "central" place to announce such a workshop, the best we could think of was the ICTMS mailing list (although this is only for 3D imaging and not exclusive to geomechanics). This is a pity.

4. Imaging techniques

Finally I would like to talk a little about new imaging technologies that may not have permeated into geomechanics yet, for example Cryo-Electron Microscopy that allows 2D and 3D imaging at extremely high resolutions.

5. Conclusion

Two years experience out of experimental geomechanics have taught me a lot about imaging across communities and I would like to share this with you in the form of an oral communication in IS-Grenoble 2024

MECHANICAL BEHAVIOUR OF LIGHTWEIGHT CEMENTED SOILS UNDER TRIAXIAL LOADING USING X-RAY MICROTOMOGRAPHY

L. Perrotta[1], E. Vitale[2], G. Russo[2], A. Tengattini[3], E. Roubin[4], G. Viggiani[4]

[1] Scuola Superiore Meridionale, Naples, Italy

[2] University of Naples Federico II, Department of Earth Sciences, Environment and Resources, Naples, Italy

[3] Université Grenoble Alpes, 3SR Lab, Grenoble, France

[4] Université Grenoble Alpes, Institut Laue Langevin, Grenoble, France

Lightweight Cemented Soils (LWCS), obtained by mixing natural soil, water and cement with air foam, are heterogeneous materials characterised by complex microstructure consisting of large foam-induced voids immersed in a cemented porous matrix (*i.e.*, soil + cement). The use of surfactants determines the formation of an artificial porosity incorporating air as almost spherical voids that leads to a reduced unit volume weight of the material. Moreover, the addition of cement as binder allows obtaining an improved mechanical strength. These peculiarities, coupled with a high workability shortly after the mixing, make LWCS suitable for many geotechnical applications, such as construction of fills [2-4] and embankments [5,6].

In the present work, in-situ x-ray microtomography (XRμCT), *i.e.*, x-ray scanning acquired during mechanical loading, on LWCS samples are carried out in order to obtain direct three-dimensional observations of foam-induced porosity changes under triaxial loading paths and the subsequent failure mechanisms. This novel experimental campaign consists of eight tests performed at different confining stress levels, i.e., from 50 kPa up to 1000 kPa, and for two percentage of foam, i.e., 20% and 40%. Scans acquired during isotropic compression and deviator stage of triaxial tests are then analysed to detect porosity maps and strain fields of the samples. In particular, the influence of confinement levels on the behaviour of cemented samples lightened with 20% of foam is presented and discussed.

At low confining stresses, *i.e.*, 50 kPa, deviatoric loading determines the local collapse of the matrix around weak regions of the specimen, consisting of large foam-induced voids or groups of voids, or shrinkage fractures developed during curing stage. Therefore, the failure essentially consists in the progressive opening of sub-vertical fractures connecting the foam-induced voids.

However, by increasing the confining stress level (150 kPa), the localisation of the shear strains is ruled by the cemented soil matrix, which determines the formation of shear bands along the directions imposed by the deviatoric loading path. Furthermore, considering higher confinement levels (namely, 500 kPa and 1000 kPa), both the formation of shear bands and densification of the material (*i.e.*, formation of compaction bands) occur due to the pore collapse (Figure 1).

Test results highlight the key role of confining levels on the failure mechanisms governing the mechanical behaviour of LWCS.

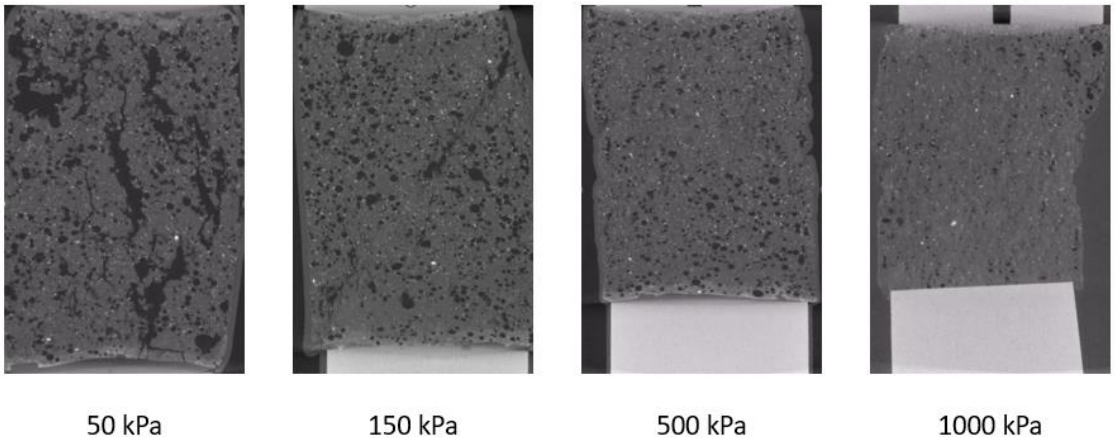

Figure 1. Final stages of the tests performed on LWCS samples with 20% foam at increasing confinement levels.

1. References

[1] De Sarno, D., Vitale, E., Deneele, D., Nicotera, M. V., Papa, R., Russo, G., & Urciuoli, G. (2019). Effects of cement and foam addition on chemo-mechanical behaviour of lightweight cemented soil (LWCS). In *E3S Web of Conferences* (Vol. 92, p. 11006). EDP Sciences.

[2] Satoh, T., Tsuchida, T., Mitsukuri, K., Hong, Z. (2001). Field placing test of lightweight treated soil under seawater in Kumamoto port. *Soils and Foundations*, **41.5**: 145-154.

[3] Tsuchida, T., & Egashira, K. (2004). *The lightweight treated soil method: new geomaterials for soft ground engineering in coastal areas*. CRC Press.

[4] Watabe, Y., Itou, Y., Kang, MS., Tsuchida, T., (2004). One-dimensional compression of air-foam treated lightweight geo-material in microscopic point of view. *Soils and Foundations*, **44.6**: 53-67.

[5] Jamnongpipatkul, P., Dechasakulsom, M., & Sukolrat, J. (2009,). Application of air foam stabilized soil for bridge-embankment transition zone in Thailand. In *Asphalt Material Characterization, Accelerated Testing, and Highway Management*: *Selected Papers from the 2009 GeoHunan International Conference* (pp. 181-193).

[6] Miki, H., Mori, M., & Chida, S. (2003). Trial embankment on soft ground using lightweight-foam-mixed in situ surface soil. In *Proc. XXIInd PIARC World Road Congress*, Durban.

[7] Vitale, E., Deneele, D., Russo, G., De Sarno, D., Nicotera, M. V., Papa, R., & Urciuoli, G. (2020). Chemo-mechanical behaviour of lightweight cemented soils. *Acta Geotechnica* **15**: 933-945.

Microstructural investigation of granular soil upon drained cyclic triaxial loading

***Ø. Torgersrud*[1,2], *E. Andò*[3], *H.P. Jostad*[2], *J.E. Andrade* [4] *and G. Viggiani*[1]**
[1] *Univ. Grenoble Alpes, 3SR, Grenoble, France*
[2] *Norwegian Geotechnical Institute, Oslo, Norway*
[3] *École Polytechnique Fédérale de Lausanne, Switzerland*
[4] *California Institute of Technology, Pasadena, CA, USA.*

1. Introduction

Existing constitutive models for sand have limited predictive capabilities for loading conditions beyond the specific stress paths for which they have been calibrated. An example is the prediction of accumulated pore pressures and shear strains that one observes in cyclic soil tests (e.g. [1]). The inability to properly predict behaviour of sand can be attributed to a lack of understanding of how sand grains interact on the micro scale, and how this interaction can be translated to the continuum scale. In this study, we investigate the behaviour of a sand subjected to drained cyclic triaxial loading, with the objective of finding evidence of microstructural changes in the sand caused by the cyclic loading. The investigation is done on triaxial experiments performed inside an x-ray tomograph, as well as from numerical simulations using the Level Set Discrete Element Method (LS-DEM) [2].

2. Methodology

Monotonic and cyclic triaxial compression tests on dry sand are performed in a miniature triaxial apparatus inside the x-ray tomograph at Laboratoire 3SR. The cyclic experiments are first run monotonically to a large mobilization, before performing a series of 10 and 100 unloading-reloading cycles in the two tests respectively. After cycling, the tests are continued monotonically to failure. To investigate the microstructural evolution in the experiments, X-ray tomography is taken at intervals of 1-2% axial strain, and at maximum and minimum stress level within selected load cycles in the cyclic tests. Image analyses are performed to identify individual particles and particle contacts [3].

Computational (LS-DEM) models of the specimens are constructed from the X-ray tomographies taken prior to triaxial shearing. Each grain is reproduced in the model with its shape, position and orientation. The membrane is modelled using bonded spheres. Special attention is given in the initialization of the model to preserve the initial fabric and hence have a simulation model that is as close as possible to a "digital twin" of its respective experiment.

3. Results

The macro response of the experiments is shown in Figure 2 in terms of deviatoric stress q and axial strain ϵ_a. A clear ratcheting effect, i.e. accumulation of axial strain due to cyclic unloading-reloading, is observed in the cyclic tests. An interesting observation is the increase in shear resistance, when monotonic loading is continued after the unloading-reloading cycles.

A microstructural investigation of the cyclic experiments indicates that the coordination number increases with increased number of cycles, while the contact fabric anisotropy slightly decreases with increased number of cycles. The void ratio is however, not changing significantly, which could mean that the increase in "post-cyclic" shear resistance is caused by changes in the contact network, rather than changes in relative density. This is further investigated with the LS-DEM model.

References

[1] Wichtmann, T. and Triantafyllidis, T. (2016). An experimental database for the development, calibration and verification of constitutive models for sand with focus to cyclic loading: part

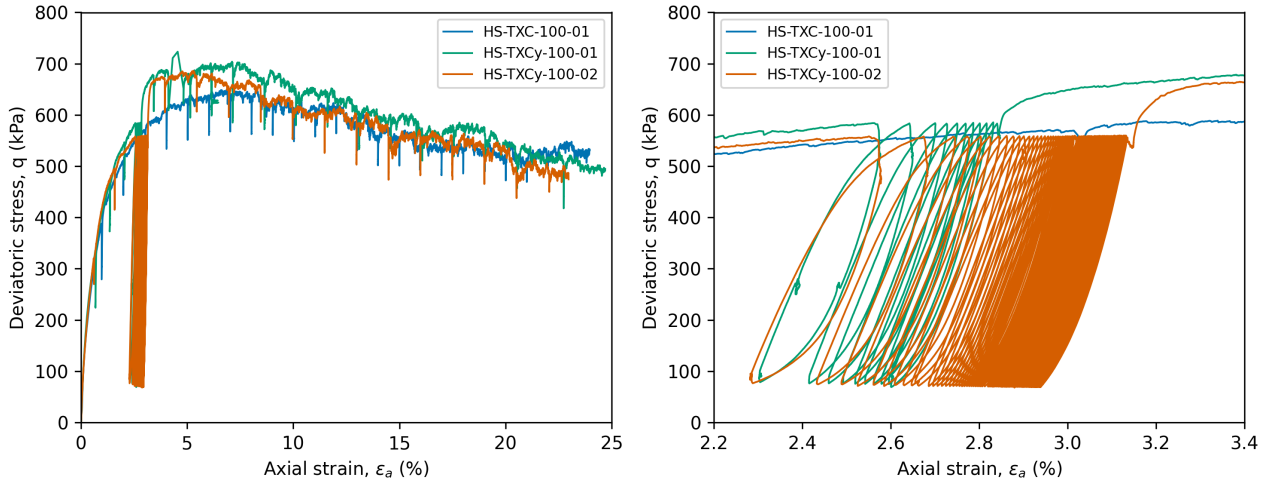

Figure 1. Force - displacement curves from LS-DEM simulations with various friction coefficient μ, compared against the experimental measurements.

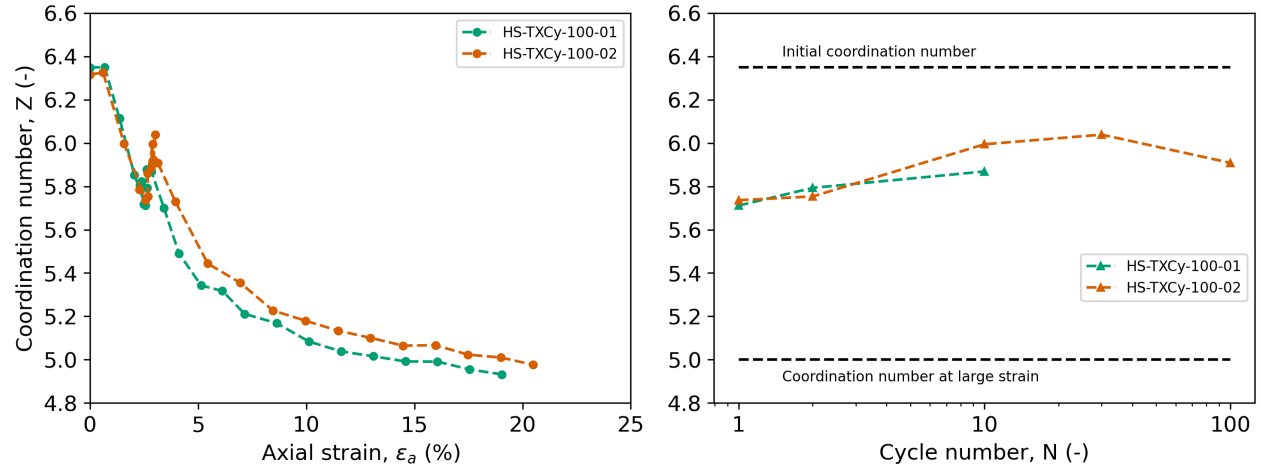

Figure 2. Coordination number versus axial strain and number of cycles.

I—tests with monotonic loading and stress cycles. *Acta Geotechnica*, **11**, 739–761, publisher: Springer Verlag.

[2] Kawamoto, R., Andò, E., Viggiani, G., and Andrade, J. E. (2016). Level set discrete element method for three-dimensional computations with triaxial case study. *Journal of the Mechanics and Physics of Solids*, **91**, 1–13.

[3] Wiebicke, M., Ando, E., Herle, I., and Viggiani, G. (2017). On the metrology of interparticle contacts in sand from x-ray tomography images. *Measurement Science and Technology*, **28**, 124007, publisher: Institute of Physics Publishing.

NEUTRON (AND X-RAY) TOMOGRAPHY FOR THE STUDY OF POROUS MEDIA

Tengattini A. [1,2*], ***Lenoir N.*** [2], ***Couture C.*** [1,2], ***Viggiani G.*** [2]
[1]*A Université Grenoble Alpes, CNRS, Grenoble INP, 3SR, Grenoble, France*
[2] *Institut Laue-Langevin (ILL), Grenoble, France,*

1. General

During the last few decades, a number of advanced experimental techniques have provided an unprecedented insight into the behaviour of geomaterials. A notable example are the so-called *full-field* techniques such as x-ray and neutron imaging, which allow the non-destructive characterisation of the 4D (3D+time) response of geomaterials undergoing hydro–chemo–thermo-mechanical loading.

While x-ray tomography over the last decade became a pillar in the domain, neutron imaging remains a comparatively less known tool. The unique properties of a neutron beam, such as high sensitivity to hydrogen (e.g., water, hydrocarbons), high penetration into metals (allowing the imposition of extreme boundary conditions), and isotope sensitivity (*e.g.*, D2O/H2O), make neutron imaging an extremely interesting tool for experimental geomechanics. Recent developments have also pushed the spatio-temporal resolution of neutron imaging [1].

A number of elements are far more (or less) visible in neutron than in X-ray imaging, making these two techniques profoundly complementary. This was acknowledged since the early days, also given the inspirational role that X-ray imaging has had on its neutron counterpart. It is nevertheless only very recently that it has been made possible to acquire Neutron and X-ray Tomography fully simultaneously [2]. This combined use is uniquely powerful, thanks to the high complementarity of their contrast. It allows not only to study different aspects of processes (*e.g.*, the interdependence between the opening of cracks and water penetration) but even aids in the identification of the different phases comprising a sample as highlighted in Fig. 1

A number of new contrast options have also been much developed recently: from monochromatic imaging to polarised neutron imaging to study the magnetic fields of materials. Grating interferometry is of particular interest as it allows the characterization of heterogeneities on the scale of 0.1 µm to 10 µm and above through dark-field imaging, while differential phase contrast can be employed to differentiate even modest variations in the refractive index of materials.

This contribution will propose an overview of recent developments in neutron imaging including the combined use of x-ray imaging, focusing on recent discoveries allowed by- and new venues opened in- the study of porous media.

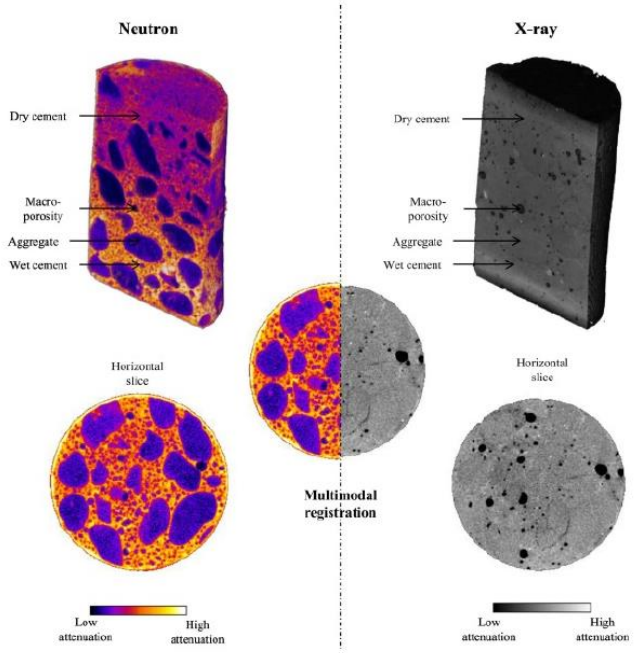

Figure 1. Example of the unique complementarity of information provided by neutrons and X-rays in the study of concrete

2. References

[1] Tengattini, A., Lenoir, N., Ando, E., & Viggiani, G. (2021). Neutron imaging for geomechanics: A review. Geomechanics for Energy and the Environment, 27, 100206.

[2] Tengattini, A., Lenoir, et al. (2020). NeXT-Grenoble, the Neutron and X-ray tomograph in Grenoble. Nuc. Inst. Meth. Phys. Res. a: A, 968, 163939.

POST FAILURE RESPONSE OF A METAMORPHIC HETEROGENOUS ROCK, AS REVEALED BY *IN-SITU* X-RAY TOMOGRAPHY

***I. Vego*[1], *S. Webster*[2,3], *N. Francois*[2], *M. Knackstedt*[2] *and M. Saadatfar*[1,2]**

[1] *School of Civil Engineering, The University of Sydney, Sydney, NSW 2006, Australia*

[2] *Department of Material Physics, Research School of Physics, The Australian National University, Canberra, Australian Capital Territory, Australia*

[3] *Northparkes Mines, Life of Mine and Exploration Department, Parkes, New South Wales, Australia*

1. Introduction

The high demand for raw materials has led to a decrease in ore grades, requiring deeper mining with associated safety concerns [1, 2]. The behaviour of materials during caving is not yet well-understood, creating a gap between predictions and actual responses, hence raising safety issues [1, 3]. The final goal would be to reduce this gap, improving safety measures during caving and possibly enhancing the efficiency of ore extraction, thereby reducing the environmental impact of mining [1, 4]. Microstructural analyses can provide insight to more accurately calibrate caving analytical and numerical models. In this context, this study aims to explore some aspects of the hydro-mechanical coupling that affect the mining industry on a daily basis. Considering significant recent advancements in imaging [1, 5], laboratory x-ray tomography and a full 3D image analysis workflow are here employed to track the mechanical response of a metamorphic rock sample undergoing axial compression, relating strain to ore distribution, and analysing joint and fracture network evolution, as they are known to strongly influence the material permeability and response [6].

2. Experimental study

A highly heterogeneous and saturated sample of hard-metamorphic rock is tested using the x-ray micro-CT high-pressure apparatus at the CTLab based at the Research School of Physics of the Australian National University [5]. A triaxial test is performed over a period of 4 months, allowing for extended relaxation between the sequential steps. As illustrated in Figure 1a, the mechanical response of the sample exhibits typical characteristics of a brittle material. 25 different x-ray tomographies are acquired, with a voxel size of approximately 45μm.

The following analyses focus on 4 specific states, encompassing S_1 (the reference configuration and initial state), along with three additional points: S_6, the failure state, and S_7 and S_8, post-failure states (see Figure 1a). Vertical slices of the reconstructed images are shown in Figure 1b, revealing the emergence of lower density regions. Compression induces joint opening, new fractures, and sliding between upper and lower regions along a higher-density preexisting thin joint. In the final step S_8, the open joints seem to fade away, as an increase of pore pressure closes them.

Image correlation is performed employing the digital volume correlation workflow implemented in the software `spam` [7]. The correlation is generally successful, although achieving convergence is challenging in areas close to joints and fractures, where there is significant variation of gray-values. From the 3D displacement field, it is then possible to compute the strain map. As shown in Figure 1, the total deviatoric strain analysis reveals the activation of the main joint at step S_6, accompanied by fracturing in surrounding regions. With further compression, the deviatoric strain increases, emphasising the opening of fractures. In the last stage S_8, when the pore pressure is increased, the results seem to suggest a partial deformation recovery. This recovery is only apparent, and it is likely due to the filling of joints by the fluid, along with the closure of fractures. These processes deceptively "flatten" the gray-values along the joints and fractures, suggesting that they have fully recovered, despite the relatively high deformation that occurred in the previous steps.

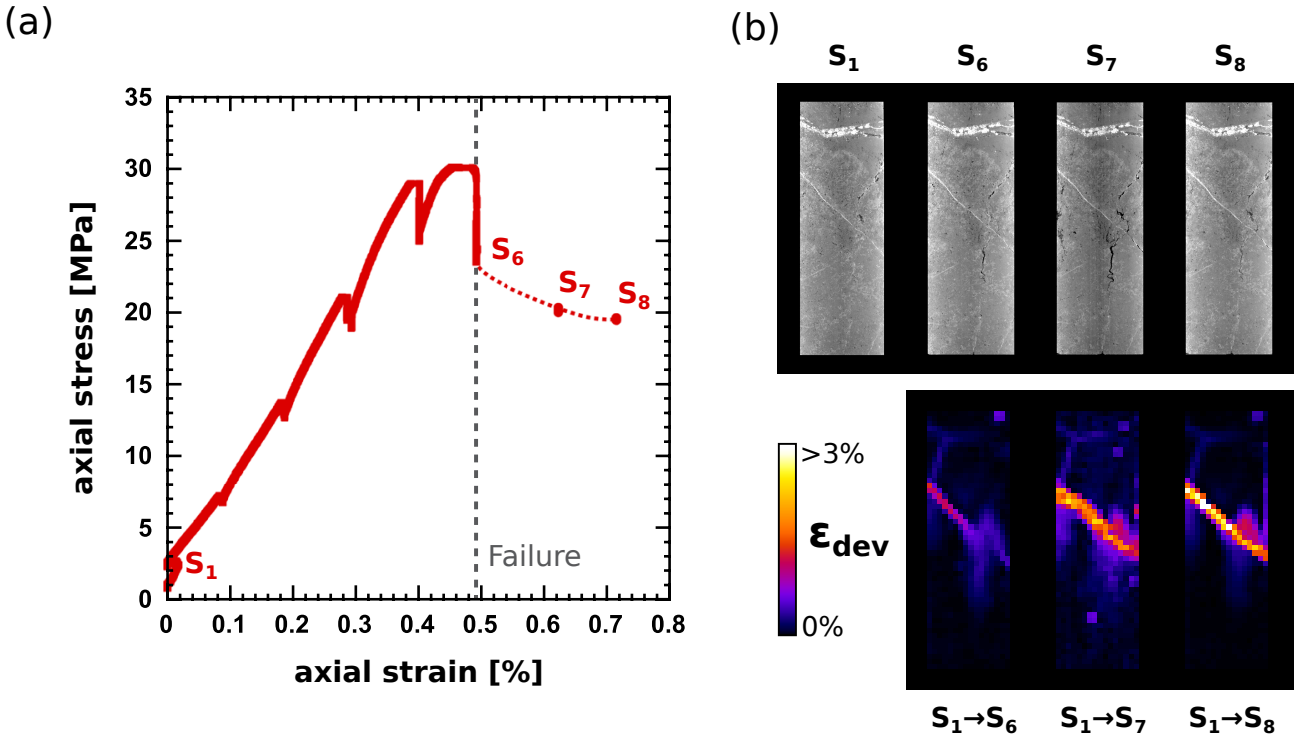

Figure 1. Stress-strain response of the sample under triaxial compression, adapted from Francois *et al.* (2022) [5] (a). Vertical slices of the crucial states and total deviatoric strain maps measured with respect to the initial state S_1 (b).

3. Conclusions

The results reveal that the main deviatoric strain is higher close to a preexisting joint characterised by higher material density. Nonetheless, higher density does not imply higher brittleness. Fractures may vanish from the images with a pore pressure increase. It is evident that the material's behaviour is influenced by joint dynamics. To better understand the dynamics of this hydro-mechanical coupling, future analyses will focus on higher-resolution images around the regions where the deviatoric strain is higher.

References

[1] Ranjith, P. G., Zhao, J., Ju, M., De Silva, R. V., Rathnaweera, T. D., and Bandara, A. K. (2017). Opportunities and challenges in deep mining: a brief review. *Engineering*, **3**, 546–551.

[2] Sonter, L. J., et al. (2023). How to fuel an energy transition with ecologically responsible mining. *Proceedings of the National Academy of Sciences*, **120**, e2307006120.

[3] Webster, S., Snyman, L., Francois, N., and Saadatfar, M. (2022). X-ray computer tomography and ground conditions at northparkes cave edges to further the understanding of the caving mechanisms of strain and hydraulic conductivity. *Caving 2022: Fifth International Conference on Block and Sublevel Caving*, pp. 635–650, Australian Centre for Geomechanics.

[4] Tavares, L. M. (2021)., Editorial for special issue "comminution in the minerals industry".

[5] Francois, N., Cruikshank, R., Herring, A., Kingston, A., Webster, S., Knackstedt, M., and Saadatfar, M. (2022). A versatile microtomography system to study in situ the failure and fragmentation in geomaterials. *Review of Scientific Instruments*, **93**.

[6] Guéguen, Y. and Boutéca, M. (2004). *Mechanics of fluid-saturated rocks*. Elsevier.

[7] Stamati, O., et al. (2020). Spam: software for practical analysis of materials. *Journal of Open Source Software*, **5**, 2286.

SELF-DRILLING X-RAY CT SCANNER FOR IN-SITU DIGITAL IMAGE SAMPLING

S. Matsumura[1], A. Kondo[2], K. Nakamura[1], T. Mizutani[1], E. Kohama[3], K. Wada[4], T. Kobayashi[5], N. Roy[6] and J.D. Frost[7]

[1] Port and Airport Research Institute, Geotechnical Engineering Division, Foundations Group, Yokosuka, Japan

[2] Port and Airport Research Institute, Earthquake Disaster Prevention Engineering Division, Earthquake and Structural Dynamics Group, Yokosuka, Japan

[3] Port and Airport Research Institute, Earthquake Disaster Prevention Engineering Division, Yokosuka, Japan

[4] Tsukuba Technology Co., Ltd., Tsukuba, Japan

[5] Ritsumeikan University, College of Science and Engineering, Department of Civil and Environmental Engineering, Kusatsu, Japan

[6] Georgia Institute of Technology, College of Computing, Atlanta, USA

[7] Georgia Institute of Technology, School of Civil and Environmental Engineering, Atlanta, USA

1. Introduction

A typical ground investigation to characterize soil properties such as void ratio, hydraulic conductivity, and shear behavior among others requires in-situ sampling of soils and various laboratory tests to determine the specific property using the sampled soils. Laboratory X-ray computed tomography (CT) has been used to non-destructively observe soils and characterize their properties using image processing, numerical analysis, or three-dimensional (3D) printing techniques based on scanned images [1−3]; however, if it became possible to scan the soils in the ground, it may enable characterization without sampling (Figure 1). Matsumura et al. [4] developed an in-situ X-ray CT scanning system, i.e., self-drilling X-ray CT scanner (SeDX) illustrated in Figure 2 and confirmed that it could drill into the subsurface and scan the soils in-situ using a prototype subsurface system of air-dried gravel. This paper summarizes the concept of SeDX for in-situ “digital image” sampling, which differs from the typical approach retrieving an actual soil core. The feasibility of the investigation approach through a model test using an air-dried gravel, and future perspectives are described.

2. Self-drilling X-ray CT scanner (SeDX)

SeDX, wherein a compact X-ray CT scanner can be installed and can excavate the soil beside the sampling tube penetrated before SeDX starts to drill (Figure 2). The installed X-ray CT scanner can scan the soil sample (sample diameter ≈ 56 mm) retained in the sampling tube underground at a given drilling depth. The sampling tube is fabricated from aluminum piping, of which the unit weight is sufficiently low to allow X-ray transmission.

3. Testing conditions and results

A model test ground was prepared by pouring an air-dried gravel (2.0–9.5 mm) to a depth of 1.1 m into a 1.0 m × 1.0 m wide × 1.3 m high container. The model test confirmed that SeDX can drill into the ground up to a target final depth of 800 mm and scan the soil samples at depths of 700, 750, and 800 mm after the sampling tube has penetrated into the ground. Figure 3 shows the vertical slice of scanned soil samples, which was processed through the procedures of image reconstitution,

noise removal, binarization, and stitching the images acquired at different depths. The gravel particles were binarized and the images acquired at different depths were stitched with no obvious gaps as seen at the boundaries indicated by the triangles. This implies that the soil sample remains undisturbed during the drilling process. The full paper will introduce more details about SeDX, the model test, and image processing, and discuss the feasibility of SeDX through evaluation of image quality.

4. References

[1] Heiko, A. et al. Digital rock physics benchmarks—Part I: Imaging and segmentation. *Comput Geosci*. 50, 25-32; https://doi.org/10.1016/j.cageo.2012.09.005 (2013a).

[2] Heiko, A. et al. Digital rock physics benchmarks—part II: Computing effective properties. *Comput Geosci*. 50, 33-43; https://doi.org/10.1016/j.cageo.2012.09.008 (2013b).

[3] Matsumura, S. et al. Manufacture of bonded granular soil using X-ray CT scanning and 3D printing. Geotech. Test. J. 40(6), 1000–1010; https://doi.org/10.1520/GTJ20160273 (2017).

[4] Matsumura, S. et al. 3D image scanning of gravel soil using in-situ X-ray computed tomography. *Sci Rep*. 13: 20007. https://doi.org/10.1038/s41598-023-46772-y (2023).

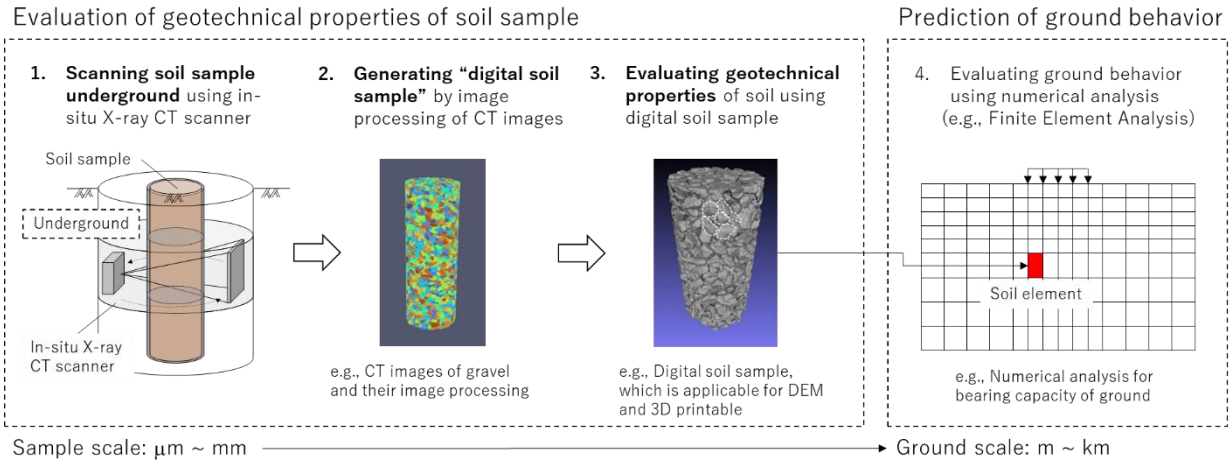

Figure 1. Concept of in-situ digital image sampling using X-ray CT scanning technique and characterization of soil based on the CT images [3, 4]

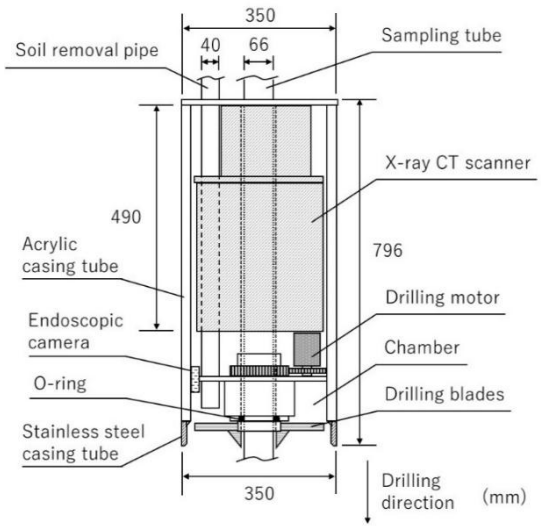

Figure 2. Schematic of SeDX

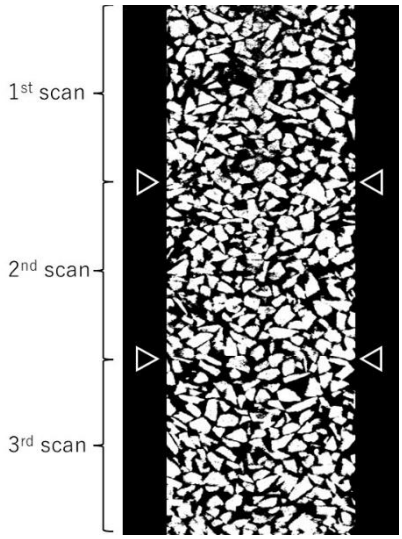

Figure 3. Vertical slice of scanned soil samples

THE INFLUENCE OF HETEROGENEITY AND CONFINING PRESSURE ON THE HYDROMECHANICS OF A SANDSTONE USING NEUTRON AND X-RAY IMAGING

F. Vieira Lima[1], S. Hall[1], J. Engqvist[1], E. Tudisco[1], R. Woracek[2], A. Tengatini3, P. Vestin[1]
[1] Lunds Tekniska Högskola, Lund University, Department of Construction Sciences, Lund, Sweden
[2]European Spallation Source, Lund, Sweden, [3]Institute Laue-Langevin (ILL), Grenoble, Franceniv.

1. Introduction

Advancing our understanding of localized deformation and heterogeneity within rocks and their profound influence on fluid flow is crucial for a range of geoenergy applications. Recent advances in 3D imaging using X-rays and neutrons at the lab scale have made significant progress.[1-3] New instruments now allow us to use both X-ray and neutron imaging together, each offering unique benefits [4]. In this study, we used X-ray and neutron tomography during permeability tests to delve into the details of how rocks evolve mechanically and hydraulically at both micro and macro scales.

2. Method

Two coupled triaxial permeability tests were conducted on Idaho Gray sandstone samples, each featuring dimensions of 25 mm in diameter and 50 mm in height. These tests were executed utilizing the NeXT instrument at the Institute Laue-Langevin, while applying confining pressures of 1 MPa (IG21) and 10 MPa (IG27). Throughout the tests, measurements of boundary force, displacement, and sample volume changes were recorded. X-ray tomography data were collected at each deformation condition, resulting in 3D image sequences with cubic voxels measuring 50 µm in width. To enhance visualization of the initial pore network, X-ray images with a cubic voxel width of 15 µm were before the campaign. Permeability tests and neutron tomography acquisition were performed on samples saturated with heavy water (D_2O) through pressure-driven percolation of distilled water (H_2O). Fluid pressure measurements were taken on both sides of the sample, and a controlled flow rate (fr) of 0.07 ml/min was applied by a syringe pump to determine bulk hydraulic conductivity (k). Rapid acquisition of tomographies within a 1-minute timeframe produced 3D images with 200 µm voxels. The reduced neutron attenuation of D_2O, compared to H_2O, enabled fluid fronts tracking in a nearly single-phase state [1] Additionally, the "cleaning process" involving pumping D_2O into an H_2O-saturated sample at a flow rate of 5 ml/min was monitored using neutron radiography.

In image analysis, porosity fields were derived from high-resolution X-ray images, enabling segmentation of the sample's volume into five quintiles of porosity. Furthermore, regular grid local Digital Volume Correlation (DVC) was performed using the SPAM [5] on pairs of in situ-acquired X-ray tomograms, deriving volumetric and deviatoric strain fields. A in-house algorithm processed the time series of neutron tomograms, generating fluid flow speed fields and local saturation degree fields for H_2O injection. The volume of active pores in the flow was estimated after fitting breakthrough curves (BTC) using neutron radiographies for H_2O and D_2O injection and assuming a non-reactive flow.

3. Results

The mechanical measurements and DVC analysis demonstrated the significant influence of confining pressure on global and local failure mechanisms. Sample IG21 experienced brittle failure with dilative-shear bands under 1 MPa, while IG27 failed through a compactive-shear band at 10

MPa. Both samples exhibited a gradual evolution of localized deformation. Analyzing strain distribution in porosity quintiles revealed that, in both samples, average deviatoric strain was higher in the least porous zones. However, IG21 displayed more contractive strain in the most porous zones, while IG27 exhibited the opposite behavior. A consistent trend emerged where the average strain of a porosity subset fell between the averages of the adjacent subsets (porosity quintiles).

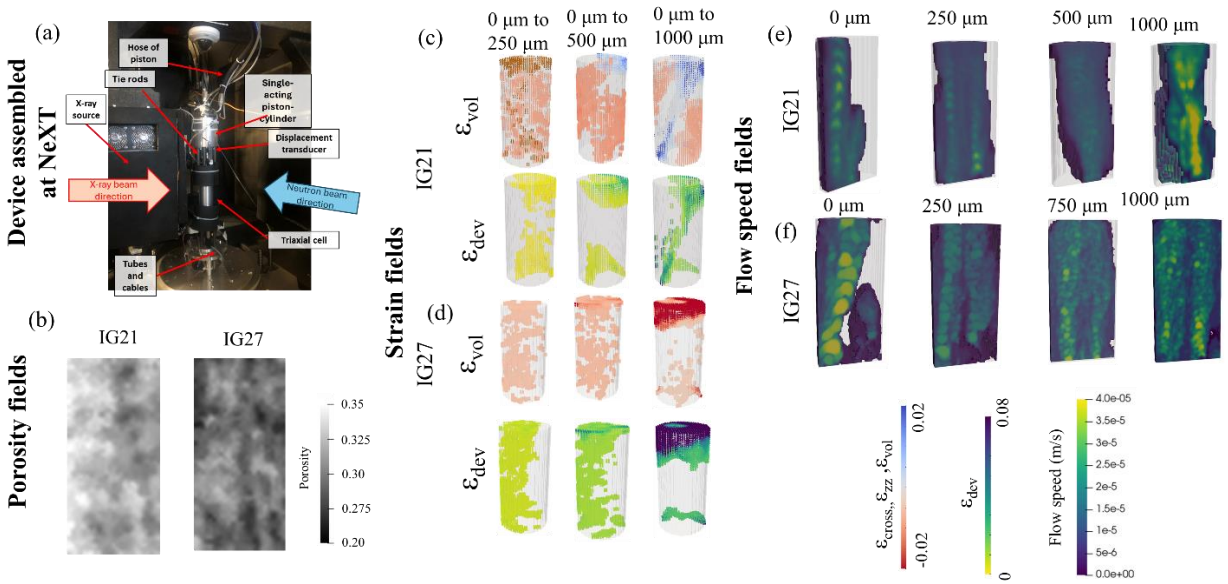

Figure 1. (a) Device assembled at NeXT – ILL, (b) Porosity fields, (c-d) Strain fields from DVC analysis, (e-f) Flow speed fields from neutron tomograms time series

Examining fluid flow data, lower flow rates (H_2O injection) reduced bulk hydraulic conductivity for both samples, with the flow path aligning with higher porosity zones. IG21 initially increased permeability until the stress peak, followed by a decrease, while IG27 displayed a continuous increase coupled with deviatoric compression. Fluid flow path geometry was influenced by strain at the inlet boundaries and strain localization, particularly the dilative shear-band.

Higher flow rates (D_2O injection) led to higher hydraulic conductivity, with IG21 showing an increase followed by a decrease post-stress peak, and IG27 experiencing a sharp decrease followed by a slight increase in k after the stress peak. Local saturation degree field analysis and BTC fitting allowed estimation of the volume of active pores. The variation in the volume of active pores was directly correlated with variation in hydraulic conductivity.

4. References

[1] M. Etxegarai, *et al*, "Characterisation of single-phase fluid-flow heterogeneity due to localised deformation in a porous rock using rapid neutron tomography," *J Imaging*, 2021,

[2] E. Tudisco *et al.*, "Fast 4-D Imaging of Fluid Flow in Rock by High-Speed Neutron Tomography," *J Geophys Res Solid Earth*, vol. 124, no. 4, pp. 3557–3569, 2019, doi: 10.1029/2018JB016522.

[3] J. McBeck, B. Cordonnier, Y. Ben-Zion, and F. Renard, "The Influence of Confining Pressure and Preexisting Damage on Strain Localization in Fluid-Saturated Crystalline Rocks in the Upper Crust," *J Geophys Res Solid Earth*, vol. 128, no. 8, Aug. 2023, doi: 10.1029/2023JB026987.

[4] A. Tengattini *et al.*, "NeXT-Grenoble, the Neutron and X-ray tomograph in Grenoble," *Nucl Instrum Methods Phys Res A*, vol. 968, no. April, Jul. 2020, doi: 10.1016/j.nima.2020.163939.

[5] O. Stamati *et al.*, "spam: Software for Practical Analysis of Materials," *J Open Source Softw*, vol. 5, no. 51, p. 2286, 2020, doi: 10.21105/joss.02286.

TRIAXIAL CYCLIC TEST WITH IN-SITU X-RAY CT SCAN FOR OBSERVATION OF RATCHETING IN GRANULAR MATERIALS

S. Li[1], H. Rattez[1], L. Simonin[1], J. Vanhulst[2], J. Soete[2] and S. François[3]

[1] Institute of Mechanics, Materials and Civil Engineering, Université Catholique de Louvain, Belgium.

[2] Department of Materials Engineering, Katholieke Universiteit Leuven, Belgium.

[3] Department of Civil Engineering, Katholieke Universiteit Leuven, Belgium.

1. Introduction

High-cyclic loading, characterized by a large numbers of load cycles (over 1000) with relatively small strain amplitudes (<0.001) [1], arises from various sources including transportation systems (e.g. high-speed and maglev trains), crane rails and machine foundations, wind and wave impacts on onshore and offshore power plants and structures, and repetitive filling and draining of structures like dams, tanks, and silos, construction activities like vibrating sheet piles, or mechanical compaction processes. Under drained conditions, high cyclic loading can result in permanent (plastic) deformations within granular foundations, a phenomenon often known as ratcheting. This presents a risk to the functionality of these foundations.

Ratcheting behavior in granular material has been studied in a number of laboratory studies [1–4], constitutive modelling [5–7] and numerical modelling [8]. These studies propose that the ratcheting primarily results from the rearrangement of particles under high cyclic loading. It is suggested that the observed reduction in the strain accumulation rate may be attribute to a gradual rearrangement of the granular structure to accommodate the applied loads more efficiently. However, a direct observation of this rearrangement process in granular materials under high-cyclic loading has yet to be achieved.

This paper presents a newly developed triaxial cyclic apparatus designed for integration with an x-ray CT scanner, enabling direct observation of particle rearrangement and macro stress-strain behaviors under monotonic compression and high-cyclic loading. Preliminary tests results are discussed by comparing them with the mechanical responses of the specimen tested on traditional triaxial apparatus. Particle contacts evolution and contacts orientation are investigated.

2. Triaxial cyclic apparatus operable with in-situ x-ray CT

Figure 1 (a) presents a schematic diagram of the triaxial cyclic apparatus operable with in-situ x-ray CT. Figure 1 (b) shows a photo of the triaxial cyclic apparatus installed in a Tescan UniTOM XL x-ray CT scanner, which enables high-through non-destructive 3D imaging. The triaxial cyclic testing apparatus, used to test cylindrical samples 20 mm in diameter and 40 mm in height, was stress/strain controlled, capable of applying cyclic stress/strain. The pore and cell pressure were applied by GDS pressure volume controllers. The axial displacement of the sample applied load and cell and pore pressures were measured by transducers linked to a PC.

3. Test material and test procedures

1 mm glass beads were selected due to their spherical shape, which facilitates contact detection. Additionally, their size not only ensures an acceptable total number of particles for image processing but also yields representative stress-strain behavior, with the voxel size being approximately 22

μm/pixel. In-situ monotonic compression tests with x ray CT scan were conducted to preliminarily validate the testing apparatus and material. The sample was subjected to monotonic compression under 200 kPa effective confining pressure. Following stress relaxation by maintaining the strain, sequential scans were performed at intervals of 1% strain increment.

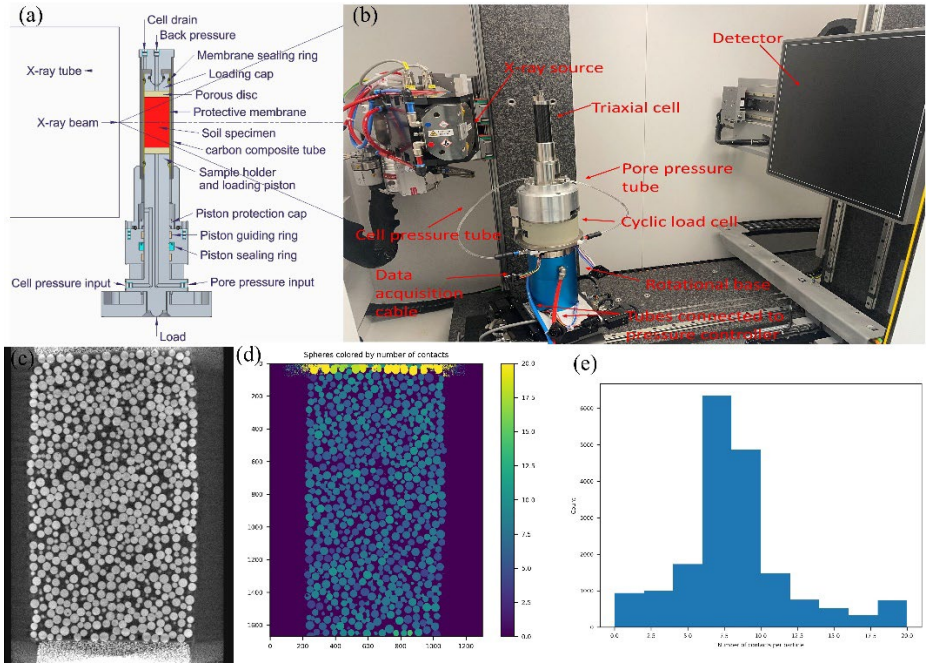

Figure 1. (a) Schematic diagram of the triaxial cyclic apparatus; (b) a photo of the triaxial cyclic apparatus installed in a x-ray CT scanner; (c) A grey-scale x-ray CT image of glass beads during triaxial compression; (d) Glass beads colored by number of contacts during compression; (e) Counts of glass beads plotted with number of contact per particle.

3. Results

The stress-strain behaviors of the testing results show comparable trend with the responses of sample tested on conventional triaxial apparatus. Particle contacts evolution and contacts orientation were calculated by registration of x-ray CT images for the entire sample in the open-source Software Analysis of Materials (SPAM) [9].

4. Conclusion.

A newly developed in-situ triaxial cyclic apparatus with x-ray CT scan capable of investigating both monotonic compression and high-cyclic loading is presented. Particle rearrangement during loading can be directly observed by sequential x-ray CT images.

5. References

1. Wichtmann T, Triantafyllidis Th, Späth L (2019) On the influence of grain shape on the cumulative deformations in sand under drained high-cyclic loading. Soils and Foundations 59:208–227. https://doi.org/10.1016/j.sandf.2018.11.001

2. Wichtmann T, Niemunis A, Triantafyllidis Th (2005) Strain accumulation in sand due to cyclic loading: drained triaxial tests. Soil Dynamics and Earthquake Engineering 25:967–979. https://doi.org/10.1016/j.soildyn.2005.02.022

3. Wichtmann T, Niemunis A, Triantafyllidis T (2010) Strain accumulation in sand due to drained cyclic loading: On the effect of monotonic and cyclic preloading (Miner's rule). Soil Dynamics and Earthquake Engineering 30:736–745. https://doi.org/10.1016/j.soildyn.2010.03.004

4. Khodair YA (2009) Lateral earth pressure behind an integral abutment. Structure and Infrastructure Engineering 5:123–136. https://doi.org/10.1080/15732470600924706

5. Wichtmann T (2005) Explicit accumulation model for non-cohesive soils under cyclic loading. PhD Thesis, Inst. für Grundbau und Bodenmechanik Braunschweig, Germany

6. He S-H, Ding Z, Sun Y, et al (2022) Cumulative deformations and particle breakage in calcareous sand subjected to drained high-cyclic loading: Experimental investigation. Soil Dynamics and Earthquake Engineering 161:107417. https://doi.org/10.1016/j.soildyn.2022.107417

7. Houlsby GT, Abadie CN, Beuckelaers WJAP, Byrne BW (2017) A model for nonlinear hysteretic and ratcheting behaviour. International Journal of Solids and Structures 120:67–80. https://doi.org/10.1016/j.ijsolstr.2017.04.031

8. Sassel TS, Patino-Ramirez F, Hanley KJ, O'Sullivan C (2023) Linking the macro-scale response of granular materials during drained cyclic loading to the evolution of micro-structure, contact network and energy components. Granular Matter 25:23. https://doi.org/10.1007/s10035-023-01308-z

9. Stamati O, Andò E, Roubin E, et al (2020) spam: Software for Practical Analysis of Materials. JOSS 5:2286. https://doi.org/10.21105/joss.02286

X-RAY MICRO CT FOR STUDYING LOCALIZED DEFORMATION IN LOESS UNDER TRIAXIAL SHEARING

Y. Y. Zhou[1], W. Fan[1] and B. Yu[1]

[1] School of Geology Engineering and Geomatics, Chang' an University, Shaanxi, China

1. Introduction

Loess is a widespread aeolian deposit consisting mainly of silt-sized quartz particles. Strain localisation is a critical factor leading to shear failure in loess, especially under low stress and water content conditions. Extensive field observations and laboratory experiments reveal a progressive failure process in loess, marked by strain concentration and substantial strength reduction, ultimately leading to the formation of shear bands [1]. Thus, advances in understanding the development of strain localization could offer important insights into the loess failure mechanism.

X-ray computed tomography which enables non-destructive examination of the microstructure of geotechnical materials, provides great benefits in studying the strain localization. With the combination of image processing techniques such as particle ID-tracking [2], strain localization within samples could be quantitatively characterised. In the context of loess, these state-of-the-art are ideal for investigating strain localization and could help to provide important insights into the failure mechanism.

In this research, the sample size was considerably reduced to achieve sufficient spatial resolution in X-ray tomography for loess microfabric characterization. The small loess sample was sheared in the compatible experimental set-up, under low confining pressure and water content, to capture the first evident localized failure mode. The sample was scanned by micro-CT at intact (ε = 0%) and deformed (ε = 15%) states, respectively. Then, based on image processing and tracking identified high-density mineral particles, the displacement field of the loess sample was measured and the localization pattern was presented, including the orientation and the thickness of the shear band.

2. Material and methodology

The undisturbed loess was collected from Gansu Province, China. For the triaxial loading test, the cylindrical sample was trimmed out of the loess block and had dimensions of 20 mm in diameter and 40 mm in height. The customized GDS triaxial loading system allows for performing loading on small samples. To examine microfabric changes within the loess sample during triaxial loading, two μ-CT scans were conducted: the first on the intact sample (ε = 0%) and the second after loading to failure (ε = 15%). The typical size of obtained three-dimensional 16-bit grayscale images is 2240×2139×3666 voxels, and the voxel size is 12.79×12.79×12.79 μm^3.

While most loess particles (D_{50} = 20.32 μm) cannot be individually visible at the current resolution, particles composed of high-density minerals can be distinguished due to their higher grayscale values. The displacement field is calculated by the difference of the high-density mineral particle centroid coordinates at the initial and deformed states. For this aim, identifying the same set of particles within the sample in different configurations is crucial. This is achieved through a particle tracking technique called 'ID-track' [2], which uses relatively invariant measurements such as particle volume as the tracking criterion to recognise particles between different configurations.

3. Results and discussion

A total of 1782 particles were successfully correlated within a selected sub-volume, which contains most of the sample axis and is normal to the shear band. Figure 1 shows the measured displacement of the tracked particles. Particles located in the upper right corner have much larger vertical displacements than those in the upper left corner due to the tilting of the porous stone and the top platen of the sample during loading. Increasing radial and vertical displacements from the top downwards within the sample showed an overall trend of lateral expansion and axis compression. Shearing results in a non-uniform response in radial and vertical displacement fields, showing two distinct regions with a tilting displacement gradient and an inclined band of localized displacement with variable thickness from around 1 to 4 mm. The unstable shear band thickness may be related to the strong structural anisotropy of loess. The inclination of the contours of equal displacement reaches a final value of around 62° from horizontal. The angle almost coincides with the shear band observed in the sample scale. These observations support the theoretical idealization of a shear band in loess as a thin layer bounded by discontinuities in the displacement gradient.

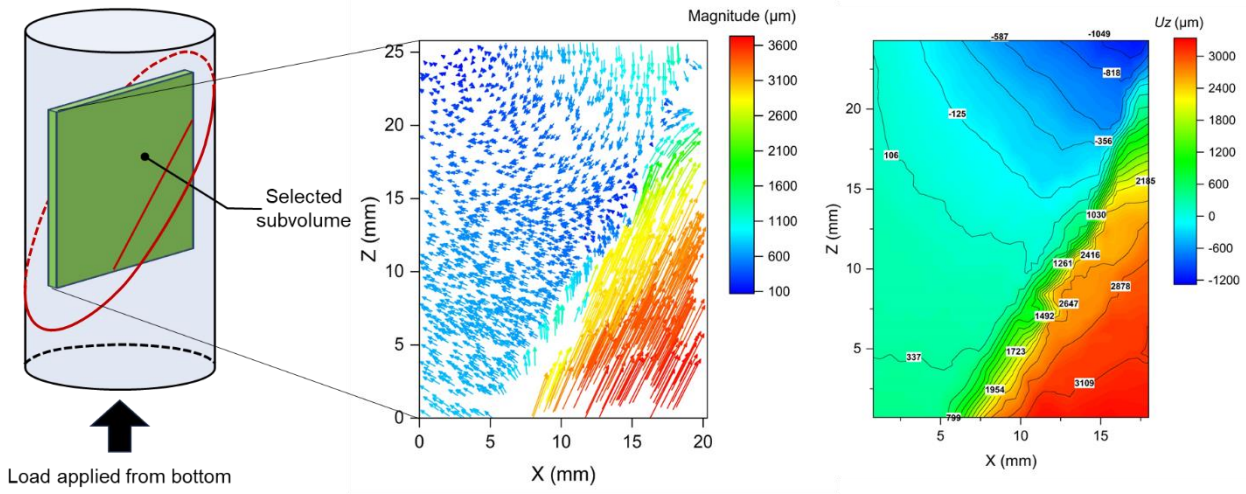

Figure 1. (a) Selected volume within loess sample for tracking particles; (b) projection of total displacement vectors plotted by identified particles; (c) vertical displacement contours.

4. Conclusions

This study investigated the microscale localization pattern in Malan loess, through a combination of triaxial shear test and X-ray micro-computed tomography (μ-CT). This approach enabled the measurement, for the first time to our knowledge, of the displacement field within the sheared loess sample. In the displacement field, the shear band was portrayed as an inclined band (62° from horizontal) of localised displacement with variable thickness ranging from 1 mm up to 4 mm. These findings offer valuable insights for multi-scale modelling of loess mechanical behaviour.

5. References

[1] Dijkstra, T., et al. (1994). The loess of north-central China: Geotechnical properties and their relation to slope stability. *Eng. Geol.*, **36**:153-171.

[2] Andò, E., et al. (2012). Grain-scale experimental investigation of localised deformation in sand: a discrete particle tracking approach. *Acta Geotech.*, **7(1)**:1-13.

Advances in experimental methods

Experimental investigations for field applications

ASSESSMENT OF UNSATURATED SOIL LIQUEFACTION RESISTANCE IN LIGHT OF THE 2023 TURKISH-SYRIAN EARTHQUAKE

***A. Gheris*[1, 2]**
[1] Univ. Souk Ahras, InfRaRes Lab., Souk Ahras, Algeria
[2] Souk Ahras University, Fac. of Science and Technology, Souk Ahras, Algeria

1. Abstract

Liquefaction of unsaturated soils during earthquakes is a significant challenge for engineers. It is widely acknowledged that soil resistance to liquefaction increases as saturation decreases. This study presents the results of a dynamic triaxial test on the sand of the Boumerdés region in Algeria under cyclical stresses, based on seismic recordings of the Turkish-Syrian earthquake of 2023. The study of behaviour under seismic stresses confirms that the degree of saturation notably affects resistance to liquefaction.

Resistance to liquefaction depends on three factors: confining pressure, pore pressure, and relative density. A relationship was discovered between liquefaction resistance ratios and volumetric strain. This relationship enables the estimation of liquefaction resistance for partially saturated sands while taking into account the effects of all three factors.

2. General

Soil deposits below the groundwater table are typically fully or nearly saturated with water [1]. However, recent investigations have shown that injecting air into the soil can significantly reduce its degree of saturation [2]. This unsaturated condition can persist for many years, often more than a decade [3]. The suggestion is that soil desaturation could effectively enhance soil resistance to liquefaction in the field. Therefore, it is necessary to establish a practical method to qualitatively estimate the liquefaction resistance of partially saturated soils.

For that, the effect of saturation degree on liquefaction resistance has been studied through laboratory tests

3. Materials and test program

Undrained cyclic triaxial tests were conducted on sand samples from the Boumerdés region. The specimens were subjected to an alternating cyclic stress rate induced by an earthquake, which was related to the maximum local acceleration (a_{max}) as noted by the equation (01):

$$\frac{\tau}{\sigma'_{v0}} = 0.65 \frac{a_{max}}{g} \cdot \frac{\sigma_v}{\sigma'_{v0}} \cdot rd \qquad (01)$$

rd=1-0.015·z (dimensionless), where z is the depth in meters. The maximum seismic acceleration amax was determined from the digital seismic signals of two earthquakes: the Boumerdés, Zemmouri earthquake of 05/21/2003 (Mw=6.8), taken as a reference earthquake, and the Turkish-Syrian earthquake of 02/06/2023 (Mw=7.8). The Fourier amplitude spectrum was calculated using a fast Fourier transform (FFT) in the frequency domain from the accelerogram to generate the optimal amplitudes and frequencies (Fig.1).

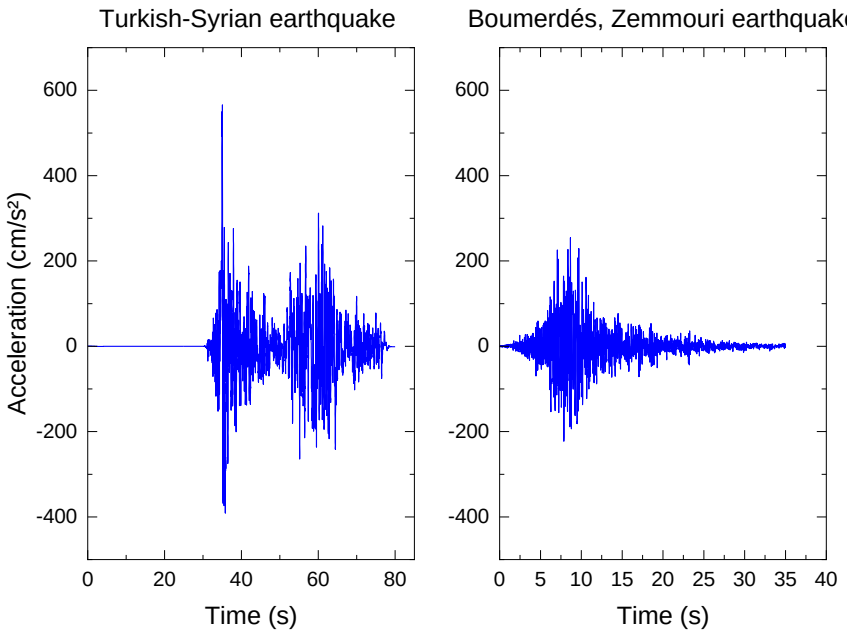

Figure1. Accelerograms, Turkish-Syrian earthquake of 2023[4], versus, Boumerdés-Zemmouri earthquake of 2003[5]

4. Results and conclusion

The impact of saturation level on sand's liquefaction resistance is confirmed. Additionally, the initial confining pressure and pore pressure also affect the liquefaction resistance. The presence of air has a more significant effect on soil's liquefaction resistance under higher confining pressure and lower initial pore pressure.

The study found a distinct correlation between the normalized liquefaction resistance and the potential volumetric strain. The relationship obtained in this study can be used to estimate the liquefaction resistance of partially saturated sand by combining it with that of fully saturated sand and the potential volumetric strain.

5. References

[1] Tsukamoto, Y., Ishihara, K., Nakazawa, H., Kamada, K. and Huang, Y. (2002). *Resistance of partially saturated sand to liquefaction with reference to longitudinal and shear wave velocities*, Soils and Foundations, **42**(6) : 93-104.

[2] Okamura, M., Ishihara, M. and Oshita, T. (2003). *Liquefaction resistance of sand improved with sand compaction piles*, Soils and Foundations, **43**(5), 175-187.

[3] Okamura, M., Ishihara, M. and Tamura, K. (2006). *Degree of saturation and liquefaction resistances of sand improved with sand compaction piles*, J. Geotech. Geoenviron. Engrg., ASCE, **132**(2): 258-264.

[4] Luzi ,L., Lanzano G., Felicetta, C., D'Amico M. C., Russo E., Sgobba S., Pacor, F., & ORFEUS Working Group 5 (2020). *Engineering Strong Motion Database (ESM) (Version 2.0)*. Istituto Nazionale di Geofisica e Vulcanologia (INGV). https://doi.org/10.13127/ESM.2.

[5] CGS Homepage, http://www.cgs-dz.org/index.php/fr/reseau-accelerometriques, last accessed 2023/08/25.

Cavitation effect of the Super Well Point method to lower the groundwater table and promote consolidation of soft soils

Masayuki Hyodo, Emeritus Professor, Yamaguchi University
Shigeyoshi Takahashi, President, Asahi Techno, Co., Ltd,
Koki Takahashi, Technical Manager, Asahi Techno, Co. Ltd.

ABSTRACT

The structure of the Super Well Point method consists of a steel pipe well of approximately 40 cm diameter, a submersible pump mounted near the bottom of the well and a vacuum pump at the top of the well. The submersible pump pumps up the water in the well and at the same time the vacuum pump at the top of the well adds vacuum pressure through a vent at the bottom of the well and through a filter wrapped around the well, creating a strong negative pressure in the ground and causing cavitation in the ground, sucking in groundwater and reducing the water content of the surrounding soil. First, a hole of about 80 cm in diameter is drilled, a casing is erected, an SWP well is inserted and boulders are placed around it. The casing is pulled out and pressurised to 80 kPa by a SWP compressor. Negative pressure is then applied and this process is repeated to clean the ground around the well and create numerous channels in the ground. This process creates natural flutter as gravel and sand with large grain sizes gather around the well at high flow velocities. A vacuum pump at the top of the well can then pump up the groundwater to promote groundwater lowering and consolidation of the soft ground. The authors have developed this method and have achieved many results in lowering the groundwater table at tunnel sites, landslide prevention and sluice gate construction, etc. The method has also been very effective in promoting consolidation of soft ground. This paper presents the effects of soil cavitation by this method and actual examples of groundwater table lowering and consolidation promotion.

EXPERIMENTAL INVESTIGATION OF UNSATURATED HYDRAULIC PROPERTIES OF SOIL COVERED BY DIFFERENT GRASSES

Xu-guang Gao[1], Xian-wei Li[1] and Ji-Peng Wang[1]
[1] Shandong University, School of Civil Engineering, China

1. Abstract

This study aims to investigate the effects of different grass species on the soil water retention curve and unsaturated permeability coefficient of the soil. Based on the indoor rainfall infiltration tests, the changes of soil water content and soil suction of bare soil and soil covered with different grasses under the effect of rainfall were investigated. The results showed that there was a large difference in the root content of the three kinds of grasses, which changed the soil pore size and thus led to the change of soil hydraulic properties. The root system can delay the increase of soil water content and the decrease of soil suction by absorbing water and occupying soil pore space under the effect of rainfall. With the increase of root content, grass roots can significantly increase the air-entry value and reduce the unsaturated permeability coefficient of the soil.

2. Introduction

Grass protection has been recognized as an ecological and environmental techniques that can improve the stability of geotechnical infrastructures, such as compacted slopes, embankments, and landfill covers [1]. Numerous studies have reported the responses of soil suction and permeability properties[2] induced by grass. However, a single grass species was mainly used in these researches, and the differences of soil water retention and permeability properties covered by different grass species are still not well understood.

The objectives of this study are to: (1) quantitatively analyze the influence of grass roots on soil water retention and permeability through rainfall infiltration test of bare soil and soil covered by grass, and then (2) analyze the difference of soil water retention and permeability properties of soils covered by different grass species.

3. Materials and methods

In this study, four vegetation boxes made of transparent plexiglass were designed (one bare and three vegetated). Soil with a thickness of 70 cm was compacted in each box, and grass was vegetated on the soil surface. Soil moisture content and soil suction sensors were installed at depths of 10 cm, 20 cm, 30 cm, 40 cm and 60 cm, respectively, to measure changes in soil moisture content and suction during rainfall. The total rainfall was set at 100 mm, with rainfall intensifies of 20 mm/h. All the vegetation boxes were filled with Yellow River alluvial silt. The grass species, *Festuca arundinaria* (FA), *Bermuda grass* (BG), *Lolium multiflorum* (LM) were selected for testing. The test was conducted after three months of cultivation in the natural environment.

4. Results

The soil water retention curves at 10 cm and 20 cm depth for bare soil and the soils covered by three kinds of grass are shown in Figure 1. It can be seen that under the same soil water content, the suction in the soil covered by three kinds of grass is higher than that in the bare soil. Moreover, among the three kinds of grass, the suction is higher in the soil covered by *Festuca Arundinaria*.

The value of α in the soil covered by three kinds of grass is smaller than that of the bare soil, which indicates that the root system of grass can increase the air intake value of the soil.

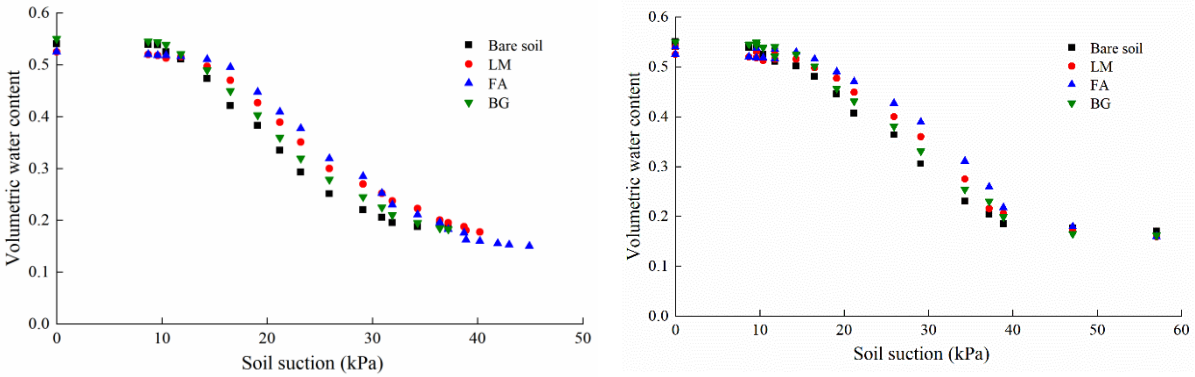

(a) 10 cm (b) 20 cm

Figure 1. Soil water retention curves of grass root zone

The instantaneous profile method was used to calculate the average permeability coefficient of the infiltration process. Figure 2 shows the unsaturated permeability coefficients at different depths in bare soil and the soils covered by three kinds of grass. It can be seen that the permeability coefficient of soil containing grass root system is smaller than that of bare soil at any depth. This is especially true at 10 cm and 20 cm depth, which is the main distribution area for the root system. However, with the increase of soil depth, the difference gradually decreases at the depth of 30 cm and 40 cm.

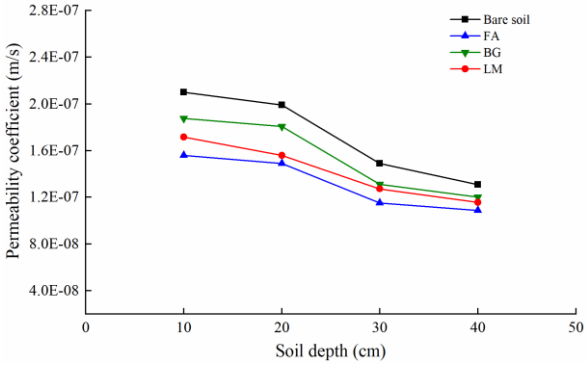

Figure 2. Unsaturated permeability coefficient at different depths

5. Conclusion

The root system of grass can increase the air intake value of the soil and decrease the soil permeability coefficient. The grass of *Festuca Arundinaria* grows fast and its root density is larger, which has the most significant effect on improving the soil water retention capacity and reducing the soil permeability coefficient.

6. Reference

[1] Wang X, Ma C, Wang Y, et al. (2020) Effect of root architecture on rainfall threshold for slope stability: variabilities in saturated hydraulic conductivity and strength of root-soil composite[J]. Landslides, 17, 1965-1977.

[2] Leung, A. K., Garg, A., & Ng, C. W. W. (2015). Effects of plant roots on soil-water retention and induced suction in vegetated soil. *Eng Geol.* 193, 183–197.

FIELD MONITORING OF ROOT-CRACK INTERACTIONS ON SOIL INFILTRATION UNDER VARYING SEASONAL CONDITIONS

Yuliana[1], Arwan Apriyono[2], Viroon Kamchoom[1*]
[1] Excellent Centre for Green and Sustainable Infrastructure, School of Engineering, King Mongkut's Institute of Technology Ladkrabang, Bangkok 10520, Thailand
[2] Department of Civil Engineering, Jenderal Soedirman University, Indonesia
[*]Corresponding author, E-mail: viroon.ka@kmitl.ac.th

1. Introduction

Accurate infiltration measurements are indispensable in geotechnical engineering, particularly for assessing slope stability. Vegetation is a widely accepted eco-friendly solution for environmental stability such as preventing shallow landslides and erosion in geotechnical structures. Numerous studies have been conducted to investigate infiltration rates in vegetated soil. However, the impact of roots on soil infiltration has contradictory findings across various research investigations. The presence of vegetation has been linked to reduce infiltration rates and saturated hydraulic conductivity (K_{sat}) [1–3]. Conversely, other studies have reported that vegetation can lead to increase infiltration rates and K_{sat} [4–6]. Furthermore, the presence of desiccation cracks has been shown to impact infiltration rates [7,8]. A comprehensive grasp of infiltration processes demands an exploration into the propagation of plant roots and their potential influence on the emergence of these cracks, especially within authentic field conditions. Additionally, infiltration rates display notable fluctuations influenced by various environmental factors, especially in rainfall and drought patterns [9]. These fluctuations are closely tied to alterations in crack intensity and distribution, the dynamics of plant roots, and the intricate interplay between plant roots and the cracks. This study aims to comprehensively investigate the interplay between plant roots and desiccation cracks, as well as the combined impact of vegetation, cracks, and seasonal variations on infiltration rates.

2. Methodology

Field monitoring was conducted at a designated test site in Khlong Sam Wa, Thailand. The flat area was divided into three square zones, each measuring 1.5 m by 1.5 m. Two identical vegetation zones, V1 and V2, were planted with vetiver grass (*Vetiveria zizanioides sp*) to assess natural

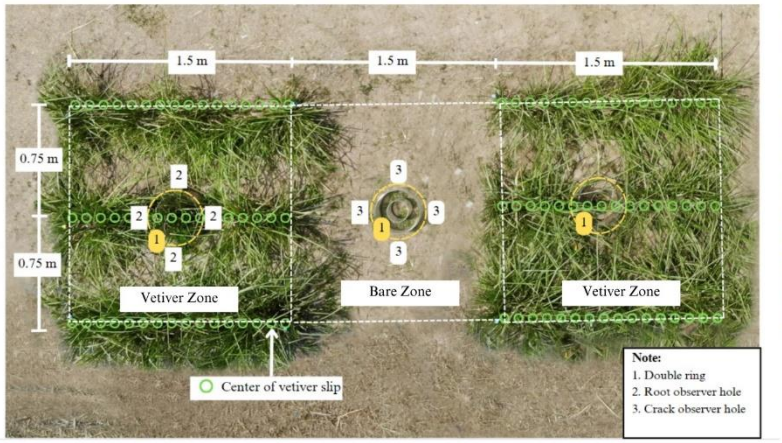

Overview of test area

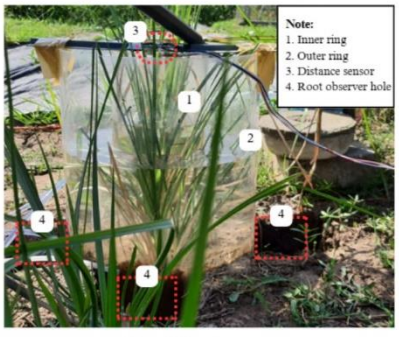

Double ring set up

Figure 1 The detail of field observation

variations, while a bare zone in the middle served for comparison (see Figure 1). Vetiver grass was planted with a spacing of 10 cm within rows and a distance of 75 cm between rows.

Employing a comprehensive six-month monitoring approach with the seasonal variations (i.e. wet, dry winter and dry summer period), this study utilized the double ring infiltration (DRI) test to directly determine infiltration rates with the falling-head standard. The inner and outer rings of the DRI test are crafted from acrylic tubes with diameters of 15 cm and 30 cm, respectively. Transparent acrylic tubes were chosen over steel for the double ring material to enable a clear observation of root and crack changes. Moreover, the rate of water flow in the inner ring was determined by measuring the temporal change in distance between the distance sensor and the water level. HC-SR04 ultrasonic distance sensors are positioned on top of the ring (refer to double ring set up in Figure 1) to observe water changes during the test. This sensor is connected to a Datalogger set up to record water level changes every second. Preceding each DRI test, both root growth and crack formation were captured using Minirhizotron. Root growth was quantitatively interpreted through Root Area Ratio (RAR), while changes in crack formation through Crack Intensity Factor (CIF) for both vegetated and bare zone.

3. Results

The finding indicates that during root growth, the existence of vetiver root potentially influenced crack distribution by minimizing up to 60% of CIF, resulting in a more irregular crack pattern compared to the bare area. In terms of infiltration rate, RAR and CIF resulted positive correlation to infiltration rate indicating that both root development and crack formation potentially enhance soil water infiltration. Furthermore, in comparison with bare zone, the final infiltration rate in the vegetated zone experiences a significant increase, approximately 1.4 times and 5 times during dry winter and summer period, respectively. During the growth period, root may minimize the likelihood of extensive cracking by promoting the formation of soil aggregates hence stabilize the soil structure. At the same time, the improved soil structure creating root creates channel as the preferential pathway leading to increase of soil infiltration.

4. References

[1] Huat B.B.K., Ali F.H.J. and Low T.H. (2006). Water infiltration characteristics of unsaturated soil slope and its effect on suction and stability. Geotech. Geol. Eng., 24 1293–306.

[2] Rahardjo H., Satyanaga A., Leong E.C., Santoso V.A. and Ng Y.S. (2014). Performance of an instrumented slope covered with shrubs and deep-rooted grass. Soils Found., 54 417–25.

[3] Leung A.K., Garg A., Coo J.L., Ng C.W.W. and Hau B.C.H. (2015). Effects of the roots of Cynodon dactylon and Schefflera heptaphylla on water infiltration rate and soil hydraulic conductivity. Hydrol. Process., 29 3342–54.

[4] Jotisankasa A. and Sirirattanachat T. (2017). Effect of grass roots on soil-water retention curve and permeability function. Can Geotech J., 54 1612–22.

[5] Rajamanthri K., Jotisankasa A. and Aramrak S. (2021). Effects of Chrysopogon zizanioides root biomass and plant age on hydro-mechanical behavior of root-permeated soils. Int. J. Geosynth. Gr. Eng., 7 1–13.

[6] Ng C.W.W., Ni J.J., Leung A.K., Zhou C. and Wang Z.J. (2016). Effects of planting density on tree growth and induced soil suction. Geotechnique., 66 711–24.

[7] Cheng Q., Tang C.S., Xu D., Zeng H. and Shi B. (2021). Water infiltration in a cracked soil considering effect of drying-wetting cycles. J. Hydrol., 593 125640.

[8] Gadi V.K, Bordoloi S., Garg A., Sahoo L., Berretta C. and Sekharan S. (2017). Effect of shoot parameters on cracking in vegetated soil. Environ. Geotech., 5 123–30.

[9] Louati F., Trabelsi H., Jamei M. and Taibi S. (2021). Impact of wetting-drying cycles and cracks on the permeability of compacted clayey soil. Eur. J. Environ. Civ. Eng., 25 696–721.

INFLUENCE OF ACTIVE AND INACTIVE INTRUDERS ON SANDY SOIL: A LINK BETWEEN RETENTION PROPERTIES AND PORE SIZE DISTRIBUTION

***F. Anselmucci*[1], *H. Cheng*[1], *Y. Zeng*[2] *and V. Magnanimo*[1]**

[1] *University of Twente, Chair of Soil Micro Mechanics, Faculty of Engineering Technology, Enschede, The Netherlands*

[2] *University of Twente, Faculty of Geo-information Science and Earth Observation, Department of Water Resources, Enschede, The Netherlands*

1. Motivation

Frequent extreme droughts pose a significant challenge for farmers who must actively adapt to these climate stress in order to preserve soil health [1, 2]. Our study aims to provide valuable insights for enhancing soil resilience in the face of climate change. We focus on understanding how soil's structure and its interaction with plants influence its capacity to retain water, a critical factor for crops production. Our objective is to develop a methodology able to predict soil behaviour under different environmental conditions. This will empower better decision-making for farming and soil conservation.

2. Experimental approach

To unravel the link between soil structure and vegetation, we conducted experiments on three configurations of sandy soil, comparing the properties of bare soil with those reinforced by crop roots (active) and nylon fibers (inactive) intruders. A key property under study is the soil's water retention capability. Tensiometers and water moisture sensors, recalibrated for precision, were used to gather data from soil samples, prepared in cylindrical containers (6.5 cm in height and 6.6 cm in diameter) and subjected to three drying and wetting cycles. All the results shown here refer to sand with the same size particles (D_{50} = 0.72mm) and the same bulk porosity (ϕ = 0.36). The measurements are taken when the growth of the roots has stopped. In the discussion that follows, we compare roots and fibers reinforced soil samples with equal intruder content (i.e. length density per soil volume).

3. Analysis

As initial step, we gather data throughout the final drying cycle, plotting soil saturation degree against matric suction, using the Van Genuchten model [3] to fit the experimental measurements. Our data show that the presence of inclusions in the soil, both roots or fibers, enhance water retention capability. Notably, the rooted soil shows a higher retention capacity with respect to the bare soil as well as fiber reinforced sand, which means that the retention capability is not due to the only presence of geometric occlusion on the pore network, but it is due to the hydraulic root activity on the matric suction of the system [4], although the root growth was stopped during the recording of the retention values in the drying cycle (i.e. no osmotic effect).

In Figure 1a, the SWRCs for the three different soil mixtures are presented. To facilitate the comparison, the SWRCs are plotted using the effective volumetric water content (VWC_{eff}), and the matric suction (ψ) is normalised to the value of the air bubbling pressure (ψ_{ae}). By using the modified Young-Laplace equation for capillary pressure in a tube, we can analytically derive the pore classes distribution d from the matric suction ψ measured to obtain the drying SWRC. The pore classes distribution is also a function of other soil properties, as the liquid contact angle θ, and the surface tension σ, as presented in Equation 1:

$$d = \frac{4\sigma \cos\theta}{\Delta\psi} \tag{1}$$

Figure 1b shows the difference in pore size distribution for the three types of soil: bare, fibers reinforced and rooted. Each pores size distribution is a direct output of the ψ values recorded for the SWRC. Compared to the bare soil, the rooted soil shows the creation of a larger network of macropores, while the fibers creates a higher microporosity.

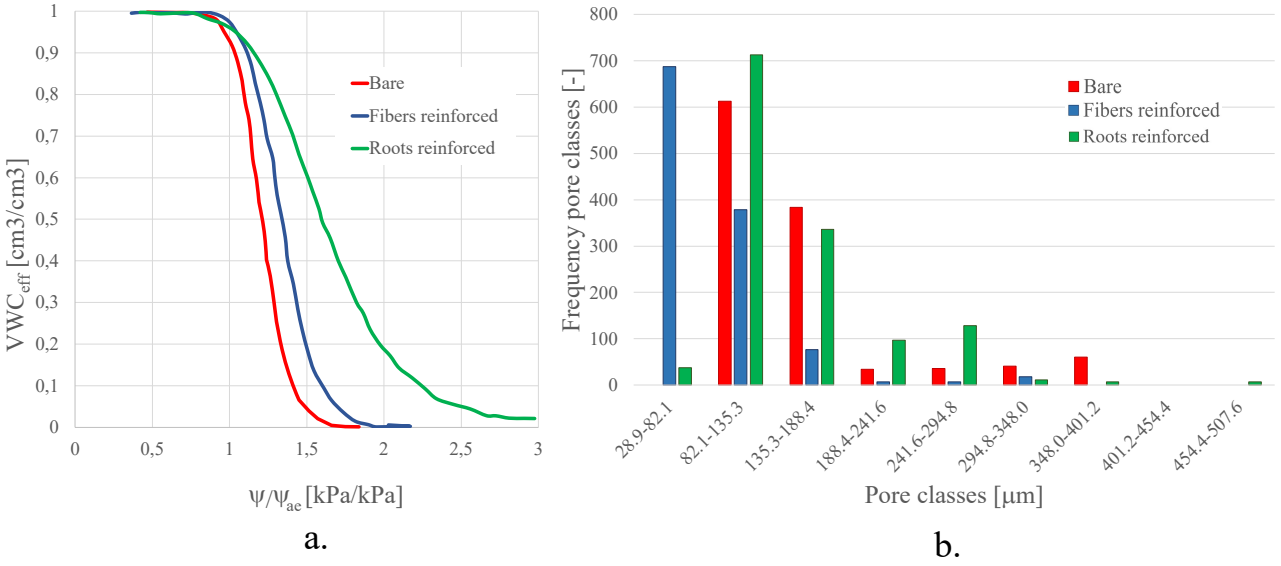

Figure 1. Comparison between the system soil water retention curves (a) and the pore size distribution (b). The results are presented for the bare soil (red), fibers reinforced soil (blue) and roots reinforced soil (green).

4. Conclusions

This study provides a comprehensive view on how changes in the soil microstructure, induced by either biological or synthetic intruders, affect soil water retention. The integration of experimental data with analytical modelling elucidates the intricate relationship between microscale modifications and macroscale soil characteristics. Although the content of intruders is equal, the presence of plant roots strongly affects the retention properties of the soil, and the overall pore network.

This approach offers a robust framework for optimising soil properties, catering to a variety of environmental and engineering applications, aligning with initiatives like the European Green Deal [5].

References

[1] Dale, V. H. (1997). The relationship between land-use change and climate change. *Ecological applications*, **7**, 753–769.

[2] Haregeweyn, N., et al. (2023). Progress and challenges in sustainable land management initiatives: A global review. *Science of The Total Environment*, **858**, 160027.

[3] Van Genuchten, M. T. (1980). A closed-form equation for predicting the hydraulic conductivity of unsaturated soils. *Soil science society of America journal*, **44**, 892–898.

[4] Cheng, H., Anselmucci, F. A., Fan, X., Zeng, Y., Luding, S., and Magnanimo, V. (2022). Down to the root of vegetated soil: challenges and state-of-the-art. *Papers in physics*, **14**, 140014–140014.

[5] European Commission, E. U. (2019)., European green deal.

SANDWICH PVC-SOIL SEISMIC ISOLATION SYSTEM: FROM ELEMENT-SCALE TESTING TO FIELD APPLICATION

B. Ge[1], Y. Sezer[1], T. Doyle[1] A. Sextos[1] and A. Diambra[1]
[1] University of Bristol, Bristol, UK

1. Introduction

Earthquake casualties are often and primarily attributed to infrastructure collapse. Unfortunately, recent seismic events in Morocco, 2023 have suggested that most buildings are not earthquake-resilient especially in low to medium-income economies where unreinforced masonries are widely used [1]. Beyond strengthening buildings with stronger materials, structural retrofitting and utilizing mass damper systems, the use of base seismic isolation is an alternative technique which can effectively reduce building displacement and transfer seismic energy during an earthquake.

Current base isolators (such as rubber bearing system and friction pendulum system) employed in construction usually involve large and complex structures, with their expensive costs being impractical and unpopular in developing countries and poverty areas. Contrarily, this paper presents a novel, low-cost "sand-wich" type PVC-sand seismic isolator system initially introduced by Tsiavos et al. [2]. Early investigation on the new system in large-scale dynamic tests conducted by [2] is briefly reviewed, demonstrating effectiveness for seismic isolation and significance of appropriately characterizing shear friction of the PVC-sand system. Then, the shear behaviour of the PVC-sand system at element level is investigated through direct shear tests, and the effects of pressure, sand properties and water content are discussed.

2. Sand-wich seismic isolation system and its early large-scale investigation

The 'sand-wich' type seismic isolation system consists of a thin layer of sand between two PVC surfaces beneath (see Figure 1). The sand particles are expected to function as a layer of 'non-perfectly rounded' ball bearings, providing flexibility of lateral motion to the upper structure during seismic events. Tsiavos et al. [2] performed large-scale shaking table tests for a low-rise structure using the proposed PVC-sand seismic isolator system. The results confirmed its effectiveness of reducing the structure acceleration compared to the fixed-base structure, when the ground motion surpassed the acceleration threshold of the isolator system, determined at $0.25g \sim 0.3g$. The system has also been employed in a typical single-story unreinforced masonry in Nepal [3]. The locally available materials and simple construction procedures suggested a promising feasibility for implementing the system in its designated regions.

3. Element-scale direct shear testing

The sliding acceleration threshold of the PVC-sand isolated buildings is strongly associated with the frictional behaviour of the sand-wich system, which should be controlled within an optimal range to balance the seismic isolation performance and the building stability under general operation loading like wind. The frictional characteristics of the PVC-sand system was investigated using the winged direct shear apparatus (WDSA), with consideration of the effects of sand particle sizes, densities, normal stresses and water contents. The results suggested the friction coefficients of systems with the given materials ranged from $0.15 \sim 0.20$. The shear friction was found more sensitive to normal stress levels than to sand densities, with higher average value found under increasing

normal stresses. Besides, fiction fluctuation was found during shearing due to particle PVC-sand interaction and re-arrangement of particles, with its extent decreasing as the normal stress and sand density increased.

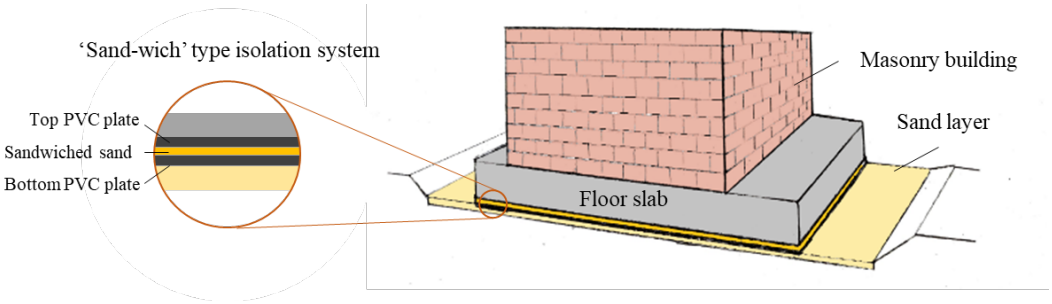

Figure 1. Schematic of a masonry building using the 'Sand-wich' type isolation system.

The friction coefficient of the system, in general, was also found to increase with the saturation ratio of the sandwiched soil sample as shown in Figure 2. However, the effect of saturation ratio on the friction coefficient varied with both sand density and normal confining stress. Due to insufficient suction developed between particles and particle-PVC interface, the effect of water content change was close to negligible for low normal stress and loose sand conditions. The outcomes in this study will provide a holistic understanding of the behaviour of the PVC-sand seismic isolation systems as the potential condition changes throughout the design, construction and operation stages and help promote this application in different regions.

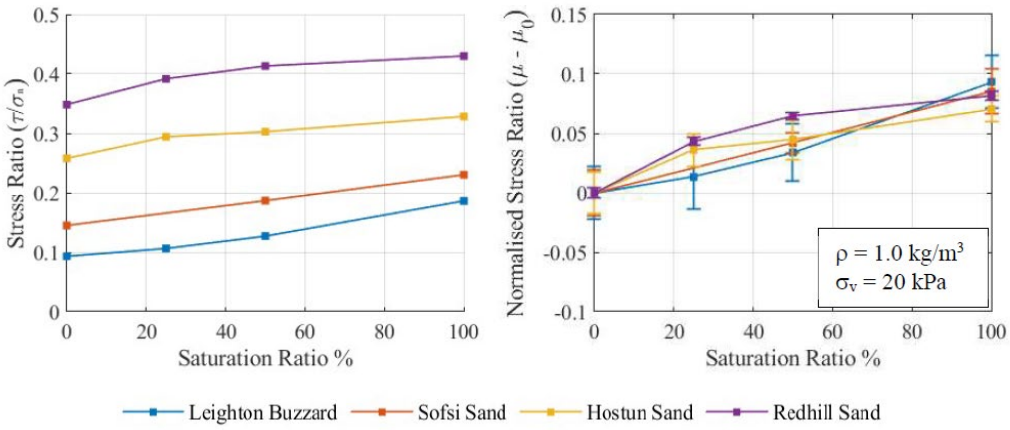

Figure 2. Friction coefficients of PVC-sand system with varying saturation ratio: (a) stress ratio and (b) normalised stress ratio.

4. References

[1] Marshall, M. (2023). Why was the Morocco earthquake so deadly? *Nature*.

[2] Tsiavos, A., Sextos, A., Stavridis, A., Dietz, M., Dihoru, L., & Alexander, N. A. (2020). Large-scale experimental investigation of a low-cost PVC 'sand-wich'(PVC-s) seismic isolation for developing countries. *Earthquake Spectra*, **36**(4): 1886-1911.

[3] Sezer, Y. M., Diambra, A., Ge, B., Dietz, M., Alexander, N. A., & Sextos, A. G. (2023). Experimental determination of friction at the interface of a sand-based, seismically isolated foundation. Acta Mechanica, 1-19.

SEASONAL WATER CONTENT VARIATION UNDER A WAFFLE RAFT FOUNDATION BUILT ON REACTIVE SOIL

S. Mediliye Gedara[1], P.L.P. Wasantha[1,2], E. Yaghoubi[1,2], R.V. Staden[1,2]

[1] Institute for Sustainable Industries & Liveable Cities, Victoria University, Melbourne, Australia

[2] College of Sport, Health and Engineering, Victoria University, Melbourne, Australia

1. Introduction

Over the years, numerous stability issues have arisen due to the shrink-swell movement of reactive soils underneath residential footing systems [1]. In Australia, about 20% of the land area is covered by reactive soil [2], and these seasonal ground movements cause severe damage to lightweight structures such as residential buildings and roads [3]. Around 1000 new residential structures were reportedly damaged in 2011 in the western suburbs of Melbourne in Victoria, Australia, due to soil heaving [3] after the millennial drought during 1996-2009 [4]. A waffle raft foundation is one of the most common footing systems used in Australia for residential structures, due mainly to their lower construction cost and time [5]. These waffle rafts utilize a grid of reinforced beams connected to the foundation, resembling a waffle. The internal beam network evenly distributes the superstructure load to the ground, and void spaces are created between internal beams. Expanded Polystyrene (EPS) pods are typically used as the void-former [5].

Developing a satisfactory solution for the stability issues of lightweight structures when built on reactive soils is constrained by the lack of knowledge of the behaviour of foundations against shrink-swell movement. The ground movement in reactive soils is a response to their existing water content. Therefore, the seasonal water content variations underneath the foundation are of critical importance to the performance of the waffle raft. Therefore, a thorough understanding of the soil water content changes underneath a waffle raft due to seasonal weather changes is imperative to the safe design of waffle rafts.

2. Aims and Objectives

This study aims to investigate the changes in soil water content underneath a model waffle raft foundation built on highly reactive soil due to seasonal weather changes to inform designers with the necessary knowledge to minimize the stability issues of lightweight structures built on reactive soils.

3. Methodology

First-hand data on volumetric water content variations were acquired through a comprehensive field-scale study. The methodology comprises five phases: site investigations, installation of moisture sensors, construction of the waffle raft, monitoring and recording data, followed by data analysis and interpretations.

The selected site for the waffle raft construction is located in Sunshine North, a western suburb of Melbourne, Australia. A site investigation was conducted following AS2870-2011 [6], and the site was classified as a H2 site class, indicating that it is a highly reactive site. Two undisturbed core specimens collected from 600mm and 800mm depths at the site were used to conduct shrink-swell tests in accordance with the AS1289.7.1.1-2003 [7]. The results showed that the shrink-swell index values were 4.7% and 4.72% clay layers at 800mm and 600mm depths, respectively. The

characteristic surface movement (y_s) was then determined using equation 2.3.1 as stipulated in AS2870-2011[6] and found to be 68mm, which confirmed the site classification to be H2 [6].

Once the site investigation was carried out, the moisture sensors were strategically installed beneath the waffle raft footing system, at varying depths and locations. Following the completion of sensor installation and waffle raft construction, the monitoring of the footing systems commenced. The data recorded by moisture sensors were then extracted using a data logger.

4. Results

To capture seasonal variations, the study took into account the four seasons: spring (September to November), summer (December to February), autumn (March to April), and winter (June to August). Average seasonal soil volumetric water contents were determined for three locations at a depth of 0.3m: outside, edge and middle of the slab. Table 1 presents the average volumetric water content values corresponding to each specific location.

Season	Outside	Edge	Middle
Winter	36.13%	29.71%	43.83%
Spring	38.44%	32.46%	37.67%
Summer	23.72%	32.17%	36.61%
Autumn	18.92%	27.18%	30.05%

Table 1. Average monthly volumetric water content values

5. Conclusion

The water content variations outside the slab exhibit a broader range, with percentage change between maximum and minimum water contents reaching up to 103%, while in the middle, the variations are confined to a narrower value of 45%. Understanding spatial differences helps in designing waffle rafts on reactive soils, and optimizing residential structure stability.

6. References

[1] Jones Jr, D.E. and W.G. Holtz, *Expansive Soils- The Hidden Disaster.* America Society of Civil Engineering, 1973. **43**(8): p. 49-51.

[2] Richards, B., Peter, P., & Emerson, W., *The effect of vegetation on the swelling and shrinking of soils in Australia.* 1983.

[3] Li, J., D.A. Cameron, and G. Ren, *Case study and back analysis of a residential building damaged by expansive soils.* Computers and Geotechnics, 2014. **56**: p. 89-99.

[4] Karunarathne, A.M.A.N., et al., *Modelling of climate-induced moisture variations and subsequent ground movements in expansive soils.* Geotechnical and Geological Engineering: An International Journal, 2018. **36(4)**: p. 2455–2477.

[5] Teodosio, B., et al., *Prefabrication of substructures for single-detached dwellings on reactive soils: a review of existing systems and design challenges.* Australian Journal of Civil Engineering, 2019. **17**: p. 120-133.

[6] Australian Standard, *AS 2870-2011 - Residential slabs and footings.* 2011.

[7] Australian Standard, *AS 1289.7.1.1-2003 - Methods of testing soils for engineering purposes, Soil reactivity tests - Determination of the shrinkage index of a soil - Shrink-swell index.* 2003.

THE APPLICABILITY OF ELECTROOSMOSIS FOR CLAY CONSOLIDATION

Y. Sugiyama[1], N. Hashimoto[1], C. Couture[2] and D. Takano[1]
[1] Port and Airport Research Institute, Yokosuka, Japan
[2] Univ. Grenoble Alpes, CNRS, 3SR Lab., Grenoble, France

1. Introduction

The use of electroosmosis in geotechnical and geo-environmental engineering has extensive application potential, such as soil consolidation and stabilization, strength improvements, soil remediation and as de-watering of sludge. Clay particles are often negatively charged in water. Therefore, during electroosmosis, the positively charged pore water near the surface of the soil particles flows towards the cathode side, causing a transient dehydration of pore water. Despite a few successful examples of applications in the field[1,2], the use of electroosmosis remains scares at the engineering scale. One of the reasons is that it remains difficult to determine the specifications for on-site application of the electroosmotic consolidation method.

In this study, in order to examine the three-dimensional effect of electroosmotic dehydration, with an electrode placement similar to potential in-situ layouts, experiments were conducted inside an acrylic cylindrical model soil tank.

3. 3D model test scale electroosmotic dehydration test

Kaolin clay with an initial water content of 100 % was used as the soil material. Figure 1 summarizes the experimental cross section. Three cases (Case Al-Al_12, Case Al-Al_6, Case Al-Fe_12) were conducted to examine the differences in the cathode material and the difference in the anode surface area. In Case Al-Al_12 and Case Al-Al_6, aluminum was used as the electrode material for both the cathode and anode. In Case Al-Fe, the cathode material was iron and the anode material was aluminum. In Case Al-Al_12, three anodes of φ12 mm were used. In Case Al-Al_6, three anodes of φ6 mm were used in order to evaluate the effect of the anode surface area on the volume of dehydrated water. In all cases, a constant current of 0.4 A was applied for 20 hours. The maximum voltage is 73.5 V.

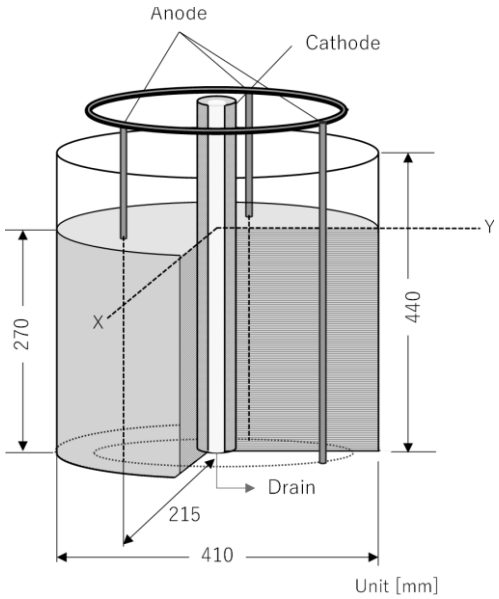

Figure 1. The experimental cross section

Figure 2 shows the results of image analysis performed using images taken with a lateral camera in order to compare the amount of settlement in Case Al-Al_12, Case Al-Al_6 and Case Al-Fe_12. The analysis was performed until the dehydrating clay started to contract laterally and separated from the wall surface. The final ground heights are similar for Case Al-Al_12 and Case Al-Al_6. The shrinkage was occurred faster in Case Al-Al_12 than Case Al-Al_6. The amount of total settlement was the largest in Case Al-Fe_12. The only difference between Case Al-Al_12 and Case Al-Fe_12 is whether the cathode material is aluminum or iron. From the results of potential measurement at the boundary between the cathode and the clay, the larger potential acting on the clay/electrode interface in Case Al-Al_12 than in Case Al-Fe_12. When the potential at the clay/electrode interface increase, the voltage acting in the clay decrease[3]. This caused differences in the final height in these cases.

A comparinson of settelement and the process of crack development on the ground surface shows that when circular cracks grow faster than radial cracks, the time it takes for the clay to peel off from the wall and start shrinking becomes shorter. Conversely, when radial cracks extend faster than circular cracks, the peel off the clay from the cathode rod is significantly delayed.

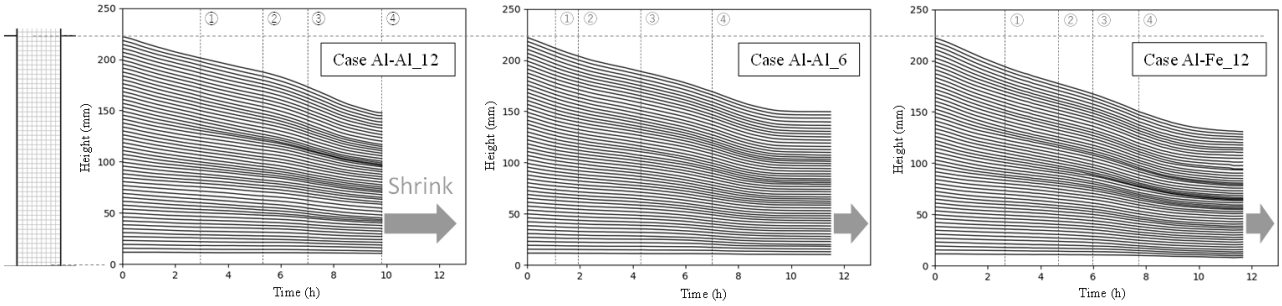

Figure 2. The results of image analysis performed using images taken with a lateral camera in order to compare the amount of settlement in Case Al-Al_12, Case Al-Al_6 and Case Al-Fe_12

4. Conclusion

The 3D model test scale electroosmotic dehydration tests, arranged in a realistic in-situ layout, are performed to study the relationship between soil dehydration, consolidation and surface crack generation. The most important factor for increasing the volume of electroosmotic dehydration is to delay shrinkage, where keeping the clay-electrode contact for a longer time period increases dehydration efficiency. When voltage gradient at the clay/electrode interface increase, the voltage acting in the clay decreased, so electroosmotic dehydration hardly occurs and the volume of dehydration don't increase. Therefore, it is also important to select the optimal electrode material for decreasing voltage loss at the clay/electrode interface.

5. References

[1] Brian, A.C. & Peter, L.B. (1975) Electro-osmosis applied to unstable embankment, *Journal of the Geotechnical engineering division*, Vol.101(8) :733-740.

[2] Chew, S.H., Karunaratne, G.P., Kuma, V.M., Lim, L.H., Toh, M.L., and Hee, A.M. (2004), A field trial for soft clay consolidation using electric vertical drains, *Geotextiles and Geomembranes*, 22(1–2) :17–35.

[3] Zhuang, Y.F. and Wang, Z. (2007) Interface electric resistance of electroosmotic consolidation, *Journal of Geotechnical and Geoenvironmental Engineering*, Vol.133(12) :1483-1640.

Advances in experimental methods

Dialog between experiments and modelling

A micromechanical Rheological Model for Pile-Frozen Soil Interface

F.Sahragard[1], M.Pouragha[1] and M.Rayhani[1]

[1] Carleton University, Department of Civil and Environmental Engineering, Ottawa, Canada

Abstract

The warming climate trends in the cold regions emphasize the critical necessity for evaluating geo-infrastructure systems in these Northern areas. Pile foundations play a pivotal role in supporting structures on frozen soils, leveraging their relatively large bearing capacity and their resistance to frost jacking. In such cold regions, performance of pile foundations is significantly impacted by the behavior of the frozen soil-pile interface. This interaction is intricately influenced by factors such as strain rate, temperature, and stress level. Therefore, any risk assessment demands a comprehensive understanding of how the interaction between the pile and frozen soil evolves with the increasing annual mean temperature.

In this study, soil mechanics and rheological theories are employed to develop an interface model that coherently integrates the influence of crucial factors. By utilizing a mixture theory approach, the overall behavior is modelled through the upscaling of characteristics for each constituent—soil, ice, and water. The interaction between the soil and pile surface is defined as frictional, while the behavior of ice is described by viscoelastic (Maxwell unit) and damage mechanisms. Based on experimental findings [1, 2, 3], it is observed that ice displays a ductile behavior at lower strain rates but undergoes brittle failure under higher strain rates.

A detailed examination of previous experimental results on ice indicate that pressure dependencies are correlated with high strain rates [1, 5]. Moreover, elevating the pressure applied to ice specimens impedes crack propagation, enhances ice strength, and induces a transition in its behavior from brittle to ductile. To account for this pressure effect, a pressure-dependent damage criterion within the elastic component of the Maxwell unit is incorporated. Moreover, following the model developed in [4] a healing mechanism has also been considered that reduces the damage in ice phase over time, which allows for more realistic long-term predictions.

The model predictions are compared to direct shear experiments on steel-frozen soil interface as documented in [6]. These experiments encompass a spectrum of subzero temperatures, strain rates, and pressure levels representative of typical conditions encountered in clod region engineering. Sample experimental results are illustrated in Figure 1. Comparisons with experiments attest to the capability of the developed model in capturing most salient characteristics of frozen soil-pile interface. More interestingly, in-depth comparison with various experimental datasets shed new lights into the nature of pressure dependency of ice and frozen soils.

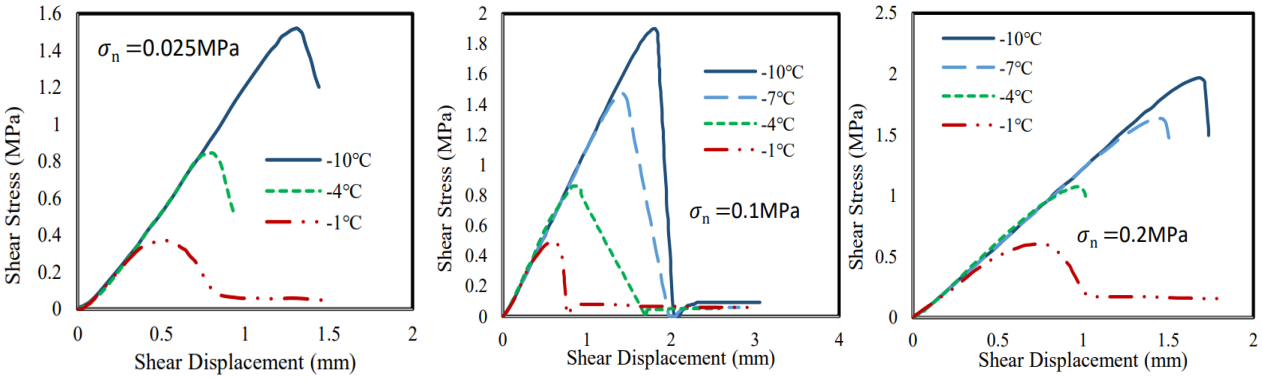

Figure 1. Typical direct shear test results under various temperature and pressure levels [6]

References

[1] Jones, S. J. (1982). The confined compressive strength of polycrystalline ice. Journal of Glaciology, 28(98), 171-178.

[2] Rist, M. A., & Murrell, S. A. F. (1994). Ice triaxial deformation and fracture. Journal of Glaciology, 40(135), 305-318.

[3] Gold, L. W. (1970). Process of failure in ice. Canadian Geotechnical Journal, 7(4), 405-413.

[4] Dansereau, V., Weiss, J., Saramito, P., & Lattes, P. (2016). A Maxwell elasto-brittle rheology for sea ice modelling. The Cryosphere, 10(3), 1339-1359.

[5] Fish, A. M., & Zaretsky, Y. K. (1997). Ice strength as a function of hydrostatic pressure and temperature: CRREL Report 97-6. US Army Corps of Engineers.

[6] Aldaeef, A.A., and Rayhani, M.T. 2021. Pile-soil interface characteristics in ice-poor frozen ground under varying exposure temperature. Cold Regions Science and Technology, 191: 103377. Elsevier.

EFFECT OF BONDED PARTICLE CLUSTERS ON FORCE TRANSMISSION IN GRANULAR ASSEMBLIES

Mohd Ilyas Bhat[1]***, Abrar Naseer***[1] ***and Tejas G. Murthy***[1]
[1] *Indian Institute of Science, Bangalore, India*

It is well documented that small amounts of inter particle cohesion significantly affects the macro-level properties of a frictional granular material and alters its kinetics - i.e. force transmission and ensemble kinematics[1, 2]. We employ a suite of experiments and simulations to study the micromechanics of granular ensembles containing bonded particle clusters. Bonded particle clusters are groups of granular particles connected by cohesive bonds[3]. Due to their morphology and imposition of kinematic constraints, bonded particle clusters enhance the strength of granular ensembles and affect their micromechanical behaviour.

Although experimental observations on weakly cemented granular materials have highlighted the macro-level signatures of bonded particle clusters in granular materials, experimental investigation of their micromechanical effects has not been explored. In this study, we employ the photo-elasticity technique to study the particle level force transmission in granular assemblies containing bonded particle clusters. Furthermore, we use our experimental data to calibrate a discrete element model and perform simulations to further explore the micromechanical behaviour of bonded particle clusters at particle level.

Our sample comprises bi-disperse 2D photo-elastic disks of radii 11mm and 15.4mm, which rest on a frictionless base and are sheared. By employing the photo-elastic technique, we evaluate the contact forces for each particle by recording the intensity field. An inverse problem is solved[4]where error between experimental and constructed image is minimised, force vector being the optimised parameter. In the second stage, small amount of cohesive bonds are introduced between randomly selected particle pairs(see Figure 1a), while preserving the contact fabric. These assemblies are loaded under bi-axial compression and their force distributions are evaluated and contrasted(See Figure 1b).

A 2D DEM model of the same scale as the experiments is calibrated from the experimental stress-strain and contact force data. Bi-axial loading simulations are performed on various ensembles generated with varying sizes and morphology of the bonded particle clusters. The evolution of various micromechanical parameters, such as force chains, contact fabric tensor, particle rotations, coordination number is evaluated to elucidate the effects of bonded particle clusters.

As the particle ensemble undergoes compression, the average contact forces in bonded particle clusters increase steadily. The proportion of dominant force chains passing through bonded particle clusters increases at higher strain levels(see Figure 1b).

References

[1] Clough, G. W., Sitar, N., Bachus, R. C., and Rad, N. S. (1981). Cemented sands under static loading. *Journal of the Geotechnical Engineering Division*, **107**, 799–817.

[2] Wu, H., Wu, W., Liang, W., Dai, F., Liu, H., and Xiao, Y. (2023). 3d dem modeling of biocemented sand with fines as cementing agents. *International Journal for Numerical and Analytical Methods in Geomechanics*, **47**, 212–240.

[3] Shen, Z., Gao, F., Wang, Z., and Jiang, M. (2019). Evolution of mesoscale bonded particle clusters in cemented granular material. *Acta Geotechnica*, **14**, 1653–1667.

[4] Majmudar, T. S. and Behringer, R. P. (2005). Contact force measurements and stress-induced anisotropy in granular materials. *nature*, **435**, 1079–1082.

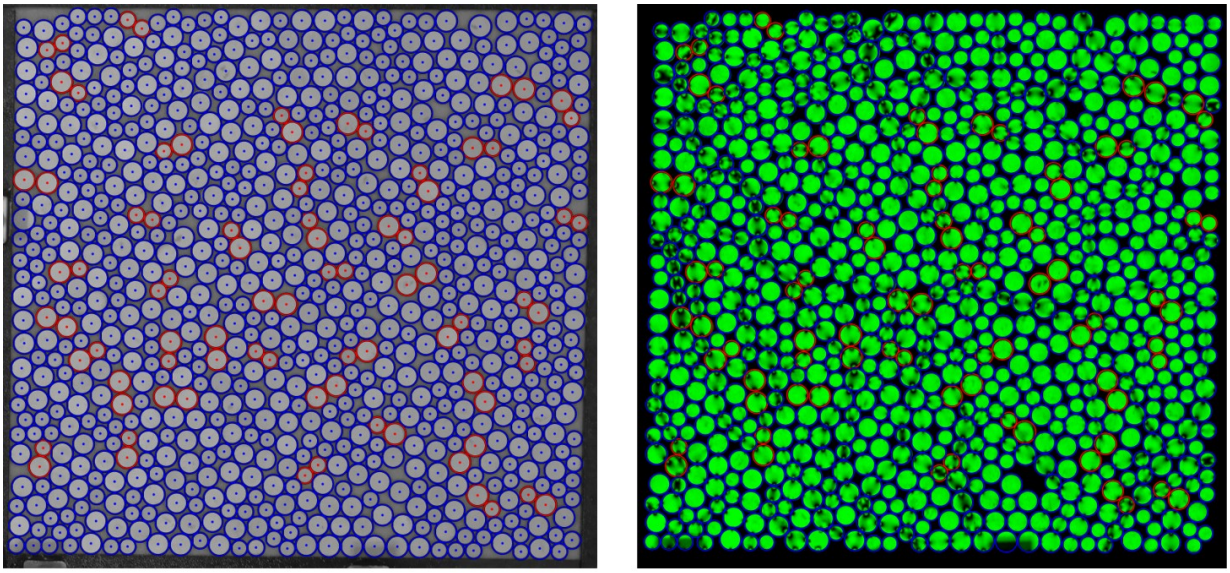

Figure 1. (a) Photo of bi-disperse photo-elastic disk assembly with bonded particle pairs. The unbonded disks and bonded disk pairs are highlighted by blue and red color circumferences respectively.(b) Fringe pattern in biaxially loaded disk assembly containing bonded disk pairs.The unbonded disks and bonded disk pairs are highlighted by blue and red color circumferences respectively. The dark-band(fringe) formation in the intensity pattern highlights the force chain propagation in the ensemble.

ESTIMATION OF SOIL WATER RETENTION CURVE BASED ON PORE FREEZING KINETICS

A. Macias[1], J. Vaunat[1] and L. Gonzalez[2]
[1]Department of Civil and Environmental Engineering, Technical University of Catalonia (UPC), Barcelona, Spain
[2]International Center for Numerical Methods in Engineering, Technical University of Catalonia (UPC), Barcelona

1. Abstract

The effect of pore radius can be observed though different processes that happen in geological media, taking a fundamental role during inter-pore ice formation and soil freezing. This can be expressed by the freezing characteristic function that relates chemical potential equilibrium and soil pore size distribution through the use of the water retention curve and the equilibrium temperature. By the analysis of temperature time evolution obtained for an undrained laboratory freezing test, and a Finite Element thermo – hydraulic model calibration, the estimation of the soil water retention curve was performed. A comparison between laboratory and the best fitted results were made and an acceptable agreement was observed between the estimated SWRC and the measured one, supporting the hypothesis of SWRC prediction through a relatively simple and rapid test.

2. Freezing process in porous media and SWRC effect

In general, free water experiences liquid-to-solid phase change when temperature reaches the freezing point at a specific pressure and the chemical potential of ice and liquid water become equilibrated. In case of pore water, due to the presence of grain/water interfaces and the rise in the chemical potential to equilibrate, water freezing point depression is observed as smaller pores tend to freeze with minor temperatures than the larger ones. This phenomenon is illustrated in Figure 1.a that shows different time evolution during freezing of soils of different nature (clay, silt and sand). This result is exploited in this paper to estimate the pore size distribution and thus the retention curve of the material from temperature measurements taken during a simple constant volume freezing test.

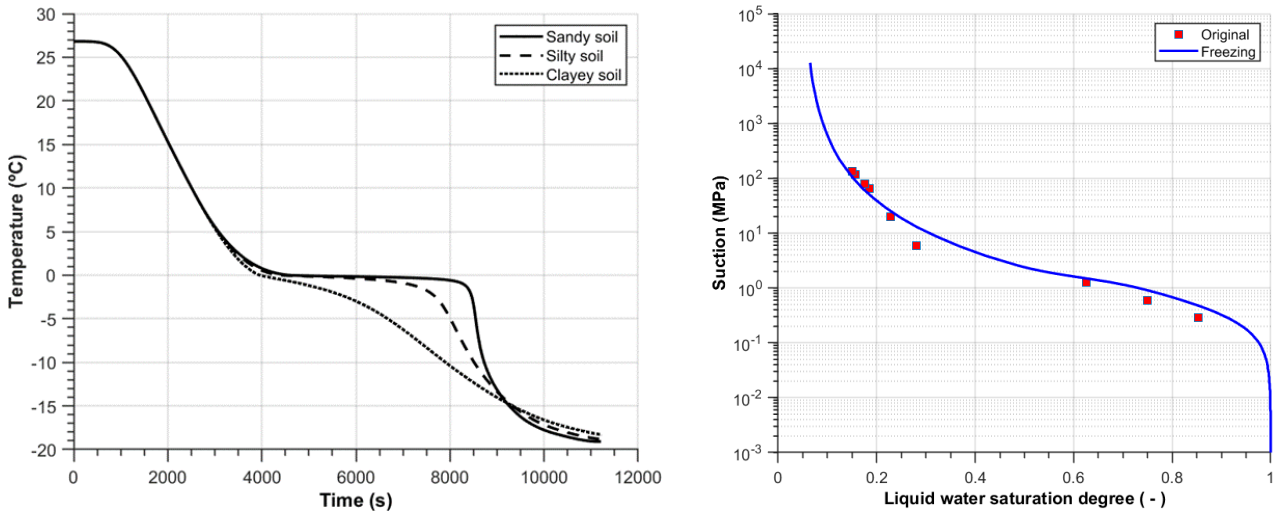

Figure 1 SWRC effect on freezing process. a) Temperature time evolution for different soil types. b) Calibrated SWRC and laboratory test comparison.

From a theoretical point of view, pore radius can be formally related to the difference in chemical potential prevailing between the solid (ice) and liquid water phase through the Young-Laplace equation. Under the assumption of the reach of equilibrium between the two phases, the difference in chemical potential is related to the temperature through the Clausius – Clapeyron equation. The combination of the two equations leads to Equation (1), which expressed the temperature *T* required to freeze water in a pore of radius *R* for a given liquid pressure P_L (Nishimura et al., 2009).

$$R = \frac{2\sigma_{T_{\alpha L}}}{1 - \left(1 - \frac{\rho_i}{\rho_l}\right) P_l - \rho_i L ln\left(\frac{T}{273.15}\right)} \quad (1)$$

ρ_i is the ice density and $\sigma_{T_{\alpha L}}$ is the water surface tension between solid and liquid phases. On the other hand, the balance of energy within the sample allows to back-analyze the amount of energy used in the latent heat of phase changes and thus the amount of liquid water that freezes at the current time. This provides a relationship between pore radius and pore volume at any time of the experiment.

The procedure of estimation of the retention curve is based on the back-analysis of the time evolution of temperature at the center of a saturated soil sample under a prescribed temperature evolution at the lateral boundaries. In a first time, the back-analysis has been carried out using a thermo-hydraulic Finite Element model considering a priori expressions for the retention curve. Figure 1.b shows a comparison of the retention curve back-analyzed by the model (blue curve) and the one obtained experimentally (red dots), using an expression for the RC based on the proposal by Casini et al. (2012) for double-structure materials:

$$S_l = 1 - S_i = (1 - w)\left[\frac{1}{1 + \left(\frac{S_{cr}}{P_M}\right)^{\frac{1}{1-M}}}\right]^M + w\left[\frac{1}{1 + \left(\frac{S_{cr}}{P_m}\right)^{\frac{1}{1-m}}}\right]^m \quad (2)$$

where P_M and *M* are the parameters proposed by van Genuchten (1980) for single structure material and applied here to soil macrostructure. P_m and *m* are the van Genuchten's parameters applied to the retention characteristics of the microstructure. w is a weighting factor to combine the micro- and macro- retention curves into the retention curve of the whole material.

The method is further extended to provide a step-by-step determination of the retention curve without defining a priori expression of the retention curve. It based on the development of an analytical solution for the equation of energy balance considering the geometry and boundary conditions of the test. Agreement between experimental and computed retentions curve for different soils is excellent and validates the considered approach that links in a simple way microstructure patterns like the Pore Size Distribution to macroscopic variable like the temperature.

3. References

[1] Casini, F., Vaunat, J., Romero, E., & Desideri, A. (2012). Consequences on water retention properties of double-porosity features in a compacted silt. Acta Geotechnica, 7, 139-150.

[2] Nishimura, S., Gens, A., Olivella, S., & Jardine, R. J. (2009). THM-coupled finite element analysis of frozen soil: formulation and application. *Géotechnique*, *59*(3), 159-171.

[3] van Genuchten, M. T. T. (1980). A closed-form equation for predicting the hydraulic conductivity of unsaturated soils. Soil Science Society of America Journal, 44(5):892.

EXPERIMENTAL AND NUMERICAL ANALYSIS OF INTERFACE BEHAVIOUR BETWEEN SAND AND CORRUGATED SURFACE

M. Nitka[1] and A. Grabowski[1]

[1] Gdańsk University of Technology, Civil and Environmental Engineering, Gdańsk, Poland

1. General

The paper deals with laboratory and numerical investigations focusing on the interaction between sand and a sinusoidal corrugated surface within a direct shear apparatus under a constant normal load. Bulk solid-structure interfaces are prevalent in various engineering constructions such as foundations, geotextiles, tunnels, and silos. These interfaces constitute a critical element in ensuring the safety of engineering systems. Key characteristics of these shear zones, including their location and thickness, play a significant role in assessing shear resistance. Understanding and characterizing these aspects are crucial for ensuring engineering systems' overall stability and reliability [1,2].

First, employing 3D printing technology, a custom-built direct shear box was created, featuring various corrugated surface topographies. Digital Image Correlation (DIC) was employed to analyse a series of interface shearing experiments involving different sinusoidal corrugated surfaces. Next, the 3D DEM model was proposed to study micro phenomena in granular material. The calculations were performed with open-source YADE code [3]. The focus was on the shear zone's shape, position and width. The micro-behaviour of the shear zone was scrutinized, revealing that an increase in the corrugation coefficient (d/l) leads to heightened forces exerted on the surface and volumetric changes.

For smooth surfaces, direct sliding of the material was observed. Conversely, rough surfaces exhibited the shear plane above the corrugation valleys, within the material, and at the corrugation peaks. This research offers unique insights into the micro-behaviour of the interface between granular material and a sinusoidal corrugated surface.

2. Experimental setup

The direct shear apparatus is a commonly employed tool in geotechnical research for assessing the frictional properties of granular materials [4,5,6]. The Matest Shearlab S276 digital shear testing machine was utilized in our research. We modified the equipment to facilitate photographic documentation, enabling Digital Image Correlation (DIC) analysis of the shearing behaviour. The side walls of the apparatus, aligned with the shear direction, were rendered transparent using 8 mm thick Perspex. This modification enabled us to capture detailed images of deformations in the contact zone between the granular material and the surface throughout the shear tests. The remaining components of the bottom and top loading frames were customized using 3D printing technology and constructed with PLA thermoplastic material. This adaptation of the shear apparatus ensures precise and detailed analysis of the granular material's behaviour during shearing while preserving the integrity of the experimental setup.

In this paper, we investigated the influence of six different surfaces. One of them was entirely flat and smooth, while the others were designed based on the geometry of silo wall corrugations. The sinusoidal corrugations shared the same wavelength (l = 15 mm), but they varied in depth (distance between the crests), denoted as d (see Figure 1). The depth was systematically altered from 0.8 mm to 6.4 mm, with an increment of 1.4 mm.

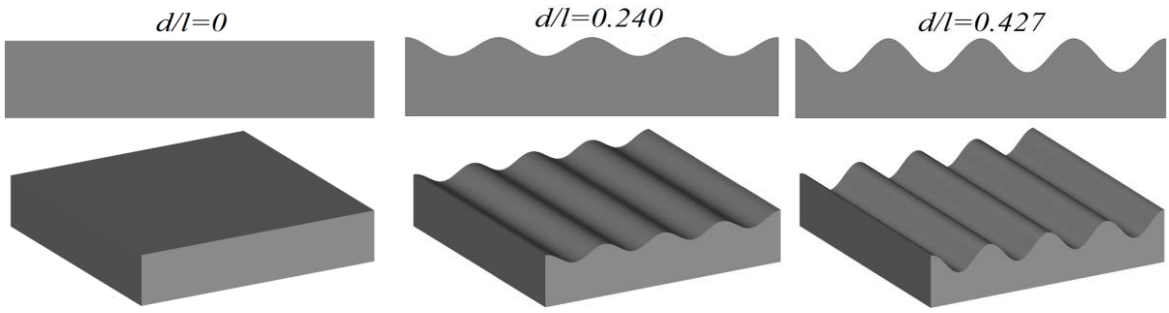

Figure 1. Exemplary cross-sections (3D STL models) of sinusoidal corrugated surfaces used in Experiments with different corrugation coefficients (*d/l*).

3. Results

The results obtained from numerical analysis were compared to laboratory one, both on micro and macro levels. The mobilized shear strain and volumetric strain curves were found in good agreement. However, the main focus was laid on microstructure. The horizontal and vertical displacement as well as horizontal, vertical and shear strains were also compared (e.g. see Figure 2).

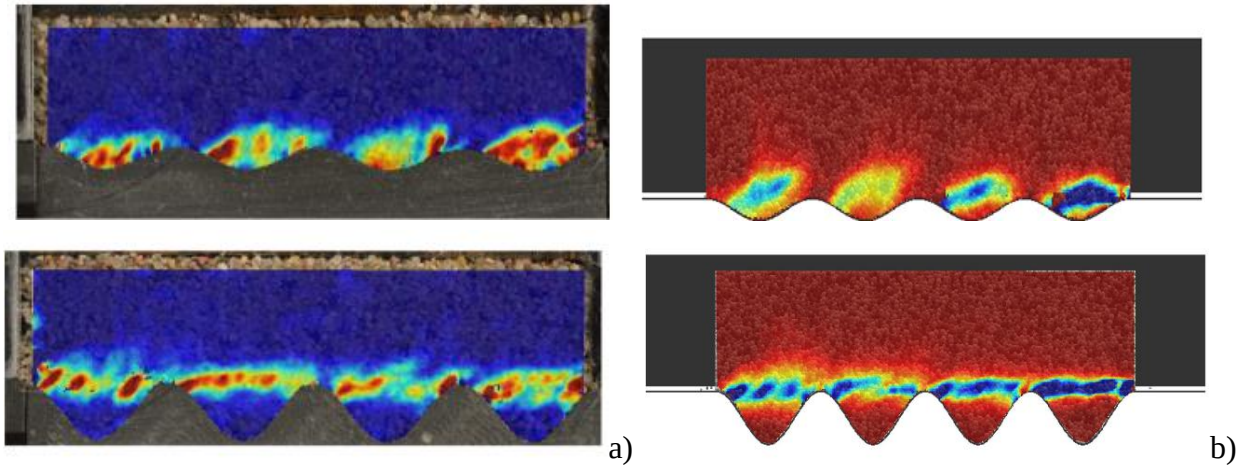

a) b)

Figure 2. Exemplary cross-sections (3D STL models) of sinusoidal corrugated surfaces used in a) experiments and b) 3D DEM model with different corrugation coefficients (*d/l*).

4. References

[1] Hu, L. & Pu, J. (2004) Testing and modeling of soil-structure interface. *Journal of Geotechnical and Geoenvironmental Engineering*, **130**(8):851–860.

[2] Su, L.J., Zhou, W.H., Chen, W.B. et al (2018) Effects of relative roughness and mean particle size on the shear strength of sand-steel interface. *Measurement*, **122**:339–19346.

[3] Kozicki, J. & Donze F.V. (2008) A new open-source software developer for numerical simulations using discrete modeling methods. *Computer Methods in Applied Mechanics and Engineering*, **197**:4429-4443.

[4] DeJong, J.T., Randolph, M.F. & White, D.J. (2003) Interface load transfer degradation during cyclic loading: A microscale investigation. *Soils and Foundations* **43**(4):81–293.

[5] Potyondy, J.G. (1961) Skin friction between various soils and construction materials. *Géotechnique* **11**(4):339–353.

[6] Zhao, C., Zhang, R., Zhao, C., et al (2019) A three-dimensional evaluation of interfacshear behavior between granular material and rough surface. *Journal of Testing and Evaluation* **49**(2):20180749.

Experimental study of the soil structure variable z used in constitutive models such as Neohypoplasticity or Sanisand

***L. Mugele*[1], *J. Zürn*[1], *A. Niemunis*[1] *and H.H. Stutz*[1]**
[1] *Institute of Soil Mechanics and Rock Mechanics, IBF, Karlsruhe Institute of Technology, KIT, Karlsruhe, Germany*

From a macroscopic point of view, the mechanical behavior of soil can be described using constitutive models with different state variables. Widely used state variables in soil mechanics are the effective stress σ_{ij} and the void ratio e. Using these, the experimentally observed soil behavior (for example, pycnotropy, barotropy, and critical state concept) can already be represented well. However, despite the same σ_{ij} and e, samples prepared using different preparation methods show different results, e.g. in monotonic undrained tests [1, 2, 3]. This reveals that additional state variables accounting for the state of the soil structure (also called fabric) should be incorporated. Several constitutive models already consider such a variable, e.g. Sanisand model [4] or the hypoplastic model after [5]. However, the constitutive description of a structure or fabric variable and its evolution equation is still not sufficiently understood because structure variables cannot be subjected to direct measurements (at least not easily). For example, in the novel neohypoplastic model [6, 7, 8], the included structure variable z_{ij} is a conjecture that needs to be verified experimentally, improved or refuted.

To clarify the underlying assumptions, the present work therefore investigates the influence of cyclic undrained preloading on a subsequent monotonic undrained triaxial compression test considering differently prepared samples. The results are compared with test without cyclic preloading. According to the hypoplastic evolution equation of the tensorial structure variable z_{ij} in Neohypoplasticity [6, 7, 8] cyclic preloading should affect the monotonic loading.

The triaxial tests are conducted using Karlsruhe Fine Sand (KFS), which is a well-known quartz sand from the literature [1]. Loose samples ($I_{D0} \approx 0.3$) with an effective isotropic initial pressure of $p_0 = 300$ kPa are considered in each test. This means that the state variables stress and void ratio are equal in all tests. Two monotonic undrained tests, which are prepared using air pluviation (AP) or moist tamping (MT) [1] serve as references. The experiments without a cyclic preloading [1] reveal the well-known dependence of contractive soil behavior on the sample preparation method, see Figure 1, which motivates the consideration of an already discussed structure variable.

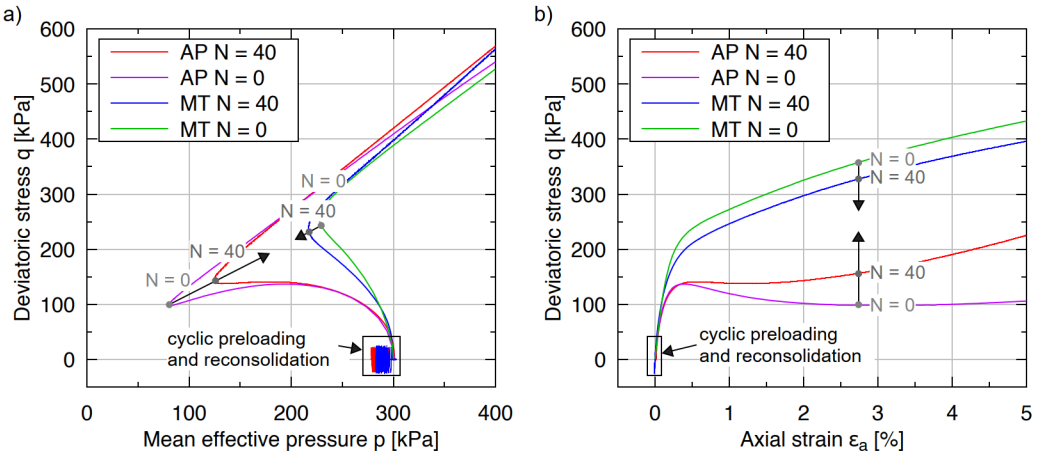

Figure 1. Undrained monotonic triaxial compression tests without and with cyclic preloading

In the presented experiments, an undrained cyclic preloading with 40 small stress cycles and a reconsolidation phase are applied before the subsequent monotonic undrained compression. In the tests with a cyclic preloading phase, the applied undrained stress cycles only lead to small strain cycles and negligible void ratio changes in the reconsolidation phase. The stress state and the void ratio are comparable at the beginning of the monotonic triaxial compression in all tests. It can be observed, that the influence of the sample preparation method reduces due to the preloading cycles. Especially the pronounced contractive behaviour of the air pluviated samples is reduced.

From the above-mentioned experiments and the literature [1, 2, 3], five qualitative requirements can be derived for a constitutive consideration of the structure effects in terms of the neohypoplastic model [6, 7, 8]. The structure variable z_{ij} should (1) only change due to shear deformations and be therefore a tensorial quantity, (2) be initialized differently for different sample preparation methods, (3) lead to a change in the contractive soil behavior, (4) reduces the initial value due to a cyclic loading with small strains, and (5) approach an asymptotic value due to a monotonic shearing to be consistent with the critical state concept.

In Neohypoplasticity, [6, 7, 8] an additional contractancy term is introduced in the stress rate - strain rate equation

$$\dot{\boldsymbol{\sigma}} = k\overline{\mathsf{E}} : \left(\dot{\boldsymbol{\varepsilon}} - \boldsymbol{m}Y\|\dot{\boldsymbol{\varepsilon}}\| - \omega \boldsymbol{m}^{z}\langle -\boldsymbol{z} : \dot{\boldsymbol{\varepsilon}}\rangle - \boldsymbol{m}^{d}Y_{d}\|\dot{\boldsymbol{\varepsilon}}\|\right) \tag{1}$$

to consider the effect of the soil structure. Thereby, the current structure of the soil is quantified using the tensorial state variable z_{ij} with the evolution equation

$$\dot{\boldsymbol{z}} = A_z \left(\dot{\boldsymbol{\varepsilon}}^{**} - \vec{\boldsymbol{z}} \left(\frac{\|\boldsymbol{z}\|}{z_{\max}}\right)^{\beta_z} \|\dot{\boldsymbol{\varepsilon}}^{**}\|\right) \left(\alpha_z + \left(\frac{\|\boldsymbol{z}\|}{z_{\max}}\right)^{n_z}\right) \tag{2}$$

whereby only a deviatoric strain rate $\dot{\boldsymbol{\varepsilon}}^{**} \propto \dot{\boldsymbol{\varepsilon}}^{*}$ is considered. As it can be seen from Equation (1-2), the above formulated requirements are qualitatively fulfilled in Neohypoplasticity. However, quantitative parameter calibration is an upcoming challenging task.

To summarize, this work describes experiments on the meso-scale aimed to detect and to investigate micromechanical processes which may affect the macromecanical material response due to both monotonic and cyclic loading.

References

[1] Wichtmann, T. (2016). *Soil behaviour under cyclic loading - experimental observations, constitutive description and applications*. Habilitation, Karlsruher Institut für Technologie, Karlsruhe.

[2] Miura, S. and Toki, S. (1982). A sample preparation method and its effect on static and cyclic deformation-strength properties of sand. *Soils and Foundations*, **22**, 61–77.

[3] Yang, Z. X., Li, X. S., and Yang, J. (2008). Quantifying and modelling fabric anisotropy of granular soils. *Géotechnique*, **58**, 237–248.

[4] Dafalias, Y. F. and Manzari, M. T. (2004). Simple plasticity sand model accounting for fabric change effects. *Journal of Engineering Mechanics*, **130**, 622–634.

[5] Liao, D. and Yang, Z. X. (2021). Hypoplastic modeling of anisotropic sand behavior accounting for fabric evolution under monotonic and cyclic loading. *Acta Geotechnica*, **16**, 2003–2029.

[6] Mugele, L., Niemunis, A., and Stutz, H. H. (2023). Neohypoplasticity revisited. *International Journal for Numerical and Analytical Methods in Geomechanics*.

[7] Niemunis, A., Grandas Tavera, C. E., and Wichtmann, T. (2016). Peak stress obliquity in drained and undrained sands. simulations with neohypoplasticity. *Holistic Simulation of Geotechnical Installation Processes*, pp. 85–114, Springer, Cham.

[8] Niemunis, A. and Grandas Tavera, C. E. (2019). Essential concepts of neohypoplasticity. Wu, W. (ed.), *Desiderata Geotechnica*, pp. 132–142, Springer eBooks Engineering, Springer.

Fundamental study on the relationship between the apex and internal immobile area during sand heap formation

S. Kajiyama[1] and Y. Nakata[2]

[1] University of Yamanashi, Graduate Faculty of Interdisciplinary Research, Kofu, Japan

[2] Yamaguchi University, Graduate School of Sciences and Technology for Innovation, Ube, Japan

1. Introduction

The authors performed an experiment on the angle of repose as a benchmark for simulations on the angle of repose in order to verify and validate the results of the discrete element method (hereafter referred to as DEM) analysis [1]. The results were compared by taking X-ray images before and after the sand heap was formed, and it was confirmed that there were areas in the sand heap where the particles had hardly moved before the start of the experiment (immobile areas). It was also found that the horizontal position of the highest particle in the immobile area (hereafter referred to as the apex of the immobile area) and the apex of the sand heap differed in the horizontal direction. It is widely known that the internal structure of sand influences its mechanical behaviour. Therefore, in this study, a DEM simulation of the angle of repose was performed based on this experiment [1], and a fundamental study on the relationship between the apex of the sand heap and the apex of the immobile area was conducted.

2. Analysis conditions and methods

The particles used in the analysis were determined based on those used in the experiments [1]. However, the shape of the particles was assumed to be spherical considering the computational cost. The specimen was box-shaped, as shown in Figure 1. The analysis was performed by lowering the sidewalls on both sides of the specimen, as shown in Figure 1, at a specified speed to allow the particles to flow. The lowering velocities of the sidewalls were 0.03 m/s and 0.0005 m/s. In this study, particles with a displacement of less than 0.001 m from the initial state in the x, y, and z directions were defined as immobile particles, with the centre position of the highest particle in the z direction among the immobile particles as the apex of the immobile area and the centre position of the highest particle in the entire sand heap as the apex.

3. Relationship between the apex of the immobile area and the apex

The results are shown for a lowering velocity of 0.0005 m/s. Figure 2 shows the relationship between the movement of the apex and the apex of the immobile area from the centre of the specimen in the x direction (Δl m) divided by the particle diameter (D = 0.01 m) and the number of steps. The figure shows that both the x coordinate of the apex of the immobile area (hereafter referred to as IN_X) and the x coordinate of the apex (hereafter referred to as EX_X) oscillate between positive and negative values during sand heap formation.

To explain the relationship between the apex of the immobile area and the apex, a Granger causality test and an impulse response were performed in this study. The Granger causality tests showed Granger causality from IN_X to EX_X, but there was no Granger causality from EX_X to IN_X. Figure 3 shows the orthogonal impulse responses for IN_X and EX_X. Note that the figure includes part of the results of the orthogonal impulse response for reasons of space limitations. From the figure, it is clear that the shock of one standard deviation in IN_X is approximately 0.5, whereas

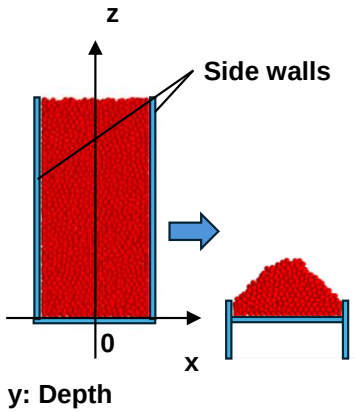

Figure 1. Simulation overview

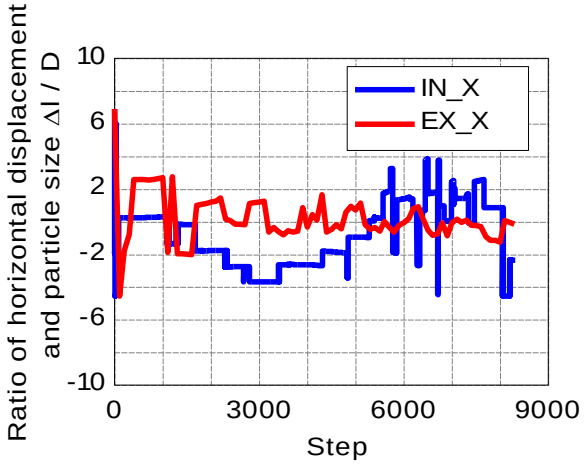

Figure 2. Relationship between particle movement and number of steps

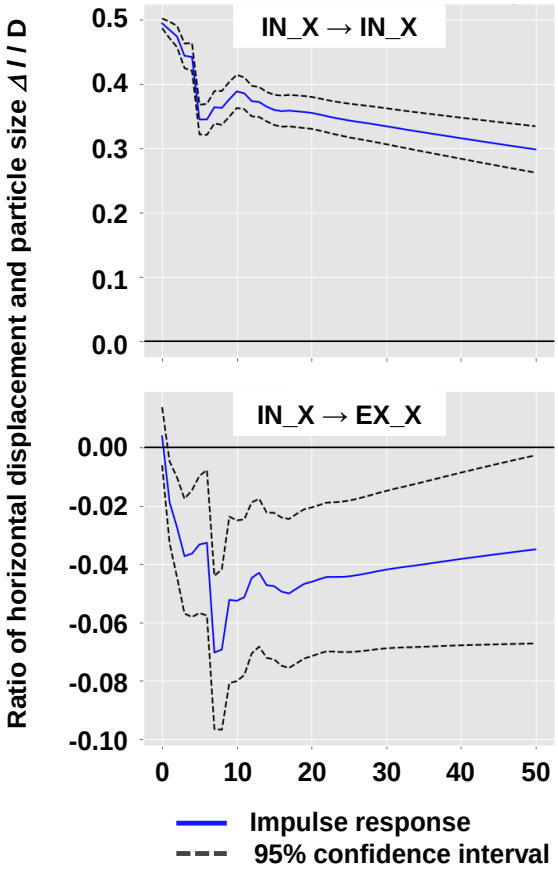

Figure 3. Results for IN_X and EX_X impulse response functions.

the impact on EX_X is approximately -0.07 after seven steps. In contrast, Granger causality was observed for both IN_X and EX_X for sidewalls, lowering the velocity by 0.03 m/s. These results suggest the possibility of causality between the apex and the apex of the immobile area. It was also shown that causality may depend on the sidewall descent velocity (i.e., the particle flow velocity).

4. Summary

The results of the Granger causality test suggest a causal relationship between the apex and the apex of the immobile area. Causality was shown to depend on the velocity of the sidewalls (particle flow velocity). However, Granger causality, by definition, indicates a temporally related relationship and not necessarily a true causal relationship. Therefore, further detailed investigations are required in the future.

5. References

[1] Nakata, Y., Moriguchi, S., Kajiyama, S., Kido, R., Kikkawa, N., Saomoto, H., Takano, D. & Higo, Y., Experimental data of 3D printed granular material for verification of discrete element modeling simulation, Soils and Foundations, Vol. 62, Issue 4, 101178, 2022

INSPECTION OF MINER'S RULE ON COARSE AND FINE-GRAINED SOILS UNDER ONE-DIMENSIONAL CONDITIONS: EXPERIMENTAL EVIDENCE AND NUMERICAL MODELLING

R. Polo-Mendoza[1] , D. Mašín[1] , J. Duque[1,2] , J. Najser[1]

[1] Charles University, Faculty of Science, Prague, Czech Republic

[2] Universidad de la Costa, Department of Civil & Environmental Engineering, Barranquilla, Colombia

Abstract

In 1945, based on experimental evidence from an aluminium alloy, Miner's rule was proposed for the first time [1]; this hypothesis states that the useful fatigue life used by repeated stress cycles at a specific stress is proportional to total cycles in the fatigue life [1]. In soil mechanics, Miner's rule can be interpreted as the hypothesis that the sequence of the load cycle packages does not affect the final strain accumulation [2], [3]. The preceding assumption allows sequentially grouping and treating irregular cyclic loads in bundles of cycles with constant amplitudes [4]. Accordingly, it simplifies the stochastic nature of the different types of loads that affect soils. Thus, it is possible to facilitate several geotechnical analysis and design. Nevertheless, Miner's rule has not yet been verified under one-dimensional (1D) conditions. The above denotes an essential gap in the state-of-the-art because the 1D condition is the most suitable approach to analyse different geotechnical problems, such as the settlement analysis of shallow foundations.

Consequently, this research studies the compliance of Miner's rule on coarse and fine-grained soils under 1D conditions through an experimental protocol combined with numerical modelling. This investigation employed Zbraslav Sand (ZS) and Malaysian Kaolin (MK) to represent typical coarse and fine-grained soils, respectively. **Table 1** shows the laboratory plan applied for both soils, i.e., stress-controlled oedometric tests following six different loading sequences. Also, advanced hypoplastic models enhanced with Intergranular Strain Improvement (ISI) were applied to inspect their capability to replicate the experimental tests. Specifically, it was employed the model for coarse-grained soils by *von Wolffersdorff* [5] and the model for fine-grained soils by *Mašín* [6], both enhanced with the ISI version by *Duque et al.* [7]. The findings from this investigation are exhibited in **Figures 1-2**. Firstly, **Figure 1** indicates that experimentally, the studied soils meet Miner's rule under 1D conditions. Meanwhile, **Figure 2** suggests that the adopted constitute models can reproduce Miner's rule for particular sets of material parameters, i.e., simulations with χ as a constant ($\chi_0 = \chi_{max}$). Accordingly, this study concludes that implementing Miner's rule for geotechnical analysis and design is a realistic and valid assumption, at least for soils under 1D conditions.

Soil sample	Test name	Loading sequence, σ_1 [kPa]		
ZS	OED1	200-100 (x10)	400-100 (x10)	800-100 (x10)
	OED2	200-100 (x10)	800-100 (x10)	400-100 (x10)
	OED3	400-100 (x10)	200-100 (x10)	800-100 (x10)
	OED4	400-100 (x10)	800-100 (x10)	200-100 (x10)
	OED5	800-100 (x10)	200-100 (x10)	400-100 (x10)
	OED6	800-100 (x10)	400-100 (x10)	200-100 (x10)
MK	OED7	200-100 (x10)	400-100 (x10)	800-100 (x10)
	OED8	200-100 (x10)	800-100 (x10)	400-100 (x10)
	OED9	400-100 (x10)	200-100 (x10)	800-100 (x10)
	OED10	400-100 (x10)	800-100 (x10)	200-100 (x10)
	OED11	800-100 (x10)	200-100 (x10)	400-100 (x10)
	OED12	800-100 (x10)	400-100 (x10)	200-100 (x10)

Table 1. Cyclic loading sequence employed for this study.

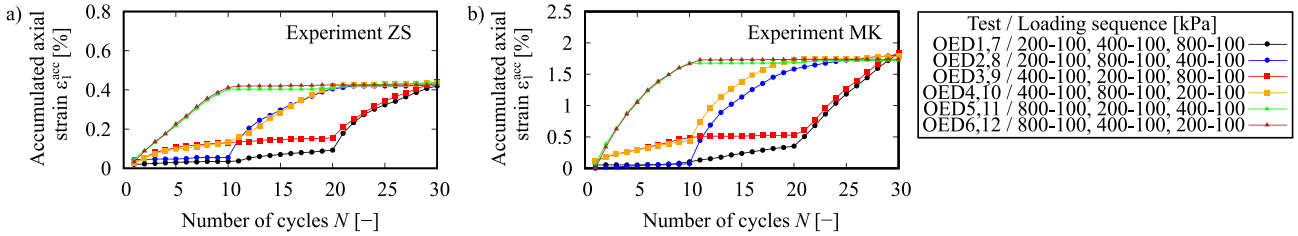

Figure 1. Laboratory results on accumulated axial strains.

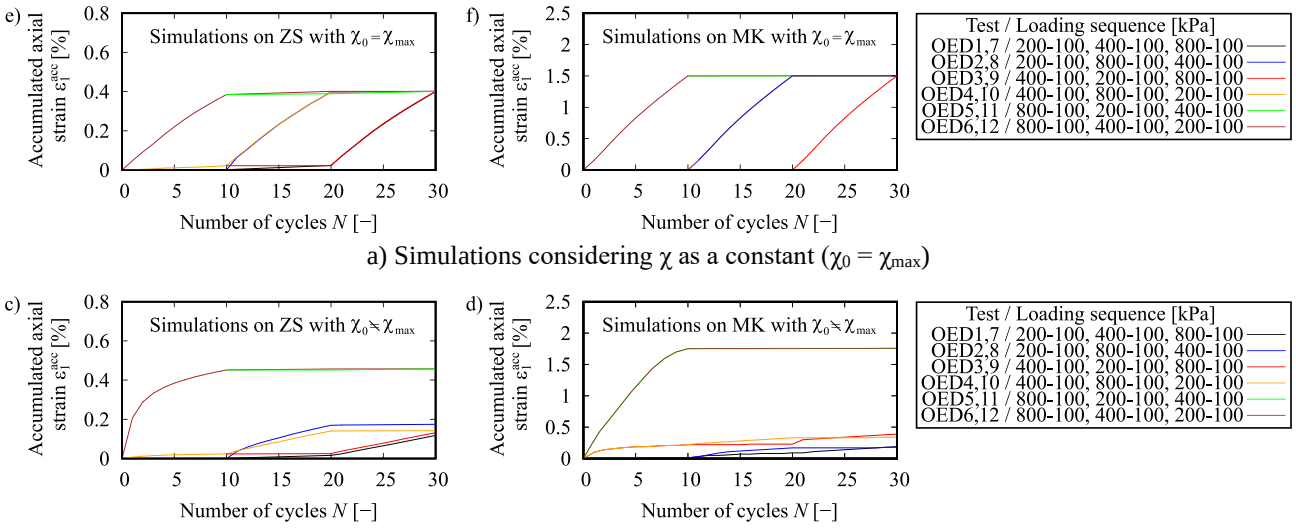

a) Simulations considering χ as a constant ($\chi_0 = \chi_{max}$)

b) Simulations considering χ as a variable ($\chi_0 \neq \chi_{max}$)

Figure 2. Numerical modelling results on accumulated axial strains.

References

[1] M. A. Miner, "Cumulative Damage in Fatigue," *J. Appl. Mech.*, vol. 12, no. 3, pp. A159–A164, 1945, doi: 10.1115/1.4009458.

[2] M. Tafili, J. Duque, M. Ochmański, D. Mašín, and T. Wichtmann, "Numerical inspection of Miner's rule and drained cyclic preloading effects on fine-grained soils," *Comput. Geotech.*, vol. 156, no. 105310, pp. 1–15, 2023, doi: 10.1016/j.compgeo.2023.105310.

[3] J. Duque, J. Roháč, D. Mašín, and J. Najser, "Experimental investigation on Malaysian kaolin under monotonic and cyclic loading: inspection of undrained Miner's rule and drained cyclic preloading," *Acta Geotech.*, vol. 17, no. 11, pp. 4953–4975, 2022, doi: 10.1007/s11440-022-01643-0.

[4] T. Wichtmann, A. Niemunis, and T. Triantafyllidis, "Strain accumulation in sand due to drained cyclic loading: On the effect of monotonic and cyclic preloading (Miner's rule)," *Soil Dyn. Earthq. Eng.*, vol. 30, no. 8, pp. 736–745, 2010, doi: 10.1016/j.soildyn.2010.03.004.

[5] P.-A. von Wolffersdorff, "A hypoplastic relation for granular materials with a predefined limit state surface," *Mech. Cohesive-Frictional Mater.*, vol. 1, no. 3, pp. 251–271, 1996, doi: 10.1002/(SICI)1099-1484(199607)1:3<251::AID-CFM13>3.0.CO;2-3.

[6] D. Mašín, "Clay hypoplasticity model including stiffness anisotropy," *Geotechnique*, vol. 64, no. 3, pp. 232–238, 2014, doi: 10.1680/geot.13.P.065.

[7] J. Duque, D. Mašín, and W. Fuentes, "Improvement to the intergranular strain model for larger numbers of repetitive cycles," *Acta Geotech.*, vol. 15, no. 12, pp. 3593–3604, 2020, doi: 10.1007/s11440-020-01073-w.

INTEGRATED ANALYSIS OF MINERALOGICAL AND TEXTURAL FACTORS ON STRESS-INDUCED FRACTAL ROCK DAMAGE: A MULTISCALE ANALYSIS

Ö. Dinç Göğüş[1], E. Avşar[2], K. Develi and A. Çalık[3]

[1] Istanbul Technical University, Fac. of Mines, Istanbul, Turkey
[2] Konya Technical University, Fac. of Engineering and Natural Sciences, Konya, Turkey
[3] Çanakkale Onsekiz Mart University, Fac. of Engineering, Çanakkale, Turkey

The construction of engineering structures within rocks exposes these materials to secondary stresses, leading to consequential deformation and potentially irreversible damage. Over a century, researchers have focused on unraveling the microscale deformations that initiate subsequent mesoscale and macroscale rock damage (e.g. Griffith 1921; Bieniawski 1967; Tapponnier and Brace 1976; Horii and Nemat-Nasser 1986; Martin and Chandler 1994; Eberhardt et al. 1998; Renard et al. 2009; Dinç Göğüş and Avşar 2022, etc.). While these investigations denote evolving interest, underscoring the concerted effort to elucidate fundamental mechanisms governing rock deformation, acquiring quantitative insights remains imperative for advancing our comprehension of rock damage mechanisms within the context of engineering applications.

In this research, we aim to quantitatively investigate the roles of textural properties, and mineralogical composition on micro and mesoscale mechanical rock behaviors by combining different methodologies such as laboratory experiments, discrete element modeling, mineralogical examinations, and fractal analysis (Figure 1). For this purpose, we focused on the initiation and propagation of cracks spanning from microscale to mesoscale in different rock types, diabase, ignimbrite, and marble. Firstly, the key macro mechanical parameters such as uniaxial compressive strength (UCS), tensile strength (UTS), elasticity modulus (E), and Poisson's ratio (ν) were determined through laboratory experiments (Figure 1a). Secondly, discrete element methodology (DEM) was employed to generate numerical models representing the stress-strain behaviors of real rocks. Critical stress thresholds (σ_{ci}, σ_{cd}, σ_{peak}) marking microscale cracking leading to meso fractures were identified within these models. Subsequently, core samples were subjected to uniaxial loading up to these critical stress levels, followed by thin section preparation for microscopic analysis—examination under a polarizing microscope allowed for inspecting mechanisms governing crack propagation (Figure 1b). Finally, a quantitative assessment of rock damage evolution was conducted through fractal analysis on crack patterns, calculating fractal dimensions (D_B) of cracking intensity at each stress level (Figure 1c). Diabase exhibited the highest D_B values on sections parallel to the loading direction, while ignimbrite and marble manifested equivalent D_B values. Conversely, diabase displayed the least tendency for cracking on sections perpendicular to the loading direction, followed by marble, with ignimbrite exhibiting the highest cracking intensity. The results show that post-critical stress (σ_{cd}) reveals the emergence of textural properties as first-order factors dictating the extent of rock damage, with mesoscale fractures aligning under mineralogical composition.

The insights derived from this research provide efficient numerical data for predicting deformation and damage mechanisms in brittle rocks during rock engineering applications. This integrative approach, combining laboratory experiments, numerical modeling, and microscopic investigations, advances our understanding of the complex interplay between mineralogical and textual controls on stress-induced fractal rock damage.

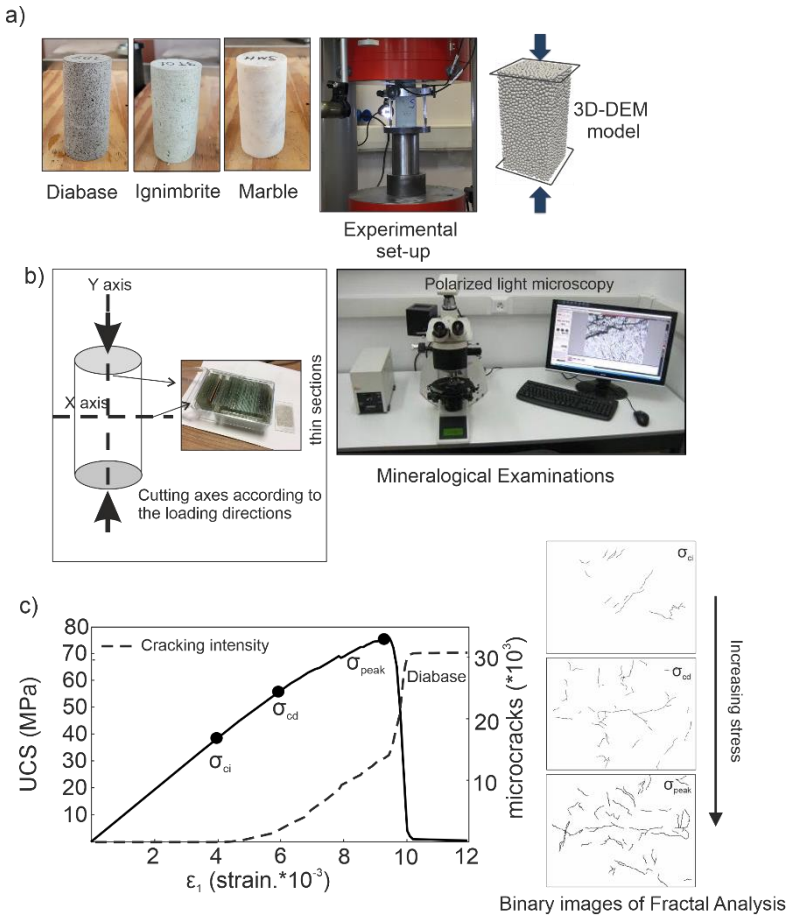

Figure 1. Integrated methodology incorporating a) laboratory and numerical experiments, b) mineralogical analysis c) fractal patterns of the cracking process during rock damage evolution.

5. References

[1] Bieniawski Z.T. (1967). Mechanism of brittle fracture of rock. Part I: Theory of fracture process. *Int. J. Rock Mech. Sci.*, 4: 395-430.

[2] Dinç Göğüş Ö., Avşar E. (2022). Stress levels of precursory strain localization subsequent to the crack damage threshold in brittle rock. *PLoSONE* 17(11), e0276214.

[3] Eberhardt E., Stead D., Stimpson B., Read R.S. (1998). Identifying crack initiation and propagation thresholds in brittle rock. *Can. Geotech. J.*, 35: 222–233.

[4] Griffith A.A. (1921). The Phenomena of Rupture and Flow in Solids. *Phil. Tran.s Roy. Soc. Ser. A.*, 221:163-198.

[5] Horii H., Nemat-Nasser S. (1986). Brittle failure in compression: splitting faulting and brittle-ductile transition. *Philos. Trans. A Math. Phys. Eng. Sci.*, 1986319337–374.

[6] Martin C.D., Chandler N.A. (1994). The progressive fracture of Lac du Bonnet granite. *Int. J. Rock Mech. Min. Sci.*, 31(6): 643-659.

[7] Renard F., Bernard D., Desrues J., Ougier-Simonin A. (2009). 3D imaging of fracture propagation using synchrotron X-ray microtomography. *Earth Planet. Sci. Lett.*, 286, 285-291.

[8] Tapponnier P., Brace W.F. (1976). Development of stress-induced microcracks in Westerly granite. *Int. J. Rock Mech. Min. Sci. Geomech. Abstr.*, 13(4), 103-112.

INFLUENCE OF PARTICLE SHAPE ON MACROSCOPIC ROTATIONAL PROPERTIES

***M. Winkelmann*[1,2], *V. Magnanimo*[2], *S. Luding*[2] *and S. Papanicolopulos*[1]**

[1] *The University of Edinburgh, Institute for Infrastructure and Environment, Edinburgh, United Kingdom*

[2] *Univeristy of Twente, Multi-Scale Mechanics, Enschede, The Netherlands*

Granular soils are made of discrete particles that interact with each other through frictional contacts. Any change of properties at grain level, the micro-scale, affects the response of the material on the macro-scale. It has been shown that the particle shape is one factor that influences the rotational behaviour of the material [1, 2].

Through discrete-to-continuum (D2C) upscaling methods, the discrete particle data such as particle mass, particle velocity and contact force can be mapped on continuous fields like density, velocity, and stress. Following the approach by Goldhirsch [3] and Weinhart [4, 5], and using a smoothening function, we develop a D2C method to transform particle properties related to rotation like discrete angular velocity, angular momentum, tangential forces, and contact torque to non-classical micropolar fields like continuum angular velocity, curvature, skew-symmetric stress, and couple stress.

However, measuring those fields in an experiment is extremely challenging, though it is possible to obtain the kinematic fields from experimental data. Triaxial tests in micro-computed tomography on sands of different shape [6] give the discrete kinematic fields that can be postprocessed via our D2C method towards continuous fields. Matching the kinematic properties of the experiment with DEM simulations allows us to obtain the static quantities as well. Via this approach, the influence of shape on rotation related macroscopic quantities is studied. This method can be used in future applications for the formulation of constitutive equations.

References

[1] Rorato, R., Arroyo Alvarez De Toledo, M., Andò, E. C. G., Gens, A., and Viggiani, G. (2020). Linking shape and rotation of grains during triaxial compression of sand. *Granular Matter*, **22**, 88.

[2] Ali, U., Kikumoto, M., Ciantia, M., Cui, Y., and Previtali, M. (2023). Systematic effect of particle roundness/angularity on macro- and microscopic behavior of granular materials. *Granular Matter*, **25**, 51.

[3] Goldhirsch, I. (2010). Stress, stress asymmetry and couple stress: from discrete particles to continuous fields. *Granular Matter*, **12**, 239–252.

[4] Weinhart, T., Hartkamp, R., Thornton, A. R., and Luding, S. (2013). Coarse-grained local and objective continuum description of three-dimensional granular flows down an inclined surface. *Physics of Fluids*, **25**, 070605.

[5] Weinhart, T., Labra, C., Luding, S., and Ooi, J. Y. (2016). Influence of coarse-graining parameters on the analysis of DEM simulations of silo flow. *Powder Technology*, **293**, 138–148.

[6] Roy, N., Frost, J. D., and Viggiani, G. (2022). Pore space evolution of granular assemblies under shear: an experimental study using X-ray tomography. *Granular Matter*, **24**, 63.

On the way to a digital soil lab: Linking geomechanical X-ray CT experiments and numerical modelling on the grain scale

M. Milatz[1]

[1] *Hamburg University of Technology (TUHH), Institute of Geotechnical Engineering and Construction Management, Hamburg, Germany*

1. Motivation

Despite its occurrence as a natural "everyday material" of our geosphere and its frequent use in construction, the physics of sand as a granular material is still not fully understood. It is common knowledge, that the material behaviour observed at the macroscopic level is a result of a multitude of intergranular and interstitial interactions on the grain or pore level of this material. As an example, the frictional nature of granular materials, leading to macroscopic shear strength and volumetric behaviours of contractancy and dilatancy upon shearing, is known to stem from intergranular friction and grain kinematics.

With the growing availability of imaging techniques, such as computed tomography (CT), new insights into granular soil behaviour on the grain and pore scale can be obtained. Highly resolved 3D image data allow to gather quantitative measurements of grain and pore shapes in granular materials. In the case of multiphase granular materials, also different constituents, such as liquids and gas in the pore space can be separated by means of image segmentation techniques. The quantitative measurements obtained on the grain and pore scale are useful to supplement the measurements on the macroscopic level in order to bridge the gap between micro mechanics/hydraulics and the macroscopic material behaviour which is of relevance for continuum mechanics-based engineering models.

In this contribution, we present experimental research on the shear behaviour of granular materials by means of miniaturised direct shear tests which are run in a CT scanning environment. The acquisition of 3D CT data during direct shearing allows to study grain kinematics of sheared granular materials and the hydro-mechanical coupling of grain motion and pore fluids in the unsaturated state. Besides the experimental analysis, we discuss discrete numerical simulations of the direct shear test by means of the Finite-Discrete Element Method (FDEM) [1]. This method allows to consider FE meshed sand grains with quasi-natural shapes based on CT data and to simulate their frictional interactions in particle scale discrete element simulations.

In the future, the combination of *in situ* CT experiments and direct numerical simulations might establish the basis for a digital soil lab where numerical models based on true granular geometries are used to study geomechanical behaviour based on digital twins and idealised boundary conditions [2].

2. Research methodology

The mechanical behaviour of granular materials, such as sand and glass beads, is studied by means of a miniaturised direct shear apparatus presented in [2]. Within the scope of this contribution, we focus on different experiments on unsaturated sand and glass bead specimens at low water content. The experimental set-up is custom-built to fit into CT scanning environments, e. g., CT systems at synchrotron radiation facilities or laboratory CT scanners as shown in Fig. 1 (a) and (b). The hardware consists of a miniature split shear cell and vertical loading system based on a guided dead load. The lower compartment of the shear box, where the shear force is measured using a load cell, is moved by a linear actuator driven by a stepper motor. The experiment is controlled by Python scripts running on a Raspberry Pi 4 single-board computer allowing for remote control of the experiment [2].

The acquired 4D CT data (3D spatial information plus time as fourth dimension) is analysed by means of dedicated Python coded image analysis algorithms allowing to measure grain kinematics

based on particle tracking, grain contacts as well as changes of capillary interactions between liquid clusters and solid grains.

In order to include natural grain shapes in discrete element simulations of the direct shear test, we apply the Finite-Discrete Element Method. In a first step, we generate FE meshes of thousands of CT scanned sand grains. Finally, these grain meshes are included as "digital soil twins" in explicit-dynamic particle based simulations of direct shearing as illustrated in Fig. 1 (c) using the commercial software Abaqus/Explicit. Following Terzaghi's idealisation of granular soils, we model sand grains as rigid bodies. Similar to the *in situ* CT experiments, the simulations allow to shed light on grain scale mechanical interactions, such as grain kinematics inside and outside of the shear zone.

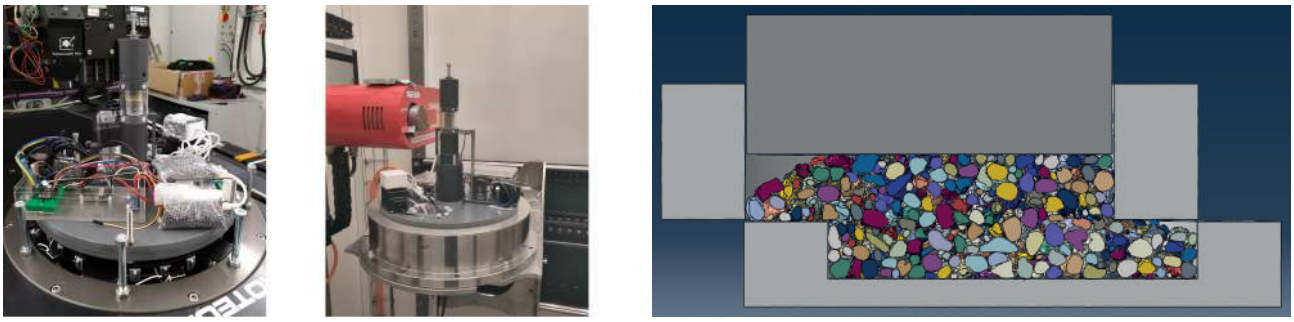

(a) (b) (c)

Figure 1. Miniaturised direct shear apparatus for *in situ* CT experiments (a) with synchrotron-based CT at the German synchrotron DESY, Hamburg, (b) with X-ray CT at Laboratoire 3SR, Grenoble, and (c) 3D sliced visualisation of a direct shear test simulation with 5 000 sand grains after shearing.

3. Experimental results

The analysis of first CT experiments with direct shearing of sand and glass beads indicate different grain kinematics inside and outside of the shear zone. The trajectories of tracer grains in sand and glass bead specimens indicate an increasing trend of "granular dilatance" with increasing vertical z-coordinate of the grain position vectors. Accordingly, grains follow very heterogeneous trajectories in the direct shear test. The rotation vectors of tracked grains yield maximum rotation angles at specimen mid height around the shear zone. Lower grain rotations are measured for sand grains as compared to glass beads. In the unsaturated case, a reduction of degree of saturation around the shear zone is measured. Furthermore, a reduction of capillary water clusters in contact with the moving tracer grains is observed, indicating that the shear process leads to changes in capillary structures on the pore level.

The FDEM simulations of the direct shear test currently only include dry granular assemblies. First simulations of the direct shear process, including a few thousands of digital sand grains from CT scans, show similar results as from the *in situ* CT experiments. Granular rotations are most pronounced in the shear zone. Furthermore, grain trajectories are similar to tracer grain trajectories in the CT experiments, revealing macroscopic volume change as a result of local grain kinematics.

References

[1] Munjiza, A. (2004). *The Combined Finite-Discrete Element Method*. John Wiley & Sons, Ltd.

[2] Milatz, M. (2022). *Investigation of capillary effects on the grain scale by means of in situ experiments, imaging and numerical simulations*. Habilitation thesis, Hamburg University of Technology.

RELATIONSHIPS BETWEEN SHEAR STIFFNESS AND THE PARTICLE SIZE DISTRIBUTION OF COARSE-GRAINED GRANULAR MATERIALS

D. Barreto[1], J. Leak[1] and E. Imre[2,3]

[1] Edinburgh Napier University, School of Computing, Engineering and the Built Environment, Edinburgh, United Kingdom

[2] Bánki Donát Faculty of Mechanical and Safety Engineering, Budapest, Hungary

[3] AIAM Doctoral School, Óbuda University, Budapest, Hungary

1. Introduction

It is well recognised that the shear stiffness at small strains in granular materials is dependent on the particle size distribution (PSD). Earlier research relates descriptors of particle size distributions and shear stiffness. For example, Wichtmann & Triantafyllidis [1] proposed relationships between the shear stiffness and the coefficient of uniformity (c_u) while Menq [2] suggested using both c_u and the mean diameter (d_{50}) for the estimation of shear stiffness. Sun et al [3] proposed a new grading parameter (c_g) that can be calculated considering the full range of particle sizes in a granular material. Furthermore, Goudarzy, et al [4] experimentally demonstrated that the shear stiffness id highly dependent on fines content and Liu, et al [5] showed a clear correlation emerged between particle size distribution and stiffness for continuous PSDs, but such correlation did not hold universally for gap-graded materials. These and other available would seem to indicate that not only the PSD is very significant on determining the shear stiffness and understanding its evolution, but also that better PSD descriptors may be required to understand its effect.

In recent years, the use of the grading entropy coordinates proposed by Lörincz [6] has gained some momentum. In this paper we postulate that grading entropy coordinates are effective PSD descriptors that are well correlated to the small strain shear stiffness of granular materials. To defend this postulate an extensive database of experiments and DEM simulations available in the literature has been compiled and examined to (i) assess the effectiveness of various PSD descriptors to predict shear stiffness from various sources, (ii) demonstrate that volumetric parameters may be also required to improve these predictions, and (iii) to meaningfully explain in a physical manner the complex relationship between shear stiffness and particle size distribution.

2. Methodology

In order to examine the effect of the particle size distribution on the shear stiffness of coarse-grained materials, first a large database of experiments and numerical simulations was compiled. Such database included physical experiments on sands with a large range of particle sizes and particle size distributions whilst considering uniform, well-graded and gap-graded PSDs. The nature of the data is quite wide. It includes different testing systems for the shear stiffness (such as conventional triaxial testing, bender element testing, resonant column testing, etc.), as well as a significant range of densities, confining stresses and particle characteristics (i.e. differences in particle shape). In terms of PSDS, the database includes standard sieving results as well as those obtained from more advanced measurements using x-ray diffraction.

Similarly to experimental results, a wide range a DEM simulations was also considered, using existing data relating (mostly) to spherical assemblies. However existing data obtained using various particle shapes (i.e. clumps, super-quadrics, etc.) has also bee included for comparison purposes. Whilst most existing DEM data relates to uniform PSDs with limited ranges of particle sizes, existing

gap-graded data and some limited better graded specimens, the present study has significantly extended the database by performing an extensive simulation campaign of DEM simulations of spherical assemblies using periodic boundaries. Both experimental and numerical databases are then comparable in terms of size and range of PSD, density and stress conditions considered. This reduced possible statistical biases but also enabled to perform detailed micro-mechanical analyses to gain further insight into the evolution of shear stiffness and its relationship with PSD, void ratio, stress and inter-particle contacts and particle characteristics.

Having assembled the database, advanced statistical analyses were performed to identify outliers and the dependence of any results on these being excluded (or not). Then multiple regression analyses between a given PSD descriptor (e.g. coefficient of uniformity, mean particle diameter, fines content, and grading entropy coordinates) or a combination of these and the value of the shear stiffness were performed and quantified in terms of various statistical parameters to determine their prediction effectiveness. Additional analysis using composite parameters of PSD descriptors, volume descriptors (e.g. void ratio, skeletal void ratio, inter-granular void ratio, etc.), and shape descriptors (e.g. sphericity, elongation, angularity, etc.) were also considered in detail.

Having examined the benefits of these relationships, their effectiveness was further assessed by predicting the stiffness obtained from both experiments and simulations which were not initially considered for their evaluation (i.e. different datasets were used for the determination of relationships and their assessment)

3. Results

The amount of results obtained in this study is extensive. It has been however possible to discern in detail the dependance of stiffness on PSD characteristics. It has been found that in order to accurately estimate the shear stiffness of coarse-grained granular materials, a description of the PSD that considers the full particle size range is required. Furthermore, these predictions are significantly improved when volume descriptors (void ratios) are simultaneously considered. In fact, volumetric response is significantly linked to the evolution of shear stiffness and necessary for its accurate prediction. The results have also enabled to further understand the inter-dependent effects of stress, density and PSD on shear stiffness at a level of detail unavailable in the existing literature.

5. References

[1] Wichtmann, T., and Triantafyllidis, T. (2009). Influence of the grain-size distribution curve of quartz sand on the small strain shear modulus Gmax . *J. Geotech. Geoenviron. Eng.*, 135:1404-1418.

[2] Menq, F. Y. (2003). *Dynamic properties of sandy and gravelly soils*. Univ. of Texas at Austin, Austin, TX

[3] Sun, Y., Yang, S. and Chen, C. (2018). A grading parameter for evaluating the grading-dependence of the shear stiffness of granular aggregates. *Particuology*, 36: 193-198.

[4] Goudarzy, M., König, D. and Schanz, T. (2016). Small strain stiffness of granular materials containing fines. *Soils and Foundations*, 56(**5**):756-764

[5] Liu, D., O'Sullivan, C. and Carraro, J.A.H. (2023). The influence of particle size distribution in granular materials. *Géotechnique,* 73(**3**): 250-264.

[6] Lörincz, J. (1986). *Grading entropy of soils*. PhD thesis, Technical Sciences, Technical niversity of Budapest, Budapest, Hungary.

TENSILE FRACTURING OF SATURATED CLAY

K. Soga[1], Y. Yang[1], C. Dong[1] and X. Sun[2]
[1] University of California Berkeley, Berkeley, USA
[2] Formerly University of California, Berkeley, Chinese Academy of Sciences, Wuhan, China

1. Introduction

Soil fracturing treatment in geotechnical engineering has historically been based on empirical methods, and academic knowledge in this area is limited compared to that of shear and compression behavior of soil. In fact, there is no formal soil fracture criteria in academic textbooks and engineering practice. This is partly because (i) non-cemented particle assembly is believed to have zero tensile capacity (in effective stress), and hence the effect is often ignored, (ii) tensile experiments are difficult to perform due to low confinement, and (iii) there are limited good geotechnical engineering case studies that analyze soil fracture failures in detail. However, many geomaterials (such as cemented soil, whether natural or man-made, and heavily overconsolidated clay) carry tensile capacity but are also brittle in nature (i.e. the stiffness/strength ratio is very large). When soil fracture occurs, it is likely to be localized and scale-dependent, and therefore the locations of the failure will be difficult to predict. This study examined a hypothesized soil-pore fluid interaction mechanism of deformation-induced soil fracture.

2. Soil-Pore Fluid Coupling Effect during Tension

Fracture or tensile tests on clayey soils are often quick and hence they are mostly in undrained conditions. When microcracks begin to form, stress concentration starts to develop near the crack tip. This stress is carried by the soil structure and water, and is associated with negative excess pore water pressure that develops in front of the fracture, as shown in Fig. 1. In this simulation, an effective stress-based cohesive crack model was used. The results show that the magnitude of negative excess pore pressure depends on the loading rate. A relationship between fracture pressure and normalized tensile index was developed using a numerical model. The normalized tensile index includes tensile strength (st), fracture toughness (J), distance from the external loading location (d), and stiffness (G). The results reveal that fluid migration plays a crucial role during fracturing, as shown in Fig. 2. For a given loading rate, a material with a low hydraulic conductivity has a higher fracture pressure than a material with a high hydraulic conductivity. Conversely, a fast loading rate to a material results in a more undrained response of the material and thus increases the fracture pressure. For a material with relatively high initial effective stress, the

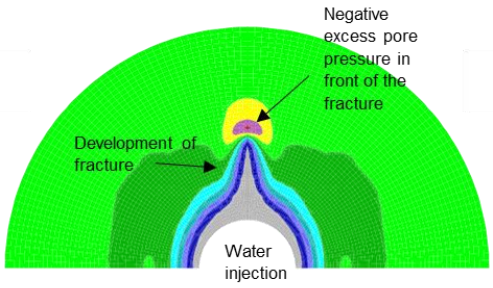

Fig.1 Numerical simulation of negative excess pore pressure developing in front of propagating soil fracture

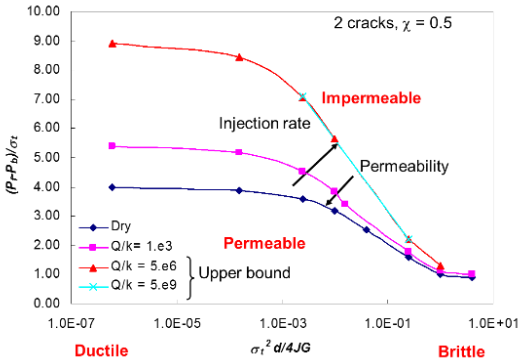

Fig.2 Normalized fracture pressure as function of fracture strength/toughness and permeability

fracture pressure is larger, and the behavior is more ductile than a material with relatively low initial effective stress. The simulation results indicate that fracture assessment should be done either by an 'effective stress' model with fully coupled soil-pore fluid coupling analysis or by a 'rate-dependent' fracture criterion based on total stress analysis. Experimental evidence to prove the validity of the proposed soil-pore fluid interaction effect on fracture initiation and propagation for soils is needed.

3. Measuring of pore pressure in front of a fracture

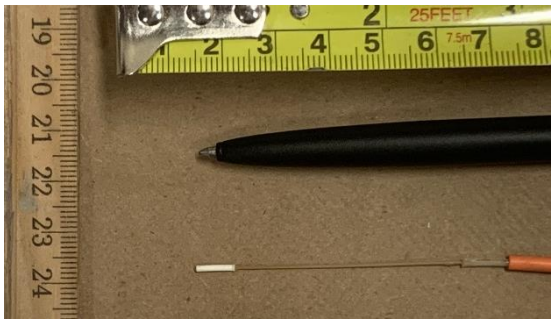

Fig. 3 A photo of FOM suction probe

It is crucial to be able to measure the negative pore pressure inside soil to find and prove an effective stress criterion for fracture initiation. Including tensiometers may cause concerns as they can act as crack raisers, and hence the sensor must be small enough to be embedded in the soil without significantly altering its behavior. A new fiber-optic-based miniature pore water suction probe was designed and manufactured with a 1.2mm diameter. The probe incorporates a pressure catheter based on the Fabry–Pérot Interferometer (FPI). The newly developed miniature pore pressure sensor uses a 0.55mm diameter miniature fiber optic pressure transducer pressure sensor manufactured by FISO. The void space between the sensor tip and the porous ceramic membrane is small enough to detect the pressure change simultaneously with the outer environment. The performance of the sensor was verified using a Hyprop testing apparatus that measures a soil moisture characteristic curve. A testing system that consists of a miniature fiber optic water pressure transducer, a 3D printed tensile box, a load cell, and a motor was developed, as shown in Fig. 4. To induce tension, a pair of loading jaws were designed between which the soil specimen was mounted. A testing apparatus with two jaws was manufactured by a 3D printer and the material is made of Polylactic acid. Interior jaws with different angles were tested. After the soil specimen was fully filled between the jaws of the loading apparatus, the miniature pore pressure transducer was then inserted at the center of the soil specimen. Fig. 5 shows the negative excess pore pressure measured in a water saturated compacted kaolin specimen as the tensile displacement increased.

Fig. 4 Fracture testing device

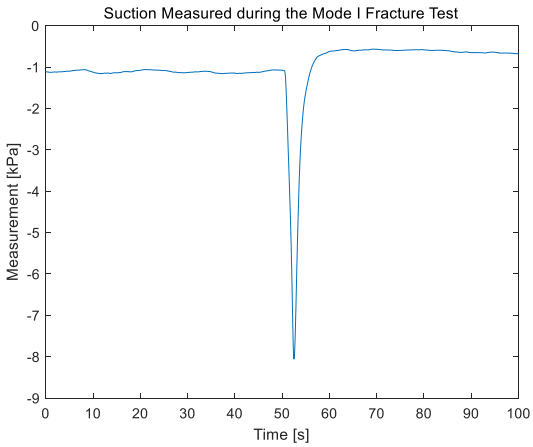

Fig. 5 Negative excess pore pressure measured in front of the crack

4. Conclusion

A novel miniature pore pressure sensor was developed to measure pressure change during soil crack development. Results show that, when soil cracking started to initiate, there was a decrease in pore pressure, which was hypothesized in this study. The pressure drop rate would depend on the rate of crack development. Further work is currently preformed to examine different magnitudes of negative pore pressure that are expected to depend on loading rate, soil conditions, and fracture modes.

WAVE VELOCITIES IN A MARTIAN SIMULANT UNDER LOW STRESS: EXPERIMENTAL AND THEORETICAL ANALYSIS

Caicedo Bernardo[1], Castillo-Betancourt Juan Pablo[1,2], Delage Pierre[2]

[1] Universidad de los Andes, Departamento de Ingeniería Civil y Ambiental, Bogotá, Colombia

[2] École des Ponts ParisTech, Navier/CERMES, Marne-la-Vallée, France

The mechanical properties of soils under low stresses (below 10 kPa) remain little explored, both from experimental and theoretical points of view, since stresses involved in terrestrial geotechnical engineering are higher. Recent attention has been paid on low stress levels during the investigation of the surface properties of Martian regolith at the InSight landing site, under reduced gravity (3.721 m/s^2) with stress as low as 1-10 kPa along the first centimeters depth. InSight was a geophysical mission on Mars (NASA – CNES – DLR) working between December 2018 and 2022, based on a lander accommodating various instruments, including a very sensitive broad band seismometer provided by France (CNES – IPGP).

This abstract presents some experimental and theoretical investigations carried out on wave transfers in a loose Martian sandy simulant made up of sub-rounded to rounded Fontainebleau sand. This simulant was chosen based on orbital Thermal Inertia measurements that indicated a sandy surface deposit with an average diameter of 170 µm (to compare to D_{50} = 220 µm for Fontainebleau sand). Due to wind saltation on Mars, surface grains are sub-rounded to rounded.

Compression and shear wave velocities (V_p and V_s, respectively) were measured by using bender elements on a loose pluviated triaxial sample (100 mm diameter and 170 mm height) on which the confining stress was applied by vacuum. To cope with low stresses, measurements were carried out on horizontal samples, with careful measurements of the stresses resulting from the membrane and from self-weight.

The changes in V_p and V_s with respect to confining stress are presented in Figure 1a, with experimental data obtained down to stresses as low as 2 kPa. To interpret these results, particular attention was paid to the effects of grain roughness at inter-grains contacts, that are suspected to be more significant under low stresses. Figure 2 presents an investigation of the roughness of a Fontainebleau sand grain determined from Atomic Force Microscopy measurements, with a most frequent asperity radius of 200 µm.

A micromechanical contact model derived from [1,2,3] was developed. Two important parameters of the model are the average roughness σ_{rms} and the fraction of non-slipping grains ξ. Figure 1a shows how the model prediction fits with our experimental data for V_p and V_s with σ_{rms} between 0.6 and 0.8 µm, two values that appear to be larger than that determined by AFM in Figure 2. Figure 1b shows how the fraction of non-slipping grains ξ affects the Poisson coefficient (determined from V_p and V_s measurements), with from our data ξ = 0.6.

The data of Figure 1a show that the model satisfactorily fits with experimental data, with however less accuracy below 10 kPa, an area where more variability is observed, due to less precision provided by bender elements. Figure 1b shows that the Poisson ratio is constant for stress between 6 and 80 kPa, with again stronger dispersion below 6 kPa. Whether or not the Poisson ratio is constant at very low stresses remains an open question that needs further investigation, in an area where bender element measurements are no longer accurate enough.

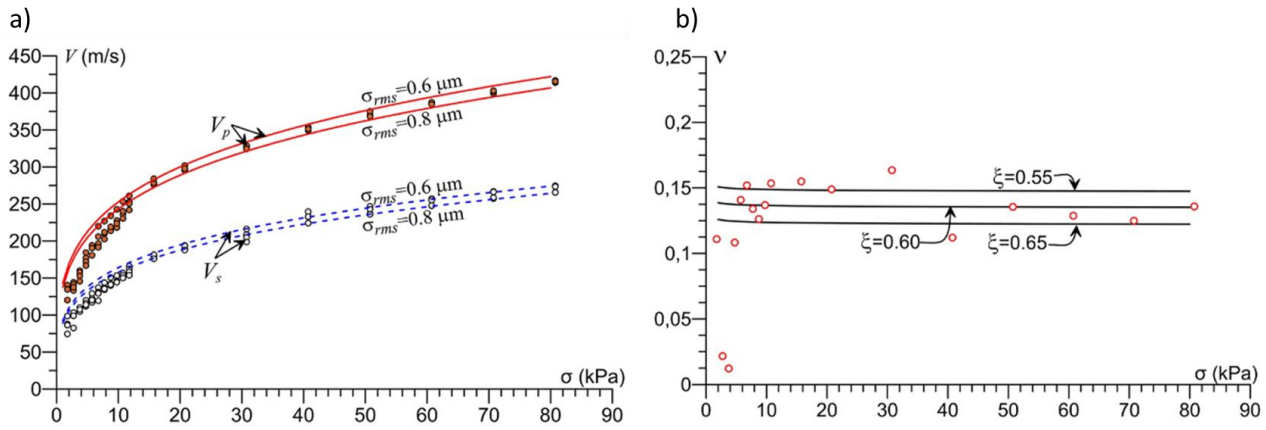

Figure 1. a) Wave velocity and b) Poisson ratio experimental results, along with the fitted theoretical models.

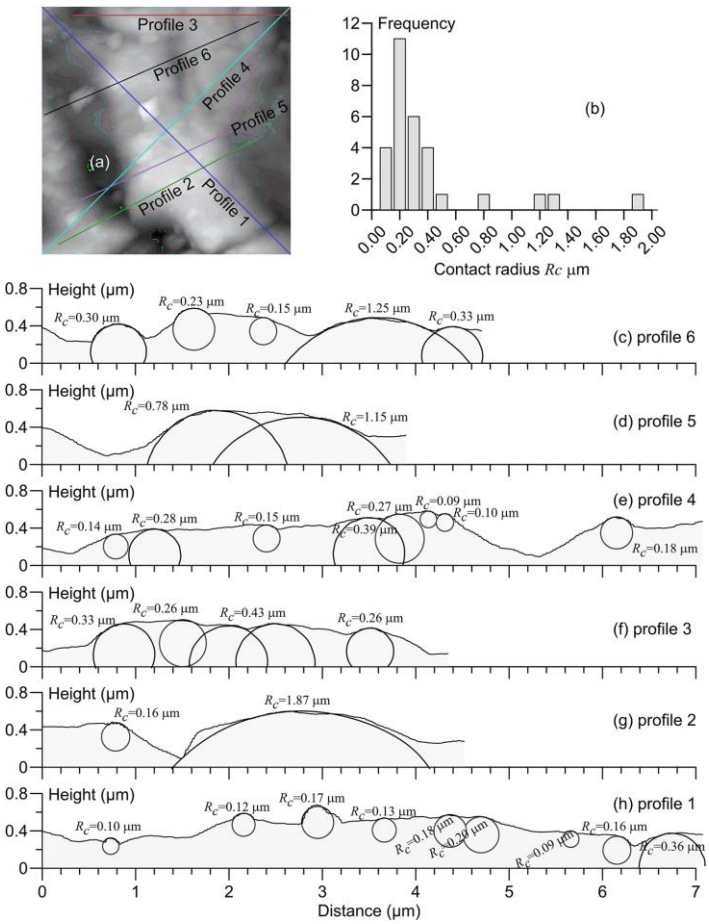

Figure 2. AFM investigation of a Fontainebleau sand grain: (a) Cross profiles on the AFM measured area; (b) Histogram of contact radius along the six profiles; (c–h) Roughness plotted along the profiles displayed in panel (a).

References

[1] Bachrach, R., Dvorkin, J. and Nur, A. M. (2000). Seismic velocities and Poisson's ratio of shallow unconsolidated sands. Geophysics, 65(2), 559–564. https://doi.org/10.1190/1.1444751.

[2] Bahrami, M., Yovanovich, M. M. and Culham, J. R. (2005). A compact model for spherical rough contacts. J. Tribol. Oct 2005, 127(4): 884-889, https://doi.org/10.1115/1.2000982

[3] Butt, S. U., Antoine, J. F. and Martin, P. (2015). Simplified stiffness model for spherical rough contacts. Tribology-Materials, Surfaces and Interfaces, 9(2), 63-70.

Wave speeds derivations for nonlinearly elastic models in dry and saturated conditions

D.M. Riley[1]***, I. Einav***[1] ***and F. Guillard***[1]
[1] *Sydney Centre in Geomechanics and Mining Materials, School of Civil Engineering, The University of Sydney, 2006, Sydney, Australia*

1. Abstract

Elastic wave speeds are fundamental in geomechanics and have historically been described by an analytic formula that assumes *linearly* elastic solid medium despite empirical findings indicating *nonlinear* stiffness. Thus, we find a mathematical and physical disconnect between the assumed wave speeds and the empirically generated stiffness constants. Recently, wave speeds were derived for energy-conserving (hyperelastic) constitutive models that generally depend on pressure and density. Under isotropic compression states, the analytical solutions converge to previously documented empirical relations. Conversely, in the presence of shear, hyperelasticity predicts changes in the longitudinal and transverse wave speed ratio. This prediction arises from terms that ensure energy conservation in the hyperelastic model without needing fabric to predict such an evolution, as was sometimes assumed in previous investigations. This work extends the previously derived wave speeds to incorporate saturated scenarios by incorporating the free energy associated with the compressibility of relevant phases. The results show that by incorporating these additional terms, the model captures both saturated wave speeds and dispersive wave velocities, as observed in experiments.

2. Introduction

Conventionally, in geotechnical engineering, wave speeds are assumed to be characterised by a homogeneous, isotropic, linearly elastic solid. After experimentally measuring the wave speeds, the stiffness moduli M_w and G_w depend on the soil's effective pressure p^e and solid fraction ϕ. Generally, these empirical relations adopt the form [1]:

$$M_w = AH(\phi)\left(\frac{p^e}{p_a}\right)^b, \tag{1}$$

$$G_w = BH(\phi)\left(\frac{p^e}{p_a}\right)^b, \tag{2}$$

where A and B are constants, $p_a = 1$ Pa is a reference stress, b is the stress exponent reflecting nonlinear pressure dependency, and $H(\phi)$ is a general function of solid fraction ϕ. Although these empirical relations have successfully captured experimental phenomena, it is crucial to note that they were determined by first assuming a linearly elastic isotropic continuum. Herein, we make no such simplifying assumptions and instead derive the wave speeds directly from nonlinear pressure and solid fraction-dependent stresses, which were determined from the internal energy.

3. Results

We adopt the form of elastic internal energy used in [2], which leads to the prediction that the ratio of longitudinal and transverse wave speeds for triaxial compression experiments as seen experimentally. We extend this derivation by incorporating the free energy associated with the compressibility of all phases as in [3]. Thus, in a saturated granular media, the longitudinal wave speed is

$$\rho\left(V_p^{hyper}\right)^2 = \bar{M}_w(\varepsilon_{ij}^e, \rho) + \frac{K^m}{\omega^2 + D^2k^4} \tag{3}$$

where $\bar{M}_w(\varepsilon_{ij}, \rho)$ is the tangent stiffness as a function of elastic strain tensor ε^e_{ij} and bulk density ρ as derived in [2], K^m is the mixture compressibility defined in [3], D is the water diffusivity, ω and k is the circular frequency and wave number, respectively. The model was fitted with experimental data for dry isotropic compression tests from [4]. Figure 1 shows the wave speeds for both dry and the predicted saturated wave speeds. Notably, the model predicts the saturated wave speeds to a high degree of accuracy.

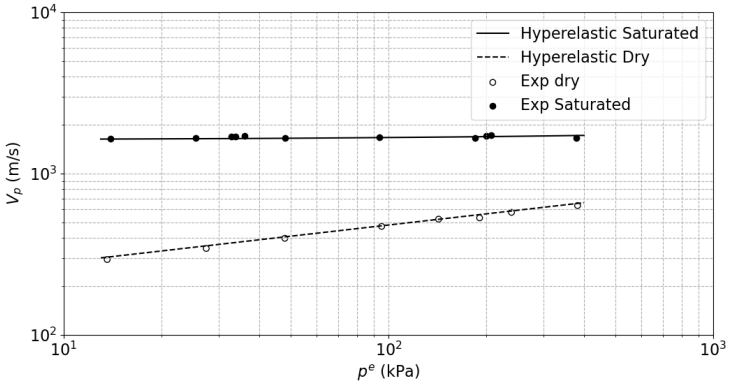

Figure 1. Longitudinal wave velocity V_p against effective pressure p^e for an isotropic stress state at a solid fraction $\phi \approx 0.63$. The experimental data was extracted from [4].

4. Conclusion

In conclusion, we have adopted the internal energy and derivation procedure from [2], extending it to include saturated scenarios. Thus, the resulting model captures the evolution of the ratios of longitudinal and transverse wave speeds, which hints that fabric may not be a necessary assumption to capture this experimental feature. Moreover, the extension to saturated scenarios reveals that the only additional information required is the compressibility of the fluid and solid phases and the fluid's diffusivity. This general formulation allows for the extension to various fluids and low-pressure limits relevant to microgravity conditions. While this publication primarily evaluates the effect of the addition of the free energy term on the group wave speed, future work will more thoroughly assess the phase wave speed and investigate the dispersion relations predicted by this model. Additionally, future research could incorporate viscous drag terms to enable fair comparisons with Biot's predictions. Finally, the model offers the potential for advancing this derivation to account for mixtures of fluids, such as partially saturated sands and other potential mixtures encountered in geophysics.

References

[1] Hardin, B. O. and Richart Jr, F. (1963). Elastic wave velocities in granular soils. *Journal of the Soil Mechanics and Foundations Division*, **89**, 33–65.

[2] Riley, D. M., Einav, I., and Guillard, F. (2023). A consistent derivation of soil stiffness from elastic wave speeds. *arXiv preprint arXiv:2312.01666*.

[3] Chen, Y., Guillard, F., and Einav, I. (2023). A hydrodynamic model for chemo-mechanics of poroelastic materials. *Géotechnique*, pp. 1–16.

[4] Valle-Molina, C. and Stokoe, K. H. (2012). Seismic measurements in sand specimens with varying degrees of saturation using piezoelectric transducers. *Canadian Geotechnical Journal*, **49**, 671–685.

Advances in numerical methods

Advances in numerical methods

DEM applications

A DEM INVESTIGATION ON THE EFFECT OF GRADATION ON THE LIQUEFACTION RESPONSE AND FABRIC EVOLUTION OF SOILS

M.S. Basson[1], A. Martinez[1] and J.T. DeJong[1]

[1] University of California Davis, Department of Civil and Environmental Engineering, Davis, USA

1. Introduction

Assessment of liquefaction triggering potential is an important aspect in the design of critical infrastructure. While soils with broad gradations are widely present in nature, the effects of soil gradation on the triggering of liquefaction and accumulation of cyclic deformations are still not fully understood. The answers to basic questions such as whether broadly graded soils have a greater resistance to liquefaction or whether they will experience smaller deformations than poorly graded soils when liquefied remain elusive. Previous research shows that increasing the breadth of soil gradation has an important effect on the packing of particles and the resulting fabric. For example, as the gradation is increased, the number of contacts per particle increases significantly [2,3]. As a result, when the response is compared based on a constant state parameter (ξ_0), soils with broader gradations have greater dilative tendencies that give them greater peak strengths and generate lower excess pore pressure magnitudes [1]. This paper uses Discrete Element Modeling (DEM) simulations to explore the effect of gradation on the liquefaction triggering and deformation accumulation in coarse-grained soils, and how these are linked to the differences in fabric.

2. DEM simulation methodology

The DEM simulations were performed on specimens with Particle Size Distributions (PSD) and particle shapes based on a range of natural broadly graded soils that have been well-characterized in the laboratory. Simulations were performed on three different materials. The 100A material has a median particle size (D_{50}) of 2.8 mm and a C_U of 2.0, 33ABC has a D_{50} of 8.8 mm and C_U of 4.5, and 25ABCD has a D_{50} of 12.7 mm and C_U of 6.4 The PSDs of the natural soils were simulated in DEM but upscaled 20 times to decrease the computational cost. Clumped particles were used to capture the effects of particle shape. The effects of gradation were isolated by using the same particle shapes in all simulations. The simulations were performed with the code Yade on cubical specimens. Periodic boundaries were used to ensure homogenous strain fields in the specimens. The simulations consisted of specimen preparation and DSS shearing stages. The friction coefficient was adjusted during the sample preparation stage to produce specimens with different densities. During the DSS stage, the sample was sheared cyclically with a Cyclic Stress Ratio (CSR), defined as the amplitude between 0.05 and 0.2. The constant volume approximation was used to simulate undrained shearing behavior. The calibrated parameters successfully reproduced the response and rate of change observed in experiments, including the decrease in mean effective stress and accumulation of shear strains with an increasing number of cycles. A detailed description of the calibration procedure is provided in [2].

3. Cyclic Direct Simple Shear Simulations

Soil gradation has an important impact on the liquefaction response. For specimens prepared at the same ξ_0, the more broadly-graded specimens required greater numbers of cycles to trigger liquefaction, and once liquefied, these specimens accumulated shear strains at lower rates. Figure 1

presents results on specimens with ξ_0 between -0.06 and -0.07 in terms of stress paths, shear stress-shear strain loops, and evolution of pore pressure ratio with cycle number. These trends are consistent for specimens prepared at different ξ_0 and sheared at varying CSR magnitudes. The differences in liquefaction response are linked to the differences in fabric. Figure 2 presents distributions of particle connectivity (PC) as a function of percent finer by particle volume for two simulation stages. PC is defined as the number of contacts per particle. The results show that the broadly graded specimen has significantly greater PC values for any percent finer by volume. Namely, the coarsest particle in the 25ABCD specimen has over 100 contacts at all simulation stages, while the corresponding particle in the 100A specimen has about 20 contacts. The greater number of contacts and contact forces carried by the larger particles produce greater dilation for the well-graded specimens, allowing them to better resist liquefaction and deformations.

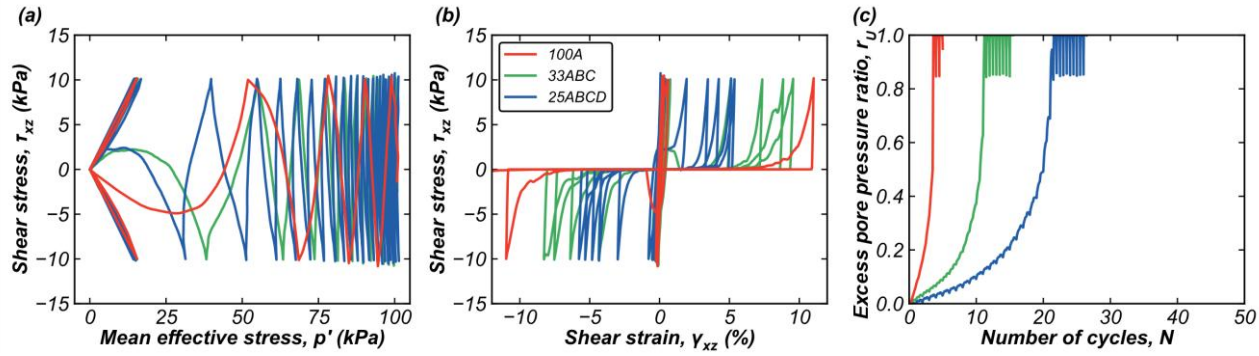

Figure 1. Comparison of DSS DEM simulation results: (a) τ_{xz} versus p', (b) τ_{xz} versus γ_{xz}, and (c) r_U versus N for specimens with ξ_0 between -0.06 and -0.07 and initial p' of 100 kPa.

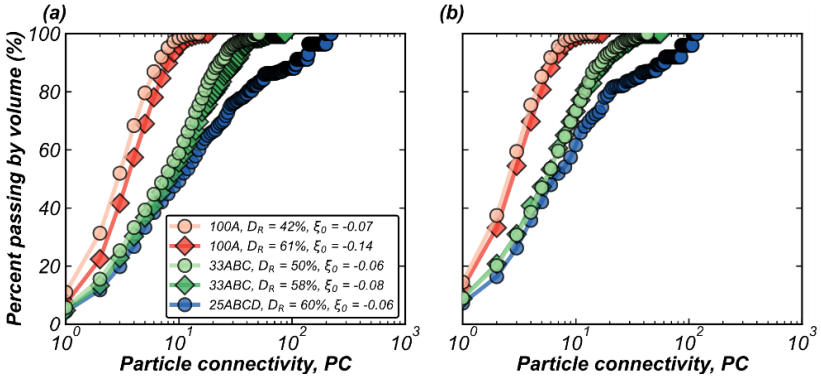

Figure 2. Cumulative distribution of PC for (a) the start of the shearing (i.e., end of consolidation), (b) dilation phase midway to triggering of liquefaction (r_U of 0.5).

4. References

[1] Ahmed, S.S., Martinez, A. & DeJong, J.T. (2023). Effect of gradation on the strength and stress-dilation behavior of coarse-grained soils in drained and undrained triaxial compression. *J. Geotech. Geoenv. Eng.* **149**(5).

[2] Basson, S.M., Martinez, A., & DeJong, J.T. DEM simulations of the liquefaction resistance and post-liquefaction strain accumulation of coarse-grained soils with varying gradations. In review for *J. Geotech. Geoenv. Eng.*

[3] Liu, D., O'Sullivan, C. & Carraro, J.A.H. (2021). Influence of particle size distribution on the proportion of stress-transmitting particles and implications for measures of soil state. *J. Geotech. Geoenv. Eng.* **147** (3).

A DEM MODEL FOR INVESTIGATING THE ELECTROMECHANICAL CHARACTERISTICS OF PARTICULATE SYSTEMS

Chao Zhang, Sadaf Maramizonouz, David Milledge, Sadegh Nadimi
School of Engineering, Newcastle University, Newcastle upon Tyne, NE1 7RU, United Kingdom

Keywords: Discrete element method; Electrical transfer; Electromechanical model; Contact model

Summary: Electromechanical coupled behaviour in geomaterials is an essential phenomenon in many industrial fields and is yet poorly understood. This study proposes an electromechanical contact model based on the formulation of electrical resistance for particle-particle and particle-wall interactions. The model is then verified and validated against published analytical solutions and experimental data.

1. Introduction

Understanding the electrical response of particulate systems under variable mechanical loading conditions is important for the optimization of compaction efficiency of geomaterials, the defects inspection of mechanical components, and the effect of sand on the electrical conduction of wheel-rail interface [1]. Several experiments have contributed to the understanding of the principle behind the electromechanical behaviour, but challenges still exist in investigating the interaction between both electrical response and mechanical actions. This paper presents an electromechanical contact model that enables the electric potential and current intensity distributions as well as variations in electrical resistance of a particulate system to be analysed from both the particle and the system scale.

2. Modelling of electromechanical model

DEM [2] is employed to track the motion of particles under mechanical loadings. In addition, the particle center is regarded as the node and the path between two contacting particles is considered as a branch to formulate the contact resistance and bulk resistance for particle-particle and particle-wall interactions. Afterwards, this model is implemented into the EDEM commercial software package for calculating the electrical conduction of the particulate system under mechanical actions at each timestep. Fig. 1a shows the simulation procedure and the schematic of resistances considered at each particle and contact.

3. Validation

Single-particle compression test, particle-particle contact test, and particle bed test are created to validate the electromechanical model. From Fig. 1b, it can be seen that the electrical resistance of the single-particle compression and particle-particle test are in agreement with the published analytical solutions. For the particle bed test, steel particles with a diameter of 2 mm are packed into a cylindrical container with a diameter of 50 mm. The 0.1 A current is fed into particle bed system with 10 particle layers. It can be seen from Fig. 1b the results of the 3D simulations are in agreement with the experimental data, while the 2D simulations differ significantly from the experimental data due to the simplification of the particle contacts. Future work will apply the electromechanical model to the high-pressure torsion (HPT) [3] test to investigate the effect of geomaterials with different conductive properties on the electrical transmission across the system.

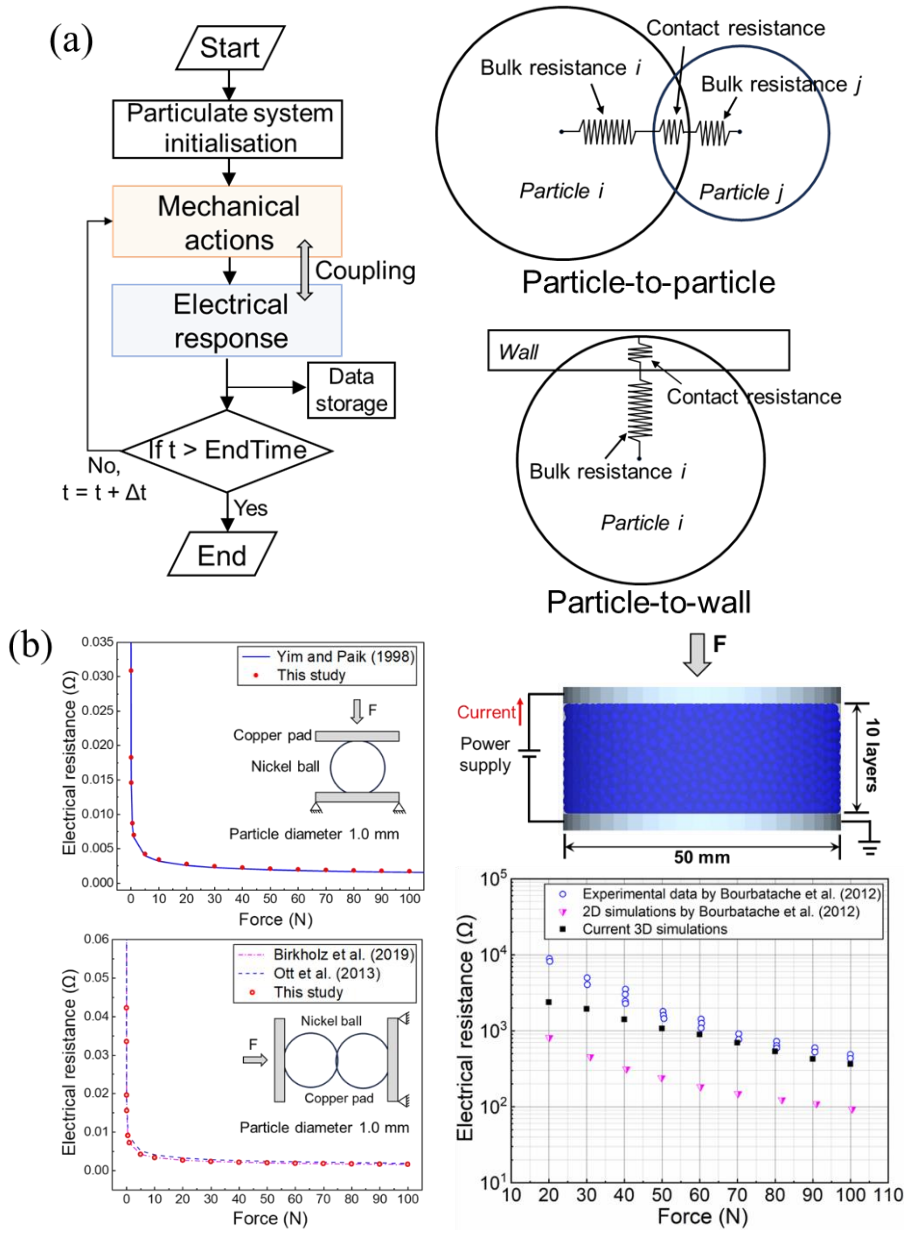

Figure 1 : a) Simulation procedure and schematic of electrical resistance modelling; b) verification and validation of the electromechanical contact model.

Acknowledgements

The authors would like to extend their gratitude to Prof. Roger Lewis and Dr William Skipper for sharing their experimental data and advices.

References

[1] Bourbatache, K., Guessasma, M., Bellenger, E., Bourny, V., Tekaya, A., 2012. Discrete modelling of electrical transfer in multi-contact systems. Granul Matter 14, 1–10.

[2] Cundall, P.A., Strack, O.D.L., 1979. A discrete numerical model for granular assemblies. Géotechnique 29, 47–65.

[3] Skipper, W., Nadimi, S., Gutsulyak, D.V., Butterfield, J.G., Ball, T., Lewis, R., 2023. Investigating the effect of different adhesion materials on electrical resistance using a high pressure torsion rig. Wear 532–533, 205116.

COUPLED PERIDYNAMICS AND DEM WITH UNSTRUCTURED GRID FOR EVALUATING THE EFFECT OF PARTICLE MORPHOLOGY ON FRACTURE BEHAVIOR

Y. Fukumoto[1], NSSP. Kalyan[2], RK. Kandasami[2] and T. Shimbo[3]

[1] Department of Civil and Environmental Engineering, Nagaoka University of Technology, Niigata, Japan

[2] Department of Civil Engineering, Indian Institute of Technology, Madras, Chennai, India

[3] National Institute of Technology, Ishikawa College, Ishikawa, Japan

1. Outline

The aim of this study was to investigate a 3-D numerical analysis technique, which combines peridynamics (PD) and the discrete element method (DEM), to handle both the fracture and post-fracture behavior of granular aggregates. In particular, the inclusion of unstructured grid into the coupled PD-DEM framework [1] to represent complex morphologies was thoroughly studied. The accuracy of the unstructured grid model was first verified through a simulation of indirect tensile tests on a cylindrical specimen. Then, structured and unstructured grid models were compared by fracturing various single particles with different morphologies and concavities. The obtained results were used to summarize the strengths and weaknesses of the unstructured grid model in assessing the fracture behavior influenced by realistic particle morphology.

2. Coupled peridynamics and DEM with unstructured grid

PD is a non-local, continuum-based, mesh-free method suitable for handling cases where cracks branch or where multiple cracks propagate simultaneously. Crack propagation is common in geomaterials [2], and PD is applied to a variety of problems in geotechnical engineering [1, 3]. In the present study, the bond-based PD is employed to reproduce the behavior from the initiation of cracks to fracturing. At the same time, the DEM is introduced to calculate the contact forces among the fragmented pieces after fracturing. The computational process of the physical contact between the wall elements and the computational nodes of the PD is also defined based on the DEM so that plane geometry boundaries can be used (see Fig. 1 (a)).

In addition to the above numerical procedure, an unstructured grid is newly introduced such that complex particle morphologies can be treated efficiently during particle breakage. Through the series of indirect tensile tests on the cylindrical specimen, the applicability of the unstructured grid to PD was examined in terms of the stress distribution and the grid resolution (see Fig.1 (b)).

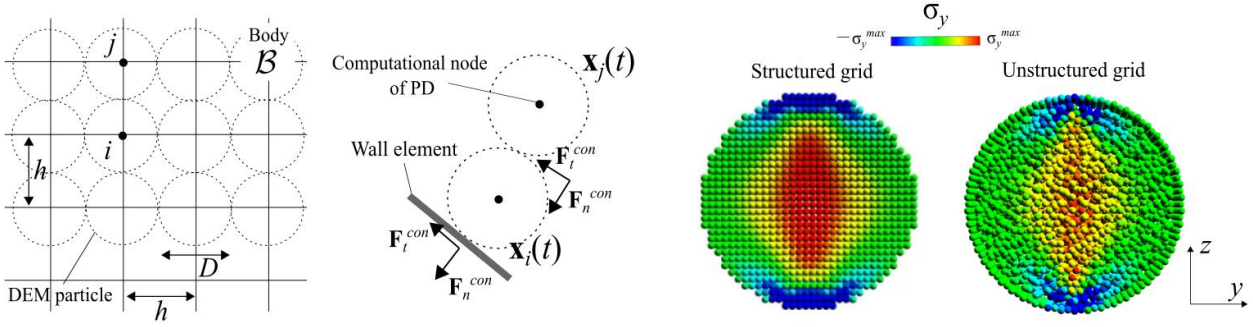

(a) Conceptual diagram of coupled PD-DEM

(b) Distribution of stress components

Figure 1. Verification of coupled PD-DEM with unstructured grid.

3. Fracture simulation of single particles with complex morphologies

A fracture simulation was conducted on single particles with complex morphologies to evaluate the effectiveness of the structured and unstructured grid models in solving engineering problems. Particle morphology, which includes roundness, the aspect ratio, angularity, concavity, and convexity, is a microscopic feature that significantly affects the macroscopic behavior of granular materials [4]. For the simulation, three distinct shapes with concave features were meshed using the structured and unstructured grids. The particles were classified into three categories based on their distinct shapes (bulky, elongated, and angular).

Figure 2 (a) depicts the initial arrangement of the computational nodes in the simulation model of the elongated shape with concavities. In the structured grid model, the nodes were placed on a regularly spaced orthogonal grid, whereas in the unstructured grid model, the nodes were placed on the vertices of the tetrahedral meshes that form the particle shape. The required number of computational nodes was 21,166 for the former case and 5,612 for the latter case, which means the unstructured grid model is advantageous in terms of the computational cost. In addition, a method of positioning the computational nodes at the mass center of the tetrahedral mesh was also considered.

An example of the calculation results is shown in Fig. 2 (b). The distribution of the local damage index is depicted for the two types of grid models. In comparing the two cases, it is seen that the final crack patterns are not the same. This is due to the difference in the contact areas and points between the loading plates and the particles. The structured grid model cannot reproduce the realistic condition of the point contacts. On the other hand, the unstructured grid model provides the advantage of realistically generating particle morphology at a lower computational cost.

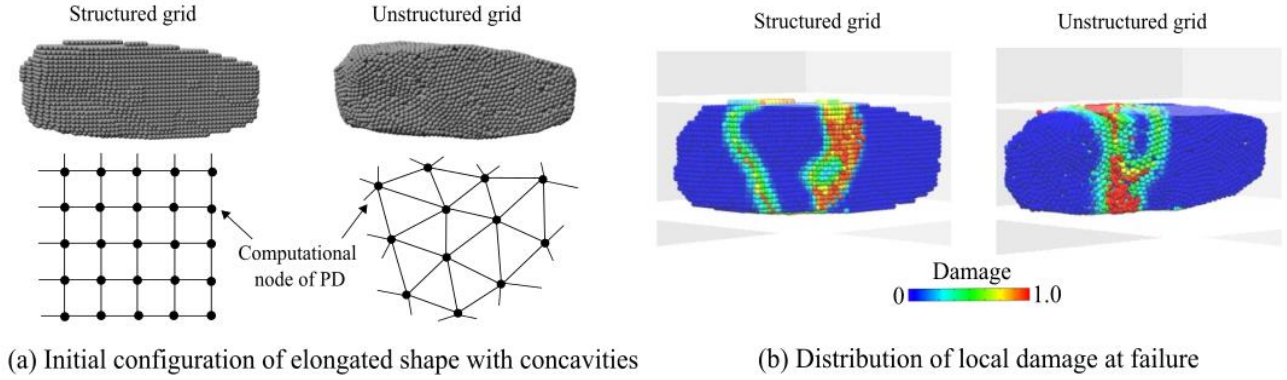

Figure 2. Numerical results of fracture simulation.

4. References

[1] Fukumoto, Y. and Shimbo, T. (2023). 3-D coupled peridynamics and discrete element method for fracture and post-fracture behavior of soil-like materials. *Computers and Geotechnics*, **158**:105372.

[2] Shimbo, T., Shinzo, C., Uchii, U., Itto, R., and Fukumoto, Y. (2022). Effect of water contents and initial crack lengths on mechanical properties and failure modes of pre-cracked compacted clay under uniaxial compression. *Engineering Geology*, **301**:106593.

[3] Shimbo, T., Itto, R., Inaba, K., Araki, K., and Watanabe, N. (2020). Seismic response analysis for ordinary state-based peridynamics in a linear isotropic elastic material. *Journal of Peridynamics and Nonlocal Modeling*, **2**:185-204.

[4] Kalyan, N.S.S.P. and Kandasami, R.K. (2023). Flow kinematics of granular materials considering realistic morphology. *Powder Technology*, **424**:118516.

DEM ANALYSIS OF PARTICLE SCALING IN DIRECT SIMPLE SHEAR TESTS

A. Sadrekarimi
University of Western Ontario, London, Ontario, Canada

1. Introduction

The direct simple shear (DSS) test is widely used to study the shearing behavior and liquefaction of saturated sands and tailings. Despite its several advantages, DSS shearing results could be affected by the limited dimensions of the sample compared to the size of soil particles being tested. This is often called "scale effect" and characterized as the ratio of sample dimensions (height, length, or diameter) to the median (D_{50}) or maximum (D_{max}) particle diameter.
This study examines scale effect associated with the number of particles and their sizes in a series of three-dimensional DEM simulations of DSS tests.

2. DEM Modeling

This study utilized the Particle Flow Code (*PFC3D*, version 6) developed by Itasca® to conduct DEM simulations of cylindrical DSS specimens. These specimens were confined within a series of 10 frictionless rings aimed at maintaining a constant cross-sectional area while enabling uniform shear deformations. Each ring, with an internal diameter (D) of 70 mm and a thickness of 2 mm, allowed for simulations of specimens initially set at a height (H) of 20 mm. The sample was then confined between two rigid frictional caps at its top and bottom surfaces.
The DEM models consisted of assemblies of numerous spheres with gradations parallel that of a Fraser River sand used in a parallel DSS laboratory testing program [1]. A cloud of overlapping spherical particles was first generated within the specimen boundaries. The specimen was then compressed by moving the upper rigid boundary downward until a vertical force correspond to the desired consolidation stress (σ'_{vc}) was achieved. The consolidation void ratio (e_c) was subsequently determined using the total volume of the specimen and the solid particles. Particle size and scale effect were examined by enlarging the particle sizes of the natural Fraser River sand by scaling factors (SF) of 7.1, 4.2, 3.7, 2.9, and 2.4. This produced DSS samples containing N = 1053, 5300, 10380, 21405, and 30,000 spherical particles with corresponding D_{max} of respectively 5.99, 3.59, 3.13, 2.48, and 2.05 mm.
Following preparation, the samples were uniformly sheared by translating the bottom wall at a prescribed rate of 6 mm/min until a shear displacement of 3 mm. Shear strain (γ) was calculated as the ratio of the horizontal displacement to the initial specimen height prior to shearing. Particles in contact with the bottom wall were forced to move with the wall to simulate a frictional boundary, minimize slippage at the specimen-wall interface (similar to the concentric blades on the top and bottom platens of the laboratory DSS device), and promote a uniform strain field within the specimen.
The DEM simulations employed five micromechanical parameters including particle density (ρ) = 2690 kg/m^3, effective modulus (E^*) = 100 MPa, normal-to-shear contact stiffness ratio (k_{ratio}) = 1.5, inter-particle friction coefficient (μ) = 0.7, and inter-particle rolling resistance coefficient (η) = 0.4. These parameters were calibrated based on the compression and shearing results of a series of laboratory DSS tests on a Fraser River sand [1].

3. Main Results

Figure 1 compares the drained stress-strain and volumetric strain behaviors of simulations carried out in this study. While the initial stiffnesses (i.e., tangent shear moduli) of the models are nearly the same, differences emerge with increasing shear strain. According to Figure 1a, large shear stress fluctuations occurred in the DEM model with the largest particle sizes (D_{50} = 1.67 mm). In samples with more particles such fluctuations however subsided, and the stress-strain trends became smoother. With additional particles and decreasing D_{50}, the mobilized shear stress (τ) and volumetric strain (ε_{vol}) respectively increased and decreased. Accordingly, models with more particles and smaller particle sizes were not only stronger but also experienced greater volumetric contraction. These changes were because of the sufficient space available for the finer particles to reorient and rearrange into a more compact fabric and form a shear zone amid the lower interference by the sample boundary. This resulted in improved particle interlocking and the mobilization of higher shear strengths. Nonetheless, the effect of particle size diminished in simulations with D_{50} of 0.69 mm (H/D_{max} = 8.1) and 0.57 mm (H/D_{max} = 9.7) as these models exhibited very similar shear stress-strain and ε_{vol} behaviors in Figure 1. While H/D_{max} = 8.1 and 9.7 at which scale effect diminished in the DEM simulations of this study are lower than the H/D_{max} threshold of 10 recommended by the ASTM D6528 standard procedure [2] for DSS testing, they are consistent with the DEM simulations of Chang et al. [3] and Li et al. [4] showing comparable shear strengths, similar principal stresses, and more uniform distributions of particle contact forces in DSS models with $H/D_{max} \geq 7.0$.

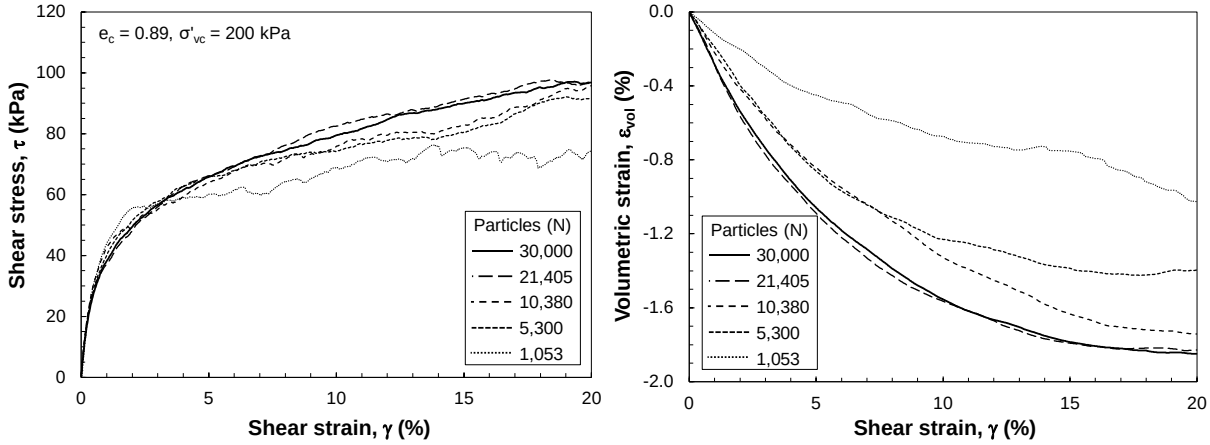

(a) (b)

Figure 1. Comparisons of (a) shear stress-strain and (b) volumetric strain behaviors of DSS simulations with different numbers of particles at σ'_{vc}= 200 kPa.

4. Reference

[1] Jones, S. (2017). *Liquefaction susceptibility analysis of Fraser River sand in miniature cone penetration tests and cyclic direct simple shear tests*, The University of Western Ontario.

[2] ASTM (2017). Standard D6528: Standard Test Method for Consolidated Undrained Direct Simple Shear Testing of Fine Grain Soils. in, *Annual book of ASTM Standards* (ASTM International: West Conshohocken, PA).

[3] Chang, W. -J., Phantachang, T. and Leong, W. -M. (2014). Evaluation of size and boundary effects in simple shear tests with distinct element method. In *World Congress on Advances in Civil, Environmental, and Materials Research (ACEM14)*. Busan, Korea.

[4] Li, Y., Li, J., Zhu, T. and Han, K. (2021). Size effect on contact behavior in DEM simple shear tests, *Nature Scientific Reports*, 11: 1 - 10.

DEM Analysis on Drained and Undrained Fabric evolution under Cyclic Loading

A.I. Theocharis[1], A. Papadimitriou[2] and E. Vairaktaris[1]
[1] National Technical University of Athens, Athens, Greece

1. General

The response of granular materials to cyclic loading is a critical aspect of geotechnical engineering, with far-reaching implications for civil engineering structures. Understanding the evolution of fabric within these materials under drained and undrained conditions is fundamental to predicting their behavior. The interplay between particle-scale interactions, pore water pressure, and fabric evolution plays a pivotal role in determining the macroscopic mechanical response of granular assemblies. In recent years, the Discrete Element Method (DEM) has emerged as a powerful tool for simulating the discrete interactions among individual particles within granular materials. This approach allows for a detailed investigation of micro-scale phenomena, enabling researchers to unravel the complex dynamics of particle contacts, forces, and porosity. This study aims to contribute into the variations in fabric evolution under drained and undrained conditions during cyclic loading. By employing the DEM, it delves into the intricate mechanics that dictate how granular materials respond to cyclic loading, considering the role of pore water pressure in shaping their fabric evolution.

2. DEM simulations and fabric evolution

The Discrete Element Method (DEM) enables a particle-scale analysis of granular mechanics, offering profound insights into fabric evolution and its significance in the macroscopic response of soils. In this study, a 2D DEM analysis is employed under both constant and changing volume conditions to simulate drained and undrained scenarios, commonly encountered in practice. Given the consistent correlation between fabric evolution in 2D and 3D, the former is deemed suitable for the current analysis, supported by periodic boundaries to mitigate localizing effects.

To ensure relevance, grains with slight elongation and a distribution providing comparable (albeit qualitative) results to 3D soil response are utilized. DEM samples are initialized as a cloud of particles isotropically consolidated to an initial state under a hydrostatic pressure of 200 kPa. Biaxial loading, initially under constant volume and subsequently under constant horizontal stress, is applied to assess stress-strain evolution. The results exhibit a typical stress-strain response, progressing with loading increments and reaching a critical state at approximately 7% vertical strain (for constant hydrostatic stress loading). In the case of constant volume loading, zero volumetric strain and an increase in stress ratio are identified. Fabric, starting from an almost zero initial value indicative of isotropic fabric, increases significantly for both loading scenarios.

After validating the sample, two cyclic loading types are applied at the isotropically consolidated state: one maintaining constant volume to simulate undrained conditions, and the other involving a constant horizontal stress (p=200 kPa) with cyclic vertical stress evolution, indicating volumetric changes. The primary focus is on fabric evolution, specifically comparing the two loading types. The macroscopic stress-strain results are depicted in Figure 1, while Figure 2 illustrates the norm evolution of fabric.

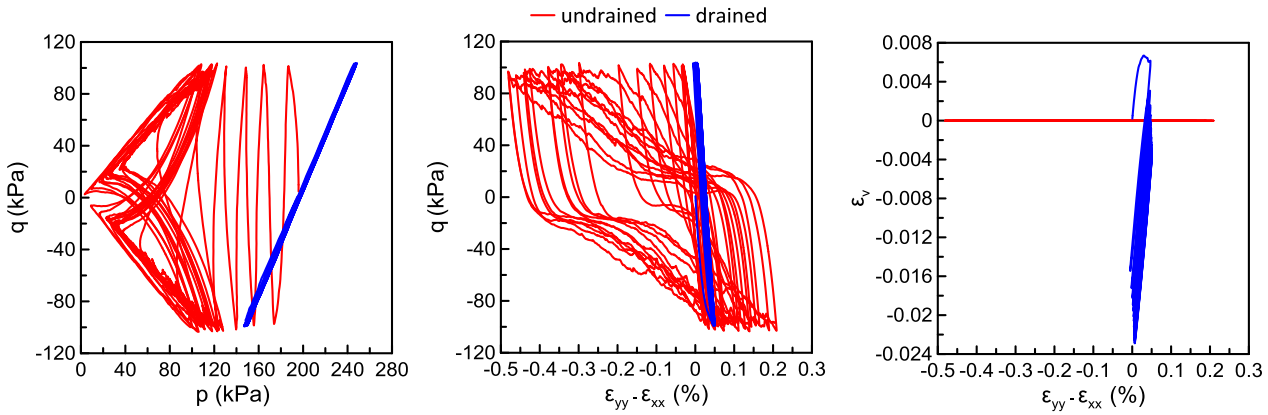

Figure 1 : Macroscopic cyclic response for constant horizontal stress and constant volume condition (a) deviatoric vs hydrostatic stress, (b) deviatoric stress and (c) volumetric strain with vertical horizontal strain difference

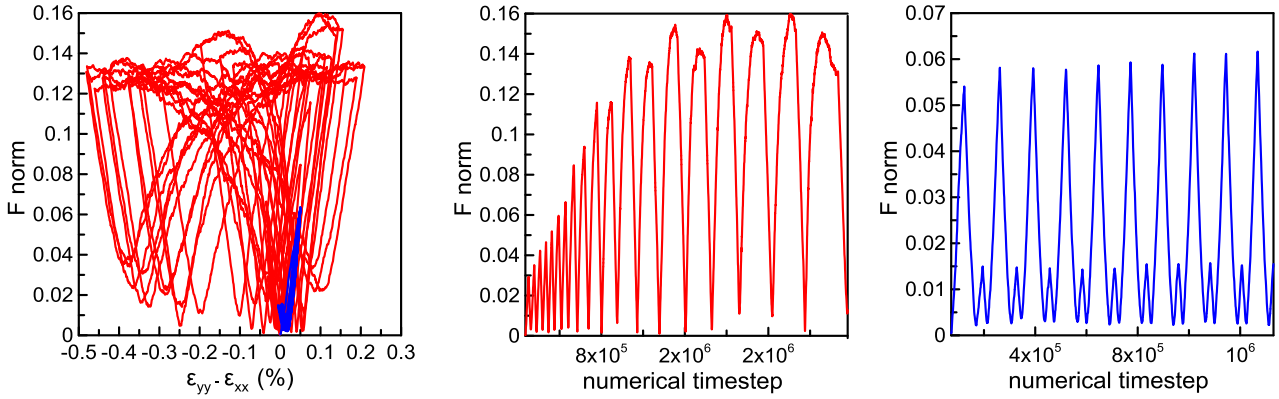

Figure 2 : Fabric norm evolution during cyclic loading for the initial 10 cycles (a) with constant volume and (b) with constant horizontal stress

3. Conclusions

Distinct fabric response is presented for the two loading conditions. For constant volume, during each loading cycle the fabric increases to one peak approximately when the deviatoric stress reaches its minimum (Figure 1(a)) and then decreases and increases to a next peak value when the deviatoric stress reaches its maximum. When the deviatoric stress passes from zero the fabric norm also decreases close to zero. The peak fabric norm that increases cycle with cycle until it reaches a maximum of about 0.15. For the drained conditions the fabric norm is more periodic from the first cycle. It reaches a maximum value approximately when the deviatoric stress reaches its minimum (Figure 1(a)) and then decreases. A second small increase takes place when the deviatoric stress reaches its maximum value. When the deviatoric stress passes from zero the fabric norm also decreases close to zero. The maximum peak fabric norm remains at approximately 0.05-0.06during all cycles.

DEM MODELING OF TRANSVERSELY ROCK AS APPLIED TO BOREHOLE STABILITY

Marte Gutierrez[1] and Guowen Xu[2]
[1] Civil & Environmental Engineering, Colorado School of Mines, Golden CO 80401, USA
[2] Southwest Jiaotong University, Chengdu 610031, Sichuan, China

1. Summary

A new numerical approach based on the particle discrete element method (PDEM) is put forward to investigate the mechanical behavior of transversely isotropic rocks with non-continuous planar fabrics. In this numerical model, the rock matrix and fabric are represented as flat joint contacts and smooth joint contacts, respectively. The following are studied using the numerical model: (1) the effects of the micro-structure of the rock matrix and the fabric micro-parameters on the shear strength and the fracture patterns of rocks under Brazilian tests, and (2) the model calibration process for determining the micro-parameters and the failure process of borehole stability in layered rock. The results show that: (1) Based on the Brazilian test results of 20 kinds of transversely isotropic rocks with non-continuous planar fabrics, six patterns regarding the relationship between the normalized failure strength (NFS) and fabric-loading angles are obtained; (2) The patterns of NFS curves are slightly affected by the coordination numbers of particle in rock matrix, while greatly affected by the amount of pre-existing micro-cracks in rock matrix, and the stiffness, strength and distributed region of the fabrics; (3) The calibrated results of six typical rocks with different patterns agreed well with the experimental results in regard to failure strength and fracture patterns; (4) The fracture of layered surrounding rock after borehole excavation is concentrated in two zones with the line connecting the center of the two zones is normal to the plane of non-continuous fabrics for isotropic geo-stress field, while the connecting line is deflected to the direction of minor principal str**.**

2. Methodology

The particle DEM is widely used to study the crack initiation, propagation and coalescence of rocks. In this article, a new numerical approach based on the particle DEM code PFC2D60 is put forward to study the mechanical behavior of transversely isotropic rocks with non-continuous fabrics under Brazilian tests. In this DEM model, the flat joint contact (FJC) model is used to represent rock matrix and the smooth joint contact (SJC) model is used to represent fabrics.

The following process was adopted to determine the micro-parameters of specific rocks:.(1) Determine the micro-parameters relating to deformation. For θ=0°, the SJC stiffness has the least impact on the rock deformation. Therefore, the stiffness of FJC and particles were calibrated to match E0 (elastic modulus for θ=0°) obtained from laboratory tests. In this stage, the stiffness of FJC and particles are set equal to reduce the number of calibrated parameters. For θ=90°, the SJC stiffness has the largest influence on the rock deformation. Thus, the SJC stiffness was calibrated through E90 (elastic modulus for θ=90°) obtained from laboratory tests. (2) Determining the micro-parameters relating to strength. For θ=90°, the SJC strength has the least influence on the rock strength. Thus, the strength of FJC($\bar{\sigma}_c$, $\bar{\tau}_c$, φ_b) was calibrated through σ90 (strength for θ=90°) obtained from laboratory tests.

3. Main Results

Figure 1 shows typical results from the DEM modeling of transversely isotropic rock under Brazil Splitting Test. The main conclusions of this study are as follows: (1) Based on the Brazilian test results of 20 kinds of transversely isotropic rocks with non-continuous planar fabrics, six patterns regarding the relationship between the normalized failure strength (NFS) and fabric-loading angles are obtained. Pattern I shows the feature of U shape distribution. The NFS of Pattern II and VII maintains a constant value from 0° to 30°-60°, then followed by a linear increase and decrease, respectively. The NFS of pattern IV fluctuates slightly within a small region, while the NFS for pattern III increases linearly with the increase of fabric-loading angles. Pattern V corresponds to an increase in NFS from 0° to 45°-70°, after which it remains unchanged. (2) The patterns of NFS curves are slightly affected by the coordination numbers of particle in rock matrix, while greatly affected by the amount of pre-existing micro-cracks in rock matrix, and the stiffness, strength and distributed region of the fabrics. (3) The calibrated results of six typical rocks with different patterns agreed well with the experimental results regarding failure strength and fracture patterns. (4) The fracture of layered surrounding rock after borehole excavation is concentrated in two zones with the line connecting the center of the two zones is normal to the plane of non-continuous fabrics for isotropic geo-stress field, while the connecting line is deflected to the direction of minor principal stress to a certain extent for non-isotropic geo-stress field.

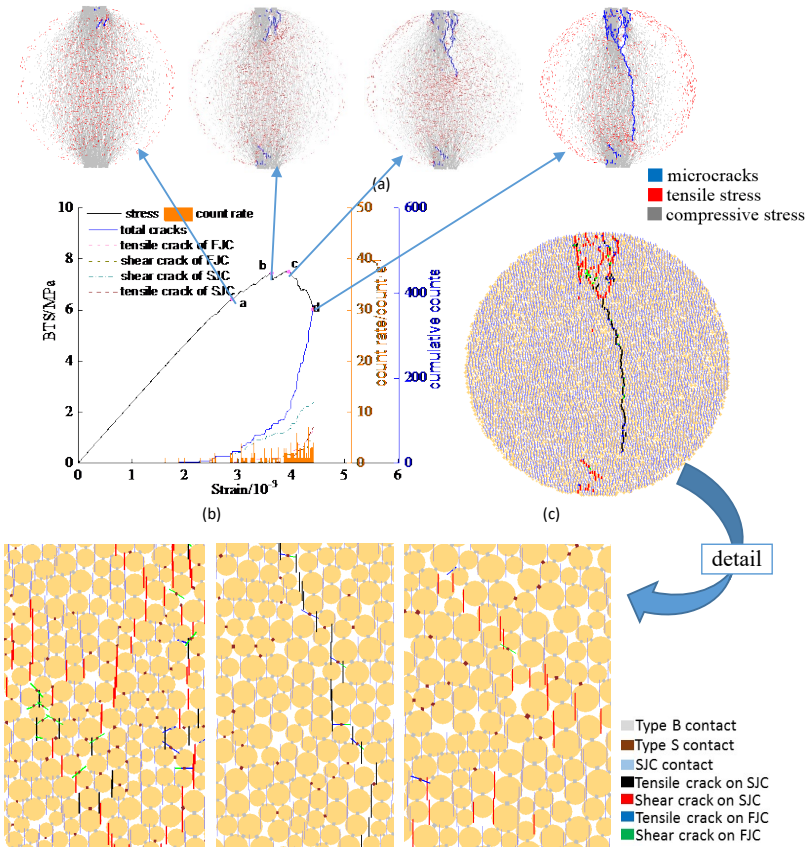

Figure 1. Failure process of specimen for LG GS with θ=45°: a contact force between particles; b failure strength versus strain and number of micro-cracks; c detailed failure pattern.

DEM analysis on soil horizontal support mechanism of monopile subjected to monotonic lateral loading.

Shogo Ishii[1], Hirokazu Akagi [1] and Koki Kitamura[1]
[1] Waseda University, Tokyo, Japan

1. Introduction

Monopiles are the dominant foundation for offshore wind turbines. Monopiles are large-diameter, stubby piles and, unlike the piles conventionally used mainly in the ocean platform, a monopile design method considering the horizontal and rotational resistance at the base of the pile is required [1]. In most of the currently proposed monopile design methods, soil reaction forces acting on the monopile are expressed using soil springs [2]. Actually, the source of the soil reaction is not the soil spring but the shear resistance of the surrounding soil. In order to establish a sophisticated monopile design method, it is necessary to understand the lateral resistance mechanism of monopile not from the soil reaction forces but generated from the resistance of the surrounding soil. In this study, the soil horizontal support mechanism of monopile was investigated through model experiment using aluminum bars and numerical simulation using Discrete Element Method (DEM) [3].

2. Model experiment

Figure 1 shows the 2D experimental apparatus. The model ground was made of a mixture of 1.6 mm and 3.0 mm diameter aluminum bars at a mass ratio of 2:1. The target density γ of the model ground was 21.6 kN/m^3. Model piles (diameter D = 20 mm, slenderness ratio L/D = 3, 4, 5, 6) were used in the experiments. The monotonic lateral load was applied to 120 mm height from the ground surface. The lateral load and displacement of monopile were measured, and the ground deformation was quantitatively evaluated by image analysis using Particle Image Velocimetry (PIV).

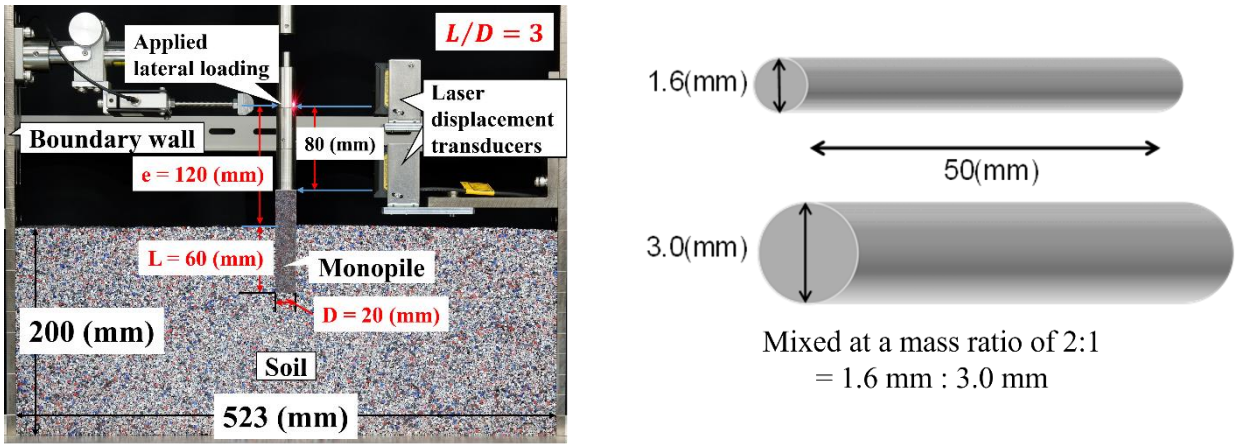

(a) Whole view (b) Allluminum rod

Figure 1. Experimental apparatus (slenderness ratio $L/D = 3$)

3. DEM analytical model

Figure 2 shows the 2D analytical model of the model experiment. In the analytical model, the soil was constituted by DEM particles and the pile and walls by rigid line elements. To evaluate soil reaction forces acting on the pile, Pisa design model [2] was used. The soil reaction forces were calculated using the divided elements at the embedded area shown in Figure 2(b).

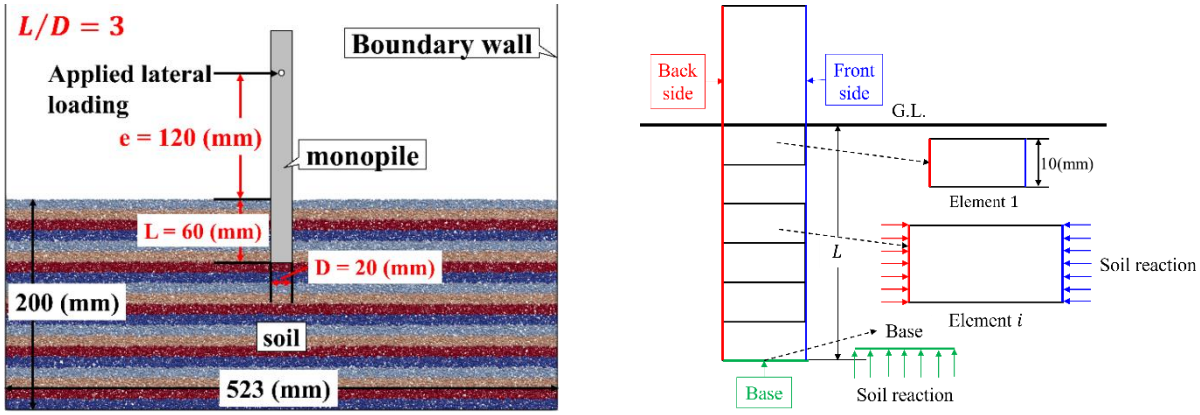

(a) Whole view (b) Divided elements of embedded area

Figure 2. 2D analytical model (slenderness ratio $L/D = 3$)

4. Resistance zone of surrounding soil around monopile

Figure 3 shows the particle displacement vector and maximum shear strain (cumulative) obtained from the DEM analysis. The particle displacement vector shows that the surrounding ground resists by forming a passive zone in front of the monopile, an active zone at the back and a rotational zone at the bottom. The maximum shear strain distribution shows that the resistance region of the surrounding ground gradually evolves to form the resistance zone in the ultimate state.

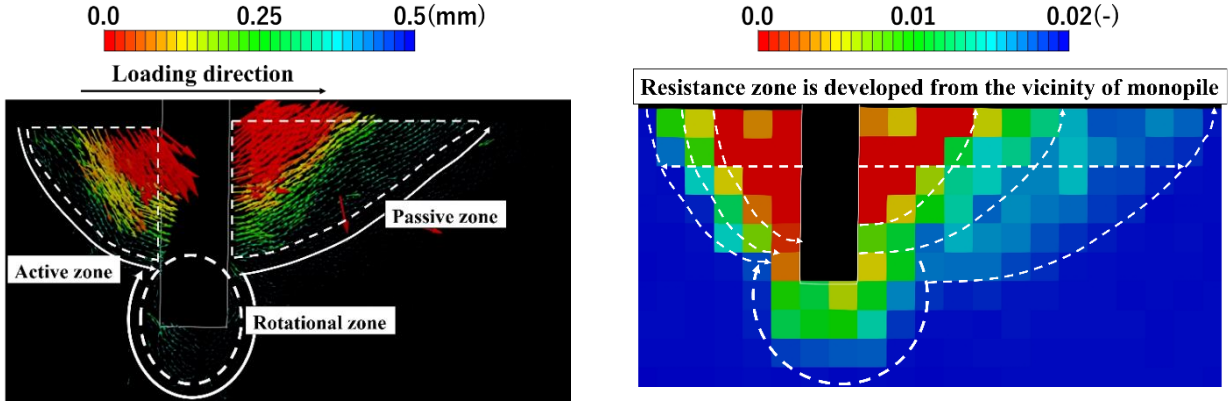

(a) Particle displacement vector (b) Cumlative maximum shear strain

Figure 3. Resistance zone of surrounding soil around monopile at ultimate state

5. References

[1] Burd, H. J., Taborda, D. M. G., Zdravkovic, L., Abadie, C. N., Byrne, B. W., Houlsby, G. T., Gavin, K. G., Igoe, D. J. P., Jardine, R. J., Martin, C. M., McAdam, R. A., Pedro, A. M. G., & Potts, D. M. (2020). PISA design model for monopiles for offshore wind turbines: application to a marine sand. Géotechnique, 70(11), 1048–1066.

[2] Cundall, P. A. and Strack, O. D. L. (1979). A discrete numerical model for granular assemblies, Géotechnique, Vol.29 (1), pp 47-65.

[3] Takahashi, A., Omura, N., Kobayashi, T., Kamata, Y., and Inagaki, S. (2022). Centrifuge model tests on large-diameter monopiles in dense sand subjected to two-way lateral cyclic loading in short-term. Soils and Foundations, 62(3), 101148.

DEM exploration of stress transmission and small strain behaviour for rubber sand mixtures

DeYun Liu[1], Zhenyu Yin[1] and Catherine O'Sullivan[2]
[1] Department of Civil & Environmental Engineering, The Hong Kong Polytechnic University, China
[2] Department of Civil & Environmental Engineering, Imperial college London, UK

1. General

This study presents a method to create rubber clumps within the framework of the Discrete Element Method (DEM), enhancing the understanding of particle-scale stress transmission and small strain stiffness in sand-rubber mixtures. The approach underwent meticulous calibration, including single particle compression, calibration of small strain stiffness, G_0, and shearing behaviour to capture the key characteristics of rubber materials, with the deformability of rubber materials being simulated. This model indicated a higher coordination number for rubber clumps, a result of their inherent deformability and significant sensitivity to stress levels compared to these of sand. Besides, the research further demonstrated that the stress transferred by the rubber remained below its volumetric content, illustrating a significant sensitivity to stress and density levels, a characteristic not observed in sand particles. Additionally, no clear threshold was identified in the transition from sand-dominated to rubber-dominated behavior, denoting a continuous shift with increasing rubber content. Analysis also shows a decrease in the small-strain stiffness values with increasing rubber content, emphasizing the negligible contributions of rubber materials to the G_0 values, especially in contrast to their substantial role in stress transmission. This study thereby offers a robust foundation for studying sand-rubber mixtures.

2. Methods

In the study, DEM simulations utilized a modified version of LAMMPS, an open-source molecular dynamics code (Plimpton, 1995). As presented before, to capture the particle scale deformability of rubber clump, a bonded sphere method was adopted. Each model is made of 12 constitutes spherical grains whose centroids are the vertices of a regular icosahedron, achieving perfect symmetry (Fig. 1a). The position vectors for these vertices were scaled down to ensure a fairly spherical rubber clump, which is quantified by its clump sphericity. This sphericity of rubber clumps is calculated by its volume and surface area, which are estimated by the Monte Carlo method (i.e., Ross & Marshak, 1991) showing a sphericity approximately of 0.9. The constituent spheres are connected by bonds with 30 same bonds being employed to create one rubber clump. This bond model of bpm/rotational model, integrated into the main LAMMPS, bonded particle models (BPM) package was used. As well as accounting for the typical normal force components, this model effectively resolves tangential forces and torques resulting from shearing behaviour, as well as bending and twisting components of the bond stemming from the rotation or displacement of particles. This BPM, with its comprehensive capabilities, emerges as a viable option for accurately representing the multifaceted deformation behaviors of rubber.

3. Key results

This study demonstrates a method of generating rubber clumps in DEM, significantly enhancing the comprehension of particle-scale stress transmission and small-strain stiffness in sand-rubber

mixtures.1. This study proposed a model for replicating the complex interactions for rubber clumps, capturing normal, tangential, bending and twisting components of rubber clump to simulate its deformability. This model underwent an extensive calibration process, including single particle compression, calibration of G_0 and shearing behaviour, showing an alignment with experimental observations. 2. A observation from this study was the higher coordination number associated with rubber clumps compared to that of sand. This characteristic was primarily a consequence of rubber's deformable nature, leading to a strong sensitivity to stress levels and packing densities for coordination number. Particularly, sand exhibits negligible response to stress level, while the coordination number associated with rubber clumps is strongly affected by stress level. 3. The study further analyzed stress transmission in sand-rubber mixtures, demonstrating that the stress carried by the rubber content consistently remained below its volume content. This phenomenon, coupled with its strong sensitivity to variations in both stress and density levels, offers a contrast to the behaviour observed in sand. Moreover, the particle scale stress transmission shows a continous shift from sand-dominated to rubber-dominated behaviour with no discernible threshold point. 4. The small strain stiffness, G_0 of sand-rubber mixtures has been studied, showing distinctive contributions from sand and rubber materials to the G_0 values. This study highlights a negligible effect of rubber clumps to G_0 values, particularly when compared to their participation in stress transmission. Refined state variables which consider rubber materials as void, show better performance in capturing the G_0 behaviour in a unified way. This detailed understanding is essential in refining the approach to engineering applications involving these mixtures.

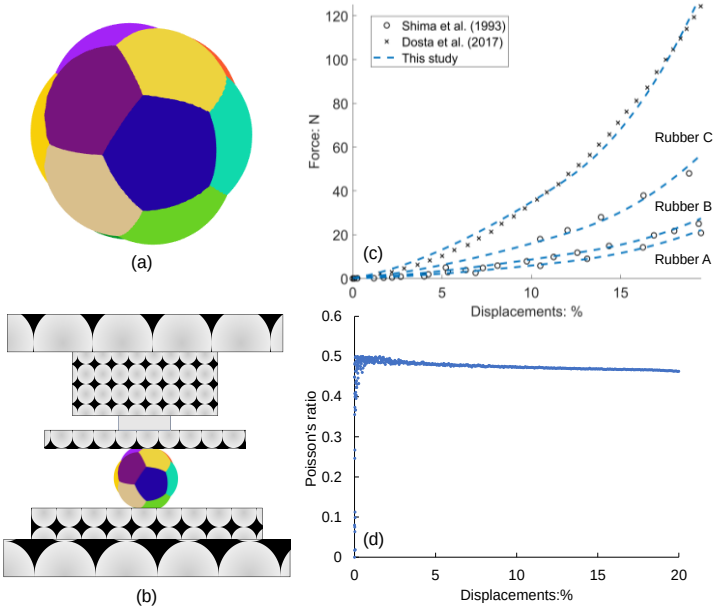

Figure 1. calibrations of rubber clumps

5. References

[1] Plimpton, S. (1995). Fast parallel algorithms for short-range molecular dynamics. Journal of Computational Physics, 117(1), 1–19.

[2] Ross, J., & Marshak, A. (1991). Monte Carlo Methods BT - Photon-Vegetation Interactions: Applications in Optical Remote Sensing and Plant Ecology (R. B. Myneni & J. Ross (eds.); pp. 441–467). Springer Berlin Heidelberg. https://doi.org/10.1007/978-3-642-75389-3_14

DEM INSIGHTS INTO CYCLIC LIQUEFACTION: EXAMINING PARTICLE SIZE DISTRIBUTION AND SHAPE

***S. Banerjee*[1], *M. Yang*[1,2], *and M. Taiebat*[1]**
[1] *University of British Columbia, Vancouver, BC, Canada*
[2] *Northwestern University, Evanston, IL, USA*

Cyclic liquefaction, a phenomenon with significant implications in geotechnical engineering, is profoundly influenced by the characteristics of granular materials. This study reports a comprehensive investigation into the isolated effects of particle size distribution (PSD) and shape on cyclic liquefaction resistance of granular materials at varying relative densities, utilizing the Discrete Element Method (DEM). Figure 1 presents snapshots of four selected samples with different size distributions or shapes used in this study.

The study begins by examining the effect of PSD on cyclic liquefaction resistance using spherical particle assemblies. The coefficient of uniformity (C_u) is employed to describe the PSD, with samples prepared to possess equivalent mean particle sizes and log-linear PSDs. Samples are meticulously prepared at different relative densities (D_r) and initial confinement pressures. These samples then undergo constant-volume cyclic simple shearing with varied cyclic stress ratios until reaching the point of initial liquefaction. Our results reveal that the relationship between C_u and cyclic liquefaction resistance demonstrates non-linear behavior, influenced again by D_r. At lower D_r, an increase in C_u from 1 to 1.5 increased the cyclic liquefaction resistance and a further increase in C_u reduced the resistance. Conversely, for samples at higher D_r, the trend was reversed, with an initial decrease in the liquefaction resistance followed by an increase beyond C_u = 2.0.

Furthermore, we investigate the influence of particle shape on the liquefaction resistance of granular materials. Superquadric particles, distinguished by two key parameters - aspect ratio (AR) and blockiness (B), are employed to model a range of particle shapes. Our findings highlight intriguing trends: the liquefaction resistance distinctly varies for different particle shapes under differing D_r conditions. In other words, the effects of particle shape, represented by varying AR and B, on cyclic liquefaction resistance did not exhibit a clear monotonic trend at different levels of D_r, and the resistance showed varying responses to changes in AR and B. For samples at lower D_r, spherical particles demonstrated higher cyclic liquefaction resistance compared to non-spherical particles. However, this trend was reversed when examining higher D_r, where spherical particles exhibited lower liquefaction resistance than non-spherical particle assemblies. Utilizing the overall regularity (OR) as a synthetic descriptor of particle shape, we observe that liquefaction strength exhibits varying correlations with OR across different D_r scenarios.

To find the link between the macro-scale observations and the initial state, we extracted initial values of various macroscopic quantities and micro-scale descriptors from the samples prior to cyclic shearing. The initial void ratio or mechanical coordination number alone did not necessarily show a clear trend with the resulting liquefaction resistance. We adopted a protocol for a monotonic simple shear test under constant mean stress to assess the void ratios and mechanical coordination numbers of the samples at the critical state, hence extracting the initial values of the macro and micro state parameters, respectively. These state parameters were observed to present a good monotone relationship with the liquefaction resistance, irrespective of relative density, particle shapes, or coefficient of uniformity. Among these, the state parameter associated with the mechanical coordination number appeared to link better with the liquefaction resistance. Additional details are presented in [1, 2]. This research provides crucial insights into the distinct influences of these granular material characteristics, enabling more precise considerations when dealing with cyclic liquefaction in diverse geological conditions.

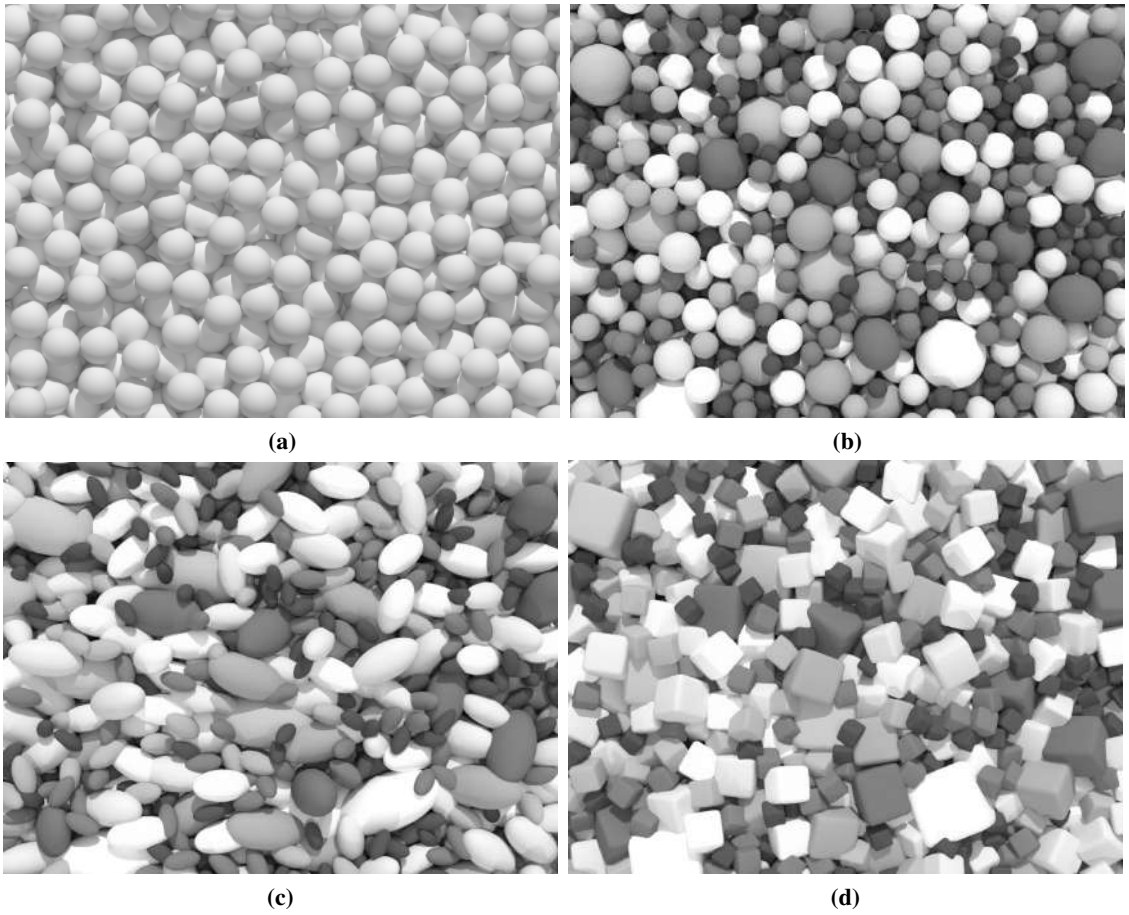

Figure 1. Snapshots of samples with different particle size distributions and shapes.

References

[1] Banerjee, S. K., Yang, M., and Taiebat, M. (2023). Effect of coefficient of uniformity on cyclic liquefaction resistance of granular materials. *Computers and Geotechnics*, **155**, 105232.

[2] Banerjee, S. K., Yang, M., and Taiebat, M. (2024). Effect of particle shape on cyclic liquefaction resistance of granular materials. *Acta Geotechnica*.

DEM modelling of highly porous soft rocks

Jinhui Zheng[1], Matteo Ciantia[1], Marco Previtali[1] and Jonathan Knappett[1]
[1] University of Dundee, DUNDEE, UK

1. Introduction

Chalk and calcarenite, typical representatives of high-porous soft rocks, are formed through sedimentation and diagenesis process of calcium carbonate microorganisms (Ciantia et al., 2015). They are often characterized by irregular-shaped grains connected by carbonate bonds, as well as intra- and inter-granular voids. Notably, these high-porous materials demonstrate loading sensitivity (Shahin et al., 2019), showing an elastic response under small loads. However, at higher loadings, the abrupt collapse of the internal structure and degradation of intergranular bonds lead to changes in void volume and the formation of compaction and or shear bands , resulting in a denser granular material.

Understanding the behaviour of these rocks is of great concern to engineering, especially for accurately predicting the driving resistance of piles. The complex responses of porous carbonate rocks can be attributed to the bond damage observed at the micro-scale (Shahin et al., 2019). Although various laboratory tests and theoretical models have been employed to investigate the underlying mechanisms, many have focused on the macro response. Recently, more detailed insights have been revealed from a micro-scale perspective using X-ray microtomography or CT-scan techniques (xxxx). These insights include correlations between the inclination angle of compaction bands and confining pressure, as well as relationships between the length of the constant stress plateau period and the formation and evolution of compaction bands (Leuthold et al., 2021). Meanwhile, many constitutive models have been proposed to describe the hardening and softening behaviour related to the degradation of interparticle bonds (Lagioia and Nova, 1995).

To better understand the macroscopic effects of high-porous soft rocks whilst revealing the underlying micromechanical mechanisms like the evolution of compaction and shear bands. A novel coupled damage-plasticity discrete element method (DEM) contact model for high-porous soft rocks implemented as a user defined model in PFC3D is presented.

2. Novel bond damage model

The interparticle contact forces (N, V) and bending moment ($\breve{M}$) are calculated based on the plastic bond displacements (u_n^p, u_s^p, θ_b^p) and are calculated as follows:

$$\begin{bmatrix} N \\ V \\ \breve{M} \end{bmatrix} = \begin{bmatrix} (1-D)k_n^0(u_n - u_n^p)A \\ (1-D)k_s^0(u_s - u_s^p)A \\ (1-D)k_b^0(\theta_b - \theta_b^p)/\bar{R} \end{bmatrix} \quad (1)$$

The bond damage variable D is calculated in the following form:

$$D = 1 - e^{-\left(\frac{\left|u_n^p\right|}{u_n^c} + \frac{u_s^p}{u_s^c} + \frac{\theta_b^p}{\theta_b^c}\right)} \quad (2)$$

The plastic displacemnts are calculated based on traditional generalised associated flow rule and more details can be found in (Zheng, et al., 2023). In addition, this model also incorporate far-field

interaction features between grains. This feature enables the consideration of physical contact distribution among irregular particles and presence of broken bonds whilst using spherical particles.

3. Model performance

The contact model was calibrated using element test results of a typical high-porous soft rock, Maastricht calcarenite (Leuthold et al., 2021). A good agreement between test and simulation is presented in Fig. 1. Under low confinement, a significant collapse after peak is captured, while under high confinement, a constant stress plateau can be found due to a transition stage of the intact rock transforms to soil-like granular material as the bond degradation evolve and the unbonded particles come into contact.

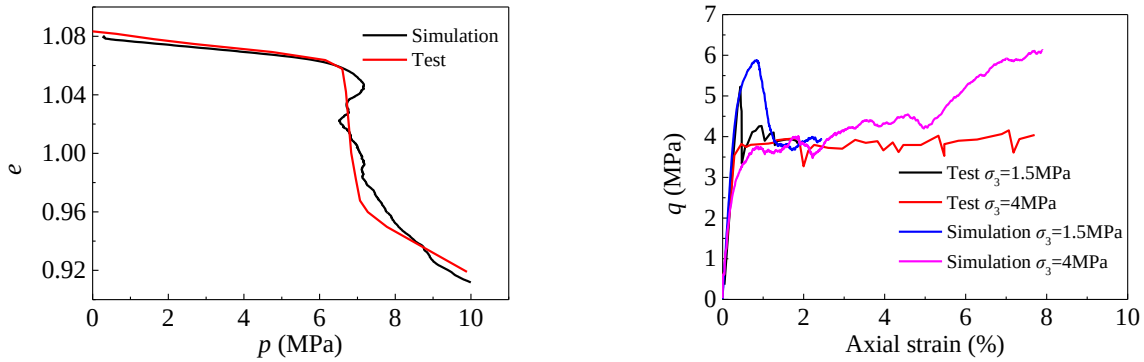

Figure 1.Calibrated results: Isotropic test (left) and Triaxial test (right).

4. Conclusion

To investigate the mechanical behaviour of high-porous rocks and identify the corresponding mechanism from a micro perspective, a novel bond damage model, which introduces a damage variable to produce strain-softening and far-field interaction, has been developed. The results show that this model can reproduce the void collapse and capture the constant stress plateau (bond degradation phase) before reaching the critical state of the debonded material.

5. References

[1] Ciantia M.O., Castellanza R., Crosta G.B., et al. (2015). Effects of mineral suspension and dissolution on strength and compressibility of soft carbonate rocks. *Engineering Geology*, **184**:1-18.

[2] Leuthold J., Gerolymatou E., Vergara M.R., et al. (2021). Effect of compaction banding on the hydraulic properties of porous rock: part I—experimental investigation. *Rock Mechanics and Rock Engineering*, **54**:2671-2683.

[3] LAGIOIA R. & NOVA R. (1995). An experimental and theoretical study of the behaviour of a calcarenite in triaxial compression . *Geotechnique*, 45(4) :633-648.

[4] Shahin, G., Papazoglou, A., Marinelli, F., & Buscarnera, G. (2019). Simulation of localized compaction in Tuffeau de Maastricht based on evidence from X-ray tomography. *International Journal of Rock Mechanics and Mining Sciences*, **121**:104039.

[5] Zheng, J., Previtali, M., Ciantia, M.O., Knappett, J.A. (2023). Micromechanical Numerical Modelling of Foundation Punching in Highly Porous Cemented Geomaterials in a Virtual Centrifuge Environment. In Palermo (Ed.), *CNRIG 2023*, **pp**:390-397.

DEM modelling of rock block impact on rock bed.

Vergara, Alvaro [1], Palma, Sergio [2] & Fuentes, Raul [1]
[1] Institute of Geomechanics and Underground Technology, RWTH Aachen, Germany
[2] Complex Fluids Laboratory, Universidad Técnica Federico Santa María, Santiago, Chile.
Research and Innovation in Mining Group (RIMG), Universidad Técnica Federico Santa María, Santiago, Chile.

Rockfall events pose significant challenges in geotechnical engineering, especially in designing protective structures for roadways and mountainous regions. While traditional studies have focused on impact forces for containment design, less attention has been given to understanding rock fracture as a result of these events. This research fills this gap by utilizing the Ansys Rocky DEM software, to analyze rock breakage under energy-based conditions in rockfall scenarios.

An integral part of this study is the application of the Fast-Breakage Method, to simulate the process of impact-induced fracture in rock systems. This method allows for the examination of a buffering layer's response when impacted by a rock block, with a special focus on energy considerations. Specifically, it examines the cumulative specific impact energy and its influence on the probability of rock block breakage, marking a departure from conventional studies that mainly focus on impact forces and block shapes.

The study explores various parameters, including the size ratio of impacting and impacted rocks and the velocity of impact, from an energy perspective. This approach facilitates a comprehensive understanding of fracture patterns and breakage probabilities under different scenarios. Findings highlight the critical role of the impacting rock's shape and size in determining fracture patterns, where even low energy levels can lead to significant rock fragmentation due to the forces generated within the system.

The implications of these findings are multifaceted. Primarily, they enhance our understanding of rockfall as a physical phenomenon, aiding in the design of more effective containment measures. Additionally, these insights are valuable for the optimization of underground mining designs, particularly in hard rock environments. Understanding rock breakage dynamics leads to improved mineral fragmentation and better geomechanical risk management.

DEM MODELLING OF SINGLE PARTICLE CRUSHING TEST OF CRUSHABLE PUMICE SAND

D. Budiman[1] and R. P. Orense[1]
[1] University of Auckland, Dept. of Civil and Environmental Engineering, Auckland, New Zealand
N. Kikkawa[2]
[2] National Institute of Occupational Safety and Health, Tokyo, Japan

1. Introduction

Pumice sand is a volcanically-derived sand that is porous, lightweight, easily crushable, and compressible. In this study, single particle crushing tests on Japanese and New Zealand pumice particles between 1 mm and 8 mm are simulated in Discrete Element Modelling (DEM) using PFC3D V6.0 to obtain representative DEM parameters for experimental simulations of laboratory tests involving this material.

2. Methodology

A 4 mm Japanese pumice sand particle [1] and 1, 2, 4, and 8 mm NZ pumice sand particles [2] are simulated as bonded agglomerates. The individual balls in the agglomerates are 0.4 mm and 0.2 mm in diameter for the Japanese and NZ pumice simulations, respectively. The linear parallel bonded element model [3] is used to bond the agglomerates, while the linear contact model [4] is used for the interactions between balls. The agglomerates are generated based on the particles' apparent porosity estimated from the apparent specific gravity of NZ pumice sands measured using vacuum extraction [5]. Based on this apparent porosity, the 4 mm agglomerate for the Japanese pumice particle is generated, comprising 472 bonded ball elements, while the agglomerates for the NZ pumice consist of 42, 324, 1690, and 8468 bonded ball elements for the 1, 2, 4, and 8 mm particles, respectively. The agglomerates are then compressed between two rigid frictionless plates at a constant velocity of 0.1 mm/s [6] until the agglomerates undergo catastrophic crushing or failure.

3. Results

Figure 1 shows the calibration result of the 4 mm Japanese pumice sand. The calibration is performed by setting the strength parameters (*pb_ten* and *pb_coh*) to a value that produces a similar peak force while the contact (*ln_kn* and *krat*) and bond (*pb_emod* and *pb_krat*) stiffness parameters are controlled to match the force-displacement response and the strain at which the peak force occurs. A similar procedure is applied to the NZ pumice particles, except that instead of calibrating to a single force - displacement plot, the results are calibrated to the average crushing force and strain of several particle-crushing test data. Table 1 summarises the calibrated DEM parameters for the 4 mm Japanese and 1 mm NZ pumice sand particles. As for the larger particle sizes of NZ pumice sands, adjusting the *pb_ten* and *pb_coh* with Weibull statistics [7], surface flaw [8], or Griffith's law [9] with m = 4.23 while keeping the contact and bond stiffness parameters the same is found to produce satisfactory force-displacement predictions.

3. Conclusions

The DEM simulations of particle crushing test using PFC3D have been performed on Japanese and NZ pumice sand particles between 1 mm and 8 mm. The pumice particles are generated using agglomerates with the DEM parameters tabulated in Table 1 for the 4 mm Japanese and 1 mm New Zealand pumice particles. Using these DEM parameters, the agglomerates satisfactorily capture the

force-displacement response. A Weibull modulus, m = 4.23, can be used with the Weibull statistics, surface flaw, or Griffith's law models on the strength parameters to predict the force-displacement response for larger New Zealand pumice particles.

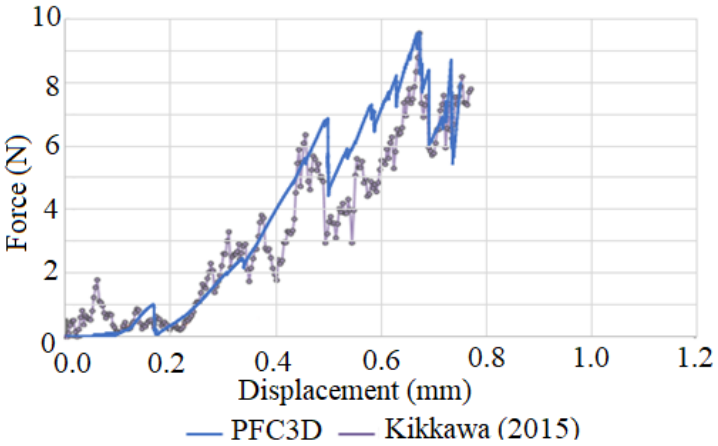

Figure 1. Force-displacement plots for 4 mm Japanese pumice sand

Table 1. Japanese and NZ pumice DEM parameters

Parameters	Unit	Japanese Pumice	New Zealand Pumice
Solid density (ρ)	kg/m^3	2490	2490
Contact Normal Stiffness (*ln_kn*)	N/m	80000	100000
Contact Stiffness Ratio (*krat*)	-	2.27	2.27
Bond stiffness ratio (*pb_krat*)	-	2.27	2.27
Bond effective modulus (*pb_emod*)	Pa	15e6	140e6
Bond tensile strength (*pb_ten*)	Pa	1.4e6	20e6
Bond cohesion (*pb_coh*)	Pa	1.4e6	20e6

4. References

[1] Kikkawa, N. (2015). Characterisation of pumice sand based on laboratory testing. *Yamaguchi University Research Seminar Oral Presentation*.

[2] Bahmani, S. H. (2021). Discrete element modelling of highly crushable pumice sand. *Doctoral Thesis*, University of Auckland.

[3] Potyondy, D. O. (2011). Parallel-bond refinements to match macroproperties of hard rock. *Proc. Second International FLAC/DEM Symposium*, 459-465.

[4] Cundall, P. A., & Strack, D. L. (1979). A discrete numerical model for granular assemblies. *Geotechnique*, 29(1): 47-65.

[5] Wesley, L. D. (2007). Geotechnical characteristics of a pumice sand. *Characterisation and Engineering Properties of Natural Soils*, 2449-2473.

[6] Orense, R. P., Pender, M. J., Hyodo, M., & Nakata, Y. (2013). Micro-mechanical properties of crushable pumice sands. *Geotechnique Letters*, 3(APRIL/JUN): 67-71.

[7] Weibull, W. (1951). A statistical distribution function of wide applicability. *Journal of Applied Mechanics*, 18(3): 293-297.

[8] McDowell, G. R., & Amon, A. (2000). The application of Weibull statistics to the fracture of soil particles. *Soils and Foundations*, 40(5):133-141.

[9] Griffith, A. A. (1921). The phenomena of rupture and flow in solids. In *Philosophical Transactions of the Royal Society of London, Series A*, 221(582-593).

DEM SIMULATION OF CARBONATE PARTICLES CONSIDERING PARTICLE SHAPE AND INTERNAL VOIDS

Z. Dong[1,2], Y. P. Cheng[2] and C. Tong[1]

[1] Central South University, School of Civil Engineering, Changsha, China

[2] University College London, Department of Civil, Environmental and Geomatic Engineering, London, UK

1. Abstract

This paper presents a detailed procedure for modelling carbonate particles through DEM simulations. The particles with four distinct shape groups are scanned, simplified, and then imported to the DEM program PFC^{3D}. To simulate particle crushing behaviour, particles with realistic shapes are subdivided into numerous small coplanar Voronoi polyhedra and bonded together. The internal porosity is assumed to follow a Gaussian distribution, and statistical data matches published values of intra-particle voids measurement of carbonate soils from the South China Sea. Simulation results show that carbonate particles typically experience four stages during compressing: particle rotation, elastic deformation, elastoplastic deformation, and post-failure. The difference in the particle shape leads to varying degrees of tensile and shear failure in the internal bonds of the particles.

2. Modelling carbonate particles with realistic shape and internal voids

To represent the real particle shape, the imported large particle is divided into many Voronoi polyhedra, the detailed procedures are (refer to Figure 1): ① import the particle mesh to PFC^{3D}; ② fill the big particle with numerous small balls; ③ subdivide the large particle into Voronoi polyhedra; ④ cut each Voronoi polyhedron using the actual particle profile, retain polyhedra that are inside of the particle profile and discard those outside; ⑤ glue all the retained polyhedra together to create the crushable real-shape particle model; ⑥ delete some inner rlocks bases on the secified internal porosity.

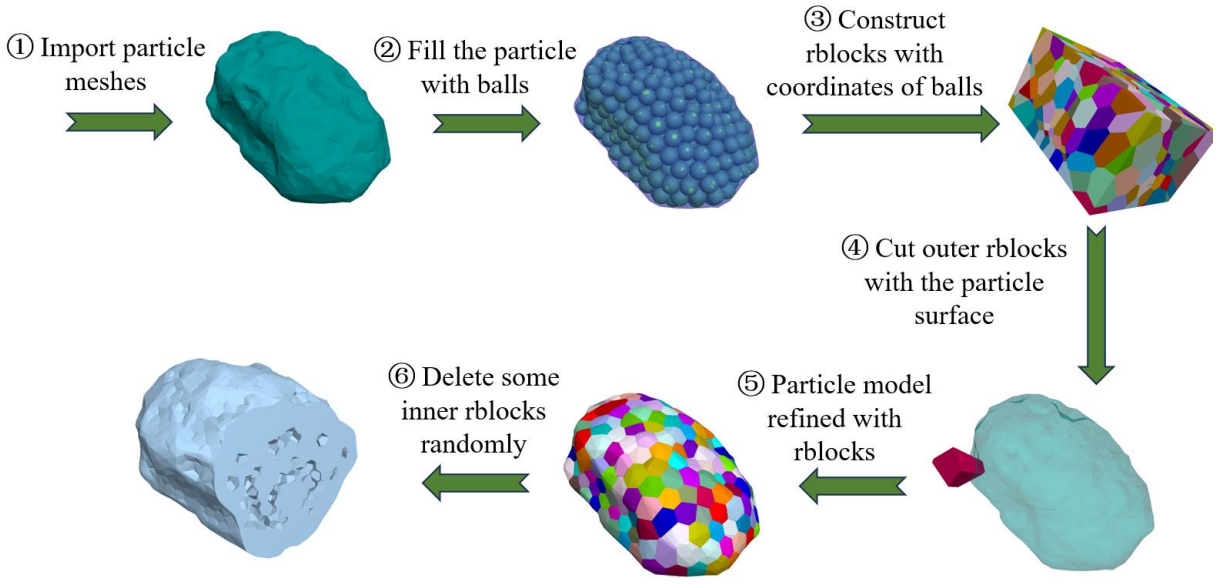

Figure 1. Schematic diagram of the modelling procedures of carbonate particles

The internal porosity p of carbonate particles collected from the South China Sea is investigated. It was found to follow a Gaussian distribution with a mean of 0.115 and a standard deviation of 0.046 (Zhou et al., 2020), as expressed in Equation (1), which was used as an asumption of the simulations in this paper.

$$f(p) = \frac{1}{0.046\sqrt{2\pi}} e^{-\frac{(p-0.115)^2}{2\times 0.046^2}} \tag{1}$$

3. Main results

Figure 2 illustrates the typical response during the single-particle crushing process of carbonate particles, comprising of distinct stages: particle rotation, elastic deformation, elastoplastic deformation, and post-failure. Firstly, the particle needs a slight rotation to achieve a stable contact state. Then, in the elastic stage, the contact force linearly increases with loading displacement. As the contact force increases, some internal bonds break, inducing fluctuations of the contact force and transitioning the single-particle crushing test into the elastoplastic state. This involves the breaking of bonds in tension and shear, leading to cracks that, when connected, trigger a catastrophic particle failure—predominantly a splitting failure, irrespective of particle shape. After the catastrophic failure, some mall fragments are generated and remain on the lower platen.

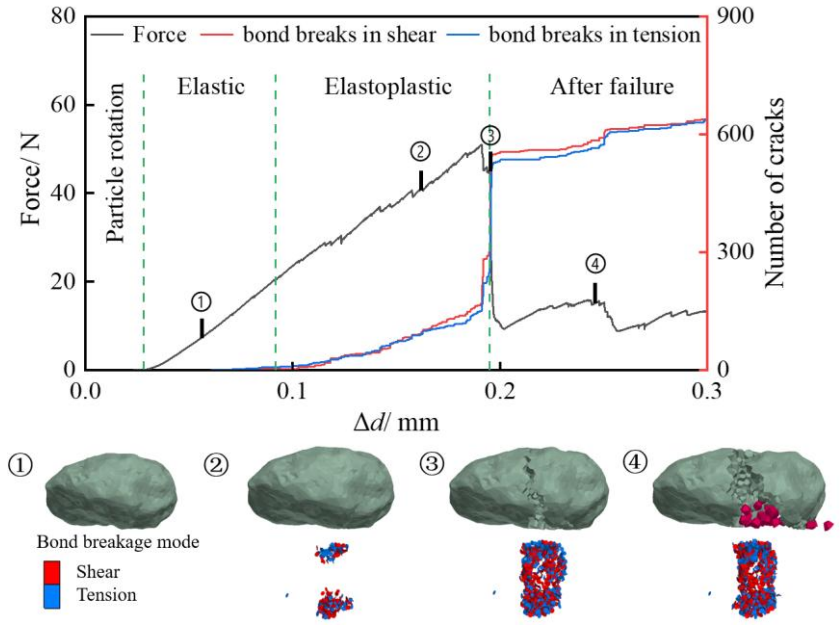

Figure 2. Schematic diagram of the modelling procedures of carbonate particles

4. References

[1] Cheng, Y. P., Nakata, Y., & Bolton, M. D. (2003). Discrete element simulation of crushable soil. *Géotechnique*, 53(7), 633-641.

[2] Fang, C., Gong, J., Jia, M., Nie, Z., Hu, W., & Li, B. (2022). Effect of the intermediate principal stress on the mechanical behaviour of breakable granular materials using realistic particle models. *Acta Geotech.*, 17(11), 4887-4904.

[3] Zhou, B., Ku, Q., Wang, H., & Wang, J. (2020). Particle classification and intra-particle pore structure of carbonate sands. *Eng. Geol.*, 279, 105889.

DISCRETE ELEMENT ANALYSIS OF ONE-DIMENSIONAL COMPRESSION TEST ON CARBON DIOXIDE HYDRATE BEARING CLAY

M. J. Jiang[1,2], S. Dong[1] and X. R. Zhang[1]
[1] School of Civil Engineering, Suzhou University of Science and Technology, Suzhou, China
[2] College of Civil Engineering, Tongji University, Shanghai, China

1. Introduction

With the continuous progress in fundamental research on hydrate, the methane (CH_4) - carbon dioxide (CO_2) replacement method has gradually attracted the global attention for its multiple advantages [1] of meeting the clean energy demand and reducing carbon emissions. However, there is still insufficient experimental data and theoretical research to improve its applicability. Moreover, the experiments are time-consuming, costly, difficult to perform, and have poor repeatability, making it difficult to accurately reveal the mechanical behavior of carbon dioxide hydrate bearing clay (CDHBC). The Discrete Element Method (DEM) can effectively simulate and analyze mechanical properties of soils, making it an indispensable and powerful tool in the field of geomechanics. However, there is still a lack of discrete element method suitable for CDHBC analyses [2].

2. DEM for CDHBC

A three dimensional thermal-hydro-mechanical-chemical bond contact model for grain-cementing type CDHBC was proposed by introducing the influence of molar fraction of carbon dioxide on the phase equilibrium line in this study. The model was implemented into a commercial DEM code, PFC, to simulate one-dimensional compression test on CDHBC under different molar fraction of carbon dioxide, different temperatures and pressures with focus on its macro and micro mechanical behaviors (e.g. compressibility, yield characteristics, bond failure number and aggregate crushing ratio, etc).

3. DEM results in 1D compression test

Figure 1 shows that the compressibility is qualitatively consistent with structured clay [3]. Before the structural yield stress, the variation of void ratio is no significant change. Beyond the structural yield stress, the variation of void ratio is significant change. And structural yield stress decreases with the increasing of the mole fraction of carbon dioxide, the increasing of temperature and the decreasing of pressure in the 1D compression tests.

Figure 2 presents the corresponding bond number of the CDHBC in the tests. Due to the internal structure, the bond number remains unchanged when the external load is lower than the structural yield stress. Beyond the structural yield stress, a significant decrease in the bond number occurs. As the mole fraction of carbon dioxide increases, the temperature increases, and the pressure decreases, the stress corresponding to the significant decrease in the bond number increases. This is essentially associated with the structural yield stress of the sample.

Figure 3 provides the corresponding aggregate crushing in the tests. At the same stress level, the aggregate number decreases with the decreasing of the mole fraction of carbon dioxide, the decreasing of temperature and the increasing of pressure, as shown in Figure 3. With the increasing of the mole fraction of carbon dioxide, the increasing of temperature and the decreasing of pressure, the stress corresponding to the significant increase in aggregate crushing ratio decreases. Because of the internal structure, aggregate crushing ratio is small when the external load is lower than the structural yield stress. Beyond the structural yield stress, the significant aggregate crushing occurs, resulting in the structure degrading.

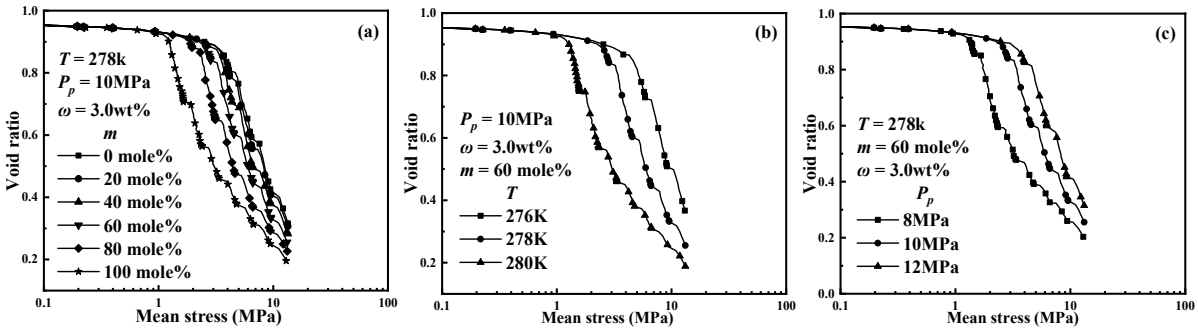

Figure 1. Compression curves for different: (a) molar fraction of carbon dioxide; (b) temperatures; (c) pressures.

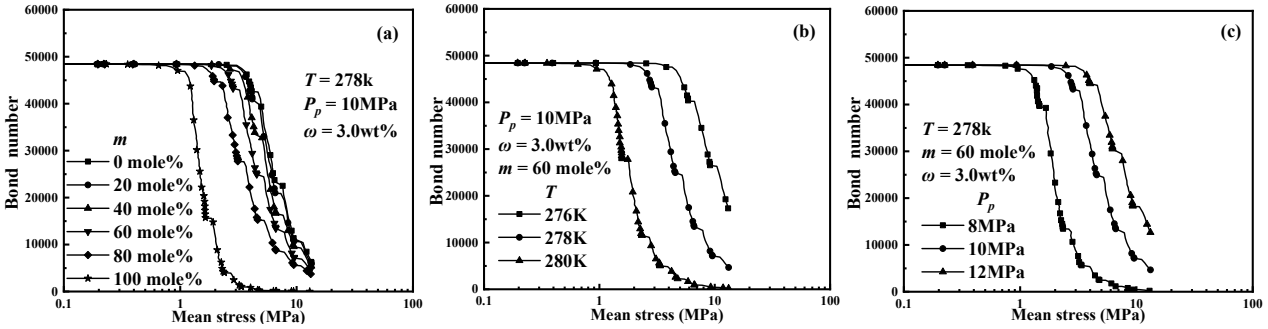

Figure 2. Bond number vs. mean stress for different: (a) molar fraction of carbon dioxide; (b) temperatures; (c) pressures.

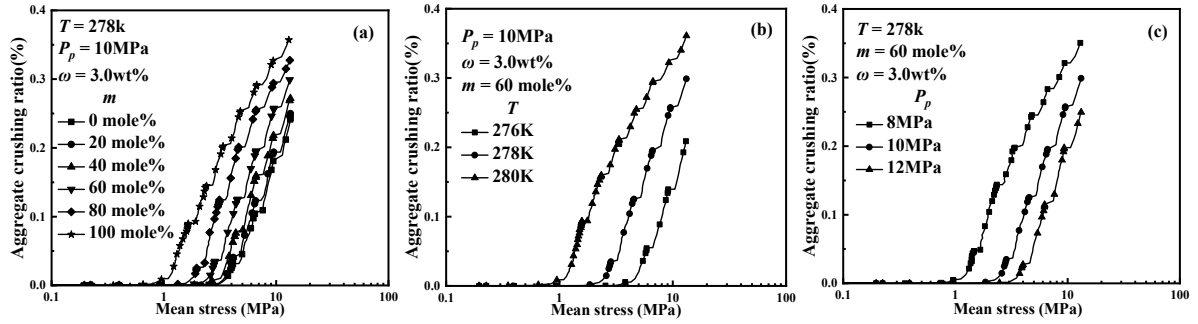

Figure 3. Aggregate crushing ratio vs. mean stress for different: (a) molar fraction of carbon dioxide; (b) temperatures; (c) pressures.

Acknowledgement: This work was financially supported by National Natural Science Foundation of China with Grant Nos. 51890911 and 52331010).

4. References

[1] Goel, N. (2006). In situ methane hydrate dissociation with carbon dioxide sequestration: current knowledge and issues. *J. Petrol. Sci. Eng.*, **51**: 169-184.

[2] Jiang, M. J., Sun, R. H., Arroyo, M., Du, W. H. (2021). Salinity effects on the mechanical behaviour of methane hydrate bearing sediments: A DEM investigation. *Comput. Geotech.*, **133**: 104067.

[3] Okewale, I. A., Grobler H. (2020). The effects of structure of Nigeria clay in one-dimensional compression: The 2020 World Congress on Advances in Civil, Environmental, & Materials Research (ACEM20).

DISSOLUTION SINKHOLE FORMATION AND ITS MICROMECHANICS

Z. Bashir[1] and L. Cui[1]

[1] Univ. of Surrey, School of Sustainability, Civil and Environmental Eng., Guildford, UK

1. Introduction

Sinkholes are geological phenomena that pose significant hazards to human lives and civil infrastructure [1]. Most sinkholes occur in areas dominated by limestone or dolomite. They are caused by anthropogenic activities such as mining and drilling, however, in some cases occur naturally due to geological and hydrological processes, such as changes in precipitation patterns and temperature, seismic activity, seawater infiltration of the subsurface caused by costal erosion of the shoreline, rapid groundwater recharge, etc. [2]. There are different types of sinkholes dependent on geological and hydrological parameters that largely influence the formation and underlying mechanism of sinkholes, including dissolution, collapse, caprock, dropout, suffusion and buried sinkholes. Understanding the mechanisms driving sinkhole formation becomes crucial for urban planning and infrastructure stability. This paper presents an investigation of dissolution sinkhole initiation and development using DEM to gain insights into the complex interactions and factors contributing to this geological hazard within karst regions.

2. Descriptions of DEM simulation

An open-source code, MatDEM [3], was employed to model sinkhole formation, incorporating dissolution processes by removing elements in the affected regions. Although MatDEM can perform 3D modelling, only 2D simulations of a layer of spherical particles were considered in the current study due to the constraint of computational costs. A 100m by 80m region is defined for sample preparation, where particles with mean diameter of 0.6m and maximum to minimum size ratio of 1.44 were generated in the region. Gravity settling was allowed to generate the initial sample. Three sets of materials macroscopic parameters (Young's Modulus E, Poisson's Ratio v, Cohesion C_u, Tensile Strength T_u, internal friction coefficient μ_i, and density ρ) were assigned to the sample to represent soil, weak rock and strong rock (Table 1). MatDEM material training function was applied to determine the five micromechanical parameters of the DEM simulations (linear elastic contact model (normal stiffness K_n, tangential stiffness K_s, breaking displacement X_b, initial shear force F_{s0}, and particle friction coefficient μ_p).

Properties	E *(GPa)*	v	C_u *(MPa)*	T_u *(MPa)*	μ_i	ρ *(kg/m^3)*	K_n (N/m)	K_s (N/m)	X_b (mm)	F_{s0} (N)	μ_p
Soil	0.02	0.14	0.02	0.002	0.6	1900	2.7e8	8.3e7	2.8	2.7e6	0.31
Weak Rock	5	0.2	20	2	0.6	2600	8.4e10	1.5e10	1.6	5.7e8	0.19
Strong Rock	10	0.15	50	5	0.6	2850	1.5e11	5.4e10	2.1	1.4e9	0.19

Table 1. Macroscopic and microscopic material parameters.

Dissolution sinkhole was initiated by eliminating particles within a prescribed shape, i.e. elliptical or triangular to assess the effect of sinkhole geometry on its stability. Both shapes grow gradually for 10 steps and soil/rock are brought to equilibrium following each step. Both types of sinkholes were simulated under no surcharge and 10MPa surcharge.

3. Simulation results and discussions

The representative displacement patterns of different scenarios were illustrated in Figure 1. Clearly, surcharge amplified the ground settlement with an obvious dip above the sinkhole. There is clear ground collapse and shear surface developed in soil and weak rock, with less fragments in weak rock; however, in strong rock, the whole ground settled more uniformly with no obvious shear surface developed. In most cases, elliptical sinkhole shows less ground settlement than triangular sinkhole, although different trend was observed in a few cases. Contact force network shows that contact force arching contributes to the higher resistance to the sinkhole collapse and lower ground settlement.

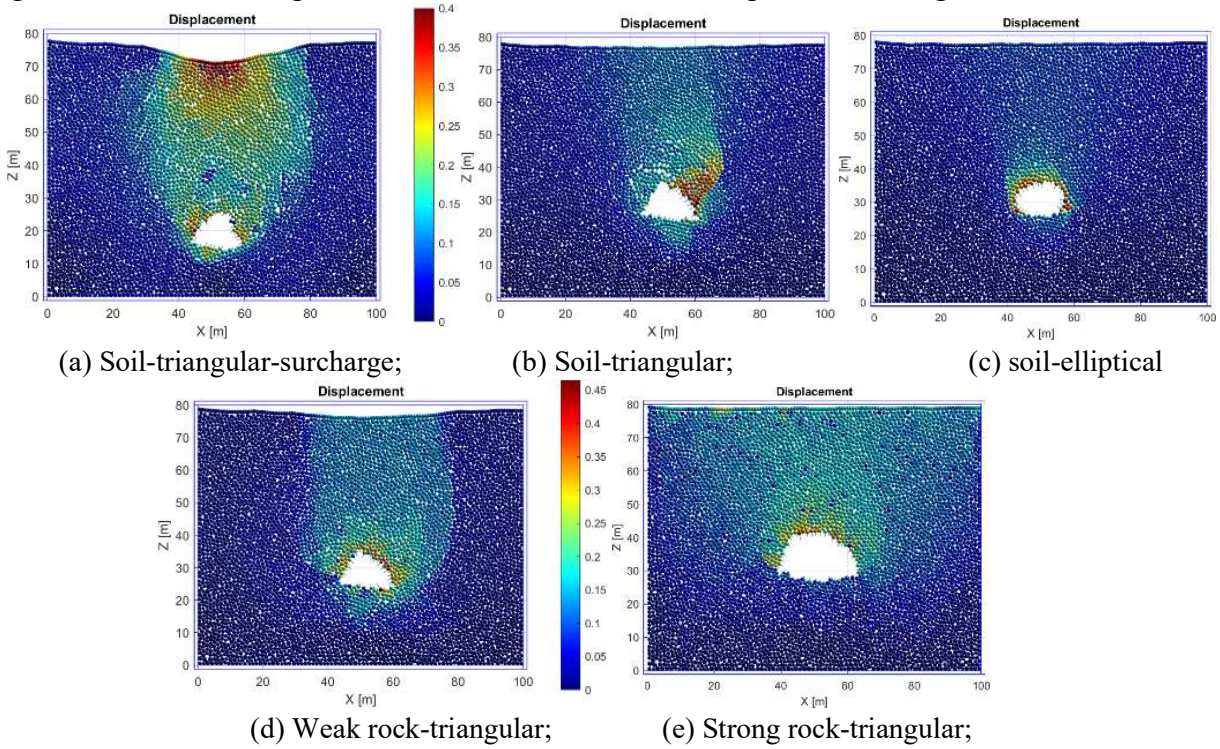

(a) Soil-triangular-surcharge; (b) Soil-triangular; (c) soil-elliptical

(d) Weak rock-triangular; (e) Strong rock-triangular;

Figure 1. Displacement patterns of sinkhole development for different scenarios.

4. Conclusions

DEM is a powerful tool to explore the microscopic mechanism underlying the development of sinkhole and its induced ground settlement. Particle bonding strength and arching effects are the main contributions to the resistance of sinkhole collapse. More parametric studies and validations will be performed in the future study.

5. References

[1] Waltham, T. (2008). "Sinkhole hazard case histories in karst terrains." Quarterly Journal of Engineering Geology and Hydrogeology 41(3): 291-300.

[2] Beck, B.F. (2003) Sinkholes and the Engineering and Environmental Impacts of Karst. ASCE.

[3] Liu, C (2021) Matrix Discrete Element Analysis of Geological and Geotechnical Engineering. Science Press.

Discrete Element Modeling of Reliquefaction Behavior of Sand Under Undrained Cyclic Simple Shear Considering Reconsolidation Effect

Wentian Xia[1], Zhijian Qiu[2], Yewei Zheng[3], and Qixin Wu[4,*]

[1] Master Student, School of Civil Engineering, Wuhan University, Wuhan, Hubei 430072, China. Email: xiawentian@whu.edu.cn

[2] Assistant Professor, School of Architecture and Civil Engineering, Xiamen University, Xiamen, Fujian 361005, China. Email: zhijianqiu@xmu.edu.cn

[3] Professor, School of Civil Engineering, Wuhan University, Wuhan, Hubei 430072 China. Email: yzheng@whu.edu.cn

[4] Lecturer, School of Civil Engineering, Wuhan University, Wuhan, Hubei 430072, China. Email: qixin931227@whu.edu.cn (corresponding author)

Abstract:

Since Niigata earthquake in 1964, a series of site surveys [4,5,11,12] show that sand liquefied during the mainshock may reliquefy during the aftershocks. Recently, on 6 February 2023, a M_w 7.8 earthquake struck southern and central Turkey and northern and western Syria. A M_w 7.7 aftershock occurred about nine hours after the mainshock. As there exists an uncertain interval between the two consecutive earthquakes, the excess pore pressure built up during the mainshock dissipates partially or completely, and the soil becomes denser after reconsolidation. However, it has been reported that the damage of sand reliquefaction caused by aftershocks may exceed that caused by mainshock [2,5,11,12]. To gain more micromechanical insights into the reliquefaction behaviors of sand, a series of discrete element simulations [1] of undrained cyclic simple shear tests were carried out on granular specimens [3,7] with different degree of reconsolidation and liquefaction history. As shown in Fig 1, polyhedral specimen configuration is employed, such that stress concentration can be greatly reduced or even eliminated by ensuring the corners between adjacent boundaries always form obtuse angles [8]. Fig 2 illustrates the loading schemes in the e-*p*' plane. In this study, liquefaction is defined as the state where the effective stress is close to zero and almost all the interparticle contacts are lost.

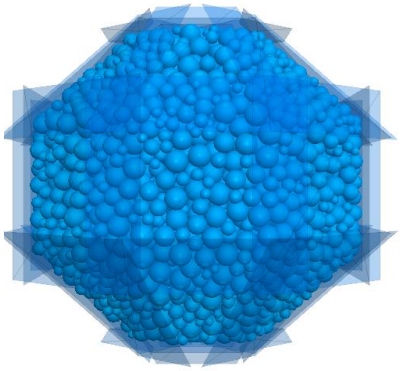

Figure 1. DEM specimen based on polyhedral configuration

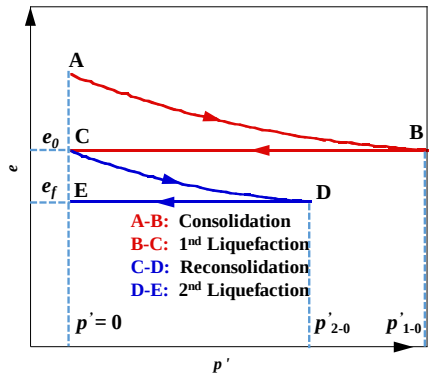

Figure 2. Loading schemes

Fig 3(a) presents the effective stress paths of specimen (with void ratio e_0 = 0.6504) during the first undrained cyclic shear with cyclic shear stress ratio *CSR* = 0.4. As shown in Fig 3(a), the butterfly-shaped stress path can be observed prior to the liquefaction until the effective stress to zero. After the first undrained cyclic shear, the liquefied specimens are reconsolidated to the target degree of reconsolidation U_r = 0.25, 0.50, 0.75, and 1.0, respectively. Fig 3(b)(c)(d)(e) present the effective stress paths of the specimens during the second cyclic shearing with *CSR* = 0.4. It can be observed that the reliquefaction resistance increases with increasing the degree of reconsolidation. However,

the number of cycles required for reliquefaction is smaller during the second cyclic shearing than that during the first cyclic shearing, even if the void ratio becomes smaller after the reconsolidation. These observations are in qualitative agreement with the results of previous experiments [13].

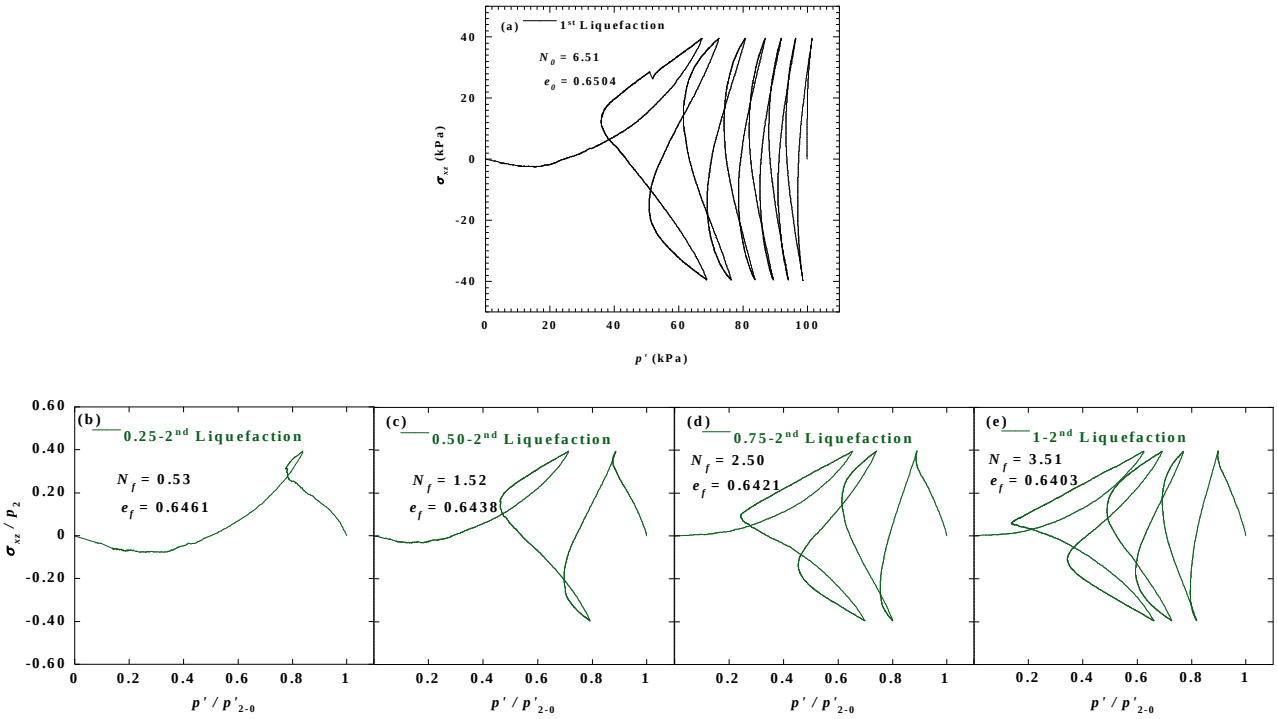

Figure 3. Effective stress paths of specimens (a) first undrained cyclic simple shear. (b)(c)(d)(e) second undrained cyclic simple shear with different degree of reconsolidation.

During both the first (mainshock) and second (aftershock) cyclic shearing process, the evolutions of the load-bearing structure of the granular specimens were quantified through a contact-normal-based fabric tensor [6,8-10], N_c and N_p are the numbers of interparticle contacts and particles, respectively.

$$CN = 2N_c / N_p \tag{1}$$

The simulation results as Fig 4(a) show that the granular specimen exhibits smaller *CN* to resist external loading during the aftershock, even if the void ratio becomes smaller after the reconsolidation. Fig 4(b) shows that the *CN* increases with increasing the degree of reconsolidation.

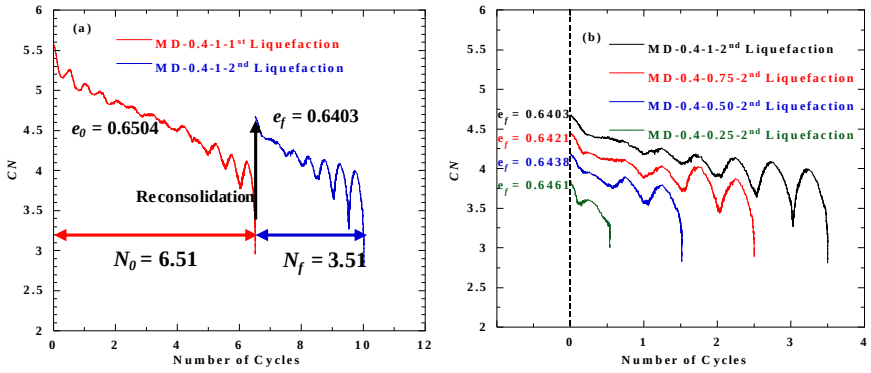

Figure 4. Evolutions of *CN* (a) first and the second undrained cyclic simple shear. (b) second undrained cyclic simple shear with the different degree of reconsolidation

References

[1] Cundall P.A., Strack O.D. (1979). A discrete numerical model for granular assemblies. *Géotechnique.* 29 (1), 47-65.

[2] Fardad A.P., Huang D.R., Wang G., Jin F. (2021). Effects of strain history and induced anisotropy on reliquefaction resistance of Toyoura sand. *J. Geotech Geoenviron.* 147 (9), 04021094.

[3] Gu X.Q., Liang X.M., Hu J. (2023). Quantifying fabric anisotropy of granular materials using wave velocity anisotropy: a numerical investigation. *Géotechnique.* In press.

[4] Görüm T., Tanyas H., Karabacak F., Yilmaz A., Girgin S., Allstadt K.E., Süzen M.L., Burgi P. (2023). Preliminary documentation of coseismic ground failure triggered by the February 6, 2023 Türkiye earthquake sequence. *Eng Geol.* 327, 107315.

[5] Ishihara K., Koga Y. (1981). Case studies of liquefaction in the 1964 Niigata earthquake. *Soils Found.* 21 (3), 35–52.

[6] Li X.S., Dafalias Y.F. (2012). Anisotropic critical state theory: role of fabric. *J. Eng Mech.* 138 (3), 263–275.

[7] Ni X.Q., Ye B., Zhang Z., Zhang S., Zhang F. (2022). An investigation of the influence of reconsolidation properties on the reliquefaction resistance of sand by element tests. *J. Geotech Geoenviron.* 148 (3), 04021191.

[8] Wu Q.X., Pan K., Yang Z.X. (2021). Undrained cyclic behavior of granular materials considering initial static shear effect: Insights from discrete element modeling. *Soil Dyn Earthq Eng.* 143, 105697.

[9] Wu Q.X., Yang Z.X. (2021). Novel undrained servomechanism in discrete-element modeling and its application in multidirectional cyclic shearing simulations. *J. Eng Mech.* 147 (3), 04020155.

[10] Wu Q.X., Yang Z.X. (2022). Undrained responses of anisotropic granular material under rotational shear by DEM. *J. Geotech Geoenviron Eng*. 148 (12), 04022112.

[11] Yasuda S., Tohno I. (1988). Sites of reliquefaction caused by the 1983 Nihonkai-Chubu earthquake. *Soils Found*. 28 (2), 61–72.

[12] Yasuda S., Harada K., Ishikawa K., Kanemaru K. (2012). Characteristics of liquefaction in Tokyo Bay area by the 2011 Great East Japan Earthquake. *Soils Found*. 52 (5), 793–810.

[13] Ye B., Ye G.L., Zhang F., Atsushi Y. (2007). Experiment and numerical simulation of repeated liquefaction-consolidation of sand. *Soils Found*. 47 (3), 547–558.

Discrete modelling of particle breakage induced pile creep in a centrifuge chamber

J. Lei[1], M. Arroyo[1] and M. Ciantia[2,3]

[1] Department of Geotechnical Engineering and Geosciences, Polytechnic University of Catalonia (UPC), Barcelona, Spain

[2] School of Science and Engineering, University of Dundee, Dundee, UK

[3] Università Degli Studi di Milano Bicocca, Milan, IT

1. Abstract

The time-dependent pile settlement under sustained service load has been reported in the literature and defined as pile creep. Particle breakage has been found as the main mechanism for pile creep in sand by Leung et al. [1]. Based on the time-to-fracture Fontainebleau sand DEM model proposed by Lei et al. [2], particle breakage induced pile creep is first investigated in a centrifuge virtual chamber using the particle refined method. The creep settlement is highly similar to the results reported by Leung et al. [1]. The model shows great potential for investigating the pile creep in a microscopic view and the relevant pile ageing (set-up) phenomenon.

2. Details of Centrifuge DEM chamber

Based on the time-to-fracture Fontainebleau sand DEM model proposed by Lei et al. [2], The Fontainebleau sand DEM chamber (30 cm diameter, 15 cm height) with 77334 particles was formed (Figure 1) using the particle refined method (PRM) proposed by McDowell et al. [3]. The chamber has seven different cylindrical sections, the boundary of the chamber was set as side walls. The smallest scaling factor S_c=5 was applied at the chamber core section with the diameter of 1.3 cm. The ratio of scaling factor from the centre section to the next was set as 1.5 to avoid particle migration following McDowell et al. [3]. Different scaled particles were first generated into each section of the chamber using radius expansion method with the initial porosity of 0.391. The particle size distribution (PSD) in all sections before scaling agrees with the real PSD curves of Fontainebleau sand. Particle friction was set as zero first, and the chamber was cycled to reach the equilibrium state (unbalanced force ratio smaller than 10^{-5}). Then, friction and particle strength properties were assigned to each particle. 50 g centrifuge acceleration and particle breakage criterion were activated. Crack propagation was only activated at the core section (S_c=5) of the chamber to ensure the computational efficiency. The system cycled again to reach the same equilibrium state and sample reached a denser state. The vertical effective stress at the bottom of the chamber was measured as 116.14 kPa, matching the theoretical stress value of a real soil column at 50 g gravity (118.73 kPa).

The pile was formed using bundled rigid wall with the diameter d_{pile} of 1cm. The chamber-to-pile diameter ratio ($D_{\text{chamber}}/D_{\text{pile}}$) is 30. Bolton et al. [4] reported that the influence of boundary effect on penetration resistance in a quartz sand centrifuge chamber can be ignored when $D_{\text{chamber}}/D_{\text{pile}}$ exceeds 25. Pile to particle ratio (D_{pile}/D_{50}) is selected as 9.5 in this study, which is larger than almost all previous studies.

The calibrated parameters for time-to-fracture DEM model can be referred to Lei et al. [2], and the parameters for modelling the pile follows the material properties of aluminium [1] with the friction μ = 0.45, the Poisson's ratio v = 0.33, the shear modulus G = 26 GPa, and the density of 2.7 kg/m^3.

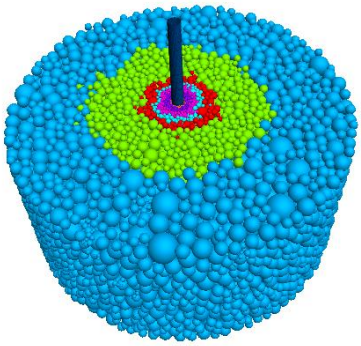

Figure 1. Fontainebleau sand DEM centrifuge chamber formed using PRM method

3. Pile creep test

The pile was jacked into three certain depths of the chamber (40 mm, 60 mm, 80 mm) before carrying out pile creep tests. Penetration velocity was selected as 1.5 m/s, which fulfils the quasi-state requirement that the inertial number I< 0.01 (critical penetration velocity 1.98 m/s) suggested by Janda & Ooi [5]. When pile reached a certain depth, the penetration resistance $F_{max}$was recorded, and pile was unloaded and re-loaded to 0.9 F_{max} to carry out pile creep. Pile load was kept constant by continually adjusting its position, and time is advanced using the off-DEM ageing scheme described in Lei et al. [1]. The pile creep settlement for one month is shown in Figure 2, which similar to the pile creep trend obtained by Leung et al. [2].

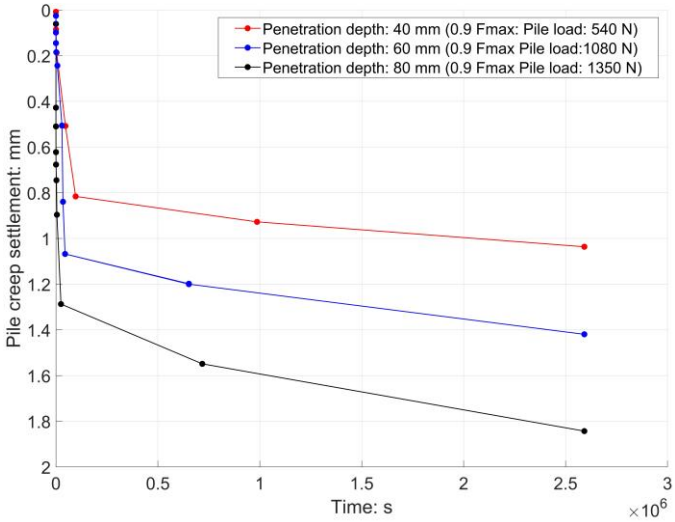

Figure 2. Pile creep settlement under upper load of 0.9 Fmax at different penetration depth

4. References

[1] Leung, C. F., Lee, F. H., & Yet, N. S. (1997). The role of particle breakage in pile creep in sand. *Canadian Geotechnical Journal* **33**(6): 888-898

[2] Lei, J., Arroyo, M., Ciantia, M & Zhang, N. A time-to-facture DEM model for simulating creep in rough crushable sand. NUMGE. University College London, UK, 2023. https://10.53243/NUMGE2023-37

[3] McDowell, G. R., Falagush, O., & Yu, H. S. (2012). A particle refinement method for simulating DEM of cone penetration testing in granular materials. *Geotechnique Letters*, **2**(7–9), 141–147.

[4] Bolton et al. (1999). Centrifuge cone penetration tests in sand. *Geotechnique*, 49(4):543-552

[5] Janda, A., & Ooi, J. Y. (2016). DEM modeling of cone penetration and unconfined compression in cohesive solids. *Powder Technology*, 293, 60–68.

EFFECT OF INITIAL CONDITIONS ON THE DEGREE OF SAMPLING DISTURBANCE IN METHANE HYDRATE-BEARING SEDMIDENT BY DEM ANALYSES

M. J. Jiang [1,2], Q. B. Xue [1], L. Han [1] and P. M. Jiang[1]

[1] School of Civil Engineering, Suzhou University of Science and Technology, Suzhou, China

[2] College of Civil Engineering, Tongji University, Shanghai, China

1. Introduction

Advances in pressure coring technique have enabled methane hydrate-bearing sediment (MHBS) samples to be retrieved under in-situ hydrostatic pressures [1]. However, due to the sampling procedure above, the effective stress applied to MHBS sample will be released from the in-situ K_0 state to the hydrostatic pressure state [2]. The effective stress release can lead to the structural disturbance for MHBS sample, namely the damage to micro-structure of MHBS sample, which will further affect their macro mechanical properties [3]. Moreover, the initial conditions of MHBS sample (i.e., in-situ effective stress σ' , the cementation strength and the hydrate saturation S_h) have significant impacts on the degree of structural disturbance (DSD), while the cementation strength can be calculated by the phase equilibrium parameter L [4]. This study aims at investigating the micro mechanisms on the structural disturbance for MHBS sample due to sampling process and exploring the effect of initial conditions above. Besides, it is also expected to find the range of initial condition with low DSD.

2. DEM simulations

In this study, the analysis tool is the distinct element method (DEM) developed for MHBS [4]. First, DEM is used to prepare the unbonded specimens via the multilayer under-compaction method (UCM) [5]. These specimens are then consolidated under in-situ stress state to simulate the samples with intact structure, while the contact model proposed by Jiang et al. (2021) for MHBS [4] is used to form bonds repeatedly at the contacts meeting the bond formation criterion, until the sample arrives at an equilibrium state. Second, these samples are unloaded to simulate sampling process [3], where DSD is characterized by the rate of bond breakage R_b. By exploring the relationship between the disturbance and initial conditions of samples, the range of initial conditions with low DSD can be obtained. Third, one-dimensional DEM tests are carried out on the MHBS sample before and after sampling a to demonstrate the proposed range of initial conditions with low DSD in view of the macro mechanical properties.

3. Main DEM results

First, the number of bond breakage N_b due to vertical unloading (see Fig. 1 (a)) is much larger than that due to horizontal unloading (see Fig. 1 (b)). Besides, during vertical unloading, the number of bond breakage tends to increase rapidly when the stress is relatively small (see Fig. 1 (a)); during horizontal unloading, the number of bond breakage will increase rapidly at the beginning and end stages of unloading (see Fig. 1 (b)). Moreover, the sampling process will reduce the anisotropy of the contact distribution induced in the sedimentation process of MHBS (see Fig. 1 (c)).

From Fig. 1 (d), it can be found that the DSD of samples will decrease with increase in both L and S_h. In addition, an inflection point can be found on the curve of R_b versus S_h (see Fig. 1 (d)), and this inflection point can be used to estimate the S_h with low DSD. In addition, one-dimensional DEM test shown that when the initial conditions of MHBS sample are within the range with low DSD, the

effect of structural disturbance due to sampling on the K_0 and yield stress of MHBS samples can be ignored.

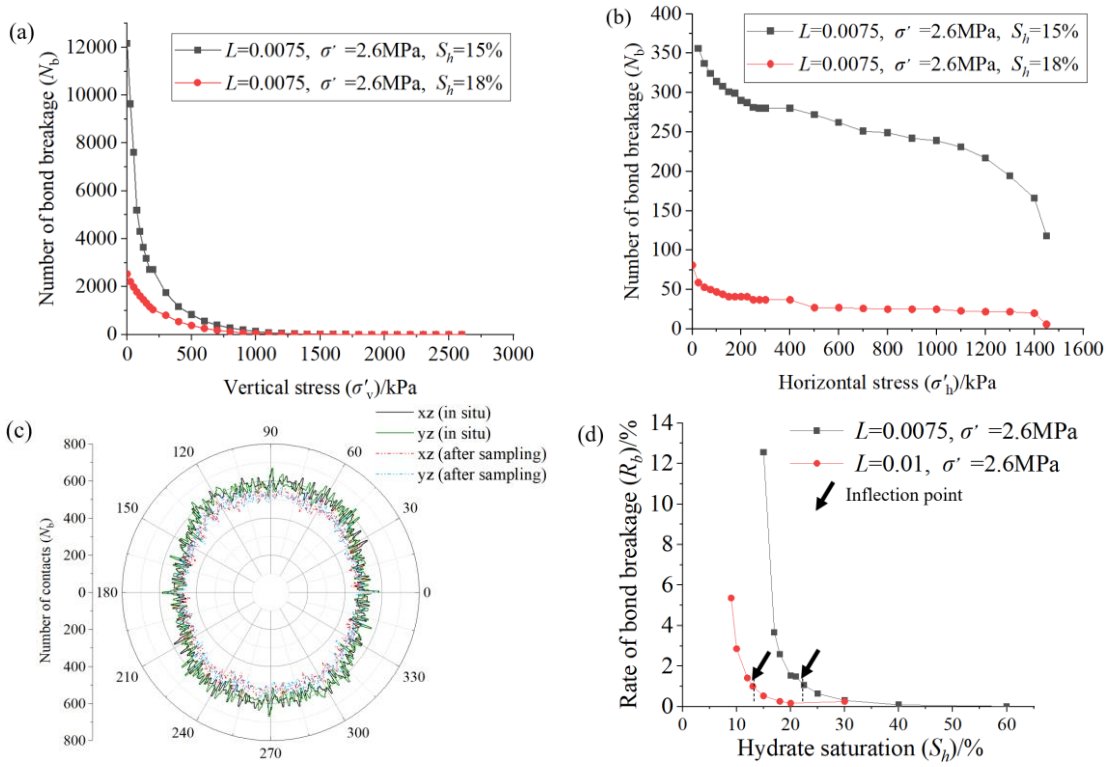

Figure 1. Results of DEM simulations: (a) the variation of N_b with σ'_v; (b) the variation of N_b with σ'_h; (c) rose diagram of contact fabric; (d) the variation of R_b with S_h.

Acknowledgement

This work was financially supported by National Natural Science Foundation of China (Grant Nos. 51890911, 52331010), and National Key Research and Development Program of China (Grant No. 2022YFC3003403). All these supports are greatly appreciated.

References

[1] Guo, D., Xie, H. P., Chen, L., Zhou, Z. Y, Lu, H. P., Dai, L., Wang, D. M., Wang, T. Y., Li, J., He, Z. Q., Hu, Y. Q., & Gao, M. Z. (2023). In-situ pressure-preserved coring for deep exploration: Insight into the rotation behavior of the valve cover of a pressure controller. *Petroleum Science*, **20**(4), 2386-2398.

[2] Yun, T. S., Fratta, D., & Santamarina, J. C. (2010). Hydrate-bearing sediments from the Krishna−Godavari Basin: physical characterization, pressure core testing, and scaled production monitoring. *Energy & Fuels*, **24**(11), 5972-5983.

[3] Holt, R. M., Brignoli, M., & Kenter, C. J. (2000). Core quality: quantification of coring-induced rock alteration. *International Journal of Rock Mechanics and Mining Sciences*, **37**(6), 889-907.

[4] Jiang, M., Sun, R., Arroyo, M., & Du, W. (2021). Salinity effects on the mechanical behaviour of methane hydrate bearing sediments: A DEM investigation. *Computers and Geotechnics*, **133**, 104067.

[5] Jiang, M. J., Konrad, J. M., & Leroueil, S. (2003). An efficient technique for generating homogeneous specimens for DEM studies. *Computers and geotechnics*, **30**, 579-597.

EFFECT OF LOADING/UNLOADING ON THE EARTH PRESSURE COEFFICIENT AT REST FOR SAND BY DEM ANALYSIS

M. J. Jiang[1,2,3], H. Li[1] and L. Han[2]

[1] School of River and Ocean Engineering, Chongqing Jiaotong University, Chongqing, China

[2] School of Civil Engineering, Suzhou University of Science and Technology, Suzhou, China

[3] College of Civil Engineering, Tongji University, Shanghai, China

1. Introduction

The earth pressure coefficient at rest (K_0) refers to the ratio of the horizontal stress (σ_h) to the vertical stress (σ_v) in the stratum. In the current laboratory tests about K_0, different loading paths have been employed to prepare the sand samples with different initial relative densities and conduct the corresponding K_0 tests [1]. Meanwhile, different loading/unloading paths are also used to study the effect of stress history on the K_0 values [2]. Actually, in the K_0 test, the relative density of sandy soil samples will change during loading/unloading, and as a result, the K_0 value will also vary accordingly [2]. However, the physical mechanisms about the issue above is still unclear. This study aims at investigating the change of K_0 for sand under loading/unloading paths and revealing the corresponding micro mechanisms via the Discrete Element Method (DEM).

2. Research method and main procedure

With focus on the effect of loading/unloading on K_0, three major steps were used to do tests on sand. First, a DEM sample for *Ottawa 50-70 sand* with the void ratio of 0.73 is prepared using the Multi-layer Undercompaction Method (UCM) [3], in which the contact model is chosen to be that proposed by Jiang, et al. (2015) [4]. This sample is prepared into a cylindrical container enclosed by two flat walls at both two ends and a cylinder wall on the side, and is allowed a period of time to arrive at an equilibrium state once it is garnered. Second, vertical load is incrementally applied to the upper wall step by step to different maximum values to simulate loading path. Third, the vertical load is reduced from the maximum vertical load to simulate unloading path. The vertical and horizontal stresses are measured at walls to calculate the K_0 value for sand at each given load during loading/unloading path. The maximum vertical load is chosen to be 1400kPa and 800kPa respectively in this study, named as Case 1 and Case 2 in the paper.

3. Main results

Figure 1(a) presents the stress path in the Case 1 and Case 2 respectively, and the mean and deviatoric stresses are calculated by the vertical and horizontal stresses measured at walls. It can be seen that the stress paths of unloading are below the path of loading in two cases, and show a hysteretic phenomenon. Figure 1(b) shows that the K_0 decreases with the increase of vertical load during both of loading/unloading paths in the two cases, and K_0 is larger during unloading. The similar results are also obtained in reference [2]. In addition, during unloading, the increasing rate of K_0 in Case 2 is larger than that in Case 1 as shown in Fig. 1(b). To reveal the micro mechanisms of K_0 responses during loading/unloading, Case 1 is taken as the example for further analyses. Here, the principal values of contact fabric tensor (Φ_{xx}, Φ_{yy}, and Φ_{zz}) and the change of principal stresses σ_{xx}, σ_{yy}, and σ_{zz} in the sample are examined for the aim. Where Φ_{xx}, Φ_{yy}, and Φ_{zz} represent the probability values of the direction distribution for contacts along three coordinate axes, respectively.

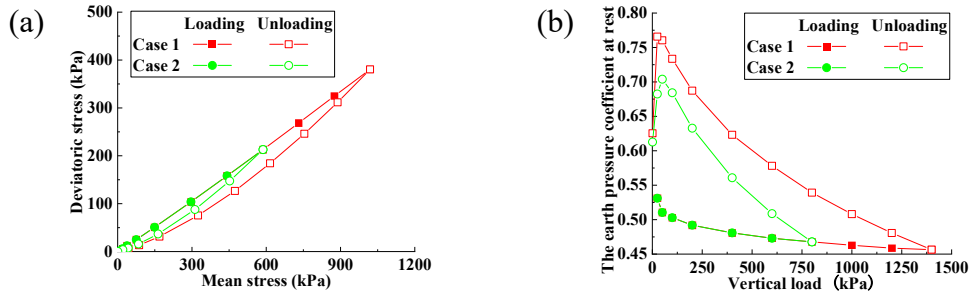

Figure 1. Macro results obtained by DEM simulation: (a) the loading/unloading paths in the K_0 tests and (b) the corresponding K_0 value for sand during the loading/unloading process.

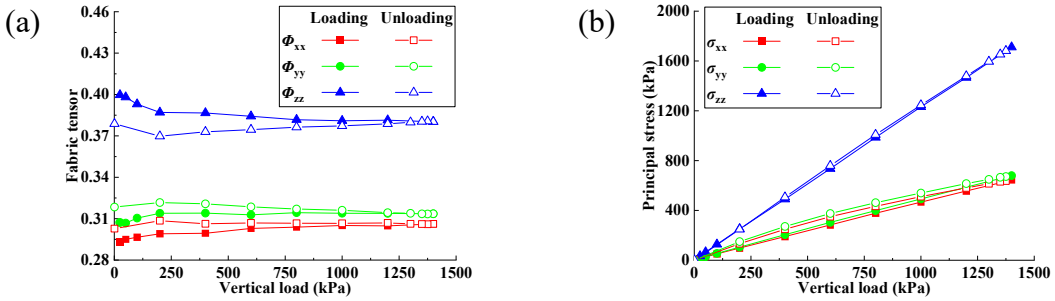

Figure 2. Micro mechanisms in K_0 test for Case 1: (a) three principal values of contact fabric and (b) horizontal/vertical stress in the sample during loading/unloading.

Figure 2(a) provides the direction distributions of contacts in the sample, which shows that Φ_{xx} is larger during loading than that during unloading but Φ_{yy} and Φ_{zz} change in an opposite manner. This reflects that the contact force chain will be more likely to transmit the stress from vertical to horizontal direction during unloading than that during loading. Figure 2(b) shows there is little difference on vertical stress between loading and unloading, while the horizontal stress is slightly greater in unloading than loading. It can be found that the change of three principal stresses is coincident with the change of three principal values of contact fabric. Accordingly, horizontal stress is always smaller than vertical stress, and the horizontal stress will be larger during unloading than that during loading under similar vertical stress, finally lead to a greater K_0 in unloading than loading.

Acknowledgement: This work was financially supported by National Natural Science Foundation of China (Grant Nos. 51890911, 52331010), and National Key Research and Development Program of China (Grant No. 2022YFC3003403). All these supports are greatly appreciated.

4. References

[1] Li, L.B., Dai, Z.Y., Liu R.M. & Jian, F.X. (2023). Experimental study on the coefficient of earth pressure at rest for sand. *Buildings*, **13**: 1276.

[2] Gao, Y. & Wang, Y.H. (2014). Experimental and DEM examinations of K_0 in sand under different loading conditions. *Journal of Geotechnical and Geoenvironmental Engineering*, **140**(5): 04014012.

[3] Jiang, M.J., Konrad, J.M. & Leroueil, S. (2003). An efficient technique for generating homogeneous specimens for DEM studies. *Computers and Geotechnics*, **30**: 579-597.

[4] Jiang, M.J., Shen, Z.F. & Wang, J.F. (2015). A novel three-dimensional contact model for granulates incorporating rolling and twisting resistances. *Computers and Geotechnics*, **65**: 147-163.

EFFECT OF ROLLING RESISTANCE ON THE MECHANICAL BEHAVIOR AND INSTABILITY RESPONSE OF SAND SUBJECTED TO TRIAXIAL COMPRESSION AND EXTENSION CONDITIONS

M.S. Negi[1] and M. Mukherjee[1]

[1] Indian Institute of Technology Mandi, School of Civil and Environmental Engineering, Mandi, India

1. Introduction

Soil elements in various geo-structure are usually subjected to different stress paths involving principal stress rotations, which include compression and extension scenarios. For characterizing the constitutive response of soil under these stress paths, various laboratory level element tests are usually conducted, such as true triaxial, hollow cylinder, triaxial compression and extension tests [1]. In order to understand the deformation mechanism associated at particle-level for the granular assembly under these loading conditions, Discrete Element Method (DEM) is widely used. Though majority of the DEM codes are formulated based on the assumption of circular or spherical particles, in reality, most of the soil particles are of irregular shape. In order to account for the rotational resistance offered by the irregular shape of soil particles, Iwashita and Oda [2] introduced the linear rolling resistance type contact model. Various studies have been conducted in the past to understand the effect of rolling resistance on the mechanical response of granular materials with a particular focus on either the plain strain biaxial condition or a triaxial compression condition [2]. However, the effect of rolling resistance under triaxial extension type of shearing condition is yet to be explored. The present study envisions to investigate the effect of rolling resistance on the mechanical behavior of granular assembly under triaxial compression and extension conditions including its impact on the associated instability response.

2. Triaxial test simulation

In the present study, 3D DEM simulations of the triaxial test have been carried out under both compression (b = 0) and extension (b = 1) stress paths, where b is the intermediate principal stress ratio, $b = (\sigma_2 - \sigma_3)/(\sigma_1 - \sigma_3)$. The DEM simulations have been validated against the experimental results of Wang and Lade [1] on the sub-angular Santa Monica beach sand specimen at 90 % relative density. Similar to the experiment, a cuboidal specimen of 76 mm × 76 mm × 186 mm with six rigid frictionless walls has been adopted in the simulation. The particle size distribution has been scaled up to 6 times of the actual particle size distribution used in the experiment, resulting in approximately 0.63 million spherical particles. In order to reduce the computation time, density scaling of 1000 has been adopted. A linear rolling resistance type contact model has been employed, which can indirectly account for the rotational resistance arising due to irregular shaped particles [2]. Two different rolling resistance coefficient values μ_r = 0.1 and 0.9 have been chosen, where higher μ_r indicates more irregularities in the particle shape.

3. Effect of rolling resistance on the mechanical behavior and instability response

Figure 1 depicts the stress-strain and volumetric response of the specimen with two different μ_r under triaxial compression (b = 0) and extension (b = 1) condition. With increase in rolling resistance, overall stresses can be noticed to increase for both b = 0 and b = 1 condition (Fig. 1a). Further, the specimen exhibits more pronounced softening for shearing with b = 1 condition in comparison to b = 0 case. Additionally, it is interesting to note that enhanced dilation has been observed with increasing rolling resistance for b = 0; whereas, for b = 1, increase in rolling resistance

leads to lesser dilative response. The genesis of this behavior has been investigated based on the particle level information captured from the DEM simulation.

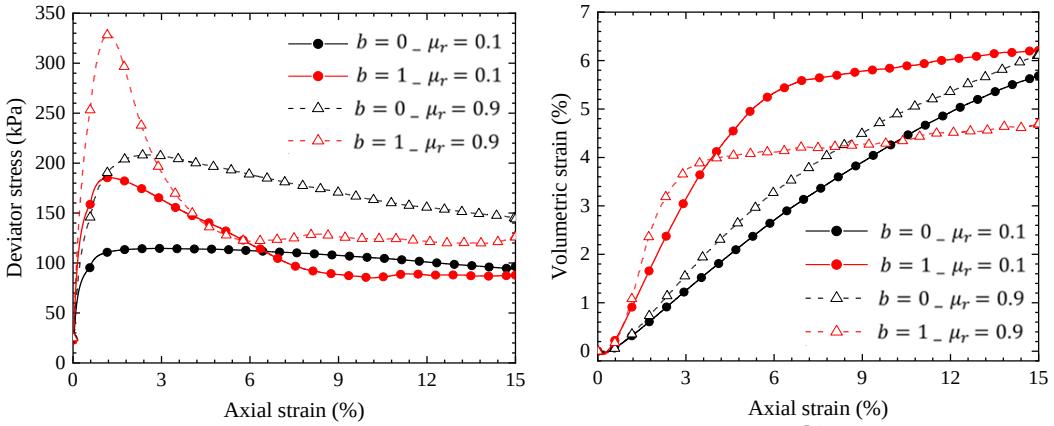

Figure 1. Evolution of (a) deviator stress and (b) volumetric strain during shearing with different rolling resistance coefficient under triaxial compression (b = 0) and extension (b = 1) conditions.

Figure 2 (a) presents the relative displacement field at the central plane of the specimen normal to the intermediate principal stress direction at an axial strain level of 12 % for shearing under both triaxial compression and extension conditions. The relative displacement (RD) field can be observed to be scattered across the specimen for shearing with μ_r = 0.1 and 0.9 in case of b = 0. On the contrary, large relative displacement has been noticed to concentrate along a specific region within the specimen when sheared under b = 1 condition indicating formation of localised instability in the form of shear band. The average normalised thickness (t/d_{50}) of the shear band has been estimated based on the relative displacement field as depicted in Fig. 2 (b). It can be observed that the thickness of the shear band reduces with increase in the rolling resistance. In this regard, it is well known that the dilation predominantly occurs within the shear band region of the dense specimens. Hence, reduction in the shear band thickness is the main reason for the lesser dilative response noticed for the specimen with high rolling resistance coefficient (Fig 1b).

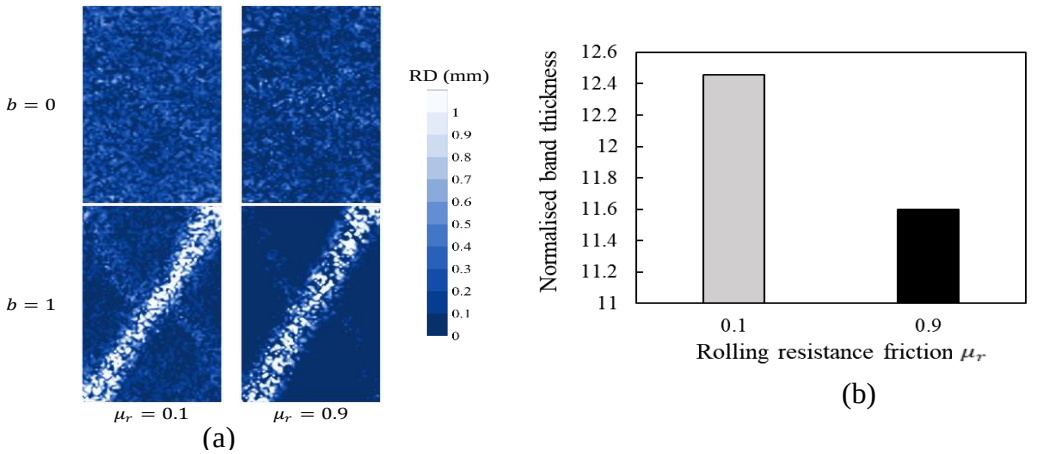

Figure 2. (a) Relative displacement (RD) field at 15 % axial strain level, (b) average normalised band thickness (t/d_{50}) of the specimen while shearing under triaxial extension (b = 1) condition.

4. References

[1] Wang, Q. & Lade, P. V. (2001). Shear banding in true triaxial tests and its effect on failure in sand. *J. Eng. Mech.*, **127**:754–761.

[2] Iwashita, K. & Oda, M. (1998). Rolling resistance at contacts in simulation of shear band. *J. Eng. Mech.*, **124**: 285–292.

EFFECT OF SHEAR DIRECITONAL ANGLES ON THE CYCLIC LIQUEFACTION OF SANDS: INSIGHT FROM DEM SIMULATIONS

Y. Zhang [1], M. J. Jiang[1,2,3,4]* M.C. Jia[4]

[1] School of Civil Engineering, Suzhou University of Science and Technology, Suzhou, Jiangsu 215009, China

[2] State Key Laboratory for Disaster Reduction in Civil Engineering, Tongji University, Shanghai 200092, China

[3] College of River and Ocean Engineering, Chongqing Jiaotong University, Chongqing 400074, China

[4] Department of Geotechnical Engineering, Tongji University, Shanghai 200092, PR, China

1. Introduction

Designing foundations for Offshore wind turbine are challenging as dynamically sensitive structures in the sense that natural frequencies of these structures are close to the environmental loads' [1]. The global natural frequency is dependent on the soil-structure stiffness, thus an investigation of soil responses under cyclic loads with varied directions is desired. Unlike the slender piles, monopile tends to rotate than bend under lateral loading. Therefore, the interactions between the monopile and the surrounding soil could be represented by cyclic simple shear tests. Cyclic responses of soil responses have been studied intensively [2, 3], but few of them were focused on the micro-mechanism underlying these responses. The aim of this paper is to study the soil stiffness responses under cyclic simple shear loading with a focus on the micromechanics. Experimental cyclic simple shear tests on typical sand are first presented. DEM simulations performed using PFC3D are then described, and the macroscopic stiffness and responses are validated against experiments. The micromechanical parameters are then analyzed to find the relationships between the micromechanical parameters and macroscopic responses.

2. Description of experimental tests and DEM setup

Cyclic simple shear apparatus was used for testing cylindrical samples of 50mm in diameter and 25mm in height. The sample height-to-diameter ratio is about 0.4 after compacting, agreeing with the ASTM D6528 [4] requirements. The tested sand with d50=0.18mm (PSD curve shown in Fig. 1), a specific gravity Gs=2.65 and minimum and maximum void ratio of 0.608 and 1.035 respectively. Cyclic simple shear tests with different shear directional angles and cyclic shear stress ratio (*CSR*) were performed.

DEM simulations of cyclic simple shear tests were performed using PFC3D [5]. The sample generated for testing is about 25mm in height and 50mm in diameter, containing 17000 balls with size ranging from 0.06mm to 0.09mm and d50=0.18mm, matching the value in experiments. Particle density is 2500 kg/m^3. Inter-particle and particle-boundary frictional coefficient, μ, is 0.5. Normal stiffness of particle is 8.0×107 N/m and shear stiffness of particle is 4.0×107 N/m. Normal and shear stiffness of boundary are 4.0×109 N/m. Two sets of samples were generated with radius

expansion approach followed by K0 consolidation with $\mu = 0.55$ to generate middle dense samples, The void ratios of dense samples at consolidation pressure of 100kPa is about 0.18, 60000 cycles were applied to each sample and 10 measurement circles were defined within the sample to measure the stress, void ratio and coordination number.

3. Discussions and Conclusions

Both experimental tests and DEM simulations of cyclic simple shear tests were performed to explore the variations of soil characteristics under cyclic loading and its underlying micro-mechanism. It has been found that:

• Shear modulus of sand decreases rapidly in the initial loading cycles as a result of cyclic loading, and then the rate of decrease diminishes when void ratio approaches constant;

• The shear modulus decreases as the angle varied from 30° to 60° , the shear strain of bidirectional shear samples developed more rapidly than that one-way loading as expected.

4. References

[1] Bhattacharya S , Adhikari S. (2011).Experimental validation of soil–structure interaction of offshore wind turbines[J].Soil Dynamics & Earthquake Engineering, 31(5-6):805-816.

[2] Vucetic M , Mortezaie A. (2015).Cyclic secant shear modulus versus pore water pressure in sands at small cyclic strains[J].Soil Dynamics & Earthquake Engineering, 70:60-72.

[3] Kong X J , Liu J M , Zou D G. et al. (2014). Experimental study of particle breakage of Zipingpu rockfill material[J].Yantu Lixue/Rock and Soil Mechanics, 35(1):35-40.

[4] ASTM D6528 – 07, (2007)

[5] Itasca, PFC3D manual 6.0 (2019)

Effect of cementation on the cyclic behaviour of sands: A 3D DEM investigation

A. Zhang, F. Collin
Urban and Environmental Engineering Research Unit, Université de Liège, Belgium

Offshore wind turbines (OWTs) play an important role in the clean energy transition. The offshore wind capacity is continuing to grow across the world to help reach the Net-zero target by 2050. The most common foundation for supporting wind turbines is monopile. The pile is subjected to cyclic loading caused by wind and sea waves. During the operational lifetime of OWTs, physio-chemical reactions may occur at the pile shaft and the adjacent sand due to the marine environments, as illustrated in Fig. 1, which can potentially affect the soil-pile interaction and hence the shaft capacity of the pile (i.e. a process termed pile ageing) [1, 2, 3, 4]. However, this effect has not yet been widely considered in the design of monopiles for OWTs since the underlying mechanisms remain to be understood.

To support the design of offshore wind piles on the operational lifetime scale, a better understanding of the underlying mechanisms of soil-monopile interaction is of importance, and therefore the intrinsic cyclic behaviour of soils around the monopile. This paper focuses on evaluating the impact of physio-chemical reactions on the mechanical performance of the soil around the monopile. For this goal, the discrete element method (DEM) is adopted in this study since it provides abundant microscopic insights which contribute to the understanding of the macroscopic mechanical behaviour. The physio-chemical effect is represented in the DEM model as a cementation process. Specifically, DEM samples without cementation (i.e. bare soil) and samples with cementation are generated. Different cementation contents are introduced to account for the accumulation of cementation in the operational lifetime of OWT. The cementing particles are modelled explicitly and assumed to grow at the grain contacts and gaps between grains [5, 6], as illustrated in Fig. 1.

The DEM samples are subjected to undrained cyclic loading to mimic the loading condition of soils around the pile shaft. The macroscopic cyclic responses of the bare soil sample and the cemented soil sample are compared. In addition, microscopic observations, such as the evolution of coordination number and bond breakage, are presented for a better understanding of the macroscopic mechanical behaviour.

This work is part of the SAGE-SAND project (Soil ageing around offshore wind turbine foundations - from operational response to decommissioning) supported by the Energy Transition Fund (ETF), Belgium.

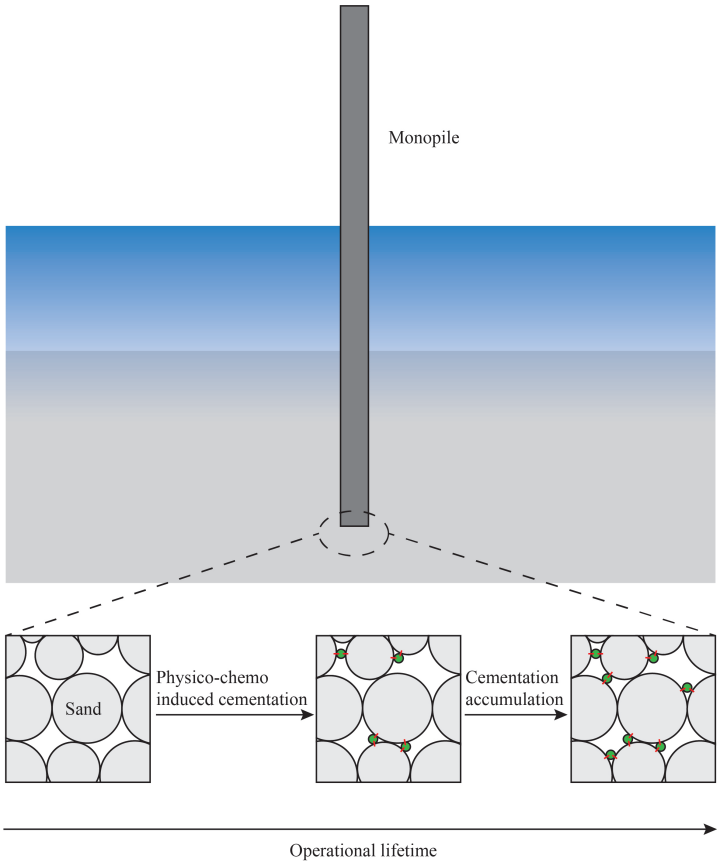

Figure 1. Schematics of cementation-induced soil ageing in offshore wind pile foundation. The grey particles represent sand grains, the green ones represent the cementing particles.

References

[1] Lehane, B. M., Schneider, J. A., Lim, J. K., and Mortara, G. (2012). Shaft friction from instrumented displacement piles in an uncemented calcareous sand. *J. Geotech. Geoenviron. Eng.*, **138**, 1357–1368.

[2] Lim, J. K. and Lehane, B. M. (2014). Characterisation of the effects of time on the shaft friction of displacement piles in sand. *Géotechnique*, **64**, 476–485.

[3] Gavin, K. and Igoe, D. (2021). A field investigation into the mechanisms of pile ageing in sand. *Géotechnique*, **71**, 120–131.

[4] Bittar, E., Lehane, B., and Zheng, H. (2023). The role of physicochemical processes in ageing of shaft friction of driven steel piles in sand. *Can. Geotech. J.*.

[5] Zhang, A. and Dieudonné, A.-C. (2023). Effects of carbonate distribution pattern on the mechanical behaviour of bio-cemented sands: A DEM study. *Comput. Geotech.*, **154**, 105152.

[6] Zhang, A. and Dieudonné, A.-C. (2023). Effects of carbonate distribution inhomogeneity on the improvement level of bio-cemented sands: A DEM study. *IACMAG*, pp. 554–561, Springer.

EFFECTS OF GRAIN SHAPE ANGULARITY ON COHESIVE STRENGTH IN SHEARED GRANULAR MEDIA

***T. Binaree*[1,2], *P. Jitsangiam*[1], *M. Renouf*[2] *and E. Azéma*[2,3]**

[1] *Chiang Mai University-Advanced Railway Civil and Foundation Engineering Center (CMU-RailCFC), Department of Civil Engineering, Faculty of Engineering, Chiang Mai University, 239 Huay Kaew Road, Muang, Chiang Mai, 50200, Thailand*

[2] *LMGC, Université de Montpellier, CNRS, Montpellier, France*

[3] *Institut Universitaire de France (IUF), Paris, France*

1. Abstract

In the realm of granular materials, cohesive interactions among particles play a pivotal role in influencing the macroscopic behavior of the material. The importance of cohesive granular media extends to a variety of fields, underpinning crucial aspects of particle processing, soil mechanics and powder technology. In the specific case of railway ballast, the presence of fine particles (resulting from the gradual degradation of the grains), combined with external agents (infiltration of water, silt, clay, climate variation), contribute to accelerate the deterioration of the ballasted track. These fine materials then act as a binder, causing the larger particles to stick together, drastically altering the stability characteristics of the ballasted track [1]. Wet or more generally cohesive granular materials have been extensively studied in the literature, using model experiments, numerical experiments, and theoretical approaches [2, 3] In general terms, local cohesive forces f_0 , whatever their origin, impart an extra cohesive strength c (also called "Coulomb cohesion") to granular materials in addition to the inherent frictional strength $\sin(\varphi)$, where φ is assumed to be the so-called macroscopic friction angle in dry condition. However, in the large majority of existing work dealing with cohesive or wet granular media, circular (in 2D) or spherical (in 3D) particles have been used. Real grains can have irregular/elongated/non-convex shapes with potentially more than one point of contact, thus increasing their net particle-particle cohesive/friction force which, in turn, will increase the cohesive/friction strength of the system by impeding particle rotations. Considering a realistic shape is even more crucial in a railway context to improve track design, maintenance practices, and overall railway system performance. How the cohesive strength, and the underlying microstructure, evolves depending on grain shape remains largely unexplored. . We present a systematic numerical investigation concerning the effects of particle shape (i.e., angularity) parameters on the quasi-static shear strength of cohesive granular packings under bi-axial conditions for various confining stress P. We consider irregular polygons with an increasing number of sides, ranging from triangles to disks. The packings behavior depends on the dimensionless number $\eta = f_0/Pd$, also known as the cohesion index, being d the average grain diameter. η is varied between 0 (dry) to 0.6 (strongly cohesive) by varying P. We find that the macroscopic friction angle increases with grain angularity and saturates at larger angularity, as in dry case. In contrast, the cohesive strength is an increasing function of grain angularity. In other word, our numerical results evidence the amplifying effect of particles shape angularity on the cohesive strength in cohesive granular media

References

[1] Trinh, V. N., Tang, A. M., Cui, Y.-J., Dupla, J.-C., Canou, J., Calon, N., Lambert, L., Robinet, A., and Schoen, O. (2012). Mechanical characterisation of the fouled ballast in ancient railway track substructure by large-scale triaxial tests. *Soils and Foundations*, **52**, 511–523.

[2] Khamseh, S., Roux, J.-N., and Chevoir, F. m. c. (2015). Flow of wet granular materials: A numerical study. *Phys. Rev. E*, **92**, 022201.

[3] Gans, A., Pouliquen, O., and Nicolas, M. (2020). Cohesion-controlled granular material. *Phys. Rev. E*, **101**, 032904.

EFFECTS OF PARTICLE SHAPE OF FALLING ROCK CLUSTERS ON THE IMPACT FORCE EXERTED ON RIGID BARRIER: INSIGHTS FROM DISCRETE ELEMENT MODELLING

Yanhao ZHENG[1,2], King Hung Michael WONG[1] and Yi Pik Helen CHENG[1]

[1] University College London, Civil, Environmental and Geomatic Engineering, London, United Kingdom

[2] Harbin Institute of Technology (Shenzhen), School of Civil and Environmental Engineering, Shenzhen, China

Rock shape plays an important role in determining the falling trajectory and dynamic behaviour of rockfall [1] [2]. Understanding the effects of the shape of falling rock particles under different conditions is of great significance for designing protective structures. In this study, three distinct shapes of clump templates with the same volume, namely sphere, tetrahedron, and cube (see Figure 1), are constructed using the discrete element method to model realistic rocks. The constricted clump consists of overlapping rigid spherical balls that do not generate contact forces, and it is a rigid entity with deformable boundaries. The effects of particle shape on the impact force acting on a vertical rigid barrier are examined by simulating two different volumes of rock clusters (containing 53 particles and 99 particles, respectively) falling down along three slopes with different inclinations (40°, 45°, and 50°, see Figure 2). The three-dimensional discrete element simulation results show that while always reaching the barrier first, the spherical particles exert the maximum peak impact force on the barrier under different slope inclination angles, followed by cubic and then tetrahedra particles. The sphericity of falling rock (by Eq. (1)) has an obvious enhancement effect on the impact force exerted on the rigid barrier, and such an effect becomes significant with the increase of the particles in the rockfall. Compared to those with low sphericity, the interaction between the particles of falling rocks with high sphericity is smaller, which causes less energy loss, thus resulting in greater impact force. In addition, the relative roughness between the rock particle and slope surface composed of small balls also affects the impact force exerted on the rigid barrier.

Figures and equations

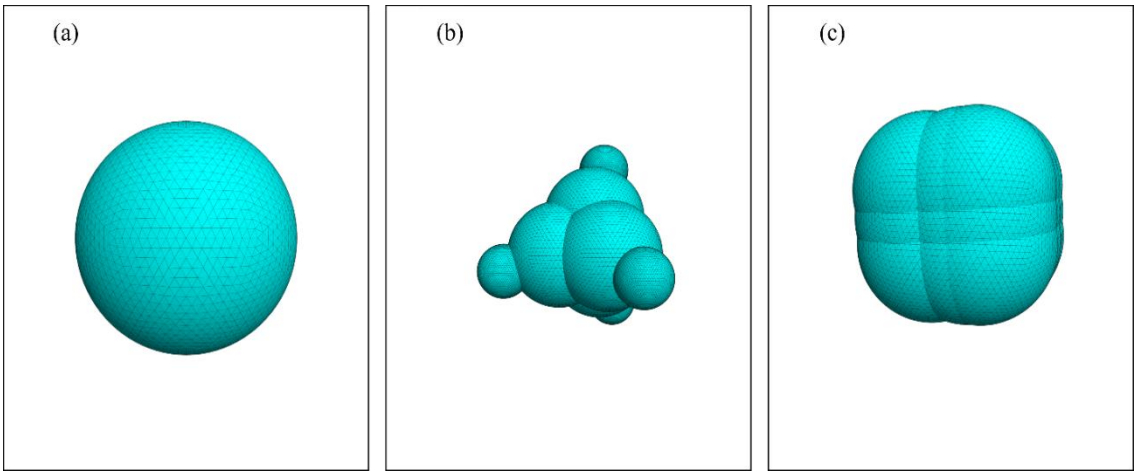

Figure 1. Three distinct shapes of clump templates for the PFC3D analysis: (a) sphere; (b) 8-ball tetrahedral clump; (c) 27-ball cubic clump

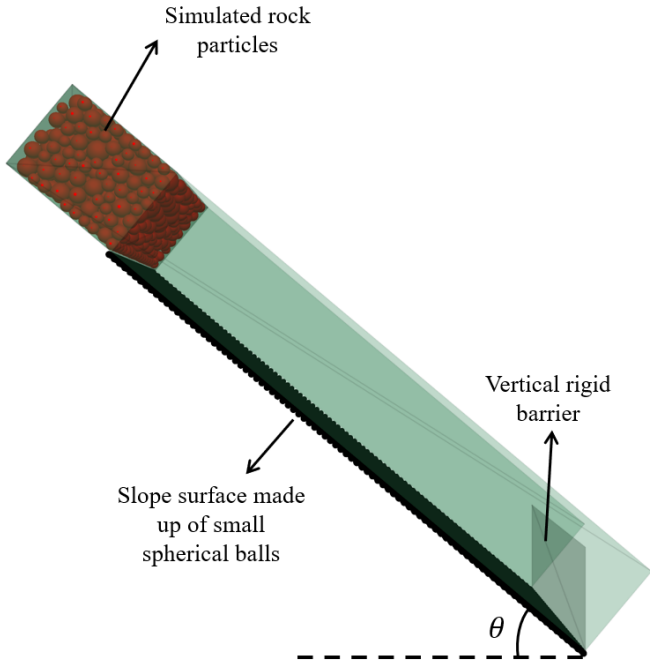

Figure 2. Numerically generated slope models with three inclination angles (θ =40°, 45° and 50°)

The sphericity of rock particles, *S*, is calculated by equation (1) [3], as follows:

$$S = \sqrt[3]{\frac{36\pi V^2}{A^3}} \tag{1}$$

where V is the Volume of rock particle and A is the total area of particle surface.

References

[1] Wang, I.T. & Lee, C.Y. (2010). Influence of slope shape and surface roughness on the moving paths of a single rockfall. *International Journal of Civil and Environmental Engineering*, 4(5), pp.122-128.

[2] Gao, G. & Meguid, M.A. (2018). On the role of sphericity of falling rock clusters—insights from experimental and numerical investigations. *Landslides*, 15(2), pp.219-232.

[3] Zheng, W., Hu, X. & Tannant, D.D. (2020). Shape characterization of fragmented sand grains via X-ray computed tomography imaging. *International Journal of Geomechanics*, *20*(3), p.04020003.

EVALUATING THE IMPACT OF DEM PARAMETERS ON THE ANGLE OF REPOSE

S. Moriguchi[1], M. Otsubo[2], A. Oya[3], A. Kono[4], M. Taue[5], H. Saomoto[6], S. Kajiyama[7], N. Kikkawa[8], and Y. Nakata[5]

[1] Tohoku University, International Research Institute of Disaster Science, Sendai, Japan
[2] Public Works Research Institute, Soil Mechanics and Dynamics Research Team, Tsukuba, Japan
[3] ITOCHU techno-solutions corporation, Science & Engineering System Division, Tokyo, Japan
[4] Railway Technical Research Institute, Railway Dynamics Division, Tokyo, Japan
[5] Yamaguchi University, Graduate School of Sciences and Technology for Innovation, Ube, Japan
[6] National Institute of Advanced Industrial Science and Technology, Research Institute of Earthquake and Volcano Geology, Tsukuba, Japan
[7] University of Yamanashi, Graduate Faculty of Interdisciplinary Research, Kofu, Japan
[8] National Institute of Occupational Safety and Health, Construction Safety Research Group, Kiyose, Japan

1. Introduction

Numerical analysis has been highly developed and recognized as a powerful tool. The Discrete Element Method (DEM) [1] is one such method and has been widely applied to engineering problems, such as understanding the relationship between micro- and macro-behavior of geomaterials and risk assessment of slope disasters. However, theoretically proving the validity of DEM analysis is generally difficult, except under simple calculation conditions. As a result, systematizing the Validation and Verification (V&V) of DEM remains challenging. To address this issue, the TC105 Japanese domestic committee conducted an international round-robin test [2] to reproduce the results of Angle of Repose (AOR) experiments [3] using artificial particles created by a 3D printer. In this study, a sensitivity analysis of DEM input parameters was performed on one of the AOR experiments to analyze the influence of DEM parameters.

2. AOR experiment

Figure 1 depicts the apparatus used in the AOR experiment examined in this study. The device was composed of acrylic boards, and the artificial particles were made of resin. A total of 2150 particles were placed in the box. Subsequently, the front panel of the box was raised at a constant speed of 43 mm per second by the motor. As a result, a portion of the particles flowed out from the box, forming the repose angle. Figure 2 shows the image of the AOR measured in the experiment.

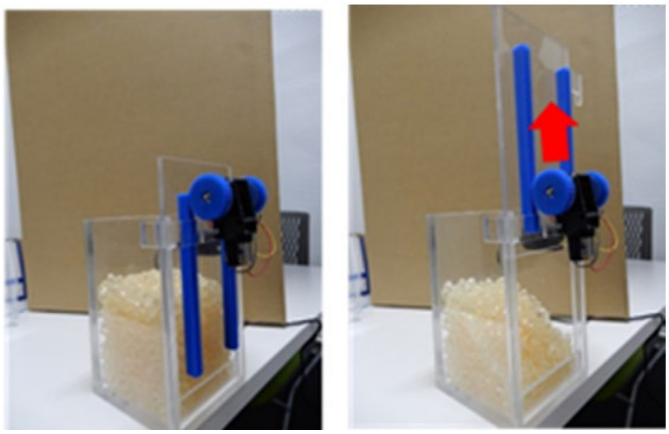

Figure 1. Experimental apparatus [3].

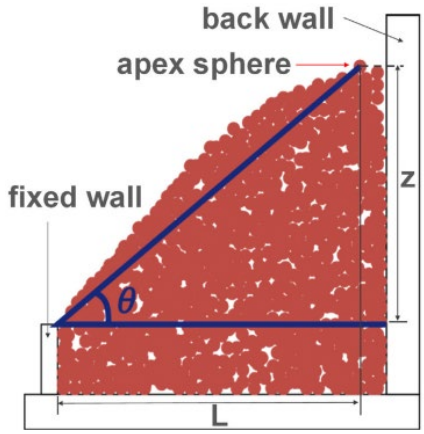

Figure 2. Schematic illustration of AOR [3].

3. Sensitivity analysis

The impact of three input parameters, such as the coefficient of restitution, friction angle between wall and particle, and friction angle between particles are quantified through DEM simulation. To enhance the generality of the discussion, we used several different analysis program codes, and 27 parameter sets were considered to generate the data for the sensitivity analysis. In the analysis, we independently utilized five different sensitivity analysis methodologies: (1) linear regression analysis (LR), (2) Random Forest (RF) [4] with the feature importance, (3) Random Forest with the permutation importance (RF-PI) [5], (4) the XGBoost [6] with the feature importance (XGB), and (5) the XGBoost with the permutation importance (XGB-PI), respectively. Obtained values in sensitivity analysis were normalized to be described as contribution ratio of the three input parameters. The contribution ratio obtained by different program codes and different sensitivity analysis methodologies are shown in Figure 3. Although there are some differences among the codes, the coefficient of restitution, the friction angle between particles, and the friction angle between wall and particle tended to have the strongest influence, in that order.

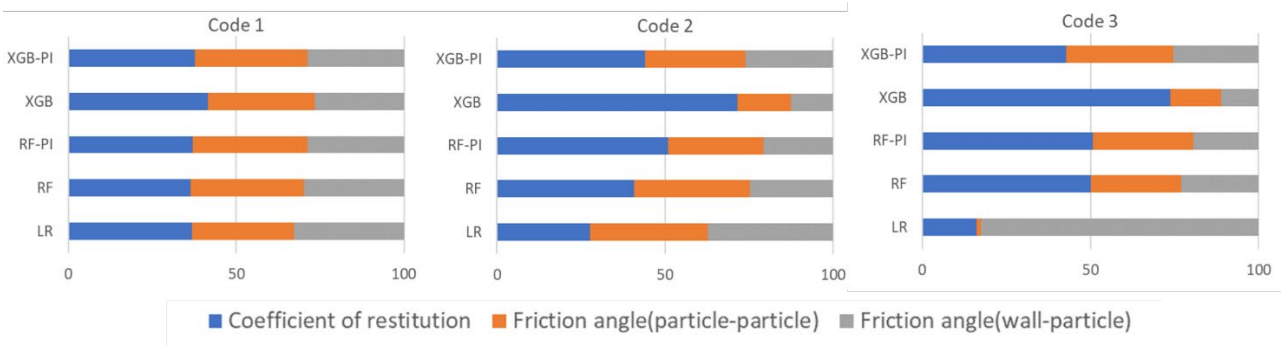

Figure 3. Quantified contribution ratio of input parameters.

5. Conclusion

This study aimed to quantify the impact of three input parameters on the AOR of artificial particles generated by a 3D printer. A series of DEM simulations were conducted using different program codes, and the sensitivity analysis was performed through five different methodologies. The results qualitatively indicated that the coefficient of restitution, the friction angle between particles, and the friction angle between wall and particle had the strongest effects, in that order. However, more detailed studies and analyses are needed in the future to further validate and refine the findings.

References

[1] Cundall, P.A., Strack, O.D.L., A discrete numerical model for granular assemblies, Géotechnique, Vol.29, Issue 1, 47–65, 1979.

[2] Saomoto, H. et al., Round robin test on angle of repose: DEM simulation results collected from 16 groups around the world, Soils and Foundations, Vol. 63, Issue 1. 101272

[3] Nakata, Y. et al., Soils and Foundations, Vol. 62, Issue 4, 101178. 2022.

[4] Breiman, Leo., Random Forests, Machine Learning, Vol. 45, Issue 1, 5–32, 2001.

[5] Altmann, André, Laura Toloşi, Oliver Sander, and Thomas Lengauer. 2010. "Permutation Importance: A Corrected Feature Importance Measure." Bioinformatics 26 (10): 1340–47.

[6] Chen, Tianqi, and Carlos Guestrin. 2016. "XGBoost: A Scalable Tree Boosting System." In Proceedings of the 22nd ACM SIGKDD International Conference on Knowledge Discovery and Data Mining, 785–94. KDD '16. New York, NY, USA: Association for Computing Machinery.

EVOLUTION OF FABRIC DUE TO SUSCEPTIBILITY OF FINE PARTICLES IN INTERNALLY UNSTABLE GAP-GRADED SOILS

R.R. Dhamne[1], M.M. Disfani[2] and A. Mehdizadeh[3]

[1,2,3] Department of Infrastructure Engineering, The University of Melbourne, Parkville, Victoria 3010, Australia

1. Area of Research

Structures such as dams and levees play a pivotal role in water supply and management. Safeguarding these paramount structures against soil erosion remains an ongoing challenge with 54% of worldwide embankment dam failures post-1950 attributed to internal erosion [1].

Suffusion, a significant mode of internal erosion, involves the transport of non-plastic fines through constrictions formed by coarser particles caused by seepage forces. Soils prone to suffusion, labeled as "internally unstable" experience fines detachment, transportation, and migration of fine particles when geometrical and hydraulic conditions are met. This can ultimately lead to alterations in soil pore structure and under certain conditions cause changes to its fabric and stress carrying matrix. The change in fabric affects the overall mechanical properties of soil through the readjustment of particles, their interparticle contacts, and pore network. This study investigates the impact of controlling parameters—such as gap ratio, fine content, and relative density—on gap-graded granular fabric under isotropic compression stress conditions. Discrete Element Modelling results indicate critical values for gap ratios, fine contents, and relative density that induce transitions in soil fabric, identified through variations in contact distributions, strong contact network and stress-transfer characteristics.

2. Methodology

To assess the erosive potential of cohesionless fines in terms of effective stresses developed on the particles, a series of three-dimensional Discrete Element Method (DEM) simulations were conducted. The simulations involved cubical assemblies of gap-graded soils composed of spherical particles. Particle Flow Code (PFC3D) [2] was used for the particulate scale simulations in this study.

3. Basic Assumptions

The samples were created by generating a cloud of non-overlapping spherical particles. Periodic boundary condition was utilized in the analyses to generate samples that mimic infinite size, eliminating boundary effects typically associated with rigid boundaries. The Hertz-Mindlin contact model was used. Particle-size distributions with gap ratios (GR) of 2 and 5, along with fine contents (f_c) ranging from 10% to 50%, were replicated in DEM using data from sieve analysis. These distributions were created by applying power-law distribution functions to randomly allocate the necessary number of particles in both the fine and coarse fractions. To avoid segregation, inhomogeneity, and anisotropy in the packing, gravitational effects were omitted. The samples were compressed isotropically and monotonically to mean normal stress of p'=140 kPa [3].

A different approach was employed to measure the relative density of gap-graded granular packings in DEM, based on modification of the interparticle friction coefficient under a constant confining pressure [3].

4. Results

From the analysis, it has been observed that the void ratio which can be obtained by bimodal samples falls as the gap ratio increases (Figure 1), in agreement with DEM simulations [3] and experimental results. Bimodal soils with GR = 2 exhibit minimal variations in void ratio, stress transfer, coordination number, and percentages of contact types.

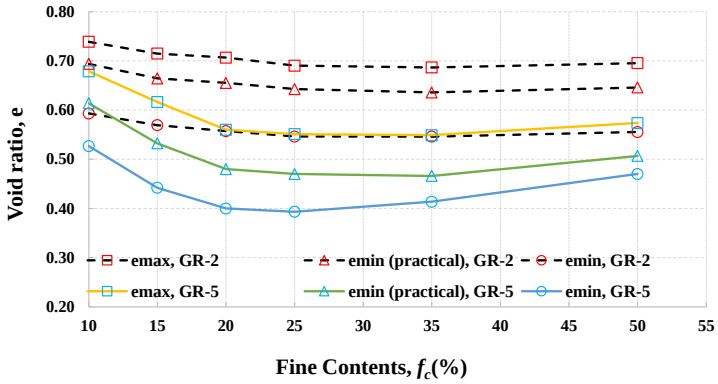

Figure 1. Variation in void ratios concerning fine content and gap ratio.

These similarities to uniform soils can be attributed to the comparable sizes of smaller pores and fine particles, where fine and coarse particles play an approximately equal role in stress transfer ($\alpha^{DEM} \approx 1$) regardless of fine contents and relative density. A soil with GR = 5 and FC ≤ 15% stays internally unstable, as the coarse fraction forms a continuous contact network, leaving most fine particles under-stressed in voids between coarse particles. α^{DEM} further remains constant ($\alpha^{DEM} \approx 1$) when FC = 50% regardless of relative density and gap ratio (Figure 2).

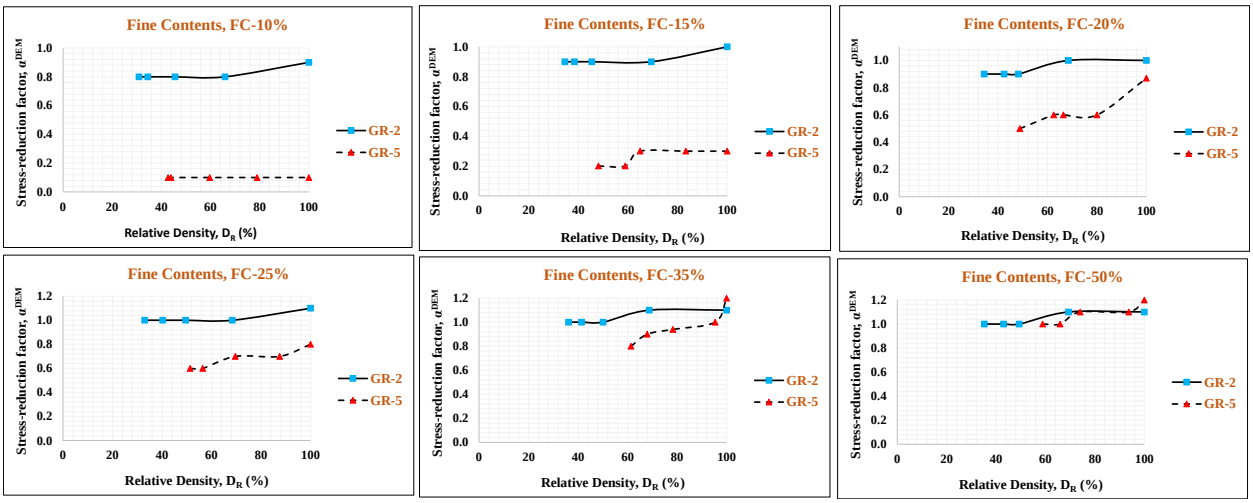

Figure 2. Variation of average stress reduction factor (α^{DEM}) with gap ratio and relative density.

5. References

[1] Foster M., Fell R. & Spannagle M. (2000). A method for assessing the relative likelihood of failure of embankment dams by piping. *Canadian Geotechnical Journal*, **37(5)**:1025-1061.

[2] Itasca Consulting Group, Inc. (2005). PFC3D, v. 3.1. Minneapolis, USA.

[3] Ahmadi M., Shire T., Mehdizadeh A. & Disfani M. (2020). DEM modelling to assess internal stability of gap-graded assemblies of spherical particles under various relative densities, fine contents and gap ratios. *Computers and Geotechnics*, **126**:103710.

EVALUATION OF ELASTIC AND PLASTIC STRAIN RATES FROM DEM SIMULATIONS AND CONSTRUCTION OF CONSTITUTIVE MODELS FROM DATA

***Xuzhen He*[1]**

[1] *School of Civil and Environmental Engineering, University of Technology Sydney, Australia*

1. General

Recently, both experiments and discrete element method (DEM) simulations confirm the existence of irreversible deformation for any finite but small stress increment, so to account for this in constitutive models, plastic strain should be specified at any state for small deformation in any direction. Traditionally, yield surfaces and flow potentials (thus can be used to determine plastic strain) are mostly summarised from experimental observations where the elastic strain is negligible. This way is impossible for states and deformation where the plastic dissipation is small.

In this study, the elastic and plastic strain rate are directly evaluated in DEM simulation, which is achieved by assuming that the rate of conservative energy defined in term of elastic strain rate equals the energy rate at contacts of granular assemblies. With these elastic and plastic strain rate data at any state for deformation in any direction, constitutive equations regarding the dilatancy, plastic deviatoric strain rate and stress rate are summarised. Simulations show that the predictions match both virtual and Toyoura sand satisfactorily in various shear tests within a board range of densities. Additionally, the calibration of parameters is extremely simple.

2. Work–energy analysis of granular assemblies

For granular assemblies, the external power input density equals the internal power density, which happens only at contacts as $\widetilde{W}_c = \frac{1}{V}\sum_{c\in V} f^{ne,c}\dot{\delta}^c + \frac{1}{V}\sum_{c\in V} \boldsymbol{f}^{te,c}\cdot\Delta\boldsymbol{v}^{c,t} + \frac{1}{V}\sum_{c\in V} \boldsymbol{M}^c\cdot\Delta\boldsymbol{\omega}^c$. Here, the rate of kinetic energy and the rate of viscous dissipation are ignored for quasi-static deformations. $\boldsymbol{f}^{e,c}$ is the non-viscous part of the contact force between internal contacts, and it can be decomposed into normal ($f^{ne,c}$) and tangential ($\boldsymbol{f}^{te,c}$) components. $\boldsymbol{M}^c$ is the contact moment. $\Delta\boldsymbol{v}^c = \boldsymbol{v}^{c,h} - \boldsymbol{v}^{c,g}$ is the relative velocity at contact *c* between two grains *h* and *g*. It can also be decomposed into normal ($\dot{\delta}^c$) and tangential ($\Delta\boldsymbol{v}^{t,c}$) components. Similar relations are defined for $\Delta\boldsymbol{\omega}^c$.

The power density of normal contact forces is always conservative and thus define $\dot{\Phi}^{fn} = \frac{1}{V}\sum_{c\in V} f^{c,en}\dot{\delta}^c$. The work done by tangential contact force at a contact can be conservative or dissipative. The tangential contact force is limited by a yield surface, the work done by it is dissipative only if the tangential contact force is on the yield surface and $\boldsymbol{f}^{c,et}\cdot\Delta\boldsymbol{v}^{c,t} > 0$. Therefore, the power density of tangential contact force is decomposed into two parts – $\dot{\Phi}^{ftc} = \frac{1}{V}\sum_{c\in Sf_c} \boldsymbol{f}^{c,et}\cdot\Delta\boldsymbol{v}^{c,t}$ and $\widetilde{\Psi}^{ftd} = \frac{1}{V}\sum_{c\in\overline{Sf_c}} \boldsymbol{f}^{c,et}\cdot\Delta\boldsymbol{v}^{c,t}$, where Sf_c is the set of contacts where the work done by the tangential contact force is conservative, and $\overline{Sf_c}$ denotes the rest dissipative contacts. Similar treatment is for contact moments – $\dot{\Phi}^{mc} = \frac{1}{V}\sum_{c\in Sm_c} \boldsymbol{M}^c\cdot\Delta\boldsymbol{\omega}^c$ and $\widetilde{\Psi}^{md} = \frac{1}{V}\sum_{c\in\overline{Sm_c}} \boldsymbol{M}^c\cdot\Delta\boldsymbol{\omega}^c$. $\dot{\Phi}^e = \dot{\Phi}^{ftc} + \dot{\Phi}^{mc}$ is the rate of energy stored as shear deformation at contacts. $\widetilde{\Psi} = \widetilde{\Psi}^{ftd} + \widetilde{\Psi}^{md}$ is the dissipation rate at contacts.

Readers are referred to He *et. al.* (2020) for detailed information about DEM setup. Figure 1a illustrates different components during the undrained shear of a loose specimen, and Figure 1b compares different mechanical rates of a dense and a loose specimen in drained tests.

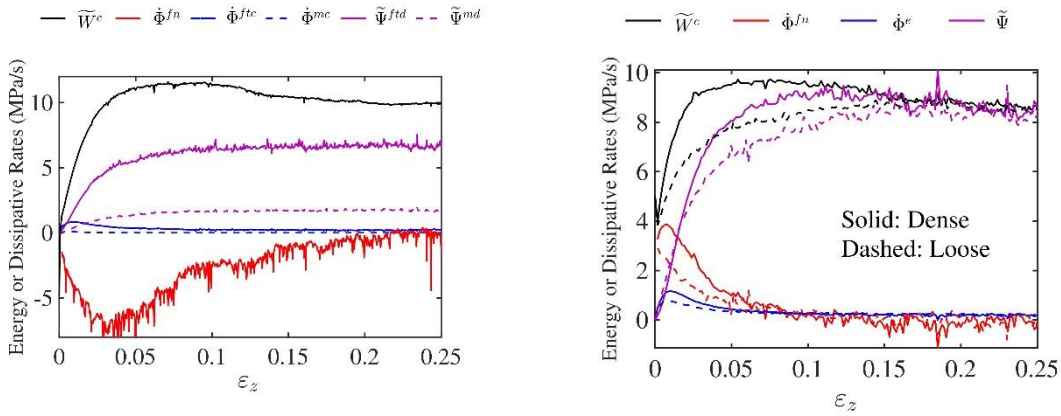

Figure 1. Conservative energy or dissipative energy rates during shearing. (a) different components in an undrained test (e = 0.655, p_0 = 2.0 MPa) (d) dense and loose specimens in drained tests.

3. Split and evaluation of strain rates

In elastoplasticity, the strain rate is split into an elastic and a plastic strain rate ($\dot{\boldsymbol{\varepsilon}} = \dot{\boldsymbol{\varepsilon}}^e + \dot{\boldsymbol{\varepsilon}}^p$) such that the energy rate is related to the elastic strain rate by $\dot{\Phi} = \boldsymbol{\sigma}: \dot{\boldsymbol{\varepsilon}}^e$ and the dissipation rate is related to the plastic strain rate by $\widetilde{\Psi} = \boldsymbol{\sigma}: \dot{\boldsymbol{\varepsilon}}^p$. Also, strain rate can be written as the sum of a volumetric part and a deviatoric part, so $\dot{\Phi} = p\dot{\varepsilon}_v^e + \mathbf{s}: \dot{\boldsymbol{\varepsilon}}^e$ and $\widetilde{\Psi} = p\dot{\varepsilon}_v^p + \mathbf{s}: \dot{\boldsymbol{\varepsilon}}^p$. So, if $p\dot{\varepsilon}_v^e$ is assumed to be identical to $\dot{\Phi}^{fn}$, an elastic volumetric strain rate is obtained directly from grain-scale data. Similarly, elastic deviatoric strain rate is obtained by assuming that $\mathbf{s}: \dot{\boldsymbol{\varepsilon}}^e$ equals $\dot{\Phi}^e$. With elastic strain rate available, the plastic strain rate is evaluated from $\dot{\boldsymbol{\varepsilon}}^p = \dot{\boldsymbol{\varepsilon}} - \dot{\boldsymbol{\varepsilon}}^e$.

Figure 2 shows some results of the evaluated strain rates for illustration. For the undrained shear of a loose specimen (Figure 2a), $\dot{\varepsilon}_v^e$ is negative, which agrees with the observation in laboratory tests that p will decrease. $\dot{\varepsilon}_v^p$ is positive and $\dot{\varepsilon}_v$ keeps zero. Vice verse for a dense specimen.

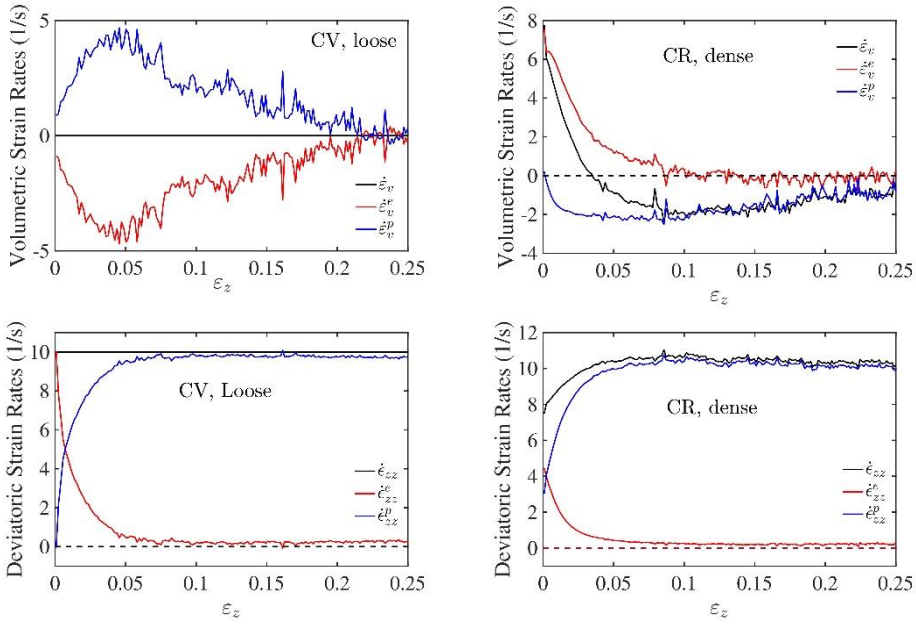

Figure 2. Evaluated strain rates. Top: volumetric; Bottom: deviatoric; Left: undrained; Right: drained.

The construction of constitutive model from the data will be discussed in the next two chapters in the full paper.

4. References

[1] He, X., Wu, W., Cai, G., Qi, J., Kim, J. R., Zhang, D., & Jiang, M. (2020). Work–energy analysis of granular assemblies validates and calibrates a constitutive model. *Granular Matter*, *22*(1), 28. https://doi.org/10.1007/s10035-019-0990-7

Exploring undrained cyclic true triaxial behaviour of granular assemblies using DEM

***M. Salimi*[1], *M. Tafili*[1], *N. Irani*[1] *and T. Wichtmann*[1]**
[1] *Ruhr-University Bochum, Bochum, Germany*

1. Introduction

Experimental investigations demonstrated that among other factors, also sand fabric anisotropy, which primarily arises from the preferred orientation of particles, vectors of contact normals, and the voids among particles [1, 2], can play a crucial role in the load-bearing capacity of shallow foundations located on anisotropic sands [3, 4] as well as strain localization in soil specimens [5]. Furthermore, the shear strength of granular soils demonstrates a clear dependency on the third deviatoric stress invariant, denoted by Lode angle (θ) [6, 7], and the corresponding effects cannot be accurately measured through conventional triaxial tests. The aforementioned studies, as well as other studies in the literature (e.g., [8, 9]), emphasize the significance of investigating soil response under undrained cyclic true-triaxial tests while considering fabric anisotropy and Lode angle effects. However, the process of loading fully saturated samples under general stress conditions in a laboratory setting has been known to pose certain difficulties [10]. Suitable test devices for such experimental studies, like hollow cylinders or true triaxial devices, are only available in specialized laboratories, and performing high-quality experiments in these devices is laborious and requires significant experience. The primary objective of this study is to investigate the undrained response of granular soil under true triaxial conditions considering the role of fabric anisotropy in terms of initial fabric and principal stress. To achieve this, a range of soil samples have been simulated with varying initial fabrics, utilizing non-spherical particle shapes, and subjected to cyclic loading along paths with different Lode angles (see Fig. 1). The coupled DEM-CFM (Coupled Fluid Method) scheme has been employed to consider the impact of fluid-solid interaction under cyclic undrained conditions. The liquefaction susceptibility of granular assemblies, the effect of the Lode angle on the undrained cyclic response of granular soils, the slope of the phase transformation and the failure line have been investigated under various loading conditions.

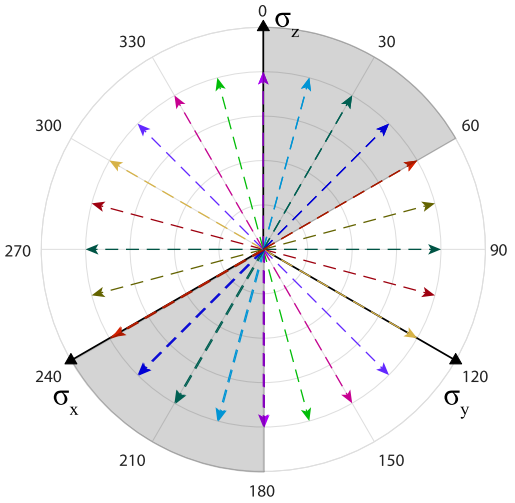

Figure 1. Illustration of applied proportional stress paths.

2. Sample preparation and methodology

For the sample preparation of the DEM simulations three overlapped spheres were used to produce non-spherical (elongated) particles (see [11, 12]). The aspect ratio (length:width) of the considered clump particles amounted 1.8:1. The diameter of pebbles was determined using an optimization method proposed by [13]. Since poorly graded sands are more prone to liquefaction than well-graded ones, a Grain Size Distribution (GSD) curve as in [11, 12] with a coefficient of uniformity $C_u = 1.5$ and a coefficient of curvature $C_c = 1.02$ is adopted in this study. Four types of specimens were created for this investigation utilizing elongated particles with different initial fabrics (say inherent anisotropy), including an isotropic specimen (ISO) and three transversely isotropic specimens (TR0, TR45, and TR90) with bedding plane angles of 0°, 45°, and 90°.

Simulations were carried out with constant total mean stress (isobaric condition) at a fixed Lode angle. It was assumed that the major principal stress is applied along the z-axis (in the vertical direction) leading to compression loading with θ ranging from 0° to 60° (stress paths are highlighted in Fig. 1).

3. Results

The coupled DEM-CFM element simulations demonstrate the combined effect of the Lode angle and anisotropic microstructure of the particulate assemblies on the accumulation of pore water pressure, mobilized shear strength, and deformation characteristics of granular soils. It was observed that the samples tend to exhibit stress paths that approach zero mean effective stress from extension loading as depicted in Fig. 2. The number of cycles required for liquefaction increases with increasing bedding plane inclination. Fig. 3 shows that excess pore water pressure generation is directly linked to the degradation of the coordination number as a result of the reduction of overall effective stress. When excess pore water pressure develops, it exerts additional forces on the soil particles, affecting their arrangement and inter-particle contacts. As the pore water pressure increases, the effective stress acting on the soil decreases, leading to a reduction in the coordination number as well as on the secant shear modulus G_{sec}. Fig. 3 presents only the results from isotropic samples, whereas considering the shear modulus degradation with the number of cycles of TR0, TR45, and TR90 samples further suggests that initial fabric is at the origin of the differences in behaviour during compression and extension. Hence, it may be suggested that with a rise in bedding plane inclination, the samples become more stiffer in the vertical direction than in the horizontal direction. The results of other samples will be provided in the extended version of this contribution.

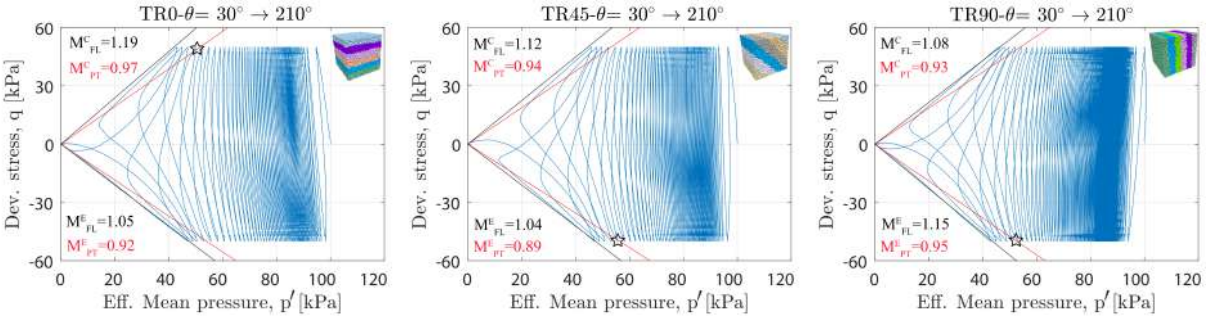

Figure 2. $q - p'$ relationship obtained from DEM simulations considering samples with different initial fabric under undrained cyclic true triaxial loading with Lode angle $\theta = 30°$ to $210°$.

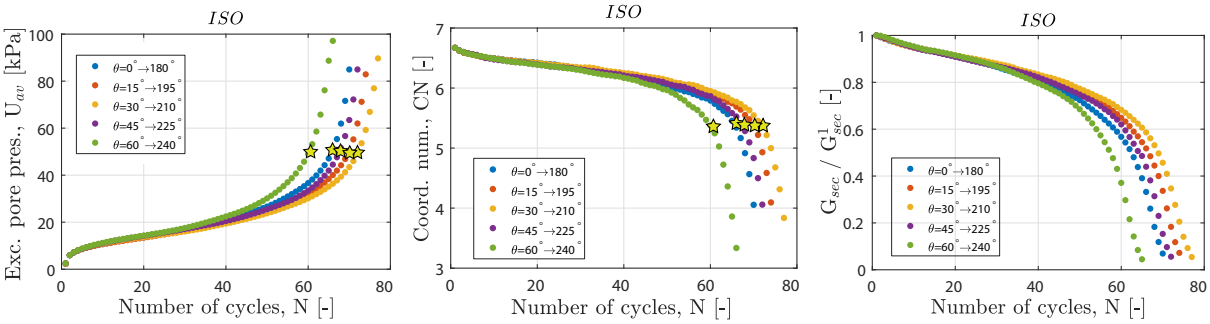

Figure 3. Excess pore water pressure, variation of coordination number CN and variation of normalised G_{sec} versus the number of cycles for medium dense ISO samples (The asterisk marks indicate the point where the phase transformation line intersects with the effective stress path.).

References

[1] Guo, N. and Zhao, J. (2013). The signature of shear-induced anisotropy in granular media. *Computers and Geotechnics*, **47**, 1–15.

[2] Jiang, M., Zhang, A., and Fu, C. (2018). 3-d dem simulations of drained triaxial tests on inherently anisotropic granulates. *European Journal of Environmental and Civil Engineering*, **22**, s37–s56.

[3] Azami, A., Pietruszczak, S., and Guo, P. (2010). Bearing capacity of shallow foundations in transversely isotropic granular media. *International Journal for Numerical and Analytical Methods in Geomechanics*, **34**, 771–793.

[4] Qin, J., Zeng, X., and Ming, H. (2016). Centrifuge modeling and the influence of fabric anisotropy on seismic response of foundations. *Journal of geotechnical and geoenvironmental engineering*, **142**, 04015082.

[5] Lu, X., Huang, M., and Qian, J. (2011). The onset of strain localization in cross-anisotropic soils under true triaxial condition. *Soils and foundations*, **51**, 693–700.

[6] Perić, D. and Ayari, M. A. (2002). On the analytical solutions for the three-invariant cam clay model. *International Journal of Plasticity*, **18**, 1061–1082.

[7] Gutta, S. K. (2003). *Modeling large three-dimensional stress reversals in cross-anisotropic sands*. University of Delaware.

[8] Vaid, Y. and Sivathayalan, S. (1996). Static and cyclic liquefaction potential of fraser delta sand in simple shear and triaxial tests. *Canadian Geotechnical Journal*, **33**, 281–289.

[9] Zhang, A., Jiang, M., and Wang, D. (2023). Effect of fabric anisotropy on the cyclic liquefaction of sands: Insight from dem simulations. *Computers and Geotechnics*, **155**, 105188.

[10] Mayne, P. W., Coop, M. R., Springman, S. M., Huang, A.-B., and Zornberg, J. G. (2009). Geomaterial behavior and testing. *Proceedings of the 17th International Conference on Soil Mechanics and Geotechnical Engineering (Volumes 1, 2, 3 and 4)*, pp. 2777–2872, IOS Press.

[11] Salimi, M. and Lashkari, A. (2020). Undrained true triaxial response of initially anisotropic particulate assemblies using cfm-dem. *Computers and Geotechnics*, **124**, 103509.

[12] Salimi, M., Tafili, M., Irani, N., and Wichtmann, T. (2023). Micro-mechanical response of transversely isotropic samples under cyclic loading. *10th European Conference on Numerical Methods in Geotechnical Engineering (NUMGE2023)*, pp. 1–6.

[13] Price, M., Murariu, V., and Morrison, G. (2007). Sphere clump generation and trajectory comparison for real particles. *Proceedings of Discrete Element Modelling 2007*.

Exploring the Validity of a DEM inspired Effective Stress Approach in Wet Polydisperse Granular Materials

D. Cantor[1,2], C. Ovalle[1,2], and Emilien Azéma[3,4]

[1] Department of Civil, Geological, and Mining Engineering, Polytechnique Montreal, QC, Canada
[2] Research Institute of Mining and Environment, RIME UQAT- Polytechnique, Montreal, QC, Canada
[3] LMGC, Université de Montpellier, CNRS, Montpellier, France
[4] Institut Universitaire de France (IUF), Paris, France

The Effective Stress Principle (ESP) stands as one of the most renowned and fundamental theories in geotechnical engineering. Attributed to Karl Terzaghi in the early 20th century [1], the ESP was developed to understand the mechanical behavior of soils whose pores are fully filled with water. Since then, the ESP has become a cornerstone theory in the field; robust and simple, it seemed natural to try to extend it to soils where both water and air occupy the pores (unsaturated soils). Over more than 70 years, researchers have tried to generalize the notion of effective stress to all types of soils [3-9]. To date, no one has fully succeeded. Only recently, by means of discrete-element modeling (DEM), several works have suggested that the ESP can still be applied to unsaturated soils [9, 10]. Modeling liquid bridge forces between grains, a capillary stress tensor (σ_{ij}^{cap}) can be obtained from a DEM model, allowing for an extension of Terzaghi's ESP as $\sigma_{ij}^{cont} = \sigma_{ij} - \sigma_{ij}^{cap}$. Thus, it has been proposed that the solid contact stress σ_{ij}^{cont} captures the effective stress [11-13]. However, these numerical works simulated granular materials with a relatively narrow particle size distribution.

Using DEM simulations, we model wet granular assemblies subjected to triaxial shearing tests. Different from previous works, we consider different particle size distributions, ranging from uniform to high polydisperse, and contact interactions that mimic pendular water bridges as measured experimentally. Through a series of macroscopic and microstructural analyses, we unveil a series of underlying factors that invalidate the recent ESP approaches to describe the shear strength of unsaturated soils. We show that the microstructure of σ_{ij}^{cont}, the effective stress candidate tensor, is radically different than the reference tensor from the dry case (i.e. without cohesive liquid bridges, $\eta = 0$ in Figure 1). Namely, Figure 1 shows that the contact and forces anisotropies, and their evolution with the grain size polydispersity $S = (d_{max} - d_{min})/(d_{max} + d_{min})$, are significantly different. Moreover, Figure 2 illustrates that the amount of grains not carrying contact forces (floating particles) is significantly higher in the dry case. This work also provides insights into potential avenues to fix and generalize the ESP based on the contact and force networks of solid contact interactions and capillary interactions.

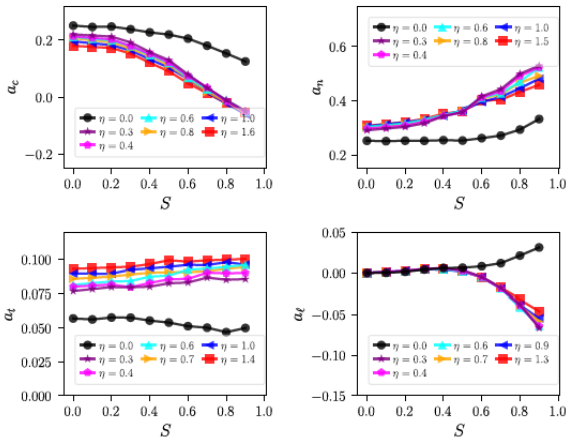

Figure 1. Evolution of anisotropies linked to contact orientations a_c, normal forces a_n, tangential forces a_t, and branch lengths for the dry material (displayed with a black line) and the 'cont ' network for increasing level of cohesive scale η.

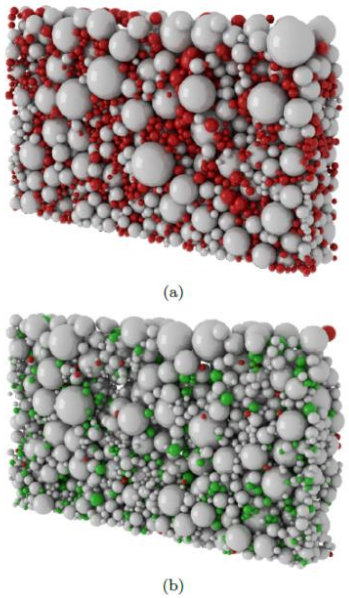

Figure 2. Slices of the samples with particle size span S = 0:8 at level of deformation of 30%, highlighting the grains carrying forces in gray and the floating particles in red for the (a) dry and (b) wet materials. For the latter case, grains that do not participate in the solid contact network are shown in green.

References

[1] K. Terzaghi, Erdbaumechanik auf bodenphysikalischer Grundlage (F. Deuticke, 1925).
[2] A. Bishop, I. Alpan, G. Blight, and I. Donald, in Proc. Research Conference on Shear Strength of Cohesive Soils (A.S.C.E, New York, U.S.A., 1960).
[3] D. G. Fredlund and N. R. Morgenstern, J. Geotech. Eng. Div. 103, 447 (1977).
[4] E. E. Alonso, A. Gens, and A. Josa, Géotechnique 40, 405 (1990).
[5] D. Sheng, D. G. Fredlund, and A. Gens, Can. Geotech. J. 45, 511 (2008).
[6] M. Nuth and L. Laloui, Int. J. Numer. Anal. Methods Geomech. 32, 771 (2008).
[7] N. Khalili, F. Geiser, and G. E. Blight, International Journal of Geomechanics 4, 115 (2004).
[8] E. Alonso, J.-M. Pereira, J. Vaunat, and S. Olivella, Géotechnique 60, 913 (2010).
[9] P.-Y. Hicher and C. Chang, Int. J. Solids Struct. 44, 2304 (2007).
[10] J.-P. Wang, G.-H. Zeng, and H.-S. Yu, Computational Particle Mechanics 6, 637 (2019).
[11] S. Khamseh, J.-N. Roux, and F. Chevoir, Phys. Rev. E 92, 022201 (2015).
[12] B. Chareyre, Phys. Rev. E 96, 016901 (2017).
[13] S. Khamseh, J.-N. Roux, and F. Chevoir, Phys. Rev. E 96, 016902 (2017).

Gyratory Shearing Compaction of Granular Materials

Teng Man[1,2]***, Zaohui Zhang***[1]

[1] *Key Laboratory of Coastal Environment and Resources of Zhejiang Province (KLaCER), School of Engineering, Westlake University, 600 Dunyu Rd, Hangzhou, Zhejiang 310024, China*

[2] *St. Anthony Fall Laboratory & Department of Civil, Environmental, and Geo- Engineering, University of Minnesota, 500 Pillsbury Dr. SE, Minneapolis, Minnesota 55455, United States*

Abstract: In this work, instead of investigating the compaction of granular materials under tapping or cyclic shearing, we focuses on the gyratory shearing compaction, where particles are subjected continuously to constant pressure and constant gyratory shear rate. Such a phenomenon is crucial to the compaction of asphalt mixtures or soils in civil engineering, and can be extended to other areas, such as powder processing and pharmaceutical engineering. In this study with discrete element simulations, we find that the gyratory speed or interstitial fluid viscosity has almost no impact on the compaction behavior, while the pressure plays a more important role. Additionally, it is the inertial time scale which dictates the compaction behavior under gyratory shearing in most cases, whereas the viscous time scale can also have influence in some conditions.

1. Introduction

Granular materials are commonly used in engineering practices such as pharmaceutical engineering, food processing, civil engineering, etc.. In civil engineering, granular materials are often subjected to complex loading conditions or loading path, or have complex particle shapes. One kind of complex loading condition is the compaction of granular materials (or granular-fluid systems). In most cases, we would like to have our concrete or asphalt pavement with as minimum amount of air voids as possible. To achieve this under both pressure and continuous shearing, the gyratory compactor and its corresponding gyratory compaction test are often used in pavement industry to achieve desired dense asphalt mixtures. However, we know very little about the physics behind the gyratory compaction when particles are subjected to continuous gyratory shearing (different from cyclic shearing where particles dilate and relax due to the cyclic excitation, i.e. the dilation/relaxation cycle).

Most previous research on granular compaction has focused on mono-disperse spherical particle systems without interstitial fluids (dry granular material) under tapping, vibrating or cyclic shearing [1]. In previous research on tapping compaction of granular systems, the reason why granular systems can evolve into a denser configuration is partly due to the dilation-relaxation cycle during the loading process. However, such a phenomenon does not exist during the gyratory compaction, where the particles are continuously subjected to constant load continuously, and it is difficult to foresee the hidden time scale inside this problem, thus, difficult to quantify the compaction behavior of a gyratory shearing process. In this article, the author will first introduce this problem and the boundary condition of the gyratory compaction. Then, the computational simulations using the discrete element method (DEM) [2] will be implemented to conduct a simple parametric study of the gyratory compaction of monodisperse granular assemblies. According to the simulation results, we can draw conclusions about the nature of the gyratory compaction of granular materials and provide some insights in the time scale governing the compaction speed.

2. Model description and preliminary results

The setup of DEM simulations is the same as shown in Fig. 1(I-IV). We can see that the particles are firstly dropped randomly (Fig. 1I) into a cylindrical box to form a random packing (Fig. 1II). Then,

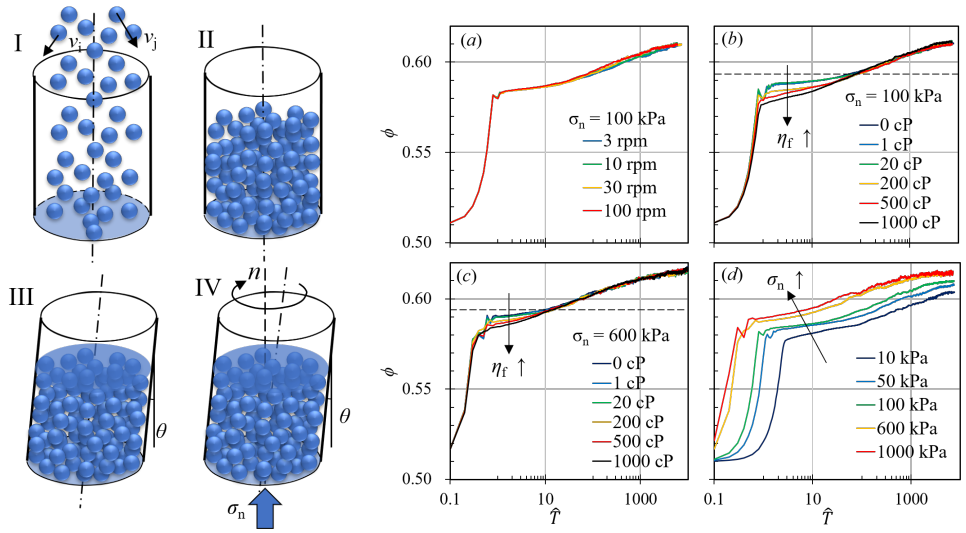

Figure 1. (I - IV) Configuration of the gyratory compactor and the model setup in the DEM simulation. (a - d) Compaction curves of granular materials with different conditions.

in the simulation, we slightly tilte the cylinder to provide a gyratory angle of θ, while adding a top plate to the cylindrical box. Finally, the loosely packed granular assemblies are loaded and sheared with constant pressure and constant gyratory speed (Fig. 1IV). In our model, two kinds of particle interactions is considered. One is the Hertz-Mindlin contact among particles calculated as follows,

$$F_c^{\mathrm{ij,n}} = -k_n \delta_n^{1.5} - \eta_n \delta_n^{0.25} \dot{\delta}_n \ , \tag{1a}$$

$$F_c^{\mathrm{ij,t}} = \min\big(-\mathrm{k_t}\delta_{\mathrm{n}}^{0.5}\delta_{\mathrm{t}} - \eta_{\mathrm{t}}\delta_{\mathrm{n}}^{0.25}\dot{\delta}_{\mathrm{t}}, \mu_{\mathrm{p}} F_c^{\mathrm{ij,n}} \big) \ . \tag{1b}$$

The other is the interstitial viscous lubrication effect calculated as[3],

$$F_v^{\mathrm{ij,n}} = 6\pi\eta_f R_{\mathrm{eff}}^2 \frac{\dot{\delta}_g}{\delta_g} \ , \tag{2a}$$

$$F_v^{\mathrm{ij,t}} = 6\pi\eta_f R_{\mathrm{eff}} v_t^{\mathrm{rel}} \big[\frac{8}{15} \ln(\mathrm{R_{eff}}/\delta_{\mathrm{g}}) + 0.9588 \big] \ . \tag{2b}$$

Figure 1(a - d) shows compaction curves of granular materials with different conditions by plotting the relationship between the solid fraction ϕ and the normalized time $\hat{T} = t\sqrt{g/\bar{r}_p}$, where $\bar{r}_p = 0.5\bar{d}$ is the average particle radius. Later in this work, we will show that the gyratory speed plays almost no effect on the gyratory compaction behavior, and that the viscosity of interstitial fluid only has secondary impact on the compaction behavior. It is the pressure which greatly influences the compaction results. During the compaction, three different time scales, the shearing time scale, $1/\dot{\gamma}$, the viscous time scale, η_f/σ_n, and the inertial time scale, $d/\sqrt{\sigma_n/\rho_p}$, have to "fight against" each other for general dominance during the compaction process. This research is particularly helpful to civil engineering industries where intensity and duration of compaction need to be determined beforehand for maximum economic gains.

References

[1] Mehta, A. and Barker, G. (1994). The dynamics of sand. *Rep Prog Phys*, **57**, 383.

[2] Man, T. (2023). Mathematical modeling of pavement gyratory compaction: A perspective on granular-fluid assemblies. *Mathematics*, **11**, 2096.

[3] Man, T., Le, J.-L., Marasteanu, M., and Hill, K. M. (2022). Two-scale discrete element modeling of gyratory compaction of hot asphalt. *Journal of Engineering Mechanics*, **148**, 04021140.

Implementing Van-der-Waals forces for polytope DEM particles

***D. Krengel*[1], *J. Chen*[2], *Y. Zhipeng*[1], *H.-G. Matuttis*[3], *and T. Matsushima*[1]**
[1] *Tsukuba University, Dept. of Engineering Mechanics and Energy, Tsukuba, Japan*
[2] *Japan Agency for Marine-Earth Science and Technology, Center for Mathematical Science and Advanced Technology, Yokohama, Japan*
[3] *The University of Electro-Communications, Dept. of Mechanical and Intelligent Systems Engineering, Chofu, Japan*

1. Introduction

Clay minerals are usually thin, elongated hexagonal platelets, which interact through attractive van der Waals forces and repulsive double layer forces [1]. They typically order into flocculated structures with large voids, with the aggregate of stacked platelets resembling a "house-of-cards". This preferred spatial arrangement of the platelets means that aggregates are highly compressible under load [2]. Two ways exist to simulate clay minerals with Discrete-Element-Models (DEM): In clumped-sphere models the implementation of van der Waals forces is computationally simple, but even aggregates of spheres cannot exactly describe the correct shape of the clay platelets. On the other hand, polygonal particle DEMs allow to model the correct shape of clay platelets (see e.g. [3]), but implementation of forces and torques is significantly more complex compared to spherical particles, and so they have seen rather limited application yet.

2. Van der Waals forces for platy particles

We implement the van der Waals forces between clay platelets by numerically integrating the London dispersion force for two identical cuboid particles,

$$F_{\text{London}} = -\frac{6C}{r^7}, \tag{1}$$

where C is the van der Waals pair potential parameter and r the distance between the molecules in the particles. When we vary the relative orientation θ between the two platelets, the van der Waals force F_{VdW} shows a strong peak for parallel plates and a minor secondary peak for perpendicular plates (see Fig. 1, a)), while for any other orientation the force decreases by several orders of magnitude. When we move the particles relative to each other, the van der Waals force shows a variation with the relative position that contains an additional dependence on the relative orientation (see Fig. 1, b)). If θ is small, then depending on the relative position of the particles F_{VdW} will either slowly decrease with increasing separation distance, or drop several orders of magnitude within a small increase of distance. On the other hand, if θ is large, then there is no jump in the force magnitude regardless of the relative position of the platelets.

3. The Anandarajah solution

For the van der Waals forces in Discrete Element Simulations, a macroscopic formulation is required. However analytical solutions in the literature [4] are available only for spherical particles or parallel, infinite half-spaces which are not representative of clay minerals. Anandarajah and Chen [5, 6, 7] analytically derived a van der Waals force for a tilted cuboid particle interacting with an infinite wall,

$$F_{\text{VdW}}(d,\theta) = \frac{A w_{\text{p}}}{6\pi \sin 2\theta} \sum_{i=1}^{8} (-1)^i \cdot \left[\frac{4}{cX_i} - \frac{1}{X_i^2} - \frac{12(X_i+c)^2}{c^4} \ln \frac{X_i + c}{X_i} \right], \tag{2}$$

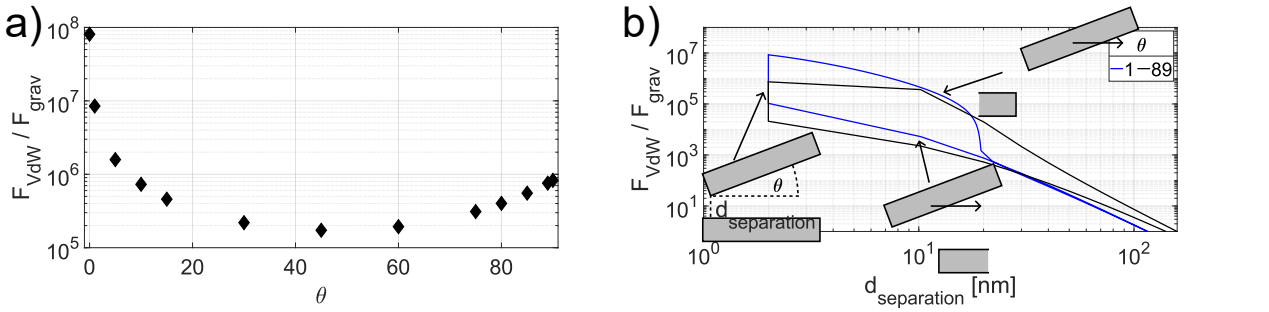

Figure 1. Van der Waals forces F_{VdW} with respect to different relative particle orientations θ in a) and with respect to different particle minimum distances $d_{\text{separation}}$, scaled with the particle weight, $F_{\text{grav}} = \varrho \cdot m$.

with the Hamaker-constant A and a variety of geometric parameters (w_{p}, c X_i). They further derived a force point on the particle based on the applying forces. However their solution is undefined for parallel and perpendicular particle orientations, and it does not consider the effect of finite particle size.

4. Numerical Implementation

The limitations in the Anandarajah approach due to particle orientation can be circumvented with a piecewise solution of the van der Waals force,

$$F_{\text{VdW}}(\theta, d) = \begin{cases} F_{\text{VdW,parallel}}(d) & \text{if } \theta = 0 \,\text{or}\, 90° \\ F_{\text{VdW}}(\theta, d) & \text{if } \theta \in]0, 90[°, \end{cases} \tag{3}$$

with the van der Waals force for two parallel plates at minimum distance d, $F_{\text{VdW,parallel}}(d)$. This produces a smooth solution for sufficiently small orientation increments. The approach can further be adopted to some degree for two particles with finite length by replacing the minimum particle distance to an infinite wall d with the minimum distance between the surfaces for two finite-sized particles, $d_{\text{separation}}$. Unfortunately, a piece-wise solution for the force point is not guaranteed to be smooth under translation and rotation and thus should not be used in numerical simulations. It is, however, possible to construct an approximate force point based on the minimum surface distance of each vertex and the projections of the vertices of the respective other particle. While this is a rather simplistic approach, the resulting force point is smooth under translation and rotation of the particle, even during contact, and thus suitable for numerical integration.

References

[1] Mitchell, J. K. and Soga, K. (2005). *Fundamentals of Soil Behaviour*. Wiley, 3 edn.
[2] Suzuki, A. and Matsushima, T. (2014). Meso-scale structural characteristics of clay deposited by 2d discrete element method. pp. 33–40.
[3] Chen, J., Krengel, D., and Matuttis, H.-G. (2023). Toward development of a plate discrete element method: Geometry and kinematics. *International Journal of Computational Methods*.
[4] Israelachvili, J. N. (2011). *Intermolecular and Surface Forces*. Academic Press, 3 edn.
[5] Anandarajah, A. and Chen, J. (1997). Van der waals attractive force between clay particles in water and contaminants. *Soils and Foundations*, **37**, 27–37.
[6] Anandarajah, A. (2000). Numerical simulation of one-dimensional behaviour of a kaolinite. *Géotechnique*, **50**, 509–519.
[7] Yao, M. and Anandarajah, A. (2003). Three-dimensional discrete element method of analysis of clays. *Journal of Engineering Mechanics*, **129**, 585–596.

INFLUENCE OF PARTICLE SHAPE IN DRY GRANULAR FLOWS AND THEIR IMPACT BEHAVIOUR AGAINST SLIT DAMS WITH BASAL UNDULATIONS

Prity Dhanai[1] ***and Debayan Bhattacharya***[1]

[1] *Department of Civil Engineering, Indian Institute of Technology Delhi, New Delhi 110016, India*

The rapid movement of granular masses, such as landslides, debris flows, rockfalls, etc., cause significant damage to human commune. To effectively mitigate these geohazards, a comprehensive understanding of the kinematic behaviour of granular mass flows and their interactions with protective barriers is essential [1, 2]. The current study employs numerical modelling within the discrete setting to replicate the interaction of granular flow with slit dams. The inherent formulation of the Discrete Element Modeling (DEM) framework seamlessly facilitates the exploration of granular mass flows for crucial understanding of flow-barrier interaction and the force transmission within the granular ensemble to optimize energy dissipation and proper designing of safety structures. Existing studies are limited to spherical particles and clumps at most, whereas particles within a granular ensemble have different morphological characteristics that significantly affect the interparticle forces and packing arrangement of granular mass [3]. Thus, micromechanical analysis plays a pivotal role in understanding the essential aspects and the underlying physics of force transmission among these particles within the granular ensemble, which finally dictates the overall system's response.

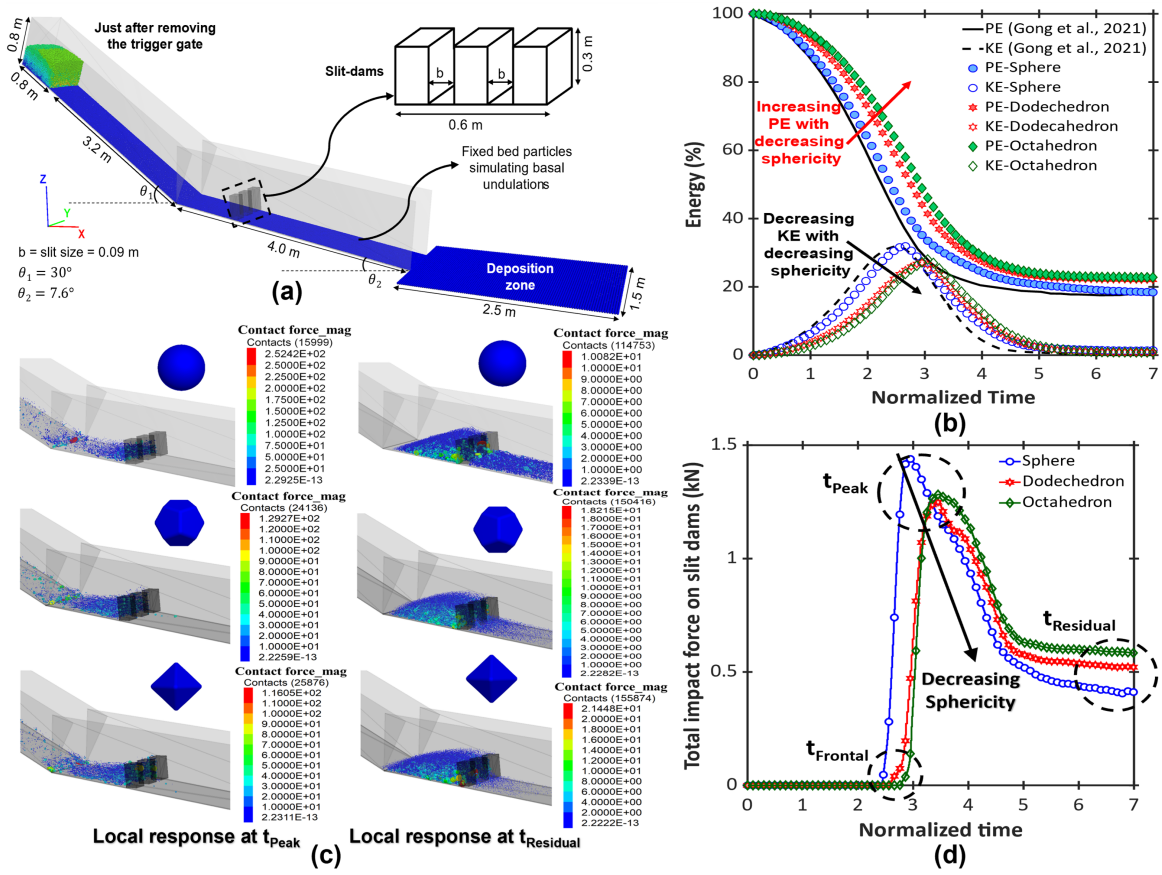

Figure 1. (a) Flume geometry (benchmarked against Gong et al.[1]); (b) particle shape effect on KE and PE of granular flow; (c) force chains at the time of peak impact force (t_{Peak}) and residual impact force $(t_{Residual})$; (d) particle shape effect on impact force (global response)

Figure 1(a) illustrates the schematic of the flume geometry, in which a layer of spherical particles is introduced on the flume base to replicate the basal undulations, a common feature found in natural terrain. This aspect is introduced to benchmark the study first in ideal conditions. Firstly, the present numerical model is validated against previously reported findings in the literature [1] by comparing the features of flow (potential energy(PE) and kinetic energy (KE)) (see Figure 1(b)). Then, the investigation is further extended to assess the particle shape effect by introducing regular polyhedral shapes (dodecahedron and octahedron), which are compared against the results obtained for spherical particles. This study uses Wadell's true sphericity as a particle shape characterization parameter [4]. Further, the effect of particle morphology on flow kinematics of dry granular flow and their interaction with the slit dams has been explored to connect how the particulate features and the underlying governing physics affect the global macromechanical response (impact force). This becomes quintessential for efficient designing of the barrier system. This aspect is presently missing in some of the design documents and strategies reported worldwide [5].

Particle Shape	True Sphericity[4]	PE_{min} (%)	KE_{max} (%)	Time of KE_{max} (s)	Time of frontal impact (s)	F_{max} (kN)	Trapping efficiency(%)
Sphere	1.0	18.5	32.1	2.67	1.1	1.44	62
Dodecahedron	0.91	22.1	27.3	2.96	1.17	1.25	80.1
Octahedron	0.86	22.8	28	3.05	1.23	1.28	90.3

Table 1. Particle shape effect on PE and KE of granular mass flow and their impact on slit dams

The carefully executed numerical simulations quite visibly capture the variation in frontal impact and peak as well as residual behaviour for different particle shapes. Quite notably, there is a decreasing trend in maximum KE and a corresponding increasing trend in PE with decreasing true sphericity (as per Wadell [4]) of particles (see Figure 1 (b) and Table 1). Moreover, our findings demonstrate that particles with lesser true sphericity lead to enhanced energy dissipation and increased trapping efficiency of slit dams, which finally results in increased residual impact force on the barrier system (see Table 1 and Figure 1 (b-d)). The gained insights become crucial for efficiently framing the design strategies for protective barriers against geophysical mass flows. The importance of incorporating particle morphology to optimize the performance of slit dams is thus demonstrated in our study. These findings carry practical implications for improving the effectiveness of such barriers by successfully exploring the intricate interplay between the micro-level responses of granular particles and the resultant macro-scale behaviour of a granular mass.

References

[1] Gong, S., Zhao, T., Zhao, J., Dai, F., and Zhao, G. (2021). Discrete element analysis of dry granular flow impact on slit dams. *Landslides*, **18**, 1143–52.

[2] Leonardi, A., Goodwin, G. R., and Pirulli, M. (2019). The force exerted by granular flows on slit dams. *Acta Geotechnica*, **14**, 1949–1963.

[3] Zhao, J., Zhao, S., and Luding, S. (2023). The role of particle shape in computational modelling of granular matter. *Nature Reviews Physics*, **5**, 505–525.

[4] Wadell, H. (1932). Volume, shape, and roundness of rock particles. *The Journal of Geology*, **40**, 443–451.

[5] CONGRESS, I. R. (2015). Engineering guidelines on landslide mitigation measures for indian roads.

INFLUENCE OF PARTICLE SHAPE REPRESENTATION IN DEM SIMULATIONS OF TORSIONAL SHEAR

***Javier E. Necochea*[1,2], *Kevin J. Hanley*[1] *Esteban Sáez*[2]**
[1] *The University of Edinburgh, School of Engineering, Edinburgh, United Kingdom*
[2] *Pontificia Universidad Católica de Chile, School of Engineering, Santiago, Chile*

1. Introduction

Particle shape has a considerable influence on the critical state behaviour and stiffness characteristics of granular soils [1, 2], and is a controlling factor on the anisotropy of elastic wave velocity [3], damping capacity [4] and many other soil properties. In order to fully understand the micromechanics of soil, particle-scale simulations, e.g., using the Discrete Element Method (DEM), are needed. DEM studies often idealise particles as spheres. However, particle shape effects can be incorporated by introducing rolling friction to the spheres [5] or by adopting non-spherical particles [6]. The different shape representations have their own advantages and limitations [7]. There are also challenges associated with representing torsional shear in DEM as energy dissipation [8, 9] becomes a major factor. In this study a torsional shear test of a real granular soil is represented in DEM using three methods to represent particle shape: spheres with rolling friction, ellipsoids and multi-sphere clumps.

2. Laboratory Testing

For this research, a poorly graduated quartz sand containing particle sizes from 1.18 to 2.00 mm was tested in a resonant column apparatus of 50 mm diameter and 100 mm height [10]. A torsional shear test was conducted on the sample with a confining pressure of 100 kPa, yielding the sample's shear modulus degradation and damping ratio evolution. Other soil properties were obtained with complementary testing. These laboratory data were used to validate the particle simulations.

3. DEM Simulations

Due to the narrow particle size distribution, three particle templates — large, medium and small — were used to represent the soil grains. Both the sphere and ellipsoid templates were generated from image analysis, while the multi-sphere templates were generated using meshes obtained from μ-CT scans [11]. Figure 1a shows an example of a reconstructed slice from such a scan.

DEM simulations were run with the open-source software LIGGGHTS (v3.7). Grains were inserted by gravitational deposition. Each sample was confined by a flexible membrane, represented as a set of bounding particles with forces applied individually to recreate the effective confinement [12, 13]. A clump of spheres was used to apply the vertical confinement and the torsional displacement. Figure 1b presents a close-up view of the top of a numerical sample. Once each sample was confined, torsional shear was applied at a frequency of 1 Hz. The torsional displacement per cycle was varied in order to recreate the stiffness degradation curve obtained in the laboratory.

4. Results

While all samples reached a fair agreement with the bulk behaviour obtained in the laboratory, substantial differences were found in the micromechanics; most notably, the rotations of particles were much higher in the samples composed of spheres than in the other two. Particle rotations were slightly greater in the sample composed of ellipsoids than in the multi-sphere clump sample. Each sample has a similar damping evolution, although this value is greatly influenced by the interparticle restitution coefficients specified in the simulations.

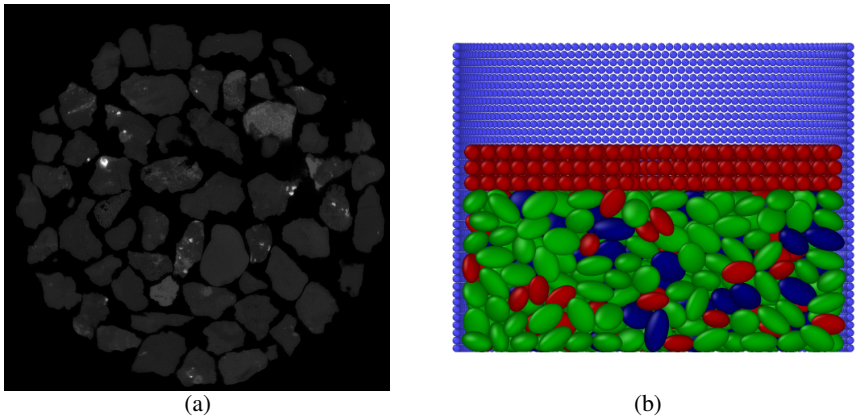

(a) (b)

Figure 1. (a) Sample slice reconstructed from µ-CT; (b) view of torsional shear model with ellipsoids.

5. Acknowledgments

The first author acknowledges funding from the Chilean Agencia Nacional de Investigación y Desarrollo (ANID) under the Doctorado Nacional scholarship, number 21200396.

References

[1] Altuhafi, F. N., Coop, M. R., and Georgiannou, V. N. (2016). Effect of particle shape on the mechanical behavior of natural sands. *Journal of Geotechnical and Geoenvironmental Engineering*, **142**, 04016071.

[2] Holubec, I. and D'Appolonia, E. (1973). Effect of particle shape on the engineering properties of granular soils. *Evaluation of Relative Density and its Role in Geotechnical Projects Involving Cohesionless Soils*, pp. 304–318.

[3] Otsubo, M., Liu, J., Kawaguchi, Y., Dutta, T. T., and Kuwano, R. (2020). Anisotropy of elastic wave velocity influenced by particle shape and fabric anisotropy under K0 condition. *Computers and Geotechnics*, **128**, 103775.

[4] Payan, M., Senetakis, K., Khoshghalb, A., and Khalili, N. (2016). Influence of particle shape on small-strain damping ratio of dry sands. *Géotechnique*, **66**, 610–616.

[5] Ai, J., Chen, J. F., Rotter, J. M., and Ooi, J. Y. (2011). Assessment of rolling resistance models in discrete element simulations. *Powder Technology*, **206**, 269–282.

[6] Nguyen, T. D. and Plimpton, S. J. (2019). Aspherical particle models for molecular dynamics simulation. *Computer Physics Communications*, **243**, 12–24.

[7] Capozza, R. and Hanley, K. J. (2021). A hierarchical, spherical harmonic-based approach to simulate abradable, irregularly shaped particles in DEM. *Powder Technology*, **378**, 528–537.

[8] Keishing, J., Huang, X., and Hanley, K. J. (2020). Energy dissipation in soil samples during cyclic triaxial simulations. *Computers and Geotechnics*, **121**, 103481.

[9] Pei, T. and Qiu, T. (2022). DEM investigation of energy dissipation at particle contacts in granular soil under cyclic torsional shear. *International Journal of Geomechanics*, **22**, 1–11.

[10] ASTM 4015-21 (2021). Standard test methods for modulus and damping of soils by fixed-base resonant column devices. *ASTM International, West Conshohocken (PA)*.

[11] Angelidakis, V., Nadimi, S., Otsubo, M., and Utili, S. (2021). CLUMP: A code library to generate universal multi-sphere particles. *SoftwareX*, **15**, 100735.

[12] de Bono, J., McDowell, G., and Wanatowski, D. (2012). Discrete element modelling of a flexible membrane for triaxial testing of granular material at high pressures. *Géotechnique Letters*, **2**, 199–203.

[13] Wilson, J. F. and Sáez, E. (2017). Use of discrete element modeling to study the stress and strain distribution in cyclic torsional shear tests. *Acta Geotechnica*, **12**, 511–526.

INSTABILITY IN WET GRANULAR MATERIALS VIA DEM MODELING

M. Farahnak*[1], *R. Wan*[1], *F. Nicot*[1,2] *and M. Pouragha [3]
[1] *University of Calgary, Department of Civil Engineering, Calgary, Canada*
[2] *University Savoie Mont-Blanc, ISTerre, Chambéry, France*
[3] *Carleton University, Department of Civil and Environmental Engineering, Ottawa, Canada*

1. Introduction

The current study presents a numerical multiscale approach to investigate bifurcation phenomena in partially saturated granular materials within the pendular regime using the Discrete Element Method (DEM) modeling. The study focuses on instability and localization phenomena in a densely packed wet granular material under triphasic (solid, water and air) conditions, accounting for the capillary effect. In a partially saturated state, defining the second-order work instability criterion is linked to the interplay between stress and strain variables, influenced by coupled hydromechanical effects. The multiphysics and multiphasic interactions at the microscale result into intricate macroscale behaviors within triphasic conditions. In this regard, the external and internal second-order works are evaluated using DEM to capture the instability with respect to the stress-strain variables in wet condition. In addition, a general hydromechanical constitutive tensor is reconstructed from DEM modeling to analyze bifurcation in elastoplasticity based on its spectral analysis. A meso-scale analysis is also provided to detect shear band localization and validate the well-known Rice criterion [1] within a micromechanical discrete modeling framework.

2. Numerical approach

Within DEM computations, the second-order work instability criterion [2] is first evaluated by applying perturbations close to the stress limit state of a plane strain loading. Three possible definitions are considered with respect to: (1) the external stress and strain increments, $W_2^{\text{ext}} = \mathrm{d}\boldsymbol{\sigma}^{\text{ext}} : \mathrm{d}\boldsymbol{\varepsilon}$, (2) the contact stress and strain increments, $W_2^{\text{cont}} = \mathrm{d}\boldsymbol{\sigma}^{\text{cont}} : \mathrm{d}\boldsymbol{\varepsilon}$, (3) a definition proposed by [3] where $\mathrm{d}\boldsymbol{\sigma}^{\text{cont}}$ is considered here as the incremental effective stress within solid skeleton, i.e., $W_2^{\text{unsat}} = \mathrm{d}\boldsymbol{\sigma}^{\text{cont}} : \mathrm{d}\boldsymbol{\varepsilon} - n\mathrm{d}s\,\mathrm{d}S_r$, with n, s, and S_r being the porosity, suction and saturation degree, respectively.

A bifurcation analysis is subsequently conducted by examining the spectral characteristics of the tangent operator reconstructed from DEM simulations. The proposed approach is presented within the elastoplasticity framework where a general incremental hydromechanical constitutive relationship, accounting for the conjugates of stress ($\boldsymbol{\Sigma}$) and strain ($\boldsymbol{E}$) variables in wet condition, is computed by performing a series of multi-directional DEM probing, and using Least Square Method (LSM) such that:

$$\begin{Bmatrix} \mathrm{d}\boldsymbol{\sigma}^{\text{cont}} \\ \mathrm{d}(ns) \end{Bmatrix} = \begin{bmatrix} \boldsymbol{D}_{mm} & \boldsymbol{D}_{mh} \\ \boldsymbol{D}_{hm} & \boldsymbol{D}_{hh} \end{bmatrix} \begin{Bmatrix} \mathrm{d}\boldsymbol{\varepsilon} \\ \mathrm{d}S_r \end{Bmatrix}, \qquad D_{ij} = \sum_{N_{probes}} \mathrm{d}\Sigma_i \mathrm{d}E_k \Big(\sum_{N_{probes}} \mathrm{d}E_j \mathrm{d}E_k \Big)^{-1} \tag{1}$$

In order to detect localization, the DEM sample is divided into meso-scale cells each regarded as a representative elementary volume so that meso-scale stress and strain can be related through a constitutive law. The localization criterion is then investigated by the vanishing of the determinant of the acoustic tensor $A_{ik} = \boldsymbol{D}_{ijkl} n_j n_l$, with $\boldsymbol{n}$ being the vector normal to the shear band [1].

3. Results and conclusions

The polar diagram depicting the normalized second-order work at stress limit state $(q^{\text{cont}}/p^{\text{cont}})_{max}$, is presented in Fig. 1. The occurrence of instability is discernible using both the expressions W_2^{ext} and W_2^{cont}. This observation supports the 'effective' role of contact stress in describing failure within wet granular materials. On the other hand, the expression W_2^{unsat} gives a generally more stable trend with higher second-order work values. This is due to the fact that the term $-n\mathrm{d}s\mathrm{d}S_r$ consistently contributes a positive value, augmenting the $\mathrm{d}\boldsymbol{\sigma}^{\text{cont}} : \mathrm{d}\boldsymbol{\varepsilon}$ term and consequently elevating W_2^{unsat}.

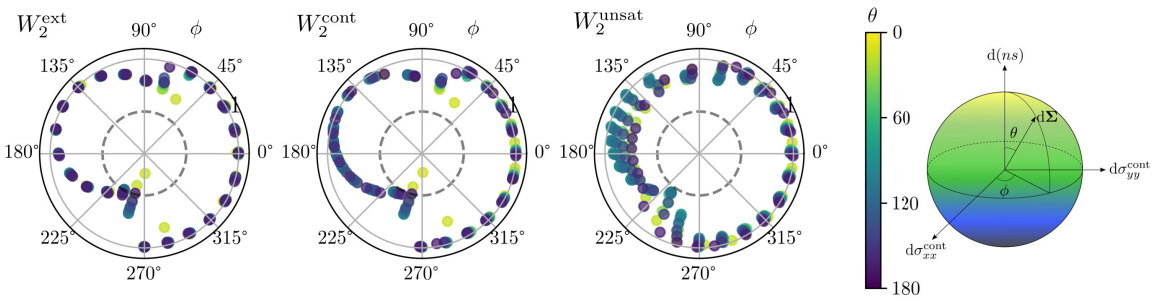

Figure 1. Polar diagrams of normalized second-order work at limit stress state.

To capture finer characteristics of the hydromechanical constitutive relationship, an octo-linear elastoplastic tensor is reconstructed across eight tensorial zones, in each of which, a bifurcation analysis is conducted by examining $\det \boldsymbol{D}^{sym} = 0$. Bifurcation occurs in three zones, resulting in the loss of positive definiteness for the mechanical part $\boldsymbol{D}_{mm}^{sym}$, and consequently the general hydromechanical tangent operator $\boldsymbol{D}^{sym}$. This is consistent with the findings of the second-order work analysis. Finally, calculating the stress/strain increments and reconstructing the tangent operator at the local mesoscale cells (Fig. 2a) enables us to proceed with the localization analysis. Figure 2b shows the calculated localization angle (α) for the cells satisfying Rice's criterion that are located along the two crossed conjugate shear band regions detected by the deviatoric strain field, as shown in Fig. 2c. Interestingly, the results indicate that Rice's criterion reasonably detecting the orientation of shear bands when applied to the mechanical part of the hydromechanical tangent operator.

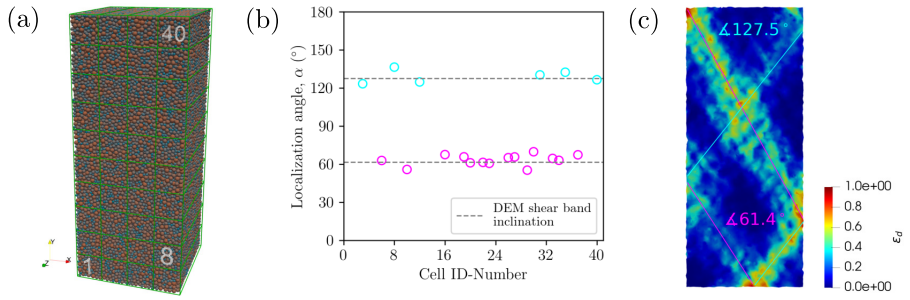

Figure 2. (a) The mesoscale cells, (b) predicted shear band inclination, and (c) deviatoric strain field.

References

[1] Rice, J. R. (1976). The localization of plastic deformation. Koiter, W. (ed.), *14th International Congress on Theoratical and Applied Mechanics*, pp. 207–229.

[2] Hill, R. (1958). A general theory of uniqueness and stability in elastic-plastic solids. *Journal of the Mechanics and Physics of Solids*, **6**, 236–249.

[3] Buscarnera, G. and Prisco, C. d. (2012). Discussing the definition of the second-order work for unsaturated soils. *International journal for numerical and analytical methods in geomechanics*, **36**, 36–49.

INFLUENCE OF CONTACT PARAMETERS ON FABRIC EVOLUTION IN TRIAXIAL DEM SIMULATIONS OF COHESIONLESS MATERIALS

A. Damon Nguyen[1], B. Yuyan Chen[1] and C. Alejandro Martinez[2]
[1] University of California, Graduate Student in Civil & Environmental Engineering, Davis, USA
[2] University of California, Associate Professor in Civil & Environmental Engineering, Davis, USA

1. Introduction

Despite computational advancements, discrete element modeling (DEM) simulations of boundary value problems commonly require simplifications such as representing complex particle shapes with spheres. By calibrating the friction (μ) and rolling resistance (μ_r) parameters of these spheres, the strength and dilatancy effects driven by the characteristics of real particle shapes can be effectively captured [1]. To this end, a parametric study is performed to evaluate the effects of friction and rolling resistance on the evolution of fabric during drained triaxial compression response of a poorly-graded granular material. The μ and μ_r parameters control the sliding and rolling interactions between particles, which influence both how particles transfer load and how the soil deforms. Deviatoric stress and volumetric strain are recorded during shearing. Particle contacts are examined to evaluate the failure mechanism (sliding or rolling) as well as the accumulated spin. The density, magnitude, and orientation of particle contacts and contact forces throughout shearing are examined to shed light on the effects of contact parameters on the anisotropy in their distributions.

2. Influence of μ and μ_r on global triaxial shearing response

The μ and μ_r parameters have coupled effects on both the mobilization of strength and volume-change responses during triaxial shearing. Within the range of μ and μ_r values considered, any increase in μ increases both peak (φ_p) and critical friction angles (φ_{cs}). Increases in μ also cause specimens to dilate more and at greater maximum dilation rates ($(\varepsilon_v/\varepsilon_a)_{max}$). The influence of μ_r on the triaxial shearing response depends on μ. At high μ values, increases in μ_r result in considerable increases in φ_p and φ_{cs}. However, at low μ values, increases in μ_r have little impact on the behavior. The reference shear modulus (G_{ref}) calculated at a shear stress of half of the peak, total volumetric strain ($\varepsilon_{v,total}$), and $(\varepsilon_v/\varepsilon_a)_{max}$ are mainly influenced by μ. Additionally, the behavior transitions from strain-hardening to strain-softening when μ is increased beyond a threshold value of around 0.35. Greater resistances to sliding and rotation at particle contacts leads to less particle mobility and thus increased stability. The restricted particle movement can also lead to mechanisms such as rotation frustration, thus resulting in dilation [3].

3. Influence of μ and μ_r on particle-level interactions during triaxial shearing

The μ and μ_r parameters control the resistance to sliding and rolling at contacts. When μ is low, sliding is the primary mechanism of failure at particle contacts. Changes in μ_r have little impact at this state as particles can slide more readily than rotate. When μ is high, rotation driven failure at particle contacts becomes more likely (see Figure 1). Changes in μ_r are more influential when μ is high, with low values of μ_r allowing for rotation and high values restricting particle movement. The simulation with a low μ and high μ_r has a probability density function of particle rotations with the greatest mean and the smallest spread, while the simulation with a high μ and low μ_r produces the smallest mean and greatest spread.

The force contact networks developed during simulations reveal that specimens with low μ mobilize a dense network of weak contacts regardless of μ_r. This contact network is slightly less anisotropic with many contact normals that may have different orientations than the vertical. However, specimens with high μ form less dense contacts networks where strong soil columns form to provide resistance against loading (see Figure 2). Increases in μ_r further boost the stability of these columns. As the soil columns take on more of the applied axial load, contacts whose normals are oriented different than vertical become weaker and less plentiful. This results in a more anisotropic fabric. These observations agree with previous similar studies [2].

4. Figures

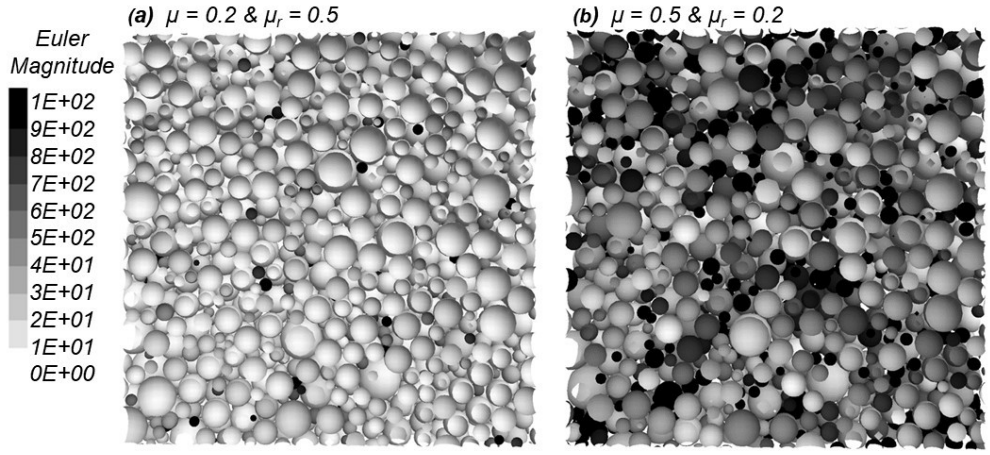

Figure 1. Accumulated spin through a central cutout at the end of select triaxial test simulations.

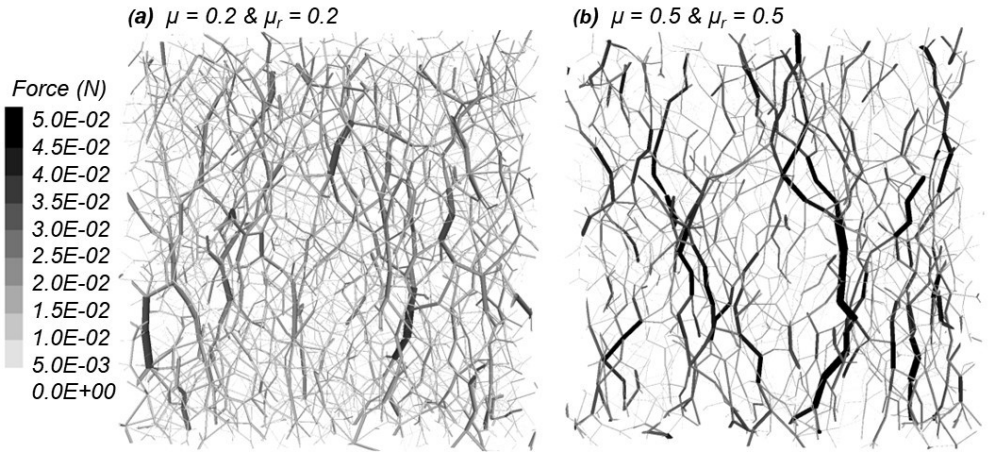

Figure 2. Force chain maps through a central cutout at the end of select triaxial test simulations.

5. References

[1] O'Sullivan, C. (2014). *Particulate Discrete Modelling: A Geomechanics Perspective*. 2 Park Square, Milton Park, Abingdon, Oxon: Spon Press.

[2] Rorato, R., Arroyo, M., Gens, A., Andò, E., & G. Viggiani. (2021). Image-based calibration of rolling resistance in discrete element models of sand. *Computers and Geotechnics* **131:**103929.

[3] Santamarina, J.C. (2003). Soil Behavior at the Macroscale: Particle Forces. *Soil Behavior and Soft Ground Construction* **1:**25-26.

Investigation into the non-coaxiality of granular material subjected to principal stress rotation by stress probing method

A. Tianhao Chen[1], B. Zhongxuan Yang[1]

[1] Computing Center for Geotechnical Engineering (COMEGE), Engineering Research Center of Urban Underground Space Development of Zhejiang Province, MOE Key Laboratory of Soft Soils and Geoenvironmental Engineering, Department of Civil Engineering, Zhejiang University, Hangzhou, Zhejiang, 310058, China

1. General

Non-coaxiality between the principal directions of plastic strain increment and stress, is often approximated to the deviation of total strain increment direction from the stress direction, owing to the challenge of separating elastic and plastic strains measured from the experimental tests [1,2]. Stress probing technique is employed in this study using the discrete element method (DEM) to extract the plastic component from the total strain response of a three-dimensional granular assembly subjected to pure rotational shear. By subtracting the elastic strain increment, the non-coaxiality can be precisely investigated, considering the influence of several factors, including stress ratio, intermediate principal stress parameter, void ratio and bedding plane angle of the samples. It is observed that a decrease in the stress ratio leads to an increase in the magnitude of non-coaxial angle, while the impact of other factors is rather insignificant. The test results also indicate that the phase angle and oscillation extent of non-coaxial angle variation with the principal stress rotation tend to increase with the increase in in-plane and out-plane bedding angles, respectively.

2. DEM modeling and stress probing technique

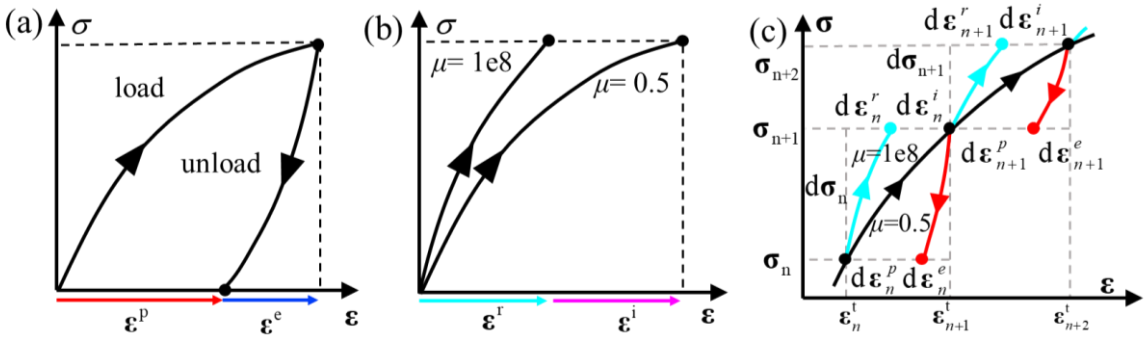

Figure 1. Schematic diagram of (a) loading-unloading scheme, (b) non-dissipative scheme and (c) stress probing in this study.

In this study, the three-dimensional particle flow code, PFC3D is used to implement the DEM numerical simulations. The basic particle is a clump formed by two identical but overlapped spheres. A 26-facet specimen consists of approximately 10,000 clumped particles is generated by multi-layer under-compaction method. Figure 1 (a) and (b) illustrate the two primary types of probing schemes, namely loading-unloading and non-dissipative[3]. Loading-unloading scheme adopts the strategy involving a closed loading-unloading cycle as its name hints. The residual strain after the full unloading is interpreted as the plastic component , while the elastic component is the portion that can be fully recovered. In the non-dissipative method, the reversible strain is obtained by running the stress probing test with the frictional dissipation being inhibited, and the rest proportion is regarded

as the irreversible strain. In this study, the stress probing technique is adopted during the entire process of pure rotational shear, as shown in Figure 1(c).

3. Non-coaxiality

Figure 2 (a) illustrates the principal directions of stress, as well as total, elastic, and plastic strain increments, as they evolve with the rotation angle of principal stresses. It is observed that all these three strain increments rotate synchronously with the rotation of principal stresses and the phase angles, in the descending order, are elastic, total and plastic strain increments. Although the magnitude of the elastic strain increment is relatively small as compared to the total strain response under a high stress ratio, the difference between $\alpha(\mathrm{d}\boldsymbol{\varepsilon}^{\mathrm{t}})$ and $\alpha(\mathrm{d}\boldsymbol{\varepsilon}^{\mathrm{p}})$ is still considerable (see Figure 2 (b)). Thus, it is inappropriate to approximately regard the direction of total strain increment as that of plastic strain increment, as what has been done in the most existing studies.

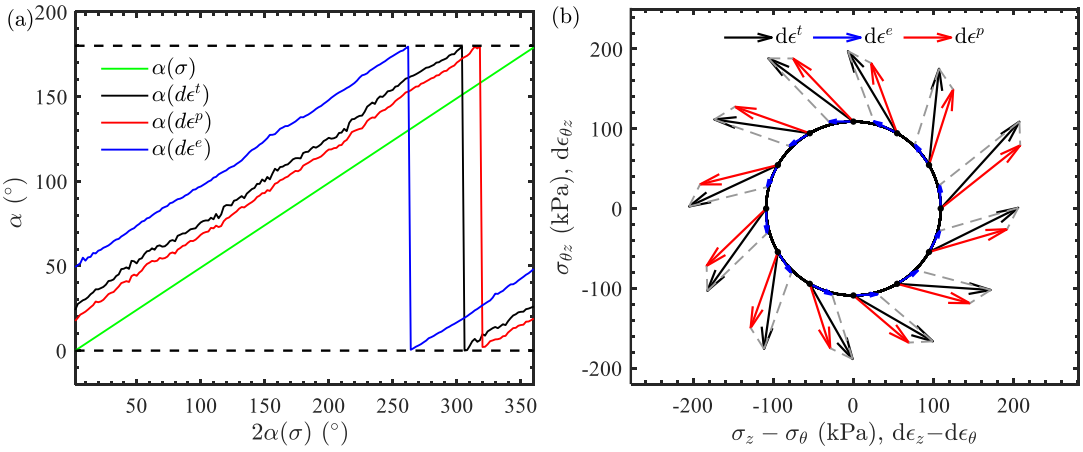

Figure 2. (a) Principal directions of stress, strain increments and (b) strain increment vector superimposed on the stress path.

To further investigate the necessity and significance of replacement of total strain increment by plastic strain increment, both the non-coaxial angle, $\beta^{\mathrm{p}} = \alpha(\boldsymbol{\sigma}) - \alpha(\mathrm{d}\boldsymbol{\varepsilon}^{\mathrm{t}})$, and approximate non-coaxial angle, $\beta^{\mathrm{t}} = \alpha(\boldsymbol{\sigma}) - \alpha(\mathrm{d}\boldsymbol{\varepsilon}^{\mathrm{t}})$ are analyzed and compared. The results reveal that β^{t} is generally greater for specimens subjected to lower stress ratios, intermediate principal stress parameter as well as specimens with lower void ratios, which are consistent with the previous studies in literature. By subtracting the elastic strain increment, it is observed that a decrease in the stress ratio leads to an increase in the magnitude of β^{p}, while the impact of other factors is rather insignificant. The test results also indicate that the magnitude of both β^{t} and β^{p} are independent of the bedding angle of the sample, but their phase angle and oscillation extent variation with the principal stress rotation tend to increase with the increase in in-plane and out-plane bedding angles, respectively.

5. References

[1] Gutierrez, M., Ishihara, K., & Towhata, I. (1991). Flow theory for sand during rotation of principal stress direction. *Soils Found.*, **31**(4), 121-132.

[2] Li, X., & Yu, H. S. (2010). Numerical investigation of granular material behaviour under rotational shear. *Géotechnique*, **60**(5), 381-394.

[3] Kuhn, M. R., & Daouadji, A. (2018). Quasi-static incremental behavior of granular materials: Elastic–plastic coupling and micro-scale dissipation. *J Mech Phys Solids*, **114**, 219-237.

Leakage behaviour of particles subjected to gravity flow with 3D filter by DEM

Y. Nakata[1], S. Kajiyama[2], I. Tokiyoshi[1], M. Yoden[1], Y. Ohta[1] and J. Yoneda[3]

[1] Yamaguchi University, Graduate School of Sciences and Technology for Innovation ,Ube, Japan

[2] University of Yamanashi, Graduate Faculty of Interdisciplinary Research, Kofu, Japan

[3] National Institute of Advanced Industrial Science and Technology, Sapporo, Japan

1. Introduction

Geomaterial filters are one of the classical issues in soil mechanics. The first study, conducted by Terzaghi[1], examined filter selection criteria for non-clogging geomaterials for fill dams and culvert drainage. There is growing interest in developing filters for granular materials. The purpose is to control the drainage function of soil structures[2], to prevent sucking and sinking, to prevent liquefaction by gravel drains[3] and to control sand outflow in the production of methane hydrate[4].

The development of high-performance filters with various functions is highly desired. That is, functions that enable long-term prevention of clogging and maintenance of drainage performance under extremely high permeability conditions. We believe that the application of a filter with a three-dimensional structure, instead of a two-dimensional mesh filter, is essential for such a highly functional filter.

In light of the above, we evaluated the basic performance of the 3D filter using DEM analysis in terms of computer aided engineering. In this study, a diamond structure was employed for the 3D structure. The applied simulation was particle leakage in a gravity field.

2. Simulation for gravity flow with 3D filter by DEM

Figure 1 shows a simulation of particle leakage. In the periodic boundary region, a diamond-structured filter was placed 10-110 mm from the bottom edge. The diamond structure filter is shown in Figure 2, with an opening of 10 mm and a wire diameter of 2.2 mm. The size of the filter was 0.04 x 0.04 x 0.10 m. 1000 particles of a given size were generated at a height of 0.25 to 1.3 m. These particles fall under the gravity force. The falling particles leaked against the installed filter. Due to the periodic boundary, the leaked particles fall again from the top edge of the boundary. So, a continuous leakage behaviour would appear depending on the size of the particles. Then we can examine the particle sizes related to clogging and the leakage rate. The same simulations were applied for a 2D filter as shown in Figure 3, and the differences between the two types of filters will be discussed. Note that the 2D and 3D filters have the same 10 mm opening size.

3. Leakage behaviour of 3D filter

Figure 4 shows the time variation of leakage mass, which is calculated by accumulating the mass of particles that pass through the filter and dividing by the cross-sectional area of the filter. From this figure, it can be seen that the minimum particle size that clogs is larger for the 3D filter. In addition, when continuous leakage behaviour is observed, the 3D filter has a higher leakage rate.

4. References

[1] Terzaghi, K.: Effect of Minor Geologic Detail on the Safety of Dams, Bulletin, American Institute of Mining Engineers, Technical Publication 215, 1926.

[2] Yasser Abdelhamid and Usama El Shamy, Pore-Scale Modeling of Fine-Particle Migration in Granular Filters, International Journal of Geomechanics, 16, 3, 2015.

[3] U El Shamy, SF Sizkow : Coupled smoothed particle hydrodynamics-discrete element methodsimulations of soil liquefaction and its mitigation using gravel drains, Soil Dynamics and Earthquake Engineering, 2021.
[4] Katagiri, J., Yoneda, J., Tenma, N. Multiobjective optimization of the particle aspect ratio for gravel pack in a methane-hydrate reservoir using pore scale simulation, Journal of Natural Gas Science and Engineeing, 35A, 920-927, 2016.

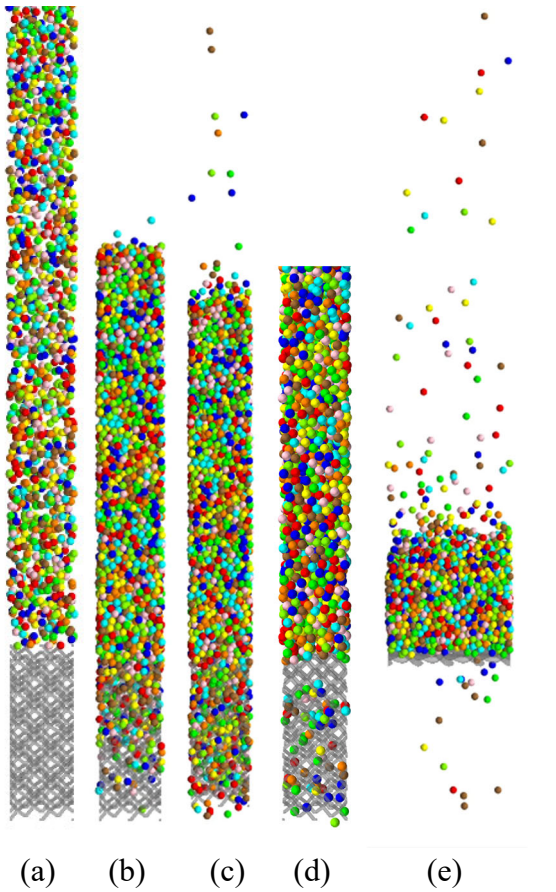

Figure 1 Particle leakage progresses to (a) initial, (b) mid, (c) later and (d) particle clogging for diamond-structured filter, and (e) for 2D filter.

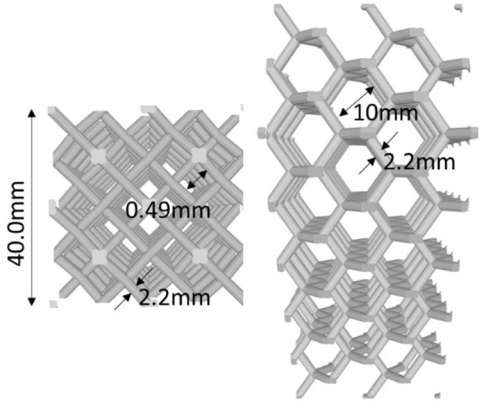

Figure 2 Geometry for diamond-structured filter

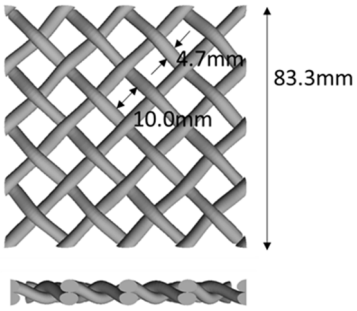

Figure 3 Geometry for 2D (mesh type) filter

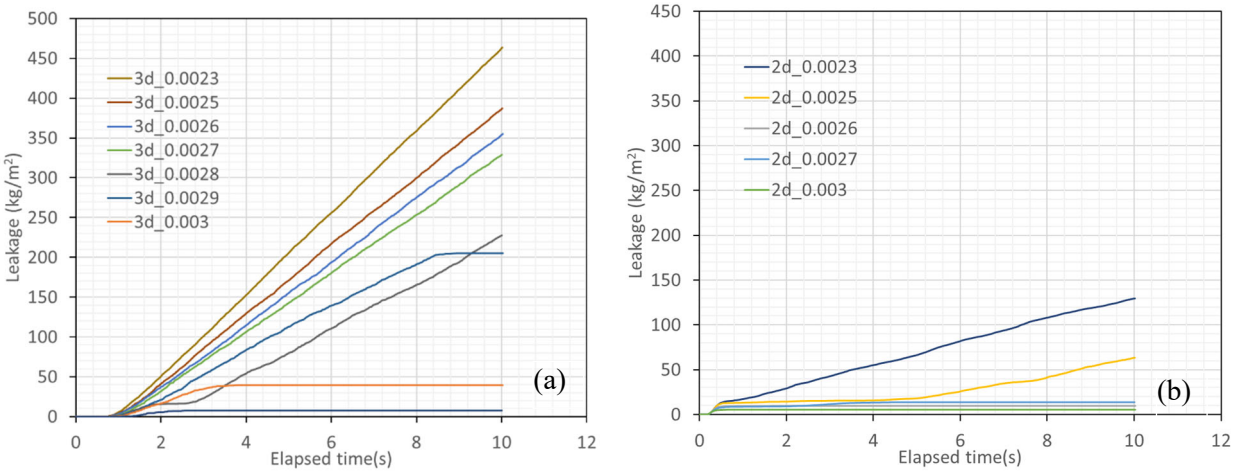

Figure 4. Leakage behaviour on flowed particles size, (a) Diamond structured and (b) 2D filters.

MICRO- AND MACRO-MECHANICAL ANALYSES OF REV IN SHEARED GRANULAR SAMPLES

P. Quiroz-Rojo[1,2,3], D. Cantor[2,3], C. Ovalle[2,3], M. Renouf[1] and E. Azéma[1,4]

[1] LMGC, Université de Montpellier, CNRS, Montpellier, France

[2] Department of Civil, Geological and Mining Engineering, Polytech. Montréal, Montréal, Canada.

[3] Research Institute of Mining and Environment (RIME), UQAT-Polytechnique, Canada

[4] Institut Universitaire de France (IUF), Paris, France

With the aim of ensuring a reliable mechanical characterization of granular materials, lab tests must be carried-out on samples having a representative elementary volume (REV). Concerning triaxial tests, the approach suggested by international geotechnical testing standards is to fulfill limiting aspect ratios between the height of the sample and its diameter (H/D), and between D and the coarsest particle ($\alpha = D/d_{max}$). While it is generally accepted that H/D should be between 2 and 2.5, common standards strongly disagree on the minimum α and the advised values might vary between 6 [1] and 20 [2]. Moreover, the effect of the particle size distribution (PSD) on REV is poorly understood and thus generally excluded from standard considerations [3].

The main objective of this article is to examine the combined effects of α and PSD on the critical shear strength of granular materials. We performed 3D DEM simulations of triaxial shearing tests on samples composed by spherical grains using the contact dynamics (CD) method [4] implemented in the LMGC90 simulation platform [5]. PSD was controlled by the span ratio $S = (d_{max} - d_{min})/(d_{max} - d_{min})$, where d_{min} is the finest particle diameter in a sample. The ranges of values tested were $\alpha = 5$ to 20, and $S = 0.0$ to 0.6. Samples were prepared in boxes of square section of side W and constant ratio $H/W = 2$. Triaxial tests were performed in two stages: first, an isotropic compression stage at constant stress $\sigma_0 = 10\ kPa$; second, triaxial quasi-static compression at constant strain rate until 60% of vertical deformation to ensure critical state conditions.

We performed macroscopic and microstructural analyses of our results. Fig. 1 shows that the normalized strength at critical state $\langle q/p \rangle$ and its standard deviation (SD) depend on both α and PSD. While a REV with $\langle q/p \rangle \sim 0.7$ is reached at $\alpha \geq 12.5$ for $S = 0$, it does at $\alpha \geq 8$ for $S = 0.6$. It is well known that the critical strength does not depend on PSD [6-7], however, here we show that this the case only once REV conditions are reached.

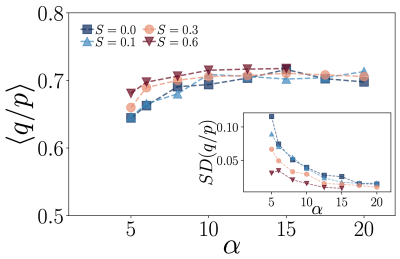

Fig. 1. Critical strength of all samples.

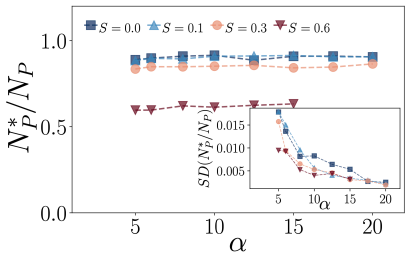

Fig. 2. Proportion of engaged particles in all samples.

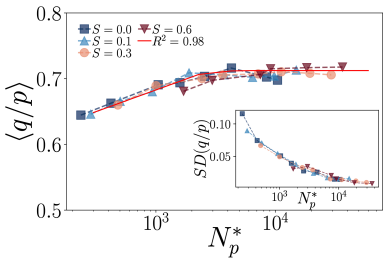

Fig. 3. Critical strength vs. N_p^*.

The microstructure of the samples at critical state indicates that the proportion of floating particles (grains not bearing forces) increases with S. In other words, the number of engaged grains

N_p^* over total particles N_p decreases with S, as illustrated in Fig. 2. Interestingly, Fig. 3 shows that a unique relationship is obtained for $\langle q/p \rangle$ as a function of N_p^*, which saturates at $\langle q/p \rangle \sim 0.7$ for $N_p^* \geq 3000$. Therefore, REV is attained only if a minimum number of particles are involved in the transmission of forces, regardless of sample size nor grading.

Our study suggests a practical viewpoint, indicating the need to reevaluate the recommendations for REV of granular soil samples in certain widely applied international testing standards. Nevertheless, our findings also suggest the necessity for additional research and the collection of experimental data on diverse granular soils to validate the conclusions drawn in this study.

References

[1] ASTM D718 (2020). Standard Test Method for Consolidated Drained Triaxial Compression Test for Soils. ASTM International Standard.

[2] JGS 0520 (2020). Preparation of specimens of coarse granular materials for triaxial tests. Japanese Geotechnical Society.

[3] D. Cantor and C. Ovalle (2024). Sample size effects on the critical state shear strength of granular materials with varied gradation and the role of column-like local structures. Géotechnique, in press.

[4] M. Jean (1999). The non-smooth contact dynamics method. Computer Methods in Applied Mechanics and Engineering, 177(3):235–257.

[5] F. Dubois and M. Jean. (2006). The non-smooth contact dynamic method: recent LMGC90 software developments and application. Springer Berlin Heidelberg, Berlin, Heidelberg,

[6] O. Polania, M. Cabrera, M. Renouf, E. Azéma, and N. Estrada (2023). Grain size distribution does not affect the residual shear strength of granular materials: An experimental proof. Phys. Rev. E, 107:L052901.

[7] J. Yang and X. D. Luo (2017). The critical state friction angle of granular materials: does it depend on grading? Acta Geotechnica, 13(3):535-547.

MEASURING AND PREDICTING THE ANGLE OF REPOSE OF GRANULAR MATTER FROM CLUMP AND POTENTIAL PARTICLES DEM APPROACHES

***V. Angelidakis*[1,2], *S. Duverger*[3], *S. Nadimi*[1], *S. Utili*[1], *S. Bonelli*[3], *P. Philippe*[3] *and J. Duriez*[3]**
[1] *School of Engineering, Newcastle University, Newcastle upon Tyne, United Kingdom*
[2] *School of Natural and Built Environment, Queen's University Belfast, Belfast, United Kingdom*
[3] *INRAE, Aix Marseille Univ, RECOVER, Aix-en-Provence, France*

1. Introduction

Depending on the applied loads granular soils may undergo phase transitions, flowing like a complex fluid before stabilizing in a heap configuration typically characterized by a linear slope, i.e., a constant angle of repose (AoR), even though such a description may bear some simplifications with respect to reality [1]. The ability of numerical Discrete Element Methods to predict the AoR has recently been benchmarked in [2, 3] in a round robin series of tests organized by the Japanese Geotechnical Society (JGS) within the activities of Technical Committee 105 (TC105: Geo-Mechanics from Micro to Macro) of the International Society for Soil Mechanics and Geotechnical Engineering (ISSMGE). Following [4], results obtained with the YADE code [5] at INRAE, Aix Marseille Univ, RECOVER (France) and at the School of Engineering, Newcastle University (United-Kingdom) are herein presented, together with new rigorous measurement methods possibly useful for evergoing AoR studies.

2. Numerical approaches

The experiments of the benchmark applied to mono-sized 3D-printed rounded tetrahedral particles with given visco-elastic-frictional properties [2]. While the particles at hand accept a direct numerical counterpart as a multi-sphere clump, i.e., a rigid aggregate of overlapping spheres, simulations have also been conducted using a convex approximation of the latter, following the potential particles (PP) approach proposed in 3D by [6] (Figure 1). In addition to particle shape, the set-up of the DEM simulations conformed the experimental configurations in terms of overall geometry (either "plane-strain" or "axisymmetric"), contact property statistical distributions and number of particles. On the other hand, the individual positions of the particles were necessarily random in the simulations, which were thus repeatedly ran and interpreted in a statistical fashion, enhancing robustness of the conclusions.

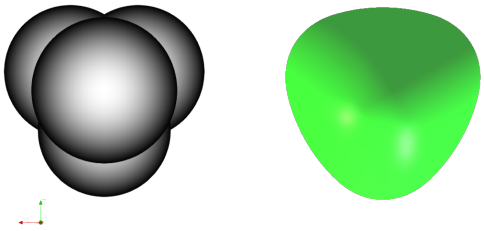

Figure 1. Considered particle as a multi-sphere clump (left) and its potential particle convex approximation (right)

Besides innovative measurement methods of the void ratio as a key parameter of the material that would possibly rule the AoR, rigorous measurement methods of the latter have also been proposed from a global consideration of outer particles forming the exterior slope through fitting techniques.

3. Results

From a methodological point of view, the proposed global measurement method of the AoR has shown itself slightly different, with no systematic trend, from the more sensitive local measure used in [2] that considered only the particles with extreme (minimal or maximal) altitudes (Table 1).

	Plane-strain	Axisymmetric
Global measure	$36.6° \pm 1.0° \in [34.1°; 37.8°]$	$37.0° \pm 0.8° \in [35.4°; 38.5°]$
Local measure	$38.1° \pm 1.1° \in [35.0°; 41.3°]$	$33.9° \pm 0.8° \in [32.0°; 36.1°]$

Table 1. Comparison of AoR measurement methods on the set of clump-based simulations. Numeric values correspond to average, standard deviation and minimum and maximum values.

From a physical point of view, the comparison between DEM simulations and experiments (using the local measurement method of the AoR which was the only one possible during experiments) first shows that the clump-based simulations successfully predict the AOR within a 8% tolerance by default, after sole prior calibration at the particle-scale. Second, it appears that neglecting local concavities of the physical particle, as with the PP, leads to further underestimation of the AoR (Table 2).

	Plane-strain	Axisymmetric
Experiments	$41.4° \pm 1.3° \in [38.3°; 46.3°]$	$35.3° \pm 0.9° \in [33.3°; 37.3°]$
Clumps	$38.1° \pm 1.1° \in [35.0°; 41.3°]$	$33.9° \pm 0.8° \in [32.0°; 36.1°]$
Potential Particles	$34.8° \pm 1.6° \in [32.5°; 38.0°]$	$29.7° \pm 0.8° \in [28.5°; 31.2°]$

Table 2. Comparison of obtained AoR values during experiments and DEM simulations with various shape descriptions (as per the "Local measurement method" of Table 1).

References

[1] Topić, N., Gallas, J. A., and Pöschel, T. (2012). Nonuniformities in the angle of repose and packing fraction of large heaps of particles. *Physical review letters*, **109**, 128001.

[2] Nakata, Y., Moriguchi, S., Kajiyama, S., Kido, R., Kikkawa, N., Saomoto, H., Takano, D., and Higo, Y. (2022). Experimental data of 3d printed granular material for verification of discrete element modeling simulation. *Soils and Foundations*, **62**, 101178.

[3] Saomoto, H., et al. (2023). Round robin test on angle of repose: DEM simulation results collected from 16 groups around the world. *Soils and Foundations*, **63**, 101272.

[4] Duverger, S., Angelidakis, V., Nadimi, S., Utili, S., Bonelli, S., Philippe, P., and Duriez, J. (2023). Investigation techniques and physical aspects of the angle of repose of granular matter. *Granular Matter*.

[5] Smilauer, V. et al. (2021). *Yade Documentation 3rd ed.*. The Yade Project, http://yade-dem.org/doc/.

[6] Boon, C. W., Houlsby, G. T., and Utili, S. (2013). A new contact detection algorithm for three-dimensional non-spherical particles. *Powder Technology*, **248**, 94 – 102.

Micro-mechanical explanation of intergranular strain

***M. Salimi*[1], *M. Tafili*[1], *N. Irani*[1] *and T. Wichtmann*[1]**
[1] *Ruhr-University Bochum, Bochum, Germany*

1. Introduction

One of the most striking shortcomings of hypoplasticity [1] is an excessive accumulation of deformation predicted for small stress cycles, and the inability of modeling small hysteretic loops in the strain-stress plane [2, 3, 4]. The hypoplastic model predicts saw-tooth-like diagrams instead of loops, such performance is often called ratcheting [5, 6, 7]. For undrained cyclic shearing the hypoplastic approach predicts a far too high build-up of pore pressure [8]. Neither the small-strain stiffness nor effects of the recent history have been adequately modeled in the reference hypoplastic model [1].
In order to improve the performance of the hypoplastic model in the range of small load cycles a new state variable called intergranular strain, $\boldsymbol{h}$, has been introduced [9, 2]. The new state variable is thought to represent the deformation of an interface layer between soil particles and is dictated by the recent history of deformation. The stiffness tensor is then increased considering the angle between intergranular strain and strain rate.
Even though this approach fulfilled its aim and is widely used to simulate cyclic processes with different hypoplastic models for clay and sand, e.g. [10, 11, 12, 13, 14, 8], criticism was raised because of its phenomenological nature. In an attempt of establishing this phenomenological concept on experimental foundations, the incremental change in anisotropy during load reversal was compared with the results from numerical simulations as well as the development of intergranular strain by Wiebicke [15]. An experimental explanation of this concept was there however not possible, at least with the contact structure, as both variables turned out to develop differently [15]. As documented there, the structure evolves more slowly than the state variable and extends far beyond the load reversal.
In the present work discrete element method (DEM) simulations with the quantification of the second-order work are conducted and used for the explanation of intergranular strain on micromechanical basis.

2. Theory

An attempt to link the macroscopic behaviour to microstructure was undertaken by [16] in order to further discuss the notion of failure in a granular assembly. Therefore, the key microstructural mechanisms which are most likely to trigger the nucleation and propagation of instabilities within a granular material were examined. For this purpose, the key variable to predict the occurrence of failure, known as second-order work, is expressed from variables on the grain scale. Even though, the intergranular strain has an opposite influence to the one of onset of failure, the second-order work proposed by [16] will be explored further. The macroscopic representation of stress within a volume V is provided by the Eulerian Love-Weber formula:

$$\sigma_{ij} = \frac{1}{V}\sum_{c=1}^{N_c} f_i^c l_j^c + \frac{1}{V}\sum_{p\in V} f_i^p x_j^p \tag{1}$$

wherein l^c is the branch vector of contacting particles in contact c, f^c is contact force, f^p is resultant force applied to the particle p and x^p is position of the particle. The micromechanical expression of the second-order work can be obtained by:

$$d^2W = \sum_{p,q} \delta f_i^c \delta l_i^c + \sum_{p\in V} \delta f_i^p \delta x_i^p \tag{2}$$

in this context, the first term introduces the intrincate link between the contact force network (denoted with f^c) and the geometrical distribution of branch vector between grains (denoted with l^c), while the second term embeds the influence of incremental unbalanced force applied to each particle. In the context of intergranular strain, $\boldsymbol{h}$ is conceptualized to modify the soil stiffness after a rapid change in the direction of the strain path. The maximum value of $\boldsymbol{h}$ is considered as a material constant denoted as R which is assumed to be unaffected by pressure [2].

3. Results

A series of drained, undrained, triaxial, and true triaxial DEM simulations have been conducted for the explanation of intergranular strain with micromechanical quantities. This abstract presents the results of one drained triaxial test with an unloading-reloading cycle, while a more detailed analysis will be covered in the extended version. Fig. 1 illustrates the predictions of the hypoplastic model coupled with intergranular strain proposed by [1, 2] (Hypo+IGS) and DEM simulations for a medium-dense sample sheared under drained triaxial conditions in the shear stress-time ($q-t$) (Fig. 1 (a-b)) and shear stress-axial strain ($q-\varepsilon_1$) plane (Fig. 1 (c-d)). Moreover, Fig. 1 (e) includes the variation of the related intergranular strain (IGS) variable during the test, showcasing a similar behaviour as the second-order work versus time (d^2W-t) obtained by the DEM data in Fig. 1 (f). In practical terms, the alterations in the stiffness of particulate media, coupled with the d^2W, may prove a systematic approach for calibrating $\boldsymbol{h}$ and most importantly for its physical explanation. Regarding the results of drained and undrained true triaxial DEM simulations, it was found that the changes in $\boldsymbol{h}$ highly depend on the level of plastic shear strain, strain rate and Lode angle.

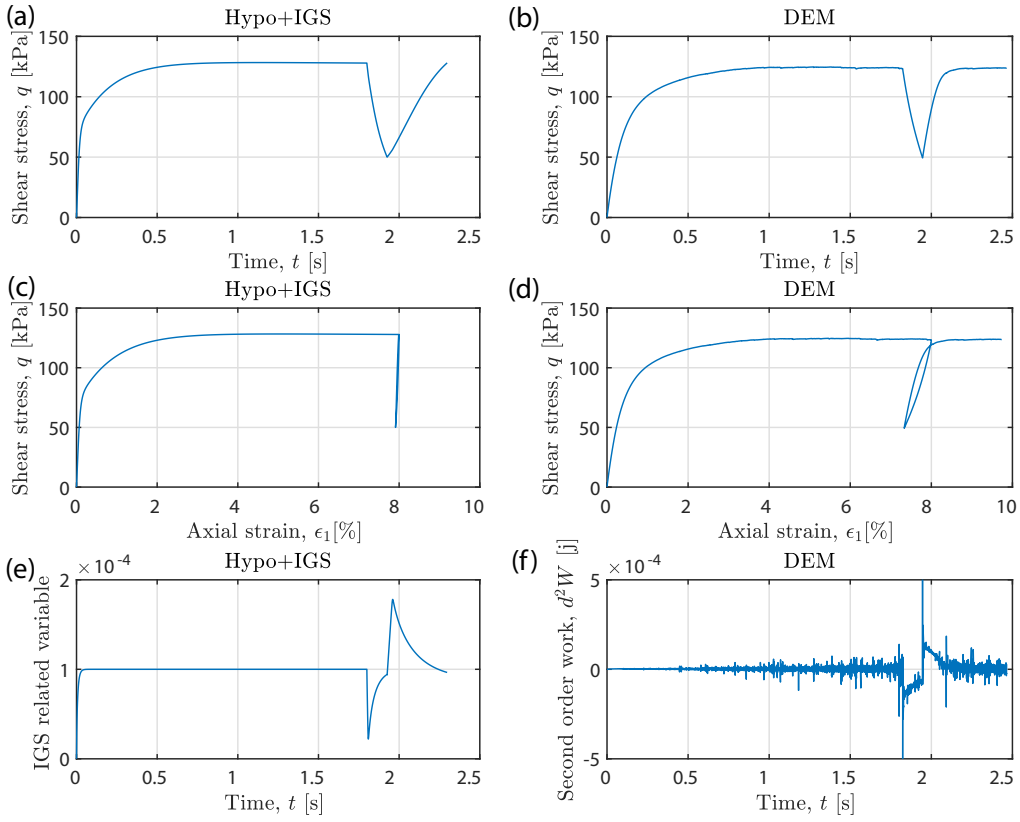

Figure 1. Hypo+IGS model predictions and DEM simulations for a medium-dense sample sheared under drained triaxial conditions in a & b: $q-t$, c & d: $q-\varepsilon_1$ plane, e & f: variation of the relate intergranular strain variable vs. time and d^2W-t from DEM data.

References

[1] Von Wolffersdorff, P.-A. (1996). A hypoplastic relation for granular materials with a predefined limit state surface. *Mechanics of Cohesive-frictional Materials: An International Journal on Experiments, Modelling and Computation of Materials and Structures*, **1**, 251–271.

[2] Niemunis, A. (2003). *Extended hypoplastic models for soils*, vol. 34. Inst. für Grundbau und Bodenmechanik Vienna.

[3] Tafili, M., Grandas Tavera, C., Triantafyllidis, T., and Wichtmann, T. (2021). On the dilatancy of fine-grained soils. *Geotechnics*, **1**, 192–215.

[4] Tafili, M. and Triantafyllidis, T. (2020). A simple hypoplastic model with loading surface accounting for viscous and fabric effects of clays. *International Journal for Numerical and Analytical Methods in Geomechanics*, **44**, 2189–2215.

[5] Medicus, G., Tafili, M., Bode, M., Fellin, W., and Wichtmann, T. (2023). Clay hypoplasticity coupled with small-strain approaches for complex cyclic loading. *Acta Geotechnica*, pp. 1–20.

[6] Duque, J., Yang, M., Fuentes, W., Mašín, D., and Taiebat, M. (2021). Characteristic limitations of advanced plasticity and hypoplasticity models for cyclic loading of sands. *Acta Geotechnica*, pp. 1–23.

[7] Knittel, L., Tafili, M., Tavera, C. G., and Triantafyllidis, T. (2023). New perspectives on preshearing history in granular soils. *Scientific Reports*, **13**, 4576.

[8] Tafili, M., Ganal, A., Wichtmann, T., and Reul, O. (2023). On the avisa model for clay–recommendations for calibration and verification based on the back analysis of a piled raft. *Computers and Geotechnics*, **154**, 105126.

[9] Niemunis, A. and Herle, I. (1997). Hypoplastic model for cohesionless soils with elastic strain range. *Mechanics of Cohesive-frictional Materials: An International Journal on Experiments, Modelling and Computation of Materials and Structures*, **2**, 279–299.

[10] Tafili, M. and Triantafyllidis, T. (2020). Avisa: anisotropic visco-isa model and its performance at cyclic loading. *Acta Geotechnica*, **15**, 2395–2413.

[11] Machaček, J., Staubach, P., Tafili, M., Zachert, H., and Wichtmann, T. (2021). Investigation of three sophisticated constitutive soil models: From numerical formulations to element tests and the analysis of vibratory pile driving tests. *Computers and Geotechnics*, **138**, 104276.

[12] Tafili, M., Medicus, G., Bode, M., and Fellin, W. (2022). Comparison of two small-strain concepts: Isa and intergranular strain applied to barodesy. *Acta Geotechnica*, **17**, 4333–4358.

[13] Duque, J., Tafili, M., Seidalinov, G., Mašín, D., and Fuentes, W. (2022). Inspection of four advanced constitutive models for fine-grained soils under monotonic and cyclic loading. *Acta Geotechnica*, **17**, 4395–4418.

[14] Duque, J., Tafili, M., and Mašín, D. (2023). On the influence of cyclic preloadings on the liquefaction resistance of sands: A numerical study. *Soil Dynamics and Earthquake Engineering*, **172**, 108025.

[15] Wiebicke, M. (2020). Experimental analysis of the evolution of fabric in granular soils upon monotonic loading and load reversals.

[16] Nicot, F., Hadda, N., Sibille, L., Radjai, F., Hicher, P.-Y., and Darve, F. (2014). Some micromechanical aspects of failure in granular materials based on second-order work. *Comptes Rendus Mécanique*, **342**, 174–188.

Microscopic Study of Factors Affecting Liquefaction Strength during Anisotropic Consolidation

Y. Han[1], R. Uzuoka[2] K. Ueda[2] and M. Nakamura[3]
[1] Kyoto University, Graduate School of Engineering, Uji, Kyoto, Japan
[2] Kyoto University, DPRI, Uji, Kyoto, Japan
[3] MAEDA Corporation, Tokyo, Japan

1. Introduction

Conventional triaxial tests [1] have been extensively conducted to elucidate the mechanisms of liquefaction. During earthquakes, vertically propagating shear waves rotate the axes of principal stress in soil elements [2], resulting in different stress states from those in triaxial tests. To address the limitations of traditional experiments, alternative testing methods, including hollow torsional shear tests [3] were utilized to study liquefaction. This study proposed a novel approach for simulating undrained hollow torsional tests using the discrete element method (DEM). It offered a microscopic perspective on how initial anisotropy influences the liquefaction strength.

2. Methodology

The initial boundary conditions, as shown in Fig. 1, involve two rigid cylindrical walls with an inner diameter of 6 cm and an outer diameter of 10 cm. The upper and lower boundaries are located 10 cm apart. Additionally, 6 blades designed for applying shear forces are positioned on the top and bottom of the apparatus.

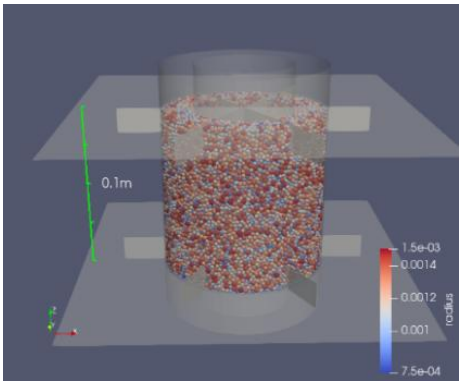

Figure 1. Specimen and apparatus in DEM simulation

To obtain anisotropically consolidated specimens, triaxial compression (K_0 < 1.0) and extension (K_0 > 1.0) shear tests were conducted on isotropic specimens under constant-p' condition. 10 cases of anisotropically consolidated specimens with K_0 values ranging from 0.3 to 3.33 were obtained. As indicated by Eq. (1), the variation of the outer and inner radii R and r was controlled proportionally to ensure a constant volume of the specimen, and t denotes time. Specimens with initial K_0 values ranging from 0.33 to 3.33 were subjected to shear forces with 7 different stress ratios (CSR) τ_{max}/p'_0 ranging from 0.225 to 0.375 until liquefaction occurred.

$$\frac{dR}{dt} = \frac{r}{R}\frac{dr}{dt} \tag{1}$$

3. Results and discussion

Fig. 2(a) depicts the relationship between deviatoric stress σ_{vM} and mean principal stress p' during the liquefaction process, and a typical stress evolution in laboratory tests has been replicated in DEM simulations, providing evidence for the effectiveness of the method proposed. Fig 2 (b) shows that an increasing initial stress anisotropy induced lower liquefaction resistance strength.

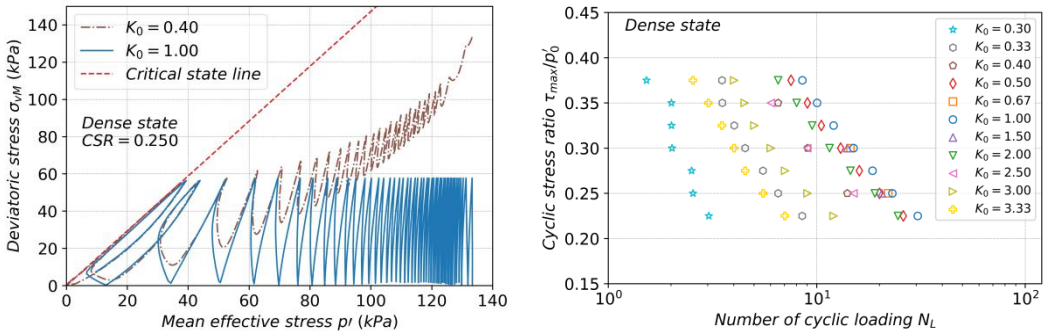

(a) Relationship between σ_{vM} and p' (b) Liquefaction resistance strength

Figure 2. Stress ralationship and liquefaction strength

The coordination number (Z) serves as an indicator reflecting the microscopic density of granular materials. Fig. 3 shows the evolution of Z under different initial stress states during the liquefaction process, and the the relationship between the number of cycles required to trigger liquefaction (N_L). The result indicates that Z contributes to the liquefaction resistance strength, and the preliminary triaxial shear produces a lower Z, thus reducing the liquefaction strength.

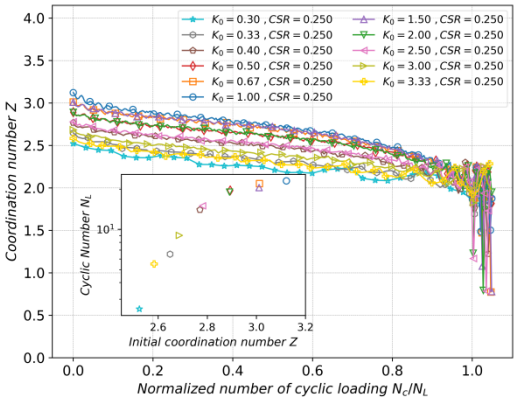

Figure 3. Evolution of Z and the relationship between Z and N_L

5. References

[1] Hyodo, M. et al. (1991). Undrained Cyclic Shear Strength and Residual Shear Strain of Saturated Sand by Cyclic Triaxial Tests. Soils and Foundations, 31(3), 60‑76.

[2] Arthur, J. R. F. et al. (1980). Principal Stress Rotation: A Missing Parameter. Journal of the Geotechnical Engineering Division, 106(4), 419‑433.

[3] Vargas, R. et al.(2020). Influence of the relative density and K0 effects in the cyclic response of Ottawa F-65 sand - cyclic Torsional Hollow-Cylinder shear tests for LEAP-ASIA-2019. Soil Dynamics and Earthquake Engineering, 133, 106111.

MICROSCOPIC MECHANISMS OF 2D ARCHING DEVELOPMENT AND DEGRADATION IN GRANULAR MATERIALS UNDER DIFFERENT RELATIVE DENSITY

Luju Liang[1,2*] and Yi Pik Cheng[3]

[1]Institute of Civil Engineering, Hangzhou City University, Hangzhou, China

[2]Key Laboratory of Safe Construction and Intelligent Maintenance for Urban Shield Tunnels of Zhejiang Province, Hangzhou City University, Hangzhou, China

[3]Department of Civil, Environmental and Geomatic Engineering, University College London, London, UK;

1. Abstract

The relative density significantly influences the arching effect on various infrastructures, such as tunnels, retaining walls, and piles in pile-supported embankments, while its mechanisms is barely analysed. This study carried out a series of DEM numerical simulations to investigate the microscopic mechanisms of arching development and degradation in granular materials with different relative density. For analysis, the granular assembly above a displacement-controlled trapdoor were divided into three zones according to particle vertical displacement normalized by the trapdoor displacement δ: (a) "zone-I" with insignificant vertical displacement of particles less than 0.1δ; (b) "zone-II" with vertical displacement of particles less than 0.9δ but larger than 0.1δ; (c) "zone-III" dominated by vertical displacement of particles larger than 0.9δ.

The microscopic mechanisms of particles in different zones are then analysed through persistence homology. The results show that the evolution of force chains and particle contact force induces shear localisation in zone-II, it plays a key part in the development and degeneration of soil arching effect. Before the maximum arching state (corresponding to the minimum arching ratio), contact forces between particles in zone-II increase rapidly and robust arched force chains with large particle contact forces are generated. The evolution of contact forces and its fabric become more obvious as the sample porosity decreases. As a result, the arching effect generated in denser particle assembly is stronger, and the minimum value of arching ratio is increased with the sample porosity. After the maximum arching state, the force chains in zone-II are degenerated gradually, leading to the decrease of particle contact forces in microscopic and the increase of arching ratio in macroscopic level. The recovery of arching ratio after the minimum value is also more significant in the simulation with larger relative density, as the degeneration of contact forces chains is more obvious in denser sample. These results indicate the importance of contact force chains stabilities in specific zone for improving soil arching in engineering practice.

NUMERICAL SIMULATION OF FLEXIBLE-BONDED GRANULAR ASSEMBLY USING DEM

Mehdi Alam[1,2], Arghya Das[2], and Mahdi M. Disfani[1]

[1] The University of Melbourne, Department of Infrastructure Engineering, Melbourne, Australia

[2] Indian Institute of Technology, Kanpur, Department of Civil Engineering, Kanpur, India

1. Outline

The present study explores the modelling of flexible binding materials for bonded granular assembly using Discrete Element Method (DEM). According to experimental findings [1], the addition of flexible polyurethane (PU) binder with geologic granular materials significantly enhances the constrained modulus of the assembly used in pavement engineering. It is noteworthy that PU binders exhibit distinct characteristics compared to cement-based binders, the latter possessing considerably higher stiffness and lower flexibility and hence a different bond breakage pattern. While numerical investigations on cement-based binders can be found in the existing literature [2], this study focuses on DEM simulations for flexible binders utilizing the soft-bond contact model [3] inbuilt in the commercially available code PFC3D[4]. The study addresses the calibration of bond parameters accounting for the contribution of bond materials in the overall porosity of the assembly. Subsequent particle-scale investigations are planned to understand the influence of PU content in the mixture.

2. Methodology

A cylindrical bonded granular assembly with dimensions of 50 mm high and 105 mm diameter is prepared in DEM similar to those outlined in experiments [1]. The soft-bond contact model is introduced at the contact points, which incorporates both rolling and twisting resistances. Notably, the bond does not immediately break upon the tensile stress at the bond periphery reaching strength; instead, it enters a softening regime (see Figure 1(a)). Figure 1(b) shows a schematic representation of the soft-bond model at the contact points. Calibration of contact parameters is performed based on the constrained modulus-axial stress response observed in experiments. The prepared sample is then subjected to loading through a servo-controlled method at various stresses from 10 kPa to 2000 kPa, replicating the conditions employed in the experiments.

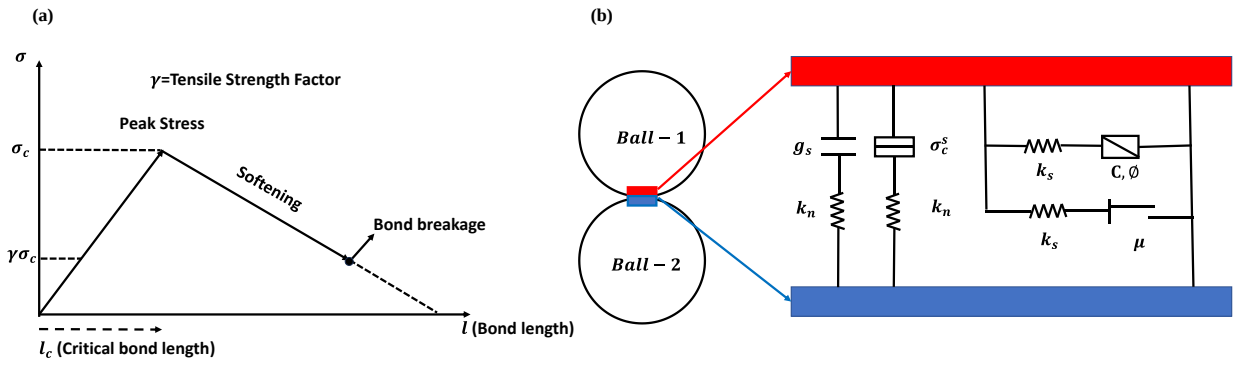

Figure 1. Soft-bond model (a) schematic of a bond response (b) schematic diagram at contact point.

The prepared sample is calibrated for three different PU content by mass, 4%, 7% and 10%. It is well known that in DEM, bond material does not contribute to mass balance or volume balance. The cross-sectional area of bond at the contacts are varied as in Figure 2 to simulate the PU content. It is assumed that with the decrease in PU content the binder will be distributed in smaller cross-sections. Also, the proximity between the particles is regulated in order to maintain the overall void ratio of the sample assuming the presence of bond.

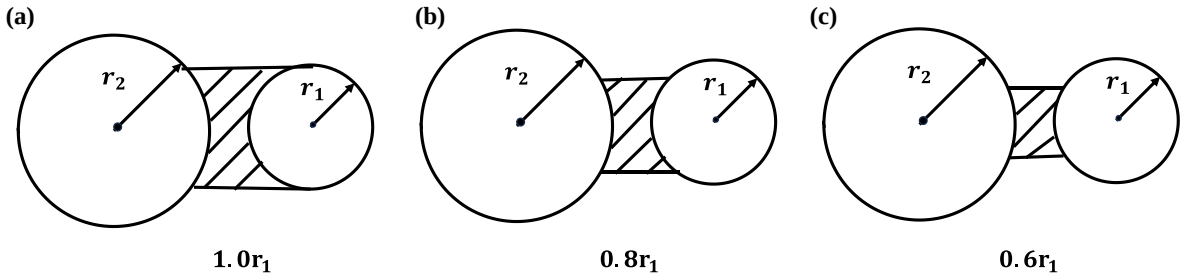

Figure 2. Cross-sectional area used to simulate different PU content (a) 10%; (b) 7%; (c) 4%.

3. Results

The calibration of the constrained modulus-axial stress is done using the contact model, and the calibrated numerical response aligns well with experimental findings across various soft contents. Figure 3 illustrates a typical comparison between the experimental representative calibrated result for 10% PU content.

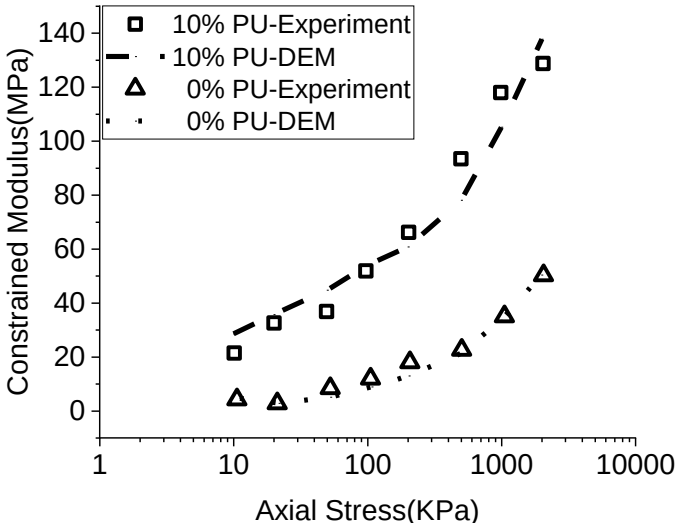

Figure 3. Calibrated experimental and numerical results for 10% PU content.

5. References

[1] Raeesi, R., Soltani, A., & Disfani, M.M. (2022) Compressibility Behavior of Soft–Rigid Granular Mixtures Bound with Polyurethane Binder. *Int. J. Geomech*. 22 (1), 04021265.

[2] Wang, Y.H. and Leung, S.C. (2008) A particulate-scale investigation of cemented sand behavior. *Can. Geotech. J*. 45 (1), 29–44.

[3] Jiang, M., Shen, Z., and Wang, J. (2015) A novel three-dimensional contact model for granulates incorporating rolling and twisting resistances. *Comput. Geotech*. 65 147–163.

[4] PFC | US Minneapolis - Itasca Consulting Group, Inc.

ON THE NUMERICAL DISCRETE MODELING OF A BOUNDARY VALUE PROBLEM USING AN ADAPTATIVE DISCRETIZATION APPROACH

***Sébastien H.E. Volcy*[1], *Christophe Dano*[1] *Luc Sibille*[1],*Bruno Chareyre*[1] *and Hamid Hosseini-Sadrabadi*[2]**

[1]*Univ. Grenoble Alpes, CNRS, Grenoble INP, 3SR F-38000 Grenoble, France*

[2]*Equaterre: Geotechnical Design Office, Annecy, France*

6 Rue de l'Euro, 74960 Meythet

The numerical modeling of a boundary value problem using the Discrete Element Method (DEM) is problematic when it involves a considerable number of particles -and hence of inter-granular contacts- which eventually generates high computational costs. It is the case, particularly, when the problem has geometrical singularities where particle sizes need to be realistic, such as interactions with tools, tips, or any object of small size within a large simulation domain. Different approaches exist to circumvent such a challenge.

One is to use multi-domain discrete-continuous coupling, with DEM around the singularity, where large deformations are expected, and another continuum mechanics method -Finite Element Method (FEM) typically- away from it. When doing so, the interfaces between DEM and FEM must be handled properly and a continuity of mechanical properties needs to be insured, which is not always easy.

Here, a simpler approach that does not require coupling computational methods is proposed. It uses an adaptative discretization approach, inspired from [1, 2]. It roughly consists of discretizing a domain with small particles within an area of interest (where large displacements, large deformations, shear band occurrence, grain crushing, ... may occur) and coarsening the particle size distribution away from it, while preserving the uniformity of mechanical properties as much as possible, using a proper scaling of the parameters of the contact models.

This approach is implemented and evaluated for the modeling of a cyclic Cone Penetration Test (CPT) in a calibration chamber as presented in Figure 1a. It is shown that relevant information such as tip/soil interactions, stress and strain fields (Figure 1b), can be obtained with a limited impact from the adaptative particle size as long as some conditions on the size gradients are satisfied, with a much smaller computational cost compared to uniform particle sizes, and with less complexity as in discrete-continuous couplings. Comparisons with experimental results obtained from "real" cyclic CPTs performed in a calibration chamber are also presented to assess the representativeness of such a numerical approach of actual problems in geomechanics.

Keywords: Cyclic CPT, Discrete Element Method, Boundary Value Problem, Adaptative Discretization

References

[1] Sadrabadi, H., Chareyre, B., Sibille, L., and Riegel, P. (2018). Modélisation du pénétromètre statique (cpt) en condition saturée: un modèle numérique discret avec couplage fluide-solide. *9èmes Journées Nationales de Géotechnique et de Géologie de l'Ingénieur-JNGG2018*.

[2] Abdallah, A., Hosn, R. A., Tfaily, B. A., and Sibille, L. (2022). Identifying parameters of a discrete numerical model of soil from a geotechnical field test. *European Journal of Environmental and Civil Engineering*, **27**, 2228–2247.

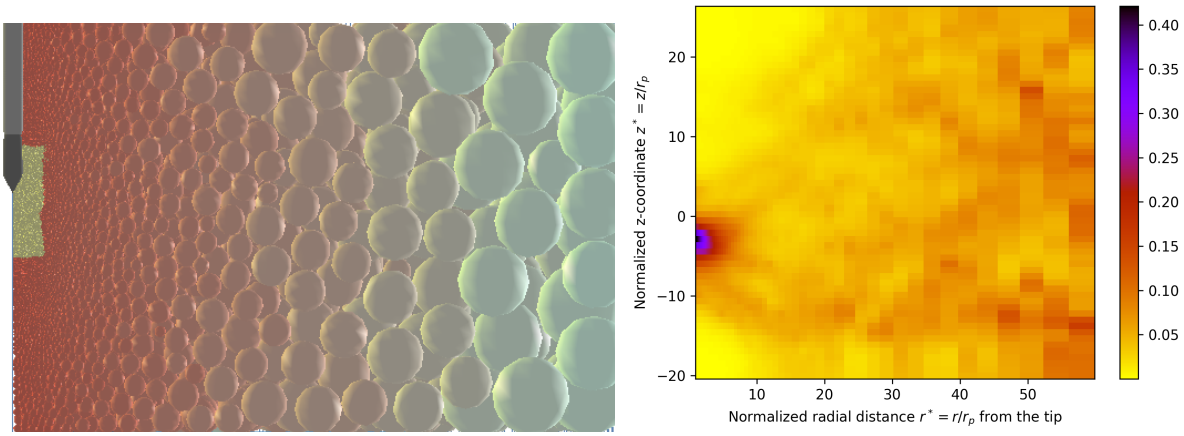

(a) (b)

Figure 1. 1a)-Discrete numerical model of a cone penetration test in a calibration chamber involving an adaptative discretization approach of the soil. 1b)-Radial stresses field, in MPa, resulting from the simulation of the cone penetration; r_p is the tip radius.

PARTICLE SCALE ANALYSIS OF THE IMPACT OF PARTIAL DRAINAGE ON UNDRAINED SHEAR RESPONSE

J. Salomon[1], F. Patino-Ramirez[1], and C. O'Sullivan[1]
[1] Imperial College London, Dept. of Civil and Environmental Engineering, London, UK

1. Introduction

Static and earthquake-induced liquefaction can have devastating economic and societal impact. It has long been recognized that undrained conditions can be simulated using the discrete element method (DEM) by imposing a constant volume condition on the simulated assembly of grains (e.g. [1]). This is a fundamentally important modelling achievement as it means that the kinematic condition that restricts deformation to be at a constant volume can trigger liquefaction in the absence of any increase in pore water pressure. Element test simulations using DEM can facilitate useful parametric studies to advance understanding of macro- (i.e. continuum) scale soil behaviour, while also providing a rich set of data which, in principle, can be used to inform fundamental understanding.

Soil desaturation, in which there is a small reduction in the in-situ degree of saturation, is one potential approach to mitigate liquefaction risk in situ [2]. This study builds upon prior experimental work (e.g. [3]) and uses DEM to explore the fundamental basis for this approach and advance understanding of the fundamental mechanisms that lead to liquefaction under constant volume and partially drained deformation.

2. Methodology

The DEM simulations used LAMMPS [4]. The virtual samples comprised approximately 5,000 spherical particles with a particle size distribution corresponding to Toyoura sand. Periodic boundaries were used and a Hertz-Mindlin contact model was adopted. A relatively loose packing (void ratio of 0.63) was attained by controlling the inter-particle friction coefficient during the initial isotropic compression phase. Once the target confining pressure of 300 kPa was achieved, identical copies of the sample were subject to monotonic triaxial shear deformation. Four scenarios were considered (i) fully drained shear (ii) constant volume (fully undrained) shear (iii) partially-drained shear with a volumetric strain of 5% of the drained volumetric strain and (iv) partially-drained shear with a volumetric strain of 25% of the drained volumetric strain. Cases (iii) and (iv) were achieved by developing a new control algorithm which imposed, at each axial strain (ε_z), a volumetric strain (ε_{vol}) that was a specified proportion of the drained volumetric strain at the same axial strain ($\varepsilon_{vol}(\varepsilon_{z,drained})$), i.e. $\varepsilon_{vol}(\varepsilon_z) = \beta\varepsilon_{vol}(\varepsilon_{z,drained})$, where $0 \leq \beta \leq 1$ is a dimensionless constant that quantifies the amount of drainage allowed. Developing this algorithm was non-trivial and the key step was to develop the overall form for an analytical expression which can capture the variation in ε_{vol} with $\varepsilon_{z,drained}$. This algorithm is a generalization of the strain-controlled linear path tests found in the DEM literature (e.g. [3]).The parameters involved in the control algorithm were then calibrated by considering the data from the fully drained simulation.

3. Results and discussions

The simulation results in terms of stress path observed are presented in Figure 1(a). The undrained sample, the sample with $\beta = 0.05$ and the sample with $\beta = 0.25$ exhibit classical features associated with static liquefaction. From the onset of shear deformation, the mean effective stress

(p') decreases. Initially the shear stress (q) increases to a peak value, then it decreases to a local minimum value at the phase transformation point, and then there is a subsequent increase in q. It is only in the case of the fully undrained (constant volume) simulation that q reduces to zero. Figure 1(b) illustrates the variation in the coordination number, Z, (average number of contacts per particle) as a function of axial strain. Interestingly it is only in the fully undrained case that Z falls beneath the value of 4 which is the minimum Z value for a statically indeterminant system. In contrast to the fully drained case where there is an initial slight increase in Z, for $\beta = 0.05$ and $\beta = 0.25$ there is a clear reduction in Z from the start of shearing, however Z remains above 4.5.

4. Conclusions

An algorithm was developed to control the volumetric strain experienced during triaxial shear deformation in DEM simulations and simulate partial drainage during triaxial shear deformation. At a macro-scale the resulting data show that classical liquefaction phenomena can be observed in the cases of small amounts of partial drainage considered here ($\beta \leq 0.25$). A greater sensitivity to the relaxation of the constant volume restraint is observed when the coordination number data are considered. Further examination of these data may provide important insight into the phenomenon of soil liquefaction. A key challenge is to extend this simulation approach to consider cyclic loading.

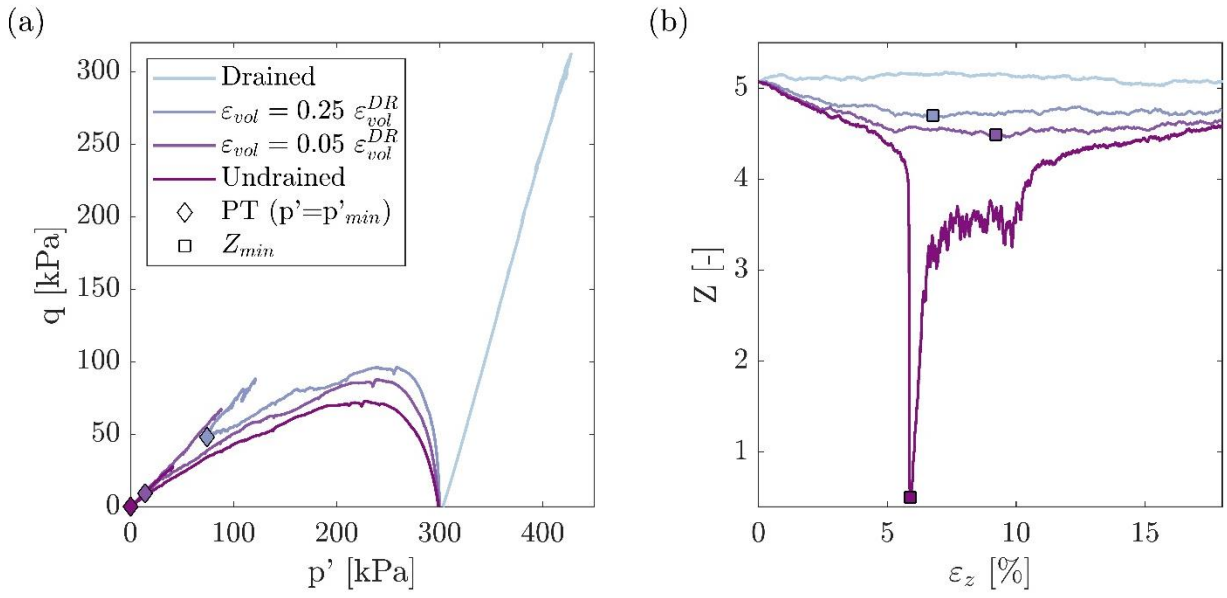

Figure 1. Observed response in triaxial shear (a) Deviator stress versus mean effective stress (b) Coordination number versus axial strain.

5. References

[1] Ng, T.T. and Dobry, R. (1994). Numerical simulations of monotonic and cyclic loading of graular soil *ASCE Journal of Geotechnical Engineering* 120 (2). 388-403

[2] Moug, D.M. et al.. (2022). Field Trials of Microbially Induced Desaturation in Low-Plasticity Silt *ASCE Journal of Geotechnical and Geoenvironmental Engineering* 148 (11). 402-410

[3] Nicot, F., Daouadji, A., Hadda, N., Jrad, M., & Darve, F. (2013). Granular media failure along triaxial proportional strain paths. *Eur. Jour. of Environ.and Civil Engineering*, 17(9), 777–790.

[4] Plimpton, S.(1995). Fast parallel algorithms for short-range molecular dynamics. Journal of Computational Physics. Vol. 117(1), 1-19. https://doi.org/10.1006/jcph.1995.1039.

PERFORMANCE OF A DEM CONTACT MODEL FOR ROUNDED AND SUBROUNDED GRANULAR MATERIALS UNDER SHEAR AND COMPRESSION

A. Uday[1], A. Peña-Olarte[1], S. Vogt[1]and R. Cudmani[1]
[1]Department of Civil, Geo and Environmental Engineering, Technical University of Munich, Germany

1. Introduction

Granular materials under shear loadings are complex to model due to their particulate nature. The discrete element method (DEM) has been identified as a promising approach to simulate distinct shear distortions by considering the microscopic behavior of granular materials. One essential key for a robust simulation is the calibration of suitable DEM contact model and hence the quantification of the contact model parameters is inevitable. The calibration procedure has to be conducted under specific boundary conditions according to certain experiments. The contact model parameters obtained by the bulk calibration method or the trial and error method lead to non-unique sets of parameters and hence the parameters calibrated from a particular experiment may be not applicable for other boundary condition [1, 2]. The present study aims to evaluate the performance of the rolling resistance linear contact model for rounded and subrounded particles for different experiments applying shear and compression loadings respectively on two granular materials.

2. Methodology

The DEM considers individual particles and their interactions. It is based on Newton's laws of motion, which provide the fundamental relationship between particle motion and the forces causing that motion [3, 4]. There are various concepts of considering the shape of the particles as they can be modelled in the form of balls, clumps, polyhedra or ellipsoids, the size of which are drawn for a particular particle size distribution. Our study uses spheres which are favourable due to the ease in contact detection hence cost-effective in terms of calculation time. Certainly, the shape of natural sand particles deviate from spheres. Our DEM simulations define spheres in combination with an additional resisting moment at the contacts, which mimics the effect of interlocking as a decisive effect for non-spherical particles. The study uses the bulk calibration approach, where the granulometric properties of the simulation like the particle size, shape, particle density along with the contact model parameter namely the contact stiffness, contact damping, contact friction coefficient and rolling resistance friction coefficient are used as input parameters such that macroscopically observeable quantities match the response from an investigated sample. Our research further focusses on the calibration of rolling resistance linear model for two materials namely Corundum, whose particles are rounded and Cuxhaven sand, made up of mainly subrounded particles. The parameters for the materials of the particle size, sphericity and roundness found by non-contact laser-scanning are given in Table 1.

The contact model parameters namely the effective modulus E^*, the normal-to-shear stiffness ratio k^*, the inter-particle friction coefficient μ and the rolling resistance friction coefficient μ_r for Corundum and Cuxhaven sand are obtained using the bulk calibration approach considering data from a set of triaxial tests. For the DEM model, a cubical container 5 mm in size was used, and approximately 10,000 spheres were created within the container without scaling the particle diameters. By the results of our experiments the parameters are first validated by simulating triaxial

tests at different relative densities and confining stresses. As a second step of validation, these parameters are applied to the simulation of compression tests (oedometer).

Table 1 : Classifying parameters for materials investigated

Material	Mean size (mm)	Specific gravity (g/cm^3)	Sphericity (-)	Roundness (-)
Cuxhaven sand	0.30	2.65	0.77	0.54
Corundum	0.80	3.62	0.88	0.92

3. Results

The calibration process of the DEM model including the quantification of the contact model parameters are discussed in [5]. The performance of the contact model parameters for simulating the triaxial test at different relative densities and confining stresses on Cuxhaven sand was notable. From the validation considering the oedometer tests, it could be observed that as already reported by [1] and [2], the agreement of the prediction of the compression curve using the calibrated contact model parameters is limited. By comparing the differences of the model prediction between the simulations of Corundum and Cuxhaven sand the discrepancy may be attributed to numerous factors which are not or only indirectly captured by the DEM model among which the most significant appears to be the particle shape of the actual material. The interlocking effect due to non-spherical particles as given by the Cuxhaven sand is different for a triaxial test compared to the oedometer test. On the scale of the particle assembly hence meso-scale, this results in an evolving network of strong force chains that obviously differs from the actual material behavior, which in turn affects the macro response of the system. On the contrary, as observed from simulations of triaxial tests on Corundum, the fit was good. Moreover the calibrated contact parameters for Corundum performed well when applied to oedometer tests. These results indicate the strong influence of particle shape on the calibration process and the DEM simulations as well as confirm the findings from [1]. For appling the cost-effective concept of modeling spherical parameters in combination with the application of an additional resisting moment at the contact to approximate the behavior of non-spherical particles, it is recommended that special care needs to be considered if the simulated boundary value problem differes significantly from the conditions considered by the calibration process of the contact model.

4. References

[1] C. Coetzee, "Review: Calibration of the discrete element method," *Powder Technology 310*, pp. 104-142, 2017.

[2] C. Coetzee, "Calibration of the discrete element method and the effect of particle shape," *Powder Technology 297*, pp. 50-70, 2016.

[3] C. O'Sullivan, Particulate discrete element modelling, Spon press, 2011.

[4] Itasca, "PFC 7.0 documentation," 2021.

[5] A. Uday and A. Peña-Olarte, "Investigation of the response of Cuxhaven sand under triaxial and ring shear boundary conditions using DEM," *Proceedings 10th NUMGE 2023*, 2023.

QUASISTATIC RESPONSE OF LOOSE COHESIVE GRANULAR MATERIALS: A DEM STUDY

J.-N. Roux[1]***, A.-M. Tang***[1]
[1] *Laboratoire Navier, UMR 8205, École des Ponts, Université Gustave Eiffel, CNRS, France*

1. Introduction

Cohesive granular assemblies, such as powders and colloids, are much less often studied than cohesionless ones, but exhibit a wider variety of static states. While the solid fraction Φ of cohesionless assemblies of identical spherical beads never reaches values < 0.55, much looser static cohesive assemblies are observed [1], in which stresses are carried by tenuous, ramified contact networks similar to colloidal gels [2]. We report on a DEM investigation of the behaviour of a simple model material, subjected to isotropic compression from a loose state and then to triaxial compression.

2. Simulated model

We use the same model system as in Ref. [1]: spherical beads of diameter d, with Hertz contact elasticity, friction coefficient $\mu = 0.3$, and adhesive forces chosen according to a simplified model of capillary attraction through small liquid bridges, which form in wet granular assemblies at low saturation. The attractive F_0 in contacts is proportional to d and to the interfacial tension. Liquid bridges form as grains come into contact and break as the separation distance reach a rupture threshold D_R (typically, $D_R = d/10$).The attractive force decreases as distance grows from $D = 0$ to D_R. The Coulomb inequality involves the elastic repulsive normal force F_N^e only. A contact with vanishing normal force ($F_N^e - F_0 = 0$) may thus transmit a tangential force as large as μF_0. This simple model agrees quantitatively with experimental observations in simple shear flow [3] and in isotropic compression [1]. As in Refs. [1, 3], reduced pressure $P^* = d^2P/F_0$, comparing the adhesive force to pressure P, is used as a dimensionless control parameter. For small P^*, strong cohesive effects stabilize tenuous, open structures [1]. Their influence gradually vanishes as P^* increases, until the properties of cohesionless systems are retrieved for $P^* \gg 1$ [2, 1]. We simulate several 8000 particle samples for each state, and use fully periodic boundary conditions. Loose systems are initially subjected to ballistic aggregation, forming a system-spanning cluster apt to support stresses [1].

3. Results

The initial mean quadratic velocity V_0 (agitation level) in the aggregation stage strongly influences the obtained microstructure (pore size distribution, coordination numbers). This effect is characterized by ratio V_0/V^*, V^* being the escape relative velocity of a grain pair in the attraction potential. For a given low initial solid fraction, it is illustrated in Fig. 1, showing samples in the two limits of large and small V_0/V^*, and the resulting different plastic compression curves. Those curves, with a linear variation of void ratio e with $\log P^*$ in some range, also depend on the initial state density [1]. They are strongly affected (as in previous 2D results [2]) by a small level of rolling resistance in contacts. We show that the influence of the initial state on this plastic compression behaviour is mainly determined by small scale features (local arrangements, angular correlations). This explains the very well identified, reproducible macroscopic behaviour despite large heterogeneities (Fig. 1).

In triaxial compression (Fig. 2), with constant lateral stresses (equal to initial pressure p_0), we measure quite a large increase of material shear strength (ratio q/p_0) due to cohesion (for which the "effective stress"approach", although poorly justified, provides correct orders of magnitude). The evolution of the material state from the initial isotropic to the final critical state is the slower the lower

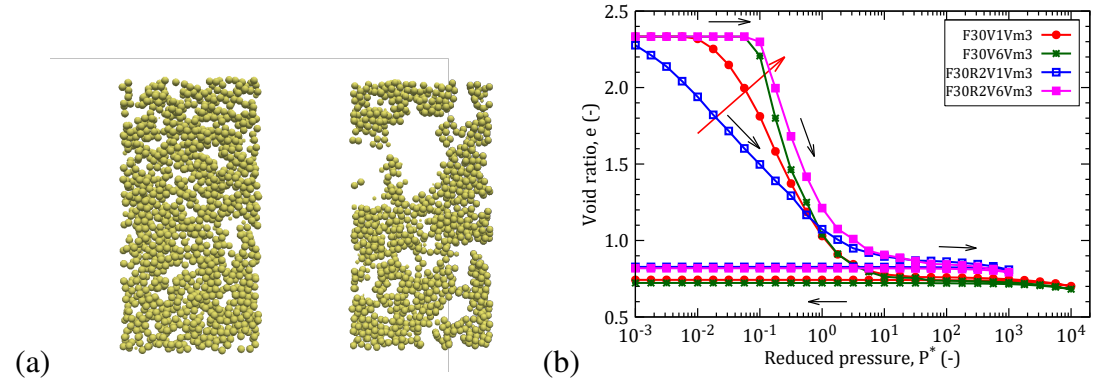

Figure 1. (a) Views of slices (thickness $3d$) cut through simulated systems compressed to $P^* = 0.1$. Left: small V_0/V^*. Right: large V_0/V^*. (b) Void ratio versus P^* in compression cycle, for those two cases (red and green curves) with $\Phi_0 = 0.3$. Also shown (extreme curves): analogous results with small resistance to rolling and pivoting in contacts.

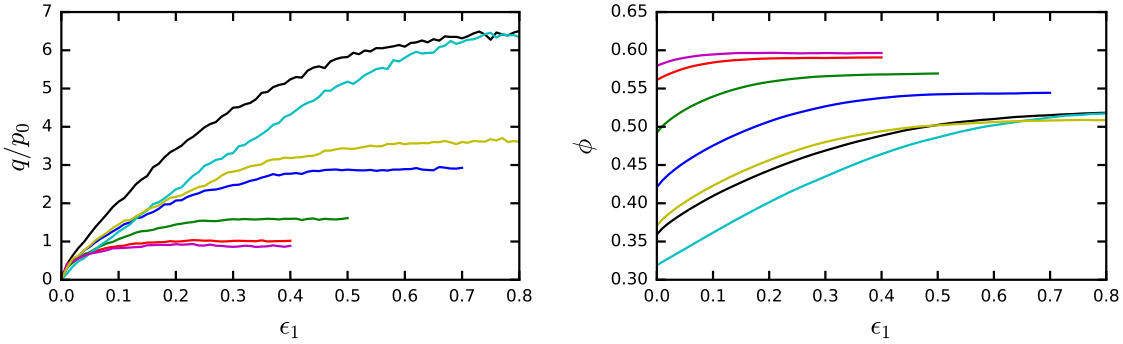

Figure 2. Left: normalised deviator stress q/p_0, versus axial strain ϵ_1, initial aggregation with small V_0/V^*. $P^* = 0.1$ (black); $P^* = 0.1$, but large V_0/V^* (only in that case, light blue); $P^* = 0.1$, without distant interactions, $D_R = 0$ (yellow); $P^* = 0.316$ (dark blue); $P^* = 1$ (green); $P^* = 6.32$ (red); $P^* = \infty$, i.e. no cohesion (purple). Right: solid fraction Φ vs. ϵ_1, same colour code.

P^*, and for $P^* = 0.1$ the influence of initial ratio V_0/V^* is not forgotten until axial stress ϵ_1 reaches about 0.8. No shear localization is observed in those markedly contractant systems. Remarkably, unlike for isotropic compression, distant interactions significantly influence the macroscopic stresses.

Both for isotropic and for triaxial compressions, the observed behaviours are discussed, related to microstructural characteristics, and compared to those of cohesive soils, powders and colloidal aggregates.

References

[1] Than, V.-D., Khamseh, S., Tang, A.-M., Pereira, J.-M., Chevoir, F., and Roux, J.-N. (2017). Basic Mechanical Properties of Wet Granular Materials: A DEM Study. *ASCE Journal of Engineering Mechanics*, **143**, C4016001.

[2] Gilabert, F. A., Roux, J.-N., and Castellanos, A. (2008). Computer simulation of model cohesive powders: Plastic consolidation, structural changes, and elasticity under isotropic loads. *Phys. Rev. E*, **78**, 031305.

[3] Badetti, M., Fall, A., Hautemayou, D., Rodts, S., and Roux, J.-N. (2018). Rheology and microstructure of unsaturated wet granular materials: Experiments and simulations. *J. of Rheology*, **62**, 1175–1186.

Sensitivity Analysis on Critical Combinations of Input Parameters in DEM Granular Flow Analysis

***Junsen Xiao*[1], *Kenta Tozato*[2], *Reika Nomura*[3], *Yu Otake*[1], *Kenjiro Terada*[3], *Shuji Moriguchi*[3]**

[1] *Department of Civil and Environmental Engineering, Tohoku university, Aza-Aoba, 468-1, Aramaki, Aoba-ku, Sendai, 980-8572, Japan*

[2] *Department of Civil Engineering and Architecture, Hachinohe Institute of Technology, 88-1 Ohbiraki, Myo, Hachinohe, Aomori, 031-8501, Japan*

[3] *International Research Institute of Disaster Science, Tohoku university, Aza-Aoba, 468-1, Aramaki, Aoba-ku, Sendai, 980-8572, Japan*

1. Introduction

This study aims to quantify the importance of four DEM input parameters, such as friction angle between elements (FABE), bottom friction (BF), coefficient of restitution (COR), and spring coefficient (SC), in determining run-out distances of granular flows. For that purpose, XGBoost feature importance is employed in consideration of the particle size distribution. The dominant parameters are identified and then comprehensively explored through the Gaussian process regression (GPR) response surfaces obtained from the results of a series of Discrete Element Method (DEM) simulations. By clarifying these mechanisms, this study attempts to identify appropriate parameter sets for landslide risk assessment throughout the entire parameter space.

2. DEM-based granular flow simulation

The polygon model is used for DEM simulations. Different particle sizes are realized by resetting the length of the short axis d_i. In the case of monodisperse flow, d_i is determined as 2.0 cm, which is the median value of the particle sizes in this study. The detailed geometrical conditions for DEM simulations are shown in Fig. 1. In this study, four particle size distribution patterns (n = 1, 2, 3, 5) are applied, where n refers to the number of particle sizes. The ranges of parameters are determined with reference to the authors' experience and values employed in related studies [1, 2]. Latin hypercube sampling (LHS) is adopted to sample 56 simulation cases that produce the training data for the response surfaces constructed in this study.

3. Parameter importance and mechanisms

The effect of each parameter is quantified by XGBoost feature importance to identify key parameters and compress the input dimension for response surfaces. Subsequently, GPR response surfaces are created to visualize the impact mechanisms of key parameters selected by XGBoost. FABE,

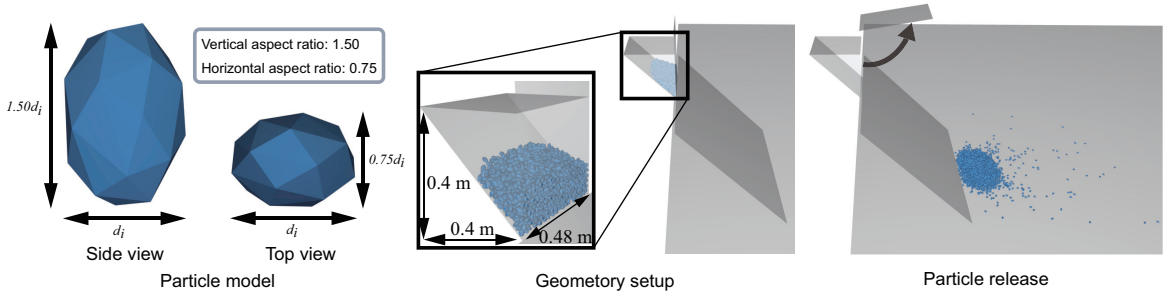

Figure 1. Geometrical conditions for the DEM simulation model.

BF, COR, SC are taken as input data for the XGBoost to calculate the feature importance with outputs, which represent 10%-100% run-out distances in terms of particle mass. Fig. 2 illustrates the feature importance of the four parameters in all run-out distance scenarios and all patterns of particle size distribution. For all the patterns, the importance of FABE and SC is relatively low, while BF and COR have relatively large impact on the run-out distance. In particular, the effect of COR increases significantly at about 80% run-out distance. The GPR response surfaces clarify the impact mechanisms of BF and COR.

Fig. 2 exhibits that for 80% run-out distance, COR and run-out distance have a nearly linear relationship, while BF shows a convex function. In this study, the effects of these two parameters are examined in all the run-out distance scenarios. Each response surface of 80% run-out distance represents the behavior of the front part in granular flow.

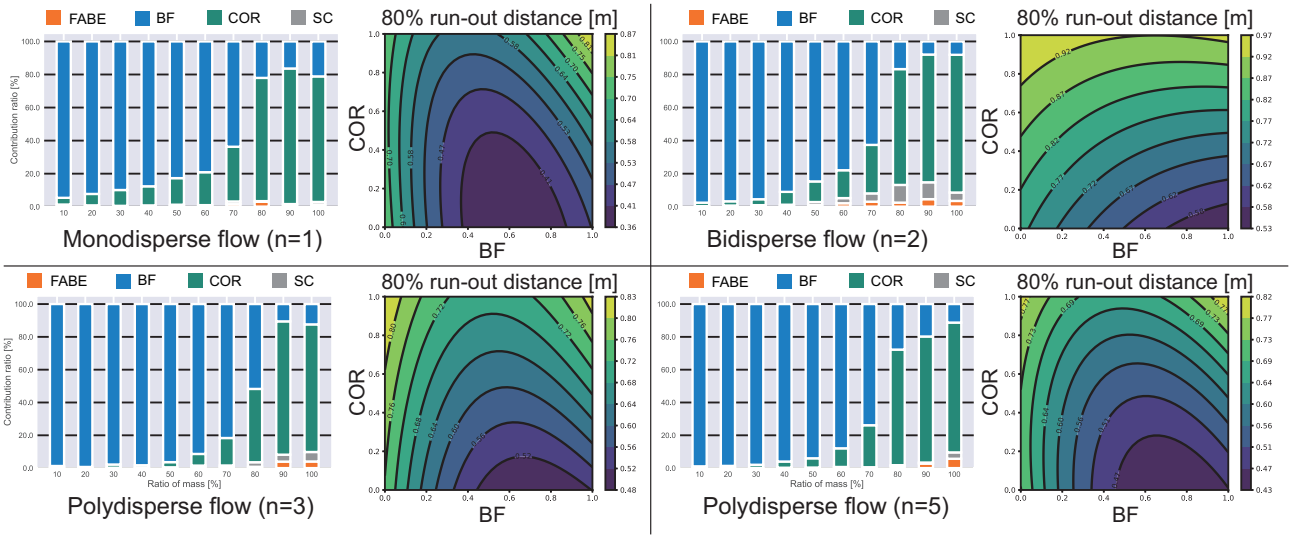

Figure 2. XGBoost feature importance and GPR response surfaces of 80% run-out distance.

4. Conclusion

According to the result of XGBoost, it is demonstrated that BF and COR are the influential factors in evaluating the run-out distance. The impact mechanism of BF is more complicated, with an approximately negative correlation in the middle and rear and an evident convex function in the front part of monodisperse flow. COR shows a nearly linear relationship with run-out distance throughout the granular flow. The value of this study is that it determines engineering priorities by quantifying the importance of various input parameters for DEM simulations. In addition, a comprehensive exploration of the impact mechanisms of key parameters leads to recommendations for appropriate parameter combinations (CORmax, BFmax and CORmax, BFmin) for risk assessment.

References

[1] Watanabe, D., Moriguchi, S., and Terada, K. (2022). A numerical study on the effects of particle size distribution on run-out distance of granular flow. *Soils and Foundations*, **62**, 101242.

[2] Xiao, J., Tozato, K., Moriguchi, S., Otake, Y., and Terada, K. (2023). Quantification of the contribution ratio of relevant input parameters on dem-based granular flow simulations. *Soils and Foundations*, **63**, 101378.

SIGNIFICANCE OF ROLLING RESISTANCE: WHEN IS IT REQUIRED ?

Usman Ali[1], Mamoru Kikumoto[1], Matteo Ciantia[2, 3], and Ying Cui[1]
[1]Department of Civil Engineering, Yokohama National University, Japan
[2]School of Science and Engineering, University of Dundee, United Kingdom
[3]Department of Earth and Environmental Sciences, University of Milano-Bicocca, Italy

Abstract

As a means to replicate the behavior of non-spherical realistic particles in the discrete element method (DEM), artificially limiting the rotations of commonly used spherical particles or circular disks by rolling resistance has gained popularity [1]. Rorato et al. [2] suggested that a rolling resistance of 0.1963 is required to replicate the triaxial response of sands composed of rounded grains representing a unit value of sphericity. This study aims to confirm whether the application of rolling resistance is essential for replicating the plane strain response of round granular media. To achieve this, the authors conducted biaxial shearing experiments on granular samples composed of dual-sized aluminum Schneebeli rods with perfectly circular cross-sections. The rotational behavior of the rods was identified through image analysis and used to check the validity of the simulation at the microscopic level. Subsequently, a DEM model of the biaxial experiment was developed to simulate the shearing response of the circular particles under the same particle size and shape distribution (as shown in Figure 1). The friction coefficient between particles was selected through a direct shear test conducted in the laboratory using aluminum disks. Initially, an attempt was made to set the rolling resistance at 0.2 while adjusting material parameters within possible ranges, such as normal and shear stiffnesses, to align stress-strain relationships with the experiment. However, this approach remained unsuccessful, and the observed results displayed increased shear strengths and an underestimation of the rotational behavior of particles compared to the actual experiments. Conversely, when no rolling resistance was applied, both the shear strengths and rotational responses closely aligned with the experimental data. Stress-strain relationships are compared in Figure 2, confirming that imitating the mechanical behavior of circular particles does not necessitate rolling resistance. The requirement for rolling resistance arises primarily from discrepancies in shape, while the DEM reasonably predicts realistic granular responses without rolling resistance for twin-shaped samples.

Keywords: Granular materials, Shearing, DEM, Rolling resistance

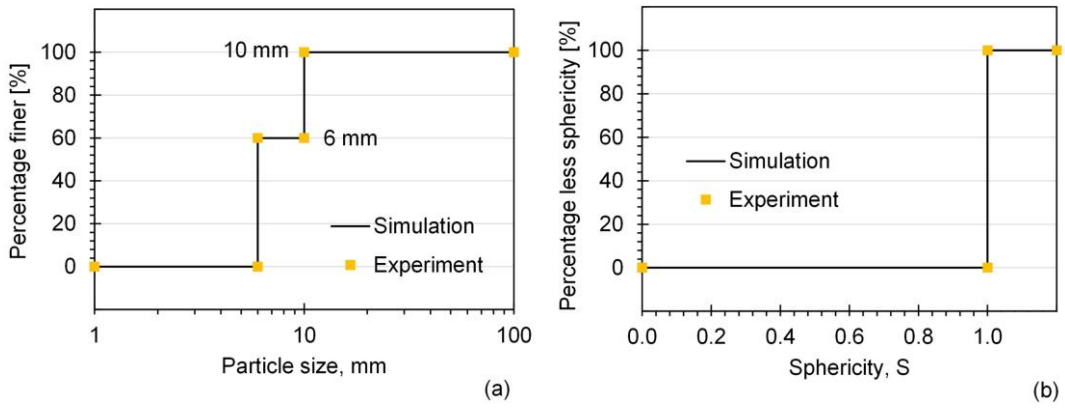

Figure 1. Comparison of (a) particle size and (b) sphericity distribution for the sample used in the experiment and equivalent DEM simulation

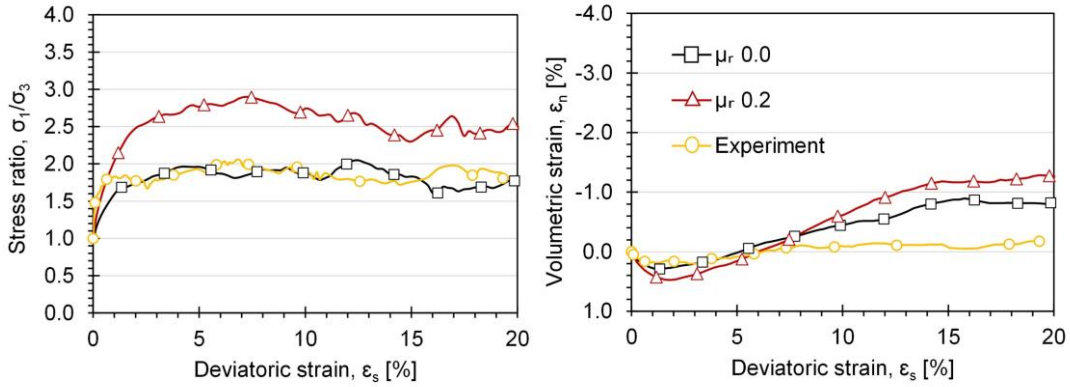

Figure 2. Comparison of stress-strain relationships and volumetric response observed in the experiment and DEM simulation (with and without rolling resistance)

References

[1] K. Iwashita and M. Oda, "Rolling Resistance At Contacts in Simulation of Shear Band," *J. Eng. Mech.*, vol. 124, no. March, pp. 285–292, 1998.

[2] R. Rorato, M. Arroyo, A. Gens, E. Andò, and G. Viggiani, "Image-based calibration of rolling resistance in discrete element models of sand," *Comput. Geotech.*, vol. 131, no. January, 2021.

STRENGTH-MICROSTRUCTURE RELATION IN COHESIVE GRANULAR MATERIALS

***M. Sonzogni*[1], *J.M. Vanson*[2], *Y. Reynier*[3], *S. Martinet*[3], *K. Ioannidou*[1] *and F. Radjai*[1]**
[1] *LMGC, University of Montpellier, CNRS, Montpellier, France*
[2] *CEA, DES, IRESNE, DEC, Cadarache, 13108 Saint-Paul-Lez-Durance, France*
[3] *University Grenoble Alpes, CEA, Liten, DEHT, 38000 Grenoble, France*

Cohesive granular materials play a major role in nature and industry. Cohesive interactions between particles have various physico-chemical origins such as capillary bonding, Van der Waals forces, and cementing matrix [1]. Despite extensive experimental and numerical work on these materials, their mechanical behavior under the action of external loading is still poorly understood, and the compaction behavior of cohesive granular materials is highly dependent on the loadings applied.

In a previous study we established a link between the material properties, applied force and porosity of a cohesive granular sample subjected to isotropic compaction [2]. Here, we study the influence of the adhesion force on the relation between strength and porosity in dense granular samples generated by isotropic compaction. We perform DEM simulations using monodisperse spherical particles confined inside a rectangular 3D box, as shown in Figure 1a. We use the microstructures obtained at the end of isotropic compaction as initial configurations, thus starting from an already compacted and stable isotropic state. These samples are subjected to triaxial compaction to measure their strength at failure. The contact force between the particles is computed through a simple elasto-adhesive contact law. A constant pressure p_h in applied on the 4 lateral walls while the top and bottom walls are fixed. Once a new stable configuration is reached, the upper wall is lowered at constant speed $\dot{\epsilon}$. The value of $\dot{\epsilon}$ is chosen as to ensure a quasi-static regime. The mean stress p and the deviatoric stress q are defined by $p = \frac{1}{3}(\sigma_1 + \sigma_2 + \sigma_3)$ and $q = (\sigma_1 - \sigma_3)$, where the σ_i are the major principal stresses of the granular sample. The shear stress q/p is close to 0 in the beginning due to the isotropic initial state, but reaches a stable value in a state of continous deformation called the critical state.

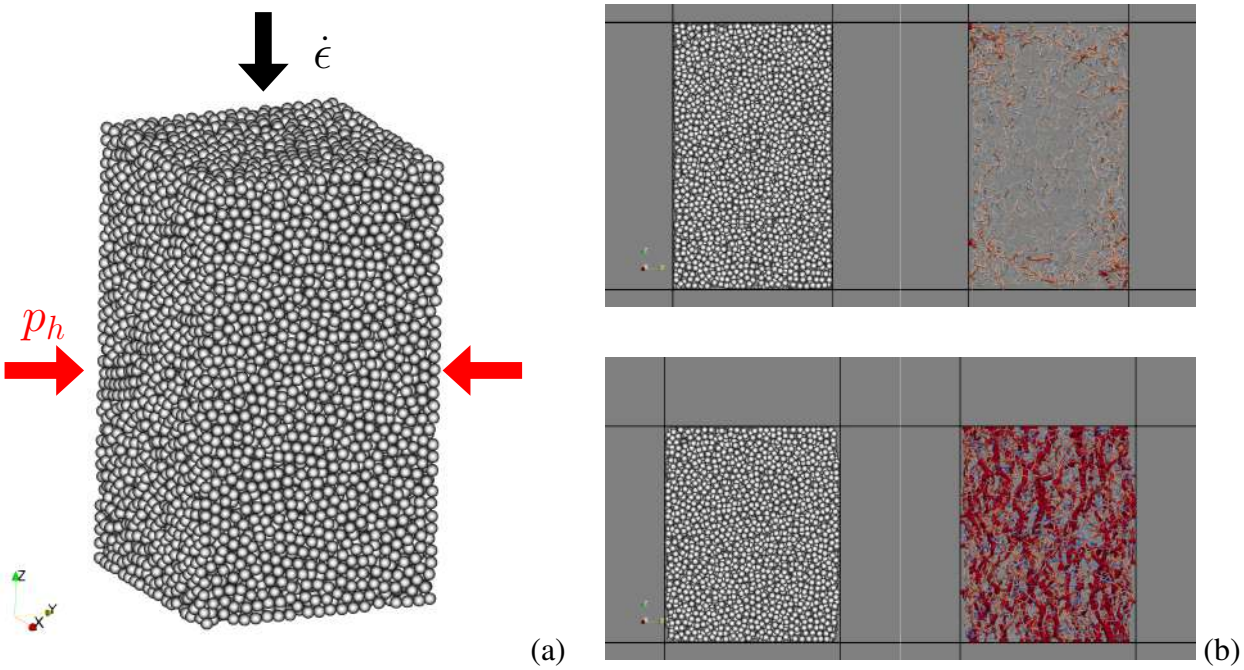

Figure 1. (a) Sample used for this study; (b) Microstructures and force networks for the adhesion force $f_c = 250\ \mu N$ at $\epsilon = 0\%$ (top) and $\epsilon = 20\%$ (bottom).

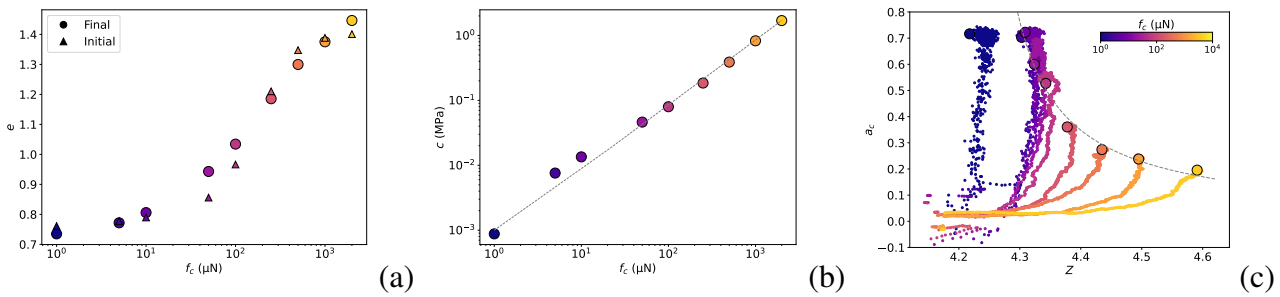

Figure 2. (a) Initial and final values of the void ratio e as a function of adhesion force f_c (b) Cohesive strength c as a function of adhesion force f_c (c) Evolution of the samples in the fabric parametric space (Z,a_c). The open circles mark the values in the critical state and the dotted line is the inverse function fitting these data points.

We find that the porosity (represented here through the void ratio e) in the critical state is nearly identical to its initial value, as shown in Figure 2a. This shows that the porosity obtained by isotropic compaction is the same as the critical porosity reached by triaxial compaction. We also find that shear stress increases linearly with void ratio in the critical state. As observed in Figure 2b, the cohesive strength c is linearly dependent on the adhesion force between the particles. We identify two limiting behaviors in the evolution of the microstructure based on the coordination number Z and the anisotropy of the contact network a_c, represented in Figure 2c : an increase of coordination number at constant anisotropy for the most cohesive cases, and an increase of anisotropy at constant coordination number for the least cohesive cases. We show that these two microstructural parameters are linked together in the fabric space as a result of steric exclusions.

References

[1] Mandal, S., Nicolas, M., and Pouliquen, O. (2020). Insights into the rheology of cohesive granular media. *Proceedings of the National Academy of Sciences*, **117**, 8366–8373.

[2] Sonzogni, M., Vanson, J.-M., Ioannidou, K., Reynier, Y., Martinet, S., and Radjai, F. (Submitted). Dynamic compaction of cohesive granular materials: Scaling behavior and bonding structures. *Soft Matter*.

STRESS NON-UNIFORMITY IN A DIRECT SIMPLE SHEAR TEST

A. Sadrekarimi
Dept. of Civil & Environmental Eng., Western University, London, Ontario, Canada

1. Area of research

The direct simple shear (DSS) test is widely used to study the shearing behavior and liquefaction of saturated sands and tailings. The main drawback of existing DSS equipment is the lack of complimentary shear stress on the side boundaries of the sample [1-3]. This leads to complex non-uniform distributions of vertical and shear stresses on the horizontal boundaries to maintain equilibrium conditions. Analysis of DSS results is, nevertheless, based on the assumption that τ and σ'_v are uniformly distribution along the specimen boundaries. In this study, the discrete element method (DEM) is used to model DSS testing of a sand and examine the uniformity of vertical and shear stresses across the sample boundary.

2. Methodology

The Particle Flow Code (PFC3, version 6) from Itasca® was used to carry out the DEM analyses of this study. As illustrated in Figure 1, DEM was used to simulate a cylindrical DSS specimen confined within a stack of 10 frictionless rings to maintain a constant cross-sectional area while allowing uniform shear deformations. These rings have an internal diameter of 70 mm and are 2-mm thick, allowing the simulation of specimens with an initial height of 20 mm. The specimen was subsequently confined at its top and bottom between two rigid boundaries.

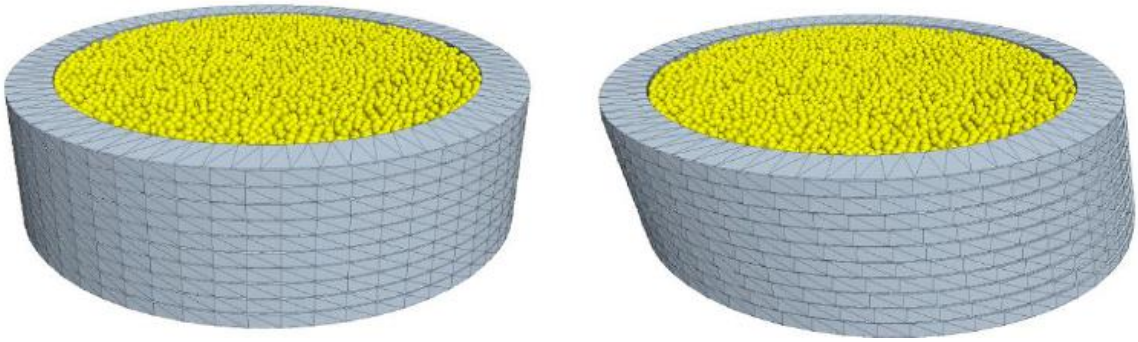

Figure 1. Schematics of the DEM model of a DSS test

The DEM model consisted of an assembly of 30,000 spheres with an upsized gradation scaled by 2.5 times that of a clean silica sand used in a series of DSS laboratory tests [4]. A cloud of overlapping spherical particles was first generated within the specimen boundaries. The specimen was then compressed by moving the upper rigid boundary downward until a vertical force corresponding to the desired vertical stress (σ'_{vc}). Several representative volume element (RVE) spheres of 4 mm in radius were placed along the top and bottom surfaces of the specimen to measure the shear and vertical stress distributions.

The specimens were uniformly sheared by translating the bottom wall at a prescribed rate of 6 mm/min until a shear displacement of 3 mm. Shear strain (γ) was calculated as the ratio of the horizontal displacement to the initial specimen height prior to shearing. Particles in contact with the bottom wall were forced to move with the wall to simulate a frictional boundary, minimize slippage at the specimen-wall interface (similar to the concentric blades on the top and bottom platens of the

laboratory DSS device), and promote a uniform strain field within the specimen. The index of unbalanced forces (I_{UF}) was monitored throughout each simulation to ensure equilibrium and quasi-static particle motion by maintaining $I_{UF} < 0.01$. No gravity was applied during any of the DEM simulation stages. The rolling resistance linear model embedded in PFC3 was used in the DSS simulations of this study. The modeling parameters were calibrated through trial-and-error to match the shear stress-strain and volumetric strain behaviors of a series of laboratory drained DSS tests on a poorly-graded (D_{50} = 0.24 mm) silica sand. The laboratory DSS experiments were carried out on cylindrical specimens with a diameter of 70 mm and a height of up to 23 mm which were enclosed in a latex membrane and supported by a stack of Teflon-coated thin (1 mm) sliding rings. The stress-strain and volumetric strain behaviors showed a favourable agreement between the calibrated DEM simulations and the drained DSS laboratory experiments.

3. Main results

As shown in the following figure, although the distributions of boundary shear (τ) and vertical (σ'_v) stresses along the top specimen boundary were non-uniform, their non-uniformity tended to reduce towards the specimens' center. Relatively larger variations of σ'_v were also observed across the specimen's top boundary compared to τ. The magnitude of these non-uniformities further decreased with increasing σ'_{vc} from 100 to 700 kPa. Additional DEM simulations showed that the uniformity of stress distributions enhanced with increasing γ, with the most uniform distributions achieved at a large strain (i.e., critical state).

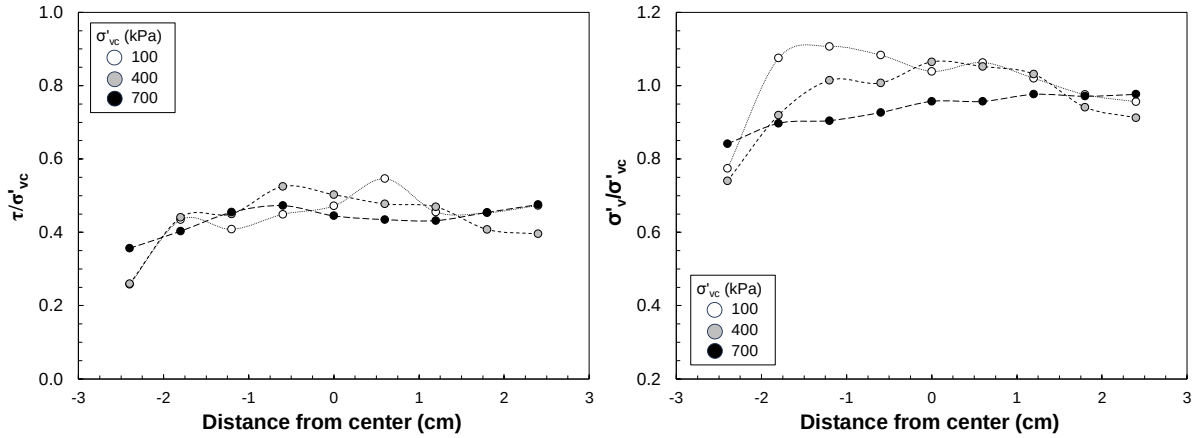

Figure 2. (a) shear and (b) vertical stress distributions at γ = 20% on the upper boundary of specimens consolidated to σ'_{vc} = 100, 400 and 700 kPa

4. References

1. Airey, D.W. and D.M. Wood, *An evaluation of direct simple shear tests on clay.* Geotechnique, 1987. **37**(1): p. 25 - 35.
2. Vucetic, M. and S. Lacasse, *Specimen size effect in simple shear test.* Journal of Geotechnical Engineering Division, ASCE, 1982. **108**(GT12): p. 1567 - 1585.
3. Budhu, M., *Non-uniformities imposed by simple shear apparatus.* Canadian Geotechnical Journal, 1984. **21**(2): p. 125 - 137.
4. Jones, S., *Liquefaction susceptibility analysis of Fraser River sand in miniature cone penetration tests and cyclic direct simple shear tests*, in *Department of Civil and Environmental Engineering*. 2017, The University of Western Ontario: London, Ontario.

TIME-DEPENDENT BEHAVIOUR AND AGEING OF SANDS – SINGLE GRAIN ANALYSIS

A. A. Peña-Olarte[1], D. Zhang[1] and S. Vogt[1]
[1] Technical University of Munich, Center for Geotechnics, Munich, Germany

1. Introduction

For more than four decades, it has been observed that changes with time in the engineering properties of soils, such as stiffness, strength, dilatancy, penetration resistance, and liquefaction resistance, are the result of ageing [1]. Meanwhile, several hypotheses have been proposed to explain the driving mechanism, but none can satisfactory explain ageing phenomena. For example, the rearrangement of particle packing is considered a main mechanism. Grain crushing or damage under high load and softening, rolling, and sliding of grains under low load contribute to packing rearrangement.

The discrete element method (DEM) is used to perform uniaxial compression tests of a single sand grain to investigate the ageing of granular materials. The time-dependent behaviour is modelled using the parallel stress-corrosion (PSC) model developed by Potyondy [1]. A series of uniaxial static-fatigue compression tests on the single grain are performed to investigate the impact of loading history. Important information such as time-to-failure, crack number, damage ratio, axial load, axial displacement/strain, and strain rate are recorded throughout the simulation process. Simulation results demonstrate that loading history significantly affects induced grain damage and grain time-dependent deformation and behaviour.

2. Methodology

Using the DEM software PFC 3D 7.0 [2] a single grain (spherical particle) is modelled as an agglomerate of sub-particles joined by parallel bonds that could resist forces and moments (including torsion). The parallel stress-corrosion (PSC) model in [1] was implemented to model the stress-corrosion process and consider the strength reduction of bonds over time. In the PSC model, the diameter and strength of the bond reduce with time when the tensile stress acting on the bond periphery exceeds a threshold value. The contact model parameters are selected equal to the values provided in [1].

The time-dependent behaviour (damage and softening) of the single grain is investigated under uniaxial static-fatigue compression test. In the static-fatigue compression test, the specimen is subjected to a constant load until failure. The static-fatigue tests were carried out at different initial loading conditions (see also Figure 1) to evaluate the influence of loading history on the time-dependent response of the single grain, namely:

(i) different initial driving-stress ratios (or percentage of the peak load under uniaxial compression)
(ii) a given driving-stress ratio after one unloading step of the specimen from an initial driving-stress ratio, and
(iii) a given driving-stress ratio after unloading and reloading of the specimen from an initial driving-stress ratio.

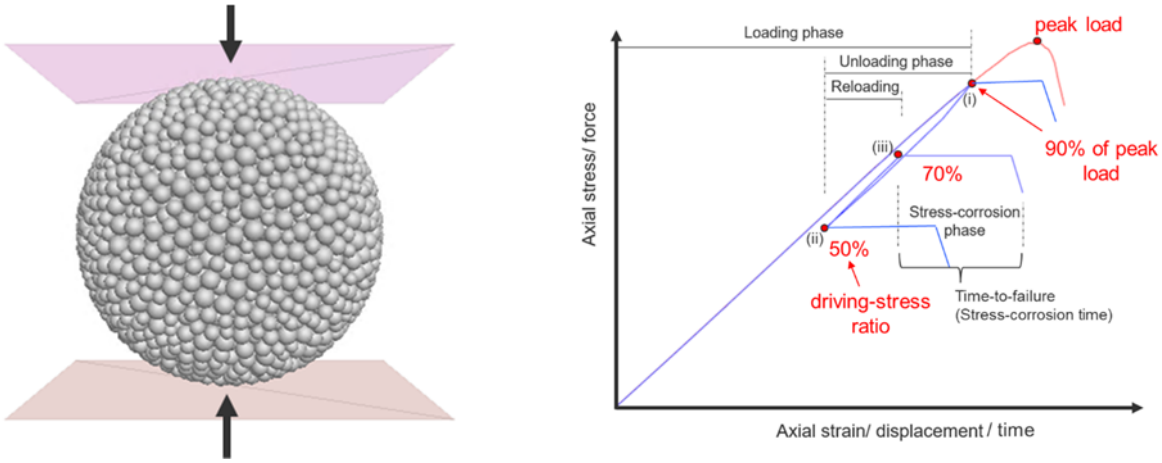

Figure 1. Compression test of single grain (left) and initial conditions for uniaxial static-fatigue compression tests (right).

3. Results and final remarks

The time-dependent response of the single grain under static fatigue compression test was monitored. The stress history highly affects the time-to-failure and the static fatigue limit (driving-stress ratio below that the specimen does not fail and the time to failure is infinite). The main results can be summarized as follows:

- For the same driving-stress ratio (i) at the static-fatigue stage, the higher the initial driving-stress ratio, the shorter the time to failure. This is related to the damage induced to the single grain through the initial driving stress.
- In the case of maintaining the driving-stress constant after unloading (ii), the higher the unloading ratio, the more significant the reduction of time-to-failure and the lower the static fatigue limit.
- For the simulations comprising unloading and reloading (iii), the time-to-failure might be larger than the time after solely unloading (ii), and even larger than the time for (i). This may relate to a more uniform stress distribution after reloading the specimen. However, this shall be further investigated as it depends, among others, on the sub-particle distribution of the agglomerate and, hence, on the stress distribution within the single grain.

Future research will consider the complex shape of real sand grains, the loading of a packing of several grains under different boundary conditions, and the effect of grain size distribution. The PSC model and its damage-rate law can also be extended by considering other failure modes for the bonds. Moreover, key work will be on setting up an experimental database to investigate the effects currently assumed to govern the ageing behaviour of sand.

4. References

[1] Mitchell, J.K. (2008). “Ageing of sand – a continuing Enigma?” 6th Int. Conf. on Case Histories in Geotechnical Engineering. Arlington, VA, Aug. 11-16, 2008, 1-21.

[2] Potyondy, D. O. (2007). Simulating stress corrosion with a bonded-particle model for rock. International journal of rock mechanics and mining sciences, 44(5), 677-691.

[3] Itasca Consulting Group, Inc. (2021) PFC — Particle Flow Code in 2 and 3 Dimensions, Version 7.0, Documentation Set of version 7.00.147. Minneapolis: Itasca.

[4] Michalowski, R. & Wang, Zhi-Jie & Nadukuru, Srinivasa. (2017). Maturing of contacts and ageing of silica sand. Géotechnique. 68. 1-13. 10.1680.

Advances in numerical methods

Innovations in numerical modelling

A NOVEL DEM-BASED COUPLED 3D THERMO-HYDRO-MECHANICAL MESOSCOPIC MODEL FOR VERY-LOW POROSITY MATERIALS

M. Krzaczek[1] and J. Tejchman[1]
[1] Gdansk University of Technology, Gdańsk, Poland

1. Introduction

Most of the physical phenomena in engineering problems occur under non-isothermal conditions. Moreover, even if the physical system is initially in a state of thermodynamic equilibrium, the physical phenomena or chemical reactions that occur may lead to local temperature changes and consequently to heat transfer. Therefore, understanding heat transfer in particulate systems is of great importance to many engineering applications such as environmental science, chemical and food processing, powder metallurgy, energy management, geomechanics and geological engineering. The need to consider the effect of heat transfer becomes critical in analyses of many multi-field problems in porous and fractured materials. The heat transfer may occur e.g. by diffusion, advection and radiation. Complex coupled thermal-hydraulic-mechanical (THM) processes, including heat transfer, fluid flow and material deformation simultaneously occur and are affected by many non-linear processes.

2. Thermo-hydro-mechanical model

A novel DEM-based pore-scale 3D thermo-hydro-mechanical model of two-phase fluid flow [1] and heat transfer in fluid and solids [2] is based on a direct numerical simulation approach. The model's original concept is based on the notion that in a physical system, two domains coexist: the 3D discrete (solid) domain and the 3D continuous (fluid) domain. Both domains are discretized into a coarse mesh of tetrahedra. The fluid flow model is simplified to a fluid flow network model in the fluid domain. The fluid flow network is created by connecting the centers of gravity of adjacent cells through channels. However, the calculated mass flow rate of the fluid phases in the channels are only used to estimate the mass flow rates of the fluid flowing through the grid cells faces.

The grid cells accumulate pressure and store both fluid-phase fractions and densities, energy, and temperature. The mass change in the grid cells is related to the density change in a fluid phase that results in pressure variations.

The equation of momentum conservation is neglected in the grid cell but the mass is still conserved in the entire volume of tetrahedron. The numerical algorithm can be divided into 5 main stages:

a) estimating the mass flow rate for each phase of fluid flowing through the cell faces (in channels surrounding a cell) by employing continuity and momentum equations,
b) computing the phase fractions and their densities in a cell by employing equations of state and continuity,
c) computing pressure in a cell by employing the equation of state,
d) solving the energy conservation equation in fluid and solids using the classical finite volume method,
e) updating material properties.

This algorithm is repeated for each fluid cell and solid cell in the grid (stage ‘d’) using an explicit formulation.

3. Model validation

The coupled thermal-hydraulic-mechanical (THM) model was validated by comparing the numerical results with the analytical solution of the classic 1D heat transfer problem. Numerical calculations were carried out for bonded granular specimens with a 3D DEM fully coupled with 3D CFD (based on a fluid flow network) and 3D heat transfer that linked discrete mechanics with fluid mechanics and heat transfer at the meso-scale. The heat transfer was related to both the fluid (diffusion and advection) and bonded particles (conduction). Bonded particle assemblies with two different grain distributions were considered. Perfect accordance was obtained between numerical and analytical outcomes. In addition, the effects of advection on the cooling of a bonded particle assembly were numerically shown (Figure 1). Finally, the authors' previously developed DEM-based 2D THM model [2] was compared with a novel 3D pore-scale THM model.

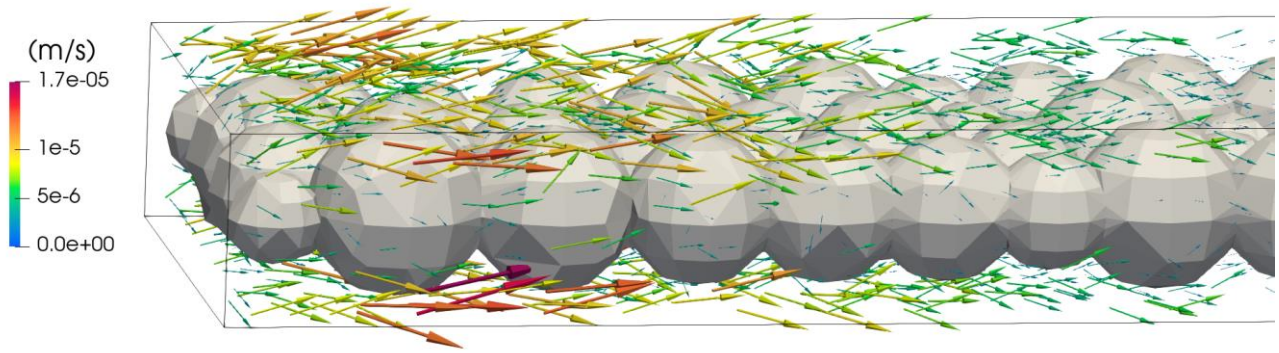

Figure 1. Distribution of fluid velocity vectors in the bonded particle assembly.

4. Conclusions

Based on mesoscale simulations, the following conclusions can be offered:

- during the 1D heat transfer problem in cooling, the largest temperature difference between numerical and analytical findings was just 0.72-0.94 K,
- advection increased the cooling of the specimen,
- in the thermal contraction of the bar specimen after cooling, the tensile failure mechanism was comparable to that of purely mechanical uniaxial tension.

5. References

[1] Krzaczek M., Nitka M. & Tejchman J. (2021). Effect of gas content in macro-pores on hydraulic fracturing in rocks using a fully coupled DEM/CFD approach. *Int. J. Numer. Anal. Methods*. **45**(2), 234-264.

[2] Krzaczek M., Nitka M. & Tejchman J. (2022). A novel DEM-based pore-scale thermal-hydro-mechanical model for fractured non-saturated porous materials. *Int. J. Solids Struct.*, Acta Geotechnica, **18**(5), 2487-2512.

A fluid-solid coupled micromechanical simulation for the analysis of piping erosion during the seabed installation of a suction bucket foundation

***S. Kemmler*[1,2], *P. Cuéllar*[1], *C. Rettinger*[2] *and H. Köstler*[2]**

[1] *Federal Institute for Materials Research and Testing, Division 7.2 for Buildings and Structures, Berlin, Germany*

[2] *Friedrich-Alexander-Universität Erlangen-Nürnberg, Chair for System Simulation, Erlangen, Germany*

Suction buckets are a promising concept for the foundations of offshore wind turbines (see Fig. 1a). These buckets are solely installed employing the self-weight of the structure and a suction pressure applied inside the bucket [1]. During the installation process of a suction bucket, localized fluidization of the granular soil (so-called piping erosion) imposes a massive risk as it is a critical failure of the installation process [2]. A three-dimensional fluid-solid coupled micromechanical simulation of a seabed foundation is presented using the waLBerla multiphysics framework [3]. We focus on the local phenomena around a representative cut of the full-scale foundation during the first meters of the suction-driven installation (see red rectangle in Fig. 1a). Due to the high computational cost, recent simulations are limited to 2D [4]. A requisite primary task first concerns the creation of the initial seabed conditions in terms of a representative granular fabric involving layered deposition, granular cementation, and a realistic state of intergranular forces and relative density throughout the embedment depth. The subsequent fully resolved simulation involves a discrete element method representation of the solid phase (i.e., the structural element and the single grains of the sandy seabed). The lattice Boltzmann method, an alternative to classical Navier-Stokes solvers, is employed for the percolating water. The coupling is attacked using the Euler-Lagrangian coupling functionality of waLBerla using geometrically resolved particles that can be generated with specified size and shape distributions. The two-way coupling employs momentum exchange between the fluid and solid phases. A cohesion model is implemented, allowing the exploitation of the influence of cohesive bonds between the grains on the occurrence of piping. The coupling scheme has been tested and validated with many carefully selected calibration and validation tests of increasing physical complexity and analytical solutions [5]. We have additionally validated our percolation physics by reproducing simulation results from the literature for dense-packed particle setups. Fig. 1 illustrates the simulation domain from different perspectives.

We simulate a rectangular representative subregion of the suction bucket foundation where a box represents the bucket wall. The outflow is governed by a time-dependent pressure boundary condition imitating the suction inside the bucket. The inflow from the outside ocean is employed using a constant pressure boundary. No-slip boundary conditions are applied on the remaining boundaries and the bucket walls. The simulation of the grain-resolved flow poses a significant computational challenge, for which we use highly optimized and parallel code utilizing the capabilities of state-of-the-art heterogeneous supercomputers containing Graphics Processing Units (GPUs). We demonstrate excellent performance and scalability on the largest supercomputers worldwide. A critical quantity for the occurrence of piping is the hydraulic gradient, which can be described as

$$i = \frac{1}{\rho_f g} \frac{\Delta P}{L_s} \tag{1}$$

with the density of the fluid ρ_f, the magnitude of the gravitational acceleration g, the pressure difference ΔP between the inside and outside of the bucket, and the length of the seepage flow L_s, i.e., the

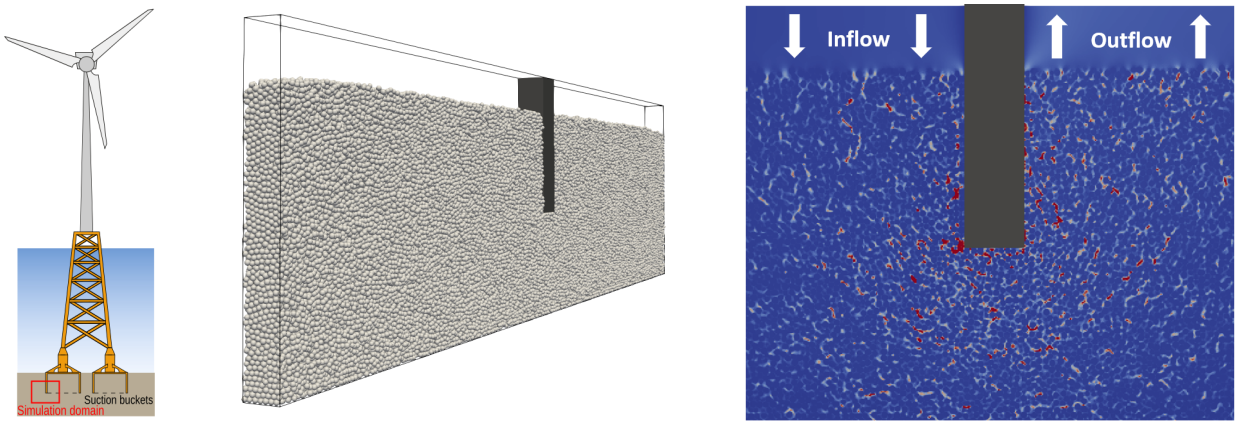

(a) Suction bucket jacket. The simulation domain is marked in red.

(b) 3D visualization of the simulation domain containing particles (grey spheres) and the bucket slice (dark box).

(c) 2D slice of the velocity field surrounding the bucket wall. Time-dependent suction pressure is applied on the right, and constant pressure on the left.

Figure 1. Visualization of the simulation domain from different perspectives.

shortest path around the bucket [4]. We investigate the behavior of the soil for varying hydraulic gradients, for instance, the change in permeability within the bucket for given pressure differences. The proposed approach enables novel insights into the triggering conditions for piping failure of suction buckets but also provides a reference open-source framework for the community for future applications in related geotechnical problems. The large-scale micromechanical simulations of the soil yield high-accuracy results since hardly any model assumptions have to be used, and many parameters, such as particle shape and size, are directly incorporated.

References

[1] Sturm, H. (2017). Design aspects of suction caissons for offshore wind turbine foundations. *Unearth the Future, Connect beyond. Proceedings of the 19th International Conference on Soil Mechanics and Geotechnical Engineering*.

[2] Ragni, R., Bienen, B., Stanier, S., O'Loughlin, C., and Cassidy, M. (2020). Observations during suction bucket installation in sand. *International Journal of Physical Modelling in Geotechnics*, **20**, 132–149.

[3] Bauer, M., et al. (2021). walberla: A block-structured high-performance framework for multiphysics simulations. *Computers & Mathematics with Applications*, **81**, 478–501.

[4] Fukumoto, Y., Yang, H., Hosoyamada, T., and Ohtsuka, S. (2021). 2-d coupled fluid-particle numerical analysis of seepage failure of saturated granular soils around an embedded sheet pile with no macroscopic assumptions. *Computers and Geotechnics*, **136**, 104234.

[5] Rettinger, C. and Rüde, U. (2022). An efficient four-way coupled lattice boltzmann–discrete element method for fully resolved simulations of particle-laden flows. *Journal of Computational Physics*, **453**, 110942.

Backward erosion piping: a focus on loosening soil

L. V. Cote[1], C. Jommi[1,2], M. A. Hicks[1], and M. Cabrera[1]
[1] Delft University of Technology, Dept. of Geoscience and Engineering, Delft, The Netherlands,
[2] Politecnico di Milano, Dept. of Civil and Environmental Engineering, Milano, Italy

1. Introduction

Flood protection structures, such as dikes or levees, are crucial for coastal and deltaic regions around the world. These structures are often situated on a low-permeable foundation layer that covers a permeable sand layer. The low-permeable layer can fracture due to uplift and heave, thereby creating an opening for the outflow of water. This process can initiate an internal erosion process known as Backward Erosion Piping (BEP), where the removal of solid grains extends over long pipes and progresses from the fracture point in a direction opposite to the seepage flow. In this work we explore, through a Discrete Element Method coupled with a Computational Fluid Dynamics solver (DEM-CFD), the initiation of BEP at the scale of the grains. Our work focuses on the critical velocity that triggers the erosion and movement of a column of grains. It considers a sand bed subjected to a vertical flow that is increased in steps until the sand particles start to move. We compare our results with those found in the experimental campaigns by [2-4].

The simulations are conducted with the DEM-CFD MigFlow software, which solves the granular phase with the non-smooth contact dynamics method, and the fluid phase with a finite element method, solving the volume Navier-Stokes equations averaged with the granular media porosity [1]. The simulations consist of a two-dimensional sand bed, that is subjected to a vertical flow that increases at a constant rate of 0.25 mm/s/s. The boundary conditions comprise two rigid and impermeable side-walls, top and bottom open boundaries with zero hydrostatic pressure, and a vertical velocity increasing over time (see Fig. 1(a)). The sand bed deposit has a slight polydispersity of $d_{min}/d_{max} = 1.2$, with a minimum diameter of $d_{min} = 0.2$ mm.

An inflection point in the response is expected, where the drag forces overcome the resisting forces and the soil becomes loose and an erosion process follows. Tracking the loosening soil formation and the erosion progression is our main goal with the simulations. We follow the loosening soil by observing the evolution of the deposit height (h), the porosity (n) of the initial deposit area, and the coordination number (z) of the granular system, which is the average number of contacts for each grain. With the increase of the fluid velocity over time, we observe an increase in the deposit height, and hence an increase in the porosity and a decrease in the coordination number. Figure 1(b) presents the inlet and outlet fluid velocity, v_{in} and v_{out}, respectively, plotted with respect to h and time. We define a critical velocity as the instant when h overcomes the initial height. Interestingly, this critical velocity is preceded by a decrease in z (see Fig. 1(c)), suggesting that the formation of a loosening region may occur before the grains at the top of the deposit start to move.

Previous studies [2-4] used different sand types and followed the deposit height to determine the critical hydraulic gradient. They found that angular grains, graded soils, and soils with higher specific gravity, have a greater resistance to erosion. In other words, these soils require a higher critical velocity in order to erode grains by up-lifting. The critical velocity is suggested to be a function of the sand bed aspect ratio (width/height), grain friction coefficient, and the grain shape. With this numerical approach, we can parametrically evaluate the effects of these parameters. The

perspective of analyzing the evolution of the coordination number instead of the deposit height can give insight into the progression of the soil loosening and become relevant for the evaluation of more complex scenarios of BEP, where a constricted exit controls the outflow of grains and fluid.

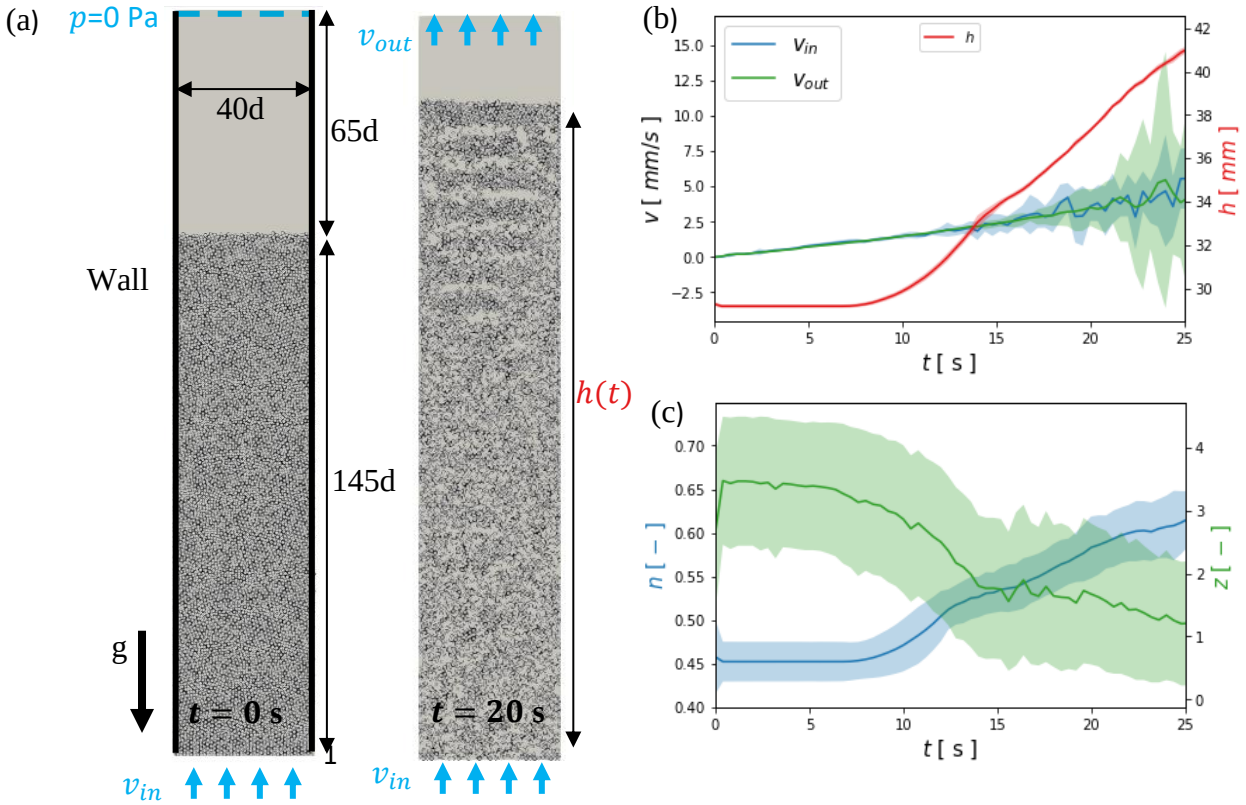

Figure 1. (a) Model setup for the CFD-DEM simulation, in an initial and middle time step; (b) fluid inlet and outlet velocity (i.e., v_{in}, v_{out}) and deposit height (h) over time; and (c) porosity (n) and coordination number (z) over time. Lines correspond to average values and shading to standard deviation among all grains.

3. References

[1] Constant, M. Dubois, F. Lambrechts, J. & Legat, V. (2018). *Implementation of an unresolved stabilised FEM–DEM model to solve immersed granular flows in Computational Particle Mechanics*. Comp. Part. Mech. 6, 213–226.

[2] Fleshman, M. S. & Rice, J. D. (2014). *Laboratory modeling of the mechanisms of piping erosion initiation*. Journal of geotechnical and geoenvironmental engineering 140 (6), 04014017.

[3] Fujisawa, K. Murakami, A. Nishimura, S. & Shuku, T. (2013). *Relation between seepage force and velocity of sand particles during sand boiling.* Geotechnical Engineering Journal of the SEAGS & AGSSEA 44 (2), 9–18.

[4] Peng, S. & Rice, J. D. (2020). *Measuring critical gradients for soil loosening and initiation of backward erosion-piping mechanism*. Journal of Geotechnical and Geoenvironmental Engineering 146 (8), 04020069.

Discrete element method and thermodynamics with internal variables: two complementary approaches to link micro- and macro-scale modelling of in anisotropic clays

A. G. Pagano[1], F. Rollo[2], V. Magnanimo[3], A. Tarantino[4] and A. Amorosi[2]
[1] James Watt School of Engineering, University of Glasgow, UK
[2] Department of Structural and Geotechnical Engineering, Sapienza University of Rome, Italy
[3]Faculty of Engineering Technology, University of Twente, Netherlands
[4]Department Civil and Environmental Engineering, University of Strathclyde, UK

Anisotropy is defined as the variation of a material property with direction. In soils, anisotropy is believed to arise from specific features evolving upon loading, including: the distribution of force chains and orientation of interparticle contacts (especially in granular materials); the orientation of particles (relevant in geomaterials made of elongated particles); the size, orientation, distribution, and cumulative volume of the pores. All these aspects are intrinsically related to the particulate nature of soils, and the mechanisms occurring upon loading or unloading at the particle or micro-scale.

To account for the anisotropy arising from microscale mechanisms, continuum constitutive models have included additional 'micro-inspired' internal variables (Fu and Dafalias, 2015; Amorosi et al., 2021), associated with experimental proxies such as the geometrical arrangement/orientation of particles (referred to as fabric), and the size and distribution of soil's porosity. These are typically observed post-mortem by means of Scanning Electron Microscopy (SEM) and Mercury Intrusion Porosimetry (MIP) respectively. However, the lack of direct experimental evidence capable of quantifying the evolution of these microstructural characteristics during the application of loads poses challenges in the formulation of the evolution law of the internal variables to be used in the constitutive models, as well as in the choice of the experimental proxy to associate with these variables.

A valuable approach to overcome the limitations of physical experiments is to carry out "virtual" (numerical) experiments where soils are modelled as discrete materials, using the Discrete Element Method (DEM). In this work, a DEM framework specifically designed to simulate non-active clays as assemblies of elongated, electrochemically interacting particles (Pagano et al. 2020), is used to explore the particle-scale mechanisms underlying the anisotropic character of the elastic properties of clay samples, determined by means of static probing. Virtual samples for static probing were obtained by compressing the assembly along different (plastic) loading paths, either isotropic ($\eta = 0$), or constant-stress-ratio virgin compression paths ($\eta = \text{const.}$). Virtual samples obtained along these paths were selected to undergo elastic probing, i.e. the application of very small strain increments to determine the corresponding reversible stress response. For each state, static probing was performed in two perpendicular directions (vertical and horizontal) to obtain the corresponding elastic properties.

The simulation results showed that: a) isotropically-compressed samples, characterised by an isotropic fabric (random particle orientations) at any state along the $\eta = 0$ loading path, exhibited an isotropic behaviour, with vertical and horizontal elastic moduli assuming similar values for each given state of stress and porosity; b) samples compressed along constant-stress-ratio loading paths, characterised by a progressively anisotropic (oriented) fabric upon loading, exhibited a gradually increasing anisotropic behaviour consistent with the evolution of fabric and particle orientations upon loading, with samples becoming stiffer along the horizontal direction (i.e., the preferential particle orientation gradually developing upon anisotropic loading), compared to the vertical direction. These

results are in line with existing experimental observations, thus confirming the validity of the DEM framework.

The particle-scale and pore-scale data directly extracted and/or inferred from the numerical simulations can be used to incorporate microscale processes and properties into a macroscopic continuum mechanics framework to improve the accuracy and reliability of constitutive models for clays. To this end, the modelling approach based on Thermodynamics with Internal Variables (TIV) (Maugin and Muschik, 1994) was adopted here, characterised by the definition of two scalar functions, namely a free energy and a rate of dissipation. Two internal variables were assumed to describe the key features of clay mechanics: *porosity*, whose evolution reflects into the isotropic hardening of the material, and *fabric*, here described by a second order tensor, that is responsible for the actual and evolving directional properties of the soil and whose evolution is controlled by a distortional hardening law (Amorosi et al., 2023). Therefore, both internal variables affect the reversible and irreversible response of clay. DEM results allowed to identify an efficient calibration procedure of the microscale model parameters, and to validate the ability of the thermodynamics-based formulation to account for the role of porosity during compression and the evolving elastic stiffness anisotropic of clays along constant-stress-ratio compression paths.

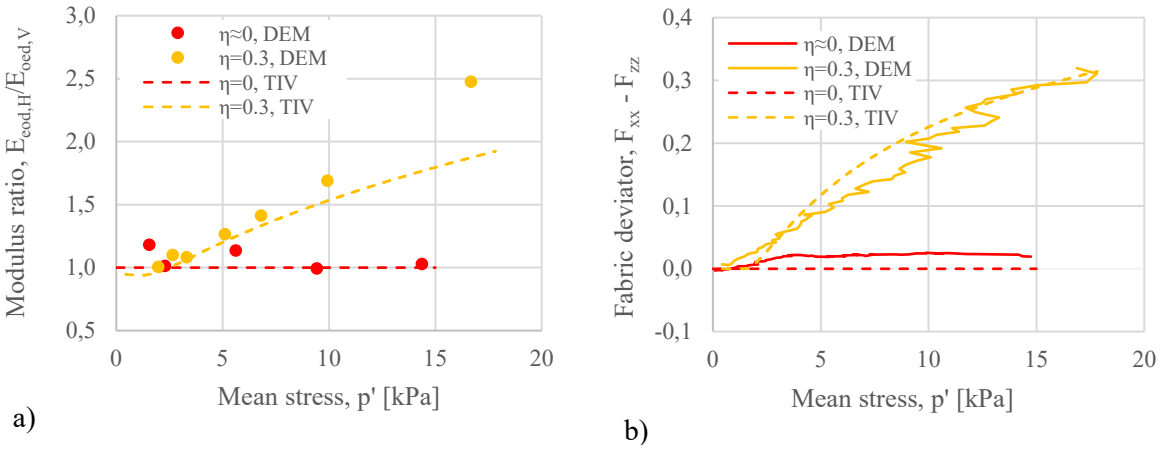

Figure 1. DEM and TIV simulation results: a) ratios of horizontal and vertical constrained Young modulus (E_{oed}) at different stress levels, and b) corresponding fabric deviator evolution

References

[1] Fu, P., & Dafalias, Y. F. (2015). Relationship between void-and contact normal-based fabric tensors for 2D idealized granular materials. *International Journal of Solids and Structures*, *63*, 68-81.

[2] Amorosi, A., Rollo, F., & Dafalias, Y. F. (2021). Relating elastic and plastic fabric anisotropy of clays. *Géotechnique*, *71*(7), 583-593.

[3] Pagano, A.G., Magnanimo, V., Weinhart, T., and Tarantino, A. (2020). Exploring the micromechanics of non-active clays by way of virtual DEM experiments. *Géotechnique*, *70*(4), 303-316.

[4] Maugin G.A., Muschik W. (1994). Thermodynamics with internal variables. I. General Concepts, II. Applications. *Journal of Non-Equilibrium Thermodynamics*. *19*, 217-249, 250-289.

[5] Amorosi, A., Rollo F., Di Santo G. (2023). A micro-inspired perspective on the constitutive modelling of clays. *Rivista Italiana di Geotecnica*, **4**.

Exploring the influence of the grain size distribution on an elemental and a macro-scale granular flow

O. Polanía[1, 2], M. Cabrera[3], E. Azéma[1, 4], M. Renouf[1] and N. Estrada[2]
[1]LMGC, Université de Montpellier, CNRS, Montpellier, France
[2]Dept. Civil and Environmental engineering, Universidad de los Andes, Bogotá D.C., Colombia
[3]Department of Geoscience & Engineering, TU Delft, Delft, The Netherlands
[4]Institut Universitaire de France (IUF), Paris, France

Granular materials are found in a wide range of Grain Size Distributions (GSD). When granular materials experience large deformations, they reach a steady state where shear strains accumulate at constant shear stress, known in the geotechnical community as the residual or critical state. The influence of GSD on the residual state has been a matter of discussion between conflicting experimental and numerical observations [1, 2, 3]. In this work we confirm, at an element scale and in dry conditions, that the residual shear strength remains independent of the GSD [4]. Then, this is further validated in dry granular flows, focusing on the mobility of a granular column collapse [5]. In this configuration, the mobility of the granular column is a macro representation of the material's effective shear strength [6, 7, 8]. On the contrary, in immersed cases, a change of the GSD is found to influence the column mobility, associated to changes in the material permeability that result in changes in the accumulation of pore pressures [9]. Hence, in immersed cases, we confirm a variation of the shear strength produced by the GSD. Therefore, in these multi-phase systems, the coupling between solid and fluid phases needs to be considered and accounted for in applications expecting multiple grain sizes and with a relative motion between both phases. We would like to motivate a discussion into the micro to macro relationships behind these relations and their further extension into more complex multi-physic processes.

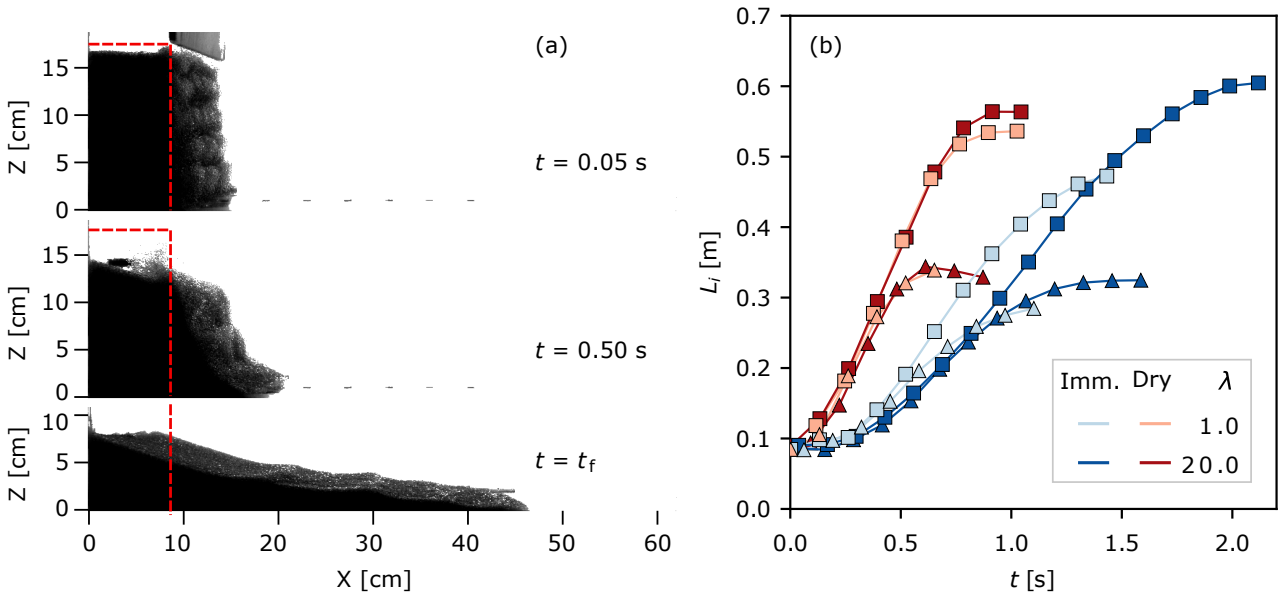

Figure 1. (a) Collapse sequence of a monodisperse granular column immersed on water with aspect ratio $A = H_0/L_0 = 2.0$, where H_0 and L_0 are the initial column height and length, respectively. The

red dashed lines indicate the column initial geometry. The fluid pore pressure measurements were done in the base of the experimental setup beneath the column's initial geometry and along the column collapse. (b) Evolution of the front position during the collapse for dry (reds) and immersed (blues) columns. The variable $\lambda = d_{max} / dmin$ stands for the ratio between the biggest (dmax) and the smallest (dmin) in the column's GSD. Squares (▲) and triangles (■) represent columns with A = 1.0 and 2.0, respectively.

References

[1] Simoni, A., & Houlsby, G. T. (2006). The direct shear strength and dilatancy of sand–gravel mixtures. *Geotechnical & Geological Engineering*, *24*, 523-549.

[2] Cantor, D., Azéma, E., Sornay, P., & Radjai, F. (2018). Rheology and structure of polydisperse three-dimensional packings of spheres. *Physical Review E*, *98*(5), 052910.

[3] Wang, H. L., Zhou, W. H., Yin, Z. Y., & Jie, X. X. (2019). Effect of grain size distribution of sandy soil on shearing behaviors at soil–structure interface. *Journal of Materials in Civil Engineering*, *31*(10), 04019238.

[4] Polanía, O., Cabrera, M., Renouf, M., Azéma, E., & Estrada, N. (2023). Grain size distribution does not affect the residual shear strength of granular materials: An experimental proof. *Physical Review E*, *107*(5), L052901.

[5] Polanía, O., Cabrera, M., Renouf, M., & Azéma, E. (2022). Collapse of dry and immersed polydisperse granular columns: A unified runout description. *Physical Review Fluids*, *7*(8), 084304.

[6] Lajeunesse, E., Monnier, J. B., & Homsy, G. M. (2005). Granular slumping on a horizontal surface. *Physics of fluids*, *17*(10).

[7] Degaetano, M., Lacaze, L., & Phillips, J. C. (2013). The influence of localised size reorganisation on short-duration bidispersed granular flows. *The European Physical Journal E*, *36*, 1-9.

[8] Cabrera, M., & Estrada, N. (2019). Granular column collapse: Analysis of grain-size effects. *Physical Review E*, *99*(1), 012905.

[9] Polanía, O., Estrada, N., Azéma, E., Renouf, M., & Cabrera, M. (2024). Polydispersity effect on dry and immersed granular collapses: An experimental study. *Under review.*

GEOMETRIC EFFECTS ON PARTICLE FRAGMENTATION: NUMERICAL PERSPECTIVE FROM COUPLED CONTINUUM-DISCRETE SIMULATIONS

NSSP. Kalyan[1], Y. Fukumoto[2] and RK. Kandasami[1]

[1]Department of Civil Engineering, Indian Institute of Technology, Madras, Chennai, India

[2]Department of Civil and Environmental Engineering, Nagaoka University of Technology, Niigata, Japan

1. Outline

The challenge of realistically simulating aggregate/particle fragmentation in response to the structural loads is well-acknowledged and often addressed through a combination of discrete and continuum methods. The mesh-based Finite Discrete Element Method (FDEM) has been an effective approach for modelling granular materials undergoing deformation and fracture [1]. Off late, meshless methods such as Peridynamics-DEM (PD) have been adopted to simulate particle fragmentation [2]. Both methods have an advantage over DEM to represent complex morphologies. Despite the merits of these methods, each presents its own set of challenges ranging from difficulties in parameter acquisition to high computational costs. In this study, both PD and FDEM models were assessed in terms of their ability to simulate the fragmentation of complex-shaped particles with specific emphasis on the meshing strategies. The morphology variation due to α-shape method was observed to influence the crushing strength and fragmentation behavior in PD and FDEM simulations. Finally, the post-fracture geometrical features such as position, surface area and shape of fragments were compared between the two numerical methods.

2. Methodology

The particle geometry forms a fundamental basis for both methods; hence, high-resolution point clouds of aggregates are obtained from X-ray CT scans. Employing the α-shape meshing technique, a surface mesh is generated from these point clouds. The α-shape, derived by constructing the Delaunay complex of the point clouds, allows control over the features on the generated surface mesh. Larger α values result in detailed concave features, while smaller values exclude finer details, leading to flat or convex surfaces (Figure 1). The presence of these fine details significantly influences breakage patterns and particle strength. The study considered complex particle morphologies with multiple α values to capture concavities on the particle surface.

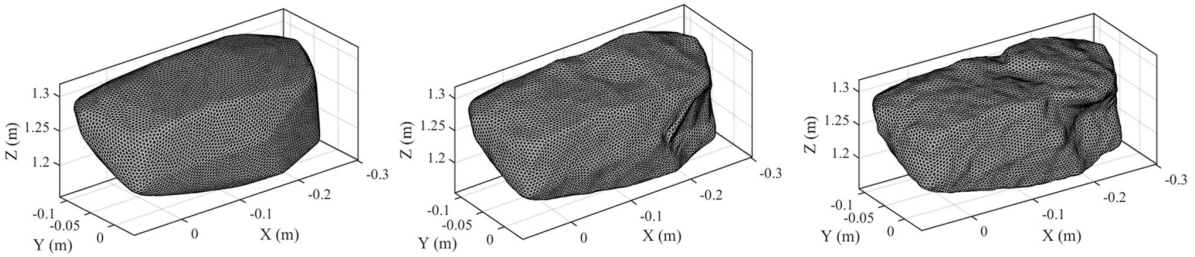

(a) Particle geometry at α = 0 (b) Particle geometry at α = 0.45 (c) Particle geometry at α = 1

Figure 1. Morphology variations generated with different α values

After obtaining the surface mesh for a given α, the volumetric geometry is constructed for each of the two numerical methods according to their respective requirements. To model fragmentation in FDEM simulations, zero-thickness cohesive elements are inserted into the

volumetric mesh created from the α-shape using constrained Delaunay tetrahedralization. In the case of PD, a bond-based framework is employed for simulating fragmentation. In both methods, DEM is utilized to deal with the interaction between the bodies (aggregate and the loading platens). Approximately 30,000 nodes in PD and 75,000 elements in FDEM were used in all simulations to capture the complex particle morphology. A single reconstructed aggregate sandwiched between two rigid plates was uniaxially loaded using both methods with similar boundary conditions (Figure 2a). A prescribed velocity of 5 mm/sec is applied to the top plate while keeping the bottom plate fixed. The stresses in the body and the load onto the wall were tracked throughout the loading period.

3. Preliminary results

The investigation into particle breakage simulations revealed a decreasing trend in breakage strength as the α value increased. This phenomenon was attributed to the localized curvatures present in particle geometries generated with high α values. Specifically, finer features such as concavities proved to be pivotal contributors to particle strength. The presence of concavities on the particle surfaces induced stress concentration, initiating faster crack opening and ultimately causing the particle to reach its critical strength. A 50% reduction in crushing strength was observed in FDEM as well as PD simulations when the parameter α was increased from 0 to 1. Consistent fracture patterns were observed between both the approaches, with FDEM producing a clear separation crack (Figure 2b) for all the α-shapes. PD, being a meshless method, effectively simulated corner breakage in geometries generated using large α values (>0.7). The simulations revealed the significance of the α value in governing the finer-level concave features, with observations indicating that, beyond an α value of 0.7, particle strength reached saturation. The computational expense in FDEM was relatively high in contrast to PD simulations, primarily attributed to the incorporation of cohesive elements in FDEM. However, the implementation of CPU/GPU parallelization strategies has the potential to reduce this computational cost substantially. Contact handling in FDEM involves surface-to-surface interactions, making this approach closely resemble a realistic contact scenario compared to the point-based contact in PD. Furthermore, both the numerical methods demonstrated an accurate simulation of particle breakage.

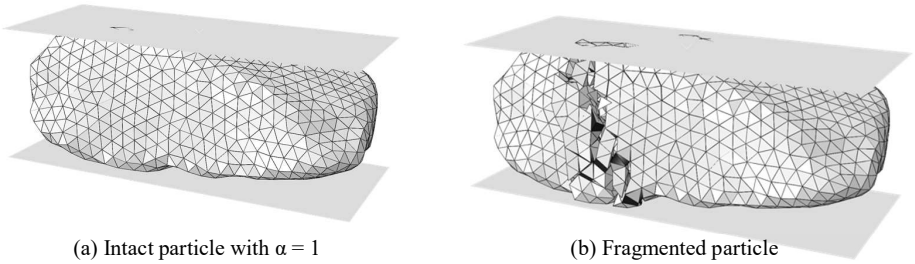

(a) Intact particle with α = 1 (b) Fragmented particle

Figure 2. FDEM simulation of a particle with complex morphology

4. References

[1] Wei, D., Zhao, B., Dias-da-Costa, D. & Gan, Y. (2023). An FDEM study of particle breakage under rotational point loading. *Engineering Fracture Mechanics.*, **212**:221-237.

[2] Fukumoto, Y. & Shimbo, T. (2023). 3-D coupled peridynamics and discrete element method for fracture and post-fracture behavior of soil-like materials. *Computers and Geotechnics.*, **158**:105372.

LEVEL SET-BASED DISCRETE ELEMENT MODELING OF SUPERQUADRICS AND ROCK AGGREGATES

***J. Duriez*[1], *C. Galusinski*[2] *and S. Bonelli*[1]**
[1] *INRAE, Aix Marseille Univ, RECOVER, Aix-en-Provence, France*
[2] *IMATH, Université de Toulon, CS 60584 83041 Toulon Cedex 9, France*

1. Introduction

In order to show predictive capabilities when modeling granular soils, the Discrete Element Method (DEM) requires a faithful description of particle shape if one wants to keep contact parameters to a minimum, as illustrated in, e.g., [1]. More precise numerical shapes than the classical sphere idealization can then be obtained using polyedra [1], rigid aggregates of possibly overlapping spheres, i.e. clumps, or an implicit surface description as the zero-contour (zero-surface in 3D) of a given function defined in space, e.g., [2]. While the latter approach relies in [2] on a so-called potential function, the consideration of the shortest-distance function in a space-discretized fashion together with its zero-level set [3] have formed a versatile shape description which avoids altogether introducing any artificial roundness (as for clumps) and the restriction to convex cases (like most polyedra approaches and the potential one), as also discussed in [4, 5]. After recalling the general principles of the Level Set approach, the focus is herein set on its capabilities for modeling convex superquadrics and 3D-scanned rock aggregates as per its implementation into the YADE code [6].

2. Discussion

In a Level Set approach, shape description starts by defining on a particle-centered grid appropriate values for the shortest distance to the particle surface, which is by convention taken to be positive outside of the particle and negative inside, while being naturally zero over its surface. Ensuring the versatility of the method, such a discrete distance field can be obtained for any surface through, e.g., a Fast Marching Method algorithm [5, 7]. For the purpose of contact detection, surface nodes furthermore discretize the particle boundary and can be obtained at will from the distance field. The method logically induces significant computational costs, either in terms of memory for the distance grid, or simulation time for looping over surface nodes when searching for overlap with another particle inner region with negative distance values. However, it is straightforward to apply to various cases stemming from convex superquadrics to non-convex rock aggregates (Figure 1).

Extending [4, 5], computational costs are herein carefully discussed for the case of convex superquadrics and optimized for lighter Level Set DEM simulations.

References

[1] Mohamed, T., Duriez, J., Veylon, G., and Peyras, L. (2022). DEM models using direct and indirect shape descriptions for Toyoura sand along monotonous loading paths. *Computers and Geotechnics*, **142**, 104551.

[2] Duverger, S., Angelidakis, V., Nadimi, S., Utili, S., Bonelli, S., Philippe, P., and Duriez, J. (2023). Investigation techniques and physical aspects of the angle of repose of granular matter. *Granular Matter*.

[3] Kawamoto, R., Andò, E., Viggiani, G., and Andrade, J. E. (2016). Level set discrete element method for three-dimensional computations with triaxial case study. *Journal of the Mechanics and Physics of Solids*, **91**, 1–13.

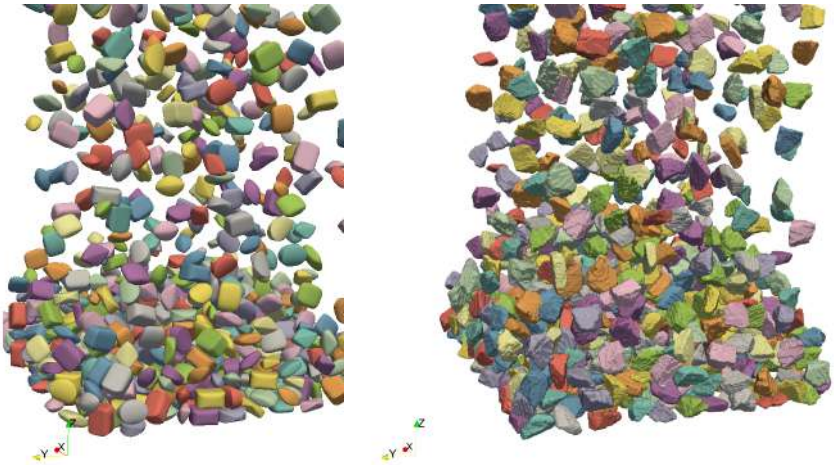

Figure 1. Level Set-based discharge simulations of convex superquadrics (left) and rock aggregates (right)

[4] Duriez, J. and Bonelli, S. (2021). Precision and computational costs of Level Set-Discrete Element Method (LS-DEM) with respect to DEM. *Computers and Geotechnics*, **134**, 104033.

[5] Duriez, J. and Galusinski, C. (2021). A Level Set-Discrete Element Method in YADE for numerical, micro-scale, geomechanics with refined grain shapes. *Computers and Geosciences*, **157**, 104936.

[6] Smilauer, V. et al. (2021). *Yade Documentation 3rd ed.*. The Yade Project, http://yade-dem.org/doc/.

[7] Sethian, J. (1996). A fast marching level set method for monotonically advancing fronts. *Proceedings of the National Academy of Sciences*, **93**, 1591–1595.

Mechanical behavior of methane hydrate bearing sediments by using DEM and PSO-BP

Chengchao Li[1,*], Liang Chen[1], Pengming Jiang[1] and Mingjing Jiang[1,2]
[1]Suzhou University of Science and Technology, School of Civil Engineering, Suzhou, China
[2]Tongji University, College of Civil Engineering, Shanghai, China

*Corresponding author: Chengchao Li;
E-mail address: ccli@usts.edu.cn (C. Li); 19962135051@163.com (L. Chen); pmjiang@usts.edu.cn (P. Jiang); mingjing.jiang@usts.edu.cn (M. Jiang)

Abstract

Estimating the mechanical behaviour of methane hydrate bearing sediments (MHBS) is important for exploiting the natural gas hydrate. In this study, the discrete element method (DEM) was first utilized to carry out a series of conventional triaxial tests on the MHBS, where a novel 3D thermo-hydro-mechanical-chemical contact model for the MHBS was employed. Then, different back pressures and hydrate saturations were simulated to capture the macro-strength and macro-stiffness of MHBS. The DEM results demonstrated that the peak shear stress increases with the increasing hydrate saturation and back pressure. In contrast, the enhancement effect of hydrate saturation on the secant modulus of MHBS is greater than that of back pressure. Besides, the numerical results were regarded as training data for the back propagation neural network combined with the particle swarm optimization (PSO-BP) to predict the mechanical response of MHBS considering different hydrate saturations. As expected, the PSO-BP shows powerful mapping ability and alleviates the time-consuming of DEM simulation for the MHBS.

Modeling soft granular materials under compaction: cohesion and strain rate effects

***S. Nezamabadi*[1,2], *F. Radjai*[1], *S. Mora*[1] *and J.-Y. Delenne*[2]**
[1] *LMGC, Univ Montpellier, CNRS, Montpellier, France*
[2] *IATE, NRAE, Montpellier SupAgro, Univ Montpellier, Montpellier, France*

1. Abstract

Numerous materials are made of a disordered arrangement of soft grains, a characteristic prevalent in various substances such as food products, metal powders, colloidal suspensions, and clays. Unlike hard-grain models, the interaction between disorder and grain deformations in these materials results in unique physical and mechanical properties. The notable deformability of soft grains under low confining pressure enables packing fractions to exceed the random close packing of hard grains. Consequently, rheological properties like compressibility and shear strength, as well as microstructure characteristics, are governed by a combination of grain rearrangements, and grain shape and volume changes. Indeed, the diverse forms of the microstructure depend on grain properties (compressibility, plasticity...) and interaction forces (friction, adhesion...) between grains.

In this work, to model the rheology and microstructure of soft granular systems, we use the Material Point Method (MPM) to compute the grain deformations and the Contact Dynamics Method (CDM) for the treatment of inter-grain interactions [1, 2, 3, 4]. An example of a deformed sample is shown in Fig. 1. We apply this approach to investigate the compaction of an assembly of elastic or plastic particles. In particular, we are interested in the behavior beyond the jamming state as a function of material parameters including the friction and cohesion between grains, and the strain rate loading.

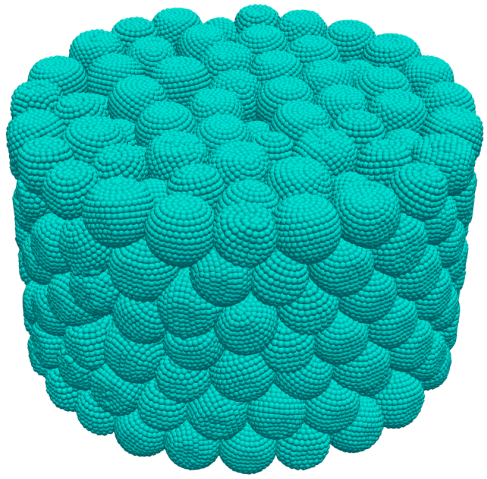

Figure 1. Compact of 400 elastic particles using the MPM-CD approach. The material points are represented by small spherical particles.

References

[1] Nezamabadi, S., Radjai, F., Averseng, J., and Delenne, J.-Y. (2015). Implicit frictional-contact model for soft particle systems. *Journal of the Mechanics and Physics of Solids*, **83**, 72–87.
[2] Nezamabadi, S., Nguyen, T., Delenne, J.-Y., and Radjai, F. (2017). Modeling soft granular materials. *Granular Matter*, **19**, 8.

[3] Nezamabadi, S., Frank, X., Delenne, J.-Y., Averseng, J., and Radjai, F. (2019). Parallel implicit contact algorithm for soft particle systems. *Computer Physics Communications*, **237**, 17–25.

[4] Nezamabadi, S., Ghadiri, M., Delenne, J.-Y., and Radjai, F. (2022). Modelling the compaction of plastic particle packings. *Computational Particle Mechanics*, **9**, 45–52.

RAY-TRACING DISCRETE ELEMENT METHOD

S. Zhao[1] and J. Zhao[1]
[1]Hong Kong University of Science and Technology, Kong Kong SAR, China

1. Introduction

Discrete element method (DEM) has been extensively employed to model granular materials in the past decades. Nevertheless, it is an outstanding issue to efficiently simulate either engineering-scale problems (e.g., landslides) or high-fidelity particulate details (e.g., particle morphology). We introduce a novel, efficient and robust approach, the ray-tracing discrete element method (RTDEM), for direct numerical simulations of granular materials. To accelerate RTDEM simulations on graphics processing units (GPUs), advanced algorithms have been developed to leverage the specific ray-tracing cores equipped on RTX GPUs. RTDEM is composed of two variants: sphere-RTDEM and mesh-RTDEM, which respectively model spherical and arbitrarily shaped particles. Sphere-RTDEM is particularly useful for simulating large-scale geotechnical problems, such as landslides and debris flow. Mesh-RTDEM uses triangular meshes to represent arbitrary shapes and introduces energy-conserving contact models, such as vertex-potential and facet-potential models, to enable robust contact resolution. These contact models benefit from our novel discrete potential field functions. RTDEM is poised to be a next-generation tool for modeling large-scale granular systems with ease and efficiency, which has been implemented in our numerical computing platform SudoSim.

2. Sphere-RTDEM

Ray tracing is a prevailing technique to render images and videos with extra realism in computer graphics. During rendering, the color of each pixel is determined by casting a ray into a model scene. The model scene most often consists of many objects, and it is computationally intensive to query a collision between a ray and all potentially touching objects. The physical RT unit was invented by NVIDIA to tackle ray-object collision on GPUs [1]. Attracted by the powerful RT unit, the authors applied the RT unit to accelerate particle-based numerical simulations in their recent work [2].

To leverage the powerful RT cores for DEM simulations, the neighbor searching procedure needs first transferring to an equivalent RT problem. Then, an imaginary short ray is cast into the model scene that has all particles organized in an accelerate structure. Next, the interparticle contact detection is identified by checking whether the cast ray is inside the expanded axis-aligned bounding box (AABB) of a neighboring particle. Such a ray-AABB collision detection is fully accelerated by the RT cores with an NVIDIA's OptiX pipeline. Interested readers are referred to [2] for more details on the implementation.

To model landslide, an efficient algorithm of particle-terrain contact detection is proposed. Specifically, the terrain is modeled by a digital elevation model, and soil particles are simplified as spheres. It is assumed that particles are smaller than the grid size of the digital elevation model to ease the particle-terrain contact detection. Thus, a particle has at most 4 grid cells (8 triangular facets) that can be identified efficiently by indexing its coordinates with respect to the regular grid cells. Moreover, a weighting scheme is applied to contact force when a particle touches with adjacent triangles, which ensures robust sliding of a particle across cells. Fig. 1 shows snapshots of a simulated dry debris flow. For the 100-second simulation, it takes only 6.5 min on a single NVIDIA RTX 3090 GPU.

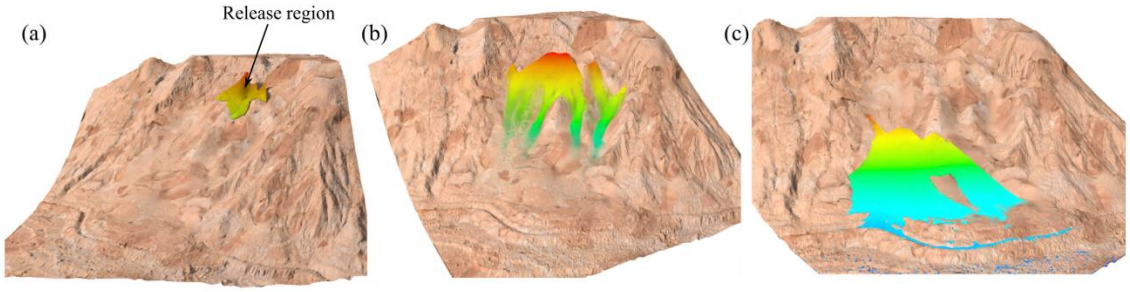

Figure 1. Simulation snapshots of dry debris flow (1.6M particles and 0.12M triangular facets) at different time instants: (a) 0 s, (b) 10 s and (c) 100 s.

3. Mesh-RTDEM

As a significant extension of sphere-RTDEM, mesh-RTDEM is proposed for efficiently modeling arbitrarily shaped particles. In addition to ray-AABB collision detection, ray-triangle collision detection is used to solve the penetration depth at each contact. Three potential-based contact models, including the vertex-potential, the facet-potential, and their combined models, make the simulations numerically stable, with the facet-potential model being the most robust. The potential-based models can be seamlessly combined with the ray-tracing contact detection, making the overall framework suitable for parallel computing on GPUs. Specifically, both shader and RT cores on GPUs can be fully leveraged to accelerate simulations, making efficient use of the computing capacity of GPUs. Interested readers are referred to [3] for detailed implementation. Fig. 2 demonstrates the capability of mesh-RTDEM to efficiently tackle arbitrarily shaped particles with extreme size ratios.

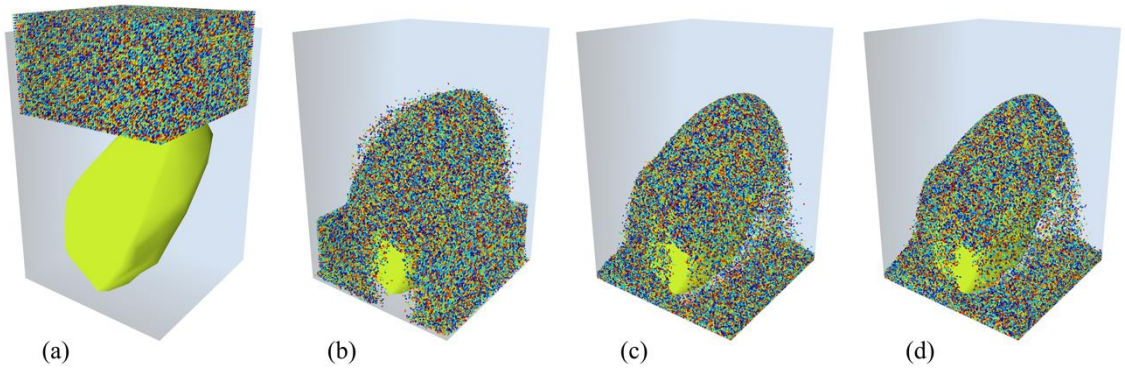

Figure 2. Configurations of 0.2M small particles impacting a big particle (with a size ratio of 100 : 1) within a box at different time instants: (a) 0 s, (b) 1 s, (c) 2 s and (d) 3 s.

4. References

[1] NVIDIA. NVIDIA Turing GPU architecture: graphics reinvented; 2018. https://bit.ly/2NGLr5t

[2] Zhao, S., Lai, Z., & Zhao, J. (2022). Leveraging ray tracing cores for particle-based simulations on GPUs. *Int. J. Numer. Meth. Eng.*, **124**(3), 696–713.

[3] Zhao, S., & Zhao, J. (2023). Revolutionizing granular matter simulations by high-performance ray tracing discrete element method for arbitrarily-shaped particles. *Comput. Methods Appl. Mech. Eng.*, *416*, 116370.

Acknowledgements This work was supported by Research Grants Council of Hong Kong (by GRF Projects No. 16211221 & No. 16206322), and the Project of Hetao Shenzhen-Hong Kong Science and Technology Innovation Cooperation Zone (Grant No. HZQBKCZYB-2020083).

Regulating Sand Trajectories in Air Jet Flow Using Particle Morphology

S. Maramizonouz and S. Nadimi
School of Engineering, Newcastle University, Newcastle upon Tyne, NE1 7RU, UK

1. Introduction

Irregular particles and their interactions with each other, the solid objects, and the fluid medium around them are the dominating components of many natural processes and industrial applications. One example is utilising irregular particulate materials as friction modifiers by the railway industry for rail-sanding application. In which, to rectify the loss of friction due to the formation of moisture, leaves, and oil on the top surface of the rail, sand particles are deposited on the top of the rail, in front of the wheel using an air jet [1].

During the rail-sanding application, the sand particles interact with the air jet as the particles flow through and exit the sander nozzle and experience forces and moments dependent on their morphological features. One such force is the drag force which for the purpose of the current application can be considered the dominant force dictating the dynamics of the particles' movement [1, 2]. At the end of their trajectory, the sand particles are entrained at the wheel-rail interface and are crushed by the train's wheel resulting in an increase in the wheel-rail friction. The efficiency of the particles' entrainment at the desired location can then be estimated using the ratio of the number of the particles that pass into the wheel-rail interface to the total number of particles [1].

In order to investigate the effects of particles' irregular morphologies on their dynamic behaviour, a mixture of air and irregular particles is numerically modelled as the particles flow through a cylindrical tube, exit the nozzle, and are entrained at a certain spot. For this purpose, a discrete element method (DEM) simulation is one-way coupled to a computational fluid dynamics (CFD) model via the drag force the particles experience when moving through the fluid.

2. Numerical Modelling and One-Way Coupling

In this study, the rail-sanding process is numerically simulated using a one-way coupled DEM-CFD model. The particles' mechanics is simulated through a DEM model using Newton's laws of motion as well as the Hertz-Mindlin contact model [3]. The dynamics of the fluid flow are modelled using the Navier-Stokes equations as the governing equations of motion [4].

To implement the effects of the fluid dynamics on particle motion, the CFD simulation is one-way coupled to the DEM simulation via the drag force the particles experience when moving through the fluid. This means that the dynamics of the fluid flow affect the particle motion but not vice versa. For this purpose, the fluid's steady-state velocity field obtained through CFD simulation is used to estimate the particles' drag force. The drag force is then added to the particles' governing equations of motion in DEM [4,5].

3. Particles' Morphology and Their Drag Force

For particles with irregular morphologies, the drag force is highly dependent on their shape characteristics. Various methods have been proposed in literature on how to implement morphological features of irregular particles in the estimation of their drag force resulting in the

introduction of more than fifteen empirical drag models each utilising various particle shape characteristics to estimate their drag force [1].

In this study, the flow and the drag force acting particles from three different shape categories of the Zingg chart [6] including compact, flat, and elongated all with the same length scale of ~1.2 mm shown in **Figure 1** are compared to the benchmark case of spherical particles with a 1.2 mm diameter. In the DEM model, the irregular particles are represented as clumps of 10 spherical fragments.

Figure 2 presents the effect of particles' morphology on their entrainment efficiency. It can be seen that irregularity in particle morphology increases their entrainment efficiencies with the flat particles presenting a maximum increase of ~ 140% in entrainment efficiency.

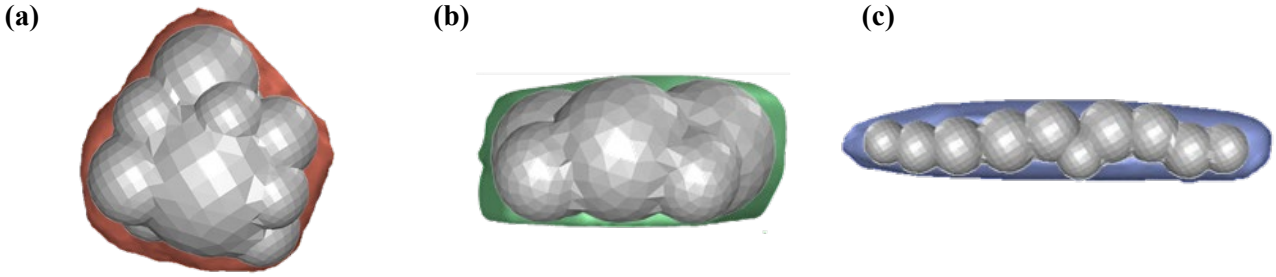

Figure 1. The three particle shapes used in the numerical modelling: **(a)** compact, **(b)** flat, and **(c)** elongated all with the same length of ~1.2 mm as their length scale.

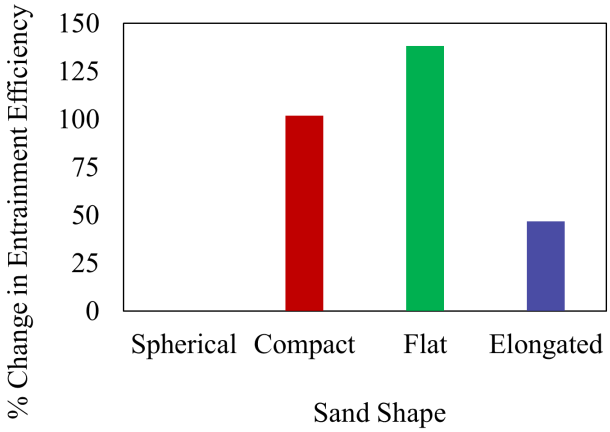

Figure 2. The percentage change in the entrainment efficiency of the three particle shapes compared to the benchmark case of spherical particle.

4. References

[1] S. Maramizonouz, S. Nadimi, W. Skipper, S. R. Lewis, and R. Lewis, (2023). Numerical Modelling of Particle Entrainment in the Wheel–Rail Interface, *Computational Particle Mechanics*, vol. 10, p. 2009-2019.

[2] S. Maramizonouz and S. Nadimi, (2022). Drag force acting on ellipsoidal particles with different shape characteristics, *Powder Technology*, vol. 412, p. 117964.

[3] Thornton, C. (2015). *Granular Dynamics, Contact Mechanics and Particle System Simulations. A DEM study*. Particle Technology Series, 24.

[4] White, F. M. (1979). *Fluid Mechanics*. Tata McGraw-Hill Education.

[5] Crowe, C. T., & Michaelides, E. E. (2006). *Multiphase Flow Handbook*. Taylor & Francis.

[6] T. Zingg, (1935). Beitrag zur Schotteranalyse, *ETH Zurich*.

Sand Behavior upon Alternating Triaxial Compression and Triaxial Extension: A Multiscale Analysis Using LS-DEM

J. Cui [1]***, K. Karapiperis***[2]***, O. Torgersrud***[3]***, E. Andò***[4]***, G. Viggiani***[3] ***and J. E. Andrade***[5]***,***
[1] *Columbia Univ., New York City, U.S.A.*
[2] *ETH Zürich, Zürich, Switzerland*
[3] *Univ. Grenoble Alpes, Grenoble, France*
[4] *École Polytechnique Fédérale de Lausanne (EPFL), Lausanne, Switzerland*
[5] *California Institute of Technology, Pasadena, CA, U.S.A.*

1. Introduction

Granular materials are subjected to cyclic loading in a range of different scenarios, and the prediction of their response is crucial for geotechnical and geophysical systems. In this study, we investigate the mechanical behavior of Hostun sand subjected to alternating cycles of triaxial compression and extension from a multiscale perspective. To this end, we construct a digital twin, using the level-set discrete element method (LS-DEM), of a specimen experiencing alternating triaxial compression and extension within an X-ray tomograph. On the basis of experimental and computational observations, we uncover the fundamental mechanisms behind fabric evolution and failure by necking.

2. Experiments and simulations

As described in [1], the Hostun sand specimen is prepared by dry pluviation and is isotropically compressed up to 430 kPa by gradually increasing the confining fluid pressure within a triaxial apparatus. Subsequently, alternating triaxial compression and extension cycles of increasing magnitude are applied by driving a loading piston up and down, until failure. To capture the microstructure variations within the specimen, X-ray scans are periodically performed during the compression and extension cycles. A series of measurements are taken including those of local strain fields using Digital Volume Correlation, as well as particle based tracking yielding the evolution of contact orientation fabric during the experiment [2].

The computational model of the specimen is constructed directly from the XRCT image of the undeformed specimen, achieving a one-to-one reproduction of the experimental sample in terms of particle shape and coordinates. LS-DEM is used to simulate the system of roughly 41,600 particles [3], whose material properties were calibrated based on a previous experiment with the same sand [4]. The membrane is modeled with bonded spheres shaped to a hollow cylinder following previous work [4]. The cyclic compression and extension of the specimen is achieved by prescribing the vertical displacement of the top platen, while keeping the bottom platen fixed in place, and imposing a constant pressure on the membrane.

3. Results

The results of the computational model are first compared against the experimental measurements at a macroscopic scale, showing good agreement as shown in Fig. 1. We then focus on uncovering the fundamental mechanisms at smaller scales including the evolution of the meso-scopic deviatoric strain field, contact fabric, as well as the particle-scale behavior, enabling an unprecedented insight into micromechanical processes during alternating cyclic loading. The contact fabric and force transmission network demonstrate a highly anisotropic pattern throughout the cycles of the test. During extension, strain localization is observed in the form of necking in both experiments and

simulations marking the failure of the specimen (Fig. 1 d). We finally discuss potential evidence of the attainment of an anisotropic critical state at the region where necking occurs.

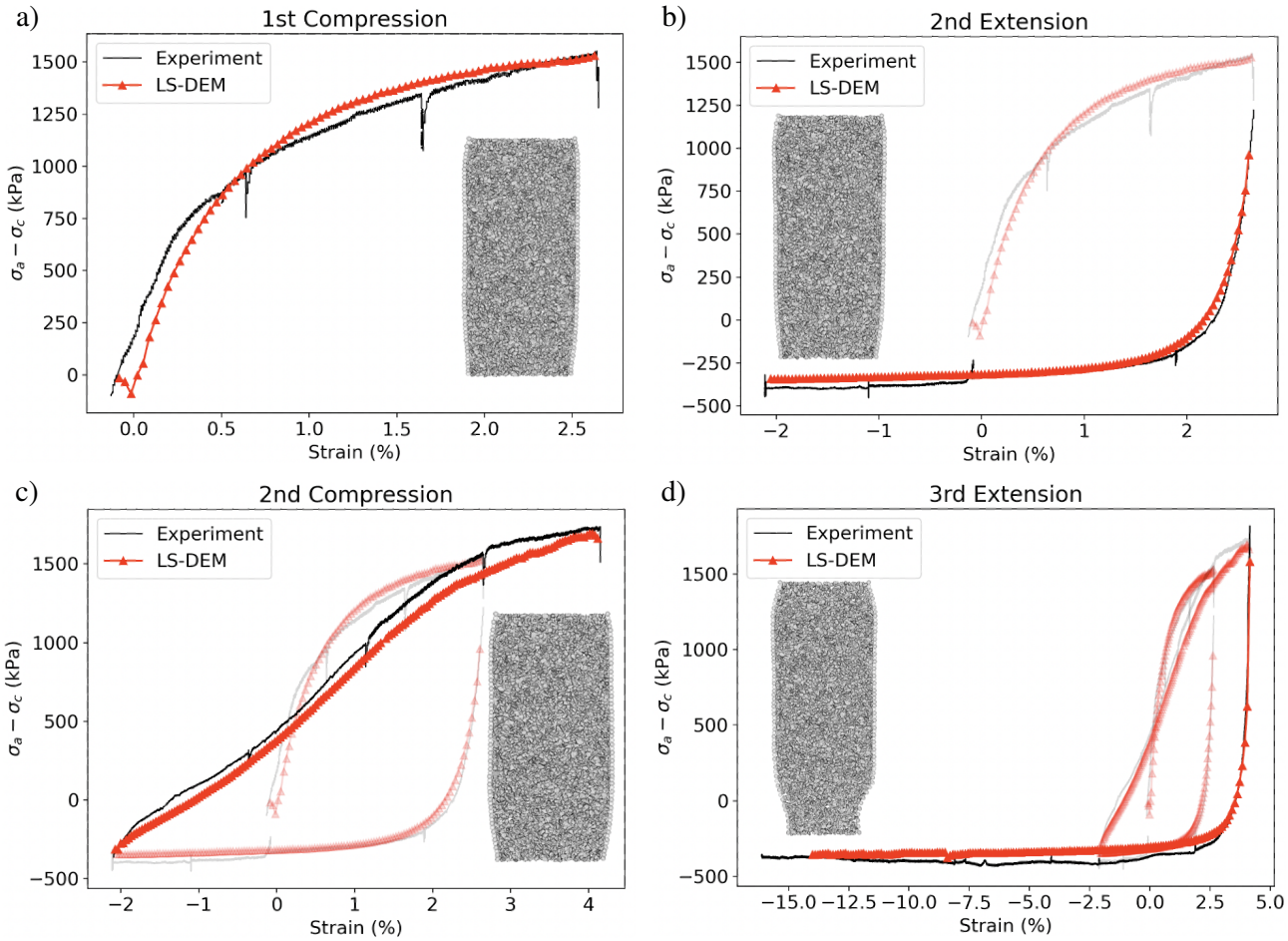

Figure 1. Macroscopic deviator stress - axial strain response during each triaxial loading cycle. (a)-(d) corresponds to the 1st compression, 2nd extension, 2nd compression and 3rd extension, respectively. Insets show the deformed virtual specimen at each stage.

References

[1] Salvatore, E., Andò, E., Modoni, G., and Viggiani, G. (2016). Micromechanical study of cyclically loaded sands with x-ray microtomography and digital image correlation. *Procedia Engineering*, **158**, 92–97.

[2] Andò, E., Hall, S. A., Viggiani, G., Desrues, J., and Bésuelle, P. (2012). Experimental micromechanics: grain-scale observation of sand deformation. *Géotechnique Letters*, **2**, 107–112.

[3] Kawamoto, R., Andò, E., Viggiani, G., and Andrade, J. E. (2016). Level set discrete element method for three-dimensional computations with triaxial case study. *Journal of the Mechanics and Physics of Solids*, **91**, 1–13.

[4] Kawamoto, R., Andò, E., Viggiani, G., and Andrade, J. E. (2018). All you need is shape: Predicting shear banding in sand with ls-dem. *Journal of the Mechanics and Physics of Solids*, **111**, 375–392.

SEEPAGE-INDUCED SUFFUSION AND SLOPE FAILURE: A MULTISCALE PERSPECTIVE USING FEM-DEM

Zheng Hu[1], Zhongxuan Yang[2], Ning Guo[2], Yida Zhang[3]

[1] Sun Yat-sen University, School of Civil Enginnering, Zhuhai, China

[2] Zhejiang University, College of Civil Enginnering and Architecture, Hangzhou, China

[3] University of Colorado Boulder, Department of Civil, Environmental and Architectural Engineering, Boulder, USA

Abstract

Suffusion, the detachment and migration of fine particles through voids among coarse particles, poses a significant threat to slope stability. This study employs a two-dimensional (2D) hierarchical multiscale finite–discrete element method (FEM–DEM) to investigate seepage-induced suffusion and its impact on slope instability. An erosion law incorporating the critical hydraulic gradient for suffusion onset is presented. Two examples, one-dimensional suffusion and biaxial compression tests, validate the proposed scheme, with a focus on reproducing suffusion and progressive slope failure under seepage flow. The results reveal the initiation of a shear band from the slope toe, extending gradually to the crest. The erosion rate directly accelerates the suffusion and slope failure process, with a higher critical hydraulic gradient playing a mitigating role. Fines loss due to suffusion predominantly occurs on the slope surface, particularly near the slope toe. Microscopic analyses on locally embedded representative volume elements (RVEs) highlight severe deformation and microstructural changes within the shear band, including soil skeleton rearrangement and variation of contact force chains. Furthermore, the 2D condition is extended to three-dimensional (3D) condition to reproduce the more realistic soil matrix, pore space and fines loss process in gap-graded soils. A novel particle removal scheme based on the internal moment tensor is presented. This scheme generates specimens with varying degrees of fines loss. Macroscopic shear responses of both eroded and non-eroded specimens are benchmarked using RVEs in a pure discrete element method (DEM). The eroded specimen exhibits a reduced peak stress ratio, yet critical state values remain almost unchanged compared to the non-eroded specimen. Fines loss restrains shear band formation, resulting in a more uniform stress and strain distribution. Interestingly, fine particles in gap-graded soils sustain only a small proportion of external loads, especially in specimens with increased fines loss. Notably, the multiscale investigation provides valuable insights into seepage-induced suffusion and fines loss, offering a comprehensive understanding of their implications on slope instability.

Simulation of non-spherical slurry particle infiltration in a sand column

Jiayuan Liu[1]***, Kevin J. Hanley***[1]
[1] *School of Engineering, Institute for Infrastructure and Environment, The University of Edinburgh, Edinburgh EH9 3JL, UK*

1. Introduction

The slurry infiltration process plays an important role in stabilising an excavation surface [1]. Laboratory column tests for slurry infiltration are frequently adopted to study the macroscopic aspects of the infiltration process and properties of filter cake [2]. A coupled computational fluid dynamics (CFD)–discrete element method (DEM) numerical approach is helpful to obtain a better understanding of the slurry and soil interaction mechanism at a particulate scale [3].

Current laboratory tests [2] and simulations [4, 5] focus on the slurry infiltration in a vertical direction, which may not accurately reflect the horizontal infiltration that is encountered in actual tunnel construction. There is limited research on the "horizontal infiltration" of slurry, i.e., the infiltration dynamics of the slurry particles and the microscopic features of the filter cake have not yet been thoroughly studied.

The objective of this research is to create a more realistic model of bentonite slurry infiltration in a sand stratum and investigate the slurry infiltration process and the properties of the filter cake. The study is carried out by comparing the slurry infiltration in coarse sand in both vertical and horizontal directions by CFD–DEM. Ellipsoidal slurry particles are adopted. The results are analysed in terms of void fraction, pressure distribution in the sand column and infiltration range of slurry particles.

2. Methodology and simulation setup

For computational tractability, the bentonite slurry particles are represented as oblate spheroids of aspect ratio 7 using superquadrics while sand particles are spheres. The drag force [6], lift force, viscous force, pressure gradient force and pitching torque [4] are included in the modelling. An adaptive cohesion model [7] is applied between the slurry particles. The Hertz contact model with mean curvature radius is used. Sand particle diameters are distributed between 2.5 mm and 5 mm. The size ratio between slurry and sand particles is 1:5. The simulation model for horizontal and vertical infiltration is illustrated in Fig. 1.

The simulation procedure for vertical infiltration in Liu and Hanley [4] is adopted. The procedure for horizontal infiltration comprises four stages. Initially, sand particles are generated in water and settle completely under gravity in the sand column. Then, a "slurry shield machine", which is represented as a cylinder, is generated and connected to the sand column. After that, the slurry particles are inserted into the cylinder with random orientations. Finally, the slurry particle infiltration is initiated when slurry particles come into contact with the sand column under pressure. A simulation is stopped upon reaching a state in which the suspended particles are still, and both the porosity and pressure drop across the column maintain a constant value. A total system energy of 10^{-7} J was chosen as the criterion for terminating each simulation.

3. Results

The infiltration area for the vertical infiltration case is fixed, being constrained to the diameter of the cylindrical column, whereas the infiltration area can expand beyond the cross-sectional area of the slurry pipe for the horizontal infiltration case. Despite this difference, the infiltration distances are similar and external filter cakes are formed in both cases. The pressure drops across the external filter

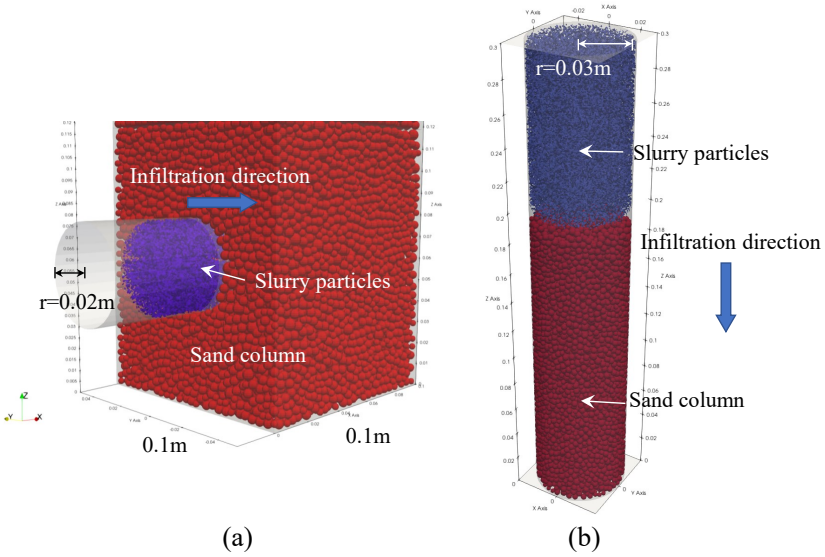

Figure 1. Simulation model of (a) horizontal infiltration and (b) vertical infiltration.

cakes are also similar: around 30 % of the total pressure drops obtained. However, there are variations in the fluid conditions and the process of particle infiltration. Although the same slurry pressure was applied in both simulations, the slurry pressure dissipated much faster in the horizontal case than in the vertical case, and the fluid velocity in the slurry pipe in the horizontal case is higher than the downward fluid velocity in the vertical case. The slurry particles, on average, have a higher initial velocity in the slurry pipe in the horizontal case; however, they slow down quickly upon contact with the sand column. The filter cake forms more quickly in the horizontal case.

This research studies the infiltration process and filter cake properties in a more realistic model. The simulation results reveal that the properties of filter cakes formed in both horizontal and vertical infiltration cases are comparable. However, essential differences were found in the infiltration process of slurry particles in both cases.

References

[1] Min, F., Liu, J., Chen, J., Liu, T., Yu, C., Ji, J., and Liu, J. (2023). A study on the excavation face failure of pressurized slurry shield. *Tunn. Undergr. Sp. Tech.*, **132**, 104900.

[2] Min, F., Du, J., Zhang, N., Chen, X., Lv, H., Liu, L., and Yu, C. (2019). Experimental study on property change of slurry and filter cake of slurry shield under seawater intrusion. *Tunn. Undergr. Sp. Tech.*, **88**, 290–299.

[3] Lin, Y., Fang, Y., and He, C. (2022). Numerical study on clogging mechanism of slurry infiltration in porous media based on coupled CFD–DEM method. *Tunn. Undergr. Sp. Tech.*, **128**, 104622.

[4] Liu, J. and Hanley, K. J. (2023). CFD–DEM modelling of the infiltration of non-spherical slurry particles in granular soils. *Comput. Geotech.*, **164**, 105845.

[5] Zhang, Z., Yin, T., Huang, X., and Dias, D. (2019). Slurry filtration process and filter cake formation during shield tunnelling: Insight from coupled CFD–DEM simulations of slurry filtration column test. *Tunn. Undergr. Sp. Tech.*, **87**, 64–77.

[6] Hölzer, A. and Sommerfeld, M. (2008). New simple correlation formula for the drag coefficient of non-spherical particles. *Powder Technol.*, **184**, 361–365.

[7] Obermayr, M., Vrettos, C., Eberhard, P., and Däuwel, T. (2014). A discrete element model and its experimental validation for the prediction of draft forces in cohesive soil. *J. Terramechanics*, **53**, 93–104.

THE STATIC/DYNAMIC RESPONSE OF PARTIALLY SATURATED CONCRETE USING A FULLY COUPLED DEM/CFD APPROACH

***M. Krzaczek*[1] *and J. Tejchman*[1]**
[1] *Gdańsk University of Technology. Gdańsk, Poland*

1. General

Concrete buildings commonly come into contact with water. Concrete is porous and has numerous macropores, capillary pores, defects, and cracks, which allow water to seep through. Due to its effects on capillary tension, pore water pressure, inter-particle cohesion, and friction, this can significantly change the static and dynamic mechanical properties of concrete. Therefore, it is essential to research how free water affects the mechanical response of concrete when building concrete buildings that must resist wet environments. Chemically bonded, physically bonded, and free water are the three forms of water that are generally present in concrete. It is a well-known fact that concrete materials perform substantially differently in laboratory tests under dynamic loading when compared with quasi-static loading conditions. In actual practice, the effect of the change in free water during concrete loading is frequently ignored. Although the mechanical properties of wet concrete have been extensively investigated, it is not still clear how water and moisture content affect these qualities at the mesoscale.

Laboratory investigations show that concrete's compressive and tensile strength, as well as its fracture toughness, both decrease as water saturation rises in static conditions and increase as water saturation rises in dynamic conditions.

2. Numerical model

In this study, the impact of free water on the static and dynamic compressive and tensile characteristics of concrete in two-dimensional (2D) mesoscale conditions is examined. On the static and dynamic mechanical properties of concrete (strength, brittleness, and fracture) during uniaxial compression and tension, the effect of free pore water content was mainly looked at. A pore-scale hydro-mechanical model based on a fully coupled DEM/CFD approach ([1]-[4]) was used to simulate the behavior of totally and partially fluid-saturated concrete. The idea behind the approach was a network of channels in a continuous area between discrete elements to create a fluid movement. A two-phase laminar fluid flow (water and air) was proposed in wet concrete that had a low porosity of 5%. Geometry and volumes of pores/cracks were considered to correctly track the liquid/gas content. A series of static and dynamic numerical simulations were run on bonded granular specimens of a simplified spherical mesostructure mimicking concrete in both dry and wet conditions. Extensive investigations into the impact of a saturation level on static and dynamic concrete strength and a fracture process were performed.

3. Numerical results

It was discovered that the saturation level had a major impact on how concrete behaved mechanically. As fluid saturation rose, so did the dynamic compressive and tensile strength. However, the static compressive and tensile strength diminished. In the dynamic range, the concrete mesostructure prevented fluid migration as a result of the rapid loading brought on by the high strain rate, and there were relatively few changes in pore fluid pressures and velocities. As a result,

the pore fluid pressures slowed the rate of fracture, which led to increased strength. In the static range, the concrete mesostructure allowed for fluid migration as a result of the slow deformation, and there were changes in pore fluid pressures and velocities. As a result, the pore fluid pressures accelerated the rate of fracture, which led to declined strength. The numerical DEM-CFD results were in agreement with the corresponding laboratory test outcomes from the literature.

The results of uniaxial compressive strengths f_c versus the fluid volume fraction are compiled in Figure 1 [4]. The numerical results show (curve 'a' in Fig.1) that when the initial fluid volume fraction α_q rose, the dynamic compressive strength and the associated vertical normal strain likewise increased in contrast to quasi-static strength results (curve 'b' in Fig.1). With rising fluid volume fraction, the static/dynamic compressive strength reduced/grew in a roughly linear way (Fig.1).

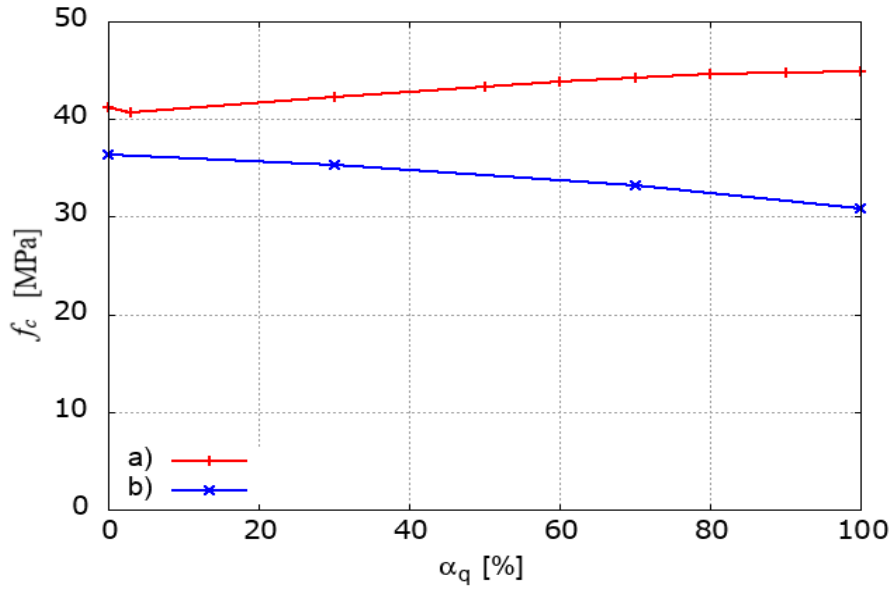

Figure 1. DEM-CFD simulation results for one-phase concrete specimen during uniaxial compression with different initial fluid volume fraction α_q: relationship between compressive strength f_c and α_q (a) dynamic tests and b) quasi-static tests).

5. References

[1] Krzaczek, M., Nitka, M. & Tejchman, J. (2021). Effect of gas content in macropores on hydraulic fracturing in rocks using a fully coupled DEM/CFD approach. *Int J Numer Anal Methods Geomech.*, **45(2)**: 234-264.

[2] Krzaczek, M., Nitka, M. & Tejchman, J. (2023). Modelling hydraulic and capillary-driven two-phase fluid flow in unsaturated concretes at the meso-scale with a unique coupled DEM-CFD technique. *Int J Numer Anal Methods Geomech.*, **47(1):** 23-53.

[3] Krzaczek, M., Nitka, M. & Tejchman, J. (2023). Hydraulic fracturing process in rocks – small-scale simulations with a novel fully coupled DEM/CFD-based thermo-hydro-mechanical approach. *Engineering Fracture Mechanics* **289**: 109424.

[4] Krzaczek, M. & Tejchman, J. (2024). Effect of free water on the quasi-static compression behavior of partially-saturated concrete with a fully coupled DEM/CFD approach. *Granular Matter* (in review).

TWO-DIMENSIONAL NUMERICAL INVESTIGATION OF THE PLUG EFFECT DURING DISPLACEMENT DOUBLE PILE-WALL PENETRATION USING A COUPLED DISCRETE ELEMENT-FINITE DIFFERENCE METHOD

Teng Xiao [1], Zijie Zhang [1]，Zhongxuan Yang [1]
[1] Dept. of Civil Engineering, Zhejiang University, Hangzhou, China

1. General

A numerical simulation using a coupled discrete element-finite difference method (DEM-FDM) is presented to investigate the plug effect during the double pile-wall penetration into sand. To increase the computational efficiency, a novel two-dimensional coupled DEM-FDM is established, in which finer DEM particles in the region near to the pile shaft while FDM elements in the further distance are used to reduce the scale effects while avoiding boundary effects. The basic idea of this coupled numerical model is to decompose the solution domain into two subdomains, i.e., DEM and FDM. Parameters used in the simulations are determined by comparing the biaxial compression test results from the DEM and FDM. Three schemes representing open-ended piles with different inner diameters but the same thickness are considered in the numerical simulations. Smaller diameter (spacing between the pile-walls) causes severer plug effect, evidenced by the lower Plug Length Ratio (PLR) and Incremental Filling Ratio (IFR). As shown in the stress contours, both horizontal and vertical stresses are concentrated near the pile-wall tip because of the plug effect. Both the principal stress and contact force distribution give further insights into the formation of the plug.

2. Basic principle of DEM and FDM coupling

The fundamental principle of DEM and FDM coupling is described as follows. First, the coupling interface which is composed of the nodes in FDM coupling surface participates in DEM calculation as boundary walls. After that, for a basic “disk–facet” contact element on the coupling interface, the equivalent force in each node is barycentric interpolated to the nodes of facets. Then, the equivalent force in each facet node is input to the corresponding FDM element node to participate in the FDM calculation. Finally, the coupling surface of FDM domain will deform as the consequence of FDM domain’s solution. Note that the nodes of the coupling wall always coincide with those of the coupling surface in FDM domain. The coupling interface composed of the FDM element nodes re-participates in the DEM calculation as a wall boundary. In this way, the compatible deformation between the boundary of DEM and FDM domains in the coupling surface can be ensured.

3. Numerical model

Figure 1 is a schematic diagram of the numerical model in this study for the investigation of the plug effect during the double pile-wall (or equivalent open-ended pile in three-dimension) penetrating into sand, which mainly contains two parts: rigid double pile-wall and sand mass field. According to the domain decomposition multi-scale perspective, DEM is used to simulate the sand in the near region of the double pile-wall, while FDM is used to simulate the far field away from double pile-walls to save computational resources. The rolling resistance contact model is adopted in the DEM domain, while the simple Mohr–Coulomb constitutive model is adopted in the FDM domain. Based on this arrangement, the ratio of pile-wall thickness to the mean particle size is 5, and the model width is increased to minimize the boundary effect.

The thickness of the pile-wall is 10 mm. Three double pile-walls with different spacings representing open-ended piles with various inner diameters are penetrated into the sand mass. Three tests are conducted with the test IDs as ‘D100’, ‘D70’ and ’D50’, and the results are illustrated in Figure 2.

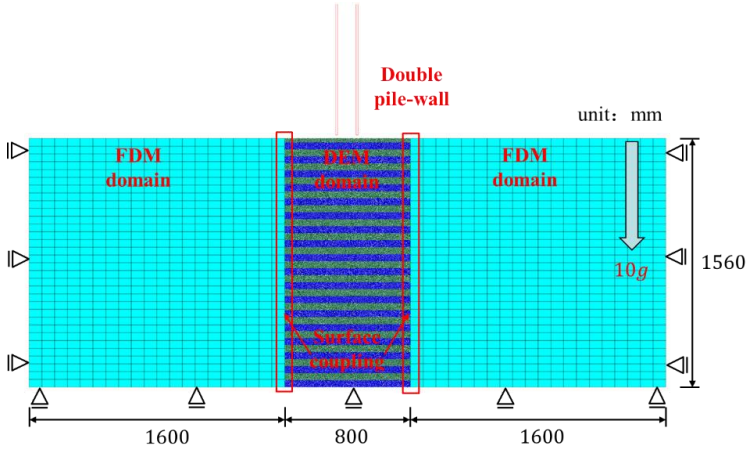

Figure 1. Numerical model diagram for two-dimensional penetration modelling of an open-ended pile into sand mass

4. Some results

The following findings can be obtained from the numerical tests.

1. Smaller diameter appears to cause severer plug effect, manifested by the lower Plug Length Ratio (PLR) and Incremental Filling Ratio (IFR).

2. Because of the plug effect, stress concentrations are observed in the vicinity of the pile-wall tips and the lower part of plug.

3. During the shallow penetration, a region with relatively large contact forces is developed beneath each pile-wall tip; For the further penetration, this region expands from the tip towards the center of the double pile-walls because of the gradual plug formation.

4. The contact force chain network indicates that the bottom part of the plug with a height of approximately 3-5 times inner diameter has high stress concentration, while the stress in the remaining part is negligibly small.

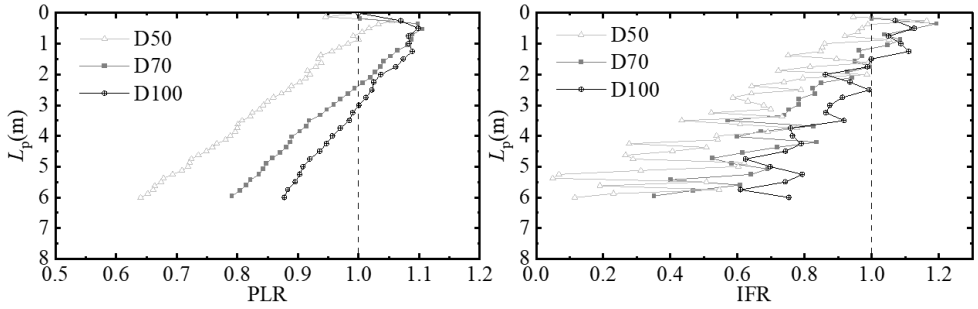

Figure 2. The development of PLR and IFR in three schemes during the double pile-wall penetration

5. References

[1] Randolph, M. F., Leong, E. C., & Houlsby, G. T. (1991). One-dimensional analysis of soil plugs in pipe piles. *Geotechnique*, 41(4), 587-598.

[2] Paik, K. H., & Lee, S. R. (1993). Behavior of soil plugs in open-ended model piles driven into sands. *Marine Georesources & Geotechnology*, 11(4), 353-373.

[3] Elmekati, A., & El Shamy, U. (2010). A practical co-simulation approach for multiscale analysis of geotechnical systems. *Computers and Geotechnics*, 37(4), 494-503.

UNIVERSALITY OF PARTICLE INFILTRATION DEPTH IN GRANULAR FILTERS

***Y. Zhang*[1,2], *A. Sufian*[1,3], *and A. Scheuermann*[1]**
[1] *The University of Queensland, Brisbane, Australia*
[2] *SMEC Australia Pty Ltd, Brisbane, Australia*
[3] *The University of New South Wales, Sydney, Australia*

Granular filters play an important role in mitigating the transport of finer base particles associated with seepage flows. This is particularly important in zoned embankment dams, where filter drains are constructed to prevent the erosion of finer core material into the coarser shell material. The design of granular filters is governed by hydraulic and geometric conditions [1]. The hydraulic condition specifies the required flow velocity or hydraulic gradient for the onset and transport of base particles, while the geometric condition specifies whether the pore space of the granular filter is sufficiently large to permit the migration of base particles.

An important consideration in granular filter design is the infiltration depth of base particles with seepage flow. Effective filters only result in minimal to no infiltration, while ineffective granular filters can experience significant and even continuing infiltration [2, 3]. The infiltration depth provides a pathway to understand the effectiveness of a granular filter, and this study employed coupled Computational Fluid Dynamics and Discrete Element Method (CFD-DEM) to demonstrate universality of infiltration depth for a range of granular filters at various hydraulic loading and geometric conditions.

CFD-DEM simulations were conducted with finer base particles underlying a coarser granular filter with upward seepage flow perpendicular to the base-filter interface (Figure 1). A wide range of size ratios were considered, from $R = 5$ to $R = 10$, where R is the ratio of the maximum to minimum particle diameter. This covered the complete breadth of filtration behaviour, including the 'no', 'some', 'excessive', and 'continuing' categories proposed by Foster et al. [4]. For each size ratio, three different ramping accelerations for the upward seepage flow was considered to investigate how infiltration is affected by the rate of hydraulic loading. Therefore, the study investigated the infiltration depth for a combined influence of geometric and hydraulic conditions.

The influence of hydraulic loading conditions and size ratios on the time-dependent infiltration depth of transported base particles was observed to be universal with respect to a newly proposed dimensionless time parameter (Figure 2). The dimensionless time parameter is given by $\tilde{t} = t\frac{a_{flow}}{d_{f,100}}$, where t is the physical time, a_{flow} is the acceleration of the upward seepage flow, and $d_{f,100}$ is the maximum size of the granular filter. In this way, the newly proposed dimensionless time parameter accounts for hydraulic and geometric conditions influence on infiltration depth. However, it is noted that the universality is only observed during the early stages of infiltration.

References

[1] ICOLD (2015). *Internal Erosion of Existing Dams, Levees and Dykes, and Their Foundations: Internal erosion processes and engineering assessment*. International Commission on Large Dams.

[2] Zhang, Y., Sufian, A., and Scheuermann, A. (2023). Influence of hydraulic and geometric conditions on the early stages of the filtration process in idealised granular soils comprising spherical particles. *International Journal for Numerical and Analytical Methods in Geomechanics*.

[3] Sufian, A., Bittner, T., Bore, T., Bajodek, M., and Scheuermann, A. (2022). Physical observations of the transient evolution of the porosity distribution during internal erosion using spatial time domain reflectometry. *Canadian Geotechnical Journal*, **59**, 1443–1458.

[4] Foster, M. and Fell, R. (2001). Assessing embankment dam filters that do not satisfy design criteria. *Journal of Geotechnical and Geoenvironmental Engineering*, **127**, 398–407.

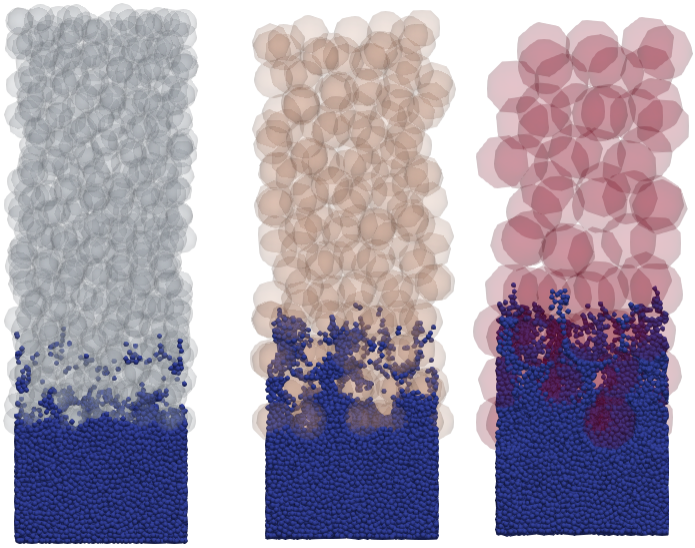

Figure 1. Visualisation at the end of the simulation for typical assemblies considered in the simulation, including $R = 5$ (left), $R = 7$ (middle), and $R = 10$ (right). The granular filter is made transparent to visualise the infiltration of finer base particles.

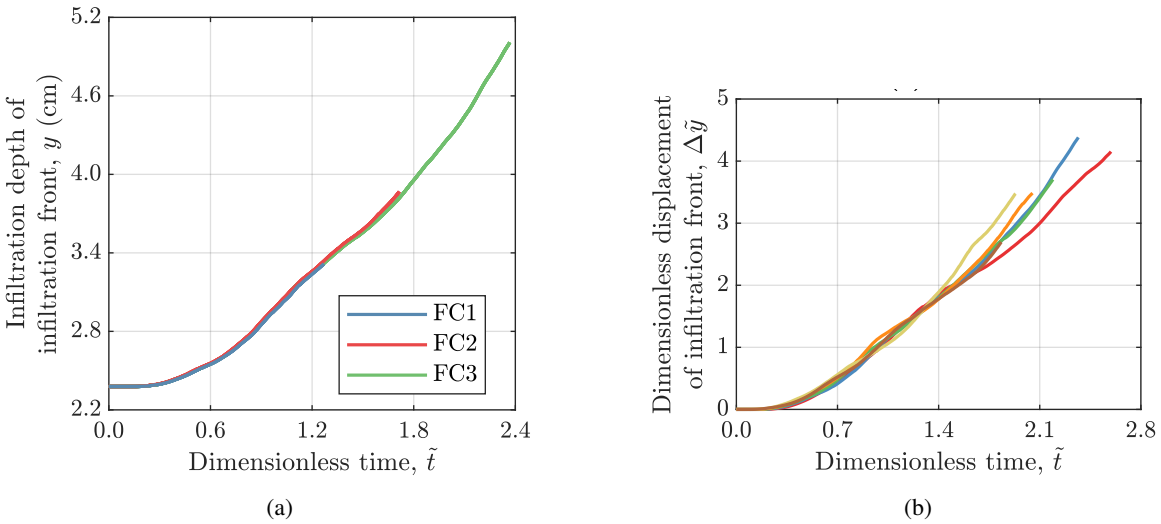

Figure 2. (a) Universality of infiltration depth with various hydraulic loading conditions (i.e. FC1, FC2, FC3). (b) Universality of infiltration depth with various size ratios from $R = 5$ to $R = 10$.

UPSCALING THE MECHANICAL PROPERTIES OF ROCK MICROSTRUCTURES DURING CYCLIC LOADING WITH DIGITAL ROCK PHYSICS

***S. Zwarts*[1], *H. Hajibeygi*[1] *and M. Lesueur*[1]**

[1] *Faculty of Civil Engineering and Geosciences, Delft University of Technology, Netherlands*

Abstract

Hydrogen, a promising vector for clean and renewable energy, can be produced emission-free using green energy sources, sidestepping carbon-based fuel influence. However, hydrogen requires large volume storage due to its lower energy density [1]. To address this, underground storage in depleted gas or oil fields, salt caverns and depleted aquifers are being studied.

This underground storage approach, vital for balancing the supply and demand of energy, introduces cyclic loading to the underground storage facilities. With the surplus of clean energy, hydrogen is produced which is stored underground. When the demand exceeds the supply of clean energy, the hydrogen can be withdrawn, leading to the cyclic loading on the rock formations.

Multiple studies have investigated the mechanical effects of cyclic loading on rocks. The cyclic deformation can be described in three distinguishable stages, as shown in Fig. 1: an initial stage (I) in which the pre-existing voids and gaps are closed, a steady stage (II) in which plasticity and time-dependent strains develop and an acceleration stage (III) in which the strain accelerates towards fatigue failure.

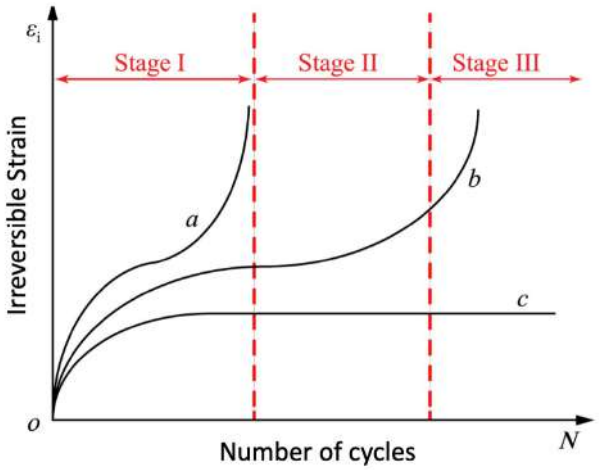

Figure 1. The irreversible strain of different rock types (curve a is correlated with brittle rocks, curve c is correlated with hard rocks and curve b falls inbetween those rock types). Taken from [2].

The deformation of rocks under cyclic loading has been described on macroscopic level, using various constitutive relationships for creep including damage parameters (e.g. [3]; [4]). Studies of cyclic loading of rocks at the micro-scale remain scarce. However, Fig. 1 illustrates well that the rock's microstructural characteristic is important to consider for the resulting mechanical behaviour. Therefore, a broader understanding of the effects of cyclic loading on a rock's microstructure is required to be able to upscale the appropriate parameters for the macroscopic constitutive creep relationship.

This study sets out to model the mechanical influence of cyclic loading on rock microstructures. The mechanical properties are upscaled during cycling loading from a digital rock physics framework.

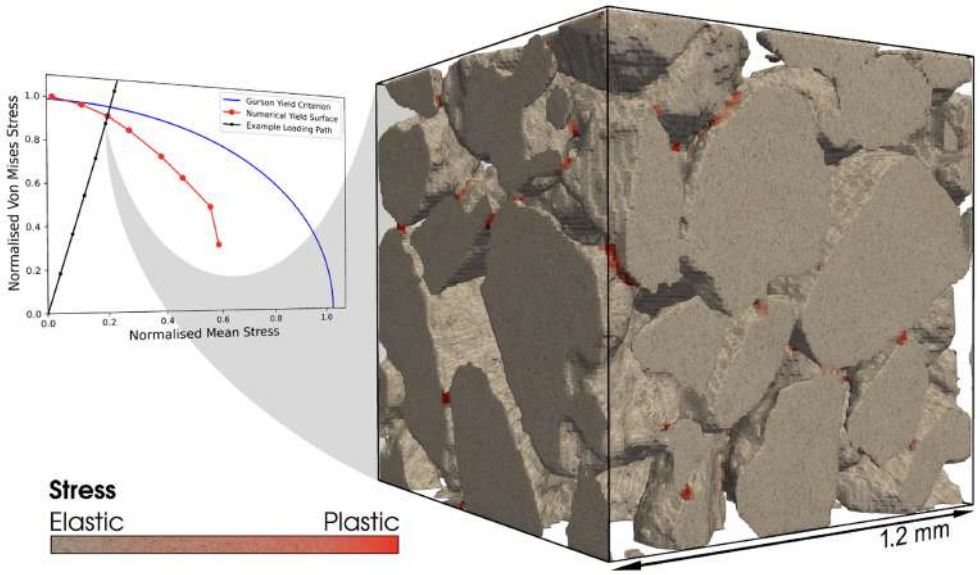

Figure 2. The plastic distribution of a digitalized rock microstructure from one point of the yield envelope, taken from [5].

To investigate the impact of cyclic loading on the mechanical properties, we conduct numerical Finite Element Method simulations on digitised rock microstructures. This method provides enhanced flexibility in addressing the multi-physics involved in underground hydrogen storage. Our simulations focus on cyclic compression tests applied to the microstructure, exploring elastic, plastic, and viscoplastic variants of the model to comprehensively assess the mechanical response. The results of these models are upscaled, and compared with the evolution of the irreversible strain development of real-life experiments.

References

[1] Reitenbach, V., Ganzer, L., Albrecht, D., and Hagemann, B. (2015). Influence of added hydrogen on underground gas storage: a review of key issues. *Environmental Earth Sciences*, **73**, 6927–6937.

[2] Liu, Y. and Dai, F. (2021). A review of experimental and theoretical research on the deformation and failure behavior of rocks subjected to cyclic loading. *Journal of Rock Mechanics and Geotechnical Engineering*, **13**, 1203–1230.

[3] Weng, M.-C. (2013). A generalized plasticity-based model for sandstone considering time-dependent behavior and wetting deterioration. *Rock Mechanics and Rock Engineering*, **47**, 1197–1209.

[4] Wang, J., Zhang, Q., Song, Z., Feng, S., and Zhang, Y. (2022). Nonlinear creep model of salt rock used for displacement prediction of salt cavern gas storage. *Journal of Energy Storage*, **48**, 103951.

[5] Lesueur, M., Poulet, T., and Veveakis, M. (2020). Three-scale multiphysics finite element framework modelling fault reactivation. *Computer Methods in Applied Mechanics and Engineering*, **365**, 112988.

Advances in numerical methods

Continuum modelling

A FULLY-COUPLED FLOW-DEFORMATION SPH FRAMEWORK FOR UNSATURATED SOILS

Yanjian Lian[1], Ha H. Bui[1], and Giang G. Nguyen[2]
[1] Monash Univ., Department of Civil Engineering MCG Lab., Melbourne, Australia
[2] The Univ. of Adelaide, School of Civil, Adelaide, Australia

Introduction

Rainfall-induced slope failures of unsaturated soil are common problems in geotechnical engineering applications. Despite significant research efforts in the past, the prediction of the entire slope failure process in unsaturated soils caused by transient seepage flow remains challenging. This paper will present a robust computational approach based on SPH to tackle these problems. The model is verified against a rainfall-induced slope failure, and the excellent agreements with the reference results are achieved, indicating that the proposed SPH framework can be readily applied to a wide range of field-scale application in rainfall-triggered failure problems.

1. Mathematics framework

1.1 Governing equations

The mathematical model is formulated following Biot's mixture theory, wherein the unsaturated soil is assumed to comprise three interconnected phases: air, water and solid phases. The governing equations for the system are subsequently established based on the ***u***-p (***u*****:** displacement, p: pore pressure) formulations and are solved using the latest SPH framework [1] developed by the authors. Within the SPH framework, the unsaturated porous mixture is represented by a single set of Lagrangian SPH particles, each of which carry all information of each phase.

1.2 SPH discretization of governing equations

The governing equations are expressed as the rates of change of porosity (n), hydraulic head (h) and solid-phase velocity ($\mathbf{v}_s$), respectively. Their SPH approximations can be written as follows:

$$\frac{d^s n_i}{dt} = \sum_{j=1}^{N} V_j \left(1 - n_j\right) \mathbf{v}_{ji}^s \widetilde{\nabla}_i W_{ij} \tag{1}$$

$$\frac{d^s h_i}{dt} = \frac{1}{\tilde{C}_{sr}} \left\{ \sum_{j=1}^{N} V_j \bar{k}_{mn}^{ji} H_{ji} \mathcal{D}^{mn} \tilde{F}_{ij} - E_{ij} - S_r^i \sum_{j=1}^{N} V_j \mathbf{v}_{ji}^s \widetilde{\nabla}_i W_{ij} + a \right\} \tag{2}$$

$$\left(\frac{d^s \mathbf{v}_s}{dt}\right)_i = \sum_{j=1}^{N} m_j \left(\frac{\boldsymbol{\sigma}_j}{\rho_j^2} + \frac{\boldsymbol{\sigma}_i}{\rho_i^2}\right) \nabla_i W_{ij} + \boldsymbol{C}_{ij} + \boldsymbol{b} \tag{3}$$

where $\widetilde{\nabla}_i W$ is the corrected first-derivative of the kernel function and $\boldsymbol{C}_{ij}$ stands the stabilisation term[1]. $\tilde{C}_{sr}$ is the specific storage term. $\boldsymbol{\sigma}$ stands for the total stress tensor, and in this paper, the suction-dependent Dracker-Prager strain softening model [2] is adopted to compute effective stress.

2. Large-scale rainfall-induced slope failure

A large-scale rainfall-induced slope failure experiment, as shown in Figure 1,is considered to demonstrate the capability of the proposed SPH model in predicting flow and large-deformation soil

behaviour in the unsaturated porous media The rainfall was applied from the top surface of the slope

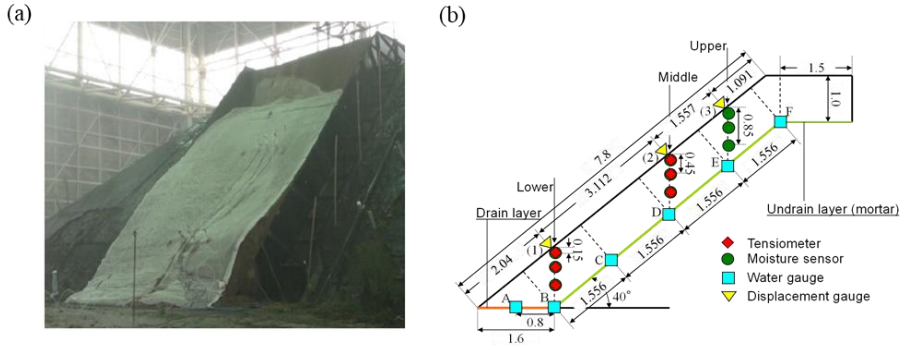

Figure 1. Problem geometry: a) Slope after failure and b) Initial setting condition

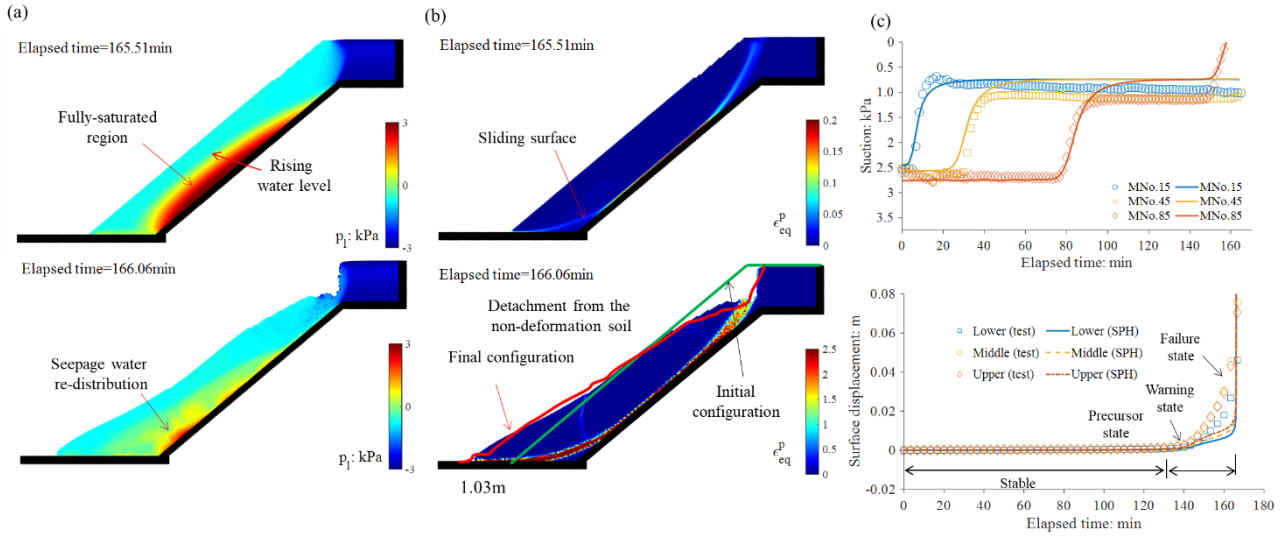

Figure 2. SPH predictions: a) Seepage flow, b) Deformation pattern, and c) Suction evolution.

which failed after around 164 minutes.The SPH results are shown in Figure 2, indicating that the SPH model captured well the hydraulic response in the slope, i.e., pore water pressure distribution in Figure 2(a). The failure response in terms of the equivelent plastic strain was also well predicted and comparable with the experiment, as shown in Figure 2(b). Finally, the evolution of suction within the slope and the surface displacement at several measuring points also match well with the experimental results, as shown in Figure 2(c). Therefore, it can conclude that the proposed coupled flow-deformation SPH framework predicts well rainfall-induced slope failure in unsaturated soils.

3. References

[1] H. H. Bui and G. D. Nguyen (2021). *Smoothed particle hydrodynamics (SPH) and its applications in geomechanics: From solid fracture to granular behaviour and multiphase flows in porous media*. *Comput Geotech*, vol. 138, no. July, p. 104315.

[2] A. Yerro, E. E. Alonso, and N. M. Pinyol (2015). *The material point method for unsaturated soils*. *Geotechnique*, vol. 65, no. 3, pp. 201–217

[3] Y. Lian, H. H. Bui, G. D. Nguyen, S. Zhao, and A. Haque (2022). *A computationally efficient SPH framework for unsaturated soils and its application to predicting the entire rainfall-induced slope failure process*. Geotechnique (in press), doi:10.1680/jgeot.21.00349.

A NEW NUMERICAL MODEL FOR THE ELASTO-PLASTIC BEHAVIOR OF CELLULAR MATERIALS

***Yohann Trivino*[1,3], *Vincent Richefeu*[2], *Farhang Radjai*[3], *Komlanvi Lampoh*[1] *and Jean-Yves Delenne*[1]**

[1] *IATE, Univ. Montpellier, INRAE, Institut Agro, Montpellier, France*

[2] *Laboratoire 3SR, Univ. Grenoble Alpes, France*

[3] *LMGC, Univ. Montpellier, CNRS, Montpellier, France*

1. Introduction

Soft particle systems encompass various materials, including plant tissues, hydrogels, colloids, and emulsions. These materials share the common ability to undergo significant deformation under the influence of external or internal forces. The study of these materials is of crucial importance, providing opportunities for creating innovative materials with engineered properties, potentially applicable in fields such as medicine, cosmetics, energy, and sustainable technologies.

The Discrete Element Method (DEM) proves indispensable in simulating granular systems, spanning granular materials, suspended particles, and moving particles in fluid media. However, the particles in DEM are perfectly rigid. In this context, we present a model based on DEM but with surface degrees of freedom, allowing thereby simulating deformable particles. The model relies on a set of equations describing the motion of surface elements in two-dimensional space. This model can be used to explore the dynamics not only of plant cell tissues and other soft particle materials.

2. Core of the Model

The model represents the surface of the particles by a set of mass points. These mass points are structured into open or closed cells, forming a network with a given 'wall' thickness ϕ. Cells are composed of interconnected vertices, each designated by a pair of indices i, k where i is the cell number and k is the local vertex number. The base element is a vertex with a mass, integrated over time using an approach similar to DEM. Bars are represented as springs and nodes as linear angular springs; see Fig. 1.

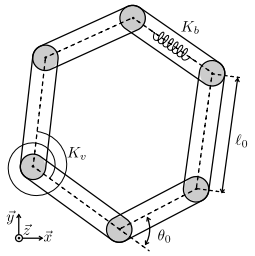

Figure 1. Representation of a cell

We also account for cell internal pressure, which enables the simulation of fluid pore pressure within cells. It is represented by an isotropic pressure depending on the cell volume and a compressibility modulus. Interaction forces between cells consider interactions solely among nodes and bars, distinguishing between the ends and the body of the bars.

Node mass is distributed at the vertex level, depending on the chosen algorithm. The mass density within the inner area of the bars or cells can be varied. The mass of a node is calculated as a

function of the homogeneous density ρ and the initial length of the bars. For simplicity, the total mass of the sample can be divided by the number of nodes. A critical time step is defined as a function of the minimum mass and maximum stiffness of the system.

The approach uses an analogy with classical beam theory to calibrate the elastic parameters. Hooke's law is used for bars, and parameters are derived for beams and nodes. Tensile plastification is assumed beyond a yield threshold σ^{Y}. In an isotropic compression test, resistance is due to the inner cell and bar stiffness. The modulus of compressibility is broken down into contributions from the cell interior and bar stiffness. A relationship between the angular threshold moment (M^Y) and the modulus of compressibility is established.

3. Mechanical behavior

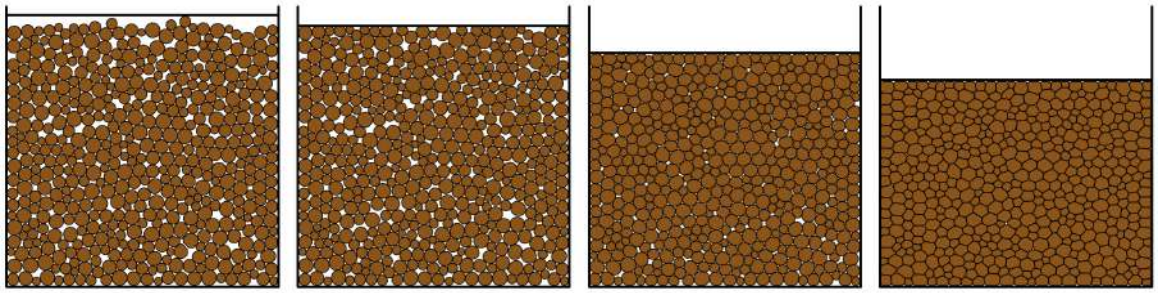

Figure 2. Uniaxial compaction simulation of a packing of soft particles.

Uniaxial compaction tests are used to assess the mechanical behavior of a packing composed of deformable particles under vertical loads; see Fig. 2. Simulations with different conditions of internal pressure, threshold moment and compressibility modulus are carried out. Compression/consolidation curves show the relationship between applied stress and deformation. Particle curvature distributions are calculated during compaction and used to characterize the elastic and plastic components of the deformation. Distinct behaviors are observed depending on the values of system parameters as shown in Fig. 3.

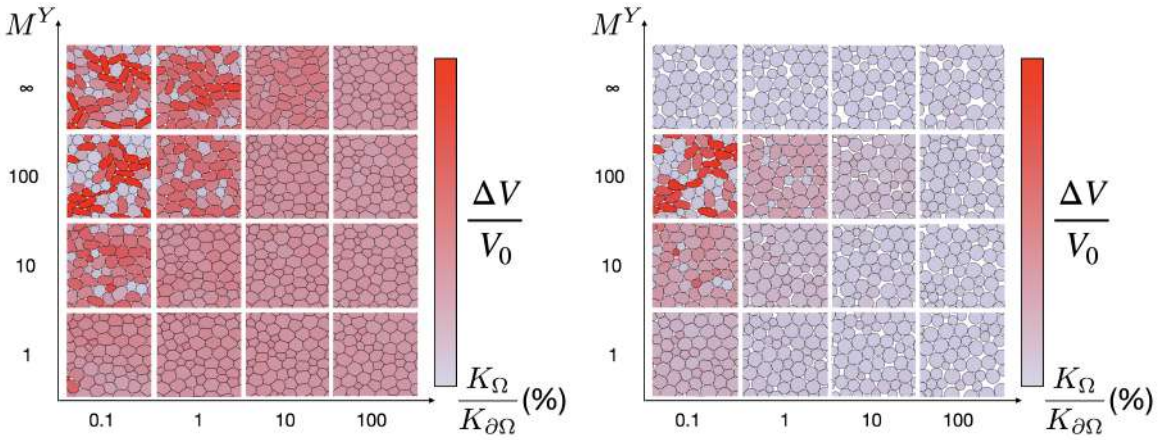

Figure 3. Snapshots of soft particles as a function of yield moment and bulk modulus in two states: the maximum compression state (left) and the unloaded state (right). The color level is proportional to the average volumetric strain.

A CONSTITUTIVE INVESTIGATION OF THE EFFECTS OF STRUCTURE ON LOESS

Runkang Zhao[1,2], Shima Atashgahi[2], Fangzhou Liu[2]
[1] Beihang University, School of Transportation Science and Engineering, Beijing, China
[2] University of Alberta, Department of Civil and Environmental Engineering, Edmonton, Canada

1. Introduction

Static liquefaction is characterized by a sudden loss of strength with large strain and excess pore pressure development under monotonic loading. Flowslides in the Chinese loess have been attributed to static liquefaction associated with the meta-stable structure [1] but it is challenging to fully capture the effects of such a meta-stable structure on the onset of flow instability. The conventional isotropically consolidated undrained (CIU) triaxial tests conducted on the silty loess indicated two separate critical state lines associated with the intact (CSL_i) and reconstituted (CSL_r) specimens in the e-lnp' plane [2], [3]. While the tests confirm the effects of structure on loess, it is impractical to directly assess the effects on the critical state parameters of loess experimentally (i.e., under the same ψ for intact and reconstituted specimens). Previous attempt to quantify such effects was conducted using the *NorSand* model [4]; however, the study treated the intact and reconstituted loess as two different materials to reflect such effects of structure. In this study, a more advanced constitutive model is employed to quantify the effects of structure on loess using the more recent triaxial datasets.

2. Unified Hardening Model for Clays and Sands (CSUM)

The Unified Hardening Model for Clays and Sands (CSUH) [5] is used in this study. The CSUH model includes a reference yield surface and a current yield surface to consider the stress history of soils. The reference yield surface ($\bar{f}$) and the hardening parameter (i.e., the plastic volumetric strain ε_v^p) can be expressed as:

$$\bar{f} = \frac{(1+\chi)\bar{q}^2}{M^2\bar{p}^2 - \chi\bar{q}^2} + 1 - \frac{\overline{p}_x}{\bar{p}} = 0 \tag{1}$$

$$p_s = \exp\left(\frac{N-Z}{\lambda}\right) - 1 \tag{2}$$

where $\bar{p}$ indicates the mean effective stress, $\bar{q}$ is deviator stress ('-' denotes to the variables associated with the reference yield surface), e_0 is the initial void ratio, χ is a control parameter for the shape of the yield surfaces, M is critical state stress ratio, λ is the slop of asymptotic line on the e-ln$p$ plane, κ is slop of the unloading line on the e-ln$p$ plane, and $\overline{p}_x$ is intersection of the reference yield surface with the p-axis. Z is the starting point of the normal compression line (NCL) and N is the intercept of the NCL asymptotic line, reflecting the effects of structure.

3. Results and Interpretation

The undrained triaxial results of the silty HFT loess [2] are used to calibrate the CSUH model, which requires 8 model parameters for the curved CSL_i and CSL_r. Fig. 1 compares the results of the undrained stress-strain responses of the intact and reconstituted HFT loess; the model captures the intense strain-softening behaviours and sharp increases of pore-water pressure and more importantly, the offset of the curved CSL_i and CSL_r that varies from low stress levels (d = 0.008 at p' = 10 kPa) with a smooth transition to the linear portion of the CSLs at high stress level (d = 0.065 when p' >

200 kPa) on the e-lnp' plane. Both contractive and dilative behaviours of the reconstituted specimens were captured by the CSUH model.

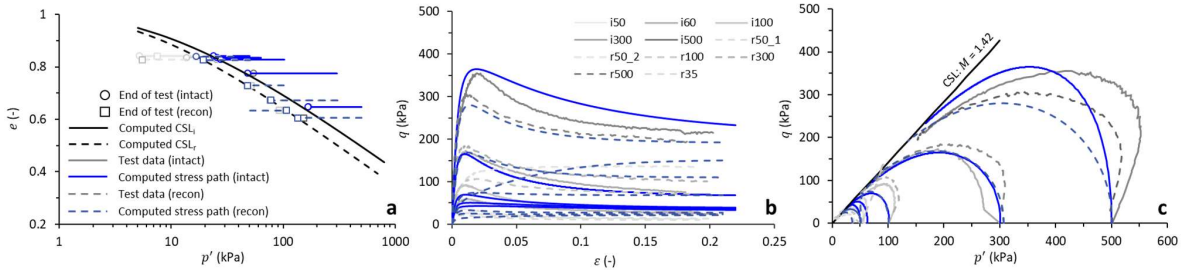

Figure 1. Simulations of undrained monotonic triaxial tests for intact and reconstituted HFT loess: (a) CSLs and the start-to-end points; (b) stress and axial strain responses; (c) undrained stress paths.

Fig. 2 compares the stress paths of HFT loess at its intact and reconstituted states with the same ψ_m, assuming the reconstituted sample precludes the effect of structure. The undrained peak strength of intact loess is slightly higher than its reconstituted state but with a lower post-peak strength, which highlights the effects of structure on the brittle response. This is also reflected by the q_{CS}/q_{max} ratio in Fig. 4c, in which the difference between the intact and reconstituted sample decreases with an increasing p'_0, suggesting a decreasing effect of structure with increasing stress.

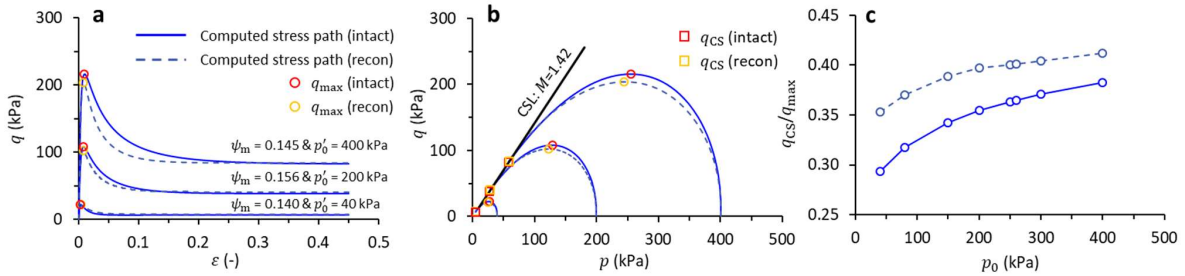

Figure 2. Simulations of undrained monotonic triaxial tests for intact and reconstituted HFT loess: (a) CSLs and the start-to-end points; (b) stress and axial strain responses; (c) undrained stress paths.

5. References

[1] F. Zhang, C. Kang, D. Chan, X. Zhang, X. Pei, and J. Peng, 'A study of a flowslide with significant entrainment in loess areas in China', *Earth Surface Processes and Landforms*, vol. 42, no. 14, pp. 2295–2305, 2017, doi: 10.1002/esp.4184.

[2] F. Liu, Q. Xu, Y. Zhang, J. D. Frost, and X. Zhang, 'State-dependent flow instability of a silty loess', *Géotechnique Letters*, vol. 9, no. 1, pp. 22–27, 2019.

[3] L. Xu, M. R. Coop, M. S. Zhang, and G. Wang, 'The mechanics of a saturated silty loess and implications for landslides', *Engineering Geology*, vol. 236, no. 5, pp. 29–42, 2018.

[4] F. Liu, J. Frost, J. Macedo, and Q. Xu, 'Effects of structure on the mechanical behavior of loess: implications for flowslides in cemented soils', in *Proceedings of the 73rd Canadian Geotechnical Conference (GeoVirtual 2020)*, 2020.

[5] Y.-P. Yao, L. Liu, T. Luo, Y. Tian, and J.-M. Zhang, 'Unified hardening (UH) model for clays and sands', *Computers and Geotechnics*, vol. 110, pp. 326–343, 2019.

A TWO-SCALE NUMERICAL MODELLING OF TIME-DEPENDENT MECHANICAL BEHAVIOUR OF CALLOVO-OXFORDIAN CLAYSTONE

Yufeng. SUN[1], Benoît PARDOEN[1] and Henry K.K. WONG[1]
[1] University of Lyon, ENTPE, LTDS, France

Abstract

In the context of underground works drilled in rock, their long-term behaviour and stability are conditioned by the time-dependent behaviour of the surrounding rock [1]. Considering clay rocks, and due to their relatively high clay mineral content [2], there is a necessity of accurately modelling the delayed viscous behaviour and creep strain of the rock. The complex microstructure and multiscale structure, with multiple characteristic lengths, of clay rocks and shales has led to the inclusion of small-scale constitutive behaviour in large-scale modelling [3,4,5,6]. This study introduces a micro-mechanics based elastoplastic and viscoplastic behaviour of the clay matrix to describe the instantaneous and time-dependent mechanical behaviour of clayey rock. The latter is considered within a two-scale finite element framework (FEMxFEM or FE²), by computational homogenisation [3]. The non-homogeneous rock is represented at the microscale as a composite material consisting of rigid elastic mineral inclusions (quartz, calcite, and pyrite) embedded in a clay matrix. To describe the damage and failure modes at small scale, interfaces between different mineral phases and within the clay matrix are considered as potential microcracks [3,4]. They are modelled by a damaged cohesive model. The microstructures of the clayey rock are generated in 2D representative elementary areas (REAs) (with 2D random Voronoi tessellation) in which several microscale morphological (elongation, orientation, granulometry, and size of mineral inclusions) and physical characteristics of the rock are numerically described [4]. The viscoplastic constitutive law for the clay matrix is an extension of Lemaitre's creep model [7] incorporating mean stress-dependency and a non-associated flow rule. Then, the overall microscale behaviour of the clay rock under mechanical solicitation is numerically obtained from equilibrated elementary area (EA) configuration and computational homogenisation. The validity of the model is verified by comparing the model prediction results with experimental data on clayey rock [1] (Figure 1). Then, the creep model of COx claystone developed at small scale (micro and meso scales) is applied to model the large-scale creep behaviour at laboratory and gallery scales. At laboratory scale, a clear three-stage creep process is reproduced, including the primary creep stage, second creep stage, and tertiary creep stage. At the gallery scale, the long-term effect of viscosity on the gallery convergences, the evolution of EDZ, and the long-term drainage and pore pressure around a gallery are investigated. It is found that the developed multiscale model is able to provide valuable insights into the large-scale creep behaviour of clay rocks through the morphological and material small-scale characterisation (at micro and meso scales) of REA.

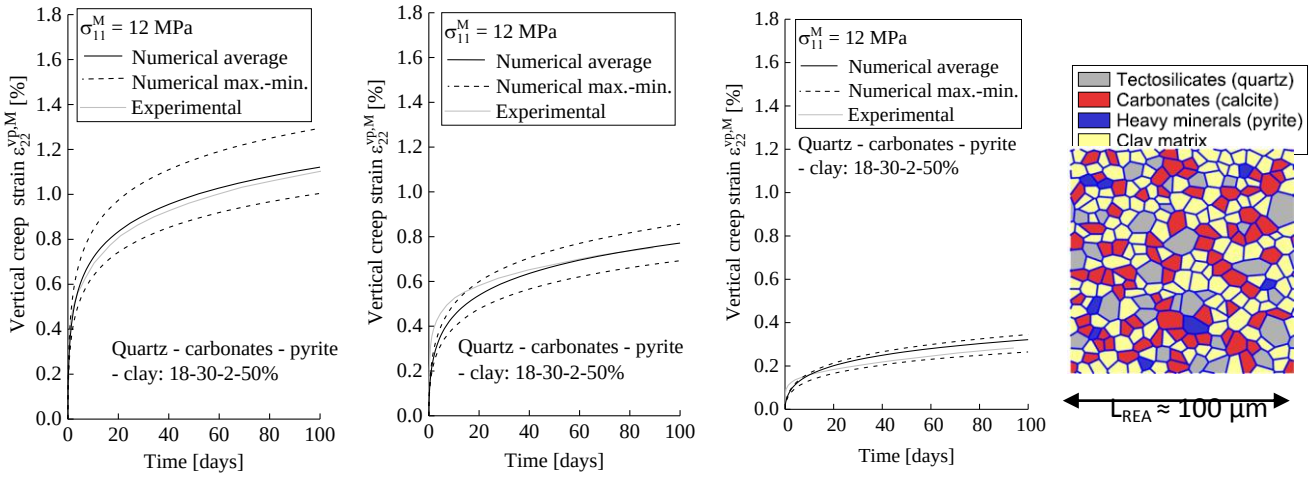

(a) 90% (b) 75% (c) 50% (d)

Figure 1. Variability of clay rock mechanical creep response at mesoscale during biaxial creep tests for three deviatoric stress levels q^M/q_{max} = (a) 90%, (b) 75%, (c) 50% of the maximum deviatoric stress q_{max} = 34.9 MPa, and (d) reference REA with average numerical creep material response.

References

[1] Armand, G., Conil, N., Talandier, J., Seyedi, D.M., (2017). Fundamental aspects of the hydromechanical behaviour of Callovo-Oxfordian claystone: From experimental studies to model calibration and validation. *Comput Geotech*., **85**:277-286.

[2] Robinet, J.C., Sardini, P., Coelho, D., et al., (2012). Effects of mineral distribution at mesoscopic scale on solute diffusion in a clay-rich rock: Example of the Callovo-Oxfordian mudstone (Bure, France), *Water Resour Res*., **48**:W05554.

[3] van den Eijnden, A.P., Bésuelle, P., Collin, F., Chambon, R., Desrues, J. (2017). Modeling the strain localization around an underground gallery with a hydro-mechanical double scale model; effect of anisotropy. *Comput Geotech*., **85**:384-400.

[4] Pardoen, B., Bésuelle, P., Dal Pont, S., et al., (2020). Accounting for small‐scale heterogeneity and variability of clay rock in homogenised numerical micromechanical response and microcracking. *Rock Mech Rock Eng*., **53(6)**:2727-2746.

[5] Abou-Chakra Guery, A., Cormery, F., Shao, J.F., Kondo, D., (2009). A multiscale modeling of damage and time-dependent behavior of cohesive rocks. *Int J Numer Anal Methods Geomech*., **33**:567–589.

[6] Zeng, T., Shao, J.F., Yao, Y., (2019). An upscaled model for elastoplastic behavior of the Callovo-Oxfordian argillite. *Comput Geotech*., **112**:81–92.

[7] Bui, T.A., Wong, H., Deleruyelle, F., et al., (2017). A thermodynamically consistent model accounting for viscoplastic creep and anisotropic damage in unsaturated rocks. *Int J Solids Struct*., **117**:26–38.

COUPLED TOTAL- AND SEMI-LAGRANGIAN PERIDYNAMICS FOR FLUID-DRIVEN FRACTURING

Changyi Yang[1], Jidong Zhao[1] and Fan Zhu[2]

[1] Department of Civil and Environmental Engineering, The Hong Kong University of Science and Technology, Hong Kong, China

[2] Department of Urban Management, Kyoto University, Kyoto

Abstract

This study introduces a fully coupled peridynamics method for simulating fluid-driven fracturing in solids. The proposed method establishes a rigorous coupling between the classical total-Lagrangian formulation and a novel semi-Lagrangian formulation within the peridynamics framework. The total-Lagrangian formulation represents the behavior of solid subjected to fluid-driven fracturing, while the semi-Lagrangian formulation effectively solves the non-local Navier-Stokes equations for fluid. To model fluid-solid interactions without introducing unphysical penetration, a coupling algorithm is developed between the two formulations. The effectiveness of the proposed method is demonstrated through extensive simulations conducted on a series of benchmark problems. Furthermore, its efficacy is showcased by successfully modeling a hydraulic fracturing problem in sandstone. The proposed method reliably captures crucial aspects such as the fracturing pattern, fracture propagation speed, and injection pressure, exhibiting good agreement with analytical solutions and experimental results. By offering a unified framework within the peridynamics theory, it provides a comprehensive approach for modeling solid, fluid, and fluid-driven fracturing processes.

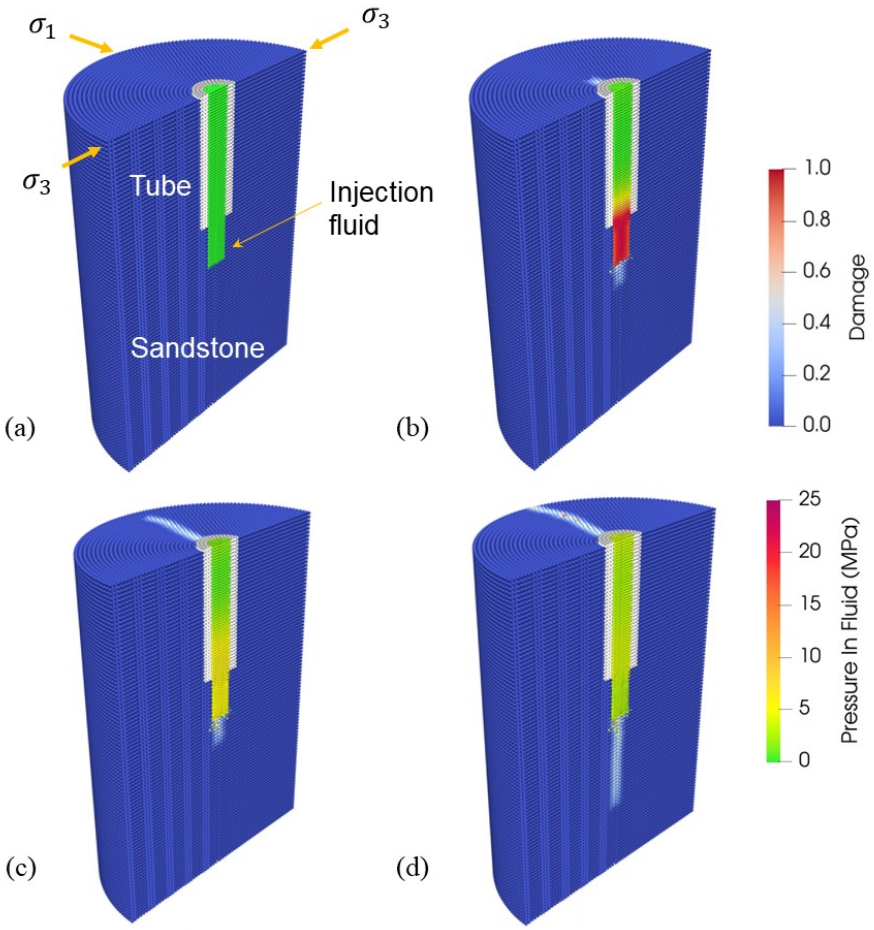

Figure 1. Evolution of fluid pressure and progress of fracture in the sandstone. (a) initial condition; (b) at step 2,000; (c) at step 4,000; (d) at step 8,000. The sandstone specimen is cut vertically at $x = 0$ for the purpose of presentation.

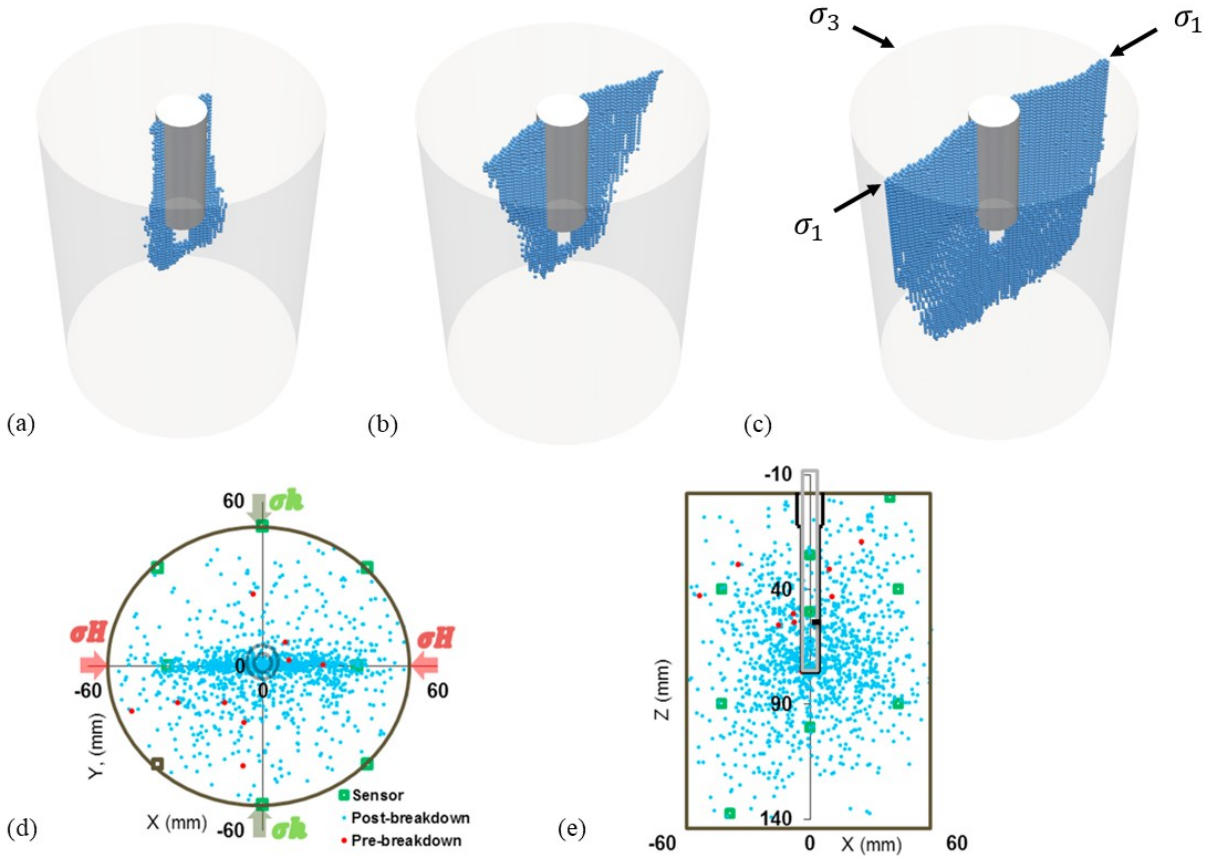

Figure 2. Interior view of the fracture surfaces in the sandstone: (a) at step 2,000; (b) at step 4,000; (c) at step 8,000; and acoustic emission events captured in experiment [4] in (d) top view; (e) side view.

References

[1] Yang, C., Zhu, F., & Zhao, J. (2024). Coupled total-and semi-Lagrangian peridynamics for modelling fluid-driven fracturing in solids. *Computer Methods in Applied Mechanics and Engineering*, 419, 116580.

[2] Bergel, G. L., & Li, S. (2016). The total and updated lagrangian formulations of state-based peridynamics. *Computational Mechanics*, *58*, 351-370.

[3] Zhu, F., & Zhao, J. (2021). Peridynamic modelling of blasting induced rock fractures. *Journal of the Mechanics and Physics of Solids*, *153*, 104469.

[4] Patel, S. M., Sondergeld, C. H., & Rai, C. S. (2017). Laboratory studies of hydraulic fracturing by cyclic injection. *International Journal of Rock Mechanics and Mining Sciences*, *95*, 8-15.

INVESTIGATING PARTICLE BREAKAGE BEHAVIOUR UNDER DIFFERENT CONTACT TOPOLOGIES USING μFE APPROACH

Bin Zhang and Sadegh Nadimi
School of Engineering, Newcastle University, Newcastle upon Tyne, NE1 7RU, UK

Keywords: particle breakage, contact topology, finite-discrete element method, cohesive interface elements

Summary: To have a better understanding of the contact topology and how it contributes to the breakage behaviour of irregular particles, this study adapts a micro finite element (μFE) model to simulate the single particle breakage under point loading. The model is first validated against an experimental test and then used for investigating the influence of contact area on breakage behaviour by altering the radius of contact curvature. The results are analysed in terms of force-displacement curve, fracture pattern and contact area.

1. Introduction

Particle breakage plays an important role in understanding the mechanical behaviour and revealing the failure modes of granular materials. In recent decades, a dedicated focus has been on modelling particle breakage using the Discrete Element Method with the assumption of spherical particles. When modelling the breakage of spherical particles, the initial contact area is invariably a point and evolves to a circle under compression. However, in natural particulate materials, the contact topologies arising from the irregular-shape particles make the numerical modelling non-trivial [1]. This study presents how the contact topology affects material fragmentation by using a numerical approach. It is an extension of μFE method proposed in [1] incorporating cohesive interface elements to gain the breaking capability [2]. By altering the radius of the rigid ball at the loading ends, various contact curvatures can be simulated. The model has been validated against the experiment and the simulation results in terms of force-displacement curve, fracture pattern and contact area have been recorded and analysed.

2. Methodology

Prior to numerical simulations, the particle shape obtained by μCT scan has been used to reconstruct the 3D particle. The cohesive interface elements (CIEs) have been utilized to simulate breakage behaviour. For the constitutive response of these elements, the traction-separation model has been adopted where the intermediate glue element is very thin and for practical purpose could be further considered as zero thickness. Thus, the particle's geometry remains unchanged after inserting CIEs, but the breakage behaviour can now be triggered by a damage initiation criterion and damage evolution law. By importing the enriched 3D particle mesh into the numerical solver (i.e. Abaqus), various loading conditions can be applied on the particle to assess the role of contact topology.

3. Simulations & results

First, the simulation results regarding the fracture pattern and force-displacement curve have been compared with the experimental data (Figure 1) obtained by Zhao et al. [3] using μCT. The plots

show an acceptable agreement between the simulation and experiment affirming the validation of the model.

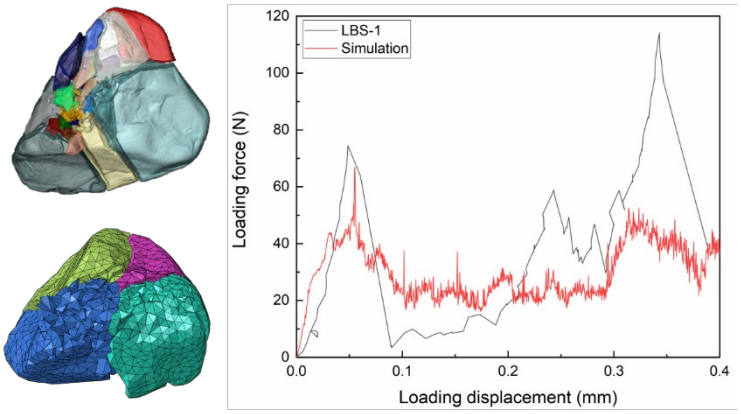

(a) (b)

Figure 1. (a) Fracture pattern from experiment and simulation, and (b) load-displacement curves.

The evolution of contact topology in terms of contact area and curvature has been investigated by altering the radius of loading balls. The simulation results including the force-displacement curve, fracture pattern and contact area have been recorded and analysed (see Figure 2). Two preliminary conclusions can be derived as follows:

1) A larger contact area leads to lower loading stiffness and higher crushing force;
2) A larger contact area contributes to splitting failure versus smaller contact area causing local crush at the loading ends.

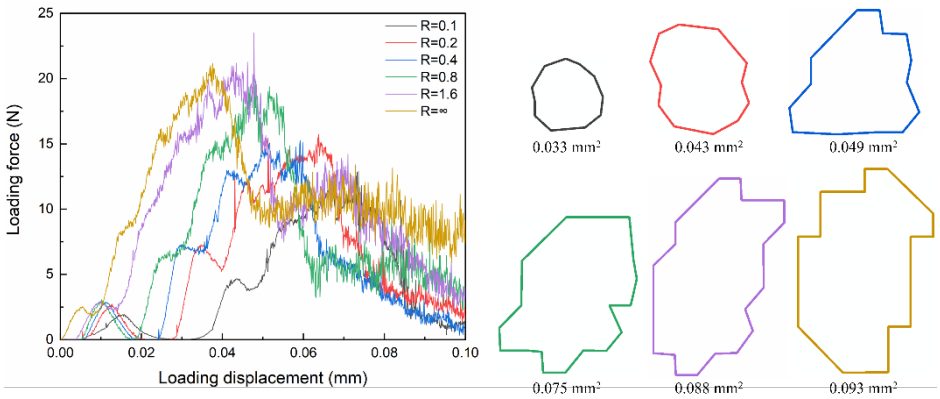

(a) (b)

Figure 2. (a) Load-displacement curves using different contact topologies and (b) colour coded contact area when the major fracture occurs.

References

[1] Nadimi, S., & Fonseca, J. (2018). A micro finite-element model for soil behaviour. *Géotechnique*, **68**(4), 290-302.

[2] Zhang, B., Nadimi, S., Eissa, A., & Rouainia, M. (2023). Modelling fracturing process using cohesive interface elements: theoretical verification and experimental validation. *Construction and Building Materials*, **365**, 130132.

[3] Zhao, B., Wang, J., Coop, M. R., Viggiani, G., & Jiang, M. (2015). An investigation of single sand particle fracture using X-ray micro-tomography. *Géotechnique*, **65**(8), 625-641.

Influence of Rock Microstructure on the Homogenisation of Mechanical Yield Strength

M. Lesueur[1], H. Rattez[2], I. Rocha[1] and W. Lindqwister[1]
[1] Delft University of Technology, Fac. of Civil Engineering and Geosciences, Delft, Netherlands
[2] Université catholique de Louvain, Institute of Mechanics, Materials and Civil Engineering, Louvain-la-Neuve, Belgium

For any concerns of safe subsurface operations, mechanical yield strength can be considered the most important material property to evaluate, a threshold not to cross to prevent plastic deformations to occur. It has been established early on that rock strength depends strongly on its microstructure. Most logically, the more porous the rock, the weaker it is. In a more rigorous manner, Gurson (1977)[1] linked through a semi-analytical relationship the compaction cap of the yield surface with the porosity. However, a more generic framework to upscale for the yield strength of porous rocks has been missing ever since. Therefore, a more profound understanding of the influence of the microstructure on rock strength is lacking. For example, it can easily be shown that two different microstructures with the same porosity can achieve different strengths. As such, more morphological parameters of the microstructure need to be taken into account to describe rock strength.

In this contribution we present a Digital Rock Physics framework to upscale yield strength from microCT-scan images of rocks (Figure 1). The simulator implements 3D semi-discrete Finite Element elasto-plasticity. As a result, more features of the yield surface were attributed to the microstructure. Investigating further, the simulator was used to generate a database[2] of computed strength for microstructures of various rocks, characterised by an extensive list of their morphological parameters. With machine learning (Gaussian Processes with anisotropic kernels for Automatic Relevance Determination or Polynomial Chaos Expansion), we show that material's strength could be explained mostly by the Minkowski Functionals of the microstructure but some minor morphological parameters, for example linked to the anisotropy of the microstructure, remain influential.

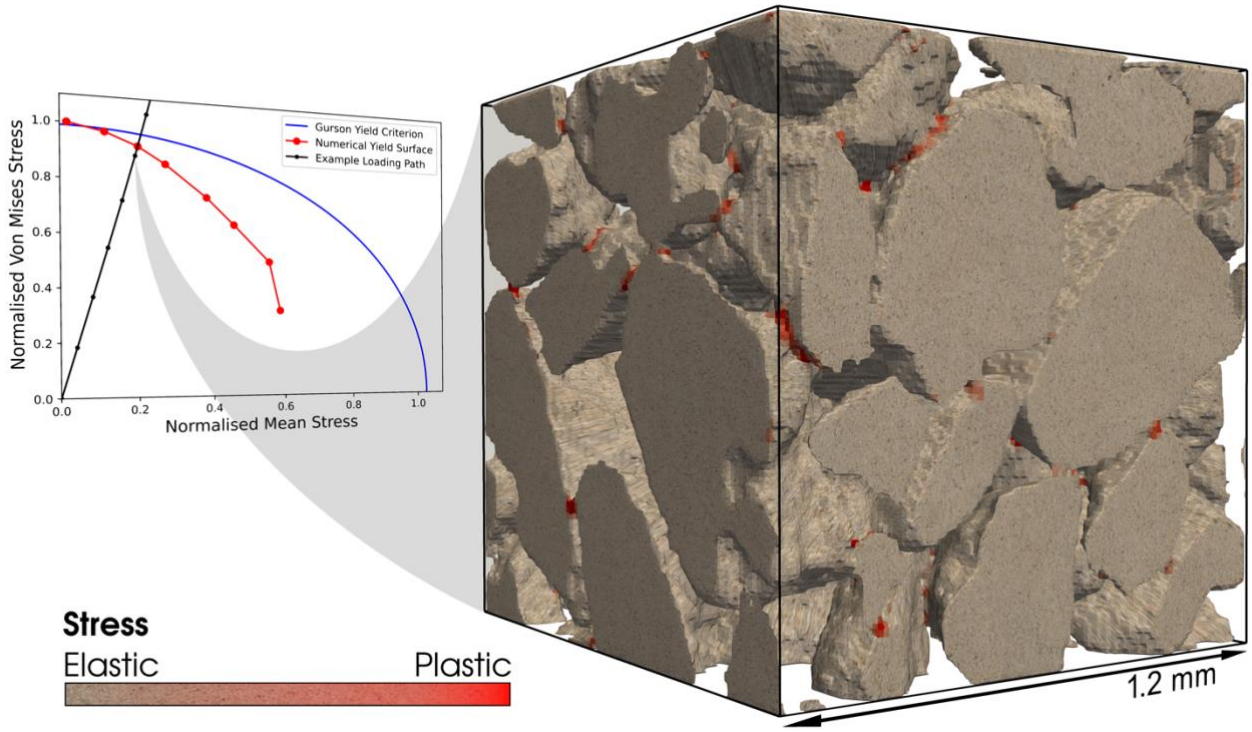

Figure 1. Plasticity distribution of a digital rock from one point of the yield envelope, taken from[3].

References

[1] A.L. Gurson. Continuum theory of ductile rupture by void nucleation and growth: Part I—yield criteria and flow rules for porous ductile media. Journal of Engineering Materials and Technology. 99: 2–15, 1977.

[2] J. Peloquin and W. Lindqwister. Neural network architecture and training data for prediction of porous material mechanical properties based on their microstructure. Mendeley Data. V1, 2023.

[3] M. Lesueur. Plasticity Distribution of Digital Rock from One Point of the Yield Envelope. Album of Porous Media: Structure and Dynamics. 2023

MICROSCOPIC COSIDERATIONS ON SUFFUSION FOR A CONTINUUM MECHANICAL DESCRIPTION

S. Buscher[1] and E. Perau[1]
[1] Univ. Duisburg-Essen, Fac. of Civil Engineering, Essen, Germany

1. Motivation

Suffusion is a special kind of internal erosion and regards the detachment, transport and attachment of small soil particles from the grain skeleton due to groundwater flow. This process leads to a creeping but durable change of permeabilities in geotechnical constructions such as dikes and dams. Moreover, it may lead to a continuously degradation of the strength of the soil. That may have a significant impact on the stability and could lead to a catastrophic dam failure, as seen in the dam breach in Brazil in 2019 [5]. A microscopic view on suffusion and drawing of conclusions for a continuum mechanical approach is topic of this presentation.

2. Conception and strategy

Firstly, some existing models for describing internal erosion, especially suffusion, will be listed and discussed. One major advance is to understand the interactions between the constituents of the soil, which could be seen in the grain skeleton, the pore water and the fine particles which can move in the pore channels of the grain skeleton.

Existing models, like [4, 7] already incorporate macroscopic parameters such as permeability of the skeleton, viscosities of fluid and suspensions, as well as volume fractions. These models regard only an advective transport of particles with the pore fluid through the grain skeleton. However, experiments [2] show that the movement of pore fluid and particles does not always happen simultaneously. Moreover, a simple microscopic consideration yields that no particle movement occurs above a certain particle diameter. If particles are larger than the continuous pore channels they cannot move, even under high hydraulic gradients. To overcome these deficits, the authors are working on a novel approach to describe particle-laden flow through porous media – following the approach by Vardoulakis [6], who incorporated microscopic effects in his equations.

In the presented project, a continuum mechanical model is developed based on the Theory of Porous Media (TPM) with individual states of motion of all constituents. The simplest considered model consists of three constituents with exchange of masses and momentums between them. Beyond that, the grain skeleton is assumed to be non-deformable. The interaction forces between the constituents, sometimes called ‘drag forces’, depend on the relative velocities and a proportional factor, called ‘resistivity’ [3]. Consequently, for three constituents three velocities, relative velocities and thus three resistivities have to be defined. Formulas for these resistivities can be derived from microscopical investigations on suffusion.

3. From Micro to Macro

Developing a novel continuum mechanical approach for suffusion, the main task was to formulate mathematical relations between different macroscopic physical variables. The following section presents selected aspects of suffusion and how suggestions and ideas are gained from microscopic considerations.

As a first example, Stokes' law for drag forces provide a microscopic approach for the interaction of momentum between the particles and the pore water. Here, a linear relation between forces and the relative velocity of the respective constituents is indicated. This is only valid for a perfect cylindrical pore channel and few non-interacting particles. It is also restricted to low Reynolds numbers [2], which suggests a non-linearity at high relative velocities. Stokes' law also leads to an insight of the role of the particle size. With increasing particle diameter, the drag force between particles and fluid becomes less dominant and the velocity difference between fluid and particles increases. In contrast, a small particle diameter in groundwater flow generates relative high volume specific interaction forces. As is well known, this phenomenon is utilized for sedimentation testing.

Another interaction mentioned here is the one between fluidized particles and grain skeleton. The pore space of the grain skeleton is defined by the tortuosity, fractured shapes of grains and pore diameter. As previously mentioned, the restriction of the grain skeleton against the particle movement has to be considered. One solution is to include a quotient in the resistivities that relates the diameters of particles and pores. Since the pore geometry is not easily measurable and changes during suffusion, a function for the pore diameter is formulated depending on the grain size distribution.

Further influences on the interaction forces originate from the interaction of a large number of particles transported by the pore fluid and the coarseness of the particles. Also, the transport of particles by dispersion is an important phenomenon. Again, a micromechanical view on the phenomena can help to formulate constitutive equations to describe suffusion.

4. Results

The novel continuum mechanical model for suffusion includes considerations on microscopic phenomena between three constituents grain skeleton, pore water and fine particles. In a special case, when particles are missing, the model is reduced to the classical equations like the well-known continuity equation and Darcy's law.

An important role in the new suffusion model is taken by the interaction forces between the constituents, which had been derived on microscopic motivated ideas. Relative movement between all constituents is regarded. Analytical results for special cases show the plausibility of the newly defined resistivity functions.

5. References

[1] Ke, L. and Takahashi, A. (2014). Experimental investigations on suffusion characteristics and its mechanical consequences on saturated cohesionless soil. *Soils and Foundations*, **54**, 713–730.

[2] Oertel, H. (2010). *Prandtl-Essentials of Fluid Mechanics.* Springer New York, New York, USA.

[3] Raats, P. A. C. (1968). Forces acting upon the solid phase of a porous medium. *J. Appl. Math. Phys.*, **19**, 606–613.

[4] Schaufler, A., Becker, C. and Steeb, H. (2012). Infiltration processes in cohesionless soils. *Z. angew. Math. Mech.*, **93**, 138–146.

[5] Silva Rotta, L. H., Alcântara, E., Park, E., Negri, R. G., Lin, Y. N., Bernardo, N., Mendes, T. S. G., Souza Filho, C. R. (2020). The 2019 Brumadinho tailings dam collapse: Possible cause and impacts of the worst human and environmental disaster in Brazil. *Int. J. Appl. Earth Obs. Geoinformation*, **90**, 102119.

[6] Vardoulakis, I. (2004). Fluidisation in artesian flow conditions. Hydromechanically unstable granular media. *Géotechnique*, **54**, 165–177.

[7] Yang, J. and Yin, Z.-Y. (2019). Modeling coupled erosion and filtration of fine particles in granular media. *Acta Geotech.*, **14**, 1615–1627.

MICROMECHANICAL MODELLING OF THE NORMAL CONTACT RESPONSE OF LEIGHTON BUZZARD QUARTZ SAND

V. Nardelli[1] and J. Bingham[2]

[1] University of Oxford, Department of Engineering Science, Oxford, United Kingdom

[2] Buro Happold Engineers Ltd., London, United Kingdom. Formerly University of Oxford, Department of Engineering Science, Oxford, United Kingdom

1. Abstract

In the last few decades, a significant number of research projects were developed in order to provide real data and results for the modelling of granular materials at the micro-scale. The earliest experimental projects in this field were carried out for either studying the breakage response of individual grains or determining the coefficient of inter-particle friction at the contact between particles. More recent research has been developed for studying the force-displacement relationships at the contact between particles, in order to verify the applicability of the existing contact laws, which were developed for ideal materials (e.g., Hertz [1]), to real soil particles. The comparisons between the theoretical and experimental results have shown some discrepancies [2], considering that soil particles have properties and features often different from those of ideal materials and their contact behaviour is affected by aspects that cannot be easily taken into account (Fig. 1). In fact, surface and mechanical features of natural soil particles are highly variable and depend on the geological history of materials, which might be relatively complex and difficult to replicate computationally.

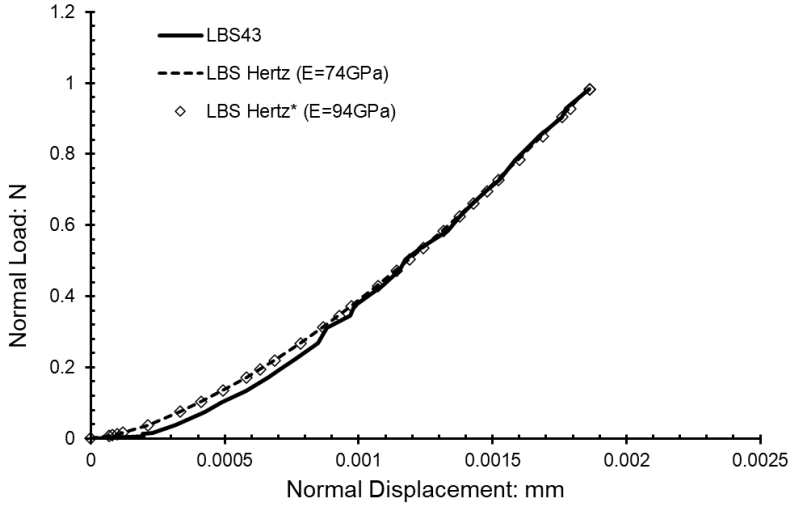

Figure 1. Comparisons between the normal loading tests LBS43 and the theoretical curves obtained from the classical Hertz theory [1] and including surface roughness (*, [2]).

Previous research studies have tried to adopt analytical models to fit the experimental results obtained in the laboratory for real soil particles tested under normal loading [2, 3], however, except for a limited number of cases, the models available in the literature do not offer a high degree of precision for this scope. In most cases, the mechanical properties (e.g., Young's modulus) required for a good curve fitting are lower than those found in the literature and the trend of the force-displacement curves is not always well captured, especially under low loads (below 1N). Some

studies [2] have also adopted more sophisticated contact models, including the effect of surface roughness into the traditional Hertz model [4], which enabled the use of material parameters closer to the real ones for a reasonable curve fitting, but did not always provide a very realistic trend for the modelling of the normal contact response (Fig. 1).

This research work has aimed at replicating the normal contact response of real sand particles by means of two elastic-plastic models developed in Abaqus, by means of the Finite Element Method (FEM). Leighton Buzzard quartz sand (LBS) has been chosen as a reference material and data from laboratory tests obtained by [2] were considered as a reference. The models developed consider the assumption that sand particles are constituted by a core, having the mechanical properties of the bulk mineral (i.e., Young's modulus and Poisson's ratio), surrounded by an outer soft layer, which represents the rough surface of the sand particle. The thickness of the outer layer was chosen to be within the typical range determined for LBS using the optical interferometer, and the hardness of the material was taken into account for the modelling of this layer. Two different models were developed, one in 2D considering the mean diameter of the individual particles in contact, and another in 3D where the individual particles were modelled as ellipsoids, considering the effect of particle shape on the contact response (Fig. 2). The particle dimensions in both models were obtained from the diameters of the real particles tested determined along the three principal axes.

The results show that, taking into account realistic surface and bulk properties of the material, an improved curve fitting of the experimental results can be obtained, in particular modelling the particles as ellipsoids.

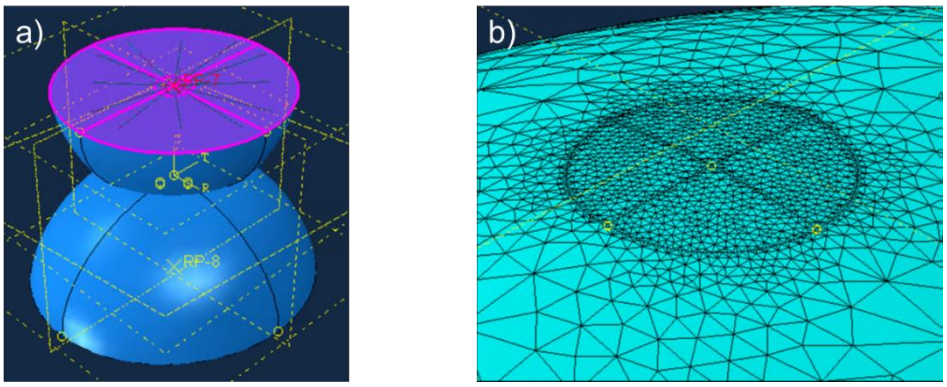

Figure 2. 3D FEM model for the normal contact response: a) geometry of the particles in contact; b) mesh adopted for one particle in the area containing the contact location.

2. References

[1] Hertz, H. (1882). Über die Berührung fester elastischer Körper. J. Reine und Angewandte Mathematik 92, 156–171 (in German).

[2] Nardelli, V., and Coop, M.R. (2019). The experimental contact behaviour of natural sands: normal and tangential loading. Géotechnique, **69** No. 8, 672–686.

[3] Altuhafi, F., Baudet, B.A. and Coop, M.R. (2023). An investigation of the applicability of contact models to the normal load-deformation behaviour of artificially shaped granite. Acta Geotechnica, published ahead of print.

[4] Greenwood, J. A., Johnson, K. L. & Matsubara, E. (1984). A surface roughness parameter in Hertz contact. Wear, **100**, No. 1–3, 47–57.

Modelling the thermo-hydromechanical behaviour of argillaceous rocks with FEM2

N. Zalamea[1], P. Bésuelle[1] , S. Dal Pont[1]and A. Di Donna[1]
[1] Univ. Grenoble Alpes, CNRS, 3SR Lab., Grenoble, France

1. Abstract

The study of argillaceous rocks is experiencing increased interest due to its potential as host rock for nuclear waste disposal facilities. Low permeability and self-sealing capabilities mitigate the risk of radioactive materials transport to the biosphere. Nevertheless, damage phenomena to the host rock need to be assessed, not only during the excavation, waste deposition, and repository sealing phases but also during the following operation, as thermal and chemical processes may affect the integrity of the repositories.

Assessing the safety and integrity of the geological seal during this thermal phase requires a deep understanding of the evolution of the permeability under thermal and mechanical solicitations. Moreover, the damage and crack propagation must be studied at scales much smaller than the repository scale. At these scales, clay rocks exhibit a complex and heterogeneous microstructure, significantly affecting macroscopic behaviour.

As a result, a multiscale approach is preferred as it considers a micromechanical description of the material with multi-physical couplings at this scale and captures the main features of clay rock macroscopic behaviour. The double-scale framework relies on replacing the material constitutive equations with the results of numerical simulations on a Representative Elementary Volume (REV), considering the microstructure heterogeneities and the constitutive behaviour of the materials at that scale.

The present work proposes a thermo-hydro-mechanical model for argillaceous rocks based on a computational homogenisation FE2 scheme. The implementation in Finite Element code Lagamine [1] is a continuation of the works from Frey, 2010 [2] and van de Eijnden, 2015 [3] on hydro-mechanical double-scale models for argillaceous rocks, where the thermal processes and the resulting couplings are introduced. The thermo-mechanical homogenisation is based on the work proposed by Ozdemir, 2008 [4], although thermally-induced damage was not considered there.

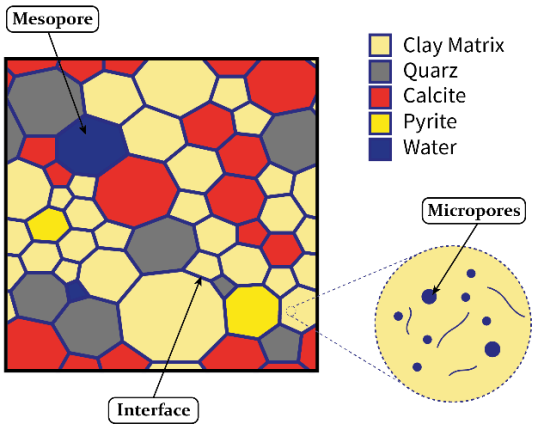

Figure 1 Example of a representative microstructure with its comnstituents.

In order to have a microstructure that is representative of porous material behaviour, not only an accurate representation of the solid components (i.e., clay matrix and mineral inclusions) but also a representation of the pore space is needed. Two pore size distributions are observed from the experimental work of Menaceur, 2020 [5]. Pores in the clay matrix (smaller than 0.01µm), and pores along the mineral inclusions (median of 12µm). A representation of the elements considered for the microstructure is shown in Figure 1.

After calibration of the microstructure to the behaviour of COx, the model is validated with simulations at the laboratory sample scale. The conditions and results at the laboratory scale are shown in figure 2.

The model shows that it is capable of modeling the failure process due to thermally induced over-pressurization, as well as the evolution of the microstructure under such solicitations.

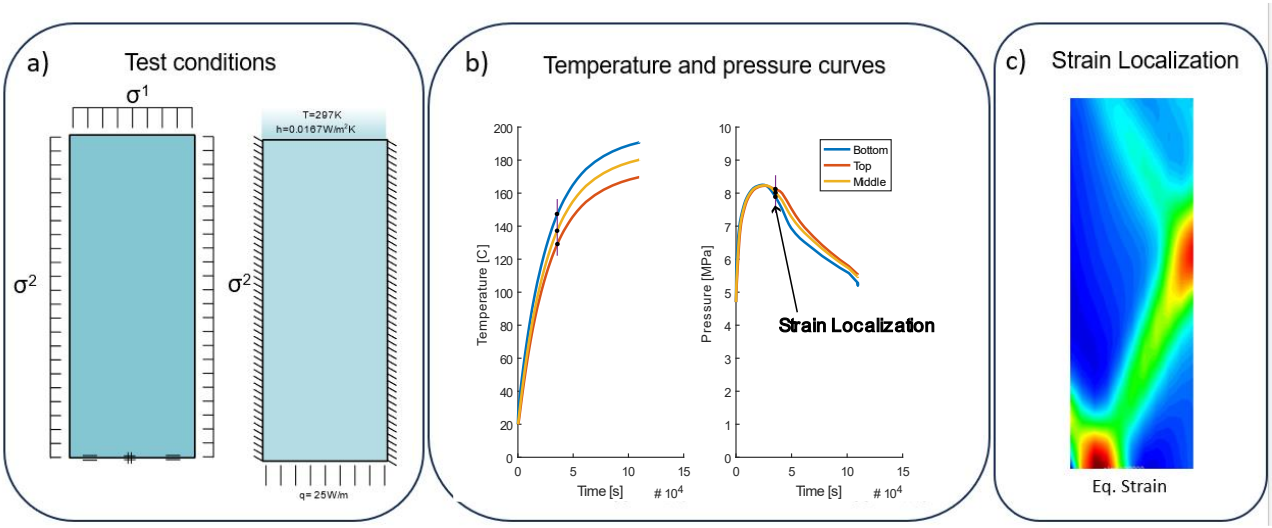

Figure 2 Validation test results. a) Boundary conditions for the simulation, b) evolution of the temperature and pressure for points on top, at the middle and at the bottom of the simple amd marking when strain localization happens, and c) von Mises equivalent strain field at the point of localization.

5. References

[1] Charlier, R. (1989). Approche unifiee de quelques problemes non lineaires de mecanique des milieux continus par la methode des elements finis.

[1] Frey, J., Chambon, R., & Dascalu, C. (2013). A two-scale poromechanical model for cohesive rocks. Acta Geotechnica, 8, 107-124.

[2] Van den Eijnden, A. P., Bésuelle, P., Chambon, R., & Collin, F. (2016). A FE2 modelling approach to hydromechanical coupling in cracking-induced localization problems. International Journal of Solids and Structures, 97, 475-488.

[3] Ozdemir, I., Brekelmans, W., and Geers, M. G. (2008). Fe2 computational ¨ homogenization for the thermo-mechanical analysis of heterogeneous solids. Computer Methods in Applied Mechanics and Engineering, 198(3-4):602–613.

[4] Menaceur, H., Delage, P., Tang, A. M., & Talandier, J. (2016). The status of water in swelling shales: an insight from the water retention properties of the Callovo-Oxfordian claystone.

NUMERICAL INVESTIGATION OF EMBANKMENT SLOPE FAILURE MITIGATION MEASURES USING THE MATERIAL POINT METHOD

T. Kiriyama[1] and K. Fukutake[1]
[1] Shimizu Corporation, Institute of Technology, Tokyo, Japan

1. Introduction

The dynamic deformation problem of embankments has long been solved numerically. During design analysis of embankment deformation, the target system is often treated as a small-deformation problem, assuming displacement/deformation is suppressed under a specific external force. However, under significant seismic forces, the actual deformation can extend beyond small deformations, introducing geometrical nonlinearity. This study reports on the use of the material point method (MPM) [1] for the seismic response analysis of embankments with slope-failure mitigation measures.

2. Material point method using a strain softening model

In this study, MPM was employed as a numerical analysis method based on continuum mechanics, capable of accounting for geometric nonlinearities. The MPM discretizes the governing equations of a solid into material points and solves the equations of motion at grid points by gathering physical quantities using interpolation functions at the grid points.

In the presence of significant deformation, the strength characteristics of the soil are assumed to decrease because of the separation of soil particles from each other, leading to a loss of connectivity among them. Subsequently, a strain-softening model [2] was employed to determine the strength characteristics.

3. Applicability of the strain softening MPM to embankment slope failure

Figure 1 shows the collapse of the embankment, obtained from both experiment and numerical analyses. The maximum shear strain distribution in the numerical model is regarded as a slip line. A comparison of the experimental and analytical results reveals similar maximum displacement and ground deformation, indicating the applicability of the numerical method. The use of the MPM for spatial discretization and Mohr–Coulomb law for a material constitutive model demonstrates its suitability for the seismic response analysis of embankments.

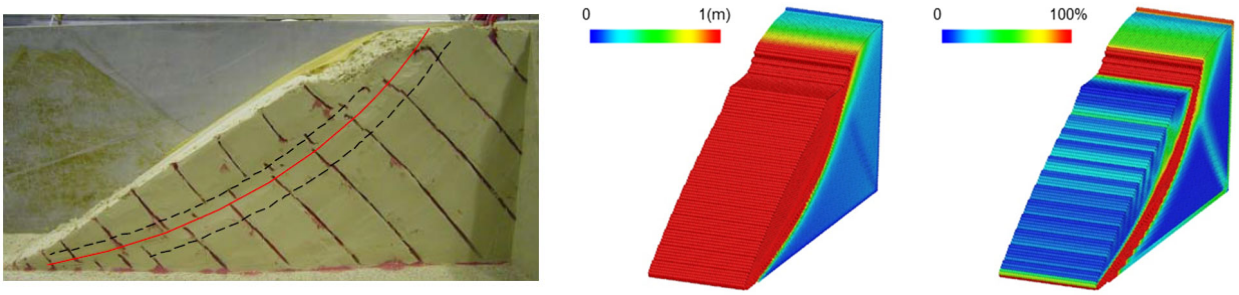

(a) Experiment by Tokida et al. [3] (b) Total disp. (c) Max. shear strain

Figure 1. Embankment slope failure after shaking.

4. Numerical investigation on embankment slope failure mitigation measures

Figure 2 shows the collapse of the full embankment for various mitigation measures: (a) no mitigation measures, (b) toe improvement, and (c) plate installation. In a previous experiment involving an one-sided embankment, both toe improvement and plate installation mitigated the settlement at the top of the embankment. However, the simulation results for the full embankment reveal that only plate installation mitigated the settlement.

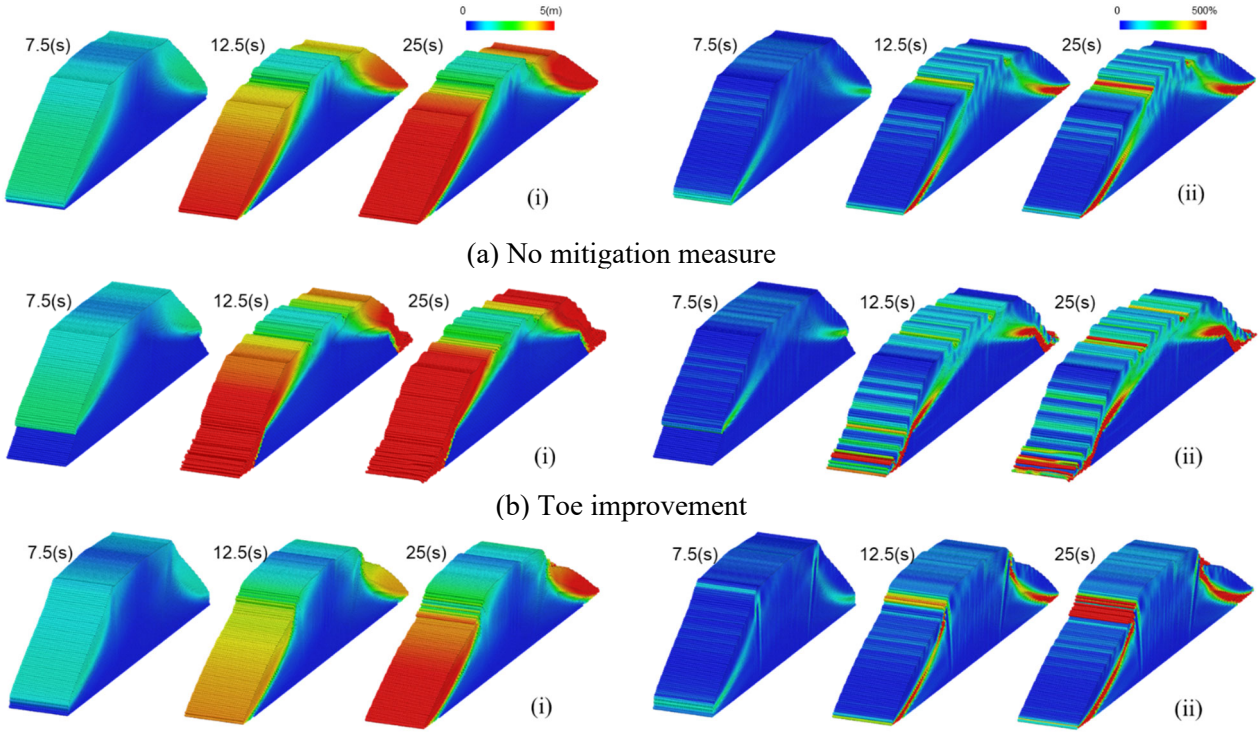

(a) No mitigation measure

(b) Toe improvement

(c) Plate installation

Figure 2. Response of embankment slope to the mitigation measures.
((i) Total displacement and (ii) maximum shear strain)

6. References

[1] Sulsky, D., Chen, Z., and Schreyer, H.L. (1994). A particle method for history-dependent materials, *Computer Methods in Applied Mechanics and Engineering*, **118**, 179-196.

[2] Kiriyama, T. and Lee, J. (2023). Soil-structure interaction analysis during thrust fault rupture propagation using the particle-element coupled method, *Proceedings of the 14th ANZ Conference on Geomechanics*, *Cairns*.

[3] Tokida, K., Jang, J., Oda, K., Nakahira, A., and Ohtsuki, A. (2007). Centrifuge test on advanced seismic performance of road embankment against sliding failure during earthquake, *Proceedings of the JSCE Earthquake Engineering Symposium*, *Japan Society of Civil Engineers*, **29**, 637-645 (In Japanese).

NUMERICAL MODELLING OF BIO-INSPIRED CONE PRESSUREMETER PROBE IN STRATIFIED SOIL

Harsha Vardhan Kurugodu[1], Debayan Bhattacharya[1], Prashanth Vangla[1] and David Frost[2]
[1] Department of Civil Engineering, Indian Institute of Technology Delhi, New Delhi 110016, India
[2] School of Civil and Environmental Engineering, Georgia Institute of Technology, 790 Atlantic Dr., Atlanta, GA 30332, USA

In recent times, geotechnical engineering community has shown deep interest in bio-inspired self-penetrating probes for site-characterization in rugged, difficult terrains and planetary exploration due to their high energy efficiency [1, 2]. In particular, the efficacy of a cone pressuremeter for bio-inspired self-penetration was explored by studying soil failure mechanisms after each stage of self-penetration [1]. These stages involve cone penetration, anchor expansion, and tip advancement (Fig. 1a). Most studies in existing literature have focused on probe advancement in single homogeneous soil layer. However, self-penetrating probes for site characterization traverse through multiple layers with different soil states, resulting in complexities in interpreting the probe response at these critical transition zones [3]. The Material Point Method (MPM) has been adopted in this study, capitalizing on the inherent advantages of particle and continuum frameworks. This study presents a viable and computationally efficient MPM framework to investigate the influence of layered strata on bio-inspired cone pressuremeter probe.

Figs. 1b & 1c represent the geometry, arrangement of stratified soil (i.e., Dense-Loose-Dense), and the schematic illustration of the numerical model adopted in this study. Taking advantage of the geometrical symmetry of the boundary value problem, only half of the geometry has been used in MPM 2D axisymmetric simulations. In this study, the soil was modelled as an elastic-perfectly plastic Mohr-Coulomb material and the cone pressuremeter probe as a rigid material to keep the modelling issues relatively handy without compromising the accuracy of numerical results. As the probe was penetrated through dense layer, cone-tip resistance (q_c) increased with depth to a peak value of around 4800 kPa (equivalent to the homogenous state) and then started reducing at around 0.06 m behind the loose layer (Fig. 1d). q_c further reduced in loose soil layer to a minimum value of around 2600 kPa (which was around 2500 kPa in case of homogenous state) and remained constant until the probe was around 0.1 m behind the subsequent dense layer (Fig. 1d). q_c slowly increased in loose layer and then rapidly in dense layer to reach a maximum value of around 4800 kPa. Fig. 1g presents the axial stresses around the cone at the end of cone penetration phase. The stresses were predominantly localized within a vicinity of 1-2 times of the probe's diameter (d_c). Interlayer movement of soil during cone penetration stage led to stress accumulation at the layer transitions (Fig. 1g).

During pressuremeter module expansion stage, maximum module pressure observed was around 530 kPa, which was below the average value of probe response in case of homogenous dense and loose media (Fig. 1e). The global responses (module pressure evolution, see Fig.1.e) observed align well with local responses, with the axial stress state variances between pressuremeter module expansion and cone penetration phases represented in Fig. 1h. Furthermore, stress relaxation was observed ahead of the pressuremeter module and near the tip which were comparable with studies from existing literature [1].

After pressuremeter module expansion stage, the tip was advanced to distance of 0.044 m ($\approx 1d_c$), while keeping the anchor and the probe behind it is stationary. During the tip advancement stage, peak q_c values of around 4100 MPa were recorded (Fig. 1f). These global responses indicate around 15% decrease in the magnitude similar to that of homogenous dense soil. Although the layered strata significantly influenced the probe's response during the penetration and expansion stages, it

had minimal impact during the tip advancement stage. Variation in axial stresses at the end of this stage were shown in Fig. 1i indicate that the increase in stresses ahead of the tip and decrease in stresses near the anchor and behind the tip.

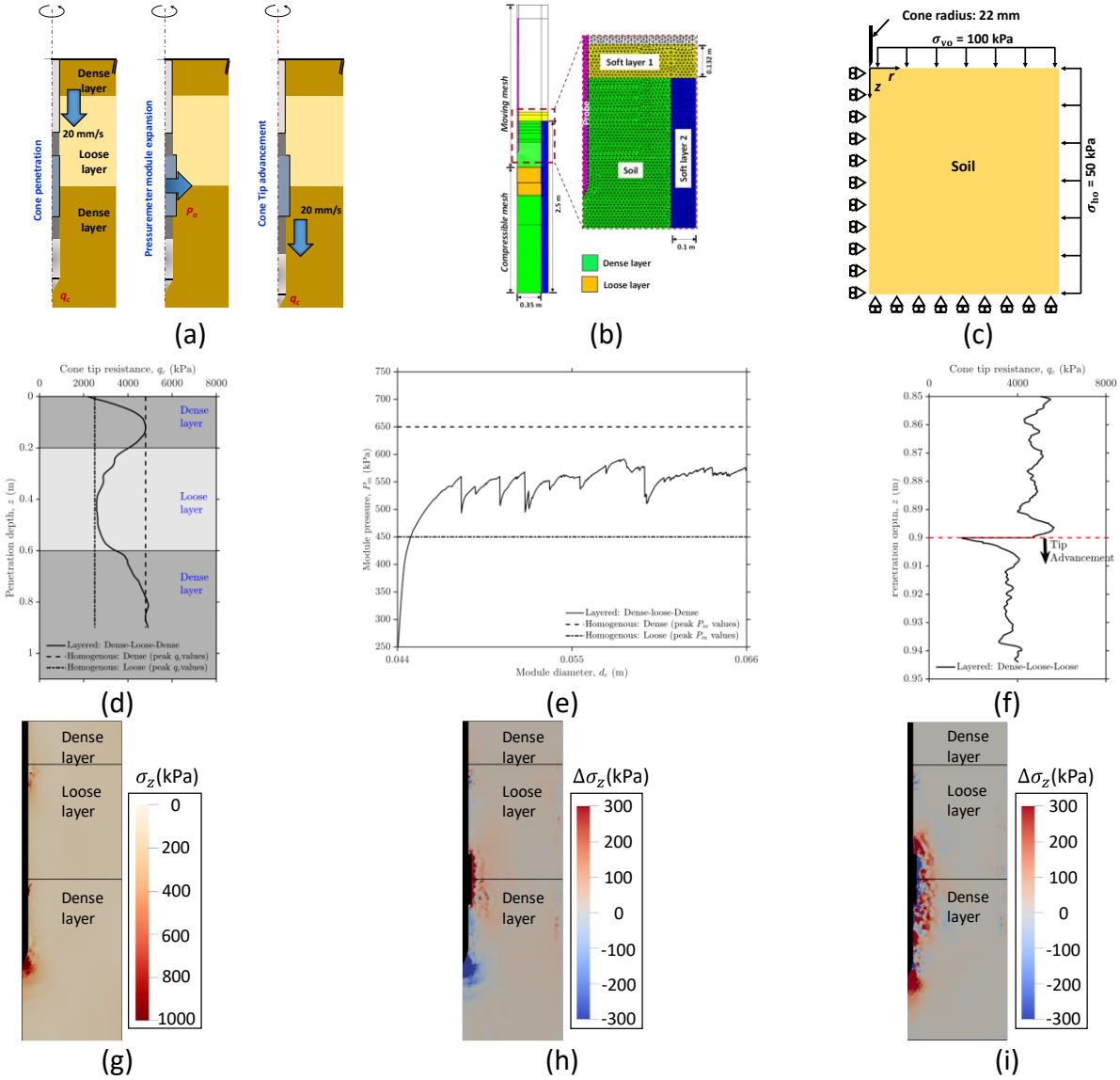

Figure 1. (a) Schematic illustration of different stages of bio-inspired self-penetrating mechanism; (b) Geometry of cone pressuremeter simulation - 2D axisymmetric idealization and mesh discretization in MPM; (c) Boundary conditions; (d) q_c vs depth during cone penetration stage; (e) Pressuremeter module pressure during expansion stage; (f) q_c vs depth during tip advancement stage; (g) Axial stress (σ_z) distribution at the end of cone penetration stage (at penetration depth of 0.9m $\approx 20d_c$); (h) $\Delta\sigma_z$ at the end of module expansion stage (module diameter of 0.066 m $\approx 1.5d_c$); (i) $\Delta\sigma_z$ at the end of tip advancement stage (at penetration depth of 0.944 $\approx 1d_c$)

References

[1] Chen, Y., Martinez, A., & DeJong, J. (2022). DEM study of the alteration of the stress state in granular media around a bio-inspired probe. *Canadian Geotechnical Journal*, **59**: 1691-1711.

[2] Wei, H., Zhang, Y., Zhang, T., Guan, Y., Xu, K., Ding, X., & Pang, Y. (2021). Review on bioinspired planetary regolith-burrowing robots. *Space Science Reviews*, **217**: 1-39.

[3] Frost, J.D., Saussus, D., and DeJong, J.T., (2006), Analytical Investigation of Friction Sleeve Length Effects on Stratigraphic Interpretation. *ASCE International Journal of Geomechanics*, **6(1)**: 11-29.

Numerical modelling of downward progressive landslides in sensitive clay

Y. Zhang[1], X. Zhang[1] and X. Li[1]
[1] University of Liverpool, Department of Civil Engineering and Industrial Design, Liverpool, United Kingdom

1. Introduction

Landslides in sensitive clay are catastrophic events worldwide, threatening lives and properties. When plastic strain occurs in sensitive clays, a significant reduction in undrained shear strength takes place. Consequently, even a minor trigger can lead to multiple progressive landslides, causing extensive devastation. Landslides in sensitive clay can be classified into single flow slides, progressive flow slides, translational progressive landslides, and spreads based on failure mechanisms [1]. They can also be categorized as upward or downward failures depending on the direction of progression [2]. Trigger factors may include erosions, surcharge loads, earthquakes, and others. Upward landslides are typically caused by erosion at the slope foot, while downward landslides usually occur on lengthy slope triggering by surcharge loads near the crest.

Investigating landslides in sensitive clay presents challenges, necessitating robust numerical methods to comprehend failure modes and collapse behaviours, particularly in the post-failure phase. Although multiple numerical methods have been developed and applied to investigate the post-failure processes of sensitive clay landslides, these studies have primarily focused on upward landslides, particularly those indicating flow slide failures or spread failures due to toe erosion of the slope, or because of seismic loading. This study focuses on the downward progressive landsides occurring on long natural slopes in sensitive clay.

2. Problem description

We consider a typical model as illustrated in Figure 1 with an inclination of 5.71°in the right slope. The total depth (H) of the model is 20 m, including a top layer of crust (H_c = 5 m) with a constant shear strength of 50 kPa, and a sensitive clay layer as the bottom layer. The unite weight, γ, of both layers is 18 kN/m^3. While the average shear strength of the sensitive clay remains constant at 40 kPa, its initial shear strength (s_{u0}) linearly increases with the depth below the ground surface (z), and k represents the strength gradient in kPa/m.The equation for strain softening from [3] is used to capture the non-linear reduction in shear strength (s_u):

$$s_u = s_{ur} + \left(s_{up} - s_{ur}\right)e^{-\eta\varepsilon_d^p} \quad (1)$$

where s_{up} and s_{ur} represent the peak and residual values of the cohesion, respectively, and the sensitivity, S_t, is defined as the ratio of s_{up}/s_{ur}. The parameter η controls the softening rate, with larger values of η indicating more rapid strain softening, and ε_d^p represents the deviatoric plastic strain.

The model experiences external disturbances due to surcharged loads from an embankment. The embankment is situated 150 m horizontally from the toe of the slope and features a top width of 20 m and a minimum height of 7.5 m. The magnitude of the surcharged load is represented by the unit weight (22kN/m^3) of the embankment.

This study used the Nodal integration based PFEM [4], and employed the rigid-perfectly plastic Tresca model with strain softening to represent the behaviour of sensitive clays. The N-PFEM simulation initially consisted of 20,437 nodes and 39,817 elements. The mesh size is 0.6 m (0.03H). A time step of 0.01 seconds was adopted for the simulations.

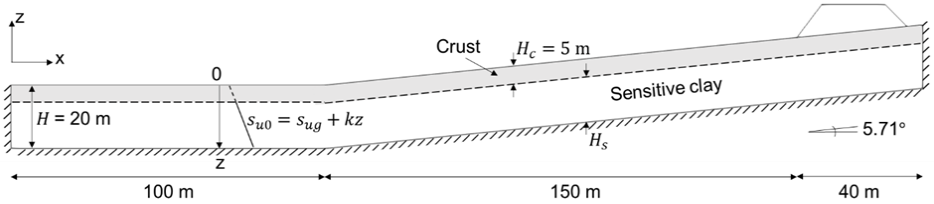

Figure 1. Geometry of the slope.

3. Simulation results

Three cases with the same values of $S_t = 2, \eta = 10$, examine the effects of the strength gradient of the sensitive clay layer with values of 1.2, 1.6 and 2.4 kPa/m, respectively. The final diffused distance of them are 88 m, 155 m and 183 m, respectively. Figure 6 presents the velocity mapping in the first 7.5 s, encompassing all progress collapses. Flow slides dominate and spreads appear in the crust layer and at the end of flow slides. A lower strength gradient result in a larger diffused distance. A reduction in the strength gradient (k) leads to an increase in the depth and span of the first flow slide, F_1(Figure 2 (a, d and g), the failure rate, and the overall number of collapses. The numbers of flow slides are 2, 3, and 4 for k = 2.4, 1.6 and 1.2 kPa/m, respectively, and collapses occur earlier with decreasing values of *k* (Figure 2). Starting from the third flow slide (F_3), collapse initiates only from the middle section to the end section of the landslide (Figure 2 (f, h and i)), resulting in a notable decrease in speed for the area near the embankment. Simulated results reveal that the slope base is a critical area for all flow slides after F_1 to pass through, and a smaller *k* corresponds to a smaller value of undrained shear strength at the slope base. Therefore, in the case of a smaller strength gradient, downward progressive flow slides are more likely to occur, and the extent of damage is also more severe.

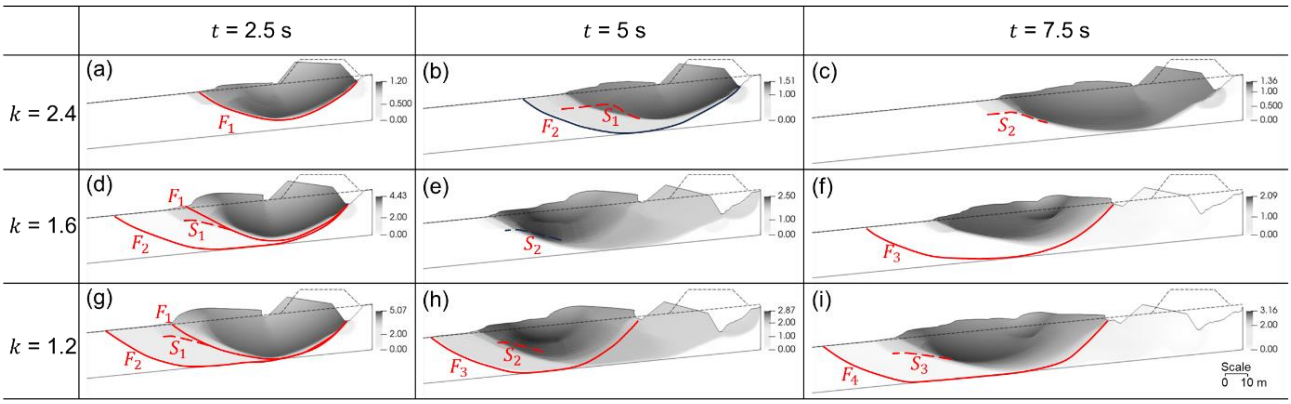

Figure 2. Effects of strength gradient (*k*) in kPa/m. Colours indicate velocities in (m/s).

4. References

[1] Bjerrum, L., *Stability of natural slopes in quick clay.* Géotechnique, 1955. **5**(1): p. 101-119.

[2] Dey, R., et al., *Numerical modeling of combined effects of upward and downward propagation of shear bands on stability of slopes with sensitive clay.* International Journal for Numerical and Analytical Methods in Geomechanics, 2016. **40**(15): p. 2076-2099.

[3] Yerro, A., E. Alonso, and N. Pinyol, *Run-out of landslides in brittle soils.* Computers and Geotechnics, 2016. **80**: p. 427-439.

[4] Meng, J., et al., *A nodal-integration based particle finite element method (N-PFEM) to model cliff recession.* Geomorphology, 2021. **381**: p. 107666.

PERFORMANCE VALIDATION OF THREE-DIMENSINONAL LIMIT EQUILIBRIUM METHOD FOR SHALLOW LANDSLIDES OVER A WIDE AREA

D. Sugo[1], S. Fujita[1], N. Dolojan[1], K. Tozato[2], R. Nomura[3], S. Moriguchi[3]and K. Terada[3]
[1] Tohoku University, Grad. Sch. of Engineering, Sendai, Japan
[2] Hachinohe Institute of Technology, Fac. of Engineering, Hachinohe, Japan
[3] Tohoku University, IRIDeS, Sendai, Japan

1. Background and Objective

Although a variety of methods have been proposed for wide-area landslide risk assessment, many of them rely on statistical models or simple physics-based models. To enhance landslide risk assessment using advanced physics-based models, it is important to examine the applicability of 3D limit equilibrium method (LEM). Under this concept, this study aims to investigate the performance of the 3D LEM-based models by comparing their results with actual landslide events.

2. Methodology

This study employs three 3D LEM-based models, such as Hovland method [1], 3D simplified Bishop method [2], and 3D simplified Janbu method [2]. These methods calculate the normal and shear forces acting on the surfaces of soil columns using the local equilibrium equations and substitute them into the global equilibrium equations for moment, vertical force, or horizontal force equilibrium equation shown in Figure 1 to obtain the factor of safety.

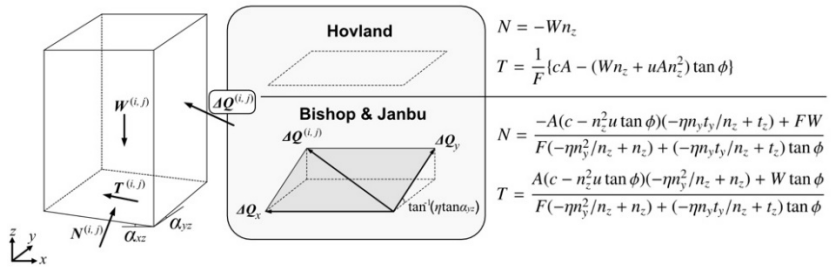

	Hovland	Bishop	Janbu
Moment eq.	○	○	
Vertical eq.		○	○
Horizontal eq.			○

A: Area of slip surface, *c*: Cohesion, *W*: Unit volume weight, *u*: Porewater pressure, ϕ: Internal friction angle, (n_x, n_y, n_z): Unit direction vector of normal force ***N***, (t_x, t_y, t_z): Unit direction vector of shear force ***T***, *F*: Factor of safety (unknown), η: Angle of ΔQ_y (unknown)

Figure 1. Assumptions of 3D LEM-based methods

3. Target area and assumption of calculation

In this study, a slope stability analysis is performed for Marumori Town, Miyagi, Japan, where numerous slope failures occurred due to heavy rainfall caused by Typhoon Hagibis in 2019. The target area, 3D geological model, and soil parameters used in this study are shown in Figure 2. The parameters were determined from databases of geological maps and borehole data. The parameters of Serpentinite areas are assumed to be the same parameters as basalt areas because no borehole data were available, and they are both classified into volcanic rock. The iterative calculation for the depth of the slip surface is constrained from 0.5 to 5.0 m since shallow landslides are generally observed under heavy rainfall conditions.

4. Results

The actual landslide map and results obtained by the three methods are shown in Figure 3. The results of TSS (True Skill Statistics) show that Hovland method overestimated the hazardous area if

the threshold of the factor of safety is set to 1.0, while the AUC (Area Under the Curve) results suggest that all the methods are almost the same in terms of accuracy when no specific threshold is set. In other words, Hovland method can output the same hazardous area and the same value of TSS obtained by the other methods by using a different threshold for the factor of safety.

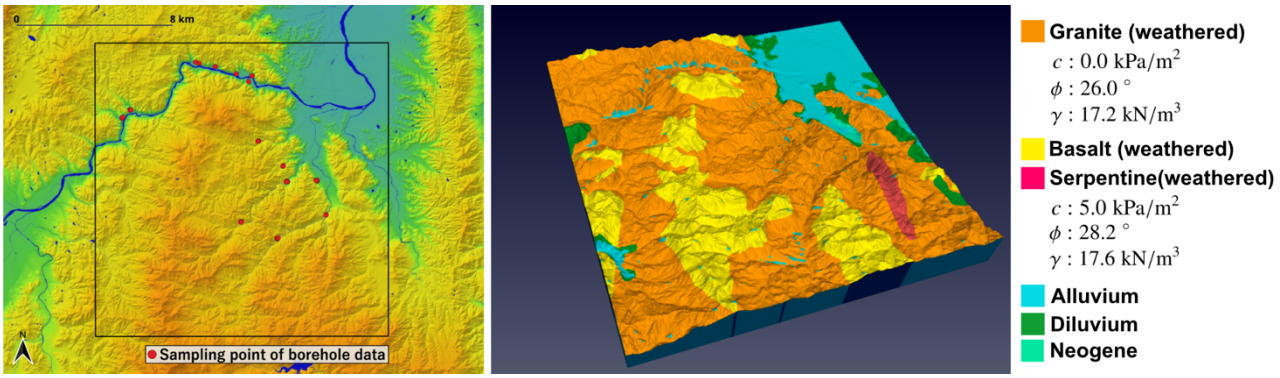

Figure 2. Terrain map and 3D-geological model of the target area.

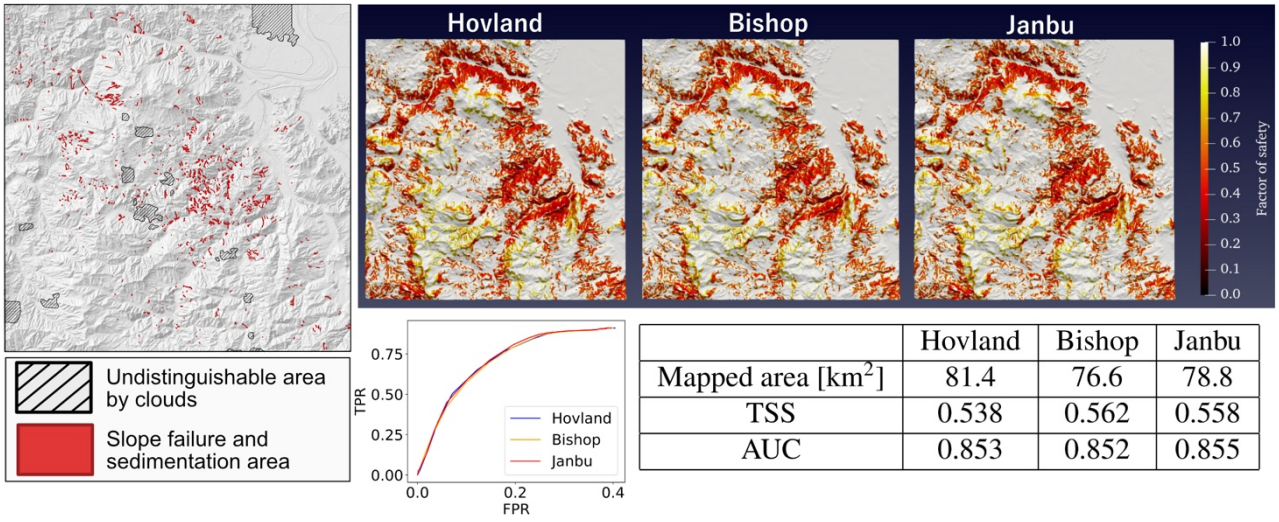

	Hovland	Bishop	Janbu
Mapped area [km^2]	81.4	76.6	78.8
TSS	0.538	0.562	0.558
AUC	0.853	0.852	0.855

Figure 3. Actual landslide map and results obtained by 3D LEM-based models.

5. Conclusions

In this study, 3D LEM-based methods were employed, and their performance for wide-area landslide risk assessment was examined by comparing with the actual landslide event. Although there are differences in the calculated factor of safety, it was confirmed that Hovland method can produce results comparable to those of more advanced methods by adjusting the threshold of the factor of safety.

6. References

[1] Hovland, H. J. (1977). Three-dimensional slope stability analysis method. *Int. J. of Mechanical Science*., Vol. 103, No. 9, pp. 971-986.

[2] Keizoh, U. & Kenji, H. (1988). Extension of simplified Bishop method, simplified Janbu method and Spencer's method to three dimensions. *Society of Civil Engineering Paper.*, No. 394, pp.21-25, 1988.

PORE SCALE STUDY OF POLYMER FLUID FLOW

***Y. Wang*[1], *C. O'Sullivan*[1], *M. Bortolotto*[1], *M. Sawada*[1,2]**
[1] *Imperial College London, Dep. Civil and Environmental Engineering, London, United Kingdom*
[2] *Tokyo Institute of Technology, School of Environment and Society, Tokyo, Japan*

Preventing the excavations from collapsing before inserting the permanent structure is essential in many geotechnical projects, including railway tunnels and deep foundations. Currently, the most used support fluid is a suspension of bentonite clay. A newer alternative has arisen that uses polymer fluids rather than suspensions of small clay particles. Compared to bentonite suspensions, support systems that use polymer fluids are economical and have a smaller environmental impact. Polymer fluids exhibit a non-Newtonian rheology. This means that, in contrast to a Newtonian fluid such as water, the viscosity depends on the shear rate. As a result, there is a complex interaction between polymer fluids and soil, which hinders the wide application of these materials in ground engineering. One key issue is quantifying the fluid-particle interaction force, which ultimately leads to the overall excavation support. The first stage of the project was to verify that computational fluid dynamics (CFD) simulations using OpenFOAM can accurately capture the behaviour of non-Newtonian fluid flow in a capillary tube. CFD simulations for regular face-centred cubic (FCC) packings were then conducted considering both Newtonian and non-Newtonian fluids with power-law rheology. These simulations provided data on the fluid-particle interaction force.

1. Flow of power-law fluids through a capillary tube

Lam et al. [1] proposed that the shear stress (τ) and the shear rate ($\dot{\gamma}$) relationship for polymer fluids at intermediate shear rates can be described by established models for non-Newtonian fluids, including the simple power-law model:

$$\tau_r = m\dot{\gamma}^n = m\left(-\frac{dU_r}{dr}\right)^n \tag{1}$$

where m is the flow consistency index (Pa s^n) and n is the dimensionless flow behaviour index. In a Newtonian fluid, $m = 10^{-3}$ and $n = 1.0$ (the dynamic viscosity, η_w of water is 1 mPa s at 20 °C). For laminar, power-law fluids in a capillary tube, dU_r/dr is the radius-dependent shear rate (s^{-1}), and U_r is the velocity (m/s) at radial distance r (m) from the tube centre:

$$U_r = \left(\frac{\Delta h \rho g}{2mL}\right)^n \frac{n}{n+1} R^{(1+n)/n}\left[1 - \left(\frac{r}{R}\right)^{(1+n)/n}\right] \tag{2}$$

Simulations were performed using the steady-state finite volume solver `simpleFoam` in the open-source CFD software OpenFOAM (version 8) [2]. A constant inlet velocity of 0.2 mm/s and a constant pressure of 0 Pa were applied at the inlet and outlet, respectively. 'No-slip' boundaries were applied to the pipe wall so that the velocities normal and tangential to the surface were constrained to be zero. The results demonstrate that CFD simulations using OpenFOAM can accurately capture the rheological behaviour of non-Newtonian fluid in a simple capillary tube (see Figure 1a).

2. Study of fluid-particle interactions

In our first analysis of the fluid-particle interaction force, we considered uniform spheres on a face-centred-cubic lattice. This allowed for validation of the simulation set-up using the data in Zick and Homsy [3], and we also could systematically control void ratio (e) with a constant fabric. The boundary conditions for the inlet and outlet were identical to the case of capillary tube validation, with 'No-slip' boundaries being applied to all particle surfaces and 'Cyclic' boundary conditions being

applied to the four sidewalls (see Figure 1b). SnappyHexMesh, an OpenFOAM mesh generation algorithm, was used [2]. Local refinement was applied to resolve the narrow channels between the spheres. The final mesh has around 1.5 million CFD cells. The fluid-particle interaction force consists of two components: a pressure component, $\mathbf{F}_p$ and a viscous component, $\mathbf{F}_v$. The fluid-particle drag coefficients for water estimated from CFD simulations were in good agreement with the numerical solutions in Zick & Homsy [3].

For the power-law fluid simulations, the values of n were chosen based on a review of literature documented in Wang [4]. Figure 1b presents the distribution of kinematic viscosity for the power-law fluid ($n = 0.7$) for $e = 0.852$. The drag forces ($|\mathbf{F}_p + \mathbf{F}_v|_{\mathrm{PL}}$) normalised by the those for water ($|\mathbf{F}_p + \mathbf{F}_v|_{\mathrm{w}}$) are shown in Figure 1c (for $n = 0.5$ and $n = 0.7$). The fluid-particle interaction forces for the power-law fluids are up to 7 times that of water. These data explain, at least in part, the fundamental mechanisms that enable polymer fluids to provide excavation support.

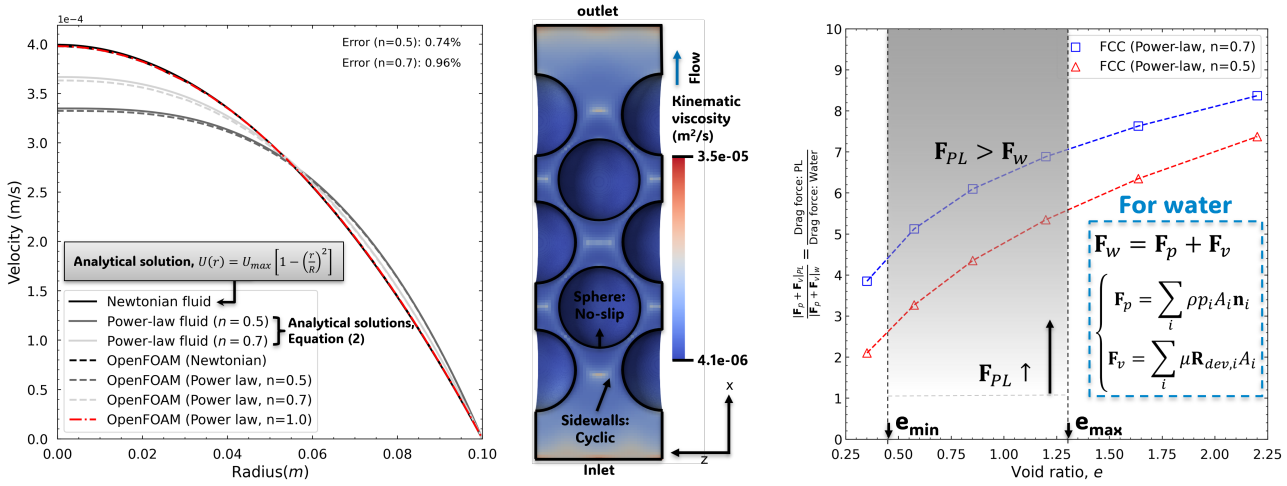

(a) (b) (c)

Figure 1. (a) Validation of capillary tube; (b) Boundary conditions for FCC packings; (c) Normalised drag forces for power-law fluids (e_{min} and e_{max} are included to give likely range of void ratio values for sand) [Note: $\mathbf{F}_{\mathrm{PL}}$ and $\mathbf{F}_{\mathrm{w}}$ are drag forces for power-law fluids and water, respectively]

3. Conclusions

The current application of polymer support fluids in geotechnical engineering is hindered by a lack of understanding of the fundamental mechanisms that provide excavation support. We have verified that OpenFOAM simulations can accurately simulate a non-Newtonian fluid flow in a capillary tube. By simulating the flow through a lattice assembly of spheres, we have shown that power-law fluids will generate larger fluid-particle interaction forces that will contribute to support an open excavation.

References

[1] Lam, C., Martin, P. J., and Jefferis, S. A. (2015). Rheological properties of phpa polymer support fluids. *Journal of Materials in Civil Engineering*, **27**, 04015021.

[2] Greenshields, C. (2020). *OpenFOAM v8 User Guide*. The OpenFOAM Foundation.

[3] Zick, A. and Homsy, G. (1982). Stokes flow through periodic arrays of spheres. *Journal of fluid mechanics*, **115**, 13–26.

[4] Wang, Y. (2023). *A pore scale understanding of polymer support fluids*. MSc dissertation, Imperial College London.

REPRESENTATIVENESS OF SAMPLES IN TRIAXIAL TESTS INVESTIGATED WITH NUMERICAL MODELS

E. Salvatore[1], M. Arciero[1,2] and G. Modoni[1]

[1] University of Cassino and Southern Lazio, Department of Civil and Mechanical Engineering, Italy

[2] Univ. Grenoble Alpes, CNRS, 3SR Lab., Grenoble, France

In engineering practice the mechanical behaviour of geomaterials is commonly studied and modelled with the representative elementary volume approach. Soil is assumed as a unique element where stress and strain are described by single tensors and physical properties are constant.

This exemplification, extremely useful in the management of a wide range of geotechnical problems, may lead in misleading observations because the observed macroscopic response is often the result of phenomena acting at the particle scale (e.g. strain localization). An emblematic example is represented by the stress path dependence of critical state of sands [7, 5].

In this framework, the paper explores the role played by the sample dimension and spatial variability of porosity on the mechanical response of sand subjected to triaxial test.

To this aim a Finite Difference code [4] together with a Critical State constitutive soil model [6, 2] has been extensively used firstly simulating compression and extension triaxial tests at different confining stress with the element test approach and subsequently implementing the model of the tests, including boundary conditions (i.e. frictional end plates and confinement latex membrane) (Figure 1), and running parametric analysis variating sample dimensions and spatial distribution of porosity by means of the random field theory [3].

Both constitutive model of soil and porosity fields are calibrated on experimental results coming a previous work where triaxial tests carried out in x-ray tomograph and interpreted at the micro scale [1, 6].

Results have proven that element test approach is not suitable to capture the correct soil response under different loading conditions and pointed out that the usual approach to determine soil properties suffers of important limitations.

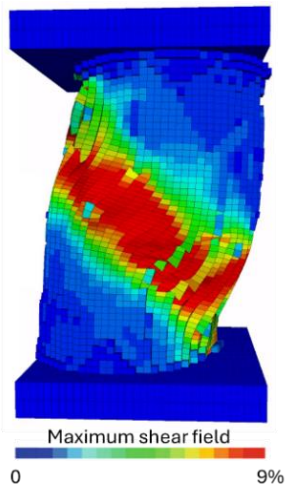

Figure 1. On the left: porosity field measured by means x-ray tomography on triaxial sample. On the right: example of simulation in terms of maximum shear field at the end of triaxial compression test.

5. References

[1] Ando, E. (2013). Experimental investigation of microstructural changes in deforming granular media using x-ray tomography (Doctoral dissertation, Université de Grenoble).
[2] Dafalias, Y.F., Manzari, M.T.: Simple plasticity sand model accounting for fabric change effects. J. Eng. Mech. 130(6), 622–634 (2004).
[3] Fenton, G. A., & Griffiths, D. V. (2002). Probabilistic foundation settlement on spatially random soil. Journal of Geotechnical and Geoenvironmental Engineering, 128(5), 381-390.
[4] Itasca Consulting Group, I.: FLAC3D—Fast Lagrangian Analysis of Continua in Three-Dimensions, Ver. 5.0. Minneapolis (2012)
[5] Salvatore, E., et al.: Determination of the critical state of granular materials with Triaxial tests. Soils Found. 57(5), 733–744 (2017).
[6] Salvatore, E., Spacagna, R. L., Andò, E., & Ochmanski, M. (2019). Geostatistical analysis of strain localization in triaxial tests on sand. Géotechnique Letters, 9(4), 334-339.
[6] Schofield, A., Wroth, P.: Critical State Soil Mechanics. McGraw-Hill, London (1968).

Revisiting the role of friction in transient granular flows through non-smooth simulations and experiments

***G. Rousseau*[1,2], *T. Métivet*[1], *H. Rousseau*[3], *G. Daviet*[1] *and F. Bertails-Descoubes*[1]**
[1] *Univ. Grenoble Alpes, INRIA, CNRS, Grenoble INP, LJK, 38000 Grenoble, France*
[2] *Inst. of Hydraulic Engineering and Water Resources Management, TU Wien, 1040 Vienna, Austria*
[3] *Department of Geography, University of Zurich, CH-8057 Zurich, Switzerland*

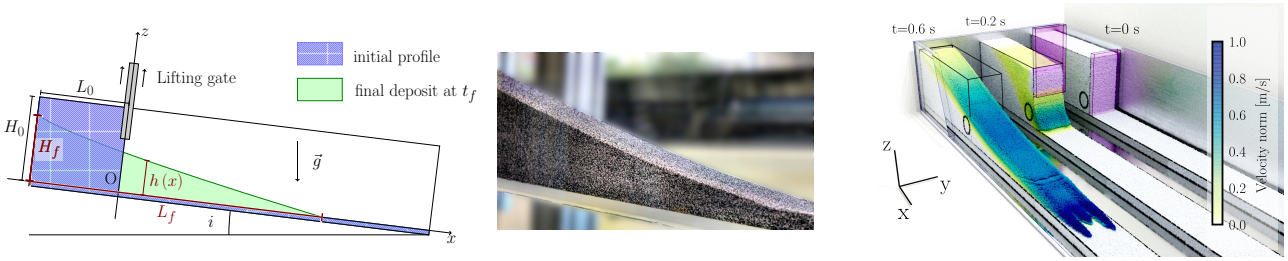

(a) Experimental setup of the granular collapses onto inclined erodible beds.

(b) 3-D simulation of a granular column collapse on a 15°-tilted bed.

Figure 1. Inclined granular column collapses: experiments and simulations [1].

The large-scale continuum simulation of granular matter is a long-standing challenge, mainly stemming from the large diversity of effects at play. Even in the simplest mono-disperse systems, the macroscopic rheology features intricate state transitions, pressure-dependent yield stress, kinetic – viscous – dissipation and hysteresis. The Drucker-Prager model [2] proposes a first-order plastic rheology, with a pressure-dependent yield-stress, close to the Mohr-Coulomb law for brittle materials. While it accurately captures the transition from rest to flow of granular matter, it does not account for the rate-dependent viscosity responsible for the existence of steady flow profiles over a range of imposed shear-rates. The celebrated $\mu(I)$ rheology [3] extends the plastic Drucker-Prager model to account for inter-grain shock dissipation by introducing an increasing dependence of the friction coefficient on the inertial number $I = \dot{\varepsilon} d\sqrt{\rho/p}$, which characterises the ratio between the inertial and deformation time-scales. As such, it effectively incorporates viscous dissipation into the model, crucial in granular flows with large strain rates or low pressure. While this visco-plastic rheology is able to accurately describe steady inertial flows, its actual role in the low I regime, in particular for transient flows subject to rest-to-flow transitions, remains unclear, all the more as these transitions display a hysteretic behaviour, characterised by the existence of a static friction coefficient larger than the dynamic one (see e.g. [4] and references therein).

In this work, we perform experiments of granular column collapses over erodible beds, along with the corresponding 3-D continuum-based numerical simulations. We carry out the collapses with different bed slopes, ranging from $0°$ to $20°$, different channel widths, and different materials, in order to carefully investigate the role of friction – within the material or with its enclosing walls – in transient flows with low inertial numbers.

Our simulation method leverages the non-smooth MPM-based continuum framework introduced in [5] to accurately resolve the plastic Drucker-Prager threshold without regularisation, and carefully accounts for all the experimental setup (c.f.fig. 1), including friction with the lateral walls and the lifting gate. We notably compare simulations obtained with the fully plastic Drucker-Prager and the viscopastic $\mu(I)$ rheologies, and compare both the resulting transient and final states with experimental measurements of the free-surface profiles and material velocities measured at the side wall.

While our results (e.g. fig. 2a) confirm the weak impact of the viscous effects introduced by the $\mu(I)$ rheology in this regime, as previously suggested in [6, 7], they also stress the importance of

setting the – constant – plastic bulk friction coefficient to the value extracted from the avalanche angle in order to accurately predict collapse rest states, instead of the stop angle measured from the steady flow experimental protocols [8], as is usually done.

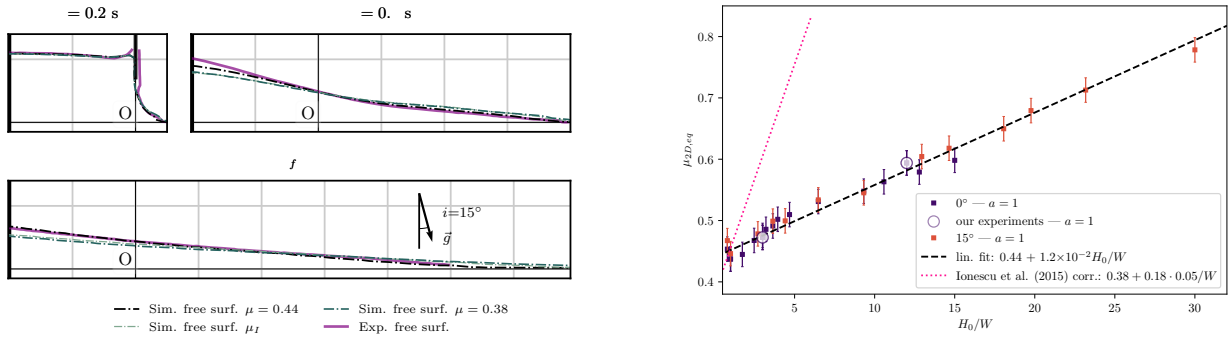

(a) 15°-tilted collapse: comparison between experiment and 3-D simulations with Drucker-Prager laws ($\mu = \mu_a = 0.44$ or $\mu = \mu_s = 0.38$), or the $\mu(I)$ law.

(b) Friction with lateral walls: scaling law of an "equivalent" 2-D friction coefficient, compared with the corresponding model extended from the steady case.

Figure 2. Investigating the role of friction by comparing experiments and simulations.

We also carefully investigate the role of friction with the enclosing walls (c.f. fig. 2b), and find it remarkably less impactful than assumed in previous studies extending the steady analysis to the transient case.

Finally, we show that a simple hysteresis model, inspired by the non-monotonous friction laws proposed in [9] can improve the simple Drucker-Prager law in the early dynamics of the collapse, thereby suggesting the high sensitivity of the actual solid-liquid transition to mechanical noise and paving the way to further analysis.

References

[1] Rousseau, G., Métivet, T., Rousseau, H., Daviet, G., and Bertails-Descoubes, F. (2023). Revisiting the role of friction coefficients in granular collapses: confrontation of 3-d non-smooth simulations with experiments. *J. Fluid Mech.*, **975**, A14.

[2] Drucker, D. C. and Prager, W. (1952). Soil mechanics and plastic analysis or limit design. *Quarterly of applied mathematics*, **10**, 157–165.

[3] Jop, P., Forterre, Y., and Pouliquen, O. (2006). A constitutive law for dense granular flows. *Nature*, **441**, 727–30.

[4] Perrin, H., Clavaud, C., Wyart, M., Metzger, B., and Forterre, Y. (2019). Interparticle friction leads to nonmonotonic flow curves and hysteresis in viscous suspensions. *Phys. Rev. X*, **9**, 031027.

[5] Daviet, G. and Bertails-Descoubes, F. (2016). Nonsmooth simulation of dense granular flows with pressure-dependent yield stress. *J. Non-Newtonian Fluid Mech.*, **234**, 15–35.

[6] Lagrée, P.-Y., Staron, L., and Popinet, S. (2011). The granular column collapse as a continuum: validity of a two-dimensional navier–stokes model with a μ (I)-rheology. *J. Fluid Mech.*, **686**, 378–408.

[7] Ionescu, I., Mangeney, A., Bouchut, F., and Roche, O. (2015). Viscoplastic modeling of granular column collapse with pressure-dependent rheology. *J. Non-Newtonian Fluid Mech.*, **219**, 1–18.

[8] Pouliquen, O. (1999). Scaling laws in granular flows down rough inclined planes. *Phys. Fluids*, **11**, 542–548.

[9] DeGiuli, E. and Wyart, M. (2017). Friction law and hysteresis in granular materials. *Proc. Natl. Acad. Sci. U.S.A.*, **114**, 9284–9289.

Shock wave loading analysis of granular material subjected to projectile impact using MPM

Ranveer Singh[a], Tanusree Chakraborty[b]

[a] Department of Civil Engineering, Indian Institute of Technology, Delhi, New Delhi, India

[b] Department of Civil Engineering, Indian Institute of Technology Delhi, New Delhi, India

Abstract

For the past few decades, the finite element method (FEM) has been widely used by researchers to solve and analyze geotechnical problems. However, granular materials subjected to blast and shock loading undergo large deformation, which causes severe mesh distortion, inefficient computation, and non-convergent solutions in FEM. The material point method (MPM) has garnered the attention of researchers as an alternative to the conventional numerical methods such as FEM to tackle the problem of large deformation analysis. In MPM, the continuum domain is discretized using a set of points instead of elements, and as a result mesh distortion problems are avoided. The need for using complicated phenomenological assumptions at high non-linearity can be avoided using the MPM framework. In this study, MPM has been used to analyze the response of the shock wave loading on granular material imparted due to a projectile. The results obtained have been compared with the existing analytical solution along with a finite element analysis to validate the effectiveness of MPM. Stresses around smaller deformation regions showed similarity for MPM and FEM, whereas for larger deformation regions MPM was able to capture the strain localization qualitatively.

Keywords: MPM, FEM, shock wave, projectile

Stability of vertical plate anchors in unsaturated sand

***M. Mushtaq*[1], *J.P. Sahoo*[1]**
[1] *Department of Civil Engineering, Indian Institute of Technology Kanpur, Kanpur, India*

1. Introduction

Vertical anchors are placed in soil to support various geotechnical structures like foundations, bridge abutments, retaining walls, slopes, and excavations. While numerous studies have been conducted to analyse the stability of vertical anchors in saturated/dry sand, it is noteworthy that real-world soil conditions often fall between these extremes. To date, no study is available to find the pullout capacity of vertical anchors in unsaturated sand.

The present study addresses the gap by conducting a numerical analysis to evaluate the stability of vertical anchors in unsaturated sand under a fully bonded condition employing the lower bound finite element limit analysis. The investigation includes a parametric study that shows the effect of various parameters like the height of the anchor plate, angle of internal friction, embedment depth and depth of water table on the pullout capacity. Additionally, the study examines the influence of other parameters, including the flow condition, van Genuchten SWRC model parameters and saturated unit weight. The modified Mohr-Coulomb yield criterion is employed to account for the effect of matric suction in unsaturated sand. Failure patterns have also been generated for some typical cases. By comprehensively analyzing these aspects, the study contributes valuable insights into the stability of vertical anchors in unsaturated sand, shedding light on their performance under various conditions and providing a basis for practical applications in geotechnical engineering.

2. Problem statement

In the current investigation, the pullout capacity of a vertical anchor plate of height b and negligible thickness placed in unsaturated sand with water table at a depth of h_w from the ground surface is obtained. The depth of the lower edge of the plate from the ground surface is d. The domain is discretized into several triangular elements. The size of the domain is chosen such that the yield zone remains within the boundary and the collapse load does not change much when the size of the domain is further increased.

3. Methodology

In the analysis, lower bound finite element limit analysis, as proposed by Sloan [5] and the second order cone optimization technique, as developed by Makrodimopoulos and Martin [2] are applied. The stresses across the entire domain are assumed to follow the element equilibrium equations, discontinuity equilibrium, boundary conditions and the specified yield criterion. The computer code for generating the mesh is written in MATLAB [3], and the conic optimization is executed using an optimization toolbox MOSEK ApS [4] available for MATLAB.

The magnitude of flow rates for evaporation, no flow and infiltration are taken equal to 1.15×10-8 m/sec, 0 m/sec and -3.14×10-8 m/sec, respectively (Lu and Likos [1]). The range of other parameters used in this study are given in Table 1.

Parameter	Range
Anchor embedment depth, d	1 m - 5 m
Angle of internal friction, ϕ'	30°, 40°
Saturated unit weight, γ_{sat}	17 kN/m^3 (when ϕ' = 30°) 20 kN/m^3 (when ϕ' = 40°)
Height of anchor plate, b	1 m, 2 m
Depth of water table from the ground surface, h_w	Depending on the value embedment depth of anchor
Residual degree of saturation, S_r	5%
Inverse of air entry pressure parameter, α	0.1 kPa^{-1} - 0.5 kPa^{-1}
Pore size distribution parameter, n	4 - 8

Table 1. Range of various parameters used

4. Results

From the analysis, the flow conditions do not affect the pullout capacity much. This is attributed to the fact that suction stress does not change much with change in flow conditions for sand. However, the anchor capacity increases with an increase in the depth of the water table, height and embedment depth of anchor and angle of internal friction. The failure patterns also show that the pullout capacity is higher for greater depths of water table and higher values angle of internal friction of sand.

5. References

[1] Lu, N. & Likos, W.J. (2004). Unsaturated soil mechanics. Wiley, New York

[2] Makrodimopoulos, A. & Martin, C.M. (2006). Lower bound limit analysis of cohesive-frictional materials using second-order cone programming. *Int. J. Numer. Methods Engng.*, **66(4)**:604–634

[3] MATLAB. (R2021a) [Computer software]. MathWorks, Natick, MA

[4] MOSEK. (2018). The MOSEK optimization toolbox for MATLAB manual. Version 8.1 (Revision 8).

[5] Sloan S.W. (1988). Lower bound limit analysis using finite elements and linear programming. *Int. J. Numer. Analyt. Meth. Geomech.*, **12(1)**:61-77.

Topology Optimization based Integrated Design of Structure-Foundation System

Xifan Li[1], Xue Zhang[1] and Yujia Zhang[1]
[1] University of Liverpool, Liverpool, UK

1. Introduction

This paper refines the conventional foundation design process, which typically treats soil foundation and above-ground turbine support structure as separate entities. This segmented approach, although standard, may result in suboptimal solutions due to its lack of a holistic view of the system. Separate treatment of these components could overlook potential synergies for improved performance or cost reduction. Li [1] introduced a method for 3D topology optimization, integrating mixed rigid-plastic analysis with a density-based approach using the smoothed finite element method. This technique, incorporating plasticity theory, has shown to yield more cost-efficient designs than traditional stress-constrained topology optimization. It also employs mesh adaptivity to boost computational efficiency.

Building upon the work in [1], this paper introduces a method to integrate two materials in plasticity-based topology optimization. This extended approach, adaptable to original formula in [1], enables an integrated design of the upper structure and underlying soil foundations. Numerical examples illustrate its robustness in design application.

2. Formulations

According to [1], density-based topology optimization in limit analysis can be formulated as a volume minimization problem by introducing a new design variable, 'density' $\rho \in [0,1]$:

$$\max_{(\boldsymbol{\sigma},\alpha)} \quad \alpha$$
$$\text{subject to:} \quad \begin{cases} \overline{\boldsymbol{B}}^{\mathrm{T}}\widehat{\boldsymbol{\sigma}} - \overline{\boldsymbol{F}}_{\mathrm{b}} = \overline{\boldsymbol{F}}_{\mathrm{t}} \\ f^i(\widehat{\boldsymbol{\sigma}}) \le 0 \qquad i = 1,2,\cdots,NN \end{cases} \tag{1}$$

where α is the collapse load factor (e.g., $\alpha\bar{\boldsymbol{t}}$ indicating the ultimate force the structure can sustain). $\widehat{\boldsymbol{\rho}} = [\rho_1, \rho_2, \cdots, \rho_{NN}]^{\mathrm{T}}$ is a vector consisting of density (i.e., ρ) at all nodes. $\overline{\boldsymbol{B}}^{\mathrm{T}}$ is the global matrix calculated based on nodal integration, $\overline{\boldsymbol{F}}_{\mathrm{b}}$, $\overline{\boldsymbol{F}}_{\mathrm{t}}$ are the body force and external force, respectively.

3. Case Study

We outline an integrated design for the soil foundation and supporting structure of offshore wind turbines, focusing on a 10m cubic domain, divided into two 10m × 5m rectangular prisms (Figure 1 a-c). The upper prism consists of reinforcing steel (yield strength 345 MPa) for the above-seabed part of the turbine structure. It includes four fixed bases (2m each) at the top corners. The lower prism is split into three zones: a deeper blue area (8m × 4m) for reinforcing steel and soil (cohesion 30kPa), a central red zone (2m × 1m) for pipelines, and a light blue area for marine soil. A circular load surface (radius 1.5m) on the top applies a pressure of 16,985 kPa. Only the upper surface is unfixed. For efficiency, we use a quarter of the domain (5 m × 10 m × 5 m) in simulations, with the upper cube for steel (zero density indicating no material) and the lower for steel or soil (zero density for soil, one for steel). Mesh adaptive techniques ensure higher mesh density in structural areas to balance simulation speed and accuracy.

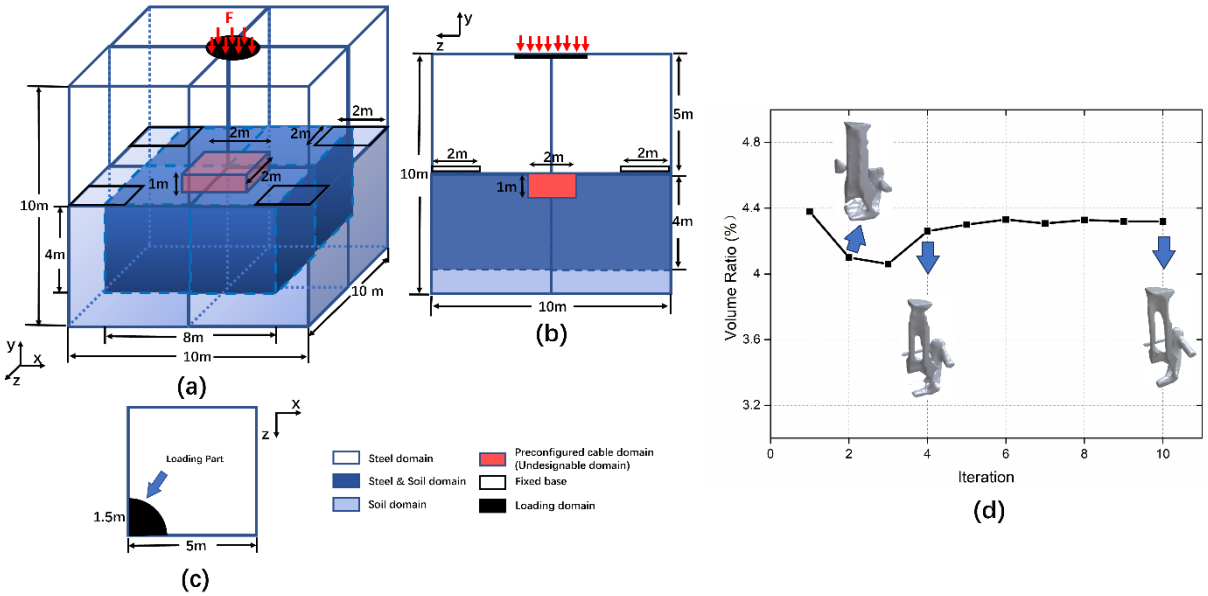

Figure 1 The integrated design domain & Topology optimization convergence history: (a) Overall domain; (b) Global Side-view; (c) Quarter section top view on loading part ; (d) Topology optimization layout & Volume Ratio under different iteration:

Figure 1 (d) shows the development of an optimized structure across various iteration counts. Initially, the first two iterations reveal an emerging structure, but with inadequate reinforcement at the bottom to resist top loads due to insufficient density penalization. By the fourth iteration, the bottom reinforcement solidifies, and the structure becomes more robust. The volume ratio's instability before the fourth iteration suggests an unstable structure, but stability is achieved as the iteration count reaches four. This indicates the algorithm's higher efficiency compared to other methods[2], needing only 4-6 iterations to stabilize the volume ratio and form a stable structure.

4. Conclusions

This paper presents a plasticity-based 3D topology optimisation method for continuous structures that can cover multiple materials. The method combines density-based topology optimisation with mixed limit analysis to promote integrated design of the upper structure and the underlying soil foundation. To improve computational efficiency, we introduce mesh adaptivity techniques using linear tetrahedral elements. A case study is shown to demonstrate the effectiveness and robustness of our approach. The results show that our method achieves satisfactory performance in integrated design, and our technique has a significant advantage over conventional methods in terms of structural convergence efficiency.

5. References

1. Li, X., X. Zhang, and Y. Zhang, *Three-dimensional plasticity-based topology optimization with smoothed finite element analysis.* Computational Mechanics, 2023: p. 1-16.

2. Wang, M.Y., X. Wang, and D. Guo, *A level set method for structural topology optimization.* Computer methods in applied mechanics and engineering, 2003. **192**(1-2): p. 227-246.

Towards the numerical modelling of the adhesion between plane steel surfaces and cohesive soils

***M. S. Narayanan*[1], *M. Schröder*[1] *and J. Grabe*[1]**

[1] *Institute of Geotechnical Engineering and Construction Management, Hamburg University of Technology, Germany*

Soil-structure interaction is a crucial phenomenon in geotechnical engineering with fundamental applications ranging from pile foundations to tunnel boring machines. Thus, a comprehensive understanding of the contact surface between a structure and the surrounding soil is essential. In the context of clayey soils, stickiness or adhesion at the soil-structure interface plays a significant role in the contact behaviour. Soil-structure adhesion is dependent on the soil characteristics, including mineralogical composition and consistency of clay. Additionally, experimental factors such as material roughness of the interface, rate of loading, temperature and contact time further influence the adhesive properties [1]. Figure 1 shows the characteristic force curve over time during a separation test with dead load.

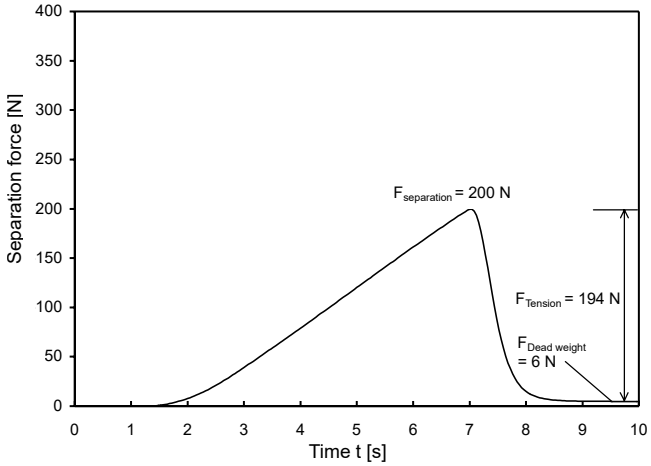

Figure 1. Exemplary progression of a separation test over time. Taken from Thewes (1999).

Numerical studies can provide detailed insights into this complex mechanism, given the adoption of appropriate constitutive models and contact laws. Generally, in the case of cohesion-less soils, a Coulomb frictional model is adopted to model the soil-structure interface. However, this approach is unrealistic when the soil of interest is cohesive in nature. To date, there have been limited numerical studies on modelling the adhesive interaction between cohesive soils and structural surfaces [2, 3]. The current study focuses on investigating the normal adhesion between a steel plate and cohesive soil through numerical modelling of separation tests using the finite element software ABAQUS. It involves separating a steel plate from a preloaded clay sample (Figure 2) and tracking the evolution of contact stresses (Figure 3). Initially, the top plate was compressed into the soil and a constant displacement boundary condition was applied to separate the plate from soil. The study assesses the effectiveness of using surface-based cohesive contact based on traction separation law for the adhesive interface. The traction-separation law governs the variation of interface stresses/traction with respect to the applied displacement/separation [4]. The adopted cohesive contact combines surface-based contact interactions and cohesive behaviour between two surfaces to capture separation and re-adhesion, thus making it suitable for addressing the current problem. This model is further validated

with the separation experiments on clays with high kaolinite content. The failure patterns observed in soil during separation are compared with the experimental specimens. Further, the effect of different non-linear traction-separation laws including bilinear, exponential and trapezoidal models, on the adhesive contact behaviour is studied.

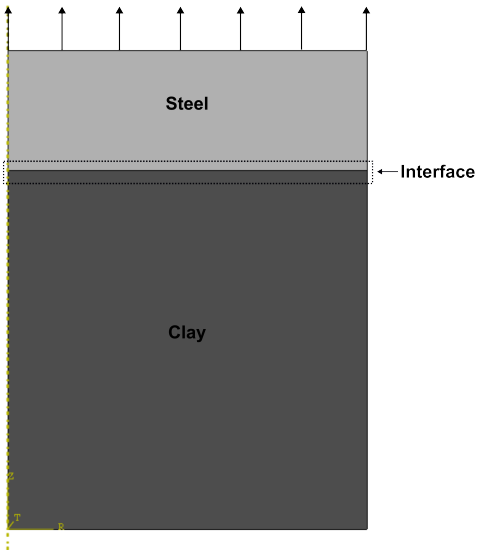

Figure 2. Numerical model: Separation test

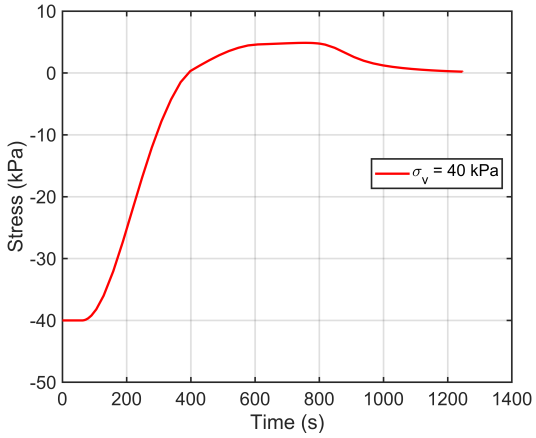

Figure 3. Preliminary results: Stress-time behaviour at the interface

References

[1] Thewes, M. (1999). *Adhäsion von Tonböden beim Tunnelvortrieb mit Flüssigkeitsschilden*. Phd thesis, Bergische Universität Wuppertal, Wuppertal, Germany.

[2] Raous, M., Cangémi, L., and Cocu, M. (1999). A consistent model coupling adhesion, friction, and unilateral contact. *Computer Methods in Applied Mechanics and Engineering*, **177**, 383–399.

[3] Nazihe, T., Berga, A., Raous, M., and Nabil, A.-B. (2018). A contact model coupling friction and adhesion: Application to pile/soil interface. *International Review of Civil Engineering (IRECE)*, **9**, 20.

[4] Sauer, R. A. (2016). A survey of computational models for adhesion. *The Journal of Adhesion*, **92**, 81–120.

Advances in numerical methods

Artificial neuron networks

A COUPLED TANN-ABAQUS METHOD FOR MULTISCALE GEOMATERIAL MODELLING

F. Rabie[1], D. Arnold[1], H. Lewis[1] and V. Demyanov[1]
[1] Institute of GeoEnergy Engineering, School of Energy, Geoscience, Infrastructure and Society, Heriot-Watt University, United Kingdom

The *multiscale* modelling framework outlined here aims to conceptualise the inherently complex constitutive response of geomaterials and demonstrate computational efficiency. The bridge between locally defined microscopic and macroscopic constitutive behaviours in multiscale geomaterial frameworks comes at a prohibitive computational cost. This is increasingly pertinent for large-scale multiscale analyses. A multiscale framework incorporating a *physics-based data-driven constitutive model* offers a computationally efficient method for large-scale geomaterial modelling, and ensures physically consistent constitutive responses (for e.g., see [1], [2], [3] and [6]).

While promising, such frameworks remain significantly underdeveloped. We present a coupled *TANN-FEM* method for multiscale geomaterial modelling in *Abaqus*. Our proposed framework leverages *Thermodynamics-based Artificial Neural Networks* (TANN), a deep learning algorithm for material constitutive modelling. TANN, based on *Generalised Thermodynamics*, adopts *internal variables* to allow for a more detailed description of the material response. The First and Second Laws of Thermodynamics are directly encoded in TANN, therefore guaranteeing the thermodynamic consistency of learnt constitutive models (refer to [4] and [5] for more).

Abaqus supports User Material (UMAT) subroutines written in Fortran for custom modelling of material constitutive behaviour. The coupled TANN-FEM method adopts a TANN-based UMAT subroutine, where a trained TANN and a Fortran-based UMAT are linked through a shared library. The presented workflow bypasses the reconstruction of the trained neural net in a Fortran-based UMAT (for e.g., see [7] and [8]). Instead, a C++ wrapper creates an interface linking TANN and Fortran, allowing the user to load and directly call the TANN model in inference mode from the Fortran-based UMAT. The C++ Application Programming Interface (API) provided by PyTorch is used to train and save the TANN model.

3D Finite Element analyses demonstrating the coupled TANN-FEM method are performed in Abaqus. The TANN training data is generated through the numerical integration of incremental thermodynamic constitutive models under random loading paths. Periodic boundary conditions are used. TANN is trained to evaluate the numerical solution of the microscale homogenisation problem, in terms of stresses and internal state variables. The assumption of scale separation, where the solution of the boundary value problem at the macroscale is separated from that of the microscale problem, must be valid for the successful implementation of this method. In this context, TANN can be used in inference mode to perform large, multiscale analyses. To evaluate the computational efficiency and prediction accuracy of the coupled TANN-FEM method, microscale reference simulations are run.

To our knowledge, our proposed method marks the first attempt at directly linking a trained Machine Learning model to a Fortran-based UMAT. The coupled TANN-FEM method supports the direct use of *autograd*, a PyTorch automatic differentiation engine, within a Fortran-based UMAT. This is particularly relevant for a TANN-based UMAT, as it relies on automatic differentiation to enforce thermodynamic constraints. The presented method is not limited to TANN and can be used

to link any trained neural network to a Fortran-based UMAT. We present this method in efforts to contribute towards accessible technical methods that bridge between Machine Learning models and commercial Finite Element tools. The coupled TANN-FEM method promises a computationally effective alternative to traditional multiscale modelling frameworks.

References

[1] Chinesta, F., Cueto, E., & Guevelou, S. (2022). Material Forming Digital Twins: The Alliance between Physics-Based and Data-Driven Models. *Key Engineering Materials, 926*, 3–14. https://doi.org/10.4028/p-234d4y

[2] Eghbalian, M., Pouragha, M., & Wan, R. (2023). A physics-informed deep neural network for surrogate modeling in classical elasto-plasticity. *Computers and Geotechnics, 159*, 105472. https://doi.org/10.1016/j.compgeo.2023.105472

[3] Fuhg, J. N., Böhm, C., Bouklas, N., Fau, A., Wriggers, P., & Marino, M. (2021). Model-data-driven constitutive responses: Application to a multiscale computational framework. *International Journal of Engineering Science, 167*, 103522. https://doi.org/10.1016/j.ijengsci.2021.103522

[4] Masi, F., & Stefanou, I. (2022). Multiscale modeling of inelastic materials with Thermodynamics-based Artificial Neural Networks (TANN). *Computer Methods in Applied Mechanics and Engineering, 398*, 115190. https://doi.org/10.1016/j.cma.2022.115190

[5] Masi, F., Stefanou, I., Vannucci, P., & Maffi-Berthier, V. (2021). Thermodynamics-based Artificial Neural Networks for constitutive modeling. *Journal of the Mechanics and Physics of Solids, 147*, 104277. https://doi.org/10.1016/j.jmps.2020.104277

[6] Rocha, I., Kerfriden, P., & Van Der Meer, F. (2023). Machine learning of evolving physics-based material models for multiscale solid mechanics. *Mechanics of Materials, 184*, 104707. https://doi.org/10.1016/j.mechmat.2023.104707

[7] Suh, H. S., Kweon, C., Lester, B. T., Kramer, S., & Sun, W. (2023). A publicly available PyTorch-ABAQUS UMAT deep-learning framework for level-set plasticity. *Mechanics of Materials, 184*, 104682. https://doi.org/10.1016/j.mechmat.2023.104682

[8] Taç, V., Sree, V. D., Rausch, M. K., & Tepole, A. B. (2022). Data-driven modeling of the mechanical behavior of anisotropic soft biological tissue. *Engineering With Computers, 38(5)*, 4167–4182. https://doi.org/10.1007/s00366-022-01733-3

MULTISCALE MODELING OF GRANULAR MATERIALS USING MESOSCALE MACHINE LEARNING APPROACH

A. Wautier[1], A. Li[1], W. Qu[1], M. Pouragha[2] and F. Nicot[3]

[1] INRAE, Aix-Marseille Université, Unité de Recherche RECOVER, Aix-en-Provence, France
antoine.wautier@inrae.fr

[2] Carleton University, Civil and Environmental Engineering Department, Ottawa, Canada

[3] Université Savoie Mont Blanc, ISTerre, Le Bourget-du-Lac, France

1. Abstract:

When it comes to deriving the constitutive behavior of a heterogeneous material from a detailed description of its microstructure, two homogenization strategies can be employed, namely spatial homogenization or statistical homogenization. On the one hand, spatial homogenization is based on the concept of the representative elementary volume (VER), and the constitutive relationships are obtained by computing the volume averages of local stresses and strains. On the other hand, statistical homogenization is based on the description of the microstructure as a collection of independent mesostructures of relatively small dimensions (several orders of magnitude smaller than the size of the REV). Macroscopic behavior is then obtained from the weighted average of the individual responses of each mesostructure. The current challenge faced by most micromechanical models based on statistical homogenization is to incorporate sufficient relevant microstructural features into the simplified mesostructures for complex properties to emerge during the upscaling process.

For granular materials, one particular example of micromechanical models is the H-model [1, 2, 3]. This model relies on elementary mesostructures that consist in hexagonal patterns of six circular grains in 2D and bi-hexagonal patterns of ten spherical grains in 3D (the "H-cell"). Because of the imposed H-cell symmetry, an analytical description of the mechanical response of the model is derivable. However, the model suffers from several known limitations, which will probably require the use of enriched mesostructures that might be too complex to allow for an analytical treatment anymore (for instance, to account for widely graded materials subjected to internal erosion).

In this work, we establish the necessary framework for inputting any kind of enriched mesostructure into the H-model, and more generally to any micromechanical model. We propose a strategy to describe the mechanical response of the mesostructures thanks to physics informed artificial neuron networks (ANN). By applying machine learning techniques at the mesoscale (instead of the REV scale), it is indeed possible to generate the necessary learning database from discrete element simulations at a cheap computation cost. We apply this modeling strategy to the standard H-model and show that the trained surrogate ANN is able to predict the response of granular materials on complex loading paths (for instance on drained biaxial and q-constant loading tests).

2. References

[1] Nicot F. & Darve F. (2011). The H-microdirectional model: accounting for a mesoscopic scale. Mechanics of materials, 43(12):918–929.

[2] Wautier A., Veylon G., Miot M., Pouragha M., Nicot F., Wan R. & Darve F. (2021). Multiscale modelling of granular materials in boundary value problems accounting for mesoscale mechanisms. Computers and Geotechnics, 134:104143.

[3] Xiong H., Nicot F. & Yin ZY (2017). A three-dimensional micromechanically based model. International Journal for Numerical and Analytical Methods in Geomechanics, 41(17):1669–1686.

Advances in numerical methods

Homogeneization

CONSTANT-VOLUME SHEAR RESPONSE OF 4-CELL ANALOGICAL MICROMECHANICS MODEL FOR GRANULAR SOIL

T. Matsushima[1], Y. Higo[2] and Y. Otake[3]

[1] University of Tsukuba, Department of Engineering Mechanics and Energy, Tsukuba, Japan

[2] Kyoto University, Department of Urban Management, Kyoto, Japan

[3] Tohoku University, Department of Civil Environmental Engineering, Sendai, Japan

1. Introduction

Constitutive modelling of quasistatic plastic shear behavior of granular solid is essential in simulating various geotechnical engineering problems. Various models describing complicated soil behaviors have been proposed mainly in the framework of phenomenological elastoplastic models as an extension of J2 flow theory in metals. Although another framework called micromechanics models have also been studied to describe the bulk behavior of granular assemblies based on grain scale mechanics, they are still under investigation. This study deals with the model of the latter type as a modification of the one proposed by Matsushima and Chang [1]. We introduce a 4-cell analogical model with which the orientational distribution of contact forces in the uniform strain model (Chang & Misra [2]) is modified to describe the plastic yielding toward critical state. In this presentation we focus on the monotonic/cyclic constant-volume response of the proposed model.

2. 4-cell analogical model

Following Matsushima and Chang [1], the proposed model adopts the finite strain formulation of the uniform-strain micromechanics constitutive model. We set a sufficient number N_c of branch vectors explicitly, and compute the elastic contact force $\boldsymbol{f}^c$ for each branch vector c due to the prescribed incremental uniform deformation field (**Fig.1**). Then, we modify the normal force component f_n^c to regulate the anisotropy of its orientational distribution. The key concept is that we introduce a regular packing granular model shown in **Fig.2**, and evaluate the ratio of the maximum and the minimum normal force, $\alpha = f_{n,\max}/\ f_{n,\min}$, by the critical ratio $(f_1/f_2)_{limit}$ when the contact slip occurs in **Fig.2**. Accordingly, the contact friction coefficient μ_c is considered as a material parameter to define f_n^c anisotropy. Second, we introduce a state parameter β that controls the dilation as a function of the porosity as $\beta = \beta_0(\theta_{\max} - \theta)/(\theta_{\max} - \theta_{\min})$, where $\theta_{\max} = 45°$ and $\theta_{\min} = 30°$. The value of β at the densest state, defined as β_0, is considered as another material parameter related to the maximum dilation of the material. Third, the structural parameter θ evolves with porosity n as $n = \pi/(6\sin 2\theta)$.

3. Constant-volume responses and discussions

The response of the constant confining pressure has been tested successfully so far (Matsushima, Higo, Otake [3]. In the present study, we tested the constant-volume response. **Table 3** shows the material parameters we used. **Fig. 3** shows the stress paths and the stress-strain relations for various initial void ratios. It can be seen that the static liquefaction occurs in loose samples, while the stress increase along the failure line is observed in dense samples. The overall behavior is quite similar to undrained triaxial compression test result of sandy soil [4]. We have confirmed that the constant-volume cyclic shear behavior can also be simulated quite nicely with the present model.

4. References

[1] Matsushima, T., Chang, C.S., 2007. In Geomechanics and Geotechnics of Particulate Media, pp. 293-298, CRC Press.

[2] Chang, C.S., Misra, A., 1990. Journal of engineering mechanics, 116(10), pp.2310-2328.

[3] Matsushima, T., Higo, Y., Otake, Y., in preparation.

[4] Yoshimine, M., Ishihara, K. Vargas, W., 1998. Soils and Foundations, 38(3), pp.179-188.

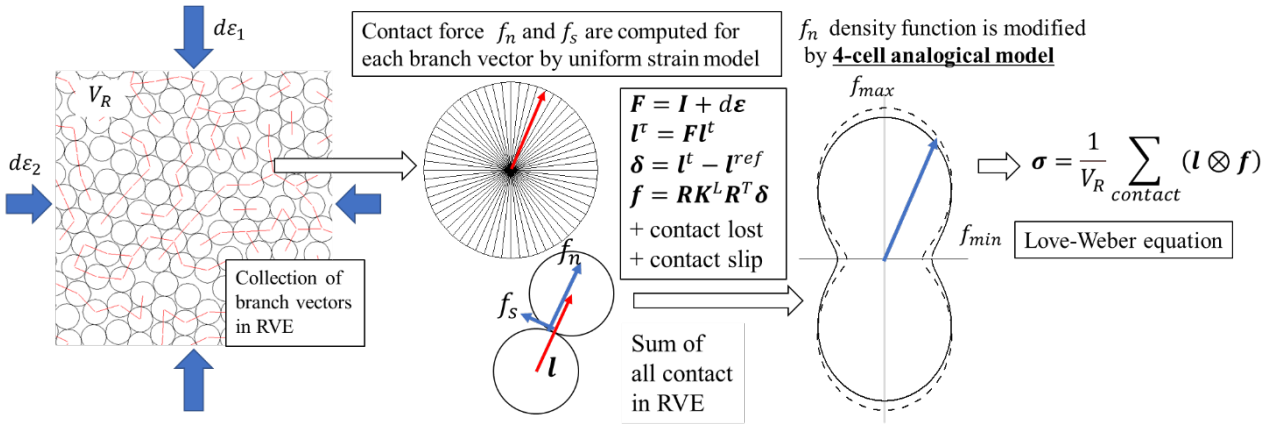

Figure 1. Basic procedure of uniform strain micromechanics model

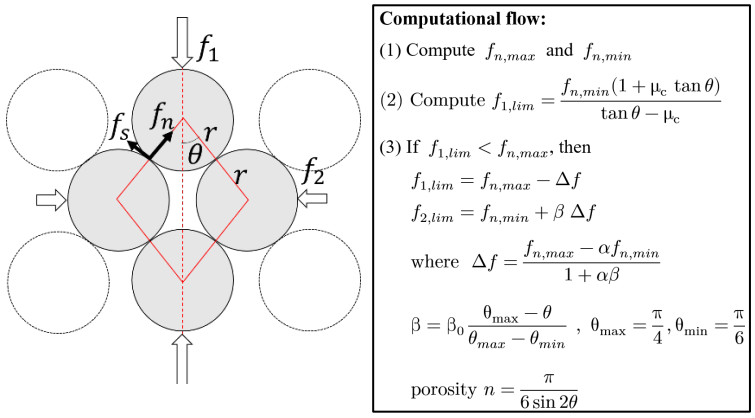

Figure 2. 4-cell analytical model

Grain size	0.1(mm)
Number of branch vectors, N_c	60
Contact spring constant, $k_n = k_s$	1.0×10^5 (N/m)
Intergranular friction μ	0.5
4-cell contact friction μ_c	0.1
β_0	2.0
Confining pressure σ_c	100 (kPa)

Table 1. Simulation parameters

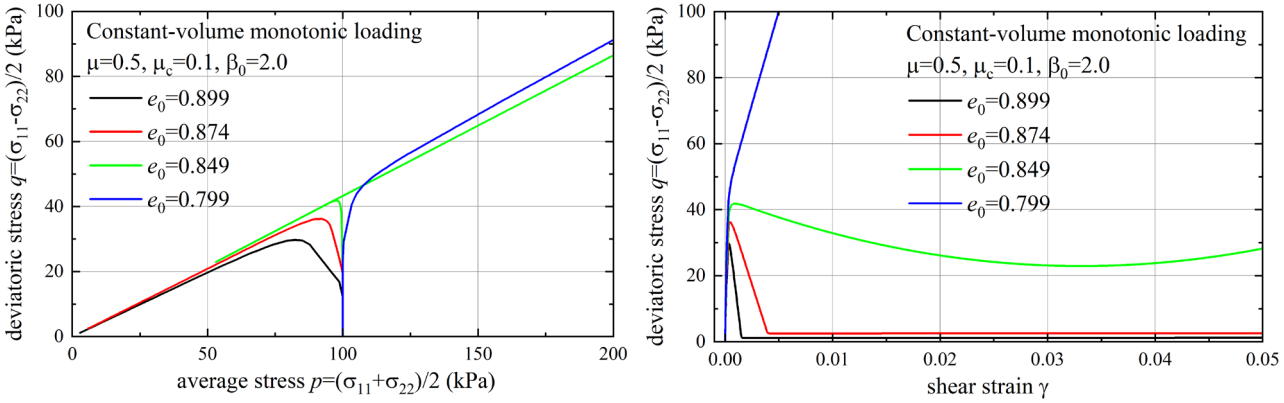

Figure 3. Stress paths (left) and stress-strain relations for various initial void ratios computed by the proposed constitutive model.

FROM PARTICLE SIMULATIONS TOWARDS A UNIVERSAL CONTINUUM THEORY ABOUT INTERMITENCE AND JAMMING, UN-JAMMING TRANSITIONS

S. Luding[1,2]

[1] *Multi-Scale Mechanics (MSM), Department of Thermal and Fluid Engineering (TFE), Faculty of Engineering Technology (ET), and MESA+, POBox 217, 7500 AE Enschede, NL*

[2] *Email: s.luding@utwente.nl ; Website: http://www2.msm.ctw.utwente.nl/sluding/*

1. General

Both the dynamic and the static behavior of particulate and granular matter (like sand, powder, suspended particles, often with a wide distribution of particle sizes) is of considerable interest in a wide range of industries and research disciplines [1-7]. Special is that granular matter can behave either solid-like or fluid-like, or a single given granular material involves both states [4] at the same time (this is not to be confused with solid-fluid coupling where different materials are in different phases). Solid fluid co-existence and transitions are a major challenge [4] for both academia and industry. The related mechanisms/processes in particle systems are active at multiple scales (from nano-meters to meters), and finding the reasons for their multiple states might lead to a better understanding of natural disasters like avalanches or of industrial problems like silo-failure.

To understand the fundamental micro-mechanics and -physics, one can use particle simulation methods [1-7]. However, large-scale applications (due to their enormous particle numbers) have to be addressed by coarse-grained models or by continuum theory. In order to bridge the gap between the scales, so-called micro-macro transition methods are necessary, which translate particle positions, velocities and forces into density-, stress-, and strain-fields. These macroscopic quantities must be compatible with the conservation equations for mass and momentum of continuum theory [4]. Furthermore, non-classical fields are needed to describe the micro-structure (fabric, force-chains) or the statistical fluctuations, e.g. of the kinetic energy [4,5] or intermittency [7], before one can reach the ultimate goal of solving application problems based on the universal granular theory combining fluid- and solid-mechanics, as well as the jamming/un-jamming transitions between the states [1-7].

2. References

[1] Luding, S. (2016) Granular matter: So much for the jamming point, *Nature Physics 12, 531-532*

[2] Kumar, N., Luding, S. (2016) Memory of jamming -- multiscale models for soft and granular matter, *Granular Matter* 18, 58

[3] Shi, H., Roy, S., Weinhart, T., Magnanimo, V., Luding, S. (2020) Steady state rheology of homogeneous and inhomogeneous cohesive granular materials, *Granular Matter* 22, 14

[4] Luding, S., Jiang, Y., and Liu, M. (2021) Un-jamming due to energetic instability: statics to dynamics, *Granular Matter* 23, 80

[5] Luding, S. (2021) How does static granular matter re-arrange for different isotropic strain rate? in: *Powders and Grains 2021*, M. A. Aguirre, S. Luding, L. A. Pugnaloni, R. Soto (Eds.), EPJ Web of Conferences 249, 10001

[6] Luding, S., Taghizadeh, K., Cheng, S., Kondic, L. (2023) Understanding slow compression &decompression of frictionless soft granular matter by network analysis, *Soft Matter* 18, 1868

[7] Luding, S. (2023) Elastic-plastic intermittent re-arrangements of frictionless, soft granular matter under very slow isotropic deformations, *Frontiers in Physics* 11, 1211394

LIGHTWEIGHT CEMENTED SOILS: MULTI-SCALE EXPERIMENTAL OBSERVATIONS AND THERMODYNAMICS-BASED CONSTITUTIVE MODELLING

L. Perrotta[1], E. Vitale[2], G. Russo[2], A. Tengattini[3], E. Roubin[4], G. Viggiani[4], F. Rollo[5], A. Amorosi[5]

[1] Scuola Superiore Meridionale, Naples, Italy

[2] University of Naples Federico II, Department of Earth Sciences, Environment and Resources, Naples, Italy

[3] Université Grenoble Alpes, Institut Laue Langevin, Grenoble, France

[4] Université Grenoble Alpes, 3SR Lab, Grenoble, France

[5] Sapienza University of Rome, Department of Structural and Geotechnical Engineering, Rome, Italy

Lightweight Cemented Soils (LWCS) are heterogeneous materials obtained by mixing natural soil, water and cement with air foam and therefore characterised by a very complex microstructure, consisting of large foam-induced voids immersed in a cemented porous matrix (i.e., soil + cement) [1]. Due to surfactants, air is incorporated as almost spherical voids (i.e., foam-induced porosity) leading to a reduced unit volume weight of the material, while the use of cement as binder allows to increase the soil strength. These features, coupled with a good workability during the mixing stage, make LWCS suitable for many geotechnical applications, such as construction of fills [2-4] and embankments [5,6].

From a chemo-mineralogical point of view, Vitale *et al*., (2020) investigated LWCS complex evolution over time, the interaction of the hydrated phases with the soil fraction and the persistence of air voids induced by the surfactant. Through multi-scale approach they highlighted that foam does not alter the chemo-physical evolution of the binder [7].

From a mechanical perspective, an insight into the link between microstructural features and macroscopic behaviour of LWCS is here summarised and provided in detail in Perrotta *et al*., 2024 [8], underlining the key role played by the foam-induced porosity on the failure mechanism of the material. However, there is still a lack of constitutive models capable of accounting for the macroscopic mechanical effects of the complex microstructure of LWCS. As such, in this paper a new formulation is developed within the framework of Thermodynamics with Internal Variables [9] through a proper choice of a micro-inspired internal variable [10]. In detail, foam-induced porosity is considered as the only internal variable controlling the evolution of the microstructure, whereas the cemented matrix is supposed to behave as a linear elastic material. Therefore, the energy dissipation is only related to volume pore changes, thus neglecting at this stage any plastic dissipation.

Finally, the predictive capability of the model is illustrated with reference to a series of numerical simulations of laboratory tests and a new strategy for the calibration of the model parameters is proposed, based on Mean Field Homogenisation Approaches [11].

References

[1] De Sarno, D., Vitale, E., Deneele, D., Nicotera, M. V., Papa, R., Russo, G., & Urciuoli, G. (2019). Effects of cement and foam addition on chemo-mechanical behaviour of lightweight cemented soil (LWCS). In *E3S Web of Conferences* (Vol. 92, p. 11006). EDP Sciences.

[2] Satoh, T., Tsuchida, T., Mitsukuri, K., Hong, Z. (2001). Field placing test of lightweight treated soil under seawater in Kumamoto port. *Soils and Foundations*, **41.5**: 145-154.

[3] Tsuchida, T., & Egashira, K. (2004). *The lightweight treated soil method: new geomaterials for soft ground engineering in coastal areas*. CRC Press.
[4] Watabe, Y., Itou, Y., Kang, MS., Tsuchida, T., (2004). One-dimensional compression of air-foam treated lightweight geo-material in microscopic point of view. *Soils and Foundations*, **44.6**: 53-67.
[5] Jamnongpipatkul, P., Dechasakulsom, M., & Sukolrat, J. (2009,). Application of air foam stabilized soil for bridge-embankment transition zone in Thailand. In *Asphalt Material Characterization, Accelerated Testing, and Highway Management*: *Selected Papers from the 2009 GeoHunan International Conference* (pp. 181-193).
[6] Miki, H., Mori, M., & Chida, S. (2003). Trial embankment on soft ground using lightweight-foam-mixed in situ surface soil. In *Proc. XXIInd PIARC World Road Congress*, Durban.
[7] Vitale, E., Deneele, D., Russo, G., De Sarno, D., Nicotera, M. V., Papa, R., & Urciuoli, G. (2020). Chemo-mechanical behaviour of lightweight cemented soils. *Acta Geotechnica*, **15**: 933-945.
[8] Perrotta, L., Vitale, E., Arciero, M., Roubin, E., Tengattini, A., Russo, G & Viggiani, G. (2024). Microstructural insights into the mechanical behaviour of Lightweight Cemented Soils using x-ray microtomography. *Submitted to Géotechnique Letters*.
[9] Maugin,G.A., Muschik,W. (1994). Thermodynamics with internal variables. I. General Concepts, II. Applications. *Journal of Non-Equilibrium Thermodynamics*, **19**: 217-249, 250-289.
[10] Amorosi, A., Rollo F., Di Santo G. (2023). A micro-inspired perspective on the constitutive modelling of clays. *Rivista Italiana di Geotecnica*, **4**.
[11] Perrotta, L., Vitale, E., Russo, G. (2023). Homogenised Elastic Properties of Lightweight Cemented Soils. *Submitted to Journal of Rock Mechanics and Geotechnical Engineering.*

Damage and healing

DEFORMATION, CRACKING AND HEALING MECHANISMS IN ROCK SALT: A MICROSCALE STUDY

N. Du[1], M. Bornert[2] P. Aimedieu[2] and A. Dimanov[1]
[1]École Polytechnique, CNRS UMR 7649, Laboratoire de Mécanique des Solides, Palaiseau, France
[2]Ecole des Ponts, Université Gustave Eiffel, CNRS UMR 8205, Laboratoire Navier, Marne-la-Vallée, France

To reach the carbon emission reduction target, there is a need to develop large scale energy storage solutions in addition to transition to low-carbon energy sources. Underground storage in salt caverns is a potential storage solution for hydrogen, considered as a promising energy carrier. This type of storage has already been in use for decades for hydrocarbons but mostly on seasonal storage time span. To smoothen the production of renewable energies, short hydrogen storage/withdrawal cycles would be required. Therefore, further studies are still needed to ensure the integrity of the caverns, both in terms of mechanical stability and tightness, over short-term storage cycles [1, 2].

Numerous earlier investigations [3-7] of the mechanical behavior of rock salt, on either single crystals or polycrystalline samples, evidenced a range of mechanisms involved during its deformation, with relative contributions depending on thermodynamic conditions including temperature, stress level and triaxiality, strain rate and water content. Indeed, rock salt has a viscoplastic behavior resulting from intra-crystalline dislocation slip at low temperature, climb at higher temperature or recrystallisation as well as from intergranular mechanisms at grain boundaries. These include grain boundary sliding and opening, inducing local damage, as well as pressure solution when brine is present. Most of these investigations relied on macroscopic measurements or post-mortem qualitative microscale observations.

More recent quantitative measurements based on grain-scale SEM observations and digital image correlation [5,6] have demonstrated that a combination of mechanisms might be involved in the deformation of polycrystalline halite. Indeed, the experimental measurement of the overall strain partitioning into intragranular crystal slip plasticity and grain-boundary sliding/opening demonstrated that both mechanisms are present from the onset of plasticity. This can be explained by the lack of easy plastic slip systems at the considered low temperature conditions, which induces local strain incompatibilities between grains which require grain boundary mechanisms for their accommodation. These investigations were however performed at the free surface of the sample and under uniaxial loading conditions, which are not fully representative of the conditions in the rock mass near caverns. Moreover, considered synthetic halite samples were essentially dry, as a consequence of their elaboration process.

The present study aims at investigating deformation mechanisms under more realistic triaxial loading conditions and considers both wet and dry samples. Grain scale observations are in addition performed in the bulk by means 3D X-rays micro-tomography imaging giving access to the evolution of microporosity and the development of micro-cracks. To do so, powder compaction processes in both dry and wet conditions have been developed to obtain synthetic salt samples with different brine content and controlled, rather uniform, grain size. In situ compression tests at different confining pressures are performed inside a lab micro-tomograph using a specifically designed triaxial cell. In situ synchrotron experiments are also planned to test a wider range of confining pressures and faster loading rates, to investigate the effects of strain rate on the formation and healing of cracks.

Our first investigations clearly show the development of a network of cracks. They appear earlier in dry samples, suggesting brine has a strong effect on the formation of cracks and the involved deformation mechanisms. Figure 1 shows that for similar loading conditions (confinement pressure of 15 MPa), at around 5% axial strain, the dry sample has already developed a well spread network of cracks whereas at about 6% axial strain no cracks are visible in the wet material. Confining pressure also seems to prevent the formation of cracks, as a sample tested in uniaxial loading conditions starts to develop micro-cracks at smaller axial strain compared to a similar sample tested in triaxial conditions. More quantitative analyses will be performed by adapting digital volume correlation and damage quantification methods to the recorded 3D images. Some microstructural observations with SEM and EBSD technics also complement the analysis.

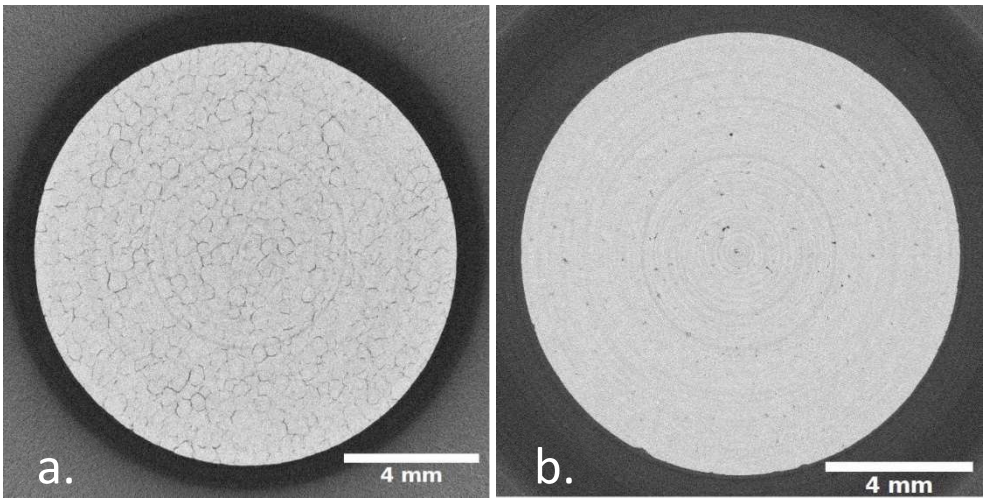

Figure 1. Cross sections through X-Ray Computed Tomography images of synthetic rock salt samples deformed under triaxial loading conditions (15 MPa confining pressure): a. dry material at ca. 5% axial strain and b. wet material at ca. 6% axial strain.

References

[1] Bérest, P. & Brouard, B. (2003). Safety of salt caverns used for underground storage blow out; mechanical instability; cavern abandonment. *Oil & Gas Science and Technology*, *58*(3), 361-384.

[2] Caglayan, D. G., Weber, N., Heinrichs, H. U., Linßen, J., Robinius, M., Kukla, P. A. & Stolten, D. (2020). Technical potential of salt caverns for hydrogen storage in Europe. *International Journal of Hydrogen Energy*, 45(11), 6793-6805.

[3]Urai, J. L., Schléder, Z., Spiers, C. J. & Kukla, P. A. (2008). Flow and transport properties of salt rocks. *Dynamics of complex intracontinental basins: The central European basin system*, 277-290

[4] Senseny, P. E., Hansen, F. D., Russell, J. E., Carter, N. L., & Handin, J. W. (1992, July). Mechanical behaviour of rock salt: phenomenology and micromechanisms. *In International journal of rock mechanics and mining sciences & geomechanics abstracts* (Vol. 29, No. 4, pp. 363-378). Pergamon.

[5] Bourcier, M., Bornert, M., Dimanov, A., Héripré, E., & Raphanel, J. (2012). Multiscale experimental investigation of crystal plasticity and grain boundary sliding in synthetic halite using digital image correlation. *Journal of Geophysical Research: solid earth*, 118(2), 511-526

[6] Gaye, A., Bornert, M., Lenoir, N., Sab, K., Dimanov, A., Bourcier, M., Héripré, E., Raphanel, J., Gharbi, H., Picard, D & Ludwig, W. (2014, June). Micromechanics of halite investigated by 2D and 3D multiscale full-field measurements. In *48th US Rock Mechanics/Geomechanics Symposium*. OnePetro.

[7] Urai, J. L., Spiers, C. J., Zwart, H. J. & Lister, G. S. (1986). Weakening of rock salt by water during long-term creep. *Nature*, *324*(6097), 554-557.

GAS TRANSPORT AND SELF-SEALING IN PLASTIC MATERIALS WITHIN A MULTI-SCALE PERSPECTIVE

L. Gonzalez-Blanco[1,2], E. Romero[1,2] and S. Levasseur[3]

[1] Centre Internacional de Mètodes Numèrics en Enginyeria (CIMNE), Barcelona, Spain

[2] Universitat Politècnica de Catalunya (UPC), Department of Civil and Environmental Engineering, Barcelona, Spain

[3] Belgian Agency for Radioactive Waste and Enriched Fissile Materials (ONDRAF/NIRAS), Brussels, Belgium

1. Introduction

Examining gas transport in plastic and low-permeability materials is gaining prominence in energy-related geotechnics, especially in managing the deep geological disposal of long-lived and heat-emitting radioactive waste. In the long-term, the generation of gases within the repository may affect the argillaceous rocks, which are investigated as potential hosts for disposal, and bentonite-based materials, as engineered barriers. The release of gases can result in an excessive pressure build-up in these saturated media, creating or reactivating fractures and fissures that establish preferential pathways for gas flow that could impair the safety assessment. However, these materials possess the capacity for self-sealing, through processes such as clay mineral swelling due to re-saturation, consolidation, or creep, thereby reducing fissure/fracture permeability and potentially restoring the barrier function [1].

2. Material and methods

This study specifically focuses on Boom Clay, a Cenozoic clay under consideration for hosting a repository in the Belgian program. The objective is to characterize the gas flow regime at relatively large pressures and the effectiveness of its self-sealing process after the gas invasion, thanks to the swelling of clay minerals during re-saturation. This plastic rock has sedimentary bedding planes that may act as preferential pathways during gas transport and different bedding orientations (parallel and orthogonal to the flow) were tested.

Gas permeability was quantified from the experimental gas injection/dissipation tests under oedometer conditions to macroscopically determine the dominant gas transport mechanism. To evaluate the self-sealing capacity, water permeability was measured before and after the gas injection stage, and the obtained values at both stages were compared. Similar values would indicate the restoration of the barrier function. Additionally, pore network analyses using mercury intrusion porosimetry (MIP), field emission scanning electron microscopy (FESEM) and micro-focus X-ray computed tomography (µ-CT) permitted visualizing and computing the potential gas pathways developed during gas injection and their possible closure upon re-saturation.

3. Results

Experimental results under oedometer conditions with lateral stress measurement indicated that samples in both orientations underwent some expansion during gas transport, even with gas pressures lower than the minor lateral stress. Computed effective gas permeability was consistently higher than the initial intrinsic water permeability which suggested the opening of preferential paths. The use of µ-CT helped in confirming the development of gas pathways following the bedding direction (Figure 1) and bridging bedding planes between them were detected with FESEM [2].

Water permeability after re-saturation showed values comparable to the initial intrinsic permeability, reflecting the recovery of the hydraulic barrier function due to clay minerals' swelling [3]. This self-sealing effect was also observed in CT images under unstressed conditions, where fissures detected after gas injection were no longer visible after re-saturation within the technique resolution (fissures > 40µm). However, a small proportion of large and disconnected pores were identified in CT images, likely resulting from some gas exsolution (Figure 1).

Finally, MIP data allowed estimating the total volume of fissures to define a multi-scale phenomenological model that relates the microstructural information to macroscopic flow transport properties capturing the intrinsic permeability increase on gas invasion and its recovery during self-sealing.

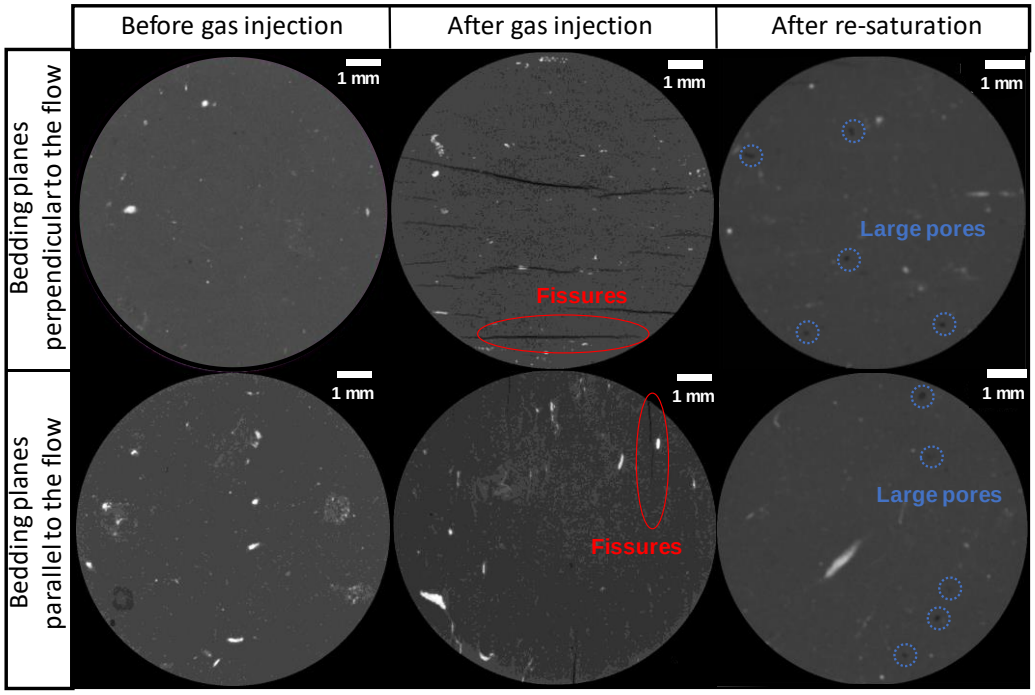

Figure 1. µ-CT images before gas injection (left), after gas injection (middle) and after re-saturation (right) of the samples with bedding planes perpendicular (top) and parallel (bottom) to the flow.

4. References

[1] Bastiaens, W., Bernier, F. & Li, X.L. (2007). SELFRAC: Experiments and conclusions on fracturing, self-healing and self-sealing processes in clays. *Phys. Chem. Earth*, 32(8–14): 600–615.

[2] Gonzalez-Blanco, L. & Romero, E. (2022) A multi-scale insight into gas migration in a deep Cenozoic clay. *Géotechnique* (Ahead of Print), 1–18.

[3] Gonzalez-Blanco, L., Romero, E. & Levasseur, S. (2023). Self-sealing of Boom Clay after gas transport. *Rock Mech. Rock Eng*, 1–17.

Acknowledgements

This project has received funding from the 'European Joint Programme on Radioactive Waste Management (EURAD)' (2019-2024) WP-Gas 'Mechanistic understanding of gas transport in clay materials' under grant agreement No. 847593 and from ONDRAF/NIRAS under contract No. CCHO 2021-0377/00/00 (2021-2024).

Insight into the micromechanisms of gas breakthrough in water-saturated clay-rich geomaterials – Implications for CO_2 sequestration

C. Allsop[1], M. Pedrotti[1] and A. Tarantino[1]
[1] University of Strathclyde, Civil & Environmental Engineering, Glasgow, Scotland

1. Abstract

The successful deployment of carbon dioxide (CO_2) geological sequestration in porous media is reliant on the sealing efficiency of the overlying, commonly, clay-rich caprock to act as a physical barrier to supercritical CO_2. Clay-rich caprock formations are considered as favorable materials to act as a seal due to them characteristically consisting of small pores providing high capillary entry pressures, hence preventing the intrusion of a non-wetting fluid (i.e., CO_2).

Due to the vast increase in CO_2 storage sites required to reach Net Zero targets, the juxtaposition and availability of deep seated (buried or highly indurated) caprock-reservoir systems to carbon capture and storage (CCS) clusters may not be available. Therefore, the assessment of shallow seated, weakly consolidated caprock-reservoir systems (e.g., Sleipner CO_2 storage field) will be required. Our experimental campaign tests analogous caprock geomaterials which have relatively high compressibility, representative of shallow seated (buried or less indurated) clay-rich caprocks.

Past experimental campaigns have focused on determining the capillary breakthrough pressure of caprock geomaterials. Only until recently have experimental campaigns demonstrated that CO_2 breakthrough is dominated by the creation of very localized channels (e.g., fractures) across the sealing barrier [1, 2, 3] and that this occurs at pressures far lower than the one predicted by the Laplace's equation (Eqn. 1). However, limited data characterizing these pathways formation exist. Furthermore, the physical indicators of susceptibility which underly the micro-mechanisms of failure (e.g., fracturing), are still only postulated for clay-rich geomaterials.

$$Pc^* = \frac{\psi\, T_s cos\theta}{d^*} \quad (1)$$

where Pc^* is the capillary breakthrough pressure [kPa], ψ, reflects pore shape [-], T_s, interfacial tension between water and gas (e.g., CO_2), and θ, represents wettability [°].

An innovative experimental set-up which allowed for the onset of surface crack formation to be captured during gas injection into intact clay-rich geomaterials is presented (representing the non-wetting fluid in CO_2 geological sequestration). The materials tested include Speswhite kaolin with plastic limit $w_P = 0.32$ and liquid limit $w_L = 0.64$, muscovite mica silt (potassium aluminium silicate) with $w_P = 0.33$ and $w_L = 0.60$, silica (quartz) silt, and a mixture of silica silt and kaolin clay with varying mass fraction, were chosen for the tests presented. This allowed for the investigation of physical indicators of susceptibility to gas breakthrough via localized pathways.

Results on different fracture patterns where non-wetting fluid (i.e., air) is injected into consolidated clay show the formation of large cracks that nucleate from within the sample (see Figure 1). Upon air pressurization, before fracture formation, the sample undergoes volumetric deformation (i.e., consolidation), as the resulting action of the vertical stress applied at the air-water interface (menisci). Once a fracture forms deformation stops and breakthrough occurs. Furthermore, gas invasion into the tested clay-rich geomaterials occurred at lower pressures than the expected air-entry-values traditionally recorded throughout the literature. The mechanisms of air intrusion are expected to be of a similar nature as CO_2 intrusion. Post-mortem assessment of the aperture, volume and

internal nature of these localized pathways was then visualized using the non-invasive and non-destructive xCT imaging technique (see Figure 1).

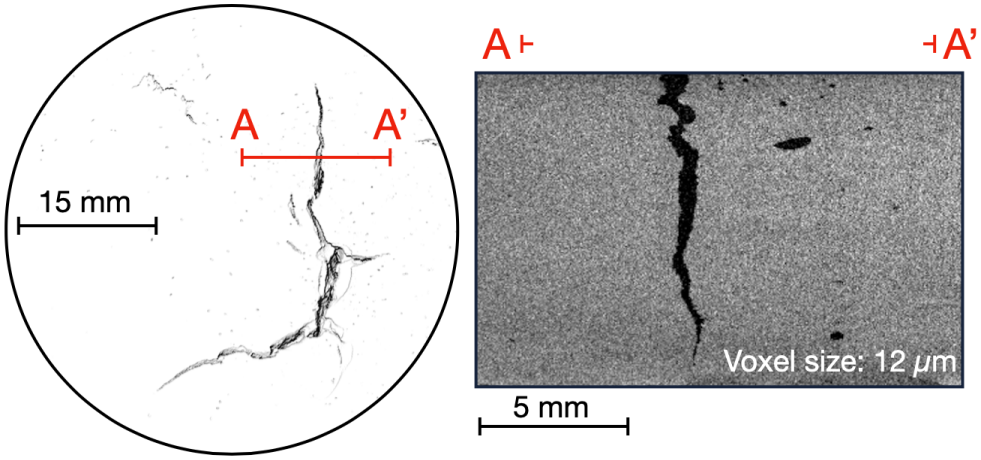

Figure 1. Representative fracture pattern of tested silica silt:kaolin clay 50:50 mixture post non-wetting gas injection. LHS: clay interface, RHS: xCT cross-section of fracture propagation.

As a continuum mechanics framework will not predict fracture formation under our test conditions, it appears that the experimental evidence support the underlying hypothesis that the disjoining pressure governs the mechanisms that ultimately control fracture formation and thus, eventually CO_2 breakthrough. The disjoining pressure is governed by the electrostatic double-layer interactions, van der Waal's dispersion forces, structural forces, and solvation forces [4].

If the pore size distribution is such that high gas pressures are required to overcome capillarity, the gas pressure will force single clay particles apart, displacing water form adjacent interparticle spaces. This processes therefore, represents a localized (imbalance) failure mechanism at the clay interface, resulting in fracture nucleation. It is expected that clay displaying large swelling pressures will subsequently display high gas entry pressure. This process is termed "pathway dilation" [4]. Therefore, pressurized gas will enter a dilated pathway at a lower pressure that the anticipated entry pressure typically recorded.

2. References

[1] Harrington, J., Milodowski, A., Graham, C., Rushton, J., & Cuss, R. (2012). Evidence for gas-induced pathways in clay using a nanoparticle injection technique. *Mineralogical Magazine, 76*(8), 3327-3336.

[2] Wiseall, A. C., Cuss, R. J., Graham C. C., & Harrington J. F. (2015). The visualization of flow paths in experimental studies of clay-rich materials. *Mineralogical Magazine, 79*(6), 1335-1342.

[3] Gonzalez-Blanco, L. and Romero, E. (2022). A multi-scale insight into gas transport in a deep Cenozoic clay. *Géotechnique*, pp. 1-18.

[4] Horseman, S.T., Higgo, J.J.W., Alexander, J.J.F.H. and Harrington, J.F. (1996). Water, gas and solute movement through argillaceous media. *Nuclear Energy Agency Rep. CC-96/1. OECD, Paris*.

NUMERICAL INVESTIGATION OF CHEMICAL DAMAGE-HEALING IN GEOMATERIALS AT THE MICROSTRUCTURAL LEVEL

***A. Sac-Morane*[1,2], *H. Rattez*[1] *and M. Veveakis*[2]**
[1] *UCLouvain, GCE, IMMC, Louvain-le-Neuve, Belgium*
[2] *Duke University, MGLab, Duke, NC, USA*

The intricate interplay between chemical and mechanical processes in soil and rocks has emerged as a key factor to consider for many engineering applications like underground storage or geothermal energy or to understand geological processes like diagenesis or earthquake nucleation. Those reactions lead to mineral dissolution (chemical damage) or to precipitation (chemical healing) that can modify the different properties of the material. This coupling between mechanic and chemistry has been investigated at the microstructural level considering two different mechanisms.

1. Debonding of cemented rocks as a chemical damage

The mechanical behavior and rupture of geomaterials is strongly affected by dissolution (chemical damage) phenomena. In the case of cemented rocks, debonding can occur during weathering and strongly weakens the material [1]. This strength degradation has also been highlighted during oedometric tests in the case of granular materials presenting no cohesion [2].

A new campaign of Discrete Element Modelization (DEM) simulations has been runned to investigate the effect of the debonding on the mechanical properties of the rock in different contexts. Those simulations consider a cohesive granular sample under oedometric conditions, while the bonds are dissolved by an acid injection. Thanks to the DEM, a lot of parameters can be easily controlled, as the initial value of the lateral earth pressure coefficient K_0 or the weakening law of the cementation.

For example, the influence of the degree of cementation, the initial state of stresses, the confining pressure or the history of the loading has been highlighted. It appears that the sample aims to reach an attractor configuration [3] with the chemical damage. This evolution of the mechanical configuration (mechanical properties and state of the stresses) can induce a modification in the stress state during the injection of a reactive fluid and lead to induced seismicity.

2. Pressure-solution phenomenon as a chemical damage-healing

Pressure solution [4] has a pivotal role in earthquake nucleation and recurrence or in diagenetic processes, among others. It involves three chemo-mechanical processes at the micro-scale: dissolution due to stress concentration at grain contacts, diffusive transport of dissolved mass from the contact to the pore space, and precipitation of the solute on the less stressed surface of the grains. These processes lead to a time-dependent compaction of the rock by changing its microstructure, pore structure and composition. It also induces a modification of the strength of a wide range of geological materials.

A new coupling between a Phase-Field method and a Discrete Element Modelization (PFDEM) has been recently developped to investigate this phenomenon [5]. The grains are modelled in the DEM part as polygonal (2D)/polyhedral (3D) particles to capture their complex shapes as they influence greatly the macroscopic mechanical behavior of the material [6]. Considering the granular material as a phase, PF is a good candidate to model with physics-based laws an addition or reduction of the quantity of material locally. The dissolution at the contact is controlled by the introduction of mechanical and chemical energy into the Allen-Cahn formulation on the phase variables, whereas the precipitation and the mass conservation are verified by a coupled diffusion formulation on the solute concentration.

This method has been applied to reproduce results from previous works on the pressure-solution phenomenon at several grains level [7]. For example, a so-called Andrade creep law has been reproduced. This new framework enables us to model chemo-mechanical couplings, considering the true shape of the grain. It is used to investigate the influence of the different physical phenomena (dissolution, precipitation or diffusion) controlling the rate of material compaction and of the macro properties evolutions, as the porosity, permeability or strength.

References

[1] Castellanza, R. and Nova, R. (2004). Oedometric tests on artificially weathered carbonatic soft rocks. *J. of Geotech. and Geoenviron. Eng.*, **130**, 728–739.

[2] Alam, M., Parol, V., , and Das, A. (2022). A dem study on microstructural behaviour of soluble granular materials subjected to chemo-mechanical loading. *Geomech. for Energy and the Environ.*, **32**, 100390.

[3] Vaughan, P. and Kwan, C. (1984). Weathering, structure and in situ stress in residual soils. *Geotech.*, **34**, 43–59.

[4] Tada, R. (1989). Pressure solution during diagenesis. *Ann. Rev. Earth Planet. Sci.*, **17**, 89–118.

[5] Sac-Morane, A., Veveakis, M., and Rattez, H. A phase-field discrete element method to study chemo-mechanical coupling in granular materials, under review in *Comput. Methods in Appl. Mech. and Eng.*

[6] Guével, A., Rattez, H., and Veveakis, M. (2022). Morphometric description of strength and degradation in porous media. *Int. J. of Solids and Struct.*, **241**, 111454.

[7] Guével, A., Rattez, H., and Veveakis, M. (2020). Viscous phase-field modeling for hcemp-mechanical microstructural evolution: application to geomaterials and pressuresolution. *Int. J. of Solids and Struct.*, **207**, 230–249.

Thermal effects

A MICROSTRUCTURAL INSIGHT OF CLAYEY SAND MIXTURES UNDER FREEZING AND THAWING CYCLES

G. Guida[1], F. Anselmucci[2], F.Casini[1] and V. Magnanimo[2]
[1] Università degli Studi di Roma Tor Vergata, DICII, Rome, Italy
[2] University of Twente, Chair of Soil MicroMechanics, ET Faculty, Enschede, The Netherlands

1. Introduction

Experimental evidence shows that soils under freezing temperatures exhibit varying susceptibility to volume expansion, depending on their fine content [1]. The reasons stem from the fact that volume expansion in frozen soils is not only attributable to the lower density of the ice (0.917 g/cm^3) compared to the liquid water (0.999 g/cm^3) but it is driven by the interface tensions generated at the freezing front, which makes the water migrate and accumulate, thereby creating ice lens [2]. With increasing fine content, the pore sizes reduce, and the interface tension rises. The volume expansion of soils induced by freezing, conventionally named "frost heave", and the severe settlements of ice-rich soils during thawing represent critical issues for the stability and functionality of the structures and infrastructures in cold regions [3].

This work investigates the complex thermo-hydro-mechanical response of clayey sand mixtures subjected to two complete cycles of freezing and thawing *in situ* in the X-ray computed tomography apparatus in TU Delft, accessible via the EPOS-NL program (https://epos-nl.nl/).

2. Experimental campaign

Four soil samples were considered. They consist of saturated Foitanbleau sand mixtures with different weight percentages of Speswhite kaolin – specifically 5, 10, 20 and 50% [4]. The samples (3.6 cm in diameter, ~3 cm in height) were prepared in Perspex cylinders (5 mm thick) sealed at the base. A water film of ~1 cm was left at the top of the sample as a reservoir. Two freezing and thawing cycles were replicated, placing the sample in contact with a cooling plate set at a temperature of - 15°C during freezing and turning it off during thawing. The top of the sample was left in contact with the environmental temperature at around 24°C. Laterally, an insulating coat was installed to avoid thermal dispersion and to allow one-dimensional conditions. The tests were performed *in situ* in the X-ray tomography room to scan the sample during the deforming stages. The steady states of the sample – namely, initial, fully frozen, and thawed – were imaged using a slow, 10-minute scan at a higher resolution (37.06 μm/px). During the deforming freezing-thawing stages, the samples were imaged using a faster 4-minute scan at a lower resolution (74.12 μm/px) to minimise image blurring caused by the high deformation rate. A few tracers (glass beads of 1.6 mm in diameter) were introduced into the mixtures to track the kinematics easily.

3. Image Analysis and micro-to-macro correlations

Interestingly, even a tiny weight percentage of fines completely changes the frost heave and the thaw contraction from a macroscopic (different displacements) and a microscopic (microstructure change) point of view. Figure 1 shows the time evolution of the sample height and tracers' position for mixtures at 5 and 10% fine content, complemented by a series of vertical cross-sections from the reconstructed three-dimensional images. These sections capture the steady states, thereby elucidating the evolution of the material internal structure over time. Both the mixtures heave during freezing

and settle during thawing without fully recovering the initial state. Points closer to the top of the sample (*e.g.*, tracer 4) undergo larger displacements, probably because of the closeness to the water reservoir at the top. The maximum cumulative heave during freezing increases significantly from the mixture with 5% clay (~0.7 cm) to 10% clay (~1.2 cm). In the mix with 10% clay, the water film at the top is adsorbed entirely during freezing. In addition, the sample segregates into two portions during thawing: a lower consolidated part in which visible pores disappear and a top part which becomes more porous than before. This microstructure change was systematically observed and became more pronounced in mixtures with higher fine percentages. Further elaboration of the images will enable the investigation of the evolution of the shape and distribution of pores throughout the process, providing a better understanding of the factors triggering the sudden change in microstructure.

Establishing a quantitative link between the macroscopic thermal loads, manifested through freezing and thawing cycles, and the irreversible changes in soil microstructure is a crucial outcome of this study. Such a finding enhances our understanding of soil behaviour under climatic stresses, paving the way for more informed soil management and predictive modelling in response to environmental changes.

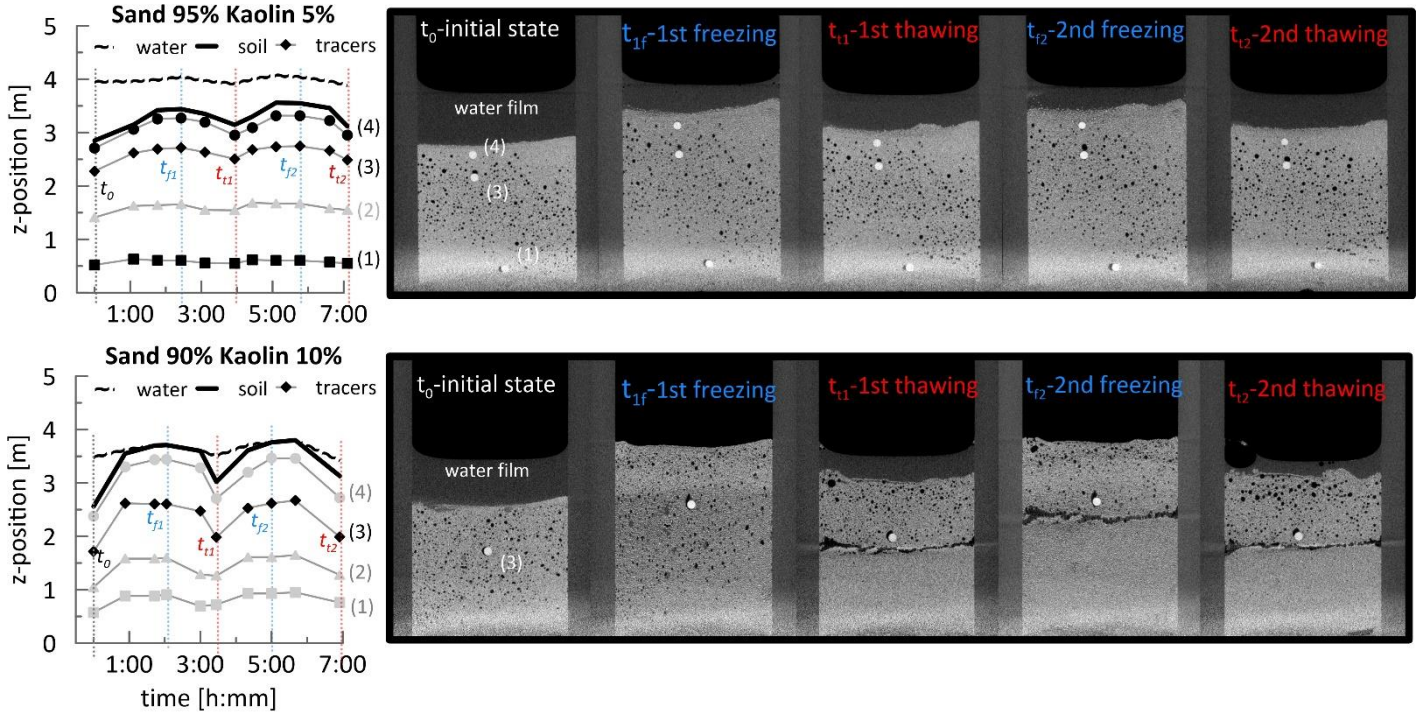

Figure 1. Time evolution of the sample height for mixtures at 5% (top row) and 10% (bottom row) fine content alongside the tracers' position, complemented by a series of vertical cross-sections from the reconstructed three-dimensional of the key steady states.

5. References

[1] Casagrande, A. (1932). A New Theory on Frost Heaving. *Discussion, Highway Research Board, (HRB), Proceedings*, No. 11, pp. 168-172.

[2] Penner, E. (1959). The mechanism of frost heaving in soils. *HRB Bulletin*, (225).

[3] Hjort, J., Streletskiy, D., Doré, G., Wu, Q., Bjella, K., & Luoto, M. (2022). Impacts of permafrost degradation on infrastructure. *Nature Reviews Earth & Environment*, 3(1), pp. 24-38.

[4] Viglianti, A., Guida, G., Casini F. (2023). Freezing-thawing response of sand-kaolin mixtures in oedometric conditions. *8th Int Symp on Deformation Characteristics of Geomaterials*, 1-6.

EFFECTS OF SALT PRECIPITATION ON SANDY SOIL THERMAL CONDUCTIVITY

H. Zhang[1], A. M. Tang[2] and B. Zhao[1]
[1] School of Civil Engineering, University College Dublin, Dublin, Ireland
[2] Laboratory Navier, École des Ponts Paris Tech, Marne-la-Vallée, France

1. Introduction

Dry climate and strong evaporation cause salinization in many arid regions. The evaporation of underground saline water in soils results in salt precipitation and accumulation on the topsoil. The precipitated salt causes cementation inside pores and alters the physical properties of soils, including strength, stiffness [1], and thermal conductivity [2]. Grains, pore fluids, air, and the contact conditions between different phases collectively contribute to the heat transfer pathway and determine the thermal conductivity of soils [3]. However, the precipitated salt crystals alter the internal structure and contact conditions of granular soils, which adds complexity to the analysis of thermal conductivity. The impact of salt precipitation on soil thermal conductivity remains to be explored.

This study adopts the transient hot wire method to determine the thermal conductivity of sand samples mixed with various initial brine contents and salt concentrations after drying through surface evaporation. The distribution of salt precipitation along the depth was determined by water rinsing for several soil layers. Additionally, we adopted X-ray microtomography to examine the pore-scale habits of salt precipitation.

2. Methodology

Fontainebleau sand with a median grain size of 0.21 mm, was utilized in this study. We mixed sand particles with NaCl solution at 1M and 6M concentrations to different initial brine content (5%, 10%, 15%, and 20%). The sand-brine mixture was filled in a cylindrical container with 30 mm in diameter and 40 mm in height. The samples were completely dried in an oven at 35℃. Thermal conductivity was then determined by inserting a thermal probe into samples and recording the heat dissipation rate while heating it at a given power. After tests, we peeled the surface salt crust and separated each sample into 4 layers from top to bottom with identical heights. The salt content of each layer was determined by comparing the weight of sand-salt mixtures and the remaining sand particles after rinsing. X-ray CT scanning was conducted to reveal pore-scale salt habits on glass bead samples.

3. Results

Figure 1a depicts the thermal conductivity of fully dried samples. At a low salt concentration (1 Mol/L), the increased initial brine saturation results in a higher thermal conductivity. The thermal conductivity rises from 0.35 W/(m·K) when the initial brine saturation is 5% to 0.45 W/(m·K) at a 20% initial brine saturation. Conversely, at a higher salt concentration (6 Mol/L), thermal conductivity is 0.52 W/(m·K) at 5% initial brine saturation but reduces to around 0.35 W/(m·K) when initial brine content is higher than 10%. Figure 1b reveals the salt precipitation distribution along the depth of each sample. At a low salt concentration (1M), the increased initial brine saturation results in more salt inside samples. However, most of the salt precipitated on the surface of the samples when the salt concentration was high (6M), which narrows the differences in salt

amount inside samples. The absence of a discernible correlation between the quantity of salt and thermal conductivity underscores the need to investigate salt habits at the pore scale.

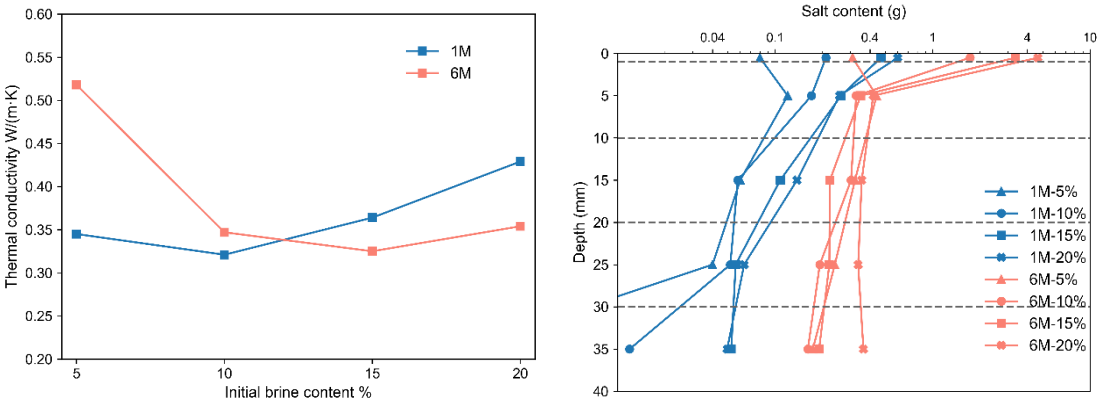

(a) (b)

Figure 1. (a)Thermal conductivity results; (b) Salt distribution along the depth.

Figure 2 presents a pore-scale depiction of a glass beads sample initially saturated by a 6M salt solution at 5% saturation. Upon drying, the precipitated salt forms salt cementation between particles which can enhance the thermal conduction. In comparison, salt precipitation prefers to accumulate in samples with high initial brine saturation, and less salt cementation was formed.

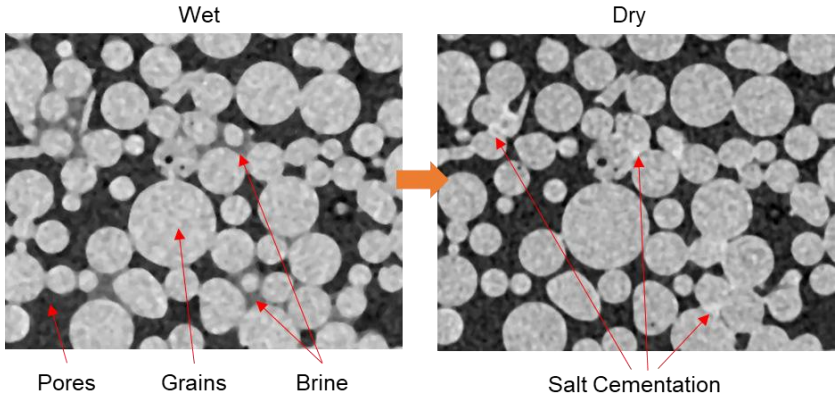

Figure 2. Pore-scale salt distribution (6M, 5%).

4. Conclusions

The influence of brine drying and salt precipitation on soil thermal conductivity has been experimentally investigated. The incremental salt content within samples did not consistently elevate thermal conductivity. Notably, pore-scale salt precipitation habits exert a more substantial influence on thermal conductivity.

5. References

[1] Truong, Q. H., Lee, C., Kim, Y. U., & Lee, J. S. (2012). Small strain stiffness of salt-cemented granular media under low confinement. *Geotechnique*, 62, 10: 949–953.

[2] Wang, Z., Zhang, N., Ding, J., Li, Q., & Xu, J. (2020). Thermal conductivity of sands treated with microbially induced calcite precipitation (MICP) and model prediction. *Int. J. Heat Mass Tran.*, 147, 118899.

[3] Roshankhah, S., Garcia, A. V., & Carlos Santamarina, J. (2021). Thermal Conductivity of Sand–Silt Mixtures. *J. Geotech. Geoenviron.*, 147(2).

INFLUENCE OF PARTICLE CONNECTIVITY ON HEAT TRANSFER IN UNSATURATED/SATURATED GRANULAR MATERIALS

Tairu Chen[1], Wenbin Fei[2,1] and Guillermo A. Narsilio[1]

[1] Department of Infrastructure Engineering, The University of Melbourne, Parkville, Australia

[2] College of Civil Engineering, Hunan University, Changsha 410082, China

1. Introduction

Heat transfer in granular materials plays an important role in many geo-engineering applications including carbon dioxide geological sequestration, hydrocarbon exploration, and geothermal energy utilisation. Connections between particles by themselves, air or water within granular materials form the main heat transfer paths and thus affect heat transfer fundamentally. Particle connection by themselves and air have been quantified and their influence on heat transfer has been studied in dry granular materials [1]. However, water bridges in unsaturated/saturated geomaterials change particle connections notably, and their contribution to heat transfer remains unknown. This study quantifies different types of particle connection in unsaturated/saturated granular assemblies based on computed tomography (CT) images, and then investigates the influence of quantified particle connection on effective thermal conductivity that indicates the ability of heat transfer.

2. Methodology

To observe connections between particles within a granular assembly, unsaturated glass bead samples were CT scanned and representative element volumes (REVs) were selected [2]. The REVs' cross-sections are shown in Figure 1 with varied degrees of saturation S_r. Considering heat transfer paths within the glass beads assemblies are attributed to 1) particles in physical contacts, and 2) particles connected by air or water bridges, six types of particle connection were found as cconceptualisedin Figure 2. Specifically, six types represent 1) particles in a physical contact with air bridge, 2) particles in a physical contact with both water and air bridges, 3) particles in a physical contact with water bridge, 4) separate particles connected by air bridge, 5) separate particles connected by both water and air bridges and 6) separate particles connected by water bridge, respectively. The water/air bridge length was selected and calibrated based on effective thermal conductivities by experiments.. Furthermore, the amount of each type within a glass assembly was quantified after recognising them by a series of image processing based on the pixel values of particle, water and air phases in CT images. Subsequently, to analyse the influence of particle connection on heat transfer, the number of each connection type was related to glass bead assemblies' effective thermal conductivities λ which were obtained by Finite Element Modelling (FEM) of heat transfer.

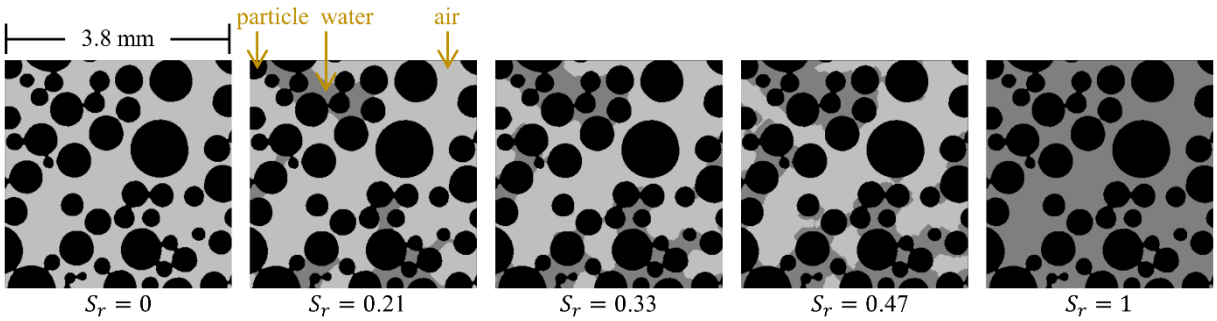

Figure 1.CT images of glass bead assemblies varying in saturation

3. Results

The relationship between the number of each particle connection type within the glass bead assemblies and thermal conductivities under varied degree of saturation is shown in Figure 2. Thermal conductivity increases with the number of type-3 (physical contact with water bridge) and type-6 (water bridge) for all range of degree of saturation. In comparison, thermal conductivity decreases with the amount of type-1 (physical contact with air bridge) and type-4 (air bridge). Especially the influence of type-1 and type-4 on thermal conductivity is more obvious in low degree of saturation (0~0.2) than high degree of saturation (0.2~1). Type-2 (physical contact with both air and water bridges) and type-5 (water and air bridges) are essentially transient types considering they are formed with the added water and eventually replaced by type-3 and type-6 with increasing degree of saturation. They contribute to the increase of thermal conductivities at low degree of saturation (0~0.2) and then their influence is negligible.

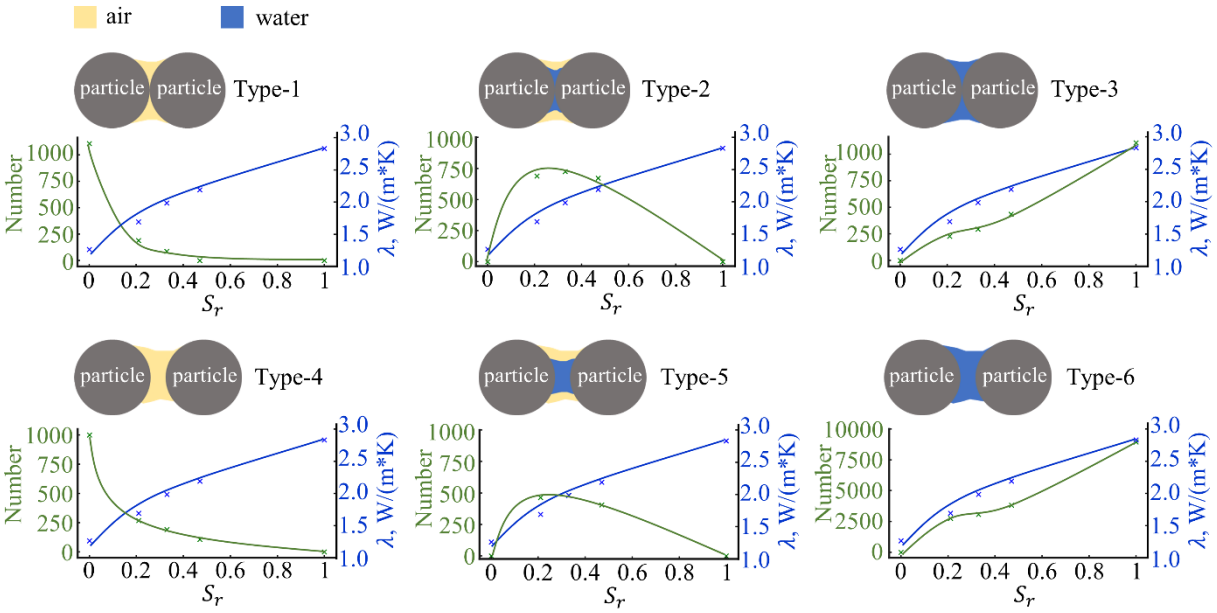

Figure 2. The change of number of different particle connection types with thermal conductivities under varied degree of saturation

4. References

[1] Fei, W., Narsilio, G. A., van der Linden, J. H. and Disfani, M. M. *Quantifying the impact of rigid interparticle structures on heat transfer in granular materials using networks*. IInt. J. Heat Mass Transf, 143 (2019), 118514.

[2] Milatz, M., Hüsener, N., Andò, E., Viggiani, G. and Grabe, J. Q*uantitative 3D imaging of partially saturated granular materials under uniaxial compression*. *Acta Geotech*, 16, 11 (2021), 3573-3600.

INVESTIGATION AND ANALYSIS OF THE MACRO- AND MICRO-RESPONSES OF BENTONITE-SAND MIXTURES TO TEMPERATURE

A. Li[1,2], W. Feng[2]*, Z. Chen[1], J. Yin[1] and C. Zhou[1]

[1] The Hong Kong Polytechnic University, Dept. of Civil and Environmental Engineering., Hong Kong, China

[2] Southern University of Science and Technology, Dept. of Ocean Science and Engineering, Shenzhen, China

1. Abstract

Bentonite-sand mixture has been proposed as a buffer material of high-level radioactive waste (HLW) repositories in many countries (Graham et al., 2001). The bentonite-based buffer material might be subjected to the elevated temperature generated by the decay heat from high-level radioactive waste in the canister and the low thermal conductivity of bentonite when the repository is closed. The temperature change will alter both fundamental hydraulic and mechanical properties of bentonite-based materials, including swelling pressure, compressibility, time-dependent behaviour, volume change behaviour, and shear strength (Watabe et al., 2011). However, to date the mechanism of temperature effects on the behaviour of the bentonite buffer is not well understood.

This study is aimed at clarifying the macro- and micro-responses of bentonite-sand mixtures to temperature. Cone penetration test, rheometer test, and flask volumetric test were carried out on bentonite-sand mixture samples with different mixing ratios for determining the liquid limit, yield stress, and bound water content at different temperatures. The evolution of microstructure for bentonite samples prepared at different temperatures was observed from the results scanning electron microscopy (SEM) and mercury intrusion porosimetry (MIP) test. The mechanisms of temperature influence on bentonite were further analyzed and discussed for both micro- and macroscopes.

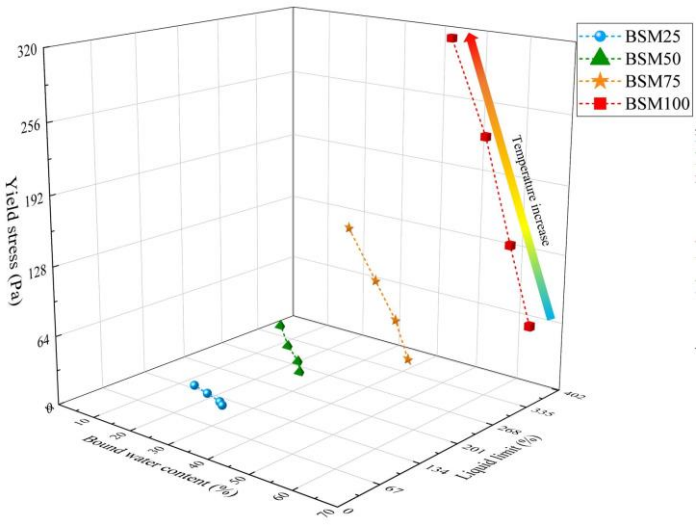

Figure 1. Relationship among liquid limit, yield stress, and bound water content for bentonite-sand mixtures at different temperatures.

The results of macro-experiments reveal that, as the temperature increases, the liquid limit and yield stress of bentonite-sand mixtures increase, while bound water content decreases (Figure 1). The normalized relationships disclose the sand content dramatically affects the degree of temperature influence on the macro-behaviour. Generally, the temperature effects on the properties of bentonite-sand mixtures are more obvious with the decreasing sand content. SEM and MIP results present that the contact manner between particles converted from edge-to-face to the edge-to-edge association and some intra-aggregate pores merged to form inter-aggregate pores as temperature increases (see Figure 2). The mechanisms of the increasing temperature influence on the responses of bentonite-sand mixtures can be inferred that: 1) the diffuse double layer is supposed to decrease since more ions were electrolyzed from montmorillonite particles, thereby, increasing the ion concentration and changing the ion valence (Ko et al., 2023); 2) the slight shrinkage of diffuse double layer produced nano-fissures, causing water-hold capacity to increase; 3) the temperature-induced transition from bound water into free water results in an increase of liquid volume; 4) increasing temperature led to increased inter-particle repulsive force. Furthermore, an empirical model was proposed to predict the yield stress of bentonite dispersion incorporating the combined effects of sand content and temperature.

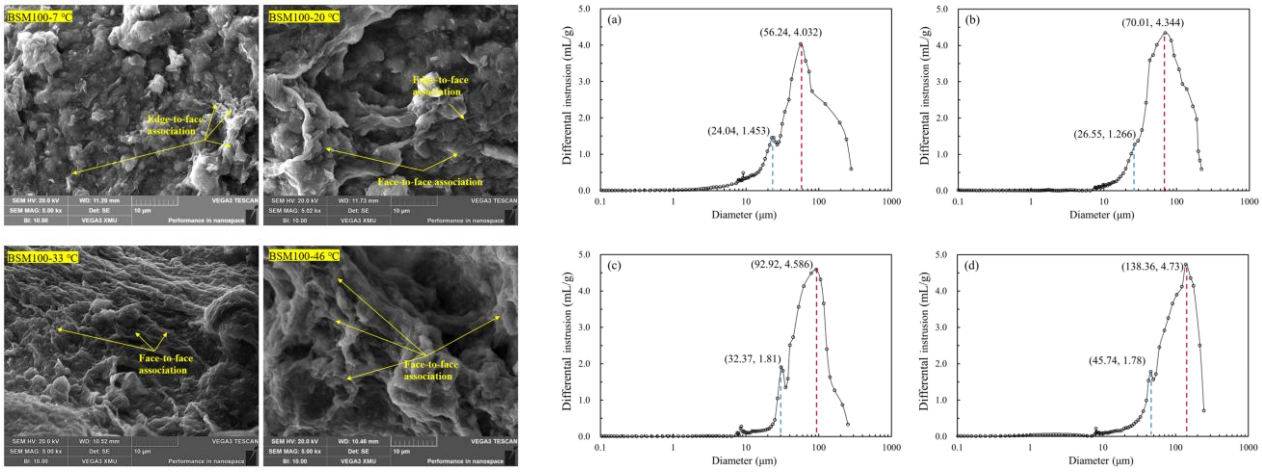

Figure 2. Evolution of microstructure and micropores from SEM and MIP tests

2. References

[1] Graham, J., Tanaka, N., Crilly, T., & Alfaro, M. 2001. Modified Cam-Clay modelling of temperature effects in clays. *Can. Geotech. J.*, 38(3), 608-621.

[2] Watabe, Y., Yamada, K., & Saitoh, K. 2011. Hydraulic conductivity and compressibility of mixtures of Nagoya clay with sand or bentonite. *Géotechnique*, 61(3), 211-219.

[3] Ko, H., Choo, H., & Ji, K., 2023. Effect of temperature on electrical conductivity of soils–Role of surface conduction. Eng. Geol., 321, 107147.

MICRO THERMO-MECHANICS OF KAOLIN CLAY

A. Di Donna[1], A. Casarella[2] and A. Tarantino[3]
[1] Univ. Grenoble Alpes, CNRS, 3SR Lab., Grenoble, France
[2] Chalmers University of Technology, Göteborg, Sweden
[3] Department of Civil and Environmental Engineering, University of Strathclyde, Scotland, UK

1. Introduction

The effect of temperature on mechanical behaviour of clay-based geomaterials is relevant in several geotechnical applications (e.g., low enthalpy geothermal systems and energy geostructures, nuclear waste disposal, and heating in rapid shear deformation). Mechanical response of (saturated) clay to temperature variation is not always intuitive. According to literature, clay exhibits irreversible contraction in normally consolidated (NC) states and reversible expansion in highly over consolidated (OC) states upon heating and subsequent cooling [1–4]. As a result, volume changes not only occur due to thermal expansion of clay constituents but also to temperature-induced changes in clay microstructure. Therefore, describing the material at scales ranging from particle level to the macroscopic system is key to understanding thermo-mechanical clay behaviour. In this work, experimental, analytical and numerical approaches are coupled to get insight into this peculiar behaviour. The chosen material is kaolin clay.

2. Micro and macro experimental evidences

A series of temperature-controlled isotropic compression tests were coupled with mercury intrusion porosimetry (MIP) tests to explore microstructural changes in remoulded non-active clay samples due to temperature changes. The macroscopic observations have been performed in a new temperature-controlled isotropic cell developed in this work with an accurate pore-water pressure monitoring system. Volumetric strain recorded upon heating at constant effective isotropic stress of 250 kPa for a normally consolidated and an overconsolidated specimen respectively are presented in Figure 1a.
The pore size distribution data in Figure 1b highlight that the thermoplastic response appears to be associated with a decrease in volume of clay macropores, a mechanism also observed in the plastic deformation associated with mechanical loading (at constant temperature). The research hypothesis put forward in this work is that volumetric collapse upon thermal loading results from two competing mechanisms: the weakening of the electrochemical attraction at the edge to-face contacts in house-card clay fabric and the destabilising effect of the external stress. The competition between the two mentioned effects would explain the non-monotonic volumetric collapse as mechanical stress increases.

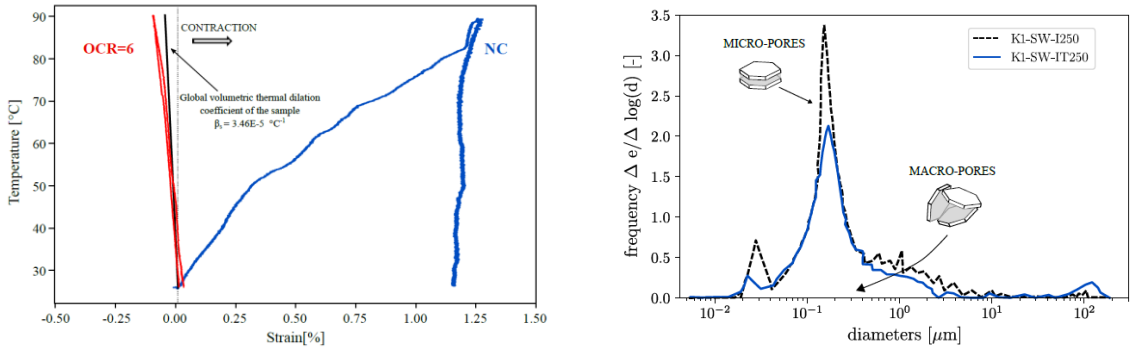

(a) (b)

Figure 1. (a) Measured volumetric strain behaviour of Speswhite Kaolin Clay during heating for a NC and a heavily OC sample; (b) pore size evolution after one heating-cooling cycle performed in NC conditions.

3. Interparticle interactions

In parallel with the experimental investigation, analytical and numerical work has been carried out to lay down the fundamentals of particle-scale models for non-active clay, capable of capturing the effect of temperature on mechanical behaviour. Clay particle interactions include non-contact forces, which are electrochemical in nature and prevail in face-to-face configuration and contact forces, which are mechanical forces transferred from one particle to another through a contact surface, typical of edge-to-face configuration. Non-contact forces include electrostatic Coulombic forces and van der Waals attractive forces. Here, we propose a combined numerical and analytical approach to quantify the elementary interactions between clay particles. The results are used to interpret typical stress-thermal paths, such as compression tests at different temperatures and heating-cooling cycles at constant mechanical stress and corroborate the research hypothesis about the ‘weakening’ of the electrochemical attraction.

4. Conclusion

It is concluded that the electrochemical interactions governing the face-to-face particle configuration can only explain the elastic volumetric response of over-consolidated clays subjected to heating. The thermo-plastic behaviour associated with the reduction of the pre-consolidation pressure with temperature and the volumetric plastic compressive strain in response to heating in normally-consolidated clays is attributed to the edge-to-face particle configurations.

5. References

[1] Cekerevac C, Laloui L. Experimental study of thermal effects on the mechanical behaviour of a clay. Int J Numer Anal Methods Geomech 2004;28:209–28.

[2] Campanella RG, Mitchell JK. Influence of temperature variations on soil behavior. J Soil Mech Found Div ASCE 1968;94:709–34.

[3] Del Olmo C, Fioravante V, Gera F, Hueckel T, Mayor JC, Pellegrini R. Thermomechanical properties of deep argillaceous formations. Eng Geol 1996;33:87–101.

[4] Di Donna A, Laloui L. Response of soil subjected to thermal cyclic loading: Experimental and constitutive study. Eng Geol 2015;190:65–76.

Geomaterials in unsaturated states

A MICROMECHANICS MODEL FOR UNSATURATED SOIL CONSIDERING LIQUID BRIDGE AND BULK WATER CONTRIBUTIONS TO SHEAR BEHAVIOR

Y. Higo[1], T. Matsushima[2], Y. Otake[3]
[1] Kyoto University, Department of Urban Management, Kyoto, Japan
[2] University of Tsukuba, Department of Engineering Mechanics and Energy, Tsukuba, Japan
[3] Tohoku University, Department of Civil Environmental Engineering, Sendai, Japan

1. Introduction

The micromechanics model (MM model) is a model that constructs macro-behaviour based on a concise and clear representation of the mechanical behaviour at the particle scale. MM model could provide clear and effective interpretation of the mechanical behaviour of geomaterials, compared to phenomenological constitutive models. MM models for unsaturated soils considering the effect of suction have been developed recently, including a model that explicitly introduces the contribution of liquid bridge to shear behaviour using the experimental data on the microscopic behaviour of the interior of specimens acquired by an X-ray micro-computed tomography (CT) [1]. The model can be applied to modelling unsaturated soils at low saturation regime where the liquid bridge contribution is significant. The aim of this study is to extend the model additionally considering the contribution of bulk water, that fills the pore spaces, to extend the applicability of the MM model to higher saturation regimes.

2. Liquid bridge and bulk water ratios

The X-ray micro-CT images of Toyoura sand loose and dense specimens acquired at different water retention states were segmented into the soil particle, pore water and pore air phases, and the morphological transition of pore water was analysed. The volumes of pore water clusters were clearly divided into two groups: smaller ones for liquid bridges and larger ones for bulk water. The ratio of liquid bridge volume to the total volume of pore water (capillary ratio, CR) with the degree of saturation as shown in Figure 1(a). The variation in CR was well reproduced by β-distribution for both the loose and dense specimens, where the ratio increases from zero at the fully saturated state to 1.0 at the residual saturation state, and then decreases down to zero at the completely dry state. The ratio of bulk water volume to the total volume of pore water (bulk ratio: BR) was defined simply as the rest of CR, i.e., BR=1-CR (Figure 1(b)). The contribution of bulk water to shear behaviour is more significant in higher saturation regime and decreases to zero at the residual saturation state. In the regime where the degree of saturation is lower than the residual one, no bulk water exists and the contribution is null.

3. Micromechanics model considering the liquid bridge and bulk water contributions

The liquid bridge contributes to increase in the inter-particle force, while the bulk water contributes to increases the confining stress. In the present study, these contributions have been introduced to the 4-cell analogical micromechanics model for granular soil [2]. Macroscopic strain increment is applied and the displacement at the grain contact is calculated using the uniform strain field hypothesis. The contact slip and f_n plasticity of 4-cell analogy model considering suction contribution are used to update the contact force at the grain contact. During the homogenisation by Love-Weber formula to update macroscopic stress, increase in effective stress due to liquid bridge

contribution is considered in the contact normal stress and the increase in confining stress due to suction of bulk water in addition to the external confining stress.

Numerical example of biaxial compression tests with various degrees of saturation is shown in Figure 2. At the early stage of the loading, axial stress quickly increases and then strain softening is observed in all cases. The peak axial stress increases as the degree of saturation decreases. The peak stress of the zero-saturation case is the lowest because of no contribution of liquid bridge and bulk water to shear behaviour.

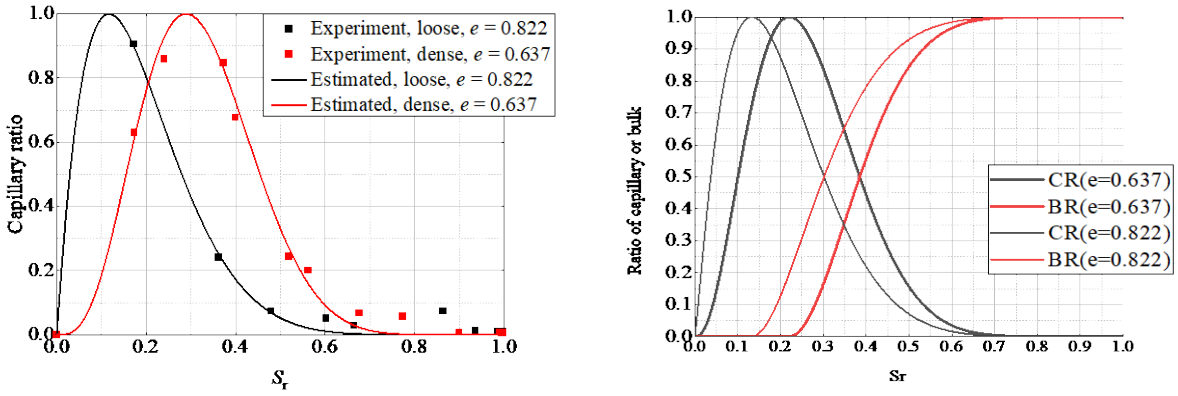

(a) Capillary ratio medelled using β-distribution (b) Bulk ratio

Figure 1 Saturation degree dependency of the liquid bridge and bulk water ratios

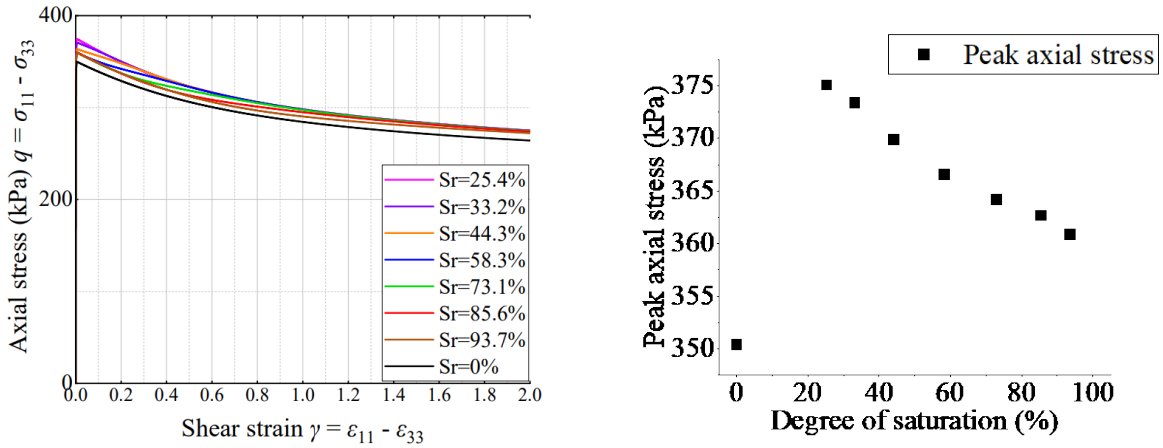

(a) Stress-strain relations (b) Peak axial stress

Figure 2 Micromechanics model performance for biaxial compression test simulation with various degree of saturation

5. References

[1] Fukushima, Y. , Higo, Y., Matsushima, T. and Otake, Y. (2021) Liquid bridge contribution to shear behavior of unsaturated soil: modeling and application to a micromechanics model. *Acta Geotechnica*, 16, 2693-2711.

[2] Matsushima, T., Higo, Y. and Otake, Y. (2024) Constant-volume shear response of 4-cell analogical micromechanics model for granular soil, IS-Grenoble 2024, submitted.

ALTERING CAPILLARY PRESSURES USING ANIONIC SURFACTANTS FOR GEOLOGICAL CARBON STORAGE APPLICATIONS: MICRO-SCALE OBSERVATIONS

J. Y. Lee[1], S. G. Gang[2], J. Ryou[2] and J. Jung[2]

[1] Korea Institute of Geoscience and Mineral Resources, Climate Change Response Division, Deajeon, South Korea

[2] Chungbuk National University, Department of Civil Engineering, Cheongju-si, South Korea

Carbon dioxide is the well-known green-house gas responsible for the global warming. Geological carbon storage utilizes readily available technique to store CO_2 in a large scale. The CO_2 storage efficiency of geological carbon storage depends on the CO_2 injection rate, the sweep efficiency, and the residual saturation of CO_2. High capillary pressures in reservoirs induces fingering phenomena and is one of the major parameters that govern sweep efficiency in reservoirs. Lower interfacial tension and higher contact angle would reduce the capillary pressure, and thus the fingering phenomena can be alleviated. The interfacial tension and contact angle between CO_2 and water can be altered by using CO_2- compatible surfactants. Surfactants have been utilized to enhance sweep efficiency by modifying capillary pressure in CO_2-EOR operations in oil fields, and recently same mechanism have been applied for enhancing sweep efficiency in geological carbon storage

Commercially available anionic surfactants, SDS and SDBS are selected to examine the performance of controlling interfacial tension and contact angle in the CO_2-water system. The interfacial tension and contact angle on quartz substrates have been experimentally measured in the pressure and temperature ranges of 25~40 °C and 4~10MPa, respectively. A high pressure micromodel experimental system has been designed and utilized for quantifying sweep efficiency enhancement with the use of surfactants. The pressure and temperature conditions for the experiment are 40°C and 8MPa, respectively, which is within those of the supercritical CO_2 condition. A numerical pore network model has been established to simulate the multiphase flow in the micromodel experiment and to predict the sweep efficiency enhancement under various flow rates, interfacial tensions, and contact angles.

Both SDS and SDBS significantly lowers interfacial tension in super-critical CO_2 condition, which will lower the capillary pressure and enhance the sweep efficiency. However, both SDS and SDBS lowers contact angles, which is not favorable phenomenon for enhancing the sweep efficiency. Micromodel and pore network model results have shown that the use of anionic surfactants can enhance the sweep efficiency, which implies the positive effect from lower interfacial tensions is more pronounced than the negative effect from lower contact angles on the sweep efficiency. Higher CO_2 injection flow rates have enhanced the sweep efficiency, but the surfactants enhance the sweep efficiency more effectively even with a very low concentration than increasing flow rate by an order of magnitude. The results have shown the significant potential of anionic surfactants for increasing CO_2 storage capacity in geological carbon storage and the reservoir scale performance will be examined numerically for further study.

Acknowledgements

This work was supported by the Korea Institute of Energy Technology Evaluation and Planning (KETEP) grant, funded by the Korean Ministry of Trade, Industry & Energy (No. 20212010200010)

EFFECT OF WETTING AND DRYING PROCESSES ON THE BEHAVIOR OF UNSATURATED GRANULAR ASSEMBLIES

***N. Younes*[1,2,3], *R. Wan*[2], *A. Wautier*[3], *O. Millet*[1], *and F. Nicot*[4]**

[1] *LaSIE, UMR CNRS 7356, University of La Rochelle, 17042, La Rochelle Cedex 1, France*

[2] *Department of Civil Engineering, Schulich School of Engineering, University of Calgary, Canada*

[3] *INRAE, Aix-Marseille University, UR RECOVER,13182 Aix-en-Provence Cedex 5, France*

[4] *University Savoie Mont-Blanc , ISTerre, Chambéry, France*

1. General Context

Earthen dikes are constructed out of granular soils that are under unsaturated conditions where capillary bridges provide additional material strength that is temporary. In particular, the interest is in shallow unsaturated regions that are permanently being subjected to wetting and drying cycles due to fluctuating events such as intense rainfalls and heat waves. Under these conditions, capillarity vanishes, thereby adversely impacting the mechanical strength of the dikes to potentially cause their collapse. It is now well recognized that failures at the macroscale have their origin in the microscale [1]. Therefore, understanding unsaturated soils where the physics operates at the pore/grain scale requires a microscale approach. In unsaturated soils, multiple regimes can be distinguished depending on the water content: pendular, funicular, and capillary regimes. While the pendular regime is well understood and documented in the geomechanics literature [2], the other two regimes are to a lesser extent and hence need a thorough analysis. The modeling of the pendular regime has been comprehensively reported in the literature, but it only represents a small portion of unsaturated soils. On the other hand, the funicular regime is more challenging to model due to complexities in geometries. Analyses in the literature seem to be restricted to only three particles, which is not viable for the simulation of real unsaturated soils. Therefore, a new approach is necessary to take into account the transitions over all possible capillary regimes and intricacies of pore geometries as capillary bridges merge and collapse to model wetting and drying cycles.

2. Proposed Numerical Model

In this study, a coupling between the Lattice Boltzmann Method (LBM) and the Discrete Element Method (DEM) is presented. The dynamics of capillary bridge formation and merging is simulated using the LBM approach, which involves solving both the Navier-Stokes and Allen-Cahn equations to tackle multiphase flow in complicated and arbitrary pore space geometries [3]. On the other hand, the kinematics of grains, here chosen to be spherical, is handled by DEM based on an elastic-plastic contact law. This coupled DEM-LBM approach has proven its capabilities in capturing numerous features, including the Soil-Water Characteristic Curve (SWCC) and the mean capillary stress p^{cap} [4]. The mean capillary stress, which is equivalent to the capillary cohesion, is defined as follows:

$$p^{\text{cap}} = \frac{1}{3}\text{Tr}\left(\boldsymbol{\sigma}^{\text{cap}}\right). \tag{1}$$

Here, the capillary stress $\boldsymbol{\sigma}^{\text{cap}}$ is calculated by subtracting the grain-to-grain contact stress $\boldsymbol{\sigma}^{\text{cont}}$ from the total stress $\boldsymbol{\sigma}^{\text{tot}}$ that is being applied to a granular sample:

$$\boldsymbol{\sigma}^{\text{cap}} = \boldsymbol{\sigma}^{\text{tot}} - \boldsymbol{\sigma}^{\text{cont}} \tag{2}$$

3. Results

We first initialize an assembly composed of several thousands of spherical particles confined at $\boldsymbol{\sigma}^{\text{conf}} = 2$ kPa. Then, the system is set in the capillary regime with a degree of saturation $S_r \approx 95\%$, where the liquid phase is continuous. The sample is first subjected to a drying process (evaporation) followed by a wetting process (condensation). Figure (1) shows both the evolution of: (a) the mean capillary stress p^{cap} and (b) the matric suction s. Although the wetting angle is the same during wetting and drying processes $\theta = 25°$, a hysteresis phenomenon is observed where the mean capillary stress and the suction are different during drying and wetting processes. Remarkably, during evaporation, Figure (1a) demonstrates that the mean capillary stress (capillary cohesion) is first close to zero and increases up to a certain threshold, at $S_r \approx 67\%$ beyond which it decreases once again. Similar behavior is observed during the wetting process, only this time the peak value of the mean capillary stress is different, as does the degree of saturation at which p^{cap} reaches its maximum value $S_r \approx 50\%$.

The example presented in this communication highlights the potential of the proposed coupled DEM-LBM model as a promising tool for computing unsaturated soils at the microscale across all the saturation regimes—pendular, funicular, and capillary regimes.

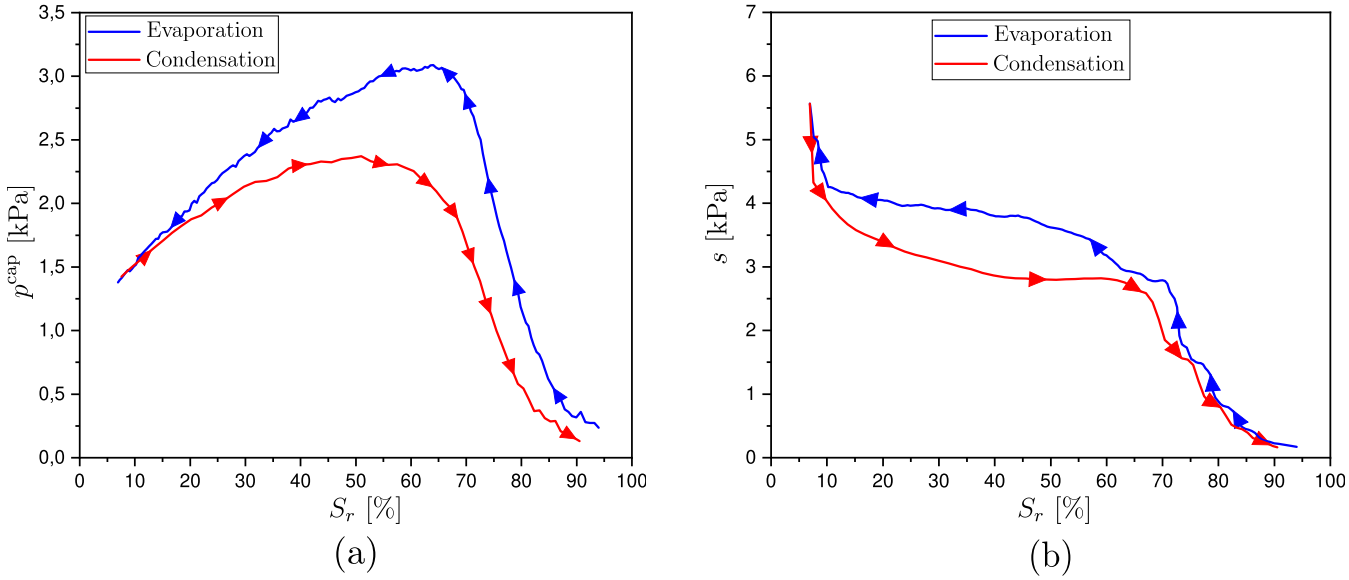

Figure 1. The evolution of (a) the mean capillary stress p^{cap} [kPa] and (b) the matric suction s [kPa] in terms of degrees of saturation S_r, during evaporation (drying) and condensation (wetting) processes for a wetting angle of $\theta = 25°$.

References

[1] Wan, R., Nicot, F., and Darve, F. (2017). *Failure in geomaterials: a contemporary treatise*. Elsevier.

[2] Duriez, J., Eghbalian, M., Wan, R., and Darve, F. (2017). The micromechanical nature of stresses in triphasic granular media with interfaces. *Journal of the Mechanics and Physics of Solids*, **99**, 495–511.

[3] Younes, N., Benseghier, Z., Millet, O., Wautier, A., Nicot, F., and Wan, R. (2022). Phase-field lattice boltzmann model for liquid bridges and coalescence in wet granular media. *Powder Technology*, p. 117942.

[4] Younes, N., Wautier, A., Wan, R., Millet, O., Nicot, F., and Bouchard, R. (2023). Dem-lbm coupling for partially saturated granular assemblies. *Computers and Geotechnics*, **162**, 105677.

EXPERIMENTAL UPSCALING OF AN ENGINEERED GAS PERMEABLE SEAL: FROM PORE-SCALE TO LAYERED/HETEROGENEOUS ZONES

E. Romero[1,2], C. Alvarado[2], A. Lloret[1], E. Toprak[2] & S. Olivella[1,2]
[1] Universitat Politècnica de Catalunya, Dep. of Civil and Env. Engineering, Barcelona, Spain
[2] Int. Centre for Numerical Methods in Engineering CIMNE, Barcelona, Spain

1. Introduction

Innovative experimental tools and physical models are required to address phenomena across various scales for observing and interpreting porous materials' multiphase (liquid, gas and solid) motion. This study mainly delves into process upscaling through experimental techniques considering an engineered gas permeable seal concept designed for a future deep geological repository for low and intermediate radioactive waste disposal (*in situ* Gas-Permeable Seal demonstration Test GAST at the Grimsel Test Site, Switzerland [1]). The seal, composed of a compacted 80/20 (dry mass) sand/bentonite (S/B) mixture, undergoes a long-term saturation and subsequent gas transport within the emplacement caverns where pollutant waste is stored. This type of seal limits the gas breakthrough pressure (generated by the degradation of organic substances and metal deterioration by corrosion) and increases its gas transport capacity through advective flow, an essential feature for preserving the seal's integrity.

2. Experimental program, numerical model, and results

A series of laboratory experiments running parallel to the *in situ* test and bridging different scales are presented and discussed together with the fully coupled numerical model. The multi-scale program aims to help interpret pore-scale phenomena (bentonite inter-sand filling and its impact on gas transport [2]), upscaling the hydromechanical and gas performance of the S/B system (gas permeability point tests at different degrees of saturation) and providing a bridge between the dm-scale mock-ups (mini-GAST's mock-ups MU-A and MU-B for gas breakthrough and subsequent dissipation process with flow parallel to compaction layers) and the full-scale GAST (numerical model). The microstructural tests, including mercury intrusion porosimetry, ESEM photomicrographs at different hydraulic states and microfocus X-ray computed tomography to estimate the degree of bentonite filling between sand grains and the connectivity of the gas pathways, were used to assess the gas transport properties at different hydraulic states. The mock-up laboratory experiments aimed to demonstrate the gas-permeable system functioning under different controlled scenarios (different stress states, gas injection pressures, volume or pressure rates for gas injection, detecting self-sealing effects after the first gas breakthrough event and detecting snap-off pressure difference that block advective gas transport). Therefore, mini-GAST mock-ups should mimic the GAST test as closely as possible and allow for a dynamically compacted and layered S/B, where water and gas should flow parallel to compaction lifts with heterogeneous properties and zigzag dry density variation on compaction. The information will be used for upscaled water and gas permeabilities of seals considering heterogeneous zones and realistic boundary conditions (back-analysed parameters with a strongly coupled numerical model using layered, anisotropic, and localised heterogeneous zones [3]).

Figure 1a shows the evolution of bentonite's volumetric degree of inter-sand filling at different degrees of saturation obtained through various microstructural techniques. This information is used to model the evolution of the effective gas permeability with the degree of saturation (Figure 1b),

which will be further implemented in a numerical, fully coupled model considering layered/heterogeneous zones (Figure 1c).

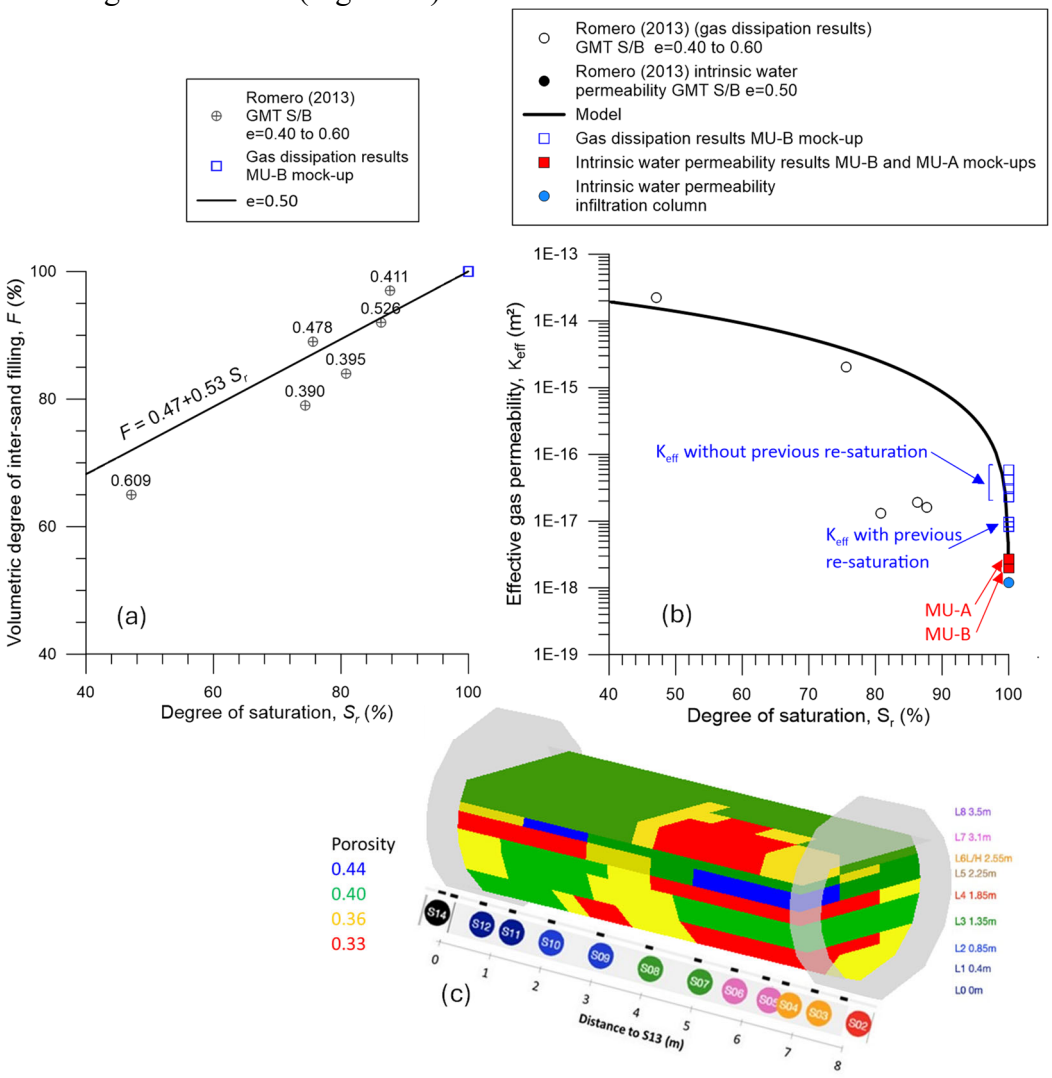

Figure 1. (a) Pore-scale phenomena. (b) Modelling the evolution of effective gas permeability based on pore-scale information. (c) Numerical model with layered/heterogeneous zones.

3. References

[1] National Cooperative for the Disposal of Radioactive Waste (Nagra), *Effects of post-disposal gas generation in a repository for low- and intermediate-level waste sited in the Opalinus Clay of Northern Switzerland.* Nagra Tech. Report NTB 08-07, Switzerland (2008).

[2] Romero E. (2013). A microstructural insight into compacted clayey soils and their hydraulic properties. *Engineering Geology* **165**: 3-19.

[3] Toprak E., Olivella S. & Romero E. *GAST in situ experiment. Code_Bright Modelling.* Final report. Nagra, Switzerland (2023).

Acknowledgements

The authors acknowledge the financial support of Nagra (Switzerland) through different research projects ('GAST–Laboratory investigation of two-phase transport in sand-bentonite mixtures' and 'GAST Modelling of gas transport in sand-bentonite mixtures') with CIMNE (Spain).

GRAIN-SCALE ANALYSIS OF HYDRO-MECHANICAL BEHAVIOUR OF SAND UNDER SUCTION-CONTROLLED TRIAXIAL COMPRESSION

J.P. Wang[1], E. Ando[2] and B. François[3]

[1] School of Civil Engineering, Shandong University, Jinan, China

[2] EPFL Center for Imaging, Ecole Polytechnique Fédérale de Lausanne, Lausanne, Switzerland

[3] Urban and Environmental Engineering, Université de Liège, Liège, Belgium

1. Introduction

In unsaturated soils, at the grain scale, the coexistence of liquid and gas phases in the voids induces capillary pressure and interfacial tension that contribute to the micro-mechanical static equilibrium between grains and, in turn, affect the macroscopic stress-strain behavior of the materials. Study of the micro-characteristics of unsaturated granular media attracts much attention in the last two decades. Those approaches are supported by numerical methods, such as discrete element modelling [1] and experimental observations at grain scale. X-ray computed tomography allows to track the micro-characteristics of granular material deformation [2] as well as to deduce the water-retention behaviour and non-homogeneous water distribution at the grain scale [3]. In this study, a customized suction controlled mini-triaxial test device is designed to be inserted in an X-Ray CT equipment [4]. The sample is scanned at different strain stages and the micro-characteristics, such as local porosity and local water distribution, are studied.

2. Experimental method

A fine sand with grain diameter ranging from 0.1 to 0.3 mm is tested in a customised mini-triaxial test device. The sample size is 10 mm in diameter and 20 mm long. Four triaxial compression tests are performed at suction of 2, 2.5, 3 and 4 kPa and a confining pressure of 16 kPa. The loading rate is slow enough (2.5×10^{-4} s^{-1}) to keep fully drained conditions. The triaxial cell is fixed on a rotational table in the micro-focus X-Ray tomography chamber in Laboratoire 3SR, Grenoble, to conduct X-ray CT scans. Scans are performed at different strain stages (0, ≈2, ≈5, ≈10 and ≈15%) when the axial loading is ceased, keeping the axial piston at a fixed position. To reach an image resolution of 9 μm/pixel, the X-Ray CT is performed on a region of interest in the middle of the sample on a height of 1.2 cm (2 h per scan). From the grey scale image, a segmentation technique adapted for three phases materials [5] is used to separate the different phases. Figure 1a shows an example of obtained segmented image with the three phases.

3. Results and analysis

The deviatoric stress evolutions of the four triaxial tests are presented in Figure 1b. The behaviour of a dry sample is also presented as a reference. The 3D images are divided in cubic representative volume elements (RVE) of 110 pixels (≈1 mm) in size (Figure 1a). Local porosity and degree of saturation are deduced in each RVE. Also, the region of interest of 1.2 cm is divided into 12 layers of elements in the vertical direction. Figure 2 shows the degree of saturation and porosity in each layer in triaxial tests for one specific test at a suction of 2.5 kPa., as an example. Initially, the porosity is uniformly distributed through all the samples around a value of 0.35. Then, during shearing, dilatancy behavior induces an increase of the porosity together with a reduction of the degree of saturation. This analysis can be generalized for all tests at all suctions.

In a more advanced study, individual grain labeling, contact detection and interface identification is performed [6]. It allows to track the inter-particle contact coordination number and fabric anisotropy all along the triaxial loading. It is then observed that an initial fabric anisotropy due to gravity and sample compaction is enlarged due to triaxial loading. It is also observed that the inter-particle contact coordination number is reduced after shearing due to the dilation behavior.

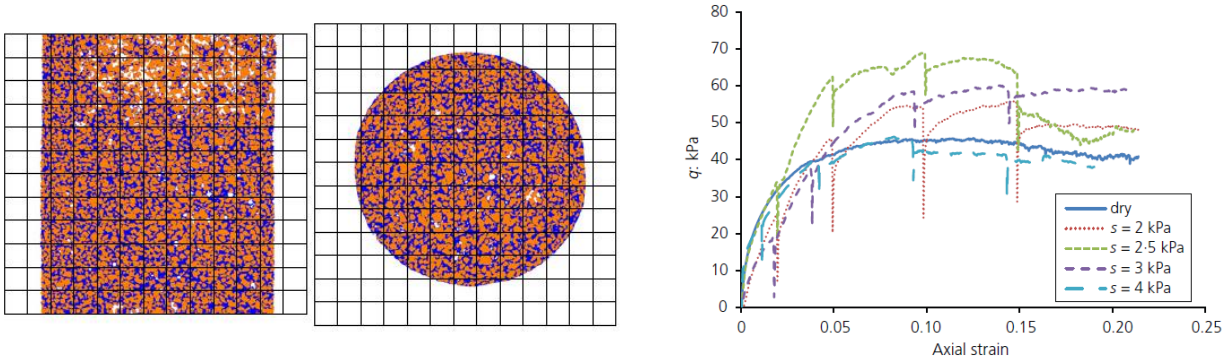

(a) (b)

Figure 1. (a) Vertical and horizontal cross-sections with the grid of 1mm-size RVE (air in white, water in blue and grain in orange), (b) Macroscopic stress-strain response of the 5 tested specimen.

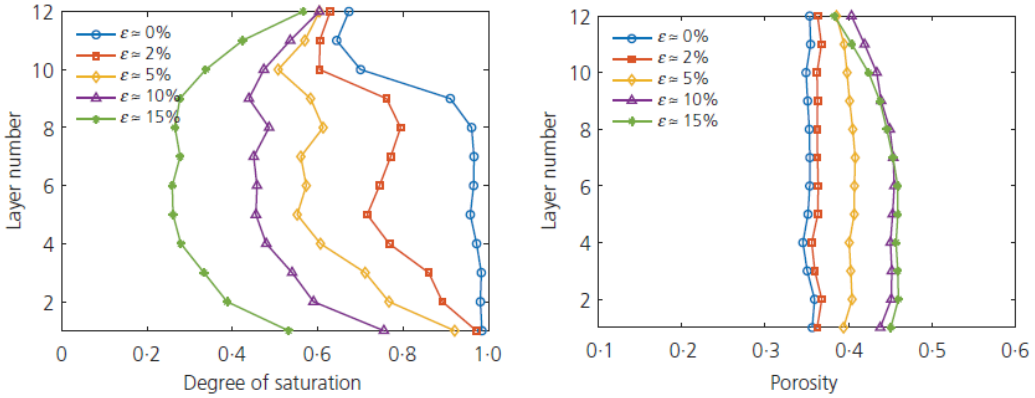

Figure 2. Degree of saturation and porosity in different layers of the sample, at a suction of 2.5 kPa

[1] Wang, J.P., Li, X. & Yu, H.S. (2018). A micro–macro investigation of the capillary strengthening effect in wet granular materials. Acta Geotech. 13(3), 513–533.

[2] Andò, E., Hall, S.A., Viggiani, G., Desrues, J. & Bésuelle, P. (2012). Grain-scale experimental investigation of localised deformation in sand: a discrete particle tracking approach. Acta Geotech. 7(1): 1–13.

[3] Khaddour, G., Riedel, I., Andò, E., Charrier, P., Bésuelle, P., Desrues, J., Viggiani, G. & Salager, S. (2018). Grain-scale characterization of water retention behaviour of sand using X-ray CT. Acta Geotech. 13(3): 497–512.

[4] Wang, J. P., Andò, E., Charrier, P., Salager, S., Lambert, P. & François, B. (2019). Micro-scale investigation of unsaturated sand in mini-triaxial shearing using X-ray CT. Géotechnique Letters, 9(4): 269-277.

[5] Hashemi, M.A., Khaddour, G., François, B., Massart, T.J. & Salager, S. (2013). A tomographic imagery segmentation methodology for three-phase geomaterials based on simultaneous region growing. Acta Geotech. 9(5): 831–846.

[6] Wang, J.P., Luan, J.Y., Gao, X.G., Liu, T.H., Ando, E., & François, B. (2022). A micro-investigation of unsaturated sand in mini-triaxial compression based on micro-CT image analysis. Acta Geotech., 17(11), 4799-4821.

HYDRO-MECHANICAL CHARACTERISATION OF THE ROMAN MADE GROUND LAYER IN UNSATURATED CONDITIONS

A. Pucci[1], G. Guida[1] and F. Casini[1]
[1] Università di Roma Tor Vergata, Dip. Ing. Civile e Ing. Inf., Rome, Italy

1. Introduction

Several monuments and buildings in the historical centre of Rome, close to the Tiber River, have suffered damages induced by differential settlements at the foundation level [1, 2]. These latter are due also to the fluctuation of the water table connected to the Tiber River hydraulic regime, which determines wetting and drying cycles in the made ground layer [3].

Upon wetting, an unsaturated soil can reversibly swell or cumulate significant compression volumetric plastic deformations (saturation collapse) depending on the stress level and porosity of the ground [4].

This work investigates the role of partial saturation of the made ground layer on the prediction of the displacements induced by the water table oscillations. The made ground is described with a critical state model extended to unsaturated conditions, where the model parameters are calibrated with unsaturated soil tests at the elementary volume scale.

2. Numerical model

The stratigraphy of the Roman subsoil close to the Tiber River comprises several lithotypes (from the top): a made ground layer (MG), 5-12 m thick, characterised by loose and very heterogeneous silty sand in unsaturated conditions, since the water table lies entirely there, a silty clay layer (SC) with an average thickness of 4 m, a silty sand one (SS) with a thickness ranging between 5 and 6 m, a layer of gravel and sand, that can be present or not, depending on the section considered, and a layer of Pleistocene clay, known as Vatican Clay, that is the bedrock for the city centre of Rome.
Figure 1a. shows the scheme of the geotechnical section adopted in the numerical model, that reproduces the stratigraphy of the Rione Trastevere area. The Tiber River regime is imposed with a time-dependent hydraulic boundary condition on the left side of the model, according to the hydraulic levels registered in the period between 2005 – 2008, containing three flood events [3]. The subsoil domain was divided into three homogeneous layers: the mechanical behaviour of the MG layer is described with the Barcelona Basic Model, while a linear elastic behaviour is adopted for the other two layers. Compared to [3], the proposed numerical model will be calibrated based on a more detailed soil hydro-mechanical characterisation on MG samples.

2. Laboratory characterisation

The water retention behaviour of the MG layer under unsaturated conditions was investigated with the HYPROP Meter apparatus. The sample is 5 cm high and 8 cm in diameter, two tensiometers of 5 cm and 2.5 cm in height, respectively, allow suction measurement over time. The sample weight is monitored with a balance. Thus, it is possible to determine the relation between suction and water content of the soil sample (Water Retention Curve, WRC) [5]. In Figure 1b., a cycle of drying (orange dots) and wetting (light blue dots) is reported, which exhibits a hysteretic behaviour related also to the irregularity of the pore network [6].

The experimental data are fitted with the Van Genuchten (1980) equation [5], for both drying (red curve) and wetting (blue curve) paths. The hydro-mechanical coupling between WRC and

mechanical behavior is fundamental to predict the behaviour of unsaturated soils upon wetting and drying (e.g. [7]).

Finally, the susceptibility of the MG layer to collapse has been investigated with oedometer tests, saturated at different vertical stress. Figure 1c. shows the evolution of the void ratio with vertical stress, where the sample has been inundated at σ_v = 50 kPa: a Δe=-0.006 of collapse is measured upon wetting. Based on a complete experimental campaign, the Barcelona Basic Model is calibrated and a numerical model at the in situ scale is developed to predict the displacement induced by ground water level variation within a finite element program.

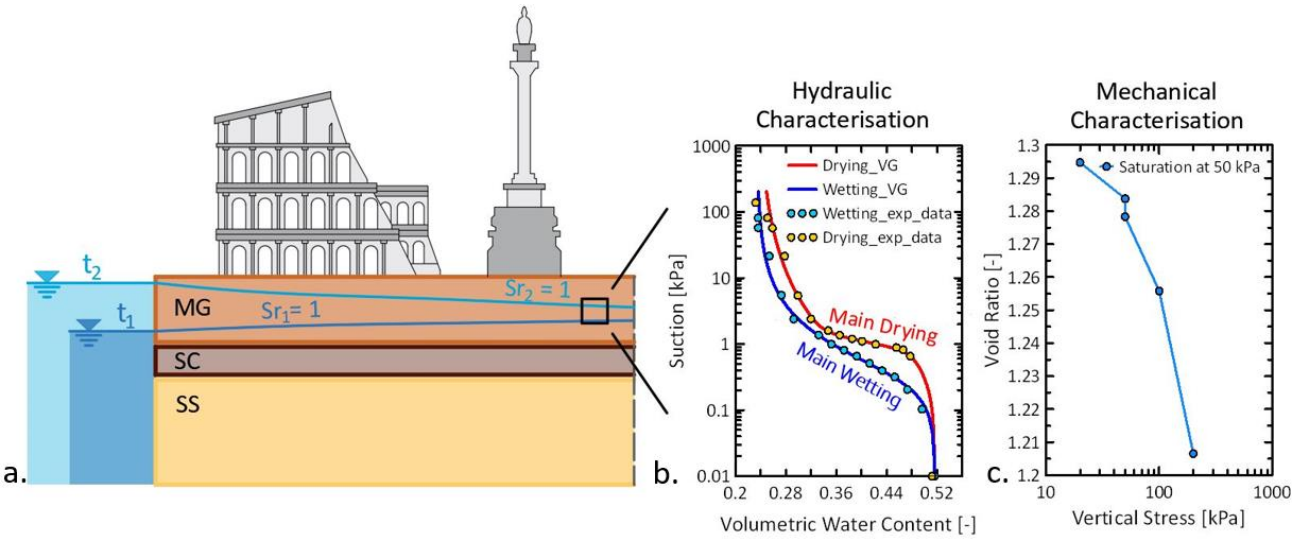

Figure 1. Scheme of the vertical section used in the numerical model and, on the right side, hydraulic hysteresis of the water retention curves and the saturation collapse in an oedometric test for the MG layer.

5. References

[1] Amanti, M., Gisotti, G., Pecci, M. (1995). I dissesti a Roma- Memorie descrittive della Carta Geologica d'Italia, **50**, 219 – 248, Rome.

[2] Calabresi, G., Cassinis, C., Nisio, P. (1980). Influenza del regime del Tevere sul comportamento di un fabbricato monumentale adiacente. *XIV Convegno Nazionale di Geotecnica*: 25-33.

[3] Pucci, A., D'Alessio, G., Giannetti, I., Moriero, I., Guida, G., Tello, J. F. G., ... & Casini, F. (2023). Geotechnical Analysis on the Effects of Tiber River Hydraulic Regime in the City Centre of Rome Within the Project Tiber'S. In *National Conference of the Researchers of Geotechnical Engineering*, 732-740.

[4] Alonso, E. E., Gens, A., Josa, A. (1990). A constitutive model for partially saturated soils. *Géotechnique*, **40(3)**: 405-430.

[5] Van Genuchten, M. T. (1980). A closed-form equation for predicting the hydraulic conductivity of unsaturated soils. *Soil Science Society of America Journal*, **44(5):** 892-898.

[6] Albadri, W. M., Noor, M. J. M., Alhani, I. J.. (2018). The importance of incorporating hysteresis effect in determining shear strength of unsaturated soil. In *AIP Conference Proceedings*, **2020(1)**. AIP Publishing.

[7] Han, K. K., Rahardjo, H., Broms, B. B. (1995). Effect of hysteresis on the shear strength of a residual soil. In *Proceedings of the first international conference on unsaturated soils*. AIP Publishing, Paris, France.

IMPACT OF WETTING AND DRYING CYCLES ON DURABILITY OF LIGHTWEIGHT CEMENTED SOILS

F. Sabatino[1], E. Vitale[2], G. Russo[2], O. Cuisinier[3] and M. V. Nicotera[1]
[1] Univ. Naples Federico II, DICEA, Naples, Italy
[2] Univ. Naples Federico II, DISTAR, Naples, Italy
[3] Univ. Lorraine, LEMTA, Nancy, France

Soils used in earthworks are generally subjected to wetting and drying cycles due to variations in climatic conditions. Such cycles can in principle alter the mechanical characteristics of soils potentially impairing their intended performance; in particular, this may occur in the case of stabilized soils for which wetting and drying cycles could significantly reduce the mechanical improvement provided by the treatment. Therefore, their mechanical response and performance may change during their service life [1, 2]. The purpose of this experimental study is to assess the impact of wetting and drying cycles on the durability of Lightweight Cemented Soils (LWCS). LWCS are prepared by mixing clayey soils with cement and foaming agent, obtaining a versatile material for different geotechnical purposes. Mechanical testing on LWCS samples has been performed after the application of wetting and drying cycles for evaluating the impact of amplitude of cycles (in terms of relative humidity) on their mechanical performance.

LWCS samples are formed by mixing clay with cement, water and foam. Speswhite kaolin it is an artificial clayey silt produced by Imerys Minerals Ltd (UK) and it is formed by kaolinite, muscovite with small amount of quartz. Portland cement (CEM II/A LL 42.5R) produced by Buzzi Unicem is used as binder. Surfactant solution (ISOCEM/S) provided by Isoltech s.r.l. is mixed with air at pressure of 3.2 bar in industrial foam generator for producing air foam of final density equal to 0.8 kN/m^3.

LWCS samples are prepared by mixing dry soil with distilled water; then grout (cement with water) is added to soil slurry and finally foam is added to the soil-cement-water system. Table 1 shows the treatment parameters adopted for this experimental samples preparation.

w_{slurry} (%)	w_c/c (%)	c/s (%)	n_f (%)
140	50	40	0-20-40

Table 1. Treatment parameters for LWCS preparation: w_{slurry} = slurry water content, w_c/c = water cement ratio, c/s = cement soil ratio, n_f = porosity induced by foam.

Two environmental load conditions are tested, namely n.3 wetting and drying cycles at 50% and 90% of relative humidity (Table 2).

Mix	Identifications	Environmental load conditions	Identifications
KC40nf20	A	3 w-d_50% RH	X
KC40nf40	B	3 w-d_90% RH	Y

Table 2. Identifications of the mix and the environmental load conditions.

Figure 1 shows the effects of different amplitude of wetting and drying cycles on shear strength of A samples. The larger the amplitude of cycles (*i.e.*, lower RH imposed during drying) the higher the shear strength, as a consequence of the increase of suction induced upon drying. The role of suction on shear strength is evidenced through the comparison with stress-strain curves on sample not submitted to any wetting and drying cycles.

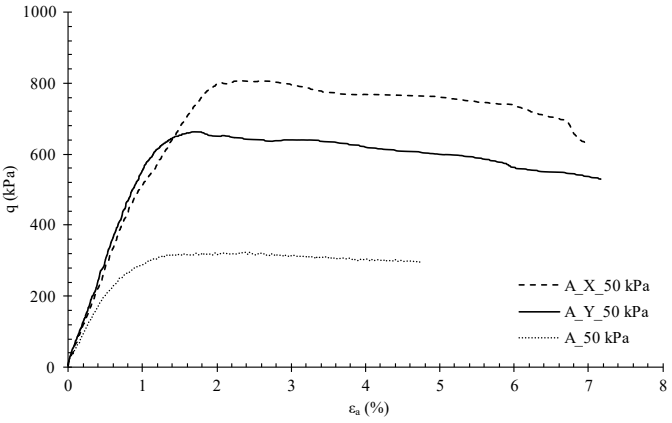

Figure 1. Increase of shear strength induced by wetting and drying cycles (X and Y) on samples at 50 kPa of confining stress.

References

[1] Chen, R. & Ng, CW.W. (2013). Impact of wetting-drying cycles on hydro-mechanical behavior on an unsaturated compacted clay. *Appl. Clay Sci.*, **86**:38-46.

[2] Tang, C-S., Wang, D-Y., Shi, B., Li, J. (2016). Effect of wetting-drying cycles on profile mechanical behavior of soils with different initial conditions. *Catena*, **139**:105-116.

[3] Vitale, E., Deneele, D., Russo, G., De Sarno, D., Nicotera, M. V., Papa, R., Urciuoli, G. (2020). Chemo-mechanical behaviour of lightweight cemented soils. *Acta Geotech.*, **15**:933–945.

INSIGHT INTO HYSTERESIS OF SOIL WATER RETENTION FROM PORE-SCALE CFD ANALYSES

M. Sawada[1,2], C. O'Sullivan[1] A. Tsiampousi[1] and J. Salomon[1]
[1] Imperial College London, Dept. of Civil and Environmental Engineering, London, UK
[2] Tokyo Institute of Technology, School of Environment and Society, Tokyo, Japan

1. Introduction

Predicting the degree of saturation in soil is important to evaluate and improve the resilience of geotechnical structures including embankments. The degree of saturation can be predicted from water retention curves, i.e., relationships between suction and water content. However, water retention curves are generally hysteretic; at a specific suction, the water content in a soil experiencing drying is higher than that in the same soil at the same suction experiencing wetting. One origin of this hysteresis is the ink-bottle effect that occurs in irregularly shaped soil pores with bulbs and constricted portions. Taylor (1948) [1] qualitatively explained the ink-bottle effect using a capillary tube with a bulb. The bulb restricts air and water entry into the tube, leading to hysteretic water retention curves.

This study aims to look into the hysteresis mechanisms caused by the ink-bottle effect from a pore-scale perspective and contribute to modeling water retention curves. The hysteresis of water retention curves in Taylor's model were simulated using a fully resolved CFD (computational fluid dynamics) code. The capillary force variation depending on the pore geometries and the mechanisms of the hysteretic air and water entries were discussed.

2. Methodology

InterFoam, an incompressible two-phase flow solver in OpenFOAM [2], was used to simulate water retention curves in a tube-single bulb system. The Navier-Stokes equation was solved with the finite volume method, and surface tension was considered at the fluid-fluid interface with the VoF (volume of fluid) method. In the VoF method, an indicator function, α, distinguished the two fluids. In the following simulations, cells with $0 \leq \alpha < 0.5$ and $0.5 \leq \alpha \leq 1$ were defined as air and water, respectively. Model validation using a straight tube without a bulb was firstly performed, followed by tube-bulb system simulations.

For the straight-tube simulations the computed capillary height was compared with theoretical values obtained with Jurin's law at several contact angles between 0º and 75º. The computed capillary heights were smaller than the theoretical values by 0.2 to 6%. The accuracy was better than in some previous studies validating *InterFoam* [3], and it was best when the contact angle was 45º. Thus, the contact angle was set at 45º in the following simulations.

For the tube-bulb simulations a numerical model of a tube (radius: 0.5 mm, height: 30 mm) with a bulb (radius: 1 mm, height: 4mm) at the middle elevation was developed. The initial water level in the tube-bulb system was set at 29 mm and negative water pressure was applied in the same manner as the laboratory water retention test using the water column method. In the drying simulation, the pressure at the tube bottom was decreased stepwise at intervals of 0.5 seconds (i.e. 100, 0, -50, -100, -180 Pa) while the tube top pressure was kept at 0 Pa. In the subsequent wetting simulation, the bottom pressure was increased in the same manner as for the drying simulation. The steady-state water volume in the tube at each step was recorded and the results were summarized in the form of water retention curves.

3. Results and discussions

Figure 1 (a) shows cross-section views of the tube during the water retention test. The capillary heights were non-reversible at the bulb which restrained wetting and drying, and thus the water retention curves were hysteretic as shown in Figure 1 (b).

The capillary force developed depending on the contact angle and tube radius, and thus it varied at the dilated part of the bulb and restricted air and water entries. During the air entry process the contact angle decreased as the contact surface changed from the vertical tube wall to the horizontal bulb top wall. The vertical component of the capillary force increased to a peak when the contact angle decreased to 0º, and thus air entry was restricted during the contact surface transition. The capillary force variation due to the tube radius increase occurred at the bulb bottom during the water entry process. Water entered the bulb when the water column coalesced with the residual water in the bulb and touched the bulb walls. A smaller capillary force developed in the bulb than in the tube, and so water entry was restricted until the bottom pressure increased sufficiently to lift the water column.

Extending the study, Figure 1 (c) shows typical simulation results of drying and wetting in face-centered-cubic packing (both images are for the same bottom pressure of 0 Pa). The water retention was hysteretic just as in the case of the single pore, and the forces acting on the particles at the wetting front were much larger than the particle weights.

4. Conclusions

The water retention hysteresis caused by the ink-bottle effect in a tube-bulb system was successfully simulated, and the mechanisms of the air and water entry restrictions at the bulb were discussed. The contact angle and tube radius variations at the dilated part of the bulb restricted air and water entries and made the water retention curves hysteretic. These preliminary results for the FCC assembly demonstrate the potential of pore-scale CFD analysis to provide useful insights into the effective stresses from the pendular to the capillary regimes.

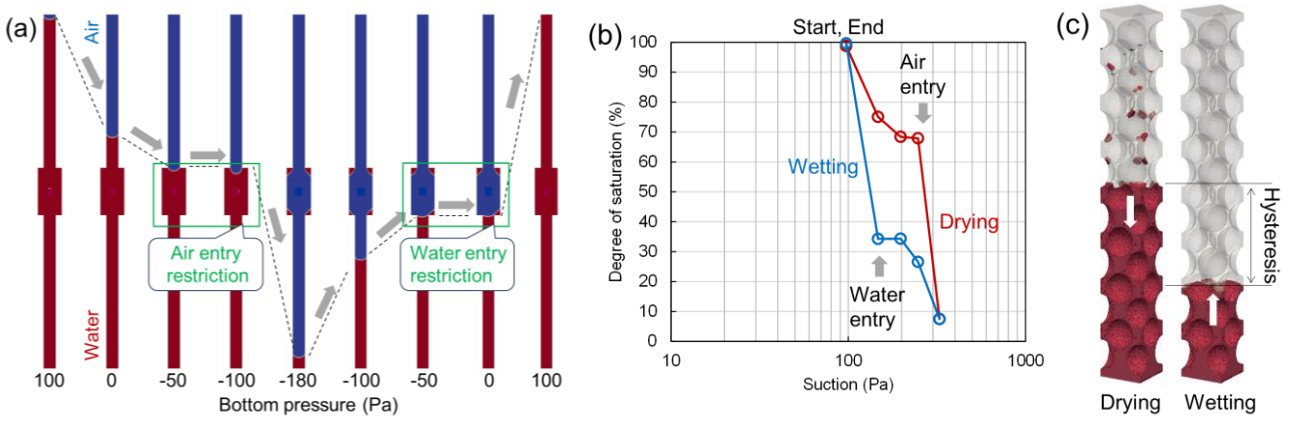

Figure 1. Computed water retention: (a), (b) single pore, and (c) FCC packing.

5. References

[1] Taylor D.W. (1948). *Fundamentals of soil mechanics*, 66 (2). LWW.

[2] Weller H.G., Tabor G., Jasak H., and Fureby C. (1998). A tensorial approach to computational continuum mechanics using object-oriented techniques. *Comput. Phys.*, 12(6), 620-631.

[3] Carrillo F.J., Bourg I.C. and Soulaine C. (2020). Multiphase flow modeling in multiscale porous media: An open-source micro-continuum approach. *J. Comput. Phys.*: X, 8, 100073.

MINIATURE TESTING DEVICE TO STUDY THE EFFECT OF EXTERNAL LOAD, AND IRRIGATION RATE AND DIRECTION ON THE CAPILLARY COLLAPSE OF UNSATURATED SOIL

L. Pérez-Jaimes[1], M. Milatz[1] and J. Grabe[1]

[1] Institute of Geotechnical Engineering and Construction Management, Hamburg University of Technology (TUHH), Germany.

1. Introduction

The capillary collapse is an irreversible volumetric deformation of partially saturated soils induced by an increase in the water content. This phenomenon has been studied for several author [1], [3], however, there are still some factor that haven't been studied yet. This paper proposes a new experimental device to study the effect of variations in the collapse behaviour due to changes in the irrigation rate and irrigation direction, as well as the presence of external death load. This device will be used in future collapse test during computational tomography to understand the phenomenon from a microscopic approach.

2. Changes in imbibition rate, direction and external loads in capillary collapse.

The rate and direction of water entry into the soil are important factors in analyzing the collapse phenomenon. This is because both factors control the change in effective stress in the soil and the distribution of capillary forces between soil particles. Understanding how these changes occur is fundamental to characterize the behaviour of the soil skeleton during the capillary collapse. Another important aspect to consider in this phenomenon is the presence of external loads on the ground, as these also generate a considerable change in the forces involved in the collapse phenomenon.

In this paper, three soil models will be studied. Two of them consist of coarse-grain sands, with one being more angular than the other. These will be referred to as Hamburg Sand I and Hamburg Sand II. The third soil model consists of a polydisperse pack of glass beads. All three soil models have a similar particle size distribution.

3. Experimental set-up

This paper presents a miniature testing device that allows the study of the effect of variations in irrigation rate and direction, and the presence of external load on the capillary collapse phenomenon in different granular unsaturated soils.

For the design of the dimensions of the testing device were developed different tests for the soils, in order to calculate the estimate water volumes necessaries for the study, as well as the estimated optimum weights and the deformations expected.

The tests were oedometer test to calculate the collapse index of each soil, and a hanging column method to have the WRC of the soils. There were also the obtention of WRC using UNSAT-PI 2, a microscopic device that allows the obtention of the WRC during cycles of wetting and drying [2]. With these laboratory tests, it was possible to characterize the soil through the WRC for the expected loose arrangements. Additionally, oedometer tests will be conducted on a larger scale, allowing for the estimation of deformations. These tests also enable control over the degree of saturation, irrigation from above and below, and the application of external loads. Vertical deformations will be measured

using image correlation methods, allowing for the estimation of saturation levels for the expected deformations in the tests.

The dimensions of the testing device are designed for future capillary collapse investigations using computed tomography to study this phenomenon from a microscopic approach.

5. References

[1] Bruchon JF, Pereira JM, Vandamme M, Lenoir N, Delage P, Bornert M (2013). Full 3d investigation and characterisation of capillary collapse of a loose unsaturated sand using X-ray CT. Granular Matter 15:783–800.

[2] Heinrich D., Milatz M. (2022): UNSAT Pi-2 - A miniaturized flow cell apparatus for measuring the water retention curve of granular media during CT imaging. In: TUHH Open Research (TORE), data repository including CAD design data, circuit diagrams and control software, DOI 10.15480/336.4394.

[3] Hüsener, N., Grabe, J. (2023). Capillary collapse of unsaturated granular soils: experimental investigation and microscale insights. E3S Web of Conferences. 382. 02004. DOI: 10.1051/e3sconf/202338202004.

MORPHOLOGICAL CHANGES IN DRAINAGE AND IMBIBITION REGIONS DURING WATER RETENTION TEST

S. Eshiro[1] and Y. Higo [1]
[1] Kyoto University, Department of Urban Management, Kyoto, Japan

1. Introduction

Water retention property is one of the key components of unsaturated soil. Recently, it has been investigated from the microscopic perspective using X-ray micro-computed tomography (μCT) [1]. In the previous studies of the morphological transitions for pore water and pore air during water retention tests, the morphology of whole pore water and air in the scan area has been investigated, and little attention has been paid so far to the water drainage and imbibition in the pore spaces. At the soil particle scale, there has been only a conceptual understanding of drainage and imbibition behaviour [2]. In this study, drainage and imbibition regions were extracted from the difference of the images in each water retention state visualised by μCT during the water retention test, and their morphology was analysed to quantitatively evaluate the behaviour of drainage and imbibition into pores.

2. Methodology

The water retention test and a series of μCT scans at each equilibrium point were carried out as described in Fukushima et al. (2021) [3]. The test sample was prepared by water pluviation technique using almost monodisperse Toyoura sand with a D_{50} of 187 μm. The CT images with a voxel size of 5.4×7.0 μm^3 were acquired at the equilibrium points during the drying process and the following wetting process, as shown in Figure 1. The CT images were segmented into three phases: soil particles, water, and air. The drainage regions during the drying process and imbibition regions during the wetting process were extracted, taking differences between the CT images at the two sequential points of different water retention states (e.g., **b-c**, **c-d**). Then, each discrete cluster of the drainage and imbibition regions was labelled to quantify each cluster's volume and surface area.

3. Results and Discussions

Figure 2 illustrates the relationship between the surface area cubed and volume squared of the clusters, depicting the morphology of the drainage and imbibition regions. In other words, for a given volume, a smaller surface area implies a simpler, sphere-like shape, whereas a larger surface area suggests a more complex shape.

The clusters of the drainage regions from point **e** to point **f** exhibit a small ratio of surface area to volume. In contrast, the clusters of the imbibition regions from points **h** to **i** demonstrate a large ratio of surface area to volume. These results indicate that the drainage occurred in a relatively simple spherical shape from near the centre of the pores during drying. During the subsequent wetting process, imbibition occurred in a complex shape near the surface of the soil particles. Such a morphological difference, probably due to the surface tension of water and the hydrophilicity of soil particles, may demonstrate the drainage and imbibition behaviour into pores along the suction change during the water retention test. The drainage and imbibition behaviour, which has been understood conceptually, can be demonstrated quantitatively.

4. Conclusions

The present study aimed to examine the morphology of drainage and imbibition regions in unsaturated soil during the water retention test with drying and wetting processes. The major findings of the study are as follows:

- The shape of the drainage and imbibition regions were quantitatively evaluated by the ratio of the surface area cubed to the volume squared.
- The morphology differences can represent the drainage and imbibition behaviour into pores during water retention tests.

5. References

[1] Kido, R., Y. Higo, F. Takamura, R. Morishita, G. Khaddour & S. Salager (2020) Morphological transitions for pore water and pore air during drying and wetting processes in partially saturated sand. *Acta Geotechnica,* **15,** 1745-1761.

[2] Childs, E. C. 1969. An introduction to the physical basis of soil water phenomena. J. Wiley.

[3] Fukushima, Y., Y. Higo, T. Matsushima & Y. Otake (2021) Liquid bridge contribution to shear behavior of unsaturated soil: modeling and application to a micromechanics model. Acta Geotechnica, 16, 2693-2711.

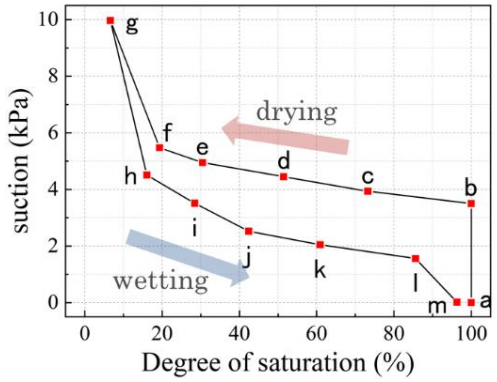

Figure 1: Suction-saturation relationship obtained from the water retention test

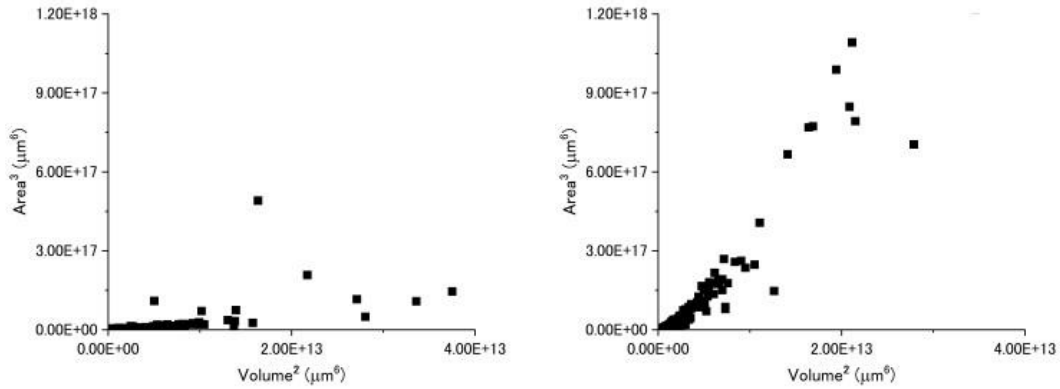

Figure 2: Surface area and volume of (a) drainage region cluster from point **e** to point **f** and (b) imbibition region clusters from point **h** to point **i**

Numerical modeling of the mechanical behavior of a partially saturated soil using a coupled DEM-LBM approach

R. Bouchard[1,4], N. Younes[1,3], O. Millet[1], A. Wautier[2], I. Stefannou[4]

[1] *LaSIE UMR CNRS7 7356, Université de La Rochelle, France, raphael.bouchard@univ-lr.fr*

[2] *INRAE, Unité de Recherche RECOVER, Aix-en-Provence, France*

[3] *Schulich School of Engineering, University of Calgary, Canada*

[4] *GeM, UMR CNRS 6183, Ecole Centrale Nantes, Nantes Université, Nantes, France*

Keywords: DEM - LBM - 3D - GPU - partially-saturated granular media - capillary bridges

The mechanical behavior of a 3D granular assembly subjected to cycles of saturation/desaturation is still poorly understood. In particular, the transition from pendular to capillary regimes and the coalescence of associated capillary bridges significantly alter its mechanical behavior.
In this work, we propose a coupled DEM-LBM approach on GPU [1, 2, 3] to simulate the behavior of a partially saturated granular assembly under different degrees of saturation. Specifically, the developed code allows simulating a drained triaxial test reaching approximately 20% deformation in about 1 hour, taking into account capillary forces precisely within the sample. The presented simulations (Fig. 1a) were carried out for initial void ratios ranging from 0.8 to 0.7, with the samples initially confined to a pressure of $5kPa$. The influence of capillary bridges and associated capillary forces at the microscopic level on the mechanical behavior of the sample is clearly highlighted. Furthermore, the performed numerical simulations and the utilized modeling enable the precise calculation of stresses solely due to capillary effects (Fig. 1b).

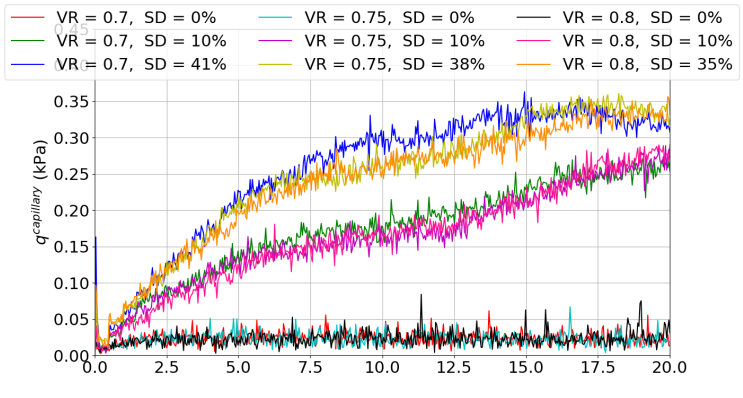

(a) *Evolution of deviatoric stress due to water for samples with different void contents and degrees of saturation*

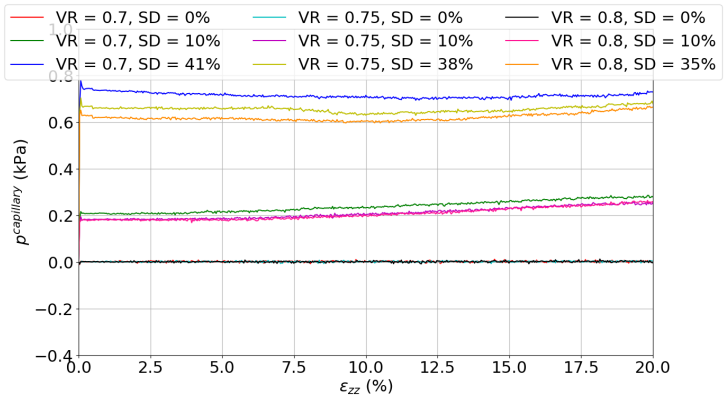

(b) *Evolution of mean water stress for samples with different void contents and degrees of saturation*

Figure 1. *Evolution of deviatoric stress and mean stress due to capillary forces only for samples with different void indices (VR) and saturation degrees (SD).*

References

[1] Benseghier, Z., Millet, O., Philippe, P., Wautier, A., Younes, N., and Liberge, E. (2022). Relevance of capillary interfaces simulation with the shan–chen multiphase lattice boltzmann model. *Granular Matter*, **24**, 1–18.

[2] Younes, N., Benseghier, Z., Millet, O., Wautier, A., Nicot, F., and Wan, R. (2022). Phase-field lattice boltzmann model for liquid bridges and coalescence in wet granular media. *Powder Technology*, p. 117942.

[3] N. Younes, A. Wautier, R. Wan, O. Millet, F. Nicot, and R. Bouchard DEM-LBM coupling for partially saturated assemblies. Preprint submitted to Computers and Geotechnics.

Partial saturation and effective stress: new insights from particle-scale simulations

B. Chareyre[1]***, C. Yuan***[2]
[1] *Univ. Grenoble Alpes, CNRS, 3SR Lab., Grenoble, France*
[2] *School of Civil Engineering, Shandong University, Jinan, Shandong 250000, China*

1. Introduction

The partial saturation of soils induces stresses and deformations, as well as changes in the mechanical strength, as a result of surface tension. To this date, the continuum-scale models taking into account these effects remain based on simplifying assumptions due to the lack of knowledge on how the three phases (minerals, water and air) interact in complex hydro-mechanical loadings. The emergence of grain-scale numerical models based on the discrete element method (DEM) enabled a new approach to this question. In this contribution, the main methods and findings are reviewed and the main advances are outlined. Namely, a meaningful definition of the effective stress in partial saturation emerge. Recent developments provide new results which tackle the limitations of the early models, generaly limited to very small saturation degrees (less that 5% typically), hence hence putting their results in perspective. In conclusion, some open questions and challenges for future research - numerical and experimental - are proposed.

2. Numerical models

2.1. Pendular state

The most common model for granular materials subjected to surface tension effects is based on the assumption that water, or any wetting liquid, is present in the form of pendular bridges connecting pairs of particles. In such case, it is possible to reflect the mechanical contribution of the bridges by attractive forces, following [1]. The forces by the *pendular* bridges are combined with the conventional contact models of the DEM to simulate stress and strain in the pendular state with thousands of particles forming a representative element volume (REV).

2.2. Generic states

Models going beyhond the pendular state are much harder to find for three dimensional problems. It is due in part to the topological complexity of the volume occupied by the wetting phase: it is no longer possible to describe it as a set of axisymmetric bridges. One solution is to use dedicated solvers such as the lattice Boltzmann method for multiphase problems yet the associatied computational costs make in not suitable for the thousands of particles present in a typical REV [2].

Alternatively, a possible solution technique uses pore-space partitionning as introduced by Yuan et al. [3]. Some results in next section were obtained by this technique, where the invasion of individual pores by one of the fluid phase is governed by local rules of drainage and imbibition which account for the local geometry of the solid skeleton. This approach produces liquid clusters of arbitrary shapes, and capillary forces forces which are no longer limited to pair interactions (Fig. 1).

3. Results

3.1. Pendular state

In the pendular state, each particle in an assembly is subjected to two types of forces (as long as gravity is neglected): contact forces and capillary forces. Both types of forces result from pair

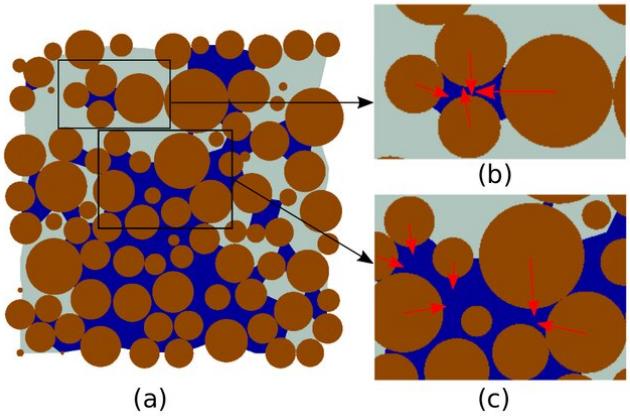

Figure 1. Distribution of wetting phase (dark blue) and a non-wetting phase (light blue) in a simulated particle system (brown). The capillary forces in two subregions are represented as red arrows [3].

interactions and, therefore, the total stress in the three phase system is given by the *virial* expression of stress, i.e. the volume averaged tensor product of forces and branch vectors:

$$\dot{\boldsymbol{\sigma}} = \frac{1}{V}\left(\sum_{ij\in contacts} \boldsymbol{f}_{ij}^{c} \otimes \boldsymbol{l}_{ij} + \sum_{ij\in bridges} \boldsymbol{f}_{ij}^{cap} \otimes \boldsymbol{l}_{ij}\right) \tag{1}$$

Note that the two sums run over distinct sets since there can be pendular bridges between particles without a contact. A striking result involving this decomposition of stress is that the contact stress $\boldsymbol{\sigma^c}$ (first term on the right hand side of Eq. 1) plays the role of the effective stress in the failure criterion. That is, substracting the capillary stress $\boldsymbol{\sigma}^{cap}$ (second term on the right-hand side of Eq. 1) from the total stress gives a stress which, if plotted at failure, satisfies a cohesionless Coulomb criterion with the same angle of friction as the dry material. This all but expected, and it introduces an unusual contribution: instead of being a spherical tensor - like excess pore pressure in the saturated case - the fluid contribution $\boldsymbol{\sigma}^{cap}$ has a significant deviatoric part. It is actually impossible to match Coulomb's failure line if this deviatoric contribution is neglected.

3.2. Generic state

It is no longer possible to evaluate Eq. 1 directly when the pendular forces are not pair interactions. However it is always possible to evaluate $\boldsymbol{\sigma^c}$ (the solid contacts are always pair interactions). When this is done, it is found that the contact stress drives the elastic deformation of the material during a simulated drainage. Hence, again and despite the complex distribution of the phases, a surprisingly simple definition of the effective stress emerges. Further, by simulating a drainage in oedometer conditions while taking into account the pendular bridges which persist behind the main drainage front, the contribution of the pendular bridges to the capillary stress is quantified. It is shown that the simulations assuming only pendular bridges can lead to situations which are not realistic, or that may be obtained only with very exotic sample preparations.

4. Conclusions

One may wonder if there exist cases where the above expression of effective stress may no longer be acceptable. We speculate that the answer to this question is: yes. In order to investigate such

cases and to propose alternative definitions, more data from simulations and experiments is needed. For the numerical models to provide new knowledge, the next challenge is to handle the evolution of the fluid phases when the soil is subjected to large deformation and failure. Only then it will be possible to analyse simultaneously pseudo-elastic response and failure for the same specimen in arbitrary hydraulic conditions.

References

[1] Lian, G., Thornton, C., and Adams, M. J. (1993). A theoretical study of the liquid bridge forces between two rigid spherical bodies. *Journal of colloid and interface science*, **161**, 138–147.

[2] Montellá, E. P., Yuan, C., Chareyre, B., and Gens, A. (2020). Hybrid multi-scale model for partially saturated media based on a pore network approach and lattice boltzmann method. *Advances in Water Resources*, **144**, 103709.

[3] Yuan, C., Chareyre, B., and Darve, F. (2016). Pore-scale simulations of drainage in granular materials: finite size effects and the representative elementary volume. *Advances in water resources*, **95**, 109–124.

REVEALING MECHANISMS OF STRESS-INDUCED WATER TRANSPORT AND SUCTION REDISTRIBUTION IN UNSATURATED SOILS BASED ON MICRO-CT IMAGING

J.B. Liu[1], A.K. Leung[1*], and Z.L. Jiang[1]

[1]Department of Civil and Environmental Engineering, the Hong Kong University of Science and Technology, Hong Kong SAR

**Corresponding author: A.K. Leung (ceanthony@ust.hk)*

Abstract

Effective stress of unsaturated soils is affected by not only the net mean stress but also matric suction associated with the surface tension of contractile skin. Recent pore-scale studies have demonstrated that the pore water in unsaturated soils can be distributed non-uniformly, leading to non-uniform matric suction distribution and affecting the evaluation of the effective stress of unsaturated soils. How fundamentally the hydromechanical loading affects the transport of pore water and the non-uniform distribution of matric suction remains unclear. Relationships among pore structure evolution, pore pressure change and water transport are yet to be explored. This paper reports the use of micro-X-ray computer tomography (μCT) to quantify the water transport processes and any redistribution of matric suction upon hydro-mechanical loading, thereby providing new physical evidence and insights into the contribution of matric suction distribution on the hydromechanical response of unsaturated soils. By using a newly-developed miniature suction-controlled triaxial cell, a series of constant-water-content (CWC) tests were conducted with simultaneous *in-situ* CT imaging. An algorithm was developed to track the transport of pore water, measure the non-uniformity of pore water and quantify the distribution of matric suction based on the Young-Laplace equation. Micro-mechanics of stress-induced water transport behaviour will be revealed through the evolution of pore structure. CT image-based estimation of the Bishop's coefficient (χ_{ij}) will be conducted to explore its relationship with the non-uniform distribution of matric suction.

Keywords: unsaturated soils, micro-hydromechanical response, matric suction distribution, water transport, X-ray computed tomography

STRATEGIES FOR EXTENDING SATURATED CONSTITUTIVE SOIL MODELS TO UNSATURATED TAILINGS

Mina Mofrad[1], Mehdi Pouragha[1] and Paul H. Simms[1]
[1] Carleton University, Ottawa, ON, Canada

1. Abstract

Constitutive modelling of tailing materials poses specific questions that can potentially go beyond the traditional soil mechanics; the presence of a wide range of particle sizes together with their hydromechanical loading history of wetting/drying cycles during self-weight consolidation necessitates a careful revisiting of models adopted to represent their response. The strength and deformation of hard rock tailings are profoundly impacted by their hydromechanical history, including recurrent cycles of desiccation and subsequent re-saturation often due to their stratified deposition methodology, which prevents the conventional simplification of behaviors solely to effective stress parameters.

Earlier studies have effectively established the foundational principles for integrating the influence of matric suction into classical continuum soil mechanics. This has led to the development of various constitutive models for unsaturated soils, including the Barcelona Basic Model [1] and the Glasgow Coupled Model [2, 3], developed based on the Cam Clay theory. Compared to granular materials, the wide particle size distribution in hard rock tailings leads to a relatively wide water retention curve and a notable capacity for hydraulic hysteresis.

In this study, we explore how previously developed framework by Glasgow Coupled Model can be adopted for extending existing saturated constitutive models to unsaturated tailings. In particular, a simple double hardening model based on Mohr-Coulomb criterion and a modified Rowe's stress-dilatancy relationship is used for reference [5]. The model is extended by; (1) considering suitable hydraulic energy conjugates including the effect of matric suction, (2) adding two hydraulic yield surfaces, and (3) including proper hydro-mechanical coupling terms in the hardening laws. Figure 1 shows the schematics of the extended 3D yield surface in $(p^* - q - s^*)$. The study addresses, different strategies for incorporating hydromechanical effects into the hardening of the yield surfaces. The trends predicted by the developed models have been compared to simple shear tests performed on unsaturated gold mine tailing undergoing drying/wetting cycles [6,7]. The comparison between model predictions and experimental results sheds new light into effective strategies for developing unsaturated constitutive models for partially saturated tailing materials.

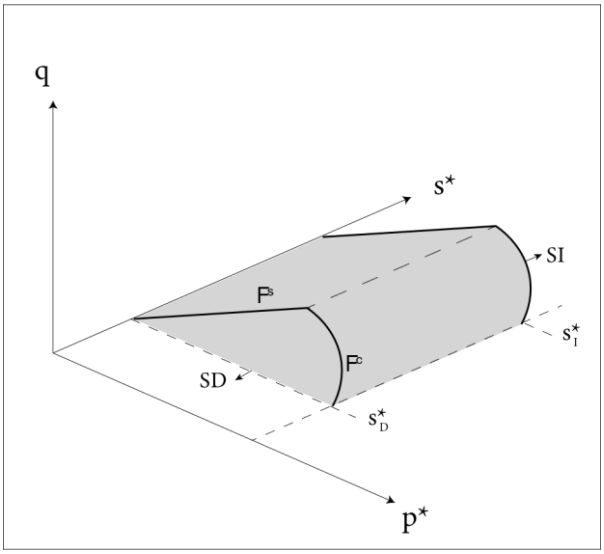

Figure 1. Yield surface of modified WG model in $(p^* - q - s^*)$ stress space

2. References

[1] Alonso, E. E., Gens, A. & Josa, A. (1990). A constitutive model for partially saturated soils. Géotechnique 40 (3) 405–430.

[2] Wheeler, S., Sharma, R. & Buisson, M. (2003). Coupling of hydraulic hysteresis and stress– strain behaviour in unsaturated soils. G´eotechnique 53 (1) 41–54.

[3] Lloret-Cabot, M., S´anchez, M., & Wheeler, S. J. (2013). Formulation of a three-dimensional constitutive model for unsaturated soils incorporating mechanical–water retention couplings. International Journal for Numerical and Analytical Methods in Geomechanics 37 (17) 3008-3035.

[5] Wan, R. & Guo, P. (1998). A simple constitutive model for granular soils: modified stress dilatancy approach, Computers and Geotechnics 22 (2) 109–133.

[6] Daliri, F., Kim, H., Simms, P. & Sivathayalan, S. (2014). Impact of desiccation on monotonic and cyclic shear strength of thickened gold tailings. Journal of Geotechnical and Geoenvironmental Engineering 140 (9).

[7] Daliri, F., Simms, P. & Sivathayalan, S. (2016). Shear and dewatering behaviour of densified gold tailings in a laboratory simulation of multi-layer deposition. Canadian Geotechnical Journal 53 (8) 1246–1257.

WATER RETENTION PROPERTIES OF DOUBLE POROSITY-VOLCANIC SOILS BY MEANS OF MICROSTRUCTURAL INVESTIGATIONS

M. Cecconi[1], A. Colella[2], C. Di Benedetto[2], L. Pappalardo[3], L. Perrotta[4], C. Sepe[2], E. Vitale[2], G. Russo[2]

[1] Univ. of Perugia, Department of Engineering, Perugia, Italy

[2] Univ. Napoli Federico II, Department of Earth Sciences, Environment, Resources, Napoli, Italy

[3] INGV- Osservatorio Vesuviano, CNR, Napoli, Italy

[4] Scuola Superiore Meridionale, Univ. of Napoli Federico II, Napoli, Italy

Fallout volcanic deposits of Somma-Vesuvius (Campania, Southern Italy), characterized by the presence of layers with contrasting textural and hydraulic properties, are frequently affected by shallow landslides during rainwater infiltration [1]. The soils of the stratigraphic sequence present intraparticle pores, originated by the gases escaped during magma decompression in the volcanic conduit, thus are characterized by double porosity (i.e., intraparticle and interparticle pores), which are expected to affect their hydraulic behaviour, and to play a key role in rainwater infiltration through layered deposits.

The role of double porosity on the hydro-mechanical behaviour of the volcanic deposits has been analysed in terms of water retention properties. Due to the characteristic grain sizes of the coarse grained materials, soil water retention properties of pumices layers were determined by semi-empirical methods proposed in literature. The method proposed by Praparhan et al. [2] was used to derive the Water Retention Curves (WRC) from the results of Mercury Intrusion Porosimetry (MIP) tests. Such method is based on the experimental evidence that mercury entry value during mercury intrusion and air entry value of the WRC are closely related, and that the equivalent pores radii from MIP tests and the pores radii from experimental WRCs can be linked through Kelvin equations [3].

In order to apply the Prapahran et al. model to coarse-grained pumices with double porosity, characterized by intra-particle and inter-particle pore sizes spanning over several order of magnitude, two different microstructural techniques have been adopted. Results from MIP tests on single pumice clasts allowed to derive the pore size distribution of intraparticle pores, whereas results from X-Ray Micro Tomography (XRMT) tests on representative samples (reconstituted at in situ bulk density) allowed the determination of interparticle pore size distribution. A unique pore size distribution of coarse-grained pumices was finally implemented in the semi-empirical model for determining the water retention curve of the representative sample.

The methodology adopted in the research combines highly reliable laboratory techniques (i.e., MIP and XRMT) finalized to the determination of fundamental properties of coarse-grained unsaturated soils such as water retention properties, difficult to be directly measured in situ

References

[1] Sepe C, Calcaterra D, Damiano E, et al. (2023) Transient infiltration tests in pyroclastic soils with double porosity. *Journal of Mountain Science* 20(11). https://doi.org/10.1007/s11629-023-7955-3

[2] Prapaharan, S., Altschaeffl, A.G., Dempsey, B.J. 1985. Mois-ture curve of compacted clay: mercury intrusion method. *Journal of Geotechnical Engineering*, ASCE, 111(9): 1139-1143

[3] Cecconi M., Russo G. 2008. Prediction of soil-water retention properties of a lime stabilised compacted silt. In D.G. Toll, C.E. Augarde, D. Gallipoli, S.J. Wheeler (eds.), *Unsaturated Soils: Advances in Geo-Engineering. 1st European Conference on Unsaturated Soils*, EU-UNSAT 2008, Durham, July 2008, 271-276, Taylor & Francis Group, London. ISBN 978-0-415-47692-8.

.

Interactions in composite geomaterials

3D INSIGHTS INTO SHEAR BEHAVIOR OF SAND-SMOOTH GEOMEMBRANE INTERFACES THROUGH X-RAY TOMOGRAPHY TESTS

Lalit Kandpal[1], Satoshi Matsumura[2] and Prashanth Vangla[1]
[1] Indian Institute of Technology Delhi, New Delhi, India
[2] Port and Airport Research Institute, Yokosuka, Japan

1. Abstract

The interface shear mechanism of geomembrane and sand particles governs the design of geosystems involving these materials, as these interfaces are the potential plane of weakness. The interaction at their interface is complex and can profoundly influence their energy efficiency, stability, and performance. Load transfer at these interfaces is mainly through friction; however, they do not obey Amontons' law of friction [1]. The sliding and plowing mechanism governs the frictional response without dilation at the interface, referred to as non-dilative interfaces. Thus, traditional soil mechanics concepts cannot describe their underlying shearing mechanism. Previous studies have revealed that the particle contacts at the interface level govern interface shear response. Therefore, it is essential to understand the shear behavior of a non-dilative interface system by studying fundamental aspects governing its macro behavior. This includes examining the sliding and plowing of particulate materials in the continuum material's surface at a micro-level within the field of tribology. Thus, comprehending the kinematics of particulate materials and tribological aspects together in a geotribological framework is essential to develop realistic force prediction models and interface friction correlation charts for non-dilative interfaces. Kandpal and Vangla [2] have experimentally investigated geotribological aspects while shearing under different influential factors for transparent continuum to demonstrate their effect on particle kinematics for transparent continuum materials. However, the literature lacks comparable studies for conventional opaque continuum materials that may lay a foundation for developing enhanced numerical models. This study presents an experimental approach that links particle kinematics and tribological aspects to understand the underlying friction mechanism of non-dilative interface shear response. To this end, interface direct shear tests accompanied by X-ray scanning are conducted on two different sands, namely, subangular sand (SA_S) and smooth glass beads (S_GB) of similar size (2-4.75 mm) but different morphologies with high-density polyethylene (HDPE) geomembrane. The effect of normal load is addressed by performing tests under three different normal loads (50, 100, and 200 kPa). The particle deformation is analyzed from the X-ray tomography data in software for practical analysis of materials (SPAM) to obtain the strain field and visualize the particle kinematics. Spatial roughness distribution is quantified using an optical microscope to correlate the shear-induced surface changes and particle kinematics with the macro shear response.

The shear force-horizontal displacement responses obtained for the interfaces with and without X-ray CT scanning for S_GB and SA_S with HDPE are shown in Figure 1. It is evident that the shear response of both the interfaces with and without scanning is similar under different normal loads, indicating the halt-and-run procedure adopted in the scanning tests is not significantly affecting the response. The shear stress increases with the increase in normal stress for both interfaces. It is also evident that the shear stress is higher for SA_S at any given normal stress than S_GB. Figure 2 shows the strain field from the top at the interface and cross-section at the centre for S_GB-HDPE and SA_S-HDPE at 50 kPa. It is evident from the strain field in Figure 2 that for both interfaces, the particle movement is at the interface only. S_GB has shown less particle kinematics while shearing than SA_S. This is attributed to the low roughness of S_GB, resulting in the development of low contact

forces to displace the particles. The post-shear roughness values are higher for the SA_S-HDPE than S_GB-HDPE due to the plowing of the geomembrane. The interface shear responses, X-ray CT image-based deformation and tracking of particle motions, and micro-topographical analysis revealed that the geotribological framework includes contact's particle kinematics and plowing, providing deeper insight into the interface shear mechanism of sand-smooth geomembrane interfaces. The effect of particle shape and normal stress on the particle kinematics, frictional mechanism, and consequentially on the friction coefficient is established. The particle kinematics are observed to reduce with an increase in the normal stress, leading to more plowing. The critical normal stress interface significantly depends on particle morphology and kinematics. These findings reconfirm with evidence that a particle's shape and contact stresses play a significant role in particle kinematics at the interface.

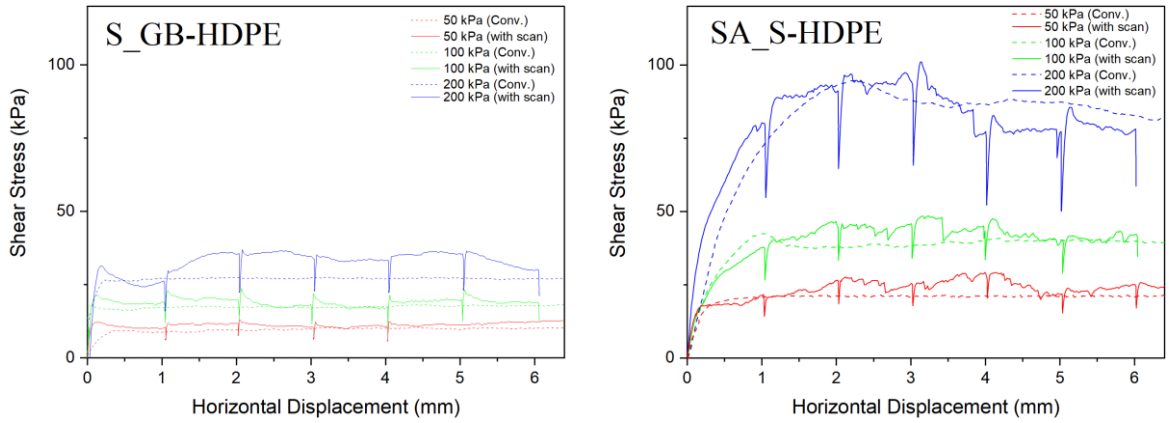

Figure 1. Shear response with and without X-ray CT scan for the interfaces

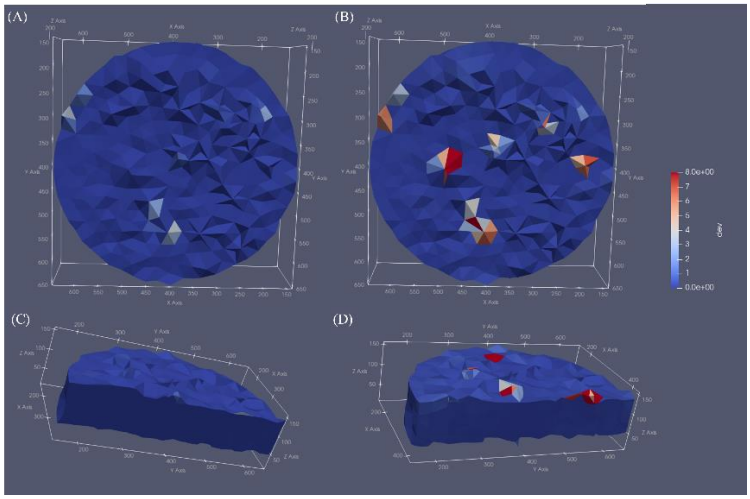

Figure 2. Strain field from the top at the interface and cross-section at the centre for (A, C) SG_B-HDPE and (B, D) SA_S-HDPE under the normal stress of 50 kPa

2. References

1. Dove JE, Frost JD (1999) Peak friction behavior of smooth geomembrane-particle interfaces. Journal of Geotechnical and Geoenvironmental Engineering 125:544–555. https://doi.org/10.1061/(ASCE)1090-0241(1999)125:7(544)

2. Kandpal L, Vangla P (2023) New insights into geotribology of non-dilative interfaces from novel experimental studies. Geosynth Int 1–17. https://doi.org/10.1680/jgein.23.00013

ACOUSTICS AND SHEAR RESPONSE OF SAND-STEEL CONTACTS THROUGH MICROMECHANICAL TESTS

Satyam Dey[1], Prashanth Vangla[1]
[1] Indian Institute of Technology Delhi, Delhi, India

Sand-metal interfaces are often seen in many geotechnical systems, such as soil-reinforced structures, buried pipelines, pile foundations, etc. Understanding their shear and acoustic responses is vital in efficiently designing and monitoring the geotechnical systems, including the soil characterisation devices that involve soil-metal interactions. The application of acoustic emission (AE) based waveguides for health monitoring of geotechnical structures is still nascent. However, its potential to accurately monitor slopes in real-time while being significantly more economical than existing methods has garnered much traction among researchers in the last decade. While [1] introduced using a metal tube as a waveguide (passive) to monitor and detect failure in soil, soil's heterogeneity and damping nature render the passive waveguide impractical. To address the issue, [2] introduced an active-waveguide system where the waveguide tube is surrounded by granular material. In an active waveguide system, the interaction between the granular material and the tube acts as the source of AE, not the host soil, which can be used to detect the failure. The active waveguide generates AE due to interactions between the tube and adjacent sand while shearing at the interface and bending the tube. While the interface shearing indicates the onset of deformation, the bending of the waveguide tube suggests large deformation. Hence, it is imperative to fundamentally study the interface shear between the metal tube and the surrounding granular material to develop efficient monitoring and provide early warning. However, most studies on active waveguides are on the bending of the tube compared to the interface shear response. Although [3] established correlations between the interface shear governing parameters and AE, the analysis was in the time domain and at a macro scale. Furthermore, to the author's knowledge, no study explored the AE response of the soil-metal interface from a micro-scale, which can reveal the fundamental source of AE and its characteristics.

To this end, a series of single particle shear tests were performed in a custom-built micromechanical direct shear testing apparatus (MDST) on geomaterial contacts made of 3 mm thick, smooth steel (ST) as the continuum material and smooth glass beads (GB) and angular quarry sand (QS) of 2-4 mm size as a granular material. The thickness of the metal plates was selected such that the AE can be travelled through it as a guided wave (Lamb wave in the kHz range) with low attenuation. GB and QS particles are selected to study the effect of their shape on the AE while shearing. Based on the image-based shape analysis technique suggested by [4], the GB and QS are classified as rounded and angular. Micromechanical shear tests are conducted at three normal loads (10, 30, 40 N) and displacement rates (1, 2, 3 mm/min). The range of the AE is selected to be 20-100 kHz to eliminate low-frequency (<20 kHz) ambience noise and high-frequency (>100 kHz) waves which attenuate rapidly. The analogue-to-digital converter’s (ADC) sampling frequency is set to 1 MHz, five times the Nyquist frequency of the highest frequency in the selected range to get distortion-free waveforms. The AE were analysed in time, frequency, and time-frequency domain using Ring Down Count (RDC), FFT and spectrogram, respectively. RDC is the number of times the digital waveform crosses a predefined threshold value based on ambient noise and sensor sensitivity.

A typical shear response of GB-ST and QS-ST interface tested at 30N normal load and 3mm/min displacement rate along with the AE waveform are illustrated in Figure 1. The shear response of both interfaces has a prominent peak followed by strain softening, and then an almost constant shear load persists. However, the peak shear load is less in the GB-ST interface, and no force drop is observed. The track formed on the continuum material and the change in surface roughness

indicates that the interface undergoes plowing while shearing. The AE response of the GB-ST is flat; no noticeable voltage peaks are observed, indicating that plowing does not generate AE. On the other hand, the shear response of the QS-ST interface contacts shows several shear force fluctuations due to the breakage of particle asperities at various intervals. The shear force rises when the particle and the continuum material's asperities interlock. In the AE response, the peaks are consistent with the force drops. During the particle breakage, the tracks are non-linear, and force drops in shear and peaks on the AE response are observed. However, no force fluctuations and AE peaks are observed when plowing occurs without asperity breakage.

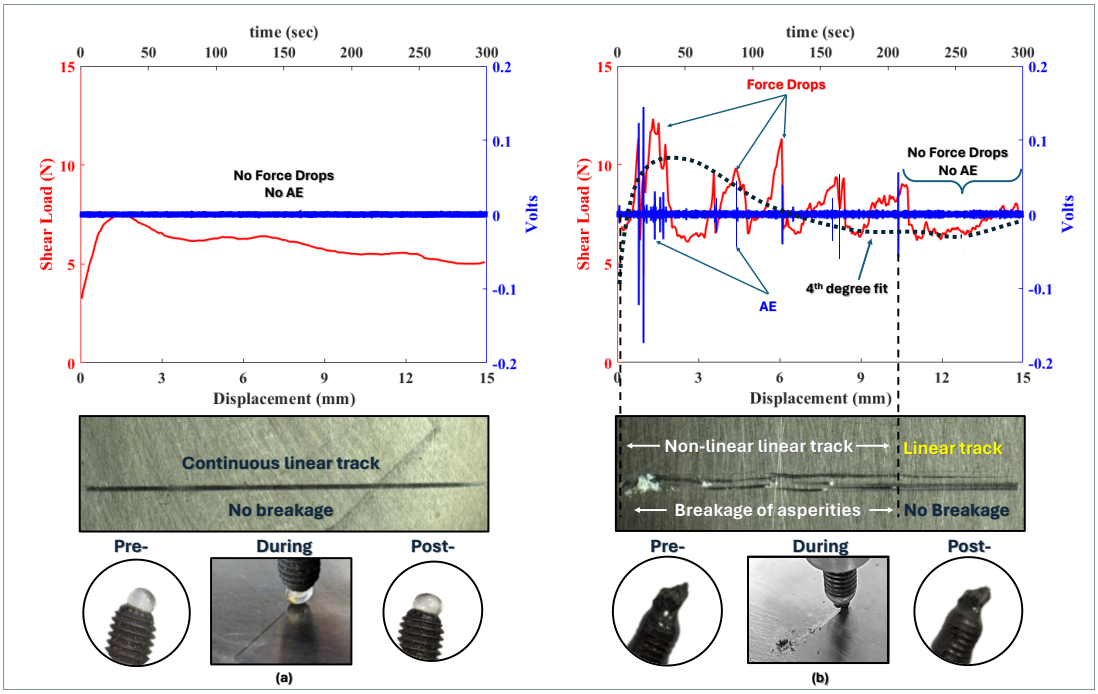

Figure 1. Single particle interface shear and AE response of (a) GB-ST and (b) QS-ST interface.

The series of tests on angular and rounded particles with steel reveal that the contact points of the QS particle and the continuum material experience high-stress concentrations, unlike GB. Additionally, these asperities break during shearing, resulting in micro-tapping and establishing new contacts. The tapping at the contacts leads to the momentarily shear load dropping and generating the AE wave. The FFT analysis of the AE signal shows that the dominating frequency of AE lies between 40 and 80 kHz. This study demonstrates that an interface generates AE only when it undergoes micro-tapping due to the breakage of interlocked contacts while shearing.

References

[1] Koerner RM, McCabe WM, Lord AE (1981). *Acoustic emission behavior and monitoring of soils*. ASTM International

[2] Dixon, N., Hill, R., & Kavanagh, J. (2003). *Acoustic emission monitoring of slope instability: development of an active waveguide system*. Geotechnical engineering, 156, 83-95.

[3] Smith A, Heather-Smith HJ, Dixon N, Flint JA, Pennie D (2020). *Acoustic emission generated by granular soil-steel structure interaction*. Geotechnique Letters 10:119–127. doi: 10.1680/jgele.19.00065

[4] Vangla P, Roy N, Gali ML (2018*) Image based shape characterization of granular materials and its effect on kinematics of particle motion.* Granular Matter. doi: 10.1007/s10035-017-0776-8

DECODING ONE-DIMENSIONAL DEFORMATION IN SOFT-RIGID GRANULAR MIXTURES

P. Badarayani[1], B. Cazacliu[1], E. Ibraim[2], P. Richard[1] and R. Artoni[1]
[1] Université Gustave Eiffel, MAST, GPEM, F-44344 Bouguenais, France
[2] Department of Civil Engineering, University of Bristol, Bristol, UK

1. Abstract

The one-dimensional loading/unloading behavior of sand-rubber mixtures is investigated by laboratory strain-controlled experiments performed for different packing densities, particle sizes, rubber contents and sand/rubber size ratios. The one-dimensional confined stiffness and the swelling behavior were then analyzed (see **Figure 1**). In the following, the authors propose a method to decompose the total deformation in three components – elastic, plastic which is recovered during the unloading and unrecovered plastic. Correlations between the two components of the plastic strain – the recoverable and the irrecoverable – and between the plastic and elastic deformation of the granular packing, independent of the packing densities, particles sizes and size ratios can further be determined using this hypothesis. The authors also propose micromechanical justifications of these experimentally observed phenomena. Granular packings exhibit one-dimensional swelling deformation during re-loading [1]. However, this deformation is not thermodynamically reversible [2]. The recoverable elastic deformation of compressed grains [1,3] is contingent on simultaneous rearrangement of surrounding particles during unloading. The deformation of the packing between two loading states is, as classically considered, the superposition of plastic and elastic components. So, the total deformation after a one-dimensional loading up to a maximum (inversion) stress σ_{max}, $\Delta\varepsilon(\sigma_{max}) = \varepsilon_{max}$, could be expressed by the sum of three contributions: the elastic (reversible) deformation directly resulted (geometrically) from the elastic deformation of the grains, $\Delta\varepsilon_g(\sigma_{max})$, the plastic deformation which is not recovered after complete unloading $\Delta\varepsilon_i(\sigma_{max}) = \varepsilon_o$, and, the plastic deformation which is recovered during the complete unloading and could be developed again if the sample is re-loaded, $\Delta\varepsilon_r(\sigma_{max})$.

$$\Delta\varepsilon = \Delta\varepsilon_i + \Delta\varepsilon_r + \Delta\varepsilon_g \quad (1)$$

In this equation, the total deformation, $\Delta\varepsilon$, and the unrecovered plastic deformation, $\Delta\varepsilon_i$, are easy to determine from the one-dimensional loading unloading curve (see **Figure 1(a)**). It remains to dissociate the elastic deformation, $\Delta\varepsilon_g$, from its associated deformation produced by the evolution of the contact network, i.e. the recovered plastic deformation, $\Delta\varepsilon_r$. The following complementary hypothesis is introduced here to further dissociate these two deformation components. It is considered that the one-dimensional recovered plastic deformation evolves linearly with the log of the vertical stress. Here, the behavior similar to overconsolidated sand packings [4] is extrapolated to packings including flexible particles, by considering that the recovered plasticity stress evolution is characterized by a stress independent "recovered plasticity swelling index":

$$C_{so} = \frac{(1+e_o)\delta\varepsilon_p}{\delta(log\sigma_v)} \quad (2)$$

One can than determine the unloading recoverable plastic deformation, $\Delta\varepsilon_r(\sigma_v)$ at any level of vertical stress σ_v, and in particular at the maximum (inversion) vertical stress σ_{max} (see **Figure 1**):

$$\Delta\varepsilon_r(\sigma_{max}) = C_{so} log(\sigma_{max}/\sigma_o) \quad (3)$$

The recovered plasticity swelling behavior does not consider the elastic deformation of the rubber-sand mixtures, which cannot be neglected. Then the swelling index C_s given by:

$$C_s = \frac{-\delta e}{\delta(log\sigma_v)} = \frac{(1+e_o)\delta\varepsilon_v}{\delta(log\sigma_v)} \quad (4)$$

and the recovered plasticity swelling behavior C_{so} (**equation 5**) are not equal, except at very low vertical stress levels where the rubber particles' elastic deformation is asymptotically vanishing. An asymptotic relation could be proposed:

$$C_{so} = \lim_{\sigma_v \to 0} C_s \quad (5)$$

Therefore, C_{so} could be obtained from the tangent behavior at the unloading curve when the vertical stress converges to zero.

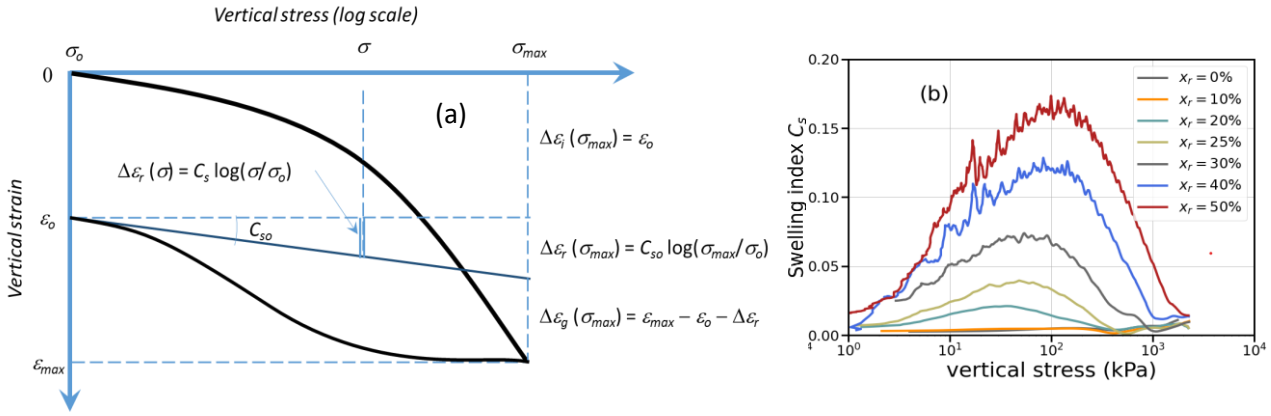

Figure 1. (a) Schematic representation of the three components of the total deformation after oedometric loading of the rubber-sand mixture at the maximum (inversion) stress σ_{max}, (b) Evolution of the swelling index at different levels of unloading vertical stress for different rubber contents [5].

Based on the above hypothesis, an expected increase of the packing elasticity with the rubber fraction can be observed, mainly for rubber fractions higher than 20%. Furthermore, strong correlation can be observed between the two components of the plastic strain: the recoverable and the irrecoverable. Finally, a correlation can be established between the plastic and elastic deformation of the granular packing.

2. References

[1] Fonseca, J. et al., (2019). Particle--scale interactions and energy dissipation mechanisms in sand-rubber mixtures. *Géotechnique Letters*, Volume 9(4), pp. 263-268.

[2] Nicot, F. & Darve, F., (2006). On the Elastic and Plastic Strain Decomposition in Granular Materials. *Granular Matter*, Volume 8, pp. 221-237.

[3] Collins, I., (2005). The concept of stored plastic work or frozen elastic energy in soil mechanics. *Géotechnique*, Volume 55, pp. 373-382.

[4] Biarez, J. & Hicher, P. Y., 1994. *Elementary mechanics of soil behaviour: saturated remoulded soils.* Rotterdam, Balkema: ISBN: 9054101571.

[5] Badarayani, P., et al., (2023). Sand Rubber Mixtures under Oedometric Loading: Sand-like vs. Rubber-like Behavior. *Applied Sciences*, *13*(6), 3867.

EXPERIMENTAL ASSESSMENT OF SOIL PROPERTIES DATABASE FOR BURROWING SOFT ROBOT DESIGN OPTIMIZATION

***I. Brodoline*[1], *F. Anselmucci*[1], *A. Sadeghi*[2] *and V. Magnanimo*[1]**

[1] *University of Twente, Chair of Soil Micro Mechanics, Faculty of Engineering Technology, Enschede, The Netherlands*

[2] *University of Twente, Soft Robotics Lab, Faculty of Engineering Technology, University of Twente, Enschede, The Netherlands*

1. Research Motivation

In recent years climate change have significantly impacted soil integrity, exposing (infra-)structu res to new challenges and our society to higher risk of severe hazards. The demand for continuous and precise soil condition monitoring has become increasingly urgent, not only for geotechnical engineers but also for diverse everyday life applications. Conventional investigation tools, although effective, are often highly invasive, constrained to predefined paths, costly, and disruptive to daily activities. In the face of these limitations, the development of less destructive methodologies for monitoring soil properties (such as strength and water content) is imperative. Innovations such as burrowing soft robots represent a significant advancement in this field [1]. This new class of robots offer a non-invasive approach to soil analysis, providing the flexibility to navigate through complex paths, reach previously inaccessible areas.

The deep-burrowing earthworm *Lumbricus terrestris* is a well-studied animal model for building burrowing robots [2, 3]. Compared to other earthworm species, *Lumbricus terrestris* has a body size of up to 1 cm in diameter and can penetrate the soil to depths exceeding one meter with minimal disruption. These properties make it a suitable target for artificial replication. However, the development of such robots is still challenging. In the last decade, there have been attempts to build earthworm-like robots [4], but only a few of them could overcome the soil penetration resistance and burrow in depth [1]. However, even these robots have shown a tendency to alter the initial soil conditions during their movement. The primary limitation in developing effective soil-investigation robots lies in understanding the interaction forces with the soil. So far, only numerical studies have been conducted to qualitatively estimate these forces [5].

In this work, we quantify and model the forces acting on an earthworm-like robot (Figure 1a) through a series of Cone Penetration Tests (CPT) and cavity expansion tests, mimicking the different stages of the robot motion. The experimental data is used to create a finite element method (FEM) model to upscale the problem and validate the stresses distribution at the interface soil-robot.

2. Experimental procedure

In this project, we built a soil properties database based on experimental measurements, investigating the soil-robot interactions which occur during burrowing. The earthworm-like robot accomplishes burrowing through a peristaltic movement, inspired by that of Lumbricus terrestris, i.e., a sequence of radial expansions and longitudinal elongations of the body segments. Thus, we hypothesize that the interaction forces acting between the robot and the soil medium can be represented by two experimental setups, as shown in Figure 1b-c. The first part of the experiment (Figure 1b) is a conventional CPT test conducted in both the vertical and horizontal directions. It corresponds to the penetration of the robot's tip into the soil. Different shapes of tips are used to measure the vertical and horizontal penetration forces at the tip Q_{cV} and Q_{cH}, and along the sleeve R_{fV}, and R_{fH}. In the second geomechanical test (Figure 1c) the expansion pressure of a balloon-like body in a sand tank is measured, to replicate the anchoring phase of the robot body.

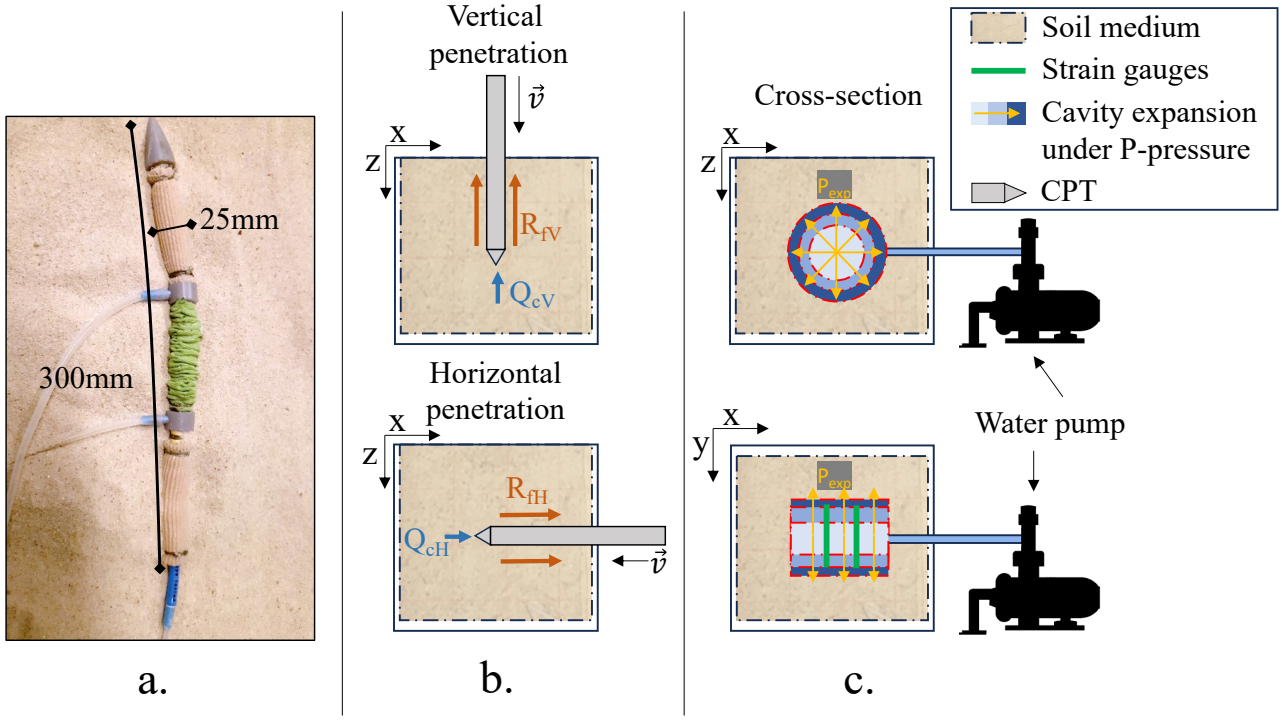

Figure 1. (a) Prototype of an earthworm-like robot developed for soil monitoring; (b) first experimental setup used to evaluate the necessary penetration stresses of the robot; (c) cavity expansion experiment, measuring the necessary anchoring pressure.

3. Conclusions

In the final stage of the project, we have integrated the information gathered from the cone penetration and cavity expansion tests within a continuum model for soil and implement the soil-robot system in a commercial finite element code, to simulate the larger scale coupled problem. This work crucially advances our understanding of the interaction forces between soil and robotic probes, particularly those inspired by earthworms.

This research lays the foundation for the deployment of earthworm-like robots in various soil environments, making substantial contributions to both scientific knowledge and practical applications in the field. It shows potential for creating novel geomechanics solutions to face challenges posed by climate change.

References

[1] Naclerio, N. D., Karsai, A., Murray-Cooper, M., Ozkan-Aydin, Y., Aydin, E., Goldman, D. I., and Hawkes, E. W. (2021). Controlling subterranean forces enables a fast, steerable, burrowing soft robot. *Science Robotics*, **6**, eabe2922.

[2] Edwards, C. A. and Arancon, N. Q. (2022). Earthworm morphology. *Biology and Ecology of Earthworms*, pp. 1–31, Springer.

[3] Quillin, K. J. (2000). Ontogenetic scaling of burrowing forces in the earthworm lumbricus terrestris. *Journal of Experimental Biology*, **203**, 2757–2770.

[4] Liu, J., Li, P., and Zuo, S. (2023). Actuation and design innovations in earthworm-inspired soft robots: A review. *Frontiers in Bioengineering and Biotechnology*, **11**, 1088105.

[5] Martinez, A., DeJong, J. T., Jaeger, R. A., and Khosravi, A. (2020). Evaluation of self-penetration potential of a bio-inspired site characterization probe by cavity expansion analysis. *Canadian Geotechnical Journal*, **57**, 706–716.

FIBER-GRAINS INTERACTION MECHANISM DURING TRIAXIAL TEST DETECTED WITH X-RAY TOMOGRAPHY

M. Arciero[1,2], E. Salvatore[1], G. Modoni[1], A. Tengattini[2] and G. Viggiani[2]
[1] University of Cassino, UNICAS, Cassino, Italy
[2] Univ. Grenoble Alpes, 3SR Lab., Grenoble, France

1. Abstract

Fiber orientation plays a key role in fiber reinforcement. Fibers must undergo tensile stress to produce enhancement and must be oriented along the minimum principal stress direction to ensure maximum interaction with the shear band. When fibers are well oriented, porosity and strain are more homogeneous and diffuse overall the specimen, and the shear band thickness is wider. The present study is focused on the detection of the interaction mechanism between sand grains and fibers, to link the behavior observed at the macroscale with the microscale. An investigation of the soil-fibers contact would disclose the mechanisms that take place locally and affect the global behavior of the soil assembly, providing great benefits for the reinforcement's design and performance predictions.

Fiber-reinforced sand is subjected to miniature triaxial compression test and CT scan. Digital Image Correlation analysis is performed to detect fiber grain interaction mechanisms.

2. Introduction and Research

Numerous studies have explored fiber-reinforced sands (FRS) to enhance properties like resistance, stiffness, and ductility in geotechnical structures, typically focusing on factors such as soil type, fiber characteristics, and ground improvement optimization. This study combines element scale analysis observed with laboratory geotechnical testing – direct shear and triaxial tests – and micro-scale analysis detected with X-ray tomography to understand the role of fibers in reinforced sands.

The reinforcement of sands by a diffuse inclusion of fibers is promoted by the idea that filaments of controlled mechanical characteristics intruded in the soil pores, somehow, inhibit the mobility of grains and provide additional properties to the assembly (e.g., resistance, stiffness, ductility, or damping) and improve the performance of geotechnical structures [1], [2], [3].

To catch the mechanism of fiber-grain interaction, several DIC procedures are performed on images from X-ray tomography of a specimen of Hostun sand HN31 reinforced with polypropylene fibers oriented along the direction of the minimum principal stress (horizontal during triaxial compression test). The procedure is strongly supported and run using SPAM, an open-source python tool for quantitative data analysis [4].

From the results at the macro-scale and the Continuum DIC analysis, porosity, and deformation maps - deviatoric and volumetric - are homogeneous and diffuse overall the specimen, generating a wider shear bandwidth. It is therefore assumed that during the shear-band evolution mechanism, fibers may be able to block the grains bordering them and increase displacements and rotations in the more distant areas. The analyses are performed at the Discrete level, i.e. analyzing each grain and its evolution during deformation.

5. References

[1] Gray, D. H., & Ohashi, H. 1983. Mechanics of fiber reinforcement in sand. Journal of geotechnical engineering, 109(3), 335-353.

[2] Maher, M. H., & Ho, Y. C. 1994. Mechanical properties of kaolinite/fiber soil composite. Journal of Geotechnical Engineering, 120(8), 1381-1393.
[3] Park, T., & Tan, S. A. 2005. Enhanced performance of reinforced soil walls by the inclusion of short fiber. Geotextiles and geomembranes, 23(4), 348-361.
[4] Stamati et al., (2020). spam: Software for Practical Analysis of Materials. Journal of Open Source Software, 5(51), 2286.

INFLUENCE OF RUBBER CONTENT ON THE MECHANICAL BEHAVIOUR OF ANGULAR AGGREGATES

NSSP. Kalyan[1], P. Badu[1] and RK. Kandasami[1]
[1]Department of Civil Engineering, Indian Institute of Technology, Madras, Chennai, India

1. General

The inclusion of tyre-driven rubber shreds into ballast aggregates has proven to be effective in improving the life span of ballast. The shear behaviour of the binary mixture of rubber and ballast aggregates is complex due to interactions at the micro-scale. However, there are limited studies examining the micromechanics of these binary aggregate mixtures and their impact on shear strength. In this study, numerical experiments were carried out using the coupled Discrete-Element Free Galerkin Method (DEM-EFG) to simulate the rubber-aggregate interaction. Granular mixtures featuring varying rubber contents were sheared to investigate changes in coordination number, fabric anisotropy, and particle rotation. The study aimed to understand the impact of individual rubber particle deformation on the dilative response of the mixture. The critical state behaviour of the mixtures was also explored by shearing the mixtures to large strains (25 %).

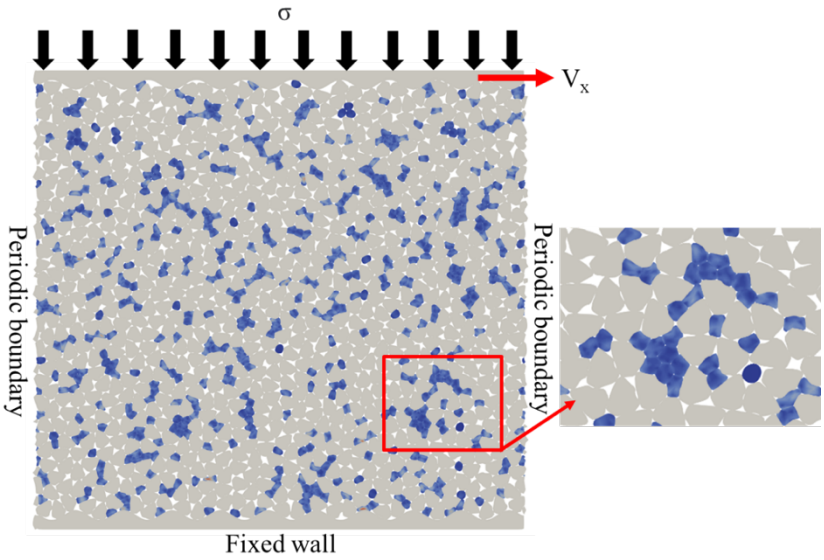

Figure 1 : Initial packing of rubber-aggregate mixture

2. Methodology

The particle-level interactions of the soft-rigid mixtures are predominantly governed by the deformability of rubber aggregates; hence, a coupled Discrete-Element Free Galerkin Method (DEM-EFG) was employed in this study. DEM considers the contact level interactions between different aggregates by utilizing traditional penalty-based stiffness-displacement laws [2]. EFG, being a meshfree method, can be used to simulate large deformations of rubber particles. The Neo-Hookean constitutive law with appropriate elastic constants was employed in the numerical simulations to replicate the deformability of rubber particles realistically. Since morphology governs the mechanical behaviour of granular media, realistic shapes of aggregate and rubber particles were captured and converted to 2D polygons to carry out plane strain-simple shear simulations. Angular morphology

was used to represent the rigid ballast aggregate, while discs were used as rubber morphology. As shown in Figure 1, the granular mixture was deposited under gravity and is sandwiched between two walls. The bottom wall was fixed, and a horizontal velocity (V_x) of 0.05 m/s was applied to the top wall in order to simulate simple shear conditions. The simulations were carried out using MELODY, a C++ based open-source code [2].

3. Preliminary results

The results obtained from numerical simulations indicate that the strength of binary granular materials decreases with an increasing rubber content. The granular assembly containing 20% rubber exhibited a less dilative response compared to the assembly with 0% rubber. This is attributed to the reduction in the rotation of the ballast aggregate (rigid) resulting from the addition of rubber. The rubber particles adopt the shape of the pores during shearing and occupy the pore space at the critical state. The cushioning effect, primarily attributed to the deformation of rubber particles, restricts the rotation of the rigid particles. Figure 2 illustrates the cushion effect on the contact force distribution in both rigid packing and the assembly with 20% rubber content. In the granular assembly consisting completely with rigid particles, strong force chains (blue in Figure 2a) were observed to be carried by few particles due to a limited number of contacts. Rattlers are notably prevalent in the rigid packing. In contrast, the force distribution in the rubber mixture assembly is less anisotropic and dispersed among contacts, owing to its high coordination number. The inclusion of deformable particles stabilizes the rattlers by increasing the contribution of weak contact force network (red in Figure 2b).

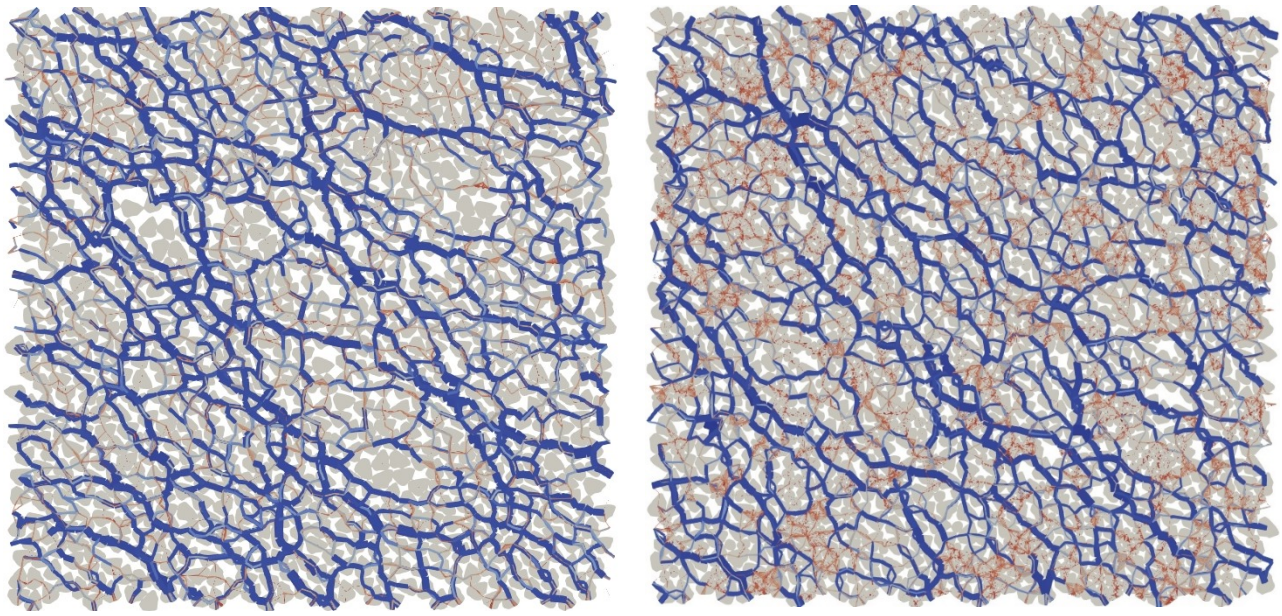

(a) Force chain network in a completely rigid particle packing

(b) Force chain network in a granular packing with 20% rubber content

Figure 2 : Contact force distribution in a granular assembly at 20% shear strain

[1] Sol-Sánchez, M., Thom, N. H., Moreno-Navarro, F., Rubio-Gámez, M. C., & Airey, G. D. (2015). A study into the use of crumb rubber in railway ballast. *Construction and Building Materials.,* 75: 19-24.

[2] Mollon, Guilhem. (2015). A unified numerical framework for rigid and compliant granular materials. *Computational Particle Mechanics.,* 5.4 : 517-527.

NANOPOROUS GELS TO PASSIVELY LIFT SUBSURFACE WATER: COLLOIDAL SILICA – PLANTS INTERACTION

Pooria Ghadir[1] and Matteo Pedrotti[1]

[1]Department of Civil and Environmental Engineering, University of Strathclyde, Glasgow G1 1XJ, United Kingdom

1. Introduction

Agriculture accounts for approximately 70% of global freshwater withdrawals [1, 2]. As the global population is projected to reach nine billion by 2050, it is estimated that agricultural production will need to expand by approximately 70% [3]. This expansion would necessitate a 15% increase in water withdrawals [2]. However, over the past few decades, there has been a consistent decline in the per capita irrigated area worldwide. This decline coupled with population growth has led to extensive extraction of groundwater. Consequently, there has been a general rise in water table depth, indicating a significant impact on our water resources [4]. These findings underscore the urgent need for sustainable water management strategies in agriculture to ensure food security for the future population [5].

Presented herein is an experimental investigation aimed at developing a bioinspired pumping system capable of passively elevating subsurface water. This system draws inspiration from the wicking mechanisms employed by plants for transpiration, utilizing emerging materials and geotechnical engineering concepts. During periods of drought or aridity, the soil undergoes desaturation, causing a reduction in its hydraulic conductivity and limiting water availability to plants [6]. In response to diminished water intake, plants close their stomata to prevent transpiration and subsequent dehydration, leading to the cessation of photosynthesis and wilting [6, 7]. To delay soil desaturation, maintain high hydraulic transmissivity, and extract water for a longer duration, some plant species are known to secrete a gelatinous substance, mucilage, around the tips of their roots [7]. This naturally engineered "grout" fills the pore spaces, reducing pore diameter and elevating the soil air-entry value by creating narrower capillaries [7].Hydrogels generally come as a suspension of nanoparticles dispersed in water that can be forced to create crosslinked polymer chains (gelation) upon physical/chemical modification of the dispersion medium. Colloidal silica hydrogels (CS) is used to create a nanoporous network within the soil designed to maintain a high degree of saturation when the water tension is high and, hence, to enable significant capillary flow. CS is a colloidal suspension of silica nanoparticles (ca 10 nm) that when irreversibly destabilised by a change in salinity or a decrease in water pH (to 5 or 6) creates a nanoporous gel. CS is non-toxic and inert, has an initial viscosity similar to water and has a highly controllable gel time [11].

The research will show how a capillary network was form through injection of CS hydrogels into vegetated soil. The interaction between the hydrogel network and the root system allows plants to withstand high negative water pressure and maintaining a water flow toward the leaves upon drying conditions.

2. Experimental methods

Colloidal silica (CS) hydrogel was used to grout a series of Runner Bean plants and study their interaction and capacity to sustain drying and wetting cycles. CS is a low-cost and environmentally friendly suspension of inorganic silica nanoparticles in water with water-like initial viscosity, nano-scale particle size, and precisely adjustable gelation period [8]. MasterRoc MP320 CS with a pH of 9.6, a density of 1.3 g/ml, a particle size of 15 nm. In this study, a 30 wt.%

concentration of CS solution was prepared. Then, a diluted acid (HCL-1M) was used to adjust the pH of the CS solution to 6 to cause gelation. Three different experimental setups were created:

- Series A. Runner Bean seeds were germinated into a gelled CS solution into petri dishes. Optical microscopy was used to investigate roots development into the CS grout and CS roots interactions upon drying-wetting paths.
- Series B: Full grown Runner Bean plants (21-day old and about 60 cm height) potted in a coarse sand-compost mixture (4/1 w/w) were grouted with CS solution. After CS gelling, plants were watered for an additional 24 days only from the bottom to force plants to withdraw water only through the CS grout. Analysis of the effect of the CS-plant interaction were made via post mortem inspection of the root system, grout network and plant health.
- Series C: Runner Bean plants were grown in soil columns (mixture of coarse and fine sand) and then grouted with CS. Each column was instrumented with Time-Domain Reflectometry sensors and High Capacity Tensiometers to measure respectively volumetric water content and pore-water tension. Different high pore-water tensions were generated by using an osmotic technique. The bottom of the column was hydraulically connected to a water reservoir containing a solution of Polyethylene Glycol – PEG). A Polythersulfon (PES) semi-permeable membrane was interposed between the reservoir and the base of the column. Upward water flow was generated by the plant and controlled by forced ventilation at the top of the leaves. For each setup water flux was controlled by measuring the change in weight of the PEG reservoir and the soil column. Post-mortem X-ray Computed Tomography will be carried out on selected columns.

Each experiment was run in triplicate and compared to control samples where no CS was added

3. Results

The experimental campaign carried out showed that the presence of CS does not hindere the growth of runner bean plants if the grout is gelled via acidification and thus salt concentration is kept at the minimum. At the microscale, roots grown do not cause any cracking into the gel, but thanks to the CS elevated deformability and self-healing ability both the pressure generated at the root tip by the advancing of the root and the pressure generated by the annular growth can be accommodated. Water flow through the CS and its low hydraulic conductivity does not represent a limiting factor for the plant growth as long as CS stays water saturated. Main drying of the grout causes an irreversible shrinking of the colloidal silica. Evidence showed that detachment occurs at the root-CS interface rather than at the interface of CS-sand grains. Further investigations are envisaged to better understand the plant coping mechanisms once that root-CS detachment occurs and the root ability to close the gap.

4. References

1. *Abobatta, W., Adv. Agric. Environ. Sci. Open Access, 2018.* ***2.*** *Egbo, O.P., et al., Environment, Development and Sustainability, 2023.* ***3.****Magnoni, P.H.J et al. Sustainable Water Resources Management, 2020.* ***4****.Gupta, D. and P.P. Patel, Geostatistics and geospatial technologies for groundwater resources in India, 2021* ***5.*** *Tabatabaei, S.-H., et al., International Journal of Recycling of Organic Waste in Agriculture, 2017. 6.Abdalla, M., et al., Annals of Botany, 2022. 7.Ahmed, M.A., et al., Functional Plant Biology, 2014. 41(11): p. 1129-1137. 8.Pedrotti, M., et al., Tunnelling and Underground Space Technology, 2017. 70: p. 105-113.*

Geomechanics below the micron

3D NANOMETRIC OBSERVATIONS OF CLAY FABRIC

***A. Casarella*[1], *V. Sadasivan*[1], *O. Stamati*[2], *J. Villanova* [2], *B. Lukić*[2,3] *and J. Dijkstra*[1]**

[1] *Chalmers university of Technology, Department of Architecture and Civil Engineering, Gothenburg, Sweden*

[2] *ESRF – The European Synchrotron, Grenoble 38043, France*

[3] *Henry Royce Institute, Department of Materials, The University of Manchester, UK*

The mechanical response of geomaterials is intricately linked to the interactions between particles. Understanding particle-scale interactions is crucial for advancing fundamental knowledge in soil mechanics and developing physics-based models corroborating existing continuum-based approaches. Exploring the microstructural origins of emerging responses at the continuum scale in soils often centers around coarse grained soils. Laboratoy X-ray micro-computed tomography [1] and particle-scale models [2] are nowadays widely used in research on the behaviour of sand.

In contrast, research in micromechanics of clayey soils has been slow to progress due to the challenges associated with studying the evolution of fabric at the submicron scale using conventional techniques such as Scanning Electron Microscopy (SEM) and Mercury Intrusion Porosimetry (MIP). While these methods provide valuable insights into the microstructure of clay, they are limited by the necessary sample preparation processes, such as pore fluid replacement and surface treatment, that alter the natural configuration of the fabric.

These limitations can be effectively overcome with non-invasive X-ray techniques, facilitated by recent advancements in 4th generation synchrotron sources that enable achieving the essential submicron spatial resolution for studying fine-grained soils. This study employs an unparalleled combination of high-resolution nano X-ray Computed Tomography (XCTs) and Small-angle X-ray Scattering (SAXS) to experimentally quantify the three-dimensional (3D) fabric of saturated kaolin clay samples that are consolidated in 1D compression.

Using the synchrotron-based imaging instrument available at the beamline ID16B of ESRF [3], it was possible to fully resolve the 3D network between kaolin particles, capturing, for the very first time, 3D images of individual clay platelets in their natural (undisturbed) state. The instrument requires miniature samples; thus, 1D-consolidated Speswhite Kaolin clay samples saturated with different pore fluids to induce diverse material fabric are carefully cored and placed into glass capillaries with a diameter of 300 µm and a wall thickness of 10 µm. The samples are then securely sealed at both ends using grease paste to maintain constant water content during the scan [4].

Local particle orientations can be computed from the direction of maximum grey level variation (i.e., highest eigenvalue) in each voxel of the 3D reconstructed volumes using the open source package *OrientationPy*. Figure 1 shows the 3D orientation map (on the left) obtained for a cropped reconstructed volume measuring 40×40x40 μm^3 (cross-section on the right), imaging a Speswhite kaolin clay sample saturated with acidic water (pH=4.1) and consolidated up to 70 kPa. The more similar the color shades in the orientation plot, the more similar the particles orientation in space.

Within the examined samples, a disordered fabric is observed, with the predominant orientation represented by a blue shade, corresponding to the direction perpendicular to the coring axis (inclined at an angle of 30 degrees relative to the vertical direction in which the sample is consolidated). Notably, diverse clusters of contrasting colours are evident. As illustrated in the diagram located in the upper right corner, this observation indicates the tendency of clay particles to adopt face-to-face configurations, forming clusters or aggregates that, in turn, exhibit a tendency to organise in an edge-to-face configuration. This observed behaviour aligns with established principles in colloid science. Specifically, the acidic pore fluid induces a positive charge at the edges of the clay platelets, as depicted in the upper left corner sketch, promoting attraction in an edge-to-face manner.

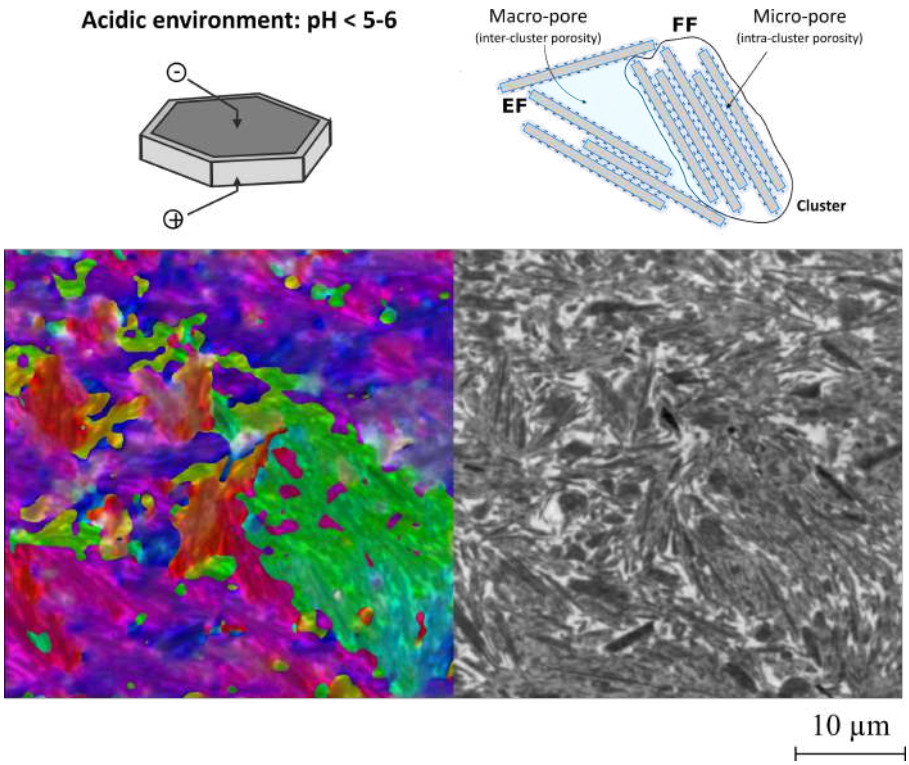

Figure 1. Measurement of the grey scale 3D orientations per pixel in a cropped volume measuring 40×40x40 µm^3 and cross-section of a reconstructed nano-CT image of a Speswhite kaolin clay sample saturated with acidic water (pH=4.1) and consolidated up to 70 kPa.

The local orientation maps are complemented and substantiated through Small-Angle X-ray Scattering (SAXS) measurements conducted on the samples subjected to tomographic analysis. Indeed, SAXS provides insight into the distribution of orientation of all the scatterers -clay particles in this case- through the path of X-rays. The Chalmers Material Analysis Laboratory X-ray scattering instrument, Mat:Nordic SAXS/WAXS, is used for the X-ray scattering measurements.

In conclusion, non-invasive X-ray based techniques that resolve submicron features pave the way for particle scale analysis and (in)operando investigation of micro-scale processes in fine-grained geomaterials. Whilst, the presented nanometric techniques are highly promising, additional experimental techniques that capture the particle-to-particle interactions remain to be developed in order to arrive at fully resolved micromechanics of clay assemblies.

References

[1] Andò, E., Hall, S., Viggiani, G., Desrues, J., and Bésuelle, P. (2012). Grain-scale experimental investigation of localised deformation in sand: A discrete particle tracking approach. Acta Geotechnica, **7**.

[2] O'Sullivan, C. (2011). Particle-based discrete element modeling: Geomechanics perspective. International Journal of Geomechanics, **11**, 449–464.

[3] Martínez-Criado, G., et al. (2016). ID16B: a hard X-ray nanoprobe beamline at the ESRF for nano-analysis. Journal of Synchrotron Radiation, **23**, 344–352.

[4] Birmpilis, G., Mohammadi, A. S., Villanova, J., Boller, E., Ando, E., and Dijkstra, J. (2022). Fabric investigation of natural sensitive clay from 3d nano- and microtomography data. Journal of Engineering Mechanics, **148**, 04021151.

GENESIS OF QUICK CLAY: A NANOMETRIC EXPERIMENTAL INVESTIGATION ON GEOLOGICAL ENVIRONMENT

***D. Saaedifar*[1], *A. Casarella*[1], *O. Stamati*[2], *J. Villanova* [2] *and J. Dijkstra*[1]**
[1] *Chalmers university of Technology, Department of Architecture and Civil Engineering, Gothenburg, Sweden*
[2] *ESRF – The European Synchrotron, Grenoble 38043, France*

Clays vary widely from soft sediments with water-filled pores to shale formations containing hydrocarbons. Among these, quick clays stand out as particularly elusive and hazardous due to their potential for abrupt loss of stability, triggering unpredictable landslides (e.g. Surte 1952; Tuve 1977; Stenungsund 2023). A quick clay is a meta-stable sensitive clay, often deposited in a marine environment, that shows an irreversible transition from solid to liquid under a hydro-mechanical perturbation. The sensitivity, denoted by the ratio S_t, which compares the undrained shear strength of a natural clay in its original, intact condition to its liquid (remoulded) state, exceeds 50 for quick clays.

The emergence of high sensitivity in a natural clay deposit is linked to geological processes controlling the formation of quick clays which are largely unknown. The deposition history directly impacts the composition and microstructure of natural (quick or sensitive) clays. Thus, the mechanical response observed at the macro-scale (metres), is linked to the processes at the nano- and micro-scale. This research takes an integrated approach to unravel the hydro-mechanical behaviour of quick clays by emphasising the crucial link between macro-scale observations and the underlying nano- and micro-scale processes that drive their unique characteristics.

Traditional limitations in experimentally observing the microstructure evolution of sensitive clays have obscured our understanding of the mechanisms that underpin the sudden transition from solid to liquid. To address this gap, this research advocates for the use of non-invasive process-monitoring techniques, particularly synchrotron-based nano X-ray Computed Tomography (XCT).

This paper examines the morphology at the nano-scale of five distinct types of natural, undisturbed sensitive clays sourced from different geological environments (marine or non-marine deposits) across five locations in the world. The primary goal is to identify the influence of geological environment and formation history on the development of sensitivity to mechanical loading. Investigations of intact natural quick clays are complemented with microstructure observations of saturated reconstituted quick clays. The objective is to establish a connection between the difference in macroscopic mechanical behaviour observed in intact and reconstituted clay [1] and the distinct nano-scale fabric characteristics, such as orientation of clay particles, void space, and/or contacts [2].

The nano-scale imaging instrument at the ID16B beamline of ESRF [3] is employed to capture nano-level features in the natural clay specimens using holotomography [4]. Phase contrast imaging is acquired using a conic and monochromatic beam with an energy of 29.6 keV and a flux of 10^{12} ph/s. Four tomographies are acquired for four different distances between the detector and the sample along the beam propagation way. For each scan, a total of 3,021 projections are recorded covering a complete 360° rotation with an exposure time of 15 ms per step. A reconstructed volume measuring 128×108x108 μm^3 with an isotropic pixel size of 50 nm is obtained using the PyNX software. The instrument requires miniature samples; thus, the natural clay are carefully placed into glass capillaries with a diameter of 300 µm and a wall thickness of 10 µm, which are then securely sealed at both ends using grease paste [5], to preserve water content.

Figure 1 shows a comparison between two representative slices from the reconstructed nanotomography scans on an intact and reconstituted natural sensitive clay sampled from a 7-m depth at the Kärra test site in Gothenburg, Sweden. The slices correspond to the horizontal cross section with the out-of-plane direction of the vertical axis in which the samples are originally deposited and

consolidated. From a visual inspection of both the intact (Figure 1a) and the reconstituted (Figure 1b) samples, Kärra clay presents large angular particles (silt grains) embedded in a clay matrix. The uneven appearance of the clay matrix suggests the presence of a discernible underlying particle network, hovering at the threshold of detection. Within this network, the largest assemblies of clay particles, likely composed of kaolinite minerals, manifest as brighter (higher intensity) fibres. The pore space, visible by the black spots with low intensity, is most probably linked to the macropore structure of natural sensitive clays (e.g., [6]). It is interesting to notice that the most evident difference between the two samples lies in the amount of macroporosity, which reduces by about 32% after remoulding and re-compaction of the material (from Figure 1a to Figure 1b). The remoulding process at natural water content irreversibly modifies the clay microstructure. This microscopic change can be ascribed as one of the possible contributing cause for the observed different macroscopic mechanical response between intact and reconstituted clay samples [1].

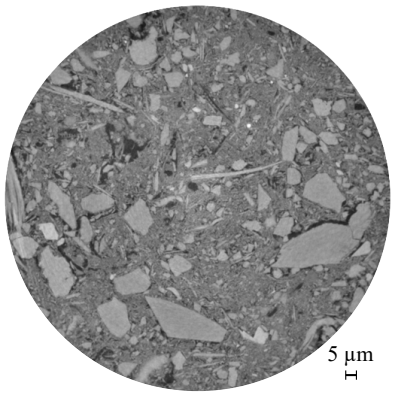

(a) (b)

Figure 1. Reconstructed horizontal cross sections from nanotomography scans on (a) an intact and (b) a reconstituted sample of Kärra clay with original size and image contrast.

The unique data from the nanotomography offers a unique insight into the characteristics that make natural clays ‘quick’, and they contribute significantly to the understanding and modelling of the macroscopic hydromechanical response of sensitive clays.

References

[1] Burland, J. B. (1990). On the compressibility and shear strength of natural clays. Géotechnique, **40**, 329–378.

[2] Ken-Ichi, K. (1984). Distribution of directional data and fabric tensors. International Journal of Engineering Science, **22**, 149–164.

[3] Martínez-Criado, G., et al. (2016). ID16B: a hard X-ray nanoprobe beamline at the ESRF for nano-analysis. Journal of Synchrotron Radiation, **23**, 344–352.

[4] Cloetens, P., Ludwig, W., Baruchel, J., Van Dyck, D., Van Landuyt, J., Guigay, J. P., and Schlenker, M. (1999). Holotomography: Quantitative phase tomography with micrometer resolution using hard synchrotron radiation x rays. Applied Physics Letters, **75**, 2912–2914.

[5] Birmpilis, G., Mohammadi, A. S., Villanova, J., Boller, E., Ando, E., and Dijkstra, J. (2022). Fabric investigation of natural sensitive clay from 3d nano- and microtomography data. Journal of Engineering Mechanics, **148**, 04021151.

[6] DELAGE, P. (2010). A microstructure approach to the sensitivity and compressibility of some eastern canada sensitive clays. Géotechnique, **60**, 353–368.

Ion transport in nanopore with overlapping electrical double layers and surface charge dependent slip boundaries

***Qingrong Xiong*[1]**
[1] *Shandong University, Jinan, China*

Abstract

Modeling of electro-chemo-mechanical transport phenomena in nanoporous media with overlapped electric double layers remains challenging. This bottleneck originates from lack of a comprehensive model to predict the local surface charge density based on the variable local solution properties or using constant physical parameters in calculations. In this work, we report the combined effect of concentration-dependent surface charge and surface charge-dependent boundary slip on the flow and ionic migration in nanoporess with overlapping EDL, unlike previous studies that focused on these physical effects, separately. The results show that the solution concentration-dependent surface charge and boundary slip apparently affect the electric conductivity and velocity distribution in the nanochannel, subsequently affect the fluid behavior and ions transport. The model performance is demonstrated using experimental data on the diffusion of species through Opalinus clay (OPA) - a complex process that involves diffusion and anionic exclusion. The accuracy of the model is validated by the simulating the reactions dependency of different species transport through OPA. The model improves the understanding of the microstructure influence on the macroscopic transport properties of porous materials. The developed model can be applied to a variety of scientific and engineering problems, such as hydraulic cracking of gas-bearing shale, radioactive nuclear waste geo-disposal, contaminated soil remediation and geological carbon storage.

THE INTERPLAY OF CLAY BEHAVIOR AND PARTICLE STRUCTURING: A MULTI-SCALE INVESTIGATION

M. Ma[1], F. Bennai[1], M. Hattab[1], P. -Y. Hicher[2], F. Nicot[3]

[1]Université de Lorraine, CNRS, Arts et Métiers ParisTech, LEM3, 57000 Metz, France
[2]Ecole Centrale de Nantes, CNRS, Research Institute of Civil Engineering and Mechanics (GeM),44300 Nantes, France
[3]Université Savoie Mont-Blanc, ISTerre, 73376 Le Bourget-du-Lac, France

Abstract

Understanding the micromechanical behavior of clay is important to better elucidate microscopic phenomena and their link with the overall mechanical behavior in order to construct relevant multiscale models for clayey materials. This study presents an experimental investigation into the clay behavior related to particle structuration.

Clay behavior is strongly associated with the particle structure, which is influenced by their surface charges. Electrostatic interactions between the charges result in different particle assembly [1]. Kaolinite particles, which have a flat plate shape, are negatively charged on the surface and positively charged at the edges. The edge charges are strongly influenced by the surrounding fluid, the positive charges could be compensated and turned to negative in high pH environment, while the surface charges remain negative in either acidic or alkaline environments [2]. The effect of these charges leads to different configurations of particle assembly that can be observed during the sedimentation processes: flocculation and dispersion [3].

In a neutral to acidic environment, the positive charges at the particle edges are attracted by the negative charges on the surface, forming an edge-to-face structure. Thus, clay particles aggregate as flocs and then sediment. Accumulation of the aggregated particles form a structure resembling a card-house- or, instead, a honeycomb-like clay fabric [4] [5]. Otherwise, the positive edge charges are neutralized and then converted to negative in an alkaline environment due to the deprotonation of the hydroxyl anions present at the particle edges. Therefore, repulsive forces dominate the interaction between clay particles, hence, the particles organize in a parallel way and form a face-to-face structure [6].

In order to create different particle structures, sedimentation tests were carried out using two appropriate solutions, prepared by adding different salts that create either an acidic or an alkaline fluid environment. In an acidic environment, where flocculation takes place, the edge-to-face structured particles sediment as flocs, whereas in an alkaline environment, where dispersion takes place, the face-to-face arranged particles sediment individually. As the dispersed particles sediment very slowly, the sedimentation tests were maintained for one week until the sediment height remained constant. The sedimented clay slurries were then collected and submitted to oedometer tests at the following levels of effective vertical stress: 120, 600, and 1000 kPa. The results showed that the compressibility of the flocculated specimens was higher than that of the dispersed specimens. [7]

Microscale analysis and observation were conducted using mercury intrusion porosimetry (MIP) technique and scanning electron microscopy (SEM). The samples collected after the oedometer tests were dehydrated using the lyophilization technique to avoid disturbing the particle structures. The samples were divided into smaller pieces and frozen in liquid nitrogen. The lyophilization process then allowed the frozen pore fluid to sublime without passing through the liquid phase. MIP analysis was used to determine the volume of voids and the pore size distribution (PSD) of the samples. The PSD results showed that the flocculated samples have larger dominant pores compared to dispersed

samples. However, they have fewer pores, as indicated by the lower void ratios obtained by either MIP or mechanical tests. The vertical planes of the specimens were observed by SEM. Specimens were gold coated to make them conductive, then microscopic observations were performed. The observations coupled with 2D image processing allowed to identify the micro properties of the clay fabric, such as the particle orientation and pore network. The SEM pictures showed a clear preferred alignment in all samples after mechanical tests along a direction perpendicular to the principal stress orientation. Some edge-to-face structures remained in the flocculated specimens, while the clay fabric exhibited a predominantly horizontal orientation. Finally, this coupling of MIP and SEM results provided a comprehensive understanding of the clay structural characteristics, opening the door toward further micromechanically-based modeling.

References

[1] Van Olphen, H. (1977). *An Introduction to Clay Colloid Chemistry: For Clay Technologists, Geologists, and Soil Scientists.* 2e edition. New York (N.Y.): Wiley, Print.

[2] Mitchell, J. K. & Soga, K. (2005). *Fundamentals of soil behavior (Vol. 3, p. USA).* New York: John Wiley & Sons.

[3] Imai, G. (1980). Settling behavior of clay suspension. *Soils and Foundations*, 20(2), 61-77.

[4] Pierre, A. C., Ma, K. & Barker, C. (1995*).* Structure of kaolinite flocs formed in an aqueous medium. *Journal of Materials Science*, 30, 2176-2181.

[5] Shakeel, A., Safar, Z., Ibanez, M., van Paassen, L. & Chassagne, C. (2020). Flocculation of clay suspensions by anionic and cationic polyelectrolytes: A systematic analysis. *Minerals*, 10(11), 999.

[6] Pedrotti, M. & Tarantino, A. (2018). An experimental investigation into the micromechanics of non-active clays. *Géotechnique*, 68(8), 666-683.

[7] Soga, K. (1994). *Mechanical behavior and constitutive modelling of natural structured soils.* University of California, Berkeley.

Triaxial compression simulations of kaolinite using coarse-grained molecular dynamics

Y. Nakamichi[1], C. O'Sullivan[1] S. Angioletti-Uberti[2] and P. Tangney[2]

[1] Imperial College London, Department of Civil and Environmental Engineering, London, United Kingdom

[2] Imperial College London, Department of Materials, London, United Kingdom

1. Background

Coarse-grained molecular dynamics (CGMD) is one approach that can be used in the particle-scale simulation of clay. Ebrahimi et al. [1] demonstrated that CGMD (modelling clay particles using flat and rigid ellipsoids) can efficiently capture the behaviour of montmorillonite particles. Bandera et al. [2] further demonstrated the efficiency of this approach by applying Ebrahimi's CGMD framework to kaolinite particles. In the CGMD framework they used, the interaction force/energy between two clay particle models (ellipsoids) are described by the Gay-Berne (GB) potential function. The GB potential is an extended version of the Leonard-Jones potential. Specially, the GB potential can consider particle shape and energy anisotropies and considers ellipsoidal particles. The GB potential cannot be directly used to model interactions which alternate between attraction and repulsion depending on particle orientation, as is the case in kaolinite for some pore water pH values (e.g. Bandera et al. [2]). To overcome this restriction Nakamichi et al. (2023) [3] developed a new potential function by modifying the GB potential. They conducted CGMD isotropic compression simulations to link the overall compression behaviour to the particle interactions. Subsequently we added inter-particle friction (Coulomb) into the potential function as Bandera et al. [4] showed that in the absence of inter-particle friction unrealistic K_0 values are obtained.

The shear behaviour of clay is as important as compression behaviour. It has been experimentally shown that clay reaches the critical state with continued shearing. Based on the concept of the critical state, examining the relationship between macroscopic shear behaviour and particle-scale behaviour may contribute to deepening our understanding of the mechanisms underlying the shear strength of clay. However, there have been few studies looking at shear deformation using coarse-grained molecular dynamics. This paucity of research can be attributed to the need to get representative element volumes and the high computational cost of the simulations.

2. Outline of the current research

Using LAMMPS [5], we conducted consolidated drained triaxial compression simulations of kaolinite to investigate the relationship between macroscopic shear behaviour and particle-scale behaviour, and to explore the applicability CGMD to particle-scale shear simulations. For the triaxial compression simulations, we used two virtual samples, each with 10,648 particles, assuming acidic (pH=4) and alkaline (pH=8) pore water conditions. In line with prior experimental observations, the pH=4 sample was a looser sample and had a flocculated microfabric where face-to-edge particle contacts were developed, while pH=8 sample was denser and had a dispersed microstructure where face-to-face particle configurations were dominant. Initially, to apply the prescribed confining pressure of 300 kPa to the samples, isotropic compression was simulated. Subsequently triaxial compression simulations were performed by imposing vertical strains at a constant rate while keeping the lateral pressure constant. Periodic boundary conditions were used in

both simulations. Figure 1(a) shows the relationship between deviatoric stress and axial strain. In both samples, the deviatoric stress converges to a steady state as the axial strain increases. As an overall trend, the pH=8 sample (denser) exhibits higher deviatoric stress than the pH=4 sample (looser). Figure 1(b) illustrates the volumetric strain variations against the axial strain. The pH=4 sample shows contractive behaviour while the pH=8 sample shows dilative behaviour, as expected. The noteworthy feature is that the pH=4 sample does not reach a steady state and continues to undergo volumetric changes even though the axial strain becomes large levels (maximum axial strain is 70%). This macroscopic behaviour is related to particle rearrangement/rotation.

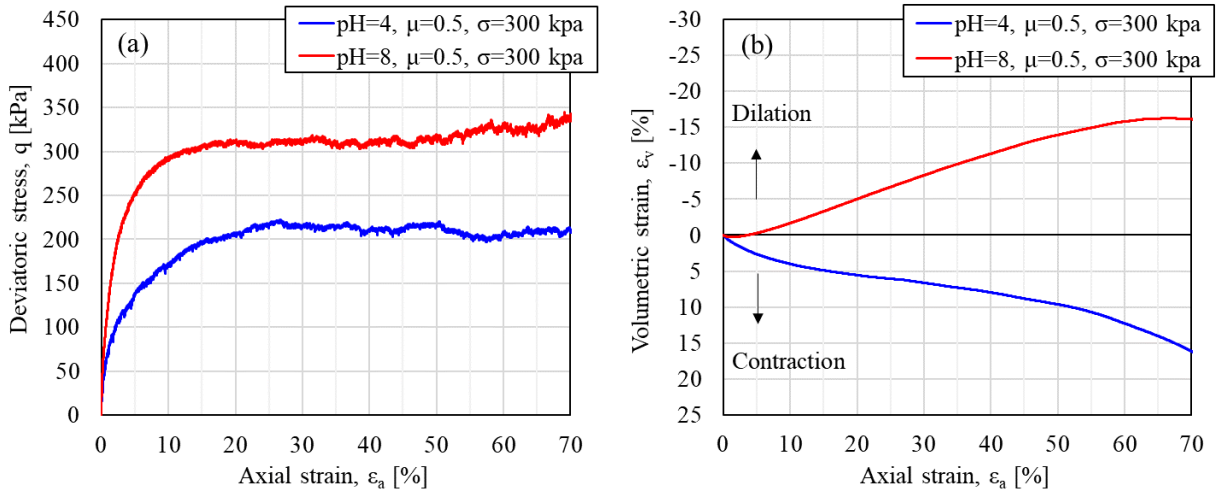

Figure 1. Results of the triaxial compression simulation (a) deviatoric stress - axial strain relationship and (b) volumetric strain - axial strain relationship

3. References

[1] Ebrahimi, D., Whittle, A. J., & Pellenq, R. J.-M. (2014). Mesoscale properties of clay aggregates from potential of mean force representation of interactions between nanoplatelets. *The Journal of Chemical Physics*, *140*(15), 154309. https://doi.org/10.1063/1.4870932

[2] Bandera, S., O'Sullivan, C., Tangney, P., & Angioletti-Uberti, S. (2021). Coarse-grained molecular dynamics simulations of clay compression. *Computers and Geotechnics*, *138*. https://doi.org/10.1016/j.compgeo.2021.104333

[3] Nakamichi, Y., O'Sullivan, C., Angioletti-Uberti, S., Tangney, P., & Bandera, S. (2023). Isotropic compression simulation of kaolinite using coarse-grained molecular dynamics. *The 8th International Symposium on Deformation Characteristics of Geomaterials*.

[4] Bandera, S. 2021. "Fundamental analysis of the influence of structure on clay behaviour", PhD thesis, Imperial College of Science, Technology and Medicine.

[5] Plimpton, S.J. 1995. "Short-Range Molecular Dynamics". J Comput Phys, 117(1), pp. 1–19. https://doi.org/10.1006/jcph.1995.1039

Stabilization and reinforcement of geomaterials

A small-strain stiffness model for bio-cemented sands

A. Zhang [1,2]***, A. C. Dieudonné*** [1]

[1] *Departement of Geoscience and Engineering, Delft University of Technology, The Netherlands*

[2] *Urban and Environmental Engineering Research Unit, Université de Liège, Belgium*

Bio-cementation soil improvement methods have gained considerable attention as alternatives to invasive, carbon-intensive stabilisation techniques. One of these methods is microbially induced carbonate precipitation (MICP), which utilises calcium carbonate minerals caused by bacterial activity to cement soil particles. MICP has demonstrated the ability to improve soil stiffness, strength and dilatancy and can be used for applications such as ground improvement and mitigation of liquefaction upon earthquake.

The small-strain stiffness plays an important role in geotechnical engineering problems, such as analysis of earthquake response and prediction of ground deformation. To advance the applications of MICP on such engineering problems, it is essential to evaluate the small-strain stiffness of MICP-treated soils, and to build a model to describe the small-strain stiffness of MICP-treated soils. The small-strain stiffness of bare soil has been comprehensively studied, with a focus on, for instance, particle size distribution [1], fine content [2, 3, 4], stress condition [5], particle shape [6] and particle surface roughness [7]. However, fewer studies have been conducted on the small-strain stiffness of (bio-)cemented soils. The small-strain stiffness of bio-cemented soil is still to be investigated, and a model is to be established.

The small-strain stiffness of bio-cemented sand depends not only on the properties of the host sand (e.g. particle size distribution, relative density) but also on the precipitated cementation (e.g. cementation content, distribution pattern [8, 9]). To evaluate the small-strain stiffness of bio-cemented sand, the discrete element method (DEM) is utilised in this study for its capacity to incorporate grain-scale features of bio-cemented sand. 3D DEM samples of bare sands with different particle size distributions and densities are first prepared. Then, cementation particles are explicitly introduced into these sand samples in different concentrations and distribution patterns to model various bio-cemented sands. The DEM samples are subjected to a static probing test to assess the small-strain stiffness. The DEM results indicate that cementation particles in different distribution patterns have different impacts on the small-strain stiffness of sand. Moreover, sands with various properties respond differently given the same amount and characteristics of the cementation. Based on the DEM results, a small-strain stiffness model for bio-cemented sands is proposed. The proposed model captures the effect of cementation on the change in small-strain stiffness of sands. In particular, the different effects on the small-strain stiffness from the cementation with various distribution patterns can also be described by the proposed model.

References

[1] Gu, X., Lu, L., and Qian, J. (2017). Discrete element modeling of the effect of particle size distribution on the small strain stiffness of granular soils. *Particuology*, **32**, 21–29.

[2] Goudarzy, M., König, D., and Schanz, T. (2016). Small strain stiffness of granular materials containing fines. *Soils Found.*, **56**, 756–764.

[3] Gong, J., Wang, X., Li, L., and Nie, Z. (2019). DEM study of the effect of fines content on the small-strain stiffness of gap-graded soils. *Comput. Geotech.*, **112**, 35–40.

[4] Shi, X., Nie, J., Zhao, J., and Gao, Y. (2020). A homogenization equation for the small strain stiffness of gap-graded granular materials. *Comput. Geotech.*, **121**, 103440.

[5] Nguyen, H., O'sullivan, C., and Otsubo, M. (2018). Discrete element method analysis of small-strain stiffness under anisotropic stress states. *Geotech. Lett.*, **8**, 183–189.

[6] Nie, J.-Y., Shi, X.-S., Cui, Y.-F., and Yang, Z.-Y. (2022). Numerical evaluation of particle shape effect on small strain properties of granular soils. *Eng. Geol.*, **303**, 106652.

[7] Otsubo, M., O'Sullivan, C., Hanley, K. J., and Sim, W. W. (2017). The influence of particle surface roughness on elastic stiffness and dynamic response. *Géotechnique*, **67**, 452–459.

[8] Zhang, A. and Dieudonné, A.-C. (2023). Effects of carbonate distribution pattern on the mechanical behaviour of bio-cemented sands: A DEM study. *Comput. Geotech.*, **154**, 105152.

[9] Zhang, A. and Dieudonné, A.-C. (2023). Effects of carbonate distribution inhomogeneity on the improvement level of bio-cemented sands: A DEM study. *IACMAG*, pp. 554–561, Springer.

ALKALINE ACTIVATION OF MUSSEL SHELLS AS AN INNOVATIVE BINDER FOR SOIL TREATMENT

P.G. Pesce[1], R. Petti[1], G. Russo[2] C. Vitone[1] and E. Vitale[2]
[1] Politecnico di Bari, DICATECh, Bari, Italy.
[2] Università degli studi di Napoli Federico II, DISTAR, Napoli, Italy.

1. Introduction

This study focuses on the use of alkali-activated binders (AABs) to improve engineering characteristics of clay-rich soils, offering an alternative to the commonly employed methods involving traditional binders like lime and Ordinary Portland Cement (OPC). The use of AABs has received increasing attention over the last decade; in fact, AABs not only mitigate CO_2 emission compared to traditional cement [1] but also allow the reuse of waste products of different origins (i.e., natural and artificial pozzolana, metallurgical waste or $CaCO_3$-rich waste limestone). When appropriately activated, these by-products can be used as cementing agents for the mechanical improvement of natural soils that would otherwise be unsuitable for construction purposes. Alkali activated binders are commonly synthesized by reacting aluminosilicate-rich precursors such as calcined clay, natural pozzolans, fly ash or blast furnace slag with an alkaline solution made of sodium hydroxide (NaOH) and/or sodium silicate (Na_2SiO_3).

Despite the growing interest in AABs, limited research has focused on the AA of $CaCO_3$-rich natural materials and waste limestone as precursors in the synthesis. Some of these studies have involved precursors containing silicate compounds [3] or alkaline solution containing silicates [2]. The presence of limestone in these binders modifies the molecular structure of the reaction products and increases their underwater stability [2]. In this context, [2] studied the activation of limestone using a commercial blend of sodium silicate and sodium hydroxide highlighting the feasibility of limestone as a precursor for producing AAB with compressive strengths ranging from 15 to 25 MPa after 360 days of curing [2]. Alkaline activation of limestone results in the formation of crystalline carbonate phases such as pirssonite, gaylussite, portlandite or thermonatrite, which are intermixed with amorphous calcium silicate hydrates (CSH), silica gel, calcium-silicate gels incorporating sodium (NCSH) and/or sodium silicate gels (NSH) [4].

2. Methodology

In this study, a multiscale experimental investigation of the chemo-mineralogical evolution and mechanical behavior of an AAB based on the activation of mussel shell powder (MSP) has been developed. Mussel shells are a widespread waste from the aquaculture industry. Their global production for human consumption is about 14% of the total marine production [5]. Rich in calcium carbonate (95%), shells are a non-biodegradable type of residue, which is difficult to compost and requires long and expensive disposal. This research is moving towards a virtuous reuse of such residues, following the encouraging results obtained by the authors when MSP was used as a partial replacement for cement in the mechanical treatment of dredged sediments [6]. Figure 1 shows the methodology followed for the two different alkaline solutions considered for the treatment of MSP (i.e., NaOH 12 M solution, Mix1, and a mixture of NaOH 12 M and sodium silicate (Na_2SiO_3) solutions, Mix2).

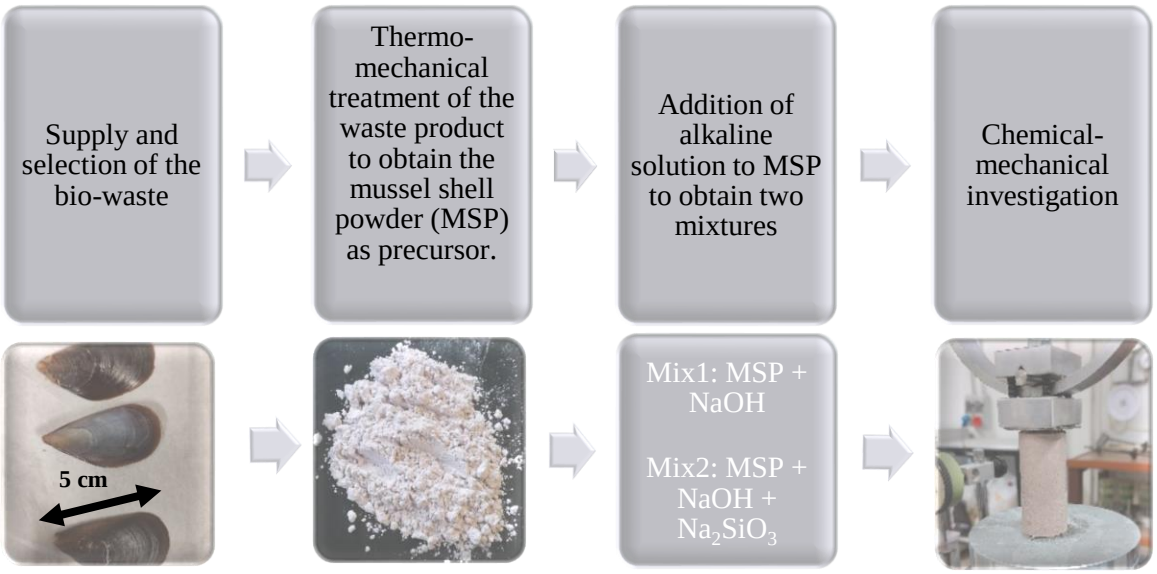

Figure 1. Sketch of the research steps.

3. Results

The reactivity of MSP was monitored over time using X-ray Diffraction (XRD) and Scanning Electron Microscopy (SEM) for both the mixtures. The mechanical behavior was instead investigated by Unconfined Compression Tests (UCT). The mineralogical analyses revealed a high reactivity of the alkali-activated MSPs as a calcium source, promoting the precipitation of new crystalline carbonate hydrated phases. SEM observations showed a progressive transformation of MSP, evidenced by a coating of gel-like phases on the particle surface and crystallization of carbonate phases. The UCS of the alkali activated MSP increases with curing time, i.e., in line with the chemo-mineralogical evolution of the binders. For a given curing time, the addition of sodium silicate solution resulted in a higher increase in the compressive strength of MSP compared to that of sodium hydroxide solution alone.

4. References

[1] Coudert E., Russo G., Deneele D., Tarantino A. (2022). Mechanical behaviour of compacted kaolin clay stabilised via alkali activated calcium-rich fly ash binder. *Geomechanics for Energy and the Environment*, **32**: article 100404.

[2] Ortega-Zavala D.E., Santana-Carrillo J.L., Burciaga-Díaz O., Escalante-García J.I. (2019). An initial study on alkali activated limestone binders, *Cement and Concrete Res.*, **120**: pp. 267–278.

[3] Menchaca-Ballinas L.E., Escalente-García J.I. (2020). Limestone as aggregate and precursor in binders of waste glass activated by CaO and NaOH. *Constr. and Build. Mat.*, **262**: article 120013.

[4] Cousture A., Renault N., Gallias J. L., Ndiaye K. (2021). Study of a binder based on alkaline activated limestone. *Construction and Building Materials*, **311**: article 125323.

[5] Wijsman J.W.M., Troost K., Fang J., Roncarati A. (2019). Global Production of Marine Bivalves. Trends and Challenges. *Goods and Services of Marine Bivalves, Springer*, chapter **2**.

[6] Petti R., Vitone C., Puzrin A., Plotze M. (2023). On the use of mussel shells as green solution to mechanically stabilise dredged sediments. *Proceedings of the 8th IS-Porto 2023*. Porto, 3rd - 6th September.

CYCLIC RESISTANCE OF LIQUEFIABLE SAND IMPROVED BY BIOPOLYMER SOIL TREATMENT

Dong-Yeup Park[1], Jeong-Uk Bang[1] Sanghoon Im[1] Ilhan Chang and Gye-Chun Cho[1]
[1] KAIST, Civil and Environmental Engineering, Daejeon, Republic of Korea
[2] Ajou University, Department of Civil Systems Engineering, Suwon, Republic of Korea

Abstract

Various methodologies have been suggested in geotechnical engineering to tackle the problem of seismic liquefaction and mitigate the magnitude of destruction resulting from earthquakes. Cement, a soil stabilizer, is used as an injection technique to build stable ground in many human applications. Nevertheless, during the cement injection technique's implementation, groundwater in the soil might have adverse effects on human health and does not effectively reduce seismic wave propagation. Biopolymer-based soil treatment (BPST) has recently gained significant traction as a sustainable geotechnical engineering method. This research examined how seismic resistance in loose sand that may become liquid can be enhanced by using polysaccharide biopolymer. The polysaccharide biopolymer's cyclic resistance ratio (CRR) was assessed using a cyclic direct simple shear device. The empirical results and seismic ground reaction study corroborate the efficacy of treating loose, liquefiable sandy grounds with polysaccharide biopolymers to mitigate seismic risk.

1. Introduction

The climate change phenomenon around the world is causing geotechnical disasters, which directly threaten human survival. Additionally, according to the USGS and NASA (2022), when glaciers melt due to climate change, the load on the crust decreases, and the number of earthquakes to relieve stress in the lower part increases. Liquefaction caused by a seismic event can cause damage such as ground subsidence, structural cracks, etc. Liquefaction occurs in loose to medium-dense sandy soil, and when cyclic shear loading is applied to the ground due to a seismic event, the bonding between particles is destroyed, and the excess pore pressure increases, which acts on the inside of the ground. This refers to a phenomenon in which vertical stress and excess pore pressure values become the same, causing it to behave like a liquid. Various cement-based construction methods have existed to prevent this. Still, in this study, an experiment was conducted using biopolymer soil treatment (BPST), one of the bio-inspired materials, to approach it from an eco-friendly ground reinforcement material perspective. In this study, the liquefaction mitigation efficiency of BPST was evaluated using the cyclic direct simple shear (CDSS) test apparatus.

2. Experimental program

The sandy soil used in this study was jumunjin sand, and the biopolymers used were xanthan gum and gellan gum. Biopolymer powder mass and water content were used at 1% and 20%, respectively, compared to the sand mass. The vertical effective stress acting on the CDSS test apparatus is 100 kPa, and the loading is fixed after the experiment begins. The decrease due to the weakening of the sample is assumed to be the increase in excess pore pressure. Liquefaction mitigation efficiency is evaluated by cyclic resistance ratio (CRR). After measuring the cycle number until the strain amplitude for a specific cyclic shear stress exceeds 5%, the same experiment

is performed for four or more types of cyclic shear stress. The cyclic shear stress value corresponding to cycle number 10 is called CRR, and the fitting curve was presented by Seed (1975) and is shown in equation (1).

$$CRR = a \cdot N^{-b} \ \#(1)$$

3. Test results and discussions

Figure 1 shows CDSS test results and CRR analysis according to various cyclic stresses of untreated, xanthan gum and gellan gum. The CRR value was calculated as the value at cycle number 10. Untreated sand and xanthan gum had a CRR value of 0.089, and it was confirmed that xanthan gum treatment was ineffective in mitigating liquefaction. On the other hand, the CRR of gellan gum treated sand is 0.334, which is about 3.8 times higher than that of untreated sand. This can be inferred from previous research that gellan gum has higher compressive and shear strength and lower permeability compared to untreated and xanthan gum treated sand. Through this study, we evaluated the utility of gellan gum among biopolymers as a liquefaction mitigation material, and it is necessary to derive an accurate recipe in the liquefiable ground through additional experiments.

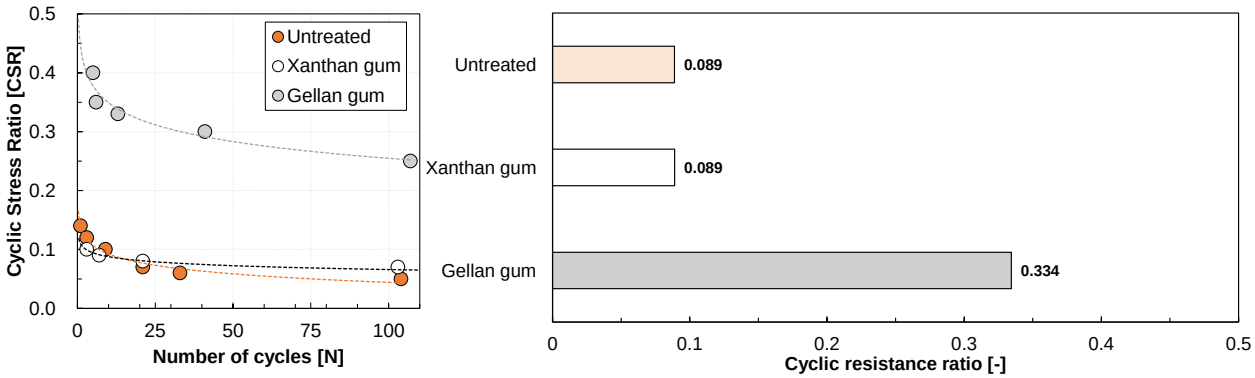

Figure 1. CDSS test results and CRR analysis

4. References

[1] Chang, I., Im, J., Prasidhi, A. K., & Cho, G. C. (2015). Effects of Xanthan gum biopolymer on soil strengthening. *Construction and Building Materials*, *74*, 65-72.

[2] Chang, I., Im, J., Lee, S. W., & Cho, G. C. (2017). Strength durability of gellan gum biopolymer-treated Korean sand with cyclic wetting and drying. *Construction and Building Materials*, *143*, 210-221.

[3] Sadhukhan, B., Chakraborty, S., & Mukherjee, S. (2022). Investigating the relationship between earthquake occurrences and climate change using RNN-based deep learning approach. *Arabian Journal of Geosciences*, *15*(1), 31.

[4] Seed, H. B., Ugas, C., & Lysmer, J. (1976). Site-dependent spectra for earthquake-resistant design. *Bulletin of the Seismological society of America*, *66*(1), 221-243.

DEGRADATION MECHANISMS OF A LIME-TREATED CLAY INDUCED BY WETTING AND DRYING CYCLES

N. Chabrat[1], G. Russo[2], E. Vitale[2],F. Masrouri[1] and O. Cuisinier[1]
[1] LEMTA (UMR 7563) CNRS, Université de Lorraine, Nancy, France
[2] DiSTAR, University of Naples Federico II, Naples, Italy

1. Introduction

Soil stabilization with lime is a common method to improve low-quality soils for the construction of earthen structures. Lime addition improves the mechanical performances of the soil [1,2] associated to the decrease of swelling and shrinkage potential [3,4].
The alteration of mechanical performances over the service life of treated soils when exposed to seasonal wetting and drying cycles is one of the major concerns associated to this technique. Indeed, several studies showed that wetting and drying cycles can alter the beneficial effects of treatments on soil performances [5,6]. However, most of the available studies on the impact of wetting and drying cycles are based on results obtained at the macroscopic scale, without deciphering the different microstructural and physico-chemical processes occurring during cycles [7,8]. There is thus a limited knowledge on the mechanisms involved in the alteration processes triggered by the exposure to successive wetting and drying cycles, and the relative importance of each process.
In this context, a laboratory study has been performed to understand the link between wetting and drying amplitude, micro-scale changes in fabric, physico-chemical properties alteration and the modification of the mechanical behaviour of a lime-treated expansive soil exposed to wetting and drying cycles. Lime-stabilised specimens were exposed to successive wetting and drying cycles of different amplitudes. The hydromechanical behaviour of the expansive soil was then determined using oedometer tests. The microstructure and some physicochemical properties were also evaluated to identify the alteration mechanisms involved.

2. Main results

The wetting and drying cycles induced a degradation of the mechanical properties of the lime-stabilized specimens, the intensity of the degradation being directly related to the maximum suction applied during the cycles. After two cycles with the largest amplitude, the yield stress of the specimen was inferior to 100 kPa, indicating the detrimental impact of the cycles (Figure 1). The results showed that the contribution of physico-chemical processes to the material degradation such as carbonation and leaching was found to be negligible.

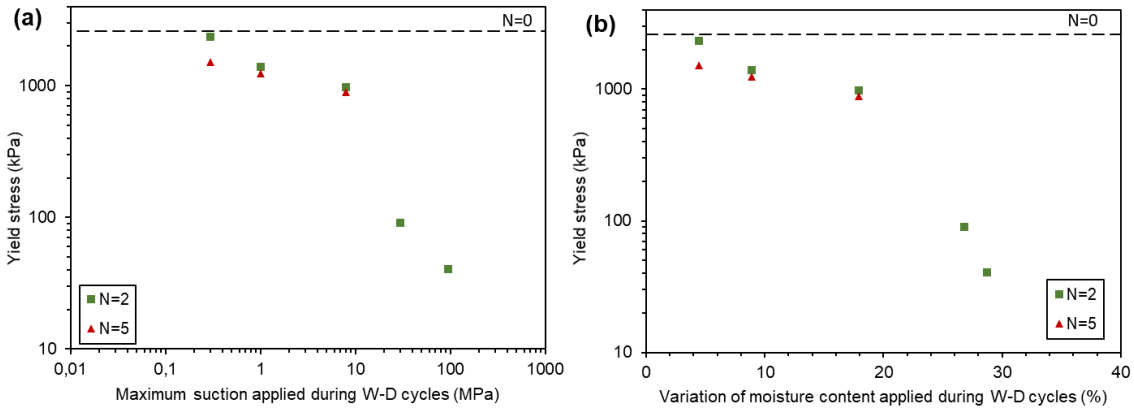

Figure 1. Effect of suction-controlled wetting and drying cycles on the stress of the quicklime-treated materials.

The SEM observations showed that the cycles altered the fabric of the soil, and that the extent of the modifications of the microstructure was linked with the degradation rate of the hydromechanical performances of the soil (Figure 2). When the maximum suction applied during the cycles remained below the air entry value (evaluated around 8 MPa), there were limited degradations in mechanical performances (Figure 1), which were associated to the modification of the macrostructure with the creation of macro-cracks (Figure 2a). When suction exceeded the air entry value, complete degradation occurred with a major reorganization of the micro-porosity (Figure 2c).

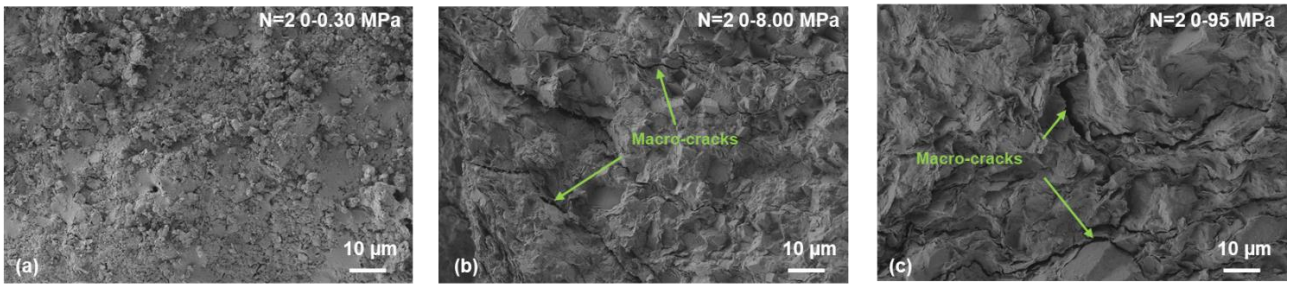

Figure 2. SEM pictures from specimens exposed to 2 wetting and drying cycles with different ranges of suctions.

3. Conclusions

This study highlighted that the main deterioration mechanism of lime-treated expansive soils exposed to cyclic wetting and drying is connected to micro-structural changes whose intensity were controlled by the amplitude of the cycles. The improved understanding of these mechanisms, as provided by this work, has the potential to more effectively forecast the conditions that could promote durability of lime-stabilized expansive soil.

4. References

[1] Brandl H. Alteration of soil parameters by stabilization with lime, 1981.
[2] Guidobaldi G, Cambi C, Cecconi M, Deneele D, Paris M, Russo G, et al. Multi-scale analysis of the mechanical improvement induced by lime addition on a pyroclastic soil. Engineering Geology 2017;221:193–201. https://doi.org/10.1016/j.enggeo.2017.03.012.
[3] Al-Mukhtar M, Khattab S, Alcover J-F. Microstructure and geotechnical properties of lime-treated expansive clayey soil. Engineering Geology 2012;139–140:17–27. https://doi.org/10.1016/j.enggeo.2012.04.004.
[4] Vitale E, Deneele D, Russo G. Microstructural Investigations on Plasticity of Lime-Treated Soils. Minerals 2020;10:386. https://doi.org/10.3390/min10050386.
[5] Gowthaman S, Nakashima K, Kawasaki S. Effect of wetting and drying cycles on the durability of bio-cemented soil of expressway slope. Int J Environ Sci Technol 2022;19:2309–22. https://doi.org/10.1007/s13762-021-03306-1.
[6] Wassermann A, Abdallah A, Cuisinier O. Impact of wetting and drying cycles on the mechanical behaviour of a cement-treated soil. Transportation Geotechnics 2022;36:100804. https://doi.org/10.1016/j.trgeo.2022.100804.
[7] Stoltz G, Cuisinier O, Masrouri F. Weathering of a lime-treated clayey soil by drying and wetting cycles. Engineering Geology 2014;181:281–9. https://doi.org/10.1016/j.enggeo.2014.08.013.
[8] Mehenni A, Cuisinier O, Masrouri F. Alteration of the Hydromechanical Performances of a Stabilized Compacted Soil Exposed to Successive Wetting–Drying Cycles. Journal of Materials in Civil Engineering 2020;32:04020349.

DEM SIMULATION OF GEOGRID PULLOUT TESTS

Harshal Verma[1,2,3], Partha Narayan Mishr[3,4], Bappaditya Manna[2] and David Williams[3]
[1] UQ-IIT Delhi academy of research, India
[2]Department of Civil Engineering, Indian Institute of Technology Delhi, India
[3] School of Civil Engineering, The University of Queensland, Brisbane, Australia
[4] Department of Civil Engineering, Indian Institute of Technology Kanpur, India

Keywords: *DEM; Geogrid; Pullout test; Reinforced Earth Structure*

Abstract

This study employs the Discrete Element Method (DEM) to simulate geogrid pullout tests in granular soil. The 3D model captures particle interactions, applying calibrated material properties and contact models. The open-source software YADE was used for simulation. Models were validated using laboratory pullout test. Results provide insights into geogrid-soil behavior, aiding in understanding pullout resistance factors. The study shows an approach to simulate pullout test using DEM.

1. Introduction

Soil-structure interaction encompasses the mutual influence between the soil and a structure situated on or within it. In geotechnical engineering, this factor holds paramount importance, as the behavior of the structure is intricately tied to the properties of the underlying soil, and, reciprocally, the presence of the structure affects the response of the soil. The consequential impact of this interaction can be substantial, directly influencing the performance, stability, and safety of the construction. Depending on the nature of the load and the reactions of the soil and structure, this interaction may manifest as either static or dynamic. In practical scenarios, however, soil-structure interactions typically involve a combination of static and dynamic effects. The comprehension and accurate consideration of soil-structure interactions play a pivotal role in the design process, ensuring the creation of resilient and cost-effective structures. A prevalent type of interaction encountered by geotechnical engineers is soil-geogrid interaction, which has been extensively studied to comprehend its nuanced behavior. The pullout test emerges as the most effective method for comprehending the interaction between geogrid and soil [1].

Various researchers have conducted different pullout tests under different conditions to understand the effect of different conditions such as effect of backfill material [2-9], moisture [10-14], compaction [15-17], length of geogrid [1, 18-23], width of geogrid [18-23] and type of geogrid material [2, 18, 24-30].

DEM simulations for pullout tests surpass traditional laboratory methods, offering cost-effectiveness, rapid experimentation, precise parameter control, and insights into micro-scale interactions. These simulations provide flexibility to explore various scenarios, particularly under extreme conditions, and allow for efficient sensitivity analyses. While physical experiments are valuable, DEM simulations excel in providing a versatile and resource-efficient approach to understanding soil-structure interactions.

2. Results and Conclusion

Numerical simulations of pullout tests were performed using an open-source code, YADE, which is an extensible tool for DEM models [31]. The aim of numerical simulation was to understand the micromechanics and soil geogrid interactions during pullout tests. The calibration was performed by comparing the numerical results with pullout test results obtained in the laboratory. The backfill material was modelled with unbonded spherical particles with the linear elastic-plastic constitutive model as proposed originally by Cundall and Strack [32]; the contact law in YADE is CundallStrack law.

The geogrids were modelled using the CohesionMoment law, which is an extended version of the CundallStrack law with cohesion and torques at contacts. CundallStrack law only has normal & shear stiffness and friction without any tensile force/strength. The geogrids were modelled similar to continuous elements as proposed by Effeindzourou, et al. [33] based on Chareyre and Villard [34] and also described and used by Bourrier, et al. [35]. This is shown in Figure 1.

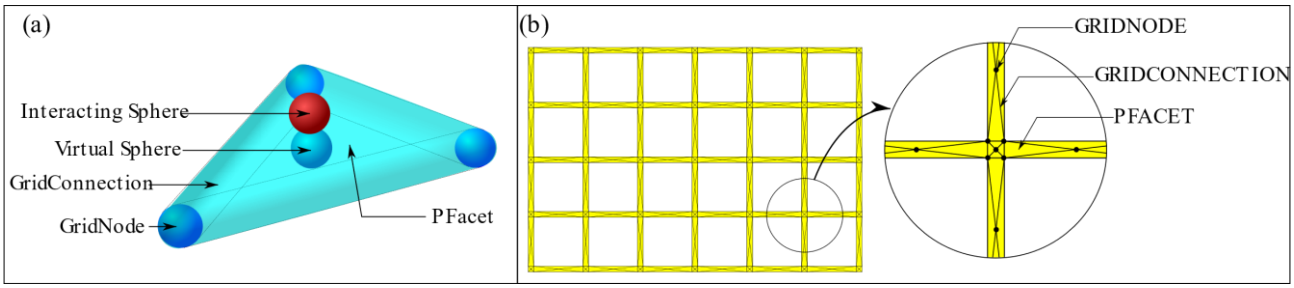

Figure 1. Geogrid generation in YADE (a) virtual sphere in PFacet element (b) geogrid in YADE using PFacet element

The results of triaxial simulation is shown in Figure 2. The numerical results are with good fit to laboratory results indicating utility of DEM for simulating pullout tests.

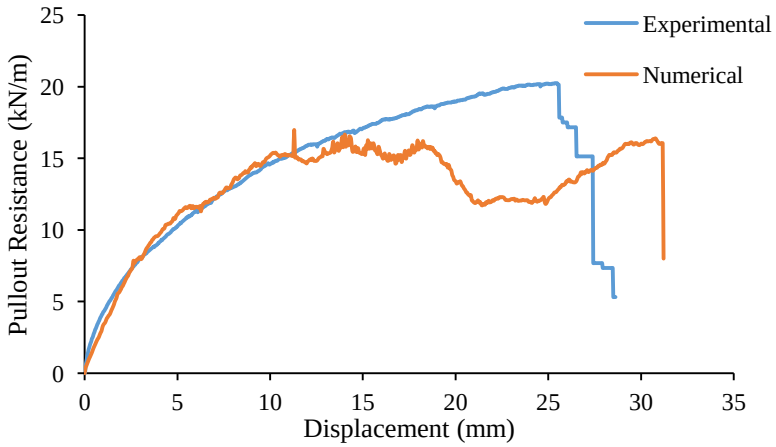

Figure 2. Comparison of numerical and experimental results from pullout tests at 75 kPa normal stress

3. References

[1] I. Yogarajah and K. C. Yeo, "Finite element modelling of pull-out tests with load and strain measurements," *Geotextiles and Geomembranes*, vol. 13, no. 1, pp. 43-54, 1994/01/01/ 1994, doi: https://doi.org/10.1016/0266-1144(94)90056-6.

[2] J. C. Chang, J. B. Hannon, and R. A. Forsyth, *Pull resistance and interaction of earthwork reinforcement and soil* (no. 640). 1977.

[3] C. Bonczkiewicz, R. CHRISTOPHER, and D. Atmatzidis, "Evaluation of soil-reinforcement interaction by large-scale pull-out tests," 1988.

[4] M. J. Goodhue, T. B. Edil, and C. H. Benson, "Interaction of foundry sands with geosynthetics," *Journal of geotechnical and geoenvironmental engineering*, vol. 127, no. 4, pp. 353-362, 2001.

[5] F. M. Nejad and J. Small, "Pullout behaviour of geogrids," *Iranian Journal of Science & Technology, Transaction B, Engineering*, vol. 29, no. B3, pp. 301-310, 2005.

[6] U. Balunaini and M. Prezzi, "Interaction of Ribbed-Metal-Strip Reinforcement with Tire Shred–Sand Mixtures," *Geotechnical and Geological Engineering*, vol. 28, no. 2, pp. 147-163, 2010/03/01 2010, doi: 10.1007/s10706-009-9288-6.

[7] M. R. Abdi and M. A. Arjomand, "Pullout tests conducted on clay reinforced with geogrid encapsulated in thin layers of sand," *Geotextiles and Geomembranes*, vol. 29, no. 6, pp. 588-595, 2011/12/01/ 2011, doi: https://doi.org/10.1016/j.geotexmem.2011.04.004.

[8] M. Pinho-Lopes, A. M. Paula, and M. L. Lopes, "Pullout response of geogrids after installation," *Geosynthetics International*, vol. 22, no. 5, pp. 339-354, 2015, doi: 10.1680/jgein.15.00016.

[9] M. R. Abdi and H. Mirzaeifar, "Experimental and PIV evaluation of grain size and distribution on soil–geogrid interactions in pullout test," *Soils and Foundations*, vol. 57, no. 6, pp. 1045-1058, 2017/12/01/ 2017, doi: https://doi.org/10.1016/j.sandf.2017.08.030.

[10] K. A. Farrag and P. Griffin, "Pull-out testing of geogrids in cohesive soils," *ASTM SPECIAL TECHNICAL PUBLICATION*, vol. 1190, pp. 76-76, 1993.

[11] H. S. Lee and A. Bobet, "Laboratory Evaluation of Pullout Capacity of Reinforced Silty Sands in Drained and Undrained Conditions," *Geotechnical Testing Journal*, vol. 28, no. 4, pp. 370-379, 2005, doi: 10.1520/GTJ12011.

[12] M. Hossain and T. Sakai, "A study on pullout behavior of reinforcement due to variation of water content of soil," 2007.

[13] G. Yin, Z. Wei, J. G. Wang, L. Wan, and L. Shen, "Interaction characteristics of geosynthetics with fine tailings in pullout test," *Geosynthetics International*, vol. 15, no. 6, pp. 428-436, 2008, doi: 10.1680/gein.2008.15.6.428.

[14] J. Zhang and N. Yasufuku, "Evaluation of Rainfall Infiltration and Compaction Effect on Soil-Geogrid Interaction Behavior," *Geosynthetics Engineering Journal*, vol. 24, pp. 61-68, 2009, doi: 10.5030/jcigsjournal.24.61.

[15] K. Farrag, Y. B. Acar, and I. Juran, "Pull-out resistance of geogrid reinforcements," *Geotextiles and Geomembranes*, vol. 12, no. 2, pp. 133-159, 1993/01/01/ 1993, doi: https://doi.org/10.1016/0266-1144(93)90003-7.

[16] M. L. Lopes and M. Ladeira, "Influence of the Confinement, Soil Density and Displacement Rate on Soil-Geogrid Interaction," *Geotextiles and Geomembranes*, vol. 14, no. 10, pp. 543-554, 1996.

[17] D. Shi and F. Wang, "Pull-out test studies on the interface characteristics between geogrids and soils," *EJGE*, vol. 18, pp. 5405-5417, 2013.

[18] D. T. Bergado, J. C. Chai, H. O. Abiera, M. C. Alfaro, and A. S. Balasubramaniam, "Interaction between cohesive-frictional soil and various grid reinforcements," *Geotextiles and Geomembranes*, vol. 12, no. 4, pp. 327-349, 1993/01/01/ 1993, doi: https://doi.org/10.1016/0266-1144(93)90008-C.

[19] R. F. Wilson- Fahmy, R. M. Koerner, and L. J. Sansone, "Experimental Behavior of Polymeric Geogrids in Pullout," *Journal of Geotechnical Engineering*, vol. 120, no. 4, pp. 661-677, 1994, doi: doi:10.1061/(ASCE)0733-9410(1994)120:4(661).

[20] M. L. Lopes and M. Ladeira, "Role of Specimen Geometry, Soil Height, and Sleeve Length on the Pull-Out Behaviour of Geogrids," *Geosynthetics International*, vol. 3, no. 6, pp. 701-719, 1996, doi: 10.1680/gein.3.0081.

[21] S. W. Perkins and E. V. Cuelho, "Soil-Geosynthetic Interface Strength and Stiffness Relationships From Pullout Tests," *Geosynthetics International*, vol. 6, no. 5, pp. 321-346, 1999, doi: 10.1680/gein.6.0156.

[22] A. Bolt and A. Duszyńska, "Soil-Geogrid Interaction in Pullout Test at 2D–Deformation Conditions," in *Proceedings of Seventh International Conference on Geosynthetics, Nice, France*, 2002.

[23] N. Moraci and P. Recalcati, "Factors affecting the pullout behaviour of extruded geogrids embedded in a compacted granular soil," *Geotextiles and Geomembranes*, vol. 24, no. 4, pp. 220-242, 2006/08/01/ 2006, doi: https://doi.org/10.1016/j.geotexmem.2006.03.001.

[24] R. Berg and R. Swan, "P4/9 Investigation into geogrid pullout mechanisms," in *Performance of reinforced soil structures*, 1991, pp. 253-257.

[25] M. J. Lopes and M. L. Lopes, "Soil-Geosynthetic Interaction - Influence of Soil Particle Size and Geosynthetic Structure," *Geosynthetics International*, vol. 6, no. 4, pp. 261-282, 1999, doi: 10.1680/gein.6.0153.

[26] A. M. N. Alagiyawanna, M. Sugimoto, S. Sato, and H. Toyota, "Influence of longitudinal and transverse members on geogrid pullout behavior during deformation," *Geotextiles and Geomembranes*, vol. 19, no. 8, pp. 483-507, 2001/12/01/ 2001, doi: https://doi.org/10.1016/S0266-1144(01)00020-6.

[27] S. H. Teixeira, B. S. Bueno, and J. G. Zornberg, "Pullout resistance of individual longitudinal and transverse geogrid ribs," *Journal of geotechnical and geoenvironmental engineering*, vol. 133, no. 1, pp. 37-50, 2007.

[28] X. Liao, G. Ye, and C. Xu, "Friction and Passive Resistance of Geogrid in Pullout Tests," in *Advances in Ground Improvement*, 2009, pp. 252-259.

[29] R. J. Bathurst and F. M. Ezzein, "Geogrid pullout load–strain behaviour and modelling using a transparent granular soil," *Geosynthetics International*, vol. 23, no. 4, pp. 271-286, 2016, doi: 10.1680/jgein.15.00051.

[30] Z. Wang, F. Jacobs, and M. Ziegler, "Experimental and DEM investigation of geogrid–soil interaction under pullout loads," *Geotextiles and Geomembranes*, vol. 44, no. 3, pp. 230-246, 2016/06/01/ 2016, doi: https://doi.org/10.1016/j.geotexmem.2015.11.001.

[31] V. Smilauer *et al.*, "Yade documentation," *The Yade Project*, 2021, doi: 10.5281/zenodo.5705394.

[32] P. A. Cundall and O. D. L. Strack, "A discrete numerical model for granular assemblies," *Géotechnique*, vol. 29, no. 1, pp. 47-65, 1979, doi: 10.1680/geot.1979.29.1.47.

[33] A. Effeindzourou, B. Chareyre, K. Thoeni, A. Giacomini, and F. Kneib, "Modelling of deformable structures in the general framework of the discrete element method," *Geotextiles and Geomembranes*, vol. 44, no. 2, pp. 143-156, 2016/04/01/ 2016, doi: https://doi.org/10.1016/j.geotexmem.2015.07.015.

[34] B. Chareyre and P. Villard, "Dynamic Spar Elements and Discrete Element Methods in Two Dimensions for the Modeling of Soil-Inclusion Problems," *Journal of Engineering Mechanics*, vol. 131, no. 7, pp. 689-698, 2005, doi: doi:10.1061/(ASCE)0733-9399(2005)131:7(689).

[35] F. Bourrier, F. Kneib, B. Chareyre, and T. Fourcaud, "Discrete modeling of granular soils reinforcement by plant roots," *Ecological Engineering*, vol. 61, pp. 646-657, 2013/12/01/ 2013, doi: https://doi.org/10.1016/j.ecoleng.2013.05.002.

EFFECT OF COAL GANGUE-CALCIUM CARBIDE RESIDUE GEOPOLYMER ON THE COMPRESSIBILITY AND PORE EVOLUTION OF SOFT SOIL

Jianfeng Li[1,2], Yi Shan[2], Yadong Li[2], Jie Cui[2*], and Pengpeng Ni[1*]
[1]School of Civil Engineering, Sun Yat-sen University, Guangzhou, China;
[2]School of Civil Engineering, Guangzhou University, Guangzhou, China.

1. The area of this research and method

As urbanization progresses, the need to construct on problematic soils becomes inevitable. Traditional methods of ground improvement involve using stabilizers such as cement, lime, and other cementitious materials. However, these stabilizers have several drawbacks, including high raw material costs, significant energy consumption during production, and substantial CO_2 emissions. To address these concerns, there is a growing interest in finding low-carbon alternatives for soil stabilization, and geopolymer has emerged as a promising technology for strengthening problematic soils.

Coal gangue (CG) is an ideal aluminosilicate precursor for geopolymer production due to its high aluminosilicate content and easy availability. Calcium carbide residue (CCR), on the other hand, provides a high pH environment and is rich in Ca^{2+}, reducing the need for NaOH and making geopolymer production cost-effective. The combination of CG and CCR in geopolymer synthesis offers potential for practical applications by minimizing the use of conventional additives. However, current research on geopolymer-stabilized soft soil primarily focuses on unconfined compressive strength index. Compressibility, which significantly affects settlement, is a crucial characteristic of soft soils. The pore diameter distribution in soil plays an important role in its mechanical properties, including compressibility. Therefore, understanding the micro-pore distribution characteristics is important to understanding the soil deformation behavior.

In this study, we utilized a series of one-dimensional tests to study the compressibility of soil stabilized with a geopolymer made from coal gangue and calcium carbide residue. We collected representative samples from crushed stabilized soil specimens for analysis using mercury intrusion porosimetry (MIP) and scanning electron microscopy (SEM) to examine the evolution of pore characteristics.

2. Main results

2.1 Compressibility behavior

The results demonstrate that the CG-CCR geopolymer significantly improves compressibility and alters pore distribution characteristics. As the geopolymer content increases, the initial void ratio of stabilized specimens decreases. For geopolymer contents of 5%, 10%, 15%, 20%, and 30%, the corresponding initial void ratios are 1.21, 1.07, 1.01, 0.96, and 0.79, respectively. The structural yield pressure, determined using the e-log σ compression curve method suggested by Casagrande, also increases with higher geopolymer content. The structural yield pressures for geopolymer contents of 5%, 10%, 15%, 20%, and 30% are 411, 556, 890, 1512, and 1925 kPa, respectively. Similar to cemented soils, increasing the geopolymer content enhances the soil's ability to withstand pressure without settlement. These findings suggest that a geopolymer content of 30% is the most effective in reducing soil compressibility.

2.2 Pore evolution

The MIP results demonstrate a decrease in the total cumulative pore volume as the geopolymer content increases, indicating that the geopolymer content primarily controls the cumulative pore volume. Additionally, the pore diameter influences the cumulative pore volume. With an increase in geopolymer content, the peak of the differential intrusion volume curve tends to shift towards smaller pore diameters, suggesting a reduction in cumulative volume and a change in pore size distribution. The majority of the pore volume is concentrated in pores ranging from 10 to 1000 nm in size. In the unstabilized soil, pore volumes for this size range account for 92.2% of the total amount, while it decreases to 72.9% for a geopolymer content of 30%. Moreover, the content of large pores decreases as the geopolymer content increases from 15% to 30%, indicating a considerable refinement of the pore structure through the addition of geopolymer.

The results of SEM showed that the unstabilized soil sample exhibited a coarse texture and large voids in the matrix, resulting in a nonuniform pore distribution and a relatively loose microstructure compared to the stabilized soil samples. This finding aligns with the MIP results. In contrast, the particles in the stabilized soil samples were coated and bonded with the reaction products, forming a strong framework regardless of the geopolymer content. The incorporation of the geopolymer significantly enhanced the mechanical contact and bonds between soil particles, transforming the scattered cluster morphology into a denser gelatinous structure.

These observations are in line with the compressibility results. The distribution of reaction products in the soil matrix led to filling of pores between soil particles. As a result, the bonds between soil particles were strengthened, leading to a denser structure and reduced compressibility of the soil.

EXAMPLES OF THREE DEEP MIXING METHODS INVESTIGATED BY X-RAY MICRO-COMPUTED TOMOGRAPHY

P. Paniagua[1,2], K. Skreien[2], S. Hov[1,2], D. Younas[2], K. Tekseth[2], B. Chattopadhyay[2] and D. Breiby[2]
[1] Norwegian Geotechnical Institute, Trondheim, Norway
[2] Norwegian University of Science and Technology, Trondheim, Norway

1. Introduction

Ground improvement of soft clays by deep mixing involves mixing and injecting a binder at the same time with the objective of increasing the soil strength and stiffness. The binder is usually made from lime, cement, and relevant industry waste products or a combination of the materials mentioned. Today, there are three main mixing methods in use, each of which has been developed in different parts of the world. Dry deep mixing (DDM) has been used in the Nordic countries for decades, while modified dry mixing (MDM) and wet deep mixing (WDM) have only started to be implemented in Scandinavia in recent years. With little to no research about the three methods in Nordic conditions, it becomes increasingly important to develop design tools and knowledge about the differences and range of applications of such methods. Knowing which method is best suited for unique projects cuts down on both design time and construction time. Previous studies [1] between laboratory and field mixed samples of sensitive clay improved with lime and cement using DDM showed clear differences in sample density and 'macro-porosity' described as entrapped air resulting from field installation and laboratory preparation.

In this study, field samples of soft clay mixed with cementitious binders by either MDM or WDM are investigated by x-ray micro-computed tomography with the objective of examining the quality and uniformity of the stabilized soil. Emphasis is given to describing the density, macro-porosity, which is the focus of the present extended abstract, and its influence on the strength and stiffness of the improved soil. This investigation adds to the knowledge of deep mixing under Nordic conditions with the aim of providing background data for further decision making and understanding of which method is ideal for different applications.

2. Materials and methods

WDM samples were collected from Sundsvall and Hjorthagen in Sweden. MDM samples were collected from Stjørdal in Norway. All the sites are located near the coast. Deposits at Sundsvall consist mostly of clay and silt, with some areas containing peat or mud. The Hjorthagen site is entirely on a land reclamation location and deposits contain mostly postglacial clay and silt, with some moraine. The deposits at Stjørdal consist mostly of marine sediments.

The samples were mixed with 100% cement in content of 100 kg/m³ for the Stjørdal site, 115 kg/m³ for the Hjorthagen site and 200 kg/m³ for the Sundsvall site. A low blade rotation number (BRN[1]) of 250 per meter was used during installation of the MDM columns at Stjørdal. This value is much lower than the recommended lower limit of 400 per meter for DDM. For the WDM columns installed at Sundsvall and Hjorthagen, the BRN was 666 and 800 per meter, respectively.

The collected samples were carefully trimmed into specimens of 100-150 mm height and 100 mm diameter prior testing by x-ray attenuation-contrast micro-computed tomography (μCT). A Nikon XT H 225 ST with a 16-bit Perkin Elmer 1620 X-ray detector was used for μCT 3D imaging.

[1]BRN refers to the total number of blades of the mixing tool passing through the soil per meter.

The field of view was 100 mm wide to match the sample diameter and the corresponding voxel size varied in the range 58-62 µm.

4. Main results

Figure 1 presents some examples of the imaged specimens for each method under study. On the 2D µCT images, pores are black while the binder and soil can be seen as varying tones of dark to light grey. Inclusions in the material are shown as white lumps of varying size and shape with high absorption compared with the rest of the sample. Some of the samples were cut after imaging and compared to the 2D µCT images. Two main materials were discovered to have high absorption: gravel of varying size like in the case of Sundsvall samples and seashells like in the case of Hjorthagen samples. Analysis of macro porosity in the imaged samples show that the WDM method produced samples with very low average macro porosity (≈ 0.1 to 0.9%). The Hjorthagen samples had lower macro porosity values than the Sundsvall samples. The average porosity in the MDM samples is higher (≈ 0.4 to 1.5 %) and the pores are more evenly distributed than in the WDM samples. A clear conclusion cannot be made because the porosity might also be affected by the longer curing time and lower binder amount, as well as installation parameters and the nature of the natural clays. However, a larger porosity in MDM samples is as expected because the MDM method uses compressed air to inject a dry binder into the soil. Previously studied DDM field samples have higher porosity values (≈ 0.5 to 1.6 %) than the WDM samples as well. These porosity values for DDM are closer to what is observed in the MDM samples.

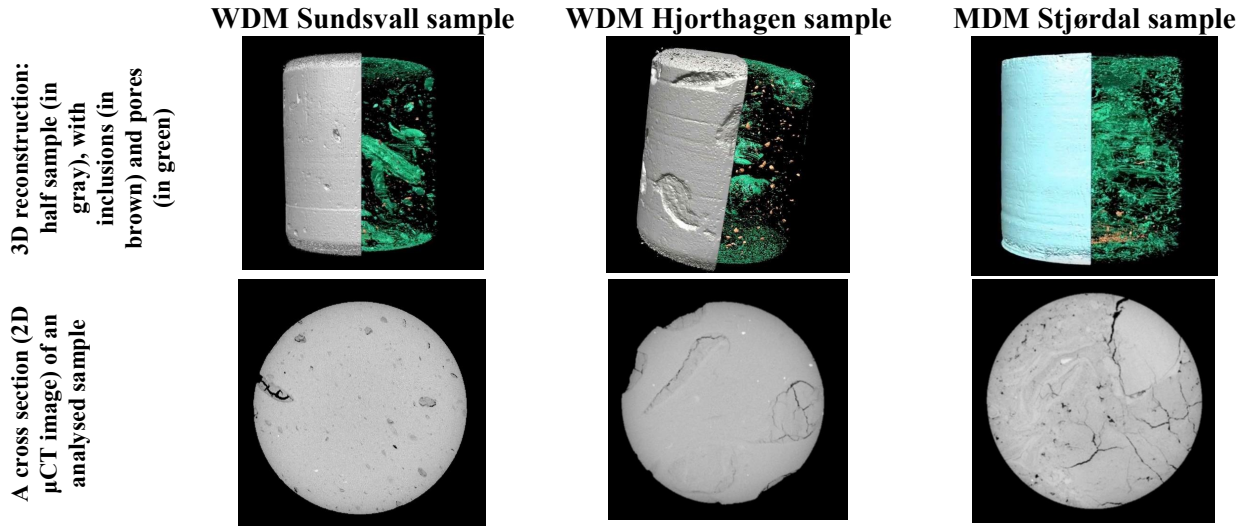

Figure 1. Images from x-ray micro-computed tomography on stabilized clays samples.

5. Conclusions

This work is an example of the application of µCT to assess homogeneity, macro porosity and other structures (i.e. inclusions). It was observed that the WDM gave a uniform texture with little to no entrapped air in the soil-binder mixture. MDM samples showed a non-uniform composition, visible binder accumulation and an even distribution of small pores and cracks.

6. References

[1] Paniagua, P., Falle, F. Å., Hov, S., Tekseth, K.R., Mirzaei, F. & Breiby, D.W. (2022). Comparing laboratory and field samples of lime–cement-improved Norwegian clay. Géotechnique Letters 12:4, 265-271. doi.org/10.1680/jgele.22.00067

INNOVATIVE BINDERS FOR TREATMENT OF DREDGED SEDIMENTS: GEO-CHEMO-HYDRO-MECHANICAL ASPECTS

R. Petti[1], C. Vitone[1], M. Plötze[2] and A. Puzrin[2]
[1] Politecnico di Bari, DICATECh, Bari, Italy
[2] ETH Zurich, Institute for Geotechnical Engineering, Zürich, Switzerland

1. Introduction

The study addresses two key challenges in coastal and port areas: the management of large quantities of dredged sediments (100-200 million m^3/year in Europe) and the disposal of mussel shells (approximately 230,000 tons/year in Europe). The first challenge involves global issues related to handling of dredged sediments, with conflicts arising between port development, environmental conservation, and tourism. Current disposal practices, treating sediments as 'waste,' are expensive and environmentally risky. While new European regulations offer waste management alternatives, concerns persist about the environmental impact, including the use of cement. Recent research explores sustainable solutions for chemo-mechanical improvement of sediments and soils, aiming to reduce reliance on cement in favour of more sustainable additives [1]. The second challenge focuses on the management of mussel shells, posing complex and expensive disposal issues due to their wet nature and non-biodegradable composition. Illegally dumped mussel shells harm ecosystems and accumulate on shorelines. Based on previous findings regarding the use of shell powder as a partial substitute for cement powder in improving the mechanical behaviour of dredged sediments [2,3,4], this study aims to extend the effectiveness for both mechanical and chemical improvement of artificially polluted sediments.

2. Method

This research involves both the multidisciplinary characterisation of dredged sediments and that of the same sediments treated with different binders after their artificial contamination by various chemicals. The experimental programme, designed to perform a geo-chemo-hydro-mechanical characterization crossing multiple investigation scales, was necessary to track the chemo-mechanical reactions between clay particles, the pollutant, and cementing agents (with and without additives) and their impact on the microstructure of the material, reflecting changes in behaviour of the mixtures at the volume element (engineering) scale. The study focuses on fine-grained marine sediments dredged from the port of Taranto (Figure 1a), Southern Italy, spiked with 8% kerosene to create artificially polluted sediment (KS). Portland cement type I 52.5 R (P) was used as the binder (8%wt.). Chemo-mechanical stabilisation of the contaminated sediment involves two bio-additives: i) mussel shell powder (MS), replacing 2% wt. of P-cement, and ii) 8% wt. of biochar (B), added to the binder alone or in a hybrid solution with cement and shell powders. The mussel shells undergo a low-temperature treatment to produce not-calcinated fine-grained shell powder (D_{50}= 6.32 µm) [2] (Figure 1b). While the use of biochar [1] and calcined shells as contaminants absorbents is documented in soil literature, further research is needed for chemo-mechanical stabilisation of marine sediments, especially using not-calcinated shells and mixed solutions. The discussion briefly covers results from mixtures of KS with i) 8% P-cement (KS8P); ii) 6% P-cement and 2% shell powder (KS6P2MS); iii) 6% P-cement, 2% shell powder, and 8% biochar (KS6P2MS8B); iv) 8% P-cement and 8% biochar (KS8P8B).

Figure 1. Materials. a-Dredged sediments, DS; b-Mussel shell powder, MS, c-Biochar, B; d-Kerosene, K.

3. Results

Figures 2a-b show the results obtained from unconfined compression tests and leaching tests of the P-mixtures after 28 days of curing in sea water. The analysis of the mixtures with the same initial water content (i.e., KS8P with KS6P2MS and KS8P8B with KS6P2MS8B) shows that the unconfined compression strength (Qu) of the mixtures with shells is only slightly lower than that with just P-cement, but this difference increases in the presence of Biochar.

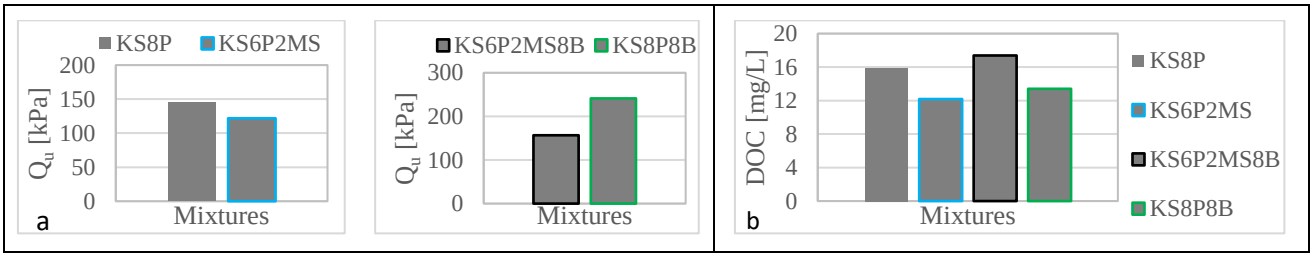

Figure 2. a) Unconfined compression strength, Q_u and b) dissolved organic carbon content, DOC, in the leachate of different mixtures after 28 days of curing.

In terms of chemical efficacy, all measured DOC concentrations are found to be below the legal limits (50 mg/L, Directive 2013/39/CE) and it seems that the addition of biochar is particularly effective in the mixtures without shells ($DOC_{KS6P2MS8B}$>$DOCK_{S8P8B}$). However, the DOC content in the eluate of the KS6P2MS sample is the lowest recorded among all the mixtures studied. Ultimately, the cement and biochar stabilisation solution (KS8P8B) showed the best mechanical performance among all the mixtures but only the second-best chemical performance (DOC).

5. References

[1] Lofrano et al., (2017). In situ remediation of contaminated marine sediment: an overview. *Environmental Science and Pollution Research*, **24** :5189–5206.

[2] Petti R., et al. (2023). Characterisation tests for mechanical stabilisation of dredged sediments using shell powder. *Proceedings of the 9ICEG*. Greece, 25-28 June.

[3] Roque, A.J., et al. (2022). Sustainable Environmental Geotechnics Practices for a Green Economy. *Environmental Geotechnics* **9**:2, 68-84.

[4] Petti R., et al. (2023). On the use of mussel shells as green solution to mechanically stabilise dredged sediments. *Proceedings of the 8th IS-Porto 2023*. Porto, 3rd - 6th September.

MECHANICAL BEHAVIOUR OF POND ASH TAILINGS BEFORE AND AFTER BIOCHEMICAL STABILIZATION

A. P. Ribera[1], S. Jain[2] , A. Peña-Olarte [1] , R. Cudmani [1] , S. K. Das [2]
[1] Technical University of Munich, Munich, Germany
[2] Indian Institute of Technology, Dhanbad, Jharkhand, India

1. General

The frequent failures of tailing dams, occurring at a rate around 100 times greater than that of traditional water retaining dams (1.2%), are a major global concern. These failures result in the release of tailing waste, causing negative economic, environmental, and ecological consequences. The main causes of such failures are insufficient characterization and the presence of loosely packed, saturated grains prone to static liquefaction. Over the last five decades, the mining industry has experienced continuous growth, with global mineral production escalating from 9.7 billion tonnes in 1985 to 17.2 billion tonnes in 2017 [1]. This increase in production is directly associated with a corresponding upswing in tailings generation. Due to this significance in the increment of the mining waste volumens, it is important to think about solutions that could lead to stabilize this type of material, and the stabilization of this dam through chemical and biological means show a promising solution for this perpouse.

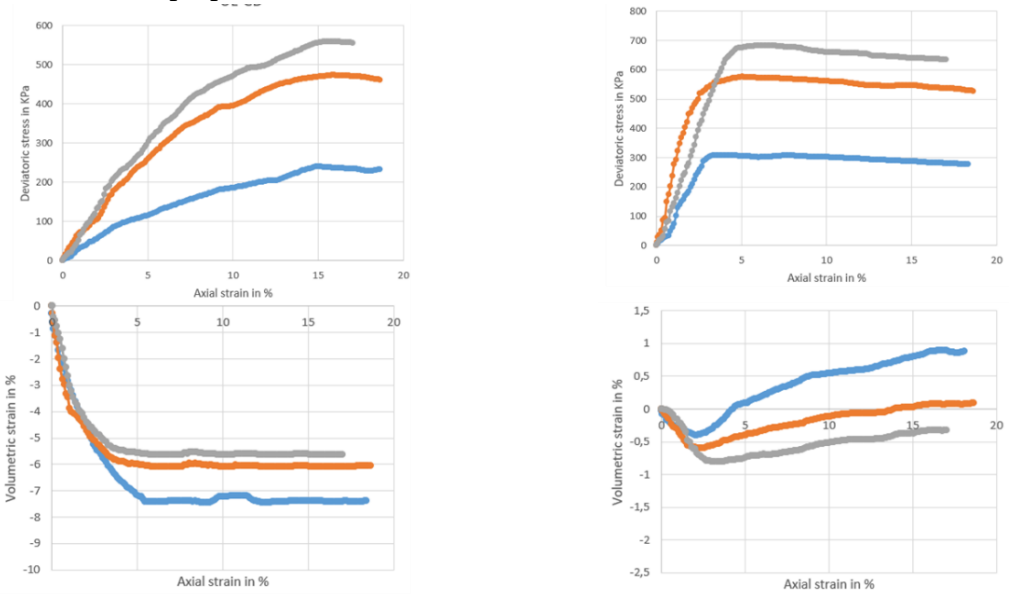

Figure 1. Experimental results of Pond Ash tailings in triaxial test for loose samples (Left) and dense samples (Right).

In this study, two methods, Enzymatic Induced Carbonate Precipitation (EICP) utilizing urease enzyme and geopolymerization employing sodium silicate and sodium hydroxide, were employed.

2. Experimental Results

The experimental outcomes demonstrate the effectiveness of both chemical and EICP methods in stabilizing pond ash against static liquefaction. Stiffness notably increases after stabilization, and the material's behavior undergoes a significant shift from being contractant to more dilatant.

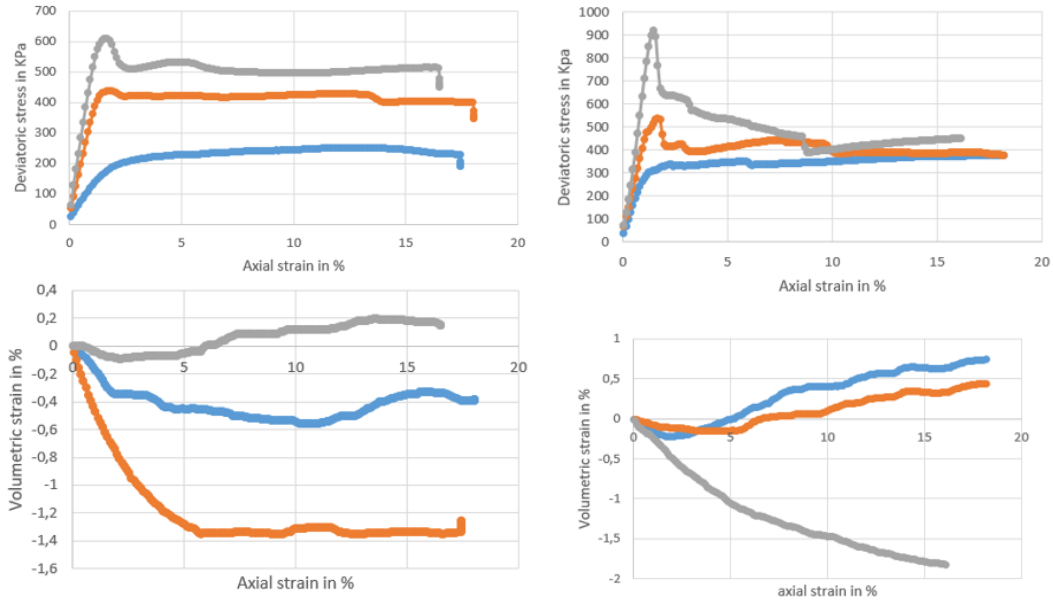

Figure 2. Experimental results of Pond Ash tailings modified with Biolymers (Left) and with Enzymes (Right) in triaxial test in loose samples.

3. Constitutive modelling

As an integral aspect of tailing dam safety management, material modeling is crucial. The study incorporates two constitutive models, Mohr-Coulomb and Hypoplasticity, to assess the behavior of untreated and bio/chemically modified tailings.

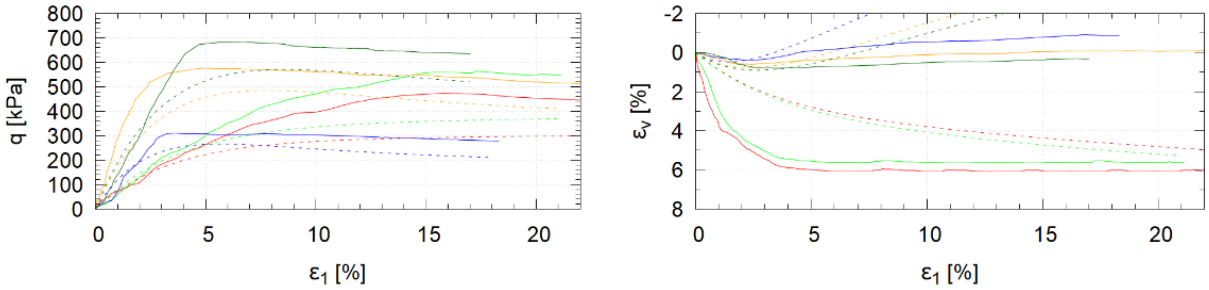

Figure 3. Element test simulation with constitutive model simulation.

However, these constitutive models, suitable for virgin pond ash, fall short in accurately representing the behavior of modified materials. Biochemical modifications alter the micro-level properties of pond ash, creating cementation between soil grains not considered in these models. Therefore, the study recommends the incorporation of advanced modeling techniques to better capture the changes resulting from bio-chemical modifications, enhancing our understanding of tailing behavior.

4. References

[1] ICOLD, U. (2001). Tailings dam–the risk of dangerous occurrences, lessons learned from practical experiences (bulletin 121). Commission Internationale des Grands Barrages, Paris, 155.

MICROMECHANICAL OBSERVATION OF BALLASTED LAYER DURING TAMPING PROCESS BY USING DEM

R.Sugai[1], A. Kono[2], T.Nakamura[1]and T.Hiroo[1]
[1] Railway Technical Research Institute, Track Technology Division, Tokyo, Japan
[2] Railway Technical Research Institute, Railway Dynamics Division, Tokyo, Japan

1. Introduction

In railway ballasted tracks, rails are fixed to sleepers, which are discretely laid in the ballasted layer. The ballasted layer of ballasted track is a granular layer composed of poorly graded crushed stone (see Fig.1), and the general layer thickness in Japan is 200 mm to 300 mm. Due to the cyclic loadings on the ballast layer under each sleeper caused by vehicle running, plastic deformation of the layer called “settlement” occurs.

Previous studies have shown that the size and arrangement of ballast grains have a significant influence on the macroscopic elasticity and plasticity of the ballasted layer. Then, in ballasted layer, there is a difference in the gradient of settlement under each sleeper, which cause track irregularity.

Along with the section of the track irregularity occurs, a kind of maintenance work called “tamping work” is carried out by a large maintenance vehicle to adjust the rail level. However, there is a difference for the gradient of settlement after the maintenance work. One of the reasons for the difference is thought to be the change in the density of the ballasted layer due to the tamping work, but there are many uncertainties, and it has not been sufficiently studied so far.

Regarding the degree of compactness of the ballasted layer, previous experimental study shows the porosity of 59.9 for the sufficiently compacted condition[1)], but it is difficult to measure the porosity of the ballasted layer at the real railway lines. Therefore, tamping work using a large maintenance vehicle is generally managed by the tamping time and the load acting on the tamping tines to determine the completion of the work.

In this study, we tried to simulate the process of tamping work using an actual large maintenance vehicle by discrete elements model of ballasted track. At the same time as observing the microscopic grains behavior of ballast particles in the tamping process, the relationship between the tamping time and the degree of compaction of the ballasted layer was also verified under the condition of a plurality of rail lift.

2. Methodology

The numerical method was a 3D-DEM, and each element of the ballast grains, sleeper, roadbed, and tamping tines were modeled by rigid clumped spheres. Ballast grains are modeled by using measurement data of the 3D shape of actual ballast grains and composed of 8 to 18 spheres per element. An overview of the analysis model is shown in Fig.2.

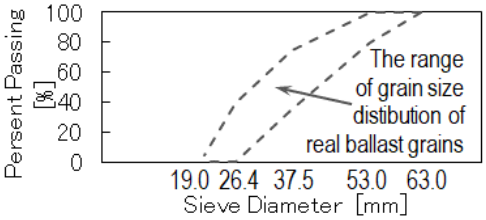

Figure 1. Grain size distribution of ballast grains

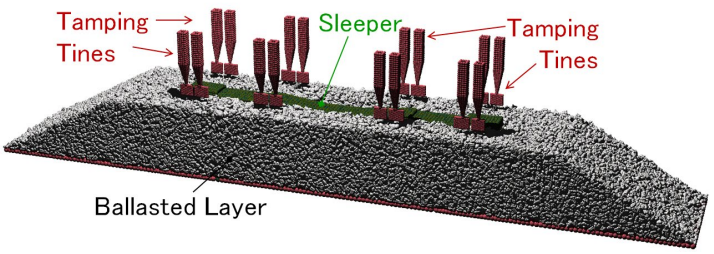

Figure 2. Overview of simulation model

The initial thickness of the ballasted layer is a) 295 mm, b) 290 mm, and c) 280 mm, respectively, and the amount of sleeper lift at each case are a) 5 mm, b)10 mm, and c)20 mm, respectively. The tamping process consisted of one set of "tines descending→ 1 second squeezing → and tines raising", then case a) have 1 set, case b) have 2set and case c) have 4 set.

The analysis code was based on DEMCS-track, which was developed through collaborative research between RTRI and the University of Tsukuba[2].

3. Examples of Simulation Results

From the simulation results, examples of the grains behavior and the change pf density of the ballasted layer during the tamping process are shown.

Fig.3 shows the arrows of grain motion before and after the tamping process in case b). In the figure, grains distributed in a cross-section with 500 mm thickness from the sleeper end are extracted, and the behavior in the sleeper cross-section direction is illustrated. From the figure, it can be confirmed that the ballast grains move from both sides of the sleeper in the direction of the void generated under the sleeper due to the lift of the sleeper.

Fig.4 shows the changes in the density distribution of the ballasted layer in cases b). From the figure, the density of the upper ballasted layer temporarily decreases due to the sleeper lift then recovers after 1 second squeezing process. However, the density of the upper ballasted layer under the center of the sleeper and between couples of tines tends to be smaller than that around tines descending position. It suggests that 1 second squeezing is not enough at the case b) with 10mm lift.

4. Conclusion

From DEM simulation of tamping work process, it was suggested that it is necessary to adjust the number of tamping processes according to the amount of sleeper lift during maintenance work, and that it is possible to reduce the difference in the gradient of the settlement of each sleeper after the maintenance work by adjusting the number of tamping processes.

5. References

[1] Sunaga, M.(1993), Density measurement of ballast layer using gamma ray, Proc. 28th Annual Conference on Geotechnical Engineering, JGS, 2383-2384, (in Japanese)

[2] A.Kono. & T.Matsushima.(2021). *Quantitative Evaluation of Estimated Residual Settlement of Poorly Graded Crushed Stone Layers by Using DEM,* JSCE, Proc. 24th Applied Mechanical Symposium, (2021) SS01A-05

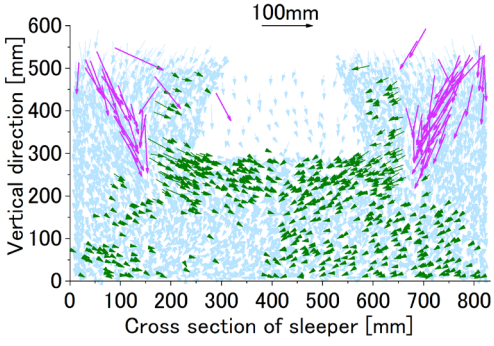

Figure 3. Motion of ballast grains

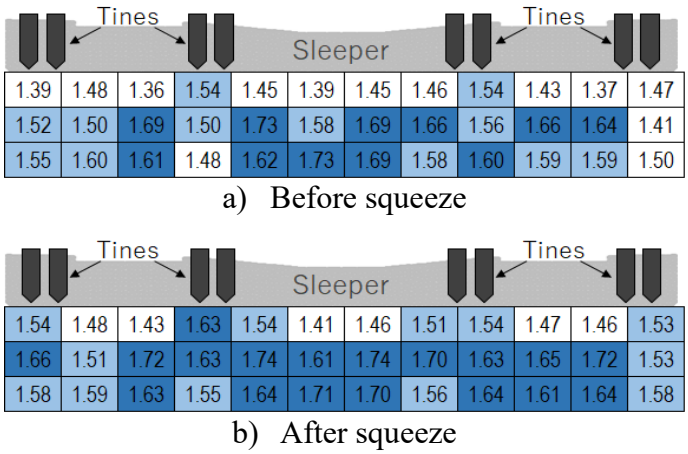

a) Before squeeze

b) After squeeze

Figure 4. Change of density of ballasted layer

NUMERICAL STUDY OF GEOTEXTILE-REINFORCED PLATFORMS LAID OVER SOFT SUBGRADE SOIL AND SUBJECTED TO CYCLIC LOADING

N. Abou Chaz[1,2], C. Silvani[2], P. Villard[1] and L. Briançon[2]
[1] Univ. Grenoble Alpes, CNRS, 3SR Lab., Grenoble, France
[2] Univ. Lyon, INSA Lyon, GEOMAS Lab. Lyon, France

1. General

Poor subgrade is a widespread issue in unpaved roads construction. The geosynthetic (GSY) is considered one of the most innovative solutions since it was used in the late 1970's. Depending on the type of the GSY used, one or many functions among the separation, the reinforcement and the soil stabilisation can be ensured. Reinforcement takes place in the road structure system when the GSY, which is under tension as taking a curved shape (membrane effect), transfers the tensile force to the location where it is anchored. Soil stabilisation is provided to the base course materials when a soil-GSY composite material is formed by interlocking and/or friction and becomes less deformable than the soil [1].

A few design methods have been presented in the literature and quantifies either the tensioned membrane effect or the confinement mechanism by friction or interlocking between the GSY and the base course material. However, all of these methods have limitations because they have been calibrated on limited GSY and soil parameters and sometimes under static loading rather than cyclic loading.

To highlight the understanding of such mechanisms and to set bases to improve existing design methods, a full-scale experimentation has been recently carried out and investigated the reinforcement performance under cyclic vertical using two types of GTXs with different tensile stiffnesses and two base course thicknesses [2]. These tests provided various ranges of displacements and stresses of granular platform and subgrade soft layer. In addition, A DEM-FEM coupled numerical model is developed to investigate the behavior of this platform reinforced by geotextile (GTX) subjected to cyclic loading. The presentation of the numerical model and the confrontation between the numerical model and the experiments are presented below and allow to give conclusions about on the reinforcement mechanisms and performance.

2. Numerical modeling

In this study, a FEM-DEM coupled numerical model [3] that considers the discrete nature of the granular material, the fibrous and continuous nature of the GTX and the frictional interaction at the interface (rolling sliding and friction) between the soil particles and the finite elements (used to restore the GTX behaviour) is adopted.

The used numerical model (Figure 1) is 1.8 m long, 1.8 m wide and 0.36 m deep and includes, from top to bottom:

1. an assembly of clumps (composed of two overlapped and unbreakable spheres of same diameter D with d is the distance between the center of two particles) describing the behaviour of the granular mattress and interacting through contact points,
2. thin, finite, triangular elements describing the membrane and tension behavior of the GTX,
3. a layer of spheres regularly distributed in a square mesh at the base of the model and associated to springs to represent the supporting soft soil which displace only vertically (no rolling admitted).

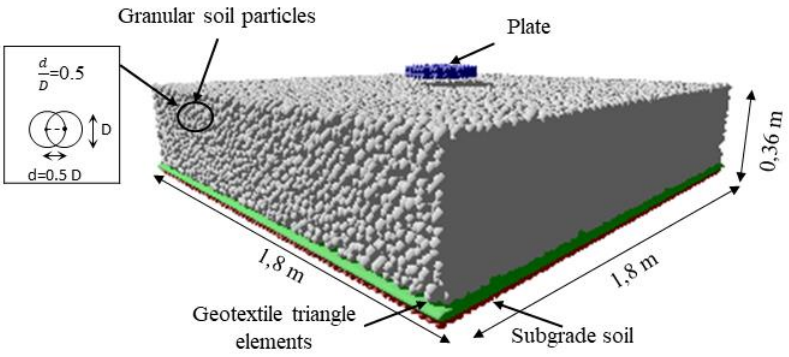

Figure 1. Geometry of the simulated sample and illustration of grain shapes used in simulations

A model for the subgrade soil is deduced from cyclic plate load tests performed directly on the subgrade soil. Based on the comparison between the numerical and experimental results in terms of displacements and stresses, the microscopic parameters of the granular platform have been calibrated. Different simulations have been performed with several number of clumps.

Several key insights are revealed. Firstly, vertical displacements of the mattress particles are observed, with a semi-cone-shaped downward movement initiated by the first loading, followed by an upward movement during unloading. Horizontal displacement primarily occurs toward the model edges in the zone around the loading plate projection where the mattress grains interacted with the geotextile. A reverse horizontal displacement in the same zones occurs after the unloading. As results permanent vertical and horizontal displacement occurs after the 1st cycle. The magnitude of permanent displacement decreases with each cycle due to an increase in subgrade rigidity.

Furthermore, the investigation delves into particle rearrangement, with patterns of densification observed under the loading plate and shear at the zones between the semi-cone and its surroundings.

In addition, principal stress orientations are explored. Shifting patterns in force directions and intensities within the mattress are revealed, suggesting complex force transmission mechanisms. Insights into load transfer through the geotextile are provided, demonstrating its increasing engagement as loading cycles advanced. In addition, the frictional forces acting on the geotextile and the forces related to the tensioned membrane effect are quantified.

Collectively, these findings underscore the capability of the numerical model to accurately represent and simulate the complex behaviours and performance of geotextile-reinforced structures. This reaffirms the valuable role of the model as a tool for comprehending how these applications are influenced under cyclic loading conditions.

3. References

[1] ISO TC221 WG6 N337 PG5 TR 18228-5 - 18 Dec 2019.

[2] Abou Chaz N., Briançon L., Villard P., Silvani C., Nancey A., Abdelouhab A. (2022). Etude expérimentale des plateformes granulaires renforcées par géosynthétique sur sol mou. 11ème Journées Nationales de Géotechnique et de Géologie de l'Ingénieur, JNGG 2022, Lyon, 28-30 Juin 2022.

[3] Villard, P., Chevalier, B., Le Hello, B., Combe, G. (2009). Coupling between finite and discrete element methods for the modelling of earth structures reinforced by geosynthetics. Comput. Geotech, **36**: 709-717.

ON THE USE OF POSIDONIA OCEANICA FIBRES FOR THE MECHANICAL IMPROVEMENT OF SEDIMENTS

J. Karimiazar[1], C. Vitone[1], E. Romero[2], J. Torres-serra[2], R. Petti[1], and A. Fraccica[3]
[1] Politecnico di Bari, DICATECh, Bari, Italy.
[2]Universitat Politècnica de Catalunya, Barcelona, Spain.
[3] Istituto Superiore per la Protezione e la Ricerca Ambientale, ISPRA, Italy.

In the contemporary world, there is a growing emphasis on conserving non-renewable resources and recycling waste materials for various applications, particularly in the field of engineering. Dredged sediments emerge as valuable resources with the potential to mitigate natural resource depletion through their reuse and recycling as secondary raw materials in various applications. Although dredging is crucial for maintaining sustainable navigation systems in marine and river environments, the continuous accumulation of dredged sediments poses environmental risks, underscoring the importance of effective management for marine and river ecosystems. Dredged sediments are complex geomaterials with low strengths, high water content and organic content, and potential contamination. They typically require chemical or chemo-mechanical treatments before their reuse. Standard treatments used for this purpose are based on ordinary Portland cement (PC) [1], but their production and use contribute significantly to CO_2 emissions. As a result, there is a growing interest in exploring alternative binders to reduce reliance on PCs, potentially offering more environmentally friendly solutions. In line with this, the efficacy of mussel shell powder (hybrid solutions), produced without calcination, has been recently demonstrated as a partial substitute for PC for the mechanical improvement of fine-grained sediments [2,3]. This contribution aims to assess the effectiveness of Posidonia Oceanica, another waste of marine origin, as a natural additive in treating fine dredged sediments. Posidonia Oceanica (PO) is an endemic Mediterranean seagrass, whose annual accumulation of leaves reaches the coastline ranges from 5 to 50 million tons [4]. Posidonia needle balls (NB) structures vary in size, ranging from a few millimetres to hundreds in diameter up to 200 mm. The fibre cross-section in balls exhibits dimensions of 100 µm with an average length of 7.7 mm. The maximum load capacity of Posidonia leaves and ball fibres is about 0.3 N and 0.025 N, respectively [5, 6]. Figures 1a-d display a representative image of Posidonia leaves, ball samples and other materials used in this study.

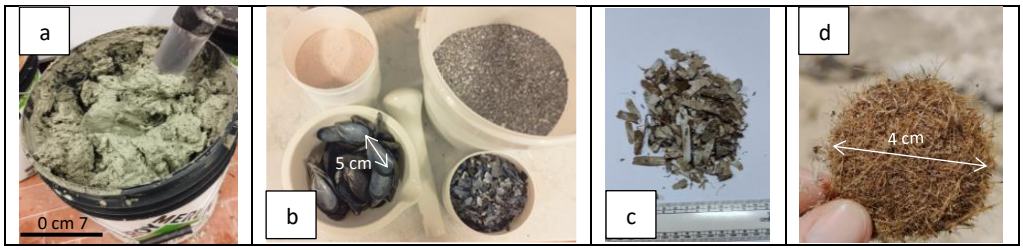

Figure 1. Materials used in this study. A) Sediment, b) Mussel shells (MS) and mussel shell powder, c) Posidonia leaves, d) Posidonia needle balls (NB).

Multiple reuses of PO have already been explored in the literature. Among the various applications, it is used to enhance the ductility of cement paste and mortar [5,7]. Straw fibres have also been tested by [8] to improve the ductility of sediment-cement mixtures. The literature on the use of either artificial (e.g., polypropylene fibre (PF), polyvinyl alcohol (PVA) fibre) or natural fibres as reinforcement of cement or soil-cement mixtures highlights the role of the fibre-length, fibre content, fibre composition on the overall mechanical efficacy of the treatment [8,9]. Moreover, when the scope of the contributions is the mechanical improvement of soils or sediments, an oven-drying

pre-treatment of the geomaterial is generally carried out before the addition of water and additives (cement, fibres, etc.) [8]. This study aims to explore the hydro-mechanical effects of the use of PO on the sediment-shell mixtures and the role of the fibre content and geometry without any pre-treatment of the base soils. The first step of the research, which here is presented, has been that of understanding how to easily select a class of fibre (needle) length starting from natural Posidonia balls collected from the beach. A comprehensive methodology, involving fibre untwisting, high-resolution scanning, and image processing using ImageJ and MATLAB, was carried out on twenty Posidonia balls of different sizes. The results reveal a clear correlation between Posidonia ball diameter and fibre length, with MATLAB preferred for microstructural analyses (Figure 2). This finding seems intriguing for selecting PO fibres for sediment treatments, especially when focusing on target hydro-mechanical properties like tensile strength, ductility, overall mixture strength, water retention and permeability properties. The research is ongoing with analysis at the microscale and hydro-mechanical testing on the fibres, their sensitivity to water content and their impact on the geotechnical properties of sediment mixtures.

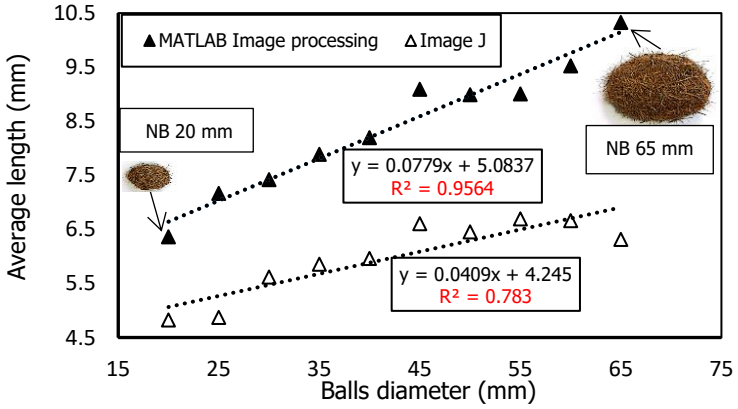

Figure 2. Correlation between the Posidonia needle balls' diameters and length of the fibres.

References

[1] Wang, D., et al. (2020). Strength properties and associated mechanisms of magnesium oxychloride cement-solidified urban river sludge. *Construction and Building Materials*, **250**: p. 118933.

[2] Petti R., et al. (2023). Characterisation tests for mechanical stabilisation of dredged sediments using shell powder. *9ICEG.*

[3] Petti R., et al. (2023). *On the use of mussel shells as green solution to mechanically stabilise dredged sediments*. *Proceedings of the IS-PORTO2023. Porto*, 3rd – 6th September.

[4] Restaino, O.F., et al. (2023). *Sustainable Exploitation of Posidonia oceanica Sea Balls (Egagropili): A Review.* International Journal of Molecular Sciences, **24**(8): p. 7301.

[5] Stefanidou, M., et al. (2021). Use of Posidonia oceanica fibres in lime mortars. *Construction and Building Materials*, **298**: p. 123881.

[6] Benjeddou, O., et al. (2022). Effect of Posidonia oceanica fibres addition on the thermal and acoustic properties of cement paste. *Buildings*, **12**(7): p. 909.

[7] Allegue, L., M. Zidi, & S. Sghaier. (2015). Mechanical properties of Posidonia oceanica fibres reinforced cement. *Journal of Composite Materials*, **49**(5): p. 509-517.

[8] Li, J.-S., et al. (2023). Evaluation of natural and artificial fibre reinforcements on the mechanical properties of cement-stabilized dredged sediment. *Soils and Foundations*, **63**(3): p. 101319.

[9] Park, S.-S., Effect of fibre reinforcement and distribution on unconfined compressive strength of fibre-reinforced cemented sand. *Geotextiles and Geomembranes*, 2009. **27**(2): p. 162-166.

REINFORCEMENT OF ERODED GRANULAR MATERIALS THROUGH FINE GRAINS INJECTION

***A. Hegde*[1], *F. Chen*[1], *N. Benahmed*[1], *A. Wautier*[1] *and P. Philippe*[1]**
[1] *INRAE, Aix-Marseille Université, RECOVER, Aix-en-Provence, France*

Internal erosion processes such as suffusion occur due to the detachment of fines under the influence of seepage forces imparted by water flowing through the soil. Though the fine grains are not a part of the weight bearing force chains, their removal from the granular medium can lead to the onset of material instabilities under certain stress conditions as illustrated by the work of Wautier et.al 2019[1], and Wang et.al. 2021[2].

One way of mitigating the onset of mechanical instabilities in such eroded soil mass would be to reintroduce the same amount of fines back into the granular medium now composing of mainly coarse particles. Addition of even small amount of fines into the soil skeleton should have a stabilizing effect on the granular medium by providing lateral support to the existing force chains.

In this work, various fines injection techniques have been systematically explored under different relative densities(20% and 40%), particle morphology(angular Hostun 1/2.5 and rounded glass beads), and flow conditions. The samples are prepared in layers using the moist-tamping technique and injection is performed with the aid of water flowing along the height of the sample inside a suffusion permeameter device[3]. After the completion of the hydraulic test, the resulting fines content in the sample is determined through sieve analysis. Irrespective of the method of injection used, density of the granular packing and morphology of the particles, the fines content inside the sample is found to be non-homogeneous, and an exponentially decaying profile of fines content is obtained for the injected samples. After the completion of the injection tests, the samples are recovered from the permeameter and subjected to mechanical tests on a triaxial apparatus along different stress paths[4]. The mechanical behavior of the injected samples is then compared against artificially reconstituted soil samples, prepared using the previously determined, mean fines content, in each layer. Note that in both cases, the tested samples are non-homogeneous which implies that the triaxial tests should not be interpreted directly as material point responses. Nevertheless, the differences in the mechanical responses are representative of the different interplay between coarse and fine grains.

In-order to obtain a micro-mechanical perspective of the injection process, Discrete Element simulations(DEM) were performed in parallel to the experiments. Numerical samples, with the same PSD as the glass beads used in our experiments, are generated under dense and loose conditions. Fines of different sizes are injected using YADE's DEM-PFV engine[5] that considers the coupling between fluid flow and grains. We analyze both the lateral and vertical displacements of the injected fine grains to understand their infiltration behaviors in terms of infiltration depth and lateral diffusion. The vertical distribution of fines within the samples is found to follow an exponential decay curve, in accordance with the experimental results. Moreover, larger the size ratio between the injected fines and coarse particle, larger is the observed penetration distance. The injected samples are then subjected to triaxial tests, and their mechanical behaviors are compared with samples generated through fine particles insertion into the coarse soil matrix, following the same vertical distribution. This digital shadow approach enable to provide micro-mechanical interpretation of the differences in microstructure to interpret the differences in the mechanical responses.

References

[1] Wautier, A., Bonelli, S., and Nicot, F. (2018). Micro-inertia origin of instabilities in granular materials. *International Journal for Numerical and Analytical Methods in Geomechanics*, **42**, 1037–1056.

[2] Wang, T., Wautier, A., Liu, S., and Nicot, F. (2021). How fines content affects granular plasticity of under-filled binary mixtures. *Acta Geotechnica*, pp. 1–15.

[3] Nguyen, C. D., Benahmed, N., Andò, E., Sibille, L., and Philippe, P. (2019). Experimental investigation of microstructural changes in soils eroded by suffusion using x-ray tomography. *Acta Geotechnica*, **14**, 749–765.

[4] Benahmed, N., Zuo, J., and Wautier, A. (2022). Instability of granular soil under conventional triaxial and constant stress paths. *International Workshop on Bifurcation and Degradation in Geomaterials*, pp. 74–83, Springer.

[5] Catalano, E., Chareyre, B., and Barthélemy, E. (2014). Pore-scale modeling of fluid-particles interaction and emerging poromechanical effects. *International Journal for Numerical and Analytical Methods in Geomechanics*, **38**, 51–71.

THICKNESS MEASUREMENT OF BIOCEMENT COVERS IN STONE DURING REHABILITATION WORKS USING PHOTOGRAMETRY AND TOMOGRAPHY

M. M. Pinto[1], R. R. Fernandez[2] and R. Cardoso[1,2]
[1] IST, University of Lisbon, Lisbon, Portugal
[2] CERIS, Lisbon, Portugal

1. Introduction

Microbiologically induced carbonate precipitation (MICP) consists of using urease producing bacteria to promote the precipitation of calcium carbonate. This technique has been proposed as an alternative to traditional rehabilitation techniques for stone or masonry old buildings and monuments. When applied to a for such purpose, bacteria must adhere to stone surfaces to act as nucleation sites for the biocement that precipitates around them, sealing cracks and reducing overall porosity [1]. The thickness of the biocement precipitated covering the surface of the treated element reflects the adhesion of this coating. Its measurement is important because biocement is a porous material and it may affect the performance of the treated element, for example to water absorption and thermal isolation. The use of any surface scanning method to inspect layers of precipitated biocement is a challenge due to the small dimensions at stake. In fact, surfaces treated by biocementation have a roughness of less than 1 mm in many cases. Therefore, although it is possible to obtain models of these surfaces and establish comparisons, the reliability of the measured values in absolute terms is not known. The feasibility of using a mobile phone and Structure from Motion photogrammetry (SfM)-based mobile phone application called Eyescloud3D [2] to measure the thickness of the biocement layer precipitated was investigated. The accuracy of the thickness computed using this method was validated through tomography analysis.

2. Methodology

Natural stone (schist) plates with dimensions of 50 x 24 mm^2 and a thickness of 3 mm were submerged for 8 days in biocementation treatment solutions made of: (i) 25 mL of bacterial solution (*Sporosarcina pasteurii)* and (ii) 25 mL of feeding solution prepared with 0.5 M urea and 0.5 M calcium chloride. This procedure allowed to obtain an almost homogeneous coating. The treatment solutions were renewed each two days of treatment. After the treatment the plates were dried in an oven under 100ºC and were completely covered by a biocement layer (Fig 1).

The thickness of this coat was measured using topographic measurements before and after the treatment. Structure from motion photogrammetry (SfM) was adopted to generate 3D topographic models from images obtained with a mobile phone camera [3], after processing the images to obtain 3D point clouds. These clouds were processed with CloudCompare v2.12 software [4]. The differences between the 3D point clouds corresponding to the initial and final surface topographies were computed and the average value corresponded to the thickness of the cover.

X-Ray tomography analysis was done using a CT-Scan equipment, being selected a small part of the plate in the face where the biocement layer was thicker (see Fig. 1). The average value was adopted considering several profiles of the face exposed to the treatment.

3. Main results

Figure 1 presents the photographs of the plate before and after the treatment, in which the

zone investigated by tomography is identified. The point clouds generated using SfM and corresponding topographies are also in this figure. The average thickness of the biocement layer computed using the difference between these two clouds in was 0.353 mm. CT scan images of the portion investigated are also in Figure 1. There it is visible the cross section the porous, almost granular, nature of the biocement, and the strata from the schist. Digital analysis of two of the cross-sections analysed to measure the average thickness of the biocement coating are also presented. The average thickness found was 0.36 mm, which is very close to that measured using SfM.

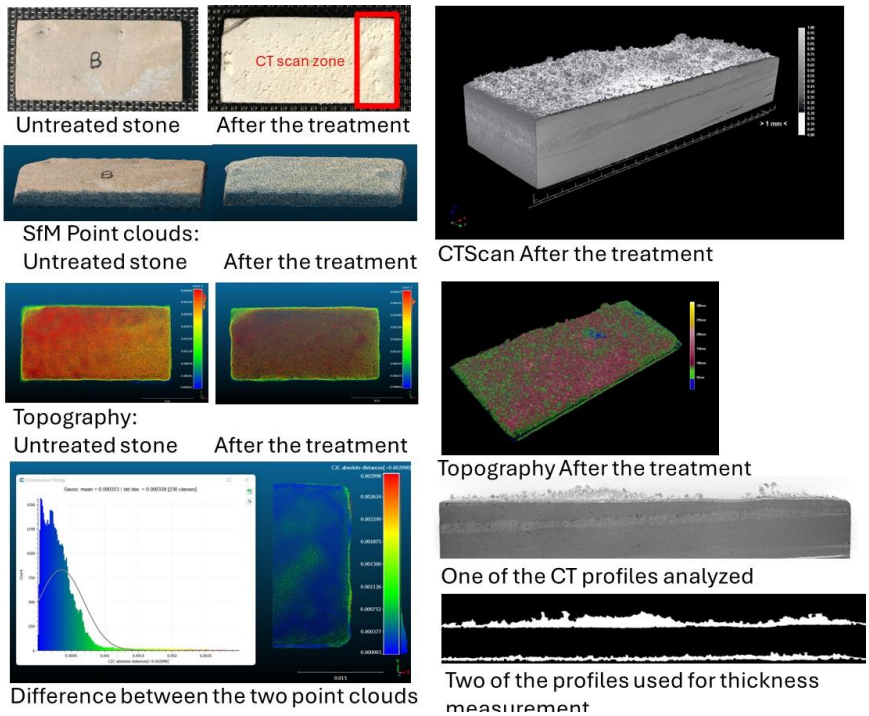

Figure 1. Schist plate covered with a biocement layer and digital analysis using SfM photogrammetry and CloudCompare (Left) and CT-scan (right).

Although only a small area was observed, the thicknesses found using both techniques were very similar. The schist plane analyzed had a flat smooth surface and this may explain such good result. Further analysis is necessary to investigate the potential and limitations of SfM, as well as the effect of the natural roughness of the stone, introducing shadows in the photographs used. A limitation of SfM photogrammetry is that details on the coating texture and porosity cannot be obtained.

The authors thank FCT, I.P. for the funding through CALCITE (Ref. PTDC/ECI-EGC/1086/2022).

References

[1] Ortega-Villamagua E, Gudiño-Gomezjurado M, Palma-Cando A. Microbiologically Induced Carbonate Precipitation in the Restoration and Conservation of Cultural Heritage Materials. *Molecules*. 2020; 25(23), 5499. https://doi.org/10.3390/molecules25235499

[2] Eyescloud3D. Retrieved from https://www.eyescloud3d.com/

[3] Carrivick J, Smith M, Quincey D. 2016. Current Applications of Structure from Motion in the Geosciences. In: Wiley, J., Sons, L. (Eds.), *Structure from Motion in the Geosciences*, pp. 124–158. https://doi.org/10.1002/9781118895818.

[4] CloudCompare (version 2.12) [GPL software]. Retrieved from http://www.cloudcompare.org/

USE OF ALKALI ACTIVATED VOLCANIC ASH BINDER FOR SOIL TREATMENT

E. Vitale[1], C. Rispoli[1], S.F. Graziano[2], P. Cappelletti[1], G. Russo[1]
[1] Department of Earth Sciences, Environment and Resources, Federico II University, Napoli, Italy
[2] Department of Pharmacy, Federico II University, Napoli, Italy

The valorization of waste materials such as natural and artificial materials with pozzolanic activity for the synthesis of alkali activated binders represents a sustainable alternative to the use of traditional binders in the field of soil treatment.

Alkali activated binders are synthesized from the chemical reaction between an amorphous precursor, which is rich in alumina (Al_2O_3) and silica (SiO_2), with a sodium or potassium-based activator [1]. During alkaline activation processes, dissolution of aluminosilicate oxides promotes a polycondensation reaction, which determines in the formation of a sodium aluminosilicate gel with cementitious properties [2, 3].

There are several secondary by-products such as fly ash (*e.g.*, ground granulated blast furnace slag, rice husk ash, crushed glass, etc.), which are commonly used as precursors for alkali activated binders for geotechnical purposes [4,5,6]. Conversely, the use of alkali activation of natural pozzolanic materials as binders for soil treatment is quite limited [7,8,9]. Valorization of natural alumina-silica sources (*i.e.*, pyroclastic deposits) is of practical interest since there is no need for materials pre-treatment (*i.e.*, calcination), with advantages in terms of lower cost, lower carbon dioxide emissions and easy access to the available resources.

In the present study, an insight into the mechanical improvement of a clayey soil induced by the treatment with an Alkali-Activated Binder (AAB) based on a volcanic ash is presented. The precursor selected is the volcanic ash from Mount Etna collected after the eruption of February 2021 [9]. An experimental multiscale analysis on the chemical and mineralogical evolution of the AAB for a deeper comprehension of its interactions with clayey soil particles is developed. Mineralogical evolution of the binder and of the clay-binder system are monitored at increasing curing times by means of X-ray Powder Diffraction (XRPD) and Scanning Electron Microscopy (SEM).

Test results shows a high reactivity of AAB treated soil to promote the formation of secondary mineralogical phases with cementitious properties. The evolution of mechanical performance of treated soils is investigated by performing unconfined compression tests on samples prepared with increasing binder contents and tested at different curing time. The addition of alkali-activated binder increases the shear strength of treated samples since the very short term. Microstructural features and mechanical properties of AAB treated clayey soil highlight the strong correlation between the alkaline activation process and macroscopic evolution of soil behavior. The efficiency of treatment is also highlighted by comparing the mechanical performance induced by alkaline activation with the one promoted by ordinary Portland cement.

References

[1] Provis, J.L., van Deventer, J.S.J. (2014). eds. *Alkali Activated Materials*. Vol.13. RILEM State of the Art Reports. Dordrecht: Springer Netherlands.

[2] Provis, J.L. & Bernal, S. A. (2014). Geopolymers and related alkali-activated materials. *Annu. Rev. Mater. Res.*, **44**:299-327.

[3] Xu, H. & Van Deventer, J.S.J. (2002). Geopolymerisation of multiple minerals. *Miner. Eng.*, **15 (12)**:1131-1139.

[4] Cristelo, N., Glendinning, S., Teixeira Pinto, A. (2011). Deep soft soil improvement by alkaline activation. *Proc. Inst. Civil Eng.-Ground Improv.*, **164 (2)**:73-82.

[5] Rios, S., Ramos, C., Viana da Fonseca, A., Cruz, N., Rodrigues, C. (2019). Mechanical and durability properties of a soil stabilised with an alkali-activated cement. *Eur. J. Environ. Civ. Eng.*, **23 (2)** :245-267.

[6] Coudert, E., Deneele, D., Russo, G., Vitale, E., Tarantino, A. (2021). Microstructural evolution and mechanical behaviour of alkali activated fly ash binder treated clay. *Construction and Building Materials*, **285**:122917.

[7] Miraki, H., Shariatmadari, N., Ghadir, P., Jahandari, S., Tao, Z., & Siddique, R. (2022). Clayey soil stabilization using alkali-activated volcanic ash and slag. *Journal of Rock Mechanics and Geotechnical Engineering*, **14(2)**: 576-591.

[8] Ghadir, P., Zamanian, M., Mahbubi-Motlagh, N., Saberian, M., Li, J., & Ranjbar, N. (2021). Shear strength and life cycle assessment of volcanic ash-based geopolymer and cement stabilized soil: a comparative study. *Transportation Geotechnics*, **31**:100639.

[9] Costa, L.T., Vitale, E., Cappelletti, P., Graziano, S.F., Rispoli, C., Russo, G. (2023). Activation of Volcanic Ash as Binder for Soil Improvement. *Springer Series in Geomechanics and Geoengineering*:792 – 799.

Microstructure characterization

A MICROSCOPIC INVESTIGATION ON THE INTRA-PARTICLE PORE DISTRIBUTION CHARACTERISTICS AND PERMEABILITY OF CARBONATE SAND PARTICLES

Yihang Wu[1] and BeiBing Dai[1,] *

[1] School of Civil Engineering, Sun Yat-sen University, Guangzhou, China

Abstract:

The presence of abundant intra-particle pores is an important feature for carbonate sand particles. A quantitative investigation is undertaken with respect to the intra-particle pore distribution based on the X-ray micro-computed tomography (μCT) technology, as well as its influence on the permeability properties of carbonate sand particles with the pore network model (PNM) simulation. The μCT image analysis results show that the particle porosity for carbonate sand particles can reach a value as high as 0.5. A size dependency of particle porosity has been identified for carbonate sands, which signifies that the particles with their sizes less than 2 mm exhibit an overall lower porosity than the ones whose sizes are larger than 2 mm. The pore structures can be classified into the open pore part and the closed pore part, with the volume of the former being the main component of intra-particle pore volume. The PNM-based simulation reveals that the permeability of pore space in a representative elementary volume is also size-dependent: there exists a positive correlation between particle porosity and absolute permeability for carbonate sand particles when their sizes are smaller than 2 mm; this positive correlation is valid as well for the particles larger than 2mm, whereas the data of permeability vs. particle size exhibit a certain degree of dispersion. It is hoped that a fundamental understanding of the microstructural and micromechanical characteristics of carbonate sand particles can be achieved in this study.

* Corresponding author, daibb@mail.sysu.edu.cn

AGGLOMERATE STRENGTH AND BREAKAGE BEHAVIOUR UNDER MICRO-COMPRESSION AS SEEN BY PHASE-CONTRAST TOMOGRAPHY TO ANALYSE CRACK PROPAGATION

J-Ph. Bayle[1], A. Egele[2], D. Favier[2], T. Weitkamp[3], L. Ramond[1], P. Kekicheff[2,3]

[1] CEA/ISEC/DMRC, Montpellier university, Bagnols sur Cèze, France
[2] Institut Charles Sadron, Université de Strasbourg, C.N.R.S., UPR22, 23 rue du Loess 67034 Strasbourg, France
[3] Synchrotron SOLEIL, Saint-Aubin, L'Orme des Merisiers, 91190 Saint-Aubin, France

(jean-philippe.bayle@cea.fr, Antoine Egele)

1. Context

The reference ceramic fabrication process behave three main stages, grinding, pressing and sintering. The macroscopic pellet compaction (pressing) is based on three main densification step, rearrangements by motion, compaction by strain and agglomerate fractures by compression. The powder took into account in this study is composed of agglomerates with a microstructure based on a mixt homogeneous of TiO_2-Y_2O_3. Each agglomerates have a microstructure composed by un-breakable elementary particles include in breakable aggregates. The agglomerates have been synthetized by the Cryogenic Granulation Synthesis Process (CGSP), **[1]**, which enables to obtain convex agglomerates with the homogeneous and porous parts. To consider the microstructure behaviour of agglomerates powders and their composition, the multi-scaling is used and based on the interactions between agglomerates and fracture phenomena inside the agglomerates due to the ultimate step during the compaction. Macroscopic models are usually used in Finite Element Method (FEM), **[2]**, simulations for the industrial pellet scale. Microscopic models are used in Discrete Element Method (DEM), **[3]**, simulations where powder's granular microstructure is directly taking into account for established the finest behaviour law. To manage these laws in FEM simulations, homogenization is done on Elementary representative volume (ERV) to mesoscopic scale.

2. Investigation

The study began by different diameter agglomerate micro-compressions in CEA Marcoule Atalante facility, with different diameters, tested by quasi-static compression with different velocities and support between the stub (fixed base) and the particle. A second part of this study was to analyse micro-compressions coupled to X-ray tomography in Charles Sadron institute. The acquired knowledge and the limit of the detection guided us to new experimentations with a more intense beam line in synchrotron Soleil, **Fig 1**.

Fig 1 : (Left to right), Agglomerates forest on stub during micro-compression tests in SEM of Atalante facility, tomograph in Charles Sadron Institute, tomograph in Anatomix beam line synchrotron Soleil.

This ultimate part is the result of a collaboration between Strasbourg University (Unistra), Anatomix beam line (Soleil synchrotron) and atomic energy office (CEA) teams. These teams pooled their skills for these investigations **[4]**.

3. Results summary

The post-treatment of micro-compressions was based on Hertz theory according to Antonyuk publications. After yield point and breakage point determinations, also the evolution of contact area during compression in order to determine elasto-plastic parameters. The Weibull distribution of the breakage stresses were plotted and the evolution of the breakage stresses depending on the agglomerates diameters is digressive when the velocities and the diameters increase. The breakage energies of each agglomerates have been computed and with number of breakage facies, a first approach of surface energy has been estimated. The first tomographic investigations enabled the elastic domain quantification where the Hertz model is calibrated. Moreover, this investigation tool is very interesting for crack propagation analyses during micro-compressions. In Link to Soleil analyses, we have been show that results are in agreement to Kendall's theory (compare to Rumpf theory), which argued that the fracture of granule is a consequence of crack nucleation at flaws leading to subsequent crack propagation through the granular structure. The 340µm agglomerate diameter was investigated by one-way cyclic micro-compression test and other agglomerates with a simple load and unload cycle until breakage have been tested. The tomographic post-treatments have enabled the porosities volumes and surfaces created after breakage, the origin of the main crack and its propagation, **Fig 2**.

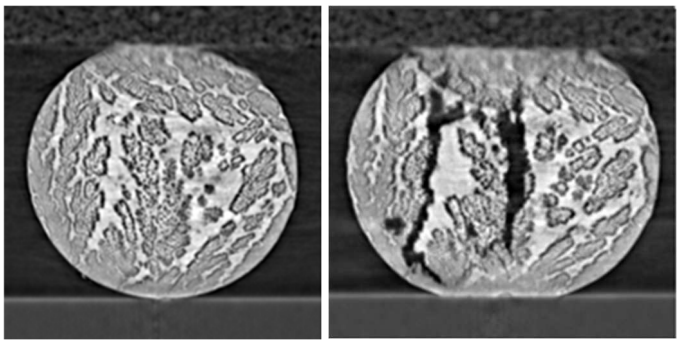

Fig 2: tomography Agglomerate before breakage (left), after breakage (right)

5. Perspectives

A parallel study involved using the discrete element method (DEM) to model the microstructure and simulate the internal interaction in the agglomerates **[3]**. The comparison between the experimental approach and the simulation approach is underway and will be the subject of a forthcoming post-doctorate.

6. References

[1] La Lumia, F., L. Ramond, C. Pagnoux, et G. Bernard-Granger. « Fabrication of Homogenous Pellets Ceramic Society 39, n° 6 (juin 2019): 2168-78.

[2] Bayle J. P., Delette G., « Finite Element Modelling and Experiments for Shaping Nuclear Powder Pellets, Application in Technological Tool Developments to Minimize Damage during Ejection, and Geometrical Tolerances ». Procedia Chemistry 7 (2012): 444-55.

[3] Tran T. D., Nezamabadi S., Bayle J. P., Amarsid L., Radjai F., Contact networks and force transmission in isotropically packed aggregates of hexapod-shaped particles, Soft Matter, 2024

[4] Dabo D., Roland T., Dalongeville G., Gauthier C., Kékicheff P., Ad-hoc modeling of closed-cell foam microstructures for structure-properties relationships, Eur. J. Mechanics A Solids 2019, 75, 128.

An investigation of the micro-mechanical contact behaviour of railway ballast particles

Aziz Hakimi[1], Saurabh Singh[1], Béatrice A. Baudet [1], Matthew R. Coop[1]
[1]University College London, WC1E 6BT, UK

Introduction

Incentives for reduced maintenance of railway ballast have prompted the need for more fundamental research in their behaviour. Ballast is made up of discrete particles, and researchers have often used the Discrete Element Method (DEM) in an attempt to predict their mechanical behaviour. Recent developments include implementing more realistic shapes of ballast into the simulations [1], however there is experimental evidence that the contact laws used in DEM may not represent well their behaviour [2,3], at least for one type of granitic ballast. It is generally the case that the source material for railway ballast is geographically close to its application, so that different countries tend to use very different types of ballast, e.g. granitic ballast in the UK, basalt ballast in Australia or andesite ballast in Iran. This paper presents unique experimental data obtained on pairs of basalt ballast from Australia subjected to normal and tangential loading, monotonic and cyclic, that will inform discrete element modellers and allow them to improve existing numerical models. The load-deflection response and evolution of particle surface roughness are presented.

Methodology

The micro-mechanical behaviour was studied through innovative experimental methods, using the inter-particle apparatus developed at UCL (Figure 1; [2]). Loading can be applied in three orthogonal directions with an accuracy of 0.01-0.02 N while deformations are measured using transducers with an accuracy of about 10^{-2} μm. A natural angular to flat contact was used in the experiments, selecting the apex of the natural ballast as the contact point. Normal loading was load-controlled while shearing was displacement-controlled. Pairs of basalt railway ballast were subjected to normal loading followed by monotonic or cyclic tangential loading, for different stress levels.

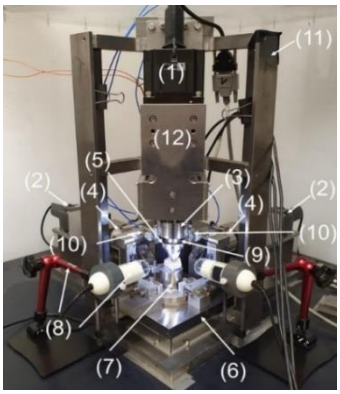

Figure 1. Interparticle loading apparatus [2]: (1) vertical and (2) horizontal linear actuator; (3) vertical and (4) horizontal load cells; (5) vertical displacement transducer; (6) sled; (7) bottom platen; (8) digital microscope camera and stand; (9) top platen; (10) horizontal displacement transducer; (11) stainless steel frame; (12) front plate

Both top and bottom particles were observed by optical microscopy before and after test, and their roughness within the contact area compiled by the use of z-stacking, with an accuracy of 6μm.

Results and Discussion

During normal loading, a softer response than that predicted by Hertz's (1882) theory is observed at the contact. The change in surface roughness during normal testing was evaluated, where the apex of the angular particle was selected as the expected area of contact against the flatter surface. Roughness was determined in terms of root mean square of heights (S_q) and fractal dimension (D_f), which indicates the density of asperities. It was found that the surface roughness S_q decreases during

compression, which was attributed to the flattening of the asperities. The value of D_f also decreased, indicating a less irregular surface.

During monotonic tangential loading, the ratio of tangential (T) to normal (N) load increases then stabilises at a coefficient of interparticle friction (μ) of about 0.5-0.6. During cyclic shearing, the value of μ changed in the first few cycles, then tended to stabilise while the vertical displacements at the contact kept increasing as the cycles continued, indicating abrasion. The coefficient of sliding resistance, μ, typically increased with the cycle number, then tended to stabilise around 0.75-0.85 (Figure 2) after about 30 cycles. Measurements of roughness before and after cyclic test show that plastic deformation has occurred, mostly at the asperities.

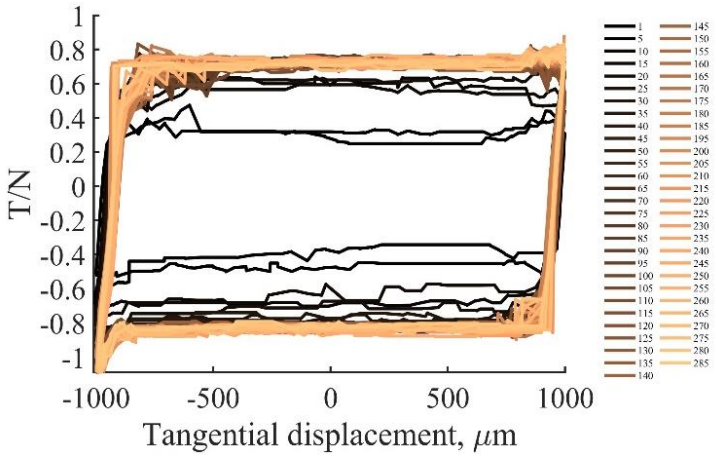

Figure 2. Evolution of load-displacement response with cycle number under a normal load of 100 N (low cycle numbers in dark colour, high cycle number in light colour)

Conclusion

The behaviour of basalt ballast shows similarities with granite ballast behaviour, such as the softer behaviour than that predicted by Hertz model, but distinct features were also found, notably the increase in surface roughness irregularity with shear loading and the smaller cycle numbers to stabilisation.

References

[1] Tolomeo, M. & McDowell, G.R. (2022). Modelling real particle shape in DEM: a comparison of two methods with application to railway ballast. *International Journal of Rock Mechanics and Mining Sciences* 159.

[2] Wong, C.P.Y., Boorman, B. & Coop, M. R. (2019). The construction and commissioning of a new inter-particle loading apparatus for the micromechanical behaviour of railway ballast. In Atlanta, USA, *IS Atlanta* 2018, a symposium on geomechanics from micro to macro in research and practice.

[3] Altuhafi, F.N., Baudet, B.A. & Coop, M.R. (2023). An investigation of the applicability of contact models to the normal load-deflection behaviour of artificially shaped granite. *Acta Geotechnica* [doi 10.1007/s11440-023-02123-9].

CHARACTERISING THE INHERENT VARIABILITY OF FILTRATION PROCESSES IN GRANULAR MEDIA USING GRAPH CONCEPTS

M. Artigaut [1] ***and A. Sufian*** [1,2]
[1] *The Univ. of Queensland, Brisbane, Australia*
[2] *The Univ. of New South Wales, Sydney, Australia*

1. Introduction

In geotechnical engineering, the structural integrity of embankment dams depends on the ability of filters to mitigate the risk of internal erosion failure. Filters are designed to trap finer particles within the pore space of coarser particles. While the Discrete Element Method (DEM) provides a platform for particle-scale investigation, current literature [1, 2, 3] does not recognise the inherent variability of the filtration process through consideration of singular experiments.

Recent findings [4] have demonstrated the importance of considering multiple stochastically generated base-filter realisations in DEM studies before drawing conclusions about the performance of filters. The initial filter particle positions of DEM simulations were shown to have a significant effect on filter performance [4]. The particle positions dictate the void space within which the filtration process occurs, and therefore, a study of the variation of void space structures would shed light on the relationship between particle positions and filter performance.

Graph concepts have the potential to quantify the inherent variability of the filtration process. Graph concepts have been used to describe complex processes on the granular particle contact network [5]. Preliminary research showed links between sample permeability and transient graph characteristics such as closeness centrality [6]. A similar study of the correlations between filter performance and pore network characteristics could yield meaningful insight into the inherent variability of the filtration process.

2. Pore Network Construction and Graph Characterisation

This study will apply graph concepts to the simulation in Holden et al. [4] to characterise the inherent variability of filter performance in granular media. A set of 12 independent filter realisations of quasi-monodisperse particles were created using the DEM package LIGGGHTS, in which the only difference was the initial particle positions. A filtration process was performed under the sole influence of gravity and the filter efficiency was assessed. The DEM simulation data produced at the steady-sate [4] will be the basis of the graph characterisation.

Pore Network (PN) models are built from the DEM data by simplifying the geometrically complex void space in to a set of individual pores (network nodes), connected via constrictions (network edges). For the current study, the individual pores are identified using a radii-weighted Delaunay tessellation [7]. The PN is optimised for the study of gravity-driven filtration by considering directed and weighted network edges. Additional geometrical information is extracted from the complex void space including constriction area, average pore characteristics and various conductance models [8, 7, 6, 9].

In this study, graph concepts are used to characterise the PN and explain the inherent variability of filtration behaviour in granular media. At the micro-scale, pore and constriction importance is investigated through centrality measures, including the closeness centrality and betweeness centrality. To tie in with the macro-scale observations of filter efficiency considered by Holden et al. [4], meso- and macro-scale characteristics are also considered: maximum-flow-minimum-cut, maximum-flow-minimum-cost, motifs and equivalence.

The preliminary findings of this investigation are:

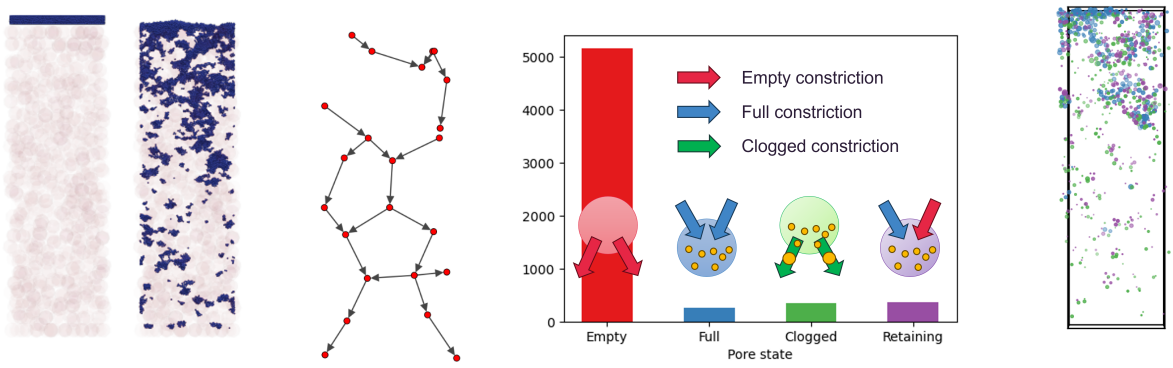

(a) (b) (c) (d)

Figure 1. (a) The filtration process at $t = 0\,s$ and $t = 10\,s$ [4]; (b) a subset of the PN with gravity-directed edges; (c) identification and (d) spatial distribution of retaining, full and clogged pores.

- The importance of considering directed weighted networks for filtration characterisation;
- The importance of spatial decomposition to account for the inherent effect of upstream behaviour on the downstream processes during filtration;
- A systematic identification of clogged, retaining and empty pores/constrictions;
- The inherent variability of the filtration process is further highlighted in the coefficient of variation of graph characteristics;
- Correlations have been observed between various graph characteristics (in particular, the max-flow-min-cost and max-flow-min-cut) and filter performance.

References

[1] Lominé, F. and Oger, L. (2006). Transport of small particles through a 3D packing of spheres: Experimental and numerical approaches. *Journal of Statistical Mechanics: Theory and Experiment*.

[2] Roozbahani, M. M., Graham-Brady, L., and Frost, J. D. (2014). Mechanical trapping of fine particles in a medium of mono-sized randomly packed spheres. *International Journal for Numerical and Analytical Methods in Geomechanics*, **38**, 1776–1791.

[3] Kerimov, A., Mavko, G., Mukerji, T., and Al Ibrahim, M. (2018). Mechanical trapping of particles in granular media. *Physical Review E*, **97**.

[4] Holden, S. A. W., Sufian, A., and Scheuermann, A. (2023). The importance of initial particle position on filter performance in granular soils. *Computers and Geotechnics*, **162**, 105632.

[5] Papadopoulos, L., Porter, M. A., Daniels, K. E., and Bassett, D. S. (2018). Network analysis of particles and grains. *Journal of Complex Networks*, **6**, 485–565.

[6] van der Linden, J. H., Sufian, A., Narsilio, G. A., Russell, A. R., and Tordesillas, A. (2018). A computational geometry approach to pore network construction for granular packings. *Computers & Geosciences*, **112**, 133–143.

[7] Chareyre, B., Cortis, A., Catalano, E., and Barthélemy, E. (2012). Pore-Scale Modeling of Viscous Flow and Induced Forces in Dense Sphere Packings. *Transport in Porous Media*, **92**, 473–493.

[8] Bryant, S. L., King, P. R., and Mellor, D. W. (1993). Network model evaluation of permeability and spatial correlation in a real random sphere packing. *Transport in Porous Media*, **11**, 53–70.

[9] Sufian, A., Knight, C., O'Sullivan, C., van Wachem, B., and Dini, D. (2019). Ability of a pore network model to predict fluid flow and drag in saturated granular materials. *Computers and Geotechnics*, **110**, 344–366.

Correction for particle surface topography in inter-particle tangential shearing tests

S. Singh[1], B.A. Baudet[1] and M.R. Coop[1]

[1] University College London, Chadwick Building, Gower Street., London, United Kingdom

1. Introduction

In the apparatus developed to investigate the contact behaviour of geomaterials, such as that described in [1, 2, 3] forces are typically applied along one or two horizontal directions and a vertical direction. The forces are resolved using the profile of particles along direction of sliding; however, the force along the out of plane (of sliding) has been generally ignored [1, 2, 3]. Here, a correction for topography of the two particles is proposed which includes force along the out of plane direction.

2. Experimental equipment and material tested

Test data were obtained from the inter-particle apparatus developed by Wong and Coop [3]. In this study, two quarzitic sands from the UK and from Germany were tested in tangential shearing.

3. Experimental procedure and correction for topography

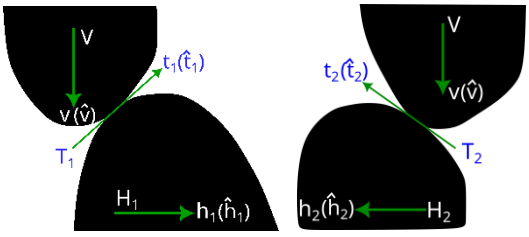

Figure 1. Particle schematic from two orthogonal directions

In the inter-particle apparatus, the top particle is restrained to move in the vertical direction and the base particle is restrained to move in the horizontal plane (two orthogonal horizontal directions) (Figure 1). In the following, the displacement (vertical) of the top particle is denoted by v, and the displacement of the base particle, along two actuators arranged orthogonally in the horizontal plane, is denoted by h_1 and h_2. The two particles are brought in contact by moving the top particle in displacement control mode until a threshold vertical force of 1-3 N, then force control is applied to achieve the desired vertical load. Subsequently, tangential shearing is carried out by moving the base particle along the h_1 direction $(\hat{h}_1)$, keeping the h_2 displacement zero while the top particle moves to keep the contact under a fixed vertical load (V). It has been misconstrued that the displacements in the plane h_1 - v is the profile of the base particle; however, it can be shown easily that it is not the case. Also, it can be shown that $\frac{dv}{dh_1}$ is the tangent $(\hat{t}_1)$ at the contact along $\hat{h}_1$, but the tangent along $\hat{h}_2$ $(\hat{t}_2)$ should also be calculated to obtain the orientation of the contact plane. The tangent $\hat{t}_2$ can give rise to a horizontal force H_2, which affects the tangential force (T) and the normal force (N) (Figure 2). During tangential shearing, the condition $h_2 = 0$, i.e. equilibrium along (h_2, v) plane, can be used to determine the tangent along the $\hat{t}_2$. Further, the direction of contact normal $\hat{n}$ can be determined by the cross product of the $\hat{t}_1$and $\hat{t}_2$. The resolved contact forces (T_1, T_2, N) along tangential and normal directions can be determined using forces (H_1, H_2, V) and orientation of contact plane $(\hat{t}_1, \hat{t}_2, \hat{n})$.

4. Experimental results

The results from the tangential shearing tests, in Figure 2, show how, when the horizontal force H_2 is non-zero, the topography correction discussed above has for effect to have T_2 going to zero, as would be expected. The H_2 force becomes significant at higher normal loads such as 50-200N (common while testing e.g. ballast particles), which results in erratic sliding force by conventional correction ([2]). Further, with proposed correction, T_1 becomes significantly stable than H_1(Figure 2).

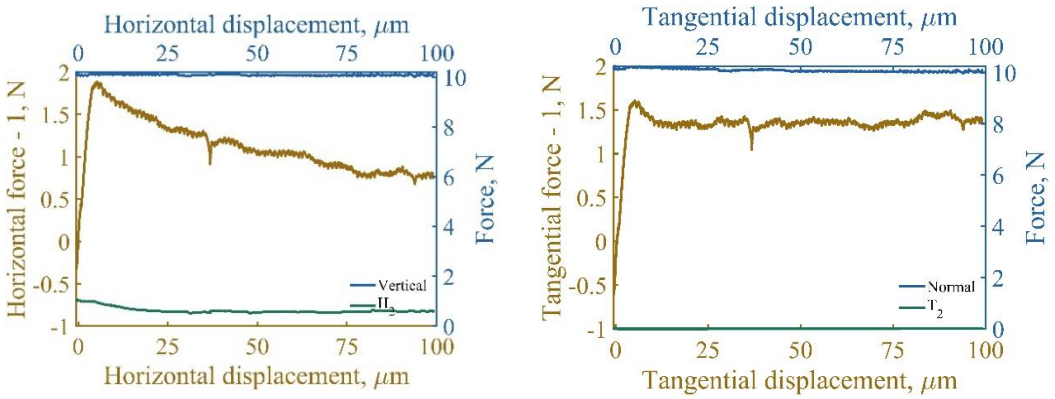

(a) UK sand (left: before correction; right: after correction)

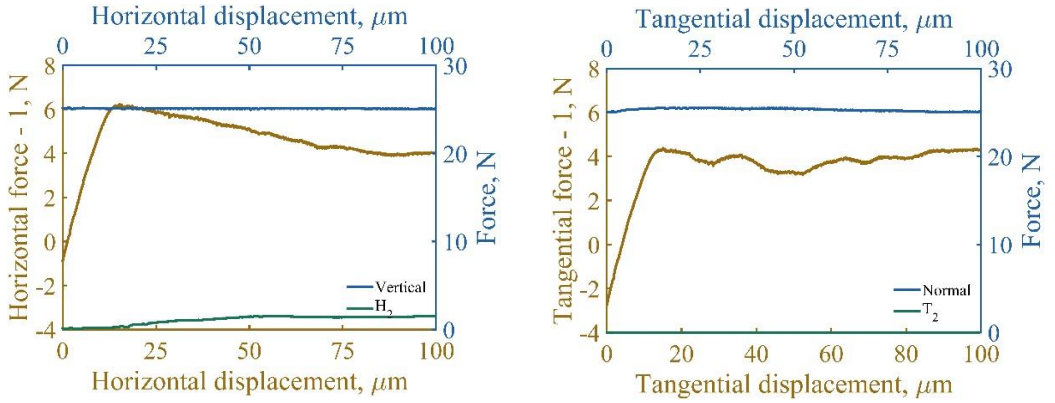

(b) German sand (left: before correction; right: after correction)

Figure 2. Tangential shearing before and after correction (H_2, V, T_2, N are on right-top axes)

5. Conclusions

This extended abstract summarizes the procedure for topography correction for tangential shear loading in inter-particle apparatus. This correction results in a more accurate set of normal and tangential forces along with consistence coefficient of friction in several tests.

6. References

[1] Cole, D.M., Mathisen, L.U., Hopkins, M.A. & Knapp, B.R. (2010). Normal and sliding contact experiments on gneiss. *Granular Matter*, **12**; 69-86.

[2] Senetakis, K., Coop, M.R. & Todisco, M.C. (2013). The inter-particle coefficient of friction at the contacts of Leighton Buzzard sand quartz minerals. *Soils and Foundations*, **53(5)**; 746-755.

[3] Wong, C.P. & Coop, M.R. (2023). The contact mechanics of a UK railway ballast. Géotechnique.

Creating Controlled-Double-Structured Soils through 3D Printing

M. Starvaggi[1], M. Rosone[2] and A. Ferrari[1,2]
[1] Department of Engineering, University of Palermo, 90138 Palermo, Italy
[2] Soil Mechanics Laboratory, Ecole Polytechnique Fédérale de Lausanne, 1015 Lausanne, Switzerland

Abstract

It is a widely held view that fabric is one of the major aspects that govern the geomechanical behaviour of soils [1] and this holds especially true for soils with clear multi-structured fabric. To date, experimental studies have used fundamentally compacted soils on the dry side of the Proctor curve to observe the behaviour of double-structured soils [2], and the way to control the openness of the two-pore size networks was to act on the value of water content and load of compaction to control the micro and the macrostructure [3]. In this context, this work assesses the feasibility of employing the concept of 3D printing of soils as an automated procedure for creating fabric-controlled samples with varying degrees of structural openness. Specifically, 3D printed soils are made with an additive manufacturing technique that involves extrusion processes. This results in a soil made of different filaments, thus a well-marked double-structure soil (Fig. 1a), where the particle arrangement inside the single filament represents the microstructure while the arrangement of multiple filaments represents the macrostructure. Previous studies on 3D printed soil have shown that for the as-printed state, the microfabric of a single filament of a 3D printed soil is highly affected by the extrusion process [4], whereas the macrostructure is governed by the designed path chosen for the printer to follow [5]. The methodology proposed in this work involves both analytical and experimental evaluation of the index properties for 3D printed samples (an example is given in Figure 1a).

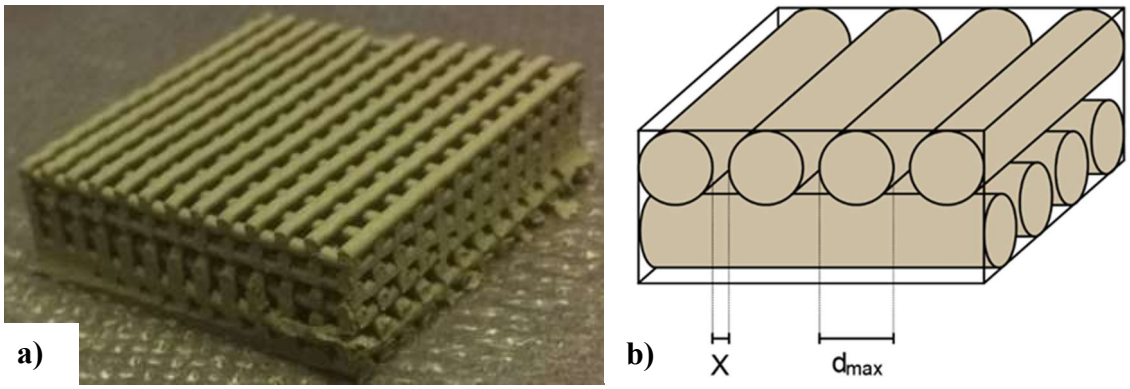

Figure 1. a) An example of a 3D printed sample. b) Schematization of the geometry for a 3D printed sample. The term X represents the distance between each filament and d_{max} is the maximum diameter of the cross-section of the filaments.

According to the geometry shown in Figure 1, macrostructural openness can be varied by changing the spacing between the filaments while keeping constant the microstructure, which means keeping constant the characteristics of single filaments. The analytical evaluation of the index properties is made possible by schematizing the geometry of Figure 1a with the one reported in Figure 1b and computing the macroporosity n^M as the ratio of the volume of macro voids to the total volume of the schematized sample. The microporosity n^m (the ratio of the volume of microvoids to the total

volume) can be evaluated by assuming full saturation of micropores inside each filament and knowing the water content, following the procedure reported in [5]. Then, the total porosity *n* is computed as the sum of micro and macroporosity. In this study, the 3D printer for soil *Delta-WASP2040-Clay* was used with commercial clayey soil as a printing material. Samples with different spacing between filaments were 3D printed and their relative index properties were measured.

To test the ability to produce samples with targeted porosities (micro and macro) by 3D printing, analytical prediction based on the printing parameters (X and d_{max}) and the experimental values of the index properties were compared. Figure 2 shows the results in terms of total porosity *n*, demonstrating a good agreement. These preliminary results prove that the creation of fabric-controlled samples by using the 3D printing technique may be a viable approach to advance the current knowledge of double-structure soils.

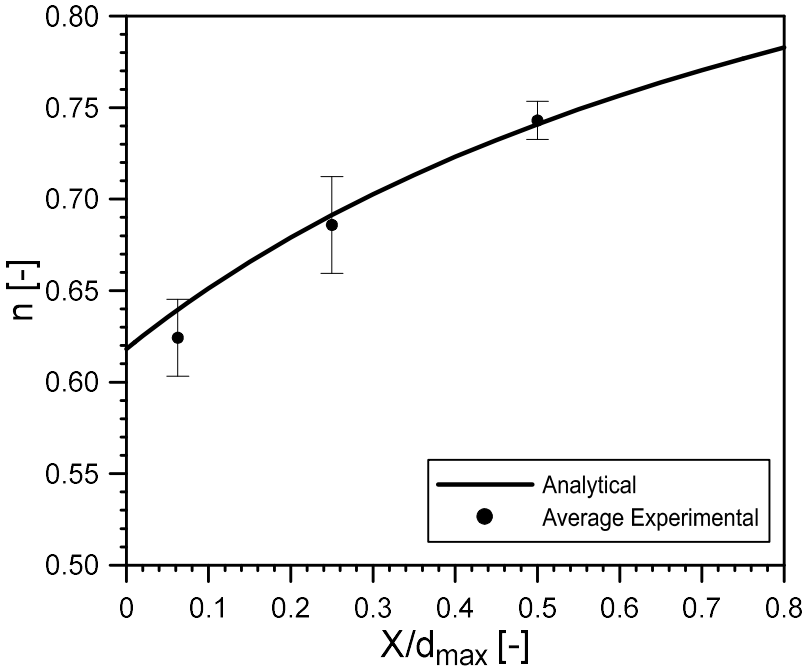

Figure 2. Analytical and average experimental value of porosity for a 3D printed soil for different openness of macrostructure.

References

[1] Collins, K. & McGrown, A. (1974). The form and function of microfabric features in a variety of natural soils. *Géotechnique* 24, No.2, **1**:223-254.

[2] Delage, P., Audiguiner, M., Cui Y. J. & Howat M. D. (1996). Microstructure of a compacted silt. *Can. Geotec. J.*, 33 **1**:150-158.

[3] Romero E. & Sims, P. H. (2008). Microstructure Investigation in Unsaturated Soils: A Review with Special Attention to Contribution of Mercury Intrusion Porosimetry and Environmental Scanning Electron Microscopy. *Geotechnical and Geological Engineering.* Vol 26, Issue 6, **1**:705-727.

[4] Ferrari, A., Rosone, M., La Rosa, S. & Sapienza, G. (2022). Microstructural characterization of a 3D-printed soil. *Soils and Rocks.*, Vol 45, Issue 4 **1**:1-6.

[5] Starvaggi, M., La Rosa, S., Rosone, M. & Ferrari A. (2023). On the Fabric of a 3D Printed Soil. *Geotechnical Engineering in the Digital and Technological Innovation Era.*, **1**:135-142.

EFFECT OF NORMAL CONFINEMENT ON THE MICROMECHANICAL CONTACT BEHAVIOUR OF NATURAL SANDS

V. Nardelli[1] and M.R. Coop[2]

[1] University of Oxford, Department of Engineering Science, Oxford, United Kingdom

[2] University College London, Department of Civil, Environmental and Geomatic Engineering, London, United Kingdom

1. Abstract

Nowadays, discrete element approaches are commonly adopted for the analysis of sands and granular materials, thanks to the increasing popularity of the Discrete Element Method (DEM, [1]). A large amount of research has been developed during the past few decades in order to refine the original method and determine aspects of the behaviour of granular materials at the particle-scale that were either unknown or fully understood previously, with the purpose of aiding DEM modellers. Several new experimental studies have been published on the micromechanical response of sand particles, after some earliest attempts carried out during the 1970's, which benefited from the development of modern technologies. Some of these studies focussed on the determination of the contact response of sands [2, 3, 4]. Data for materials having different composition and origin were obtained, studying mostly the response of particle pairs in compression and shearing. These results have also been compared to those predicted using analytical models and discrepancies were sometimes found, considering that natural sands are complex materials, and that the most popular contact models were not developed for soils, but for materials that were ideal.

This study investigates the role of normal confinement on the contact response of real sand particles. The experimental data were obtained carrying out laboratory tests on real sand grains using a custom-made inter-particle loading apparatus, which was capable of applying different combinations of loads and displacements at the particle contacts [4]. The apparatus was equipped with three linear actuators for the application of either forces or displacements along three orthogonal directions and, along each directions, a set of high-resolution load cells and non-contact eddy-current displacement sensors was installed, for the measurements of forces and displacements, respectively. Particle pairs were tested at their contacts, and the typical experiments carried out were normal loading tests, for the determination of the particle pairs response in compression, and tangential loading tests, during which one particle was sheared over another after the application of a constant normal load at their contact.

In order to understand the role of normal confinement on the mechanical response of natural sands, some additional test types were performed. Cyclic normal loading tests up to large contact loads (above 20 N) were carried out for determining the impact of the loading history on the contact response in compression and the so-called "friction tests" were performed for studying the effect of normal loading during shearing. The friction tests were performed increasing the magnitude of normal confinement while shearing one particle over another at their apexes. Different materials were tested, highlighting the differences between particles characterised by hard minerals and relatively low roughness (e.g., Leighton Buzzard sand, LBS) and particles that were softer and rougher (e.g., carbonate sand, limestone).

The results show that harder and relatively less rough materials, such as LBS, exhibit a behaviour that is almost fully reversible in normal loading. On the other hand, for softer and rougher materials, such as limestone, significant plastic deformations and surface damage could be observed

(Fig. 1). The results of tangential loading and friction tests have shown that the coefficient of inter-particle friction decreases for increasing normal confinement during shearing and this suggests that a curved failure envelope might provide a better interpolation of the results compared to the typical linear fitting. Also, the results suggest that the tangential stiffness does not increase linearly with the increase of normal confinement.

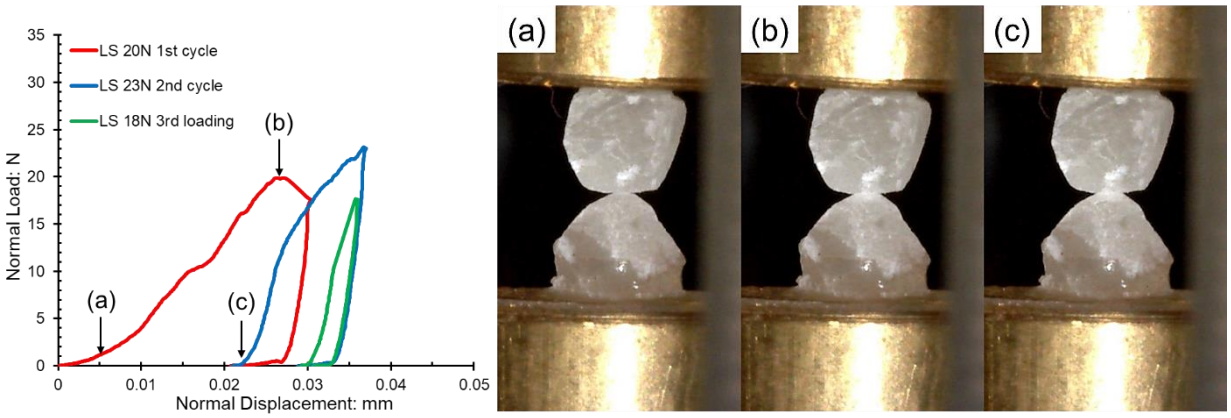

Figure 1. Cyclic normal loading test performed on limestone particle pairs and evolution of damage at the particle contact (a to b). The opening of a fissure right below the contact on the lower particle can be observed after the removal of the normal load (c).

2. References

[1] Cundall, P. A. and Strack, O. D. L. (1979). A discrete numerical model for granular assemblies. Géotechnique, **29**, No. 1, 47–65.

[2] Cavarretta, I., Coop, M. R. and O'Sullivan, C. (2010). The influence of particle characteristics on the behaviour of coarse-grained soils. Géotechnique, **60**, No. 6, 413–423.

[3] Senetakis, K., Coop, M. R. and Todisco, M. C. (2013). Tangential load–deflection behaviour at the contacts of soil particles. Géotechnique Letters, **3**, No. 2, 59–66.

[4] Nardelli, V., and Coop, M.R. (2019). The experimental contact behaviour of natural sands: normal and tangential loading. Géotechnique, **69** No. 8, 672–686.

EVOLUTION OF PARTICLE MORPHOLOGY OF PUMICE SUBJECTED TO TORSIONAL SHEAR

H. Hashimoto[1], M. Otsubo[2] and R. Kuwano[3]
[1] The University of Tokyo, Dept. of Civil Engineering, Tokyo, Japan
[2] Public Works Research Institute, Soil Mechanics and Dynamics Research Team, Tsukuba, Japan
[3] The University of Tokyo, Institute of Industrial Science, Tokyo, Japan

1. Introduction

Volcanic pumice soils are widely distributed throughout the world and often cause landslides, debris flows and other geo-disasters. Pumice particles are characterized by their porous structure and high crushability. In recent years, many studies have been carried out on the phenomenon of particle morphology changes in sand due to particle breakage. However, studies on the porous pumice particles have been very limited [1], and the effects of shearing and particle breakage have not been considered. In this study, a series of torsional shear tests of pumice soils was carried out and the changes in particle shape and intra-void ratio were quantitatively analyzed using X-ray μCT of randomly selected particles from the pre-test and post-test samples.

2. Testing procedure

In this study, an artificial pumice soil with porous and crushable particles was used. It was made by mixing non-plastic silt (DL clay), high-early strength cement and water and curing it for seven days. The results of single particle crushing tests showed that the particle crushing strength of most of the 1.18-2.00 mm particles was very weak, below 1 MPa. Hollow cylindrical specimens (15 cm in height, 10 cm in outer diameter, and 6 cm in inner diameter) were prepared from reconstituted samples of artificial pumice soil using the air-pluviation method. Then, the specimen was saturated, isotropically consolidated at 500 kPa and subjected to drained torsional shear to a shear strain of 30 %.

Sixteen particles of artificial pumice soil, 1.18-2.00 mm in diameter, were randomly selected before and after the test and X-ray μCT scans were performed using Skyscan 1172 with a resolution of 3 μm/voxel. The intra-particle void ratio of the particles was calculated as follows:

$$e_{\text{intra}} = (V_{\text{app}} - V_{\text{solid}})/V_{\text{solid}} = (V_{\text{app}} - M/\rho_s)/(M/\rho_s) \quad (1)$$

where V_{app} is the apparent volume of the particle, determined by extracting the contours of the particles; V_{solid} is the estimated solid volume of the particle, calculated by dry mass of the particle M and solid density of the particle ρ_s. ρ_s was determined to be 2.691 by standard density test of soil particle using pumice particles that had been crushed to reduce the internal voids as much as possible. Three principal dimensions (a>b>c) was obtained using principal component analysis (PCA), and two aspect ratio indices were used, i.e., elongation index ($EI = b/a$) and flatness index ($FI = c/b$). Particle compactness was quantified with convexity index $C_X = V_{\text{app}}/V_{\text{CH}}$, where V_{CH} is the volume of the particle's convex hull.

3. Results and conclusions

The relationships between shear stress, volumetric strain, axial strain and shear strain are shown in Figure 1. A photograph of the specimen after shearing and the particle size distribution (PSD) curves before and after the test are shown in Figure 2. The specimens exhibited significantly

contractive behavior due to shear-induced particle breakage, leading to a residual shear strength without any clear peaks. The void ratio of the specimen was initially 2.33 (Dr = 64%), but contraction due to consolidation reduced it to 1.71, and contractancy during shearing further reduced it to 1.38. The reduction in the void ratio was attributed to particle breakage, and the amount of particle breakage was particularly large in the shear band.

Table 1 shows the average values of the intra-particle void ratio and shape indices of randomly selected 16 particles from the pre-test samples and the post-test shear band samples, respectively. For particle shape indices, standard deviations are given in brackets. The average intra-particle void ratio of the particles became smaller, suggesting that even if the particles did not undergo particle breakage, they might have been deformed and the void space within the particles was decreased. Not much change was observed in *EI* and *FI* values. The C_X values became larger, indicating that particles might have become more compact as a result of chipping or abrasion. Future studies will be conducted for various types and grain sizes of pumice soils.

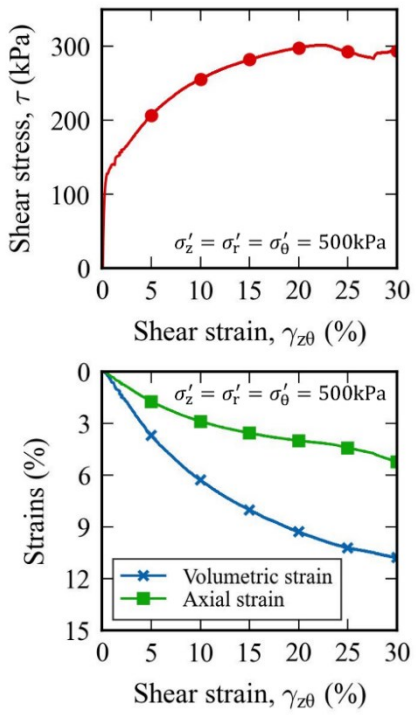

Figure 1. Stress-strain relationships.

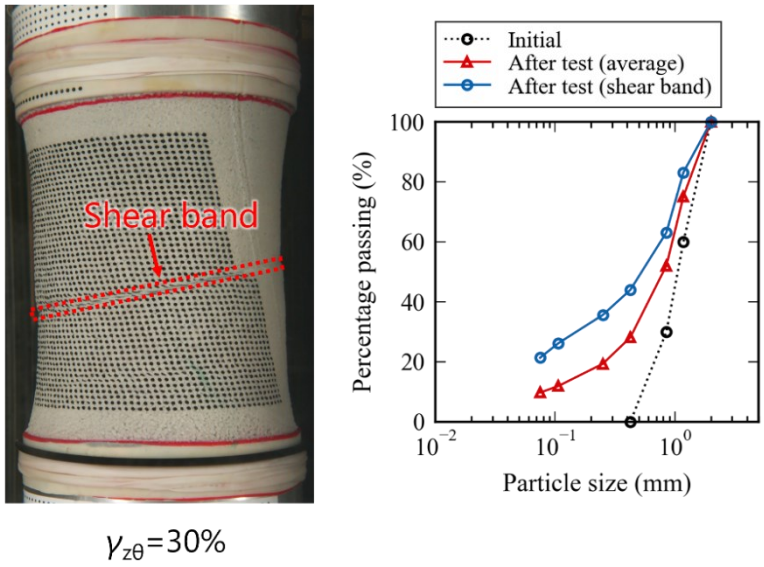

Figure 2. Image of the specimen and evolution of PSD.

Particles	Intra-particle void ratio	*EI**	*FI**	C_x*
Before tests	0.73	0.82 (0.09)	0.80 (0.10)	0.73 (0.06)
After tests (shear band)	0.66	0.83 (0.09)	0.84 (0.11)	0.81 (0.03)

* The number in brackets represents the standard deviation.

Table 1. Evolution of the average value of intra-particle void ratio and particle shape indices.

4. References

[1] Kikkawa, N., Orense, R.P., Pender, M.J. (2013). Observations on microstructure of pumice particles using computed tomography. *Can. Geotech. J.,* **50**:1109–1117.

Examination of Silt-size Particle Matrices Using X-ray µ-CT Imaging: Advancements, Selected Findings, and Challenges.

Ana Valverde[1], Dharma Wijewickreme[2*]
(1) Geotechnical Engineer, WSP Canada, Canada. (2) Professor, University of British Columbia, Canada.
*corresponding author: dharmaw@civil.ubc.ca

Recent resarch work has shown that the mechanical behaviour of silts, including earthquake response, is significantly influenced by the soil particle fabric (i.e., spatial arrangement of individual particles) in addition to the well-known effects arising from void ratio and effective confining stress. Although the fabric of sandy soils have been studied widely, the research work conducted on the fabric of silt matrices (particle size ~2 to 74 µm) is scarce. With this background, a research program is underway at the University of British Columbia (UBC), Vancouver, Canada to systematically investigate the fabric of silt particle matrices. The work is accompished with the aid of non-destructive, X-ray micro-computed tomography (micro-CT) imaging technology. The end objective is to pave the way to fundamentally examine the silt particle matrices of natural silts, and in turn, support the characterization of the mechanical (stress-strain) behavior of silts in geotechnical engineering.

This paper presents some selected findings from the micro-CT imaging of matrices of commercially available, pre-calibrated, standard size silt material. Due to the lack of previous experience on the imaging of silt matrices, much of the initial research effort at UBC had to be expended in developing procedures and protocols for imaging and digital segmentation of particles from the images. The visualizations performed on images of spherical silt particle matrices having uniform gradation (mean particle size of 50 µm) provided useful insights on the capability of micro-CT imaging to capture the key particle parameters (e.g., particle size, shape, volume), confirm the uniformity of specimens, and determine scalar fabric parameters of the silt matrix such as void ratio. This demostration also provided the confidence needed to extend the imaging technology to non-spherical standard particles as well as natural silt. Challenges in using this technology, including the importance of the scanning parameters on the image quality and the need for optimizing these parameters on a silt-specific basis to obtaining high-quality images is also highlighted. The enhancements to imaging arising through these findings provide a stepping-stone towards studying the fabric of silts, and in turn, understanding its relationship with the mechanical behavior of this complex soil.

Keywords: X-ray micro-computed tomography, segmentation, visualization, silt, soil fabric, 3D image analysis, particle fabric.

Extracting the fabric-strain relationship from a shear band inside a sand specimen using μCT and representative elementary volumes

S. Schmidt[1] ***and I. Herle***[1]
[1] *Institut für Geotechnik, Technische Universität Dresden, Germany*

1. Introduction

Almost 30 years ago, Desrues et al. [1] were one the first researchers using x-ray computed tomography (CT) to analyse sand specimens after triaxial testing. Among numerous interesting results in their work they underlined that, in fact, the critical state is only reached inside the shear bands. Thus, the shear band is the only active deformation zone in the critical state, i.e. the strain is mostly concentrated in this zone.

Since then, x-ray CT has been used extensively to gain a better understanding of the mechanisms inside the shear band. Tools, such as discrete digital image correlation (DDIC) [2], enable the tracking of individual grains and give further information on the grain kinematics inside the localised zone.

This work focuses on the extraction of the material behaviour inside the evolving shear band using μCT images of a sand specimen in triaxial compression. It is motivated by the idea that the full material behaviour can only be found inside the shear band. For this purpose, the size of a representative elementary volume (REV) is determined inside the shear band regarding void ratio, contact fabric and strain. The REV is then extracted from the initial state of the triaxial test and the set of grains contained in the REV is tracked throughout the test.

2. Determination of the REV size

The basis for the determination of the REV size is the approach presented in Schmidt et al. [3]. This procedure has been enhanced to face the issues arising once localisation zones develop inside the specimen. Cubic elements with increasing size are extracted from the specimen and the chosen variables are determined for each element size. This allows the analysis of the convergence of each variable with increasing element size.

To improve the procedure, the positions of the elements are chosen so that their center is in the center of the localisation (cf. Figure 1). Consequently, the variables converge towards a constant value and, once the element is large enough to reach the boundaries of the localisation, they start to slowly decrease or increase. As the width of the localisation is different for each variable (see [3]), this might happen at different element sizes. The REV should not be larger than the localisation width in order to extract the material behaviour inside the localised zone without any influences from the localisation boundaries.

The variables analysed in this work are the void ratio, the contact fabric and the strain. The void ratio is calculated by counting void and solid voxels after binarising the original greyscale μCT image. In order to characterise the contact fabric, the coordination number and the scalar anisotropy factor are used. For a reliable determination of the contacts and their orientation, the procedure developed by Wiebicke et al. [4] is used. The strain is calculated for tetrahedra which are a result of a tesselation of all grain centers. Bagi's average displacement gradient tensor [5] is used here. The grain displacements forming the basis for the strain calculations have been determined using DDIC. The local deviatoric strain for the last global strain increment is displayed in Figure 1.

Alternatively, the REV size is also determined for sets of grains which have been tracked throughout the triaxial test. The sets of grains are defined at the initial state as all grains with their center of mass inside a cubic element of a certain size. In this case, the void ratio and the contact fabric are determined and attributed to each single grain and then, an average for the set is calculated.

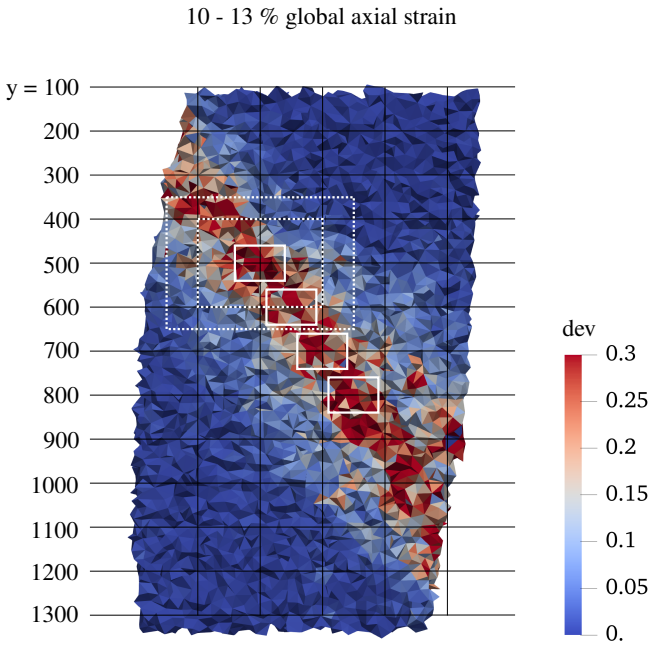

Figure 1. Element positions used to determine the REV size for the last strain increment from 10 to 13 % of global axial strain. The elements are displayed on top of a visualisation of the local deviatoric strain inside the specimen for the same increment. The 2D slice was chosen to contain the shear band.

3. Extraction of the fabric-strain relationship

After the determination of the REV size, the REV is placed in a region where the shear band will eventually form and the set of grains inside the REV is determined at the initial state. The grains assigned to the REV are then tracked throughout the triaxial test and the evolution of the variables is obtained with a grain-based approach as described above. Finally, this results in the identification of the fabric-strain relationship inside the shear zone.

This fabric-strain relationship can now be used for the calibration and maybe even development of constitutive models as it represents the full scale of the material behaviour. Although, the stress evolution cannot be directly derived from μCT images, the evolution of the contact orientation anisotropy is closely connected to the stress evolution and could serve as a basis for an indirect determination of the stress evolution. Furthermore, this analysis could be coupled with the DEM to access stresses and provide a full stress-strain-fabric relationship.

References

[1] Desrues, J., Chambon, R., Mokni, M., and Mazerolle, F. (1996). Void ratio evolution inside shear bands in triaxial sand specimens studied by computed tomography. *Géotechnique*, **46**, 529–546.

[2] Hall, S., Bornert, M., Desrues, J., Pannier, Y., Lenoir, N., Viggiani, G., and Bésuelle, P. (2010). Discrete and continuum analysis of localised deformation in sand using X-ray μCT and volumetric digital image correlation. *Géotechnique*, **60**, 315–322.

[3] Schmidt, S., Wiebicke, M., and Herle, I. (2022). On the determination and evolution of fabric in representative elementary volumes for a sand specimen in triaxial compression. *Granular Matter*, **24**, 97.

[4] Wiebicke, M., Andò, E., Šmilauer, V., Herle, I., and Viggiani, G. (2019). A benchmark strategy for the experimental measurement of contact fabric. *Granular Matter*, **21**, 54.

[5] Bagi, K. (1996). Stress and strain in granular assemblies. *Mechanics of Materials*, **22**, 165–177.

Fabric evolution in granular assemblies: Role of particle aspect ratio, drainage condition and Lode angle

***M. Salimi*[1], *N. Irani*[1] *M. Tafili*[1], *and T. Wichtmann*[1]**
[1] *Ruhr-University Bochum, Bochum, Germany*

1. Introduction

The macro-scale mechanical behaviour of granular materials is significantly influenced by microstructure, i.e., grain-scale entities such as the geometrical arrangement and orientation of particles in a soil assembly known as "fabric" [1, 2, 3]. The measurement of fabric and observation of its evolution in experimental setups is challenging due to the required advanced apparatuses and techniques (e.g., [4, 5, 6]. As a result, only limited experimental evidence is available regarding the effect of Lode angle on fabric evolution in the literature. Employing Discrete Element Method (DEM) offers an effective solution to track soil fabric under general stress paths. While prior DEM studies explored the development of fabric under drained true triaxial stress paths [7, 8], undrained simulations often focus on axisymmetric conditions or fixed variations of principal stresses. It is worth mentioning that particle shape has a substantial impact on the packing structure of granular assemblies, and non-spherical particles exhibit significantly different mechanical behaviour than spherical ones [9, 10, 11]. Therefore, considering the influence of shape effects elevates the scope of investigating the fabric anisotropy of granular soils.
This study pursues tow primary objectives: firstly, exploring the influence of anisotropy in terms of initial fabric and principal stress on the undrained response of granular assemblies; secondly, investigating the impact of Lode angle (θ) particle Aspect Ratio (AR) and drainage condition on fabric evolution under continuous shearing.

2. Numerical procedure of DEM simulations

Utilizing the 3D Particle Flow Code (PFC3D) [12], this study employs numerical simulations to investigate the behavior of granular assemblies under drained and undrained true triaxial conditions. The simulation integrates the DEM-CFM coupling scheme proposed by [13], utilizing Darcy's law to simulate the behaviour of particulate assemblies under prescribed undrained stress paths. The simulation setup involves generating particles to fill a confined cubic space, subjected to stress applied by pairs of frictionless faceted walls. Three distinct particle AR are considered: assemblies with three overlapped spheres (AR=1.8), assemblies with two overlapped spheres (AR=1.5), and assemblies with spherical particles (AR=1). Specimens with isotropic initial fabrics labeled 'ISO' and three transversely isotropic ones labeled 'TR0,' 'TR45,' and 'TR90' with bedding plane angles of 0°, 45°, and 90°, are examined. A second-order fabric tensor based on inter-particle contact orientations tracks fabric evolution during loading. In total, 640 simulations were conducted to explore fabric evaluation's interplay with varying void ratios, mean effective stress, and particle arrangements within granular assemblies under diverse loading conditions. This abstract presents results from initially isotropic samples (ISO). A more detailed analysis will be covered in the extended version.

3. Results

Fig. 1 illustrates the results of the undrained true triaxial tests for medium-dense specimens with AR=1.8. The observations underscore the influence of the stress path on the strength characteristics of soil samples under undrained loading conditions. Fig. 2 demonstrates the changes in the diagonal components of fabric tensor versus deviatoric strain for undrained condition. Each component of the

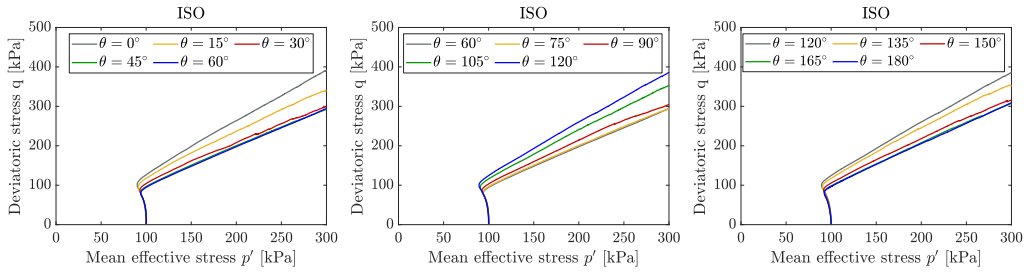

(a) (b) (c)

Figure 1. Mechanical response of a medium-dense assemblies with $e_0 = 0.59$, $p'_0 = 100$ kPa and AR=1.8 under undrained true triaxial condition for (a): $\theta = 0°$ to $60°$, (b): $\theta = 60°$ to $120°$, (c): $\theta = 120°$ to $180°$.

fabric tensor represents contact intensity in a specific direction. Regarding Fig. 2, the fabric components continuously evolve towards an ultimate value during shear loading, with the evolution trend primarily influenced by the Lode angle. Fig. 3 illustrates the visualized fabric for medium-dense sam-

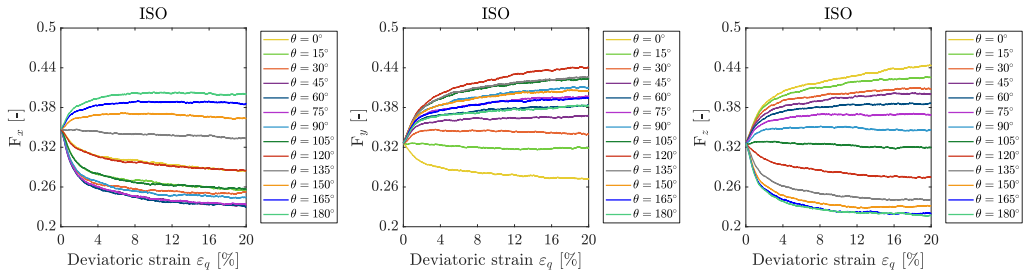

(a) (b) (c)

Figure 2. Evolution of components of fabric tensor with respect to the reference axes of (a):x, (b):y, (c):z for a medium-dense assemblies with $e_0 = 0.59$, $p'_0 = 100$ kPa and AR=1.8 under undrained true triaxial condition.

ples with different particle AR under undrained true triaxial tests. A comparison between Fig. 3(a) and Fig. 3(b) reveals that AR has a considerable impact on the degree of fabric anisotropy as well as its evolution pattern.

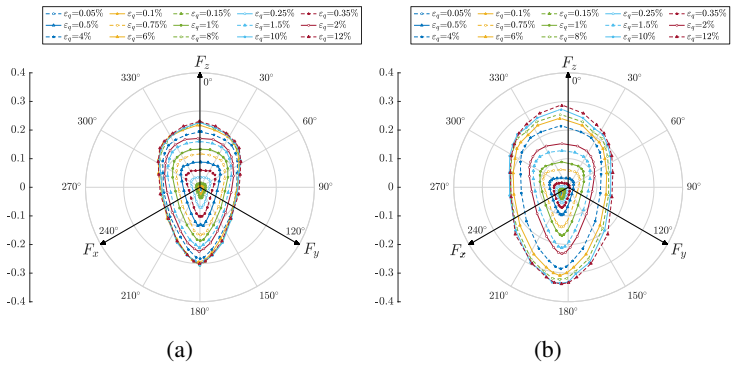

(a) (b)

Figure 3. Visualization of the fabric anisotropy of ISO samples in the octahedral plane for the sample sheared under undrained condition with $e_0 = 0.59$, $p'_0 = 100$: a: AR=1.0 and b: AR=1.8.

4. Citing references

References

[1] Subhash, G., Nemat-Nasser, S., Mehrabadi, M., and Shodj, H. (1991). Experimental investigation of fabric-stress relations in granular materials. *Mechanics of Materials*, **11**, 87–106.

[2] Li, X. and Li, X.-S. (2009). Micro-macro quantification of the internal structure of granular materials. *Journal of engineering mechanics*, **135**, 641–656.

[3] Fu, P. and Dafalias, Y. F. (2011). Fabric evolution within shear bands of granular materials and its relation to critical state theory. *International Journal for numerical and analytical methods in geomechanics*, **35**, 1918–1948.

[4] Zhao, C.-F., Pinzón, G., Wiebicke, M., Andò, E., Kruyt, N. P., and Viggiani, G. (2021). Evolution of fabric anisotropy of granular soils: X-ray tomography measurements and theoretical modelling. *Computers and Geotechnics*, **133**, 104046.

[5] Drescher, A. and De Jong, G. D. J. (2006). Photoelastic verification of a mechanical model for the flow of a granular material. *Soil Mechanics and Transport in Porous Media: Selected Works of G. de Josselin de Jong*, pp. 28–43.

[6] Calvetti, F., Combe, G., and Lanier, J. (1997). Experimental micromechanical analysis of a 2d granular material: relation between structure evolution and loading path. *Mechanics of Cohesive-frictional Materials: An International Journal on Experiments, Modelling and Computation of Materials and Structures*, **2**, 121–163.

[7] Yuan, R., Yu, H.-S., Yang, D.-S., and Hu, N. (2019). On a fabric evolution law incorporating the effects of b-value. *Computers and Geotechnics*, **105**, 142–154.

[8] Liu, Y., Zhang, D., Wu, S., and Yu, P. (2020). Dem investigation on the evolution of fabric under true triaxial conditions in granular materials. *International Journal of Geomechanics*, **20**, 04020110.

[9] Wouterse, A., Williams, S. R., and Philipse, A. P. (2007). Effect of particle shape on the density and microstructure of random packings. *Journal of Physics: Condensed Matter*, **19**, 406215.

[10] Kyrylyuk, A. V. and Philipse, A. P. (2011). Effect of particle shape on the random packing density of amorphous solids. *physica status solidi (a)*, **208**, 2299–2302.

[11] Vairaktaris, E., Theocharis, A. I., and Dafalias, Y. F. (2020). Correlation of fabric tensors for granular materials using 2d dem. *Acta Geotechnica*, **15**, 681–694.

[12] Itasca, P. (2014). Version 5.0. *Itasca Consulting Group Inc. Minneapolis, United States*.

[13] Salimi, M. and Lashkari, A. (2020). Undrained true triaxial response of initially anisotropic particulate assemblies using cfm-dem. *Computers and Geotechnics*, **124**, 103509.

FINE GRAIN DISPERSION BEHAVIOR IN 3D SOIL PACKING-NUMERICAL AND EXPERIMENTAL INVESTIGATIONS

***F. Chen*[1], *A. Hegde*[1], *A. Wautier*[1], *N. Benahmed*[1], *and P. Philippe*[1]**
[1] *INRAE, Aix-Marseille Université, RECOVER, Aix-en-Provence, France*

Filtration of particles using granular media has applications in a wide variety of engineering disciplines such as design of reusable filters in waste water treatment [1], purification of drinking water [2], storage of radioactive pollutants and microplastics [3, 4], and design of filters for embankments and dykes in-order to prevent internal erosion of the base soil [5]. Due to its significance, the filtration process through granular materials merits an in-depth micro-mechanical study, exploring the impact of the underlying pore geometry of the filter, grain shape of the filter as well as infiltrating particles, the role of diffusion, as well as the infiltration method employed.

Utilizing the discrete element method (DEM) and Pore-scale Finite Volume (PFV) scheme [6], the process of spherical fine infiltration into a coarse sand column is analyzed under gravity and hydraulic forces. The study considers various fine/coarse size ratios and void ratios of sand columns. Key factors like infiltration depth, penetration velocity, and distribution of retained fines are examined. An probabilistic model based on pore-constriction size is proposed to interpret the decaying characteristics of the infiltration results. The effect of column packing density and hydraulic conditions on lateral dispersion of fine grains is also studied. Furthermore, the particle-scale dynamics, including bouncing and falling, are linked to macroscopic parameters like pore and constriction size estimation.

Complementary, experimental studies in the laboratory analyze the infiltration pattern under additional conditions, including relative densities, particle morphology (angular Hostun 1/2.5 and rounded glass beads), flow conditions (constant or fluctuation flow rates) and injection method (deposited layer of fine or fine in suspension in the fluid). Post hydraulic testing, the fine content in the samples is determined through sieve analysis. The findings reveal a non-homogeneous fine content in the samples, that depends on the material and loading conditions. Exponentially decaying profiles of fine content in the injected samples align consistently with the numerical results.

References

[1] McDowell-Boyer, L. M., Hunt, J. R., and Sitar, N. (1986). Particle transport through porous media. *Water resources research*, **22**, 1901–1921.

[2] Adin, A. (2003). Slow granular filtration for water reuse. *Water Science and Technology: Water Supply*, **3**, 123–130.

[3] Painter, S. L., Cvetkovic, V., and Pensado, O. (2008). Time-domain random-walk algorithms for simulating radionuclide transport in fractured porous rock. *Nuclear technology*, **163**, 129–136.

[4] Keller, A. S., Jimenez-Martinez, J., and Mitrano, D. M. (2019). Transport of nano-and microplastic through unsaturated porous media from sewage sludge application. *Environmental science & technology*, **54**, 911–920.

[5] Indraratna, B. and Locke, M. (1999). Design methods for granular filters—critical review. *Proceedings of the institution of civil engineers-geotechnical engineering*, **137**, 137–147.

[6] Catalano, E., Chareyre, B., and Barthélemy, E. (2014). Pore-scale modeling of fluid-particles interaction and emerging poromechanical effects. *International Journal for Numerical and Analytical Methods in Geomechanics*, **38**, 51–71.

IMPACT OF FLUID MIGRATION STRATEGIES ON WATER RETENTION CURVE IN POROUS MEDIA: A LATTICE BOLTZMANN ANALYSIS

***S. Joseph*[*], *H. Cheng*[*], *J. Harting*[+], *S. Luding*[**], *V. Magnanimo*[*]**

[*] *University of Twente, Chair of Soil MicroMechanics, Faculty of Engineering Technology, Enschede, The Netherlands*

[**] *University of Twente, Chair of MultiScale Mechanics, Faculty of Engineering Technology, Enschede, The Netherlands*

[+] *Helmholtz Institute Erlangen-Nürnberg for Renewable Energy, Forschungszentrum Jülich Erlangen, Germany*

1. Introduction

The relationship between capillary pressure and saturation in a porous material is described by the retention characteristic curve (WRC). Due to the varying fluid migration between imbibition and drainage processes, the retention curve displays hysteresis, which correlates with the specific pore geometry [1, 2]. In the present work, the WRC is obtained by conducting imbibition and drainage analysis using the Colour Gradient Lattice Boltzmann Method [3], which allows for a pore-scale analysis of the processes. Imbibition starts when water is first introduced into pores with the greatest potential for trapping. Next, two different methods of expanding the water patches are used: uniform and differential expansion. The latter accounts for the connection of pores. The two approaches are contrasted according to the degree of hysteresis seen. The comparison emphasizes how crucial it is to model realistic fluid distribution patterns while studying immiscible fluid migration. The study is further extended to analyze the influence of tortuosity on fluid migration and subsequently on hysteresis. The work's findings are valuable in fields where fluid distribution and retention are critical.

2. Methodology

The porous medium under consideration is a randomly generated 3D sample consisting of 640 particles, as illustrated in Figure 1a. The system also comprises two types of fluids: water, which is wetting, and oil, which is non-wetting (see Figures 1b and 1c). The fluids are numerically modeled using the Colour Gradient Lattice Boltzmann Method. A highly parallelized code, LB3D is used to solve the hydrodynamics of the multiphase system [4]. Surface tension is incorporated into this process to ensure that the fluids remain separated and do not mix. The hydrophobic and hydrophilic nature of solids is explored by varying the wetting strengths (adhesion) between fluids and solids.

The ability of a porous media to hold water in its pores is called water retention capacity. In the current context, water retention is a complex interplay between capillary forces, saturation degree, pore distribution, and connectivity. Pores of a specific size, shape, and connection can capture more water than others. Smaller pores with higher capillary pressure, smaller throats connected to larger pore bodies, and less connected pores can trap more water. Hence, the pores with maximum trapping efficiency contribute the most to the water retention in the medium. An initial state before imbibition will consist of pores with maximum trapping efficiency filled with water. To create such an initial state, the trapping efficiency of the pores is analyzed. Within the complex pore network, this is done by setting thresholds for pore size, shape, and connectivity. The pores with the highest water retention capacity are then filled with water and equilibrated. Following the first approach, i.e., the uniform expansion, the existing water patches in the low saturated medium are uniformly extended in a controlled manner, ensuring that no preferential flow pathways exist, other than hydrodynamic equilibrium. Drainage follows a similar procedure, except that it begins with an almost saturated

medium and focuses on spreading oil patches. On the other hand, when the differential expansion methodology is adopted for imbibition, the existing water patches are differentially expanded while considering pore connectivity. The pore connectivity is mapped together with the water patches, and the patches are then ranked, with patches in highly connected pores receiving more water than isolated ones. Because water distribution is related to pore connectivity, this approach provides greater control over the states naturally achieved in a heterogeneous medium.

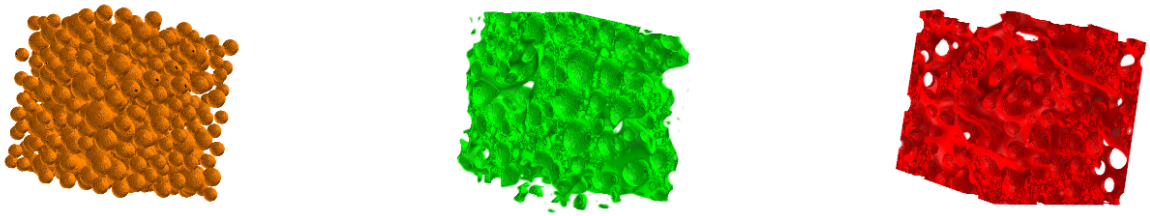

(a) (b) (c)

Figure 1. Snapshot of a multiphase simulation at 50% saturation in a porous medium, depicting (a) the solid matrix, (b) water distribution, and (c) oil distribution.

3. Main Findings

When studying representative volumes at the microscale, it is appropriate to increase/decrease water within existing patches rather than from boundaries. Pore connectivity can serve as a reliable predictor for anticipating the required water addition across various patches. The addition/removal has to occur at an optimal rate to capture the highest number of states on the retention curve and reach high accuracy in the analysis. The comparative study reveals the strengths and limitations of the two water distribution strategies. Moving forward, future studies will also focus on exploring the role of local saturation alongside pore connectivity in influencing differential expansion.

Finally, the attention is devoted to the role of tortuosity. Compaction reduces porosity, which in turn makes the pores network more convoluted. With higher tortuosity, water movement, and retention will be more influenced by the pore network's size, shape, and connectivity. Given such a scenario, the way fluids are added/removed and how they move is more strictly related to the geometrical features of the pore. Since hysteresis has been linked to phenomena like the ink-bottle effect, pore connectivity, and tortuosity, this study can give the extent of the influence of these migration strategies on hysteresis.

References

[1] Hosseini, R., Kumar, K., and Delenne, J.-Y. (2022). Investigating the source of hysteresis in the soil-water characteristic curve using the multiphase lattice boltzmann method. *arXiv preprint arXiv:2204.07174*.

[2] Perrier, E., Rieu, M., Sposito, G., and de Marsily, G. (1996). Models of the water retention curve for soils with a fractal pore size distribution. *Water Resources Research*, **32**, 3025–3031.

[3] Gunstensen, A. K., Rothman, D. H., Zaleski, S., and Zanetti, G. (1991). Lattice boltzmann model of immiscible fluids. *Physical review A*, **43**, 4320.

[4] Schmieschek, S., Shamardin, L., Frijters, S., Krüger, T., Schiller, U. D., Harting, J., and Coveney, P. V. (2017). Lb3d: A parallel implementation of the lattice-boltzmann method for simulation of interacting amphiphilic fluids. *Computer Physics Communications*, **217**, 149–161.

Impact of Sand-Hydrogel Mixtures Swelling on Shearing Behaviour: An X-ray CT Study

M.K.L. Masango[1], M. Long[1], J. Wang[2], S. Tracy[3], and B. Zhao[1]
[1] University College Dublin, School of Civil Engineering, Dublin, Ireland
[2] City University of Hong Kong, Department of Architecture and Civil Engineering, Hong Kong
[3] University College Dublin, School of Agriculture and Food Science, Dublin, Ireland

1. Introduction

Hydrogels, also known as superabsorbent polymers, are crosslinked hydrophilic polymers characterized by a three-dimensional structure capable of absorbing water up to a thousand times their own weight. The use of hydrogels has recently been found to have increased utility in diverse fields, including agriculture, ecology, environmental science, and civil engineering [1]. The key attraction of these applications lies in their capacity to absorb substantial amounts of water, thereby enhancing soil water retention, promoting plant growth, attracting, and binding to pollutants, and facilitating soil particle aggregation [1, 2].

During the wetting process, previous studies have consistently demonstrated that swelling can induce a restructuring of the soil structure, including decreased soil stiffness, increased erodibility, and reduced shear strength [2-3]. However, we lack a more comprehensive understanding of the complex micromechanical processes that govern the behaviour of hydrogel-treated soils during wetting. This knowledge gap hinders our understanding of the interaction of hydrogels with soil and the effective use of hydrogels in soil remediation and geotechnical engineering applications.

Our research seeks to bridge this critical knowledge gap by meticulously examining the swelling behaviour of hydrogels in soils and swelling under various stress conditions. We aim to unravel the processes which lead to soil restructuring during wetting and elucidate the impact of swelling on the shear behaviour of the soil. Employing X-ray computed-tomography (CT), we will unveil a three-dimensional perspective on the complexities of these processes, thus contributing to a more comprehensive understanding of hydrogel-soil interactions during wetting cycles.

2. Materials and methods

Materials tested in this experiment are Leighton Buzzard sand (LBS) treated with a super absorbent polymer (SAP), polyacrylic acid. The swelling of hydrogel in soil was investigated using a miniature triaxial cell compatible with an X-ray CT scanner. The humid air was delivered to the sample through a peristaltic pump. The sample was prepared by mixing fine sand (D_{50} = 0.603 mm) with dry SAP particles (D_{50} = 0.750 mm) at a mass ratio of 1%. The mixture was then spooned into a latex membrane stretched into a mould to form a sample of 20 mm in diameter and 40 mm in height. The sample is placed between two perforated plates to allow the free flow of humid air into the sample.

The testing procedure consisted of three stages: (a) In the first stage, the sample was subjected to isotropic confinement of 50 kPa. Then, the sample is loaded axially until it reaches 20% of the peak deviatoric stress; (b) In the second stage, the stepping motor was stopped to maintain a constant vertical strain. Meanwhile, the sample is exposed to humid air to allow the SAP particles to absorb moisture and swell until the swelling reaches equilibrium; and (c) the sample is further loaded until it reaches shear failure in the last stage. Throughout the test, X-ray tomographies are acquired, and during scanning, the axial load is halted.

3. Results

The impact of swelling of hydrogel-treated soils resulting from wetting is analysed phenomenologically based on the stress-strain curves and qualitatively based on X-ray CT grayscale images in Figure 1. The stress-strain curves show a clear decrease in shear strength between natural and hydrogel-treated soils Figure 1a. These results indicate that hydrogel swelling during saturation can induce failure even before the soil reaches its peak strength.

Figures 1b, c and d are grayscale images acquired at the end of three stages after confinement, saturation, and shear failure, and they clearly illustrate the direct impact of hydrogel swelling in soils. During the saturation stage, the hydrogel swells, and the dilatation of particles causes the sand particles' packing to decrease. Figure 1c shows that swelling is generally uniform along the height of the sample. The soil restructuring causes the formation of weak zones that are later activated during shearing as shear bands. The localized deformation occurs as conjugate shear bands forming a friction cone because of friction between the wire mesh and the sample (see Figure 1c and Figure 1d).

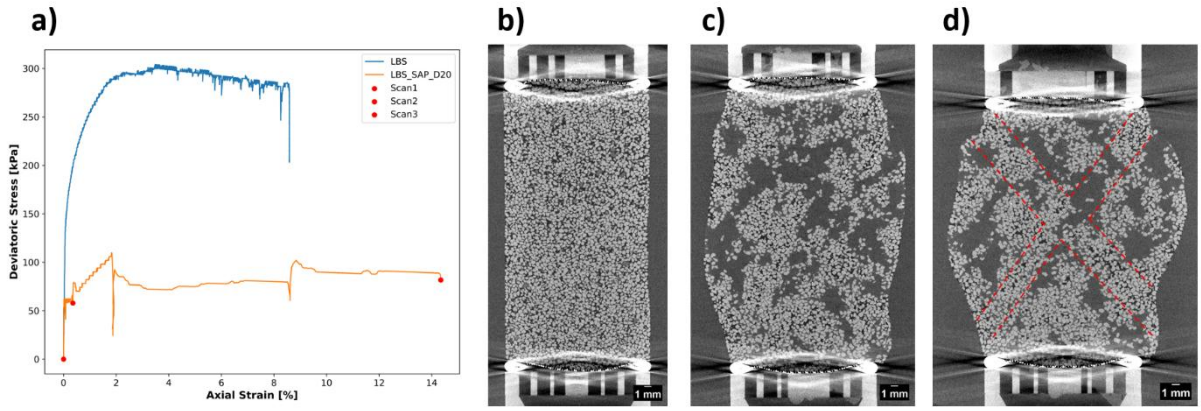

Figure 1 : a) Stress-strain curves showing the macroscopic response of natural and hydrogel-treated soils, with corresponding points of X-ray CT scan. b), c), and (d) Vertical slices were acquired during the three stages of the experiment and correspond to the three scanning points.

4. Conclusions

The study highlights the relationship between hydrogel swelling and the shearing behaviour of soils during wetting conditions. The impact of hydrogel on soil showed that swelling significantly alters the stress-strain characteristics of the soil, as swelling leads to soil particle restructuring, which induces failure before reaching peak strength and leading to the activation and formation of shear bands. The results underscore the importance of considering hydrogel-induced changes in soil behaviour during wetting.

5. References

[1] Zohuriaan-Mehr M.J., Omidian H., Doroudiani S., Kabiri K. (2010). Advances in non-hygienic applications of superabsorbent hydrogel materials. *J. Mater Sci.*, **45**:5711-5735.

[2] Saha A., Sekharan S., Manna U. (2010). Hysteresis model for water retention characteristics of water-absorbing polymer-amended soils. *J. Geotech. Geoenviron. Eng.*, **148**(4):5711-5735.

[3] Louf J-F., Lu N.B., O'Connell M.G., Cho H.J., Datta S.S. (2021). Under pressure: Hydrogel swelling in granular medium. *Sci. Adv.*, **75**(7): eabd2711.

INVESTIGATION OF SHAPE FOR THE BALTIC SEA COASTAL AREA SAND PARTICLES USING SPHERICAL HARMONICS

U. Radvilaitė[1], Š. Skuodis[1], T. Tamošiūnas[1] and R. Kačianauskas[1]
[1] Vilnius Gediminas Technical University, Vilnius, Lithuania

1. Introduction

Soils present specific class of naturally existing materials. Understanding of their behavior and quantitative description of their properties is very important for many applications in different technical areas. Major part of soils present composition of mineral grains. Macroscopic behavior of granular soils (GS) and their actual mechanical properties are significantly affected by a shape of particles. Large variety of mineral grains and their properties requires to all strata behavior characterization. They should be tested individually for each construction site. Generally, microstructure of GS is site-specific and contains specific shape of particles [1]. Sand particles of Baltic Sea coastal area are formed by the waves and are considered in this report.

Since performing real shape investigation experiments is very costly, computer simulations can help investigate granular material reducing amount of expensive experiments. Handling of particle shape is rather two-fold. Firstly, description of shapes is considered in relation to context of DEM simulations. Thus, particle shape must be convenient for a contact calculation and the simplest surface models are developed using clusters of discs and spheres [2]. These multi-sphere as well as polyhedral models yield non-smooth description of the shape. Another demand is related to have an analytical description of shape and important parameters suitable for storing particle data in database. The description of shape by spherical harmonics (SH) is considered. Spherical harmonics yield smooth description of the star-shaped particles with finite number of harmonics [3].

2. Investigation of sand particles

As the suitability of spherical harmonics to represent differently shaped particles has been demonstrated in study [3], this method can be applied for geomaterials. Furthermore, its application to smooth particle tends to be suitable for the non-convex and smooth particles of coastal sands.

Properties of sand considered below are related to the area located on seaside of Baltic Sea in the southern part of the Lithuanian mainland northwards from the Klaipėda city. The samples of sand particles have been extracted from the immediate near coast area that contains a sandy strip of Holocene marine sediments (m IV), which occur as deep as to 4–5 meters in the sea [4]. The recent marine sediments (m IV) formed in the coastal zone, which mineralogical composition of sand contains ~85% quartz and ~6% feldspar with remaining contribution of carbonate, mica and some other minerals [5]. Investigated sand uniformity coefficient C_U = 1.47, coefficient of curvature C_C = 0.93.

Due to continuous rolling effect because of the sea waves in the coastal zone, investigated non-convex particles have smooth surface. This kind of shape is suitable for SH models.

The images of investigated sand particles were taken with scanning electronic microscope (SEM) Quanta 250 (FEI Company). On the basis of scanned images sand particles are generated. The sample of 2D image of a particle is given in Fig. 1a. The coordinates of surface points are used as input for SH expansion model.

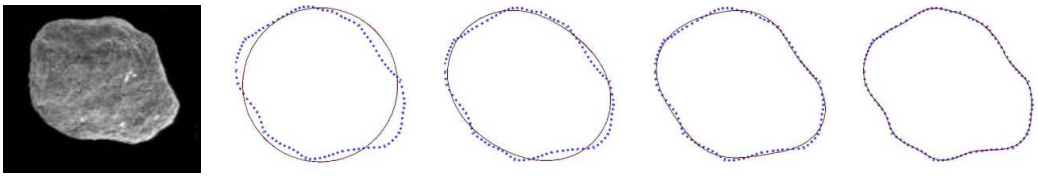

a) b) c) d) e)

Figure 1. SH models (from left to right) with 3, 5, 9 and 21 SH functions.

The shapes obtained using 3, 5, 9, and 21 SH functions are illustrated in Fig. 1b-e. Additionally, the area, perimeter and sphericity have been calculated for 2D models of sand particles. Using only 3 SHs in a model (Fig. 1b), the area of 2D particle is 0.786, perimeter is 3.143. The area in a model with 5 SHs (Fig. 1c) is equal to 0.791 and perimeter is 3.183. Increasing number of SH functions to 9 and 21 (Fig. 1d and 1e) gives similar accuracy: area is equal to 0.793, while perimeter changes slightly: from 3.225 to 3.261. Sphericity changes in these models from 0.999 to 0.937.

The application of SH 3D particle models will be presented in the full version of the paper. Here, important characteristics as particle volume, surface area, sphericity, etc., will be demonstrated.

3. Conclusions

The investigation demonstrates the suitability of SH functions to represent shapes of sand particles taken from the area of Baltic Sea. The accuracy as well as complexity of a SH model is controlled by expansion degree. The results presented in this paper demonstrated that the required accuracy can be retained by smaller number of SH functions. Because of high sphericity number of SHs limited to 10 demonstrates convergence.

SH model being an analytical mathematical tool to reconstruct a shape of a particle is a powerful tool enabling to derive any necessary shape characteristics or properties. Furthermore, these SH models of particles can be implemented in DEM simulations to model the behavior of geomaterials.

4. References

[1] Anusree, K. & Latha, G. M. (2023). Characterization of Sand Particle Morphology: State-of-the-Art. *Bull. Eng. Geol. Environ.* 82, 269.

[2] Adesina, P., O'Sullivan, C. & Wang, T. (2023). DEM study on the effect of particle shape on the shear behaviour of granular materials. *Comp. Part. Mech.*

[3] Radvilaitė, U., Ramírez-Gómez, Á. & Kačianauskas, R. (2016). Determining the shape of agricultural materials using spherical harmonics. *Comput Electron Agric* 128:160-171.

[4] Skuodis, Š., Markausas, D., Norkus, A., Žaržojus, G. & Dirgėlienė, N. (2014). Testing and numerical simulation of Holocene marine sand uniaxial compression at Lithuanian coast. *Baltica* 27(1):33–44.

[5] Amšiejus, J., Kačianauskas, R., Norkus, A. & Tumonis, L. (2010). Investigation of the sand porosity via oedometric testing. *Balt. J. Road Bridge Eng.* 5(3): 139-147.

INVESTIGATION OF THE BREAKAGE BEHAVIOUR OF COMPLETELY DECOMPOSED GRANITE UNDER SHEAR USING X-RAY TOMOGRAPHY

Zhiren Zhu[1], Jianfeng Wang[1]
[1] City Univ. of Hong Kong, Dept. of Architecture and Civil Engineering, Hong Kong, China

Abstract

Noise reduction and extraction of microscopic details have been persistent challenges in microstructure visualization. This study monitors the breakage behaviour of a reconstituted completely decomposed granite (CDG) sample within a medium-sized triaxial loading device using X-ray microtomography techniques (CT). We use a new filter, non-local means (NL-means), to denoise CT images. NL-means shows a better performance in noise reduction and edge sharpening than traditional filters such as median and Gaussian filters. Microfractures within the particles are extracted by the black top-hat (BTH) transformation and introduced into particle fragmentation analysis to investigate the effect of microstructure on particle fragmentation patterns. We further study the degree of particle fragmentation with relative breakage, fractal dimension, and mass loss. The particle mass loss shows a bilinear evolution pattern. Changes in CDG particle morphology are analyzed by observing the evolution of aspect ratio, convexity, and sphericity at different strains.

1. Introduction

CDG is highly weathered in situ from the granite rock and is widely distributed in many countries and regions, especially in Hong Kong [5]. CDG is commonly used locally in the land formation works and the marine reclamations as a construction fill material. Due to the presence of clay, inner defects, pre-cracks in CDG, the material is fragile and easily breaks into fine particles under a small load [5]. Notably, the pre-existing microfractures have a great influence on the particle fragmentation pattern [5]. Therefore, a medium-sized triaxial test was conducted on a reconstituted CDG sample at Shanghai synchrotron radiation facility (SSRF) to investigate their breakage behaviour under shear.

2. Methodology and results

A reconstituted CDG sample from Hong Kong underwent a drained consolidated (CD) triaxial test with in-situ CT scanning. Comprising primarily of quartz, feldspar, biotite, and mica, CDG particles have experienced severe weathering, resulting in a clay matrix. There are three main types of particle: Type I, individual high-strength quartz particles, constituting approximately 30% of the sample (Fig. 1(a)); Types II and III, agglomerates (50% and 20% of the sample, respectively) consisting of quartz, feldspar, silt, clay, and fines. Specifically, Type II agglomerates consist of one or multiple large quartz particles with attached clay and fines (about 50% of the sample), while Type III agglomerates involve several small particles agglomerated by clay (about 20% of the sample), as depicted in Figs. 1(b) and (c). Both agglomerate types are breakable, attributed to the diminished cohesiveness of silt and clay, and the release of fines during reconstitution. The release process results in the formation of voids within the cement, contributing to additional weakness (Fig. 1(d)) [3]. Their fragmentation pattern results from the loss of cohesiveness. Notably, after

breaking, Type I and Type II particles maintain strength, contributing to the granular skeleton, while Type III particles completely lose load-carrying capacity.

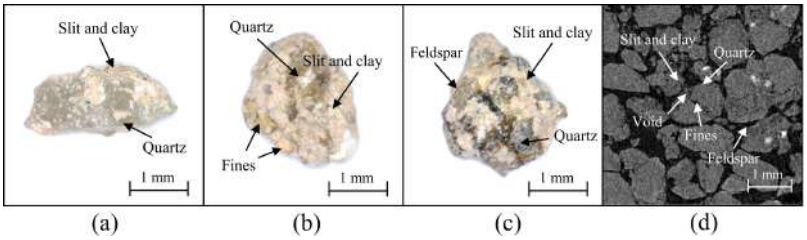

Figure 1. The reconstituted CDG particle: (a) Type I; (b) Type II; (c) Type III; (d) CT image.

Due to the low X-ray energy, raw CT images are highly blurred and noisy (Fig. 2(a)). Firstly, the NL-means filter [1] was applied to the images to reduce noise and sharpen edges (Fig. 2(b)). Specifically, noise reduction is achieved by scanning the entire image to find all pixels similar to those that need denoising and then performing a weighted average. Next, microfractures were successfully identified and extracted using the BTH transformation [2] (Fig. 2(c)). Subsequently, the Otsu thresholding algorithm [4] was employed to distinguish CDG particles from other materials by selecting an appropriate grayscale interval in the grayscale histogram, as each material has its unique grayscale interval in the histogram. The effect of microfractures on particle fragmentation was considered during image processing by subtracting the microfracture results from the CDG particle results (Fig. 2(d)). A comparison between Fig. 2(a) and Fig. 2(d) shows that the edge features and internal microfractures of the CDG particles are well-rendered with the BTH transformation, and some closely contacted particles are clearly distinguished, facilitating subsequent object segmentation. Finally, the marker-based watershed segmentation algorithm was applied to address the over-segmentation problem. As shown in Fig. 2(e), each CDG particle was labeled with different colors after segmentation and recognition.

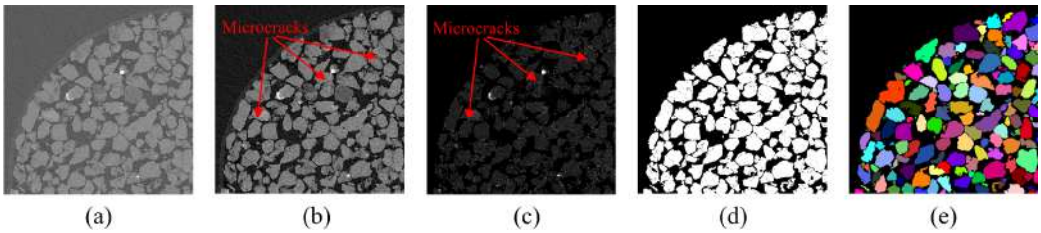

Figure 2. Image processing procedure: (a) raw CT image; (b) after NL-means denoising; (c) after BTH transformation; (d) after Otsu thresholding; (e) labelled individual particles.

3. References

[1] Buades, A., Coll, B., & Morel, J.-M. (2011). Non-Local Means Denoising. *Image Processing On Line*, **1**: 208–212.

[2] Jackway PT. (2000). Improved morphological top-hat. *Electron Lett*, **36**:1194–5.

[3] Madhusudhan, B. N., & Baudet, B. A. (2014). Influence of reconstitution method on the behaviour of completely decomposed granite. *Géotechnique*, **64**(7), 540–550.

[4] Otsu, N., (1979). A Threshold Selection Method from Gray-Level Histograms. *IEEE Transactions on Systems, Man, and Cybernetics*, C (**1**): 62–66.

[5] Zhao, B.D. (2016). Investigation of Sand Particle Breakage Using X-ray Micro-tomography. PhD thesis, City University of Hong Kong.

INVESTIGATION OF THE FABRIC EVOLUTION OF BOUND SOFT-RIGID MIXTURES USING IMAGING ANALYSIS

Abbas Rezamand[1], Mahdi M. Disfani[1] and Amirhassan Mehdizadeh[1]
[1]Department of Infrastructure Engineering, The University of Melbourne, Parkville, VIC, Australia

1. Area of Research

Mixtures of soft and rigid aggregates have shown promising potential in engineering applications in recent years. Prior research has extensively investigated the mechanical properties and behaviours of unbound soft-rigid mixtures [1]. So far, most studies on bound soft-rigid mixtures have primarily been on cemented mixtures [2 ,3], while limited research has been done on the behaviour of soft-rigid mixtures bonded with non-brittle binders [4]. There is still a gap in explaining the fabric change of mixtures with different types of binders and relating this change of fabric to the observed mechanical behaviour. This study aims to investigate the fabric evolution of bound soft-rigid granular mixtures, bonded with different types of binder, through computed tomography (CT) imaging, aiming to expand insights into their behaviour beyond the scope of mechanical testing.

2. Methodology

To study the effects of type of binder on the behaviour of mixtures, three different binders, varying in stiffness and elasticity, were used. First, through conducting one-dimensional compression tests on bound samples, the variation of constrained modulus versus applied vertical stress was explored. Through use of CT imaging techniques, detailed fabric change of each mixture was captured to explain and visualize the different stages of deformation behaviour. Based on the obtained CT images, the relevant fabric information such as particle arrangement, binder distribution and breakage, and change in internal voids and contact areas between soft and rigid particles were processed and interpreted to explain the behaviour trends observed in constrained modulus tests.

3. Basic Assumptions

The tested mixtures were prepared using three binders of different degree of elasticity. Meticulous sample preparation was undertaken to obtain repeatable results. Additionally, the imaging analysis was conducted under the assumption of consistent density and homogeneity of used material.

4. Main Results

Figure 1(a) shows an example of test results for the deformation behaviour of different types of binder, presented in terms of the variation of the normalized height of samples (H/H_0) versus applied vertical stress (σ_v). It indicates that among samples with different binder types, flexible binders showed greater vertical deflection under vertical stresses but lower plastic deformation after unloading, attributed to their highly deformable nature. Additionally, Figure 1(b) compares the evolution of constrained modulus on completion of each stage, based on the following equation:

$$M_{(i)} = \frac{\delta\sigma_{v(i)}}{\delta\varepsilon_{v(i)}} = \frac{\delta\sigma_{v(i)}}{-\frac{\delta H_{(i)}}{H_0}} \quad (1)$$

where $M(i)$ = constrained modulus at the end of the (i)th stage; $\delta\sigma_v(i)$ = change in vertical stress in the (i)th stage (between the (i)th and (i-1)th stages); $\delta\varepsilon_v(i)$ = change in vertical strain in the (i)th stage; $\delta H(i)$ = change in sample height in the (i)th stage; and H_0 = initial height of the sample.

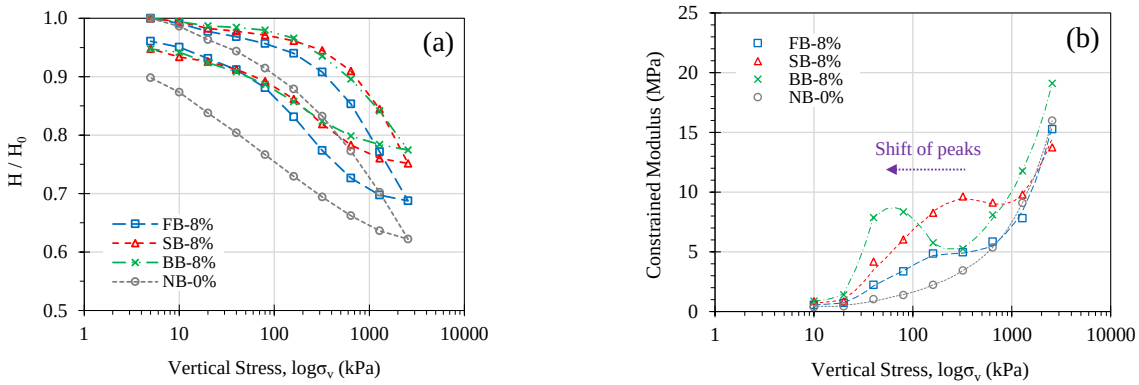

Figure 1. Response of tested mix designs under applied vertical stresses: (a) variation of the normalized height of samples; and (b) evolution of constrained modulus.

The CT scan images provided insights into the deformation mechanism and fabric change of bound soft-rigid granular mixtures, under different levels of applied vertical stresses. Figure 2 shows preliminary observations on particle arrangement and change in internal voids and contact areas between soft and rigid particles, using CT scan images. Results are further analyzed to quantitatively show the impact of binder type on change in modulus, yield point and post yield behaviour.

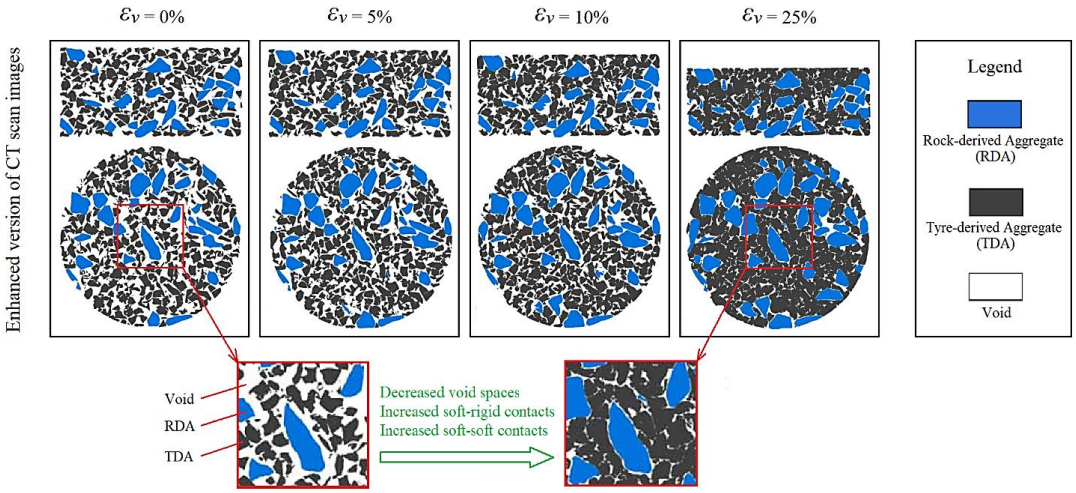

Figure 2. CT scan images at various applied stresses.

5. References

[1] Mohammadinia, A., Disfani, M.M., Narsilio, G.A. & Aye, L. (2018). Mechanical behaviour and load bearing mechanism of high porosity permeable pavements utilizing recycled tire aggregates. *C & B Materials*. 168:794-804.

[2] Lee, C., Truong, Q.H. & Lee, J.S. (2010). Cementation and bond degradation of rubber–sand mixtures. *Canadian Geotech J*. 47(7):763-74.

[3] Zhang, T., Cai, G., Liu, S. & Duan, W. (2016). Laboratory observation of engineering properties and deformation mechanisms of cemented rubber-sand mixtures. *C & B Materials*. 120:514-23.

[4] Raeesi, R., Soltani, A. & Disfani, M.M. (2022). Compressibility Behavior of Soft–Rigid Granular Mixtures Bound with Polyurethane Binder. *Int. J. Geomechanics*. 22(1).

INFLUENCE OF GRAIN ROUNDNESS OR ANGULARITY ON THE LIQUEFACTION RATIO OF DUMP SOILS IN THE LUSATIAN MINING DISTRICT (GERMANY)

G. Erdmann[1] and M. Groeschke[1]

[1] Federal Institute for Geosciences and Natural Resources (BGR), Research and Development Centre for Post-Mining Areas, Cottbus, Germany

1. Introduction

As a result of the groundwater-level recovery following the end of mining activities in the Lusatian lignite mining district after the German reunification in 1990, an increase in the number of sudden and severe soil subsidence events due to soil liquefaction was observed. Since 2010, the events mainly occurred on the inner dumps of the disused open-pit mines. Subsequently, large areas (~ 30,000 ha) were closed off against unauthorized entry and are to date not available for their post-mining land use (agriculture, forestry, tourism) according the legally binding land use plans.

To better localize the potential zones of risk, and develop and carry out targeted rehabilitation measures, comprehensive investigations have been carried out in the past decade with regard to the causes, boundary conditions, and extent of these liquefaction landslips. In this context, numerous sediment and water samples were collected, laboratory tests and analyses were conducted, and the results were evaluated taking into account the existing data from each dump. Based on this assessment, hazard categories were assigned to the closed-off areas [1], which ultimately influence the prioritization of the necessary remediation measures. The conditions that dump soils must fulfill in order to be classified as potentially at risk of liquefaction can therefore be described as sufficiently known. Nevertheless, there must be differences between the mine dumps in terms of grain structure, compactness, groundwater levels, and/or possibly groundwater chemistry, which - under otherwise similar boundary conditions - lead to a liquefaction event at one site and not at another site.

2. Current state of research and further investigations

It is well established that soils with a round grain shape are generally more sensitive to liquefaction than soils with an angular grain shape [2]. However, this might only hold true when comparing sediments with the same void ratio, but that an increasing void ratio can lead to a decreasing liquefaction resistance even in sediments with angular grains [3],[4]. A much broader range of void ratios can be observed in sediments with angular grains, so that these sediments can form very stable or collapsible fabrics [5]. In order to investigate how it behaves in the dump soils from the Lusatian open-pit mines, laboratory tests on grain roundness and angularity are carried out in 2-D and 3-D camsizers on selected, potentially liquefaction-sensitive dump soils.

The sample material comes from former and from active open-pit mines in the Lusatian mining area, which differ from each other in terms of depth and dumping technology. The focus of the sample selection is on the mine dumps, which in the past have reacted very sensitively to a trigger event. These are in the Schlabendorf and Seese open-pit mines in Brandenburg and in the Spreetal and Lohsa open-pit mines in Saxony. The results obtained will be compared with each other as well as with previous microscopy data and – in further investigations to evaluate the liquefaction behavior – evaluated with regard to the derivation of a critical grain shape or roundness for the dump soils of the Lusatian mining area. The knowledge gained from this should serve to better understand the spontaneously occurring liquefaction events. Furthermore, it can be used to check the existing hazard categorization.

References

[1] Weißbach, J. & Kudla, W. (2022). Risk assessment for spontaneous soil liquefaction on dump sites. In Rahman, M. & Jaksa, M. (eds) *Proceedings of the 20th International Conference on Soil Mechanics and Geotechnical Engineering*, pp. 4661-4666.

[2] VE BKK Senftenberg & Bergakademie Freiberg (1989). Beurteilung der Setzungsfließgefahr und Schutz von Kippen gegen Setzungsfließen [Assessment liquefaction susceptibility and protection of mine dumps against liquefaction]. *Unpublished report*, 66 pp.

[3] Hird, C.C. & Hassona, F.A.K. (1990). Some factors affecting the liquefaction and flow of saturated sands in laboratory tests. *Eng. Geol.*, **28**(1): 149-170.

[4] Wei, X., Yang, J., Zhuang, Y.S., Zhou, Y.G. & Chen, Y.M. (2019). Effects of particle shape on the liquefaction resistance of sand. In Silvestri, F. & Moraci, N. (eds), *Earthquake Geotechnical Engineering for Protection and Development of Environment and Constructions*, pp. 5656-5663.

[5] Ashmawy, A., Sukumaran, B. & Hoang, V. (2003). Evaluating the Influence of Particle Shape on Liquefaction Behavior Using Discrete Element Modeling. *Proc. Offshore and Polar Engineering Conference*. Paper No. 2003-PCW-05.

INVESTIGATION ON MICROMECHANISM OF BIO-CEMENTED MATERIALS UNDER DIFFERENT SATURATIONS BY DEM SIMULATION

M. Li[1], M. Qi[1], J. Wang[1]*

[1] Shandong University, School of Civil Engineering, Jinan, China

1. Introduction

Microbial-induced calcium carbonate precipitation (MICP) is a new biotechnology that can be used to improve the strength of soils [1]. In addition to the concentration of calcium carbonate, the degree of effective cementation between soil particles is a key factor in MICP efficiency [2]. More effective cementation can be produced when MICP is under low saturation with the same amount of calcium carbonate. Therefore, it is of great significance to establish a model that can depict the precipitation distribution and failure mechanism in bio-cemented sands under different saturations. In the present study, a 3D Discrete Element Method (DEM) model for bio-cemented sand under different saturations is proposed based on real contact properties that have been obtained from 3D X-ray computed tomography (CT) images with different saturations. With this model, the microstructural characteristics and their evolution upon external loading can be investigated.

2. Experiments

The effect of saturation is hard to simulate directly in DEM simulation. Therefore, CT technology can be used to observe the microstructural properties which help to establish the DEM model of bio-cemented materials under different saturations. The samples under different saturation conditions were made using the microfluidic experiment system (see Figure 1). The whole MICP reinforcement test equipment and the test sample are miniaturized (diameter 10mm, height 20mm) for global CT scanning to get the complete information of the microstructure. The microbial reinforcement was carried out to control the saturation of the samples. The mechanical behaviour was tested using an unconfined compressive strength test. The spatial distribution of effective cementation was obtained through image processing on the original image matrix obtained by CT scanning.

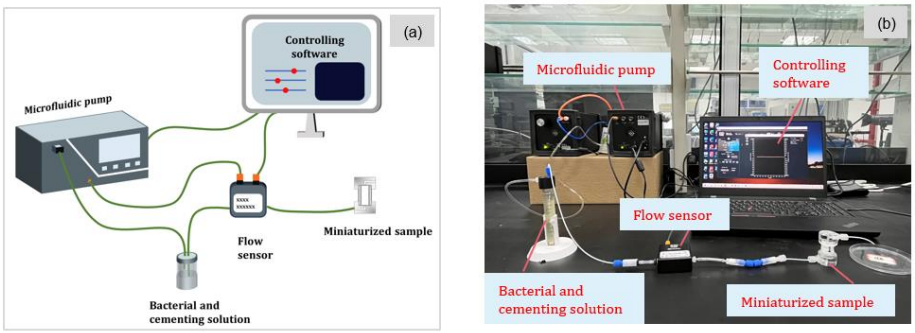

Figure 1. Microfluidic-experiment system (a) schematic diagram (b) real products

3. DEM model

The micromechanics would be observed through DEM simulation using LIGGGHTS software. The parallel bond model was used to simulate the cementation. The difference in effective cement distribution under different saturation conditions was obtained from the CT image. The different

patterns of calcium carbonate precipitation in DEM simulation are shown in Figure 2 and were characterized by changing the position of calcium carbonate. To be precise, when the sample was generated, the small particles (calcium carbonate) were added to an attractive force to change the position to simulate the effect of suction. The unconfined compressive test was reproduced to test its mechanical properties.

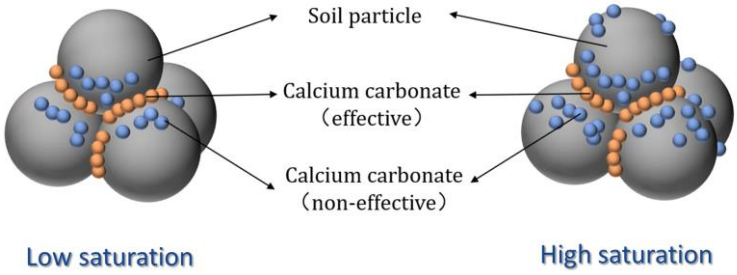

Figure 2. Discrete element model of microbially cemented sand under different saturations

4. Results and conclusion

The contact information between soil particles and calcium carbonate was extracted after establishing the DEM model. The contact types are divided into three types, namely effective cementation, surface cementation, and pore filling (see Figure 3). As can be seen from Figure 3, this method can effectively change the proportion of different contact types, which lays a foundation for future research.

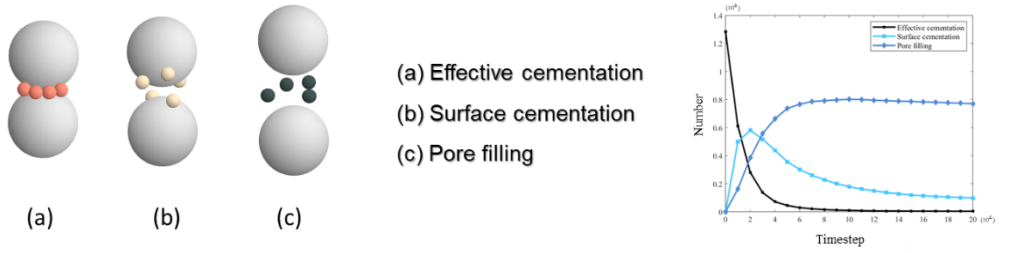

Figure 3. DEM modeling results

5. References

[1] Wang, Z. Y., Zhang, N., Cai, G. J., Jin, Y., Ding, N. & Shen, D. J. (2017). Review of ground improvement using microbial induced carbonate precipitation (MICP). *Mar. Georesour. Geotechnol.*, **35**:1135-1146

[2] Cheng, L., Cord-Ruwisch, R. & Shahin, M. A. (2013). Cementation of sand soil by microbially induced calcite precipitation at various degrees of saturation. *Can. Geotech. J.*, **50**:81-90.

JAMMING IN A GRANULAR COLUMN WITH VARIABLE FUID SATURATION: FROM MICRO TO MACRO.

J. S. Olafsen[1], M. H. McKenna Taylor[2], and O-D. S. Taylor[3]
[1]Baylor University, Department of Physics, Waco, TX USA
[2]U.S. Army Engineer Research and Development Center, U.S. Army ST Near-Surface Phenomenology, Vicksburg, MS USA
[3]ECS Southeast, LLC Baton Rouge, LA USA

1. Introduction

Understanding how porous structures become rigid and retain their strength or fail over variable saturation rates is crucial for designing materials with targeted performances under different construction conditions. This is especially true for the development of materials with time-dependent viscosities and the emerging science behind manipulatable advanced geometamaterials. Modeling unconstrained granular columns traversing from the microscale (granular temperature) to the mesoscale (internal granular force chains and interactions with pore fluid) and defining the macroscale properties, characteristics and behaviors are key to the development of a universal picture.

2. Methodology

Here, we experimentally investigate how an unconstrained granular column can retain structure over a range of saturations. Analyzing a suite of 487 macroscale tests, sigmoid saturation models were developed that define state variable interactions within the mesoscale mechanical domain (Figure 1). Both granular (dry) structure and pore-fluid (wet) structure contributions to the strength and stability are determined by experimental parameters obtained for bulk measurements from previously published studies. Physical quantities that are controlled by granular-dominant parameters or controlled by fluid-dominant parameters can be fit to sigmoid functions (Figure 2(a)) that produce a phase space envelope of strength and stability for a particular column [1].

3. The tanh Model

This led to the formulation of an energy balance model based on microscale interactions via a 1D thermostatistical picture applied to a granular temperature defined from the analysis [2]. This low-dimensional “phase space” energy model is presented that outlines contributions to relative strength and stability of jammed granular+fluid columns spanning a wide range of columns from one of small, fine, nearly monodisperse grains to one of larger, coarse, more polydisperse grains. The difference between strength and stability can thus be independently assessed simultaneously. The two domains are not necessarily synonymous (i.e., strong columns may not be stable), and the energy cost to change the stability state on the microscopic scale becomes a quantifiable physical property that manifests in macroscopic granular behavior. The model demonstrates the overall role that granular temperature plays in both the relative strength and stability of the system in a manner that allows the two characteristics to be distinguished. The quasi-one-dimensional phase space produced by the hyperbolic tangent model is nearly identical to the phase space produced by the sigmoid functions (Figure 2(a)). However, there are important differences between the two that demonstrate the tanh model as being even more revealing to the overall response of the jammed column, particularly in the

extrema of no saturation and maximum saturation. As such, the tanh model, while a macroscopic representation of the column that lacks many of the obvious two- and three- dimensional details of the real column, is a powerful way to analyze the response of the structure (Figure 2(b)).

4. Results

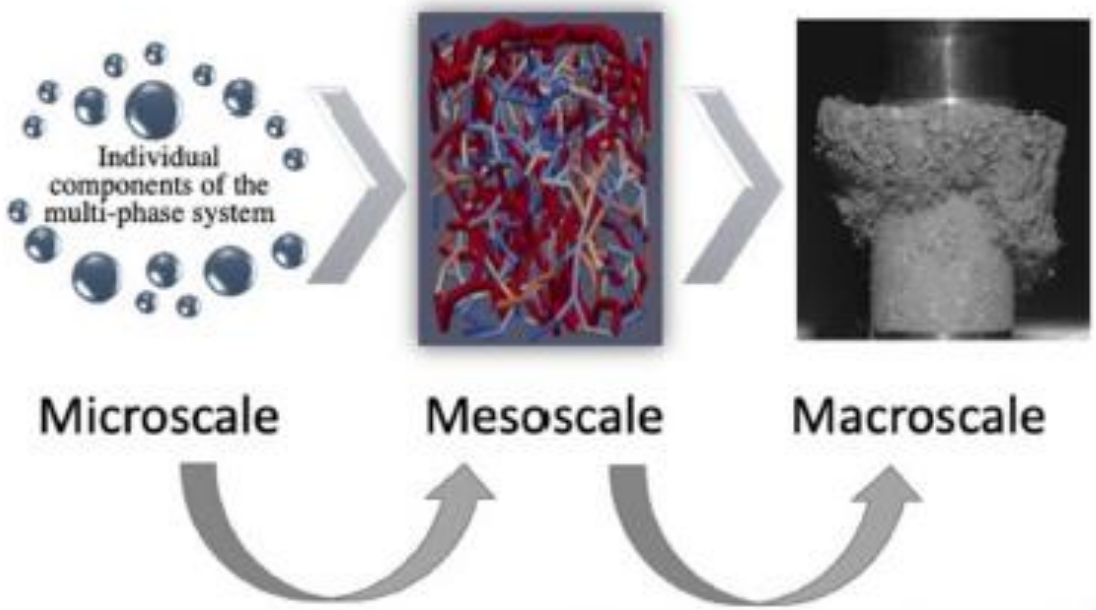

Figure 1. Microscopic measures in a mesoscopic model can predict macroscopic behavior.

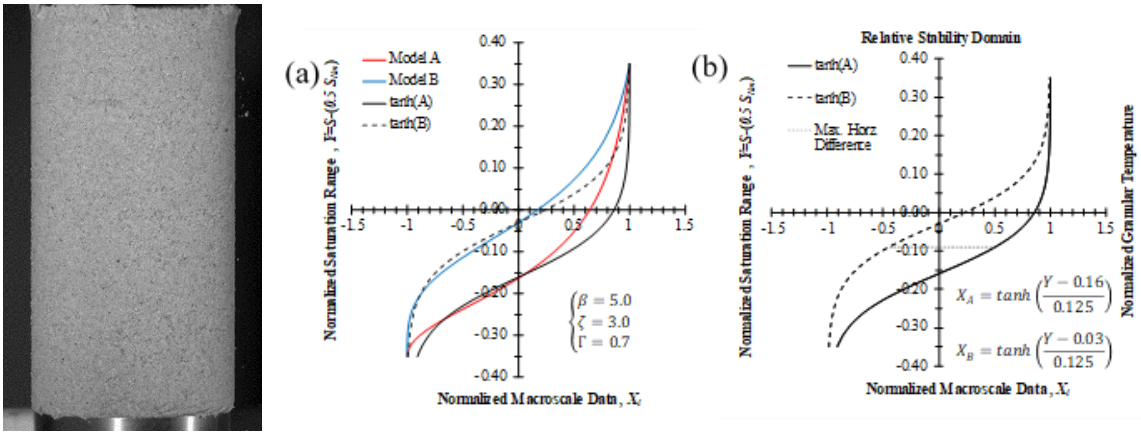

Figure 2. (a) Sigmoid curves (colored) and (b) the tanh curves (black) model phase spaces.

5. References

[1] Oliver-Denzil S. Taylor, J. S. Olafsen and M. H. McKenna Taylor, "To Fall or Not to Fall: The Physics of Sandcastles." Granular Matter **24**, 13 (2022).

[2] J. S. Olafsen, O-D. S. Taylor, and M. H. McKenna Taylor, "A low-dimensional energy model to distinguish strength and stability in a jammed column." Powder Technology, **429**, 118907 (2023). https://doi.org/10.1016/j.powtec.2023.118907.

MICROSCOPIC DISTRIBUTION OF BENTONITE IN PORE SPACES OF SAND AFTER INFILTRATION OF STABILIZING SOLUTION WITH DIFFERENT CONCENTRATIONS

R. Kido[1] and H. Ueda[1]
[1] Kyoto University, Kyoto, Japan

1. Introduction

When cast-in place pile foundations are constructed using an earth drilling technique, ground excavation is conducted using stabilizing solution made by bentonite slurry. As shown in Figure. 1, a thin mud film is formed on the excavated wall, and then the stabilizing solution pressure works well to resist to lateral earth pressure and groundwater pressure, resulting in a stable state of the excavated wall. It is possible, however, that the excavated wall collapses because solution pressure is reduced due to the infiltration of the solution into the excavated caused by incomplete formation of mud film. A previous study [1] has investigated the effective conditions to form mud film by experiments, and they found that small grain size, low permeability of soils, large water level difference, large concentration of the stabilizing solution contributes to stability of the soil wall. From microscopic viewpoint, the mud film formation probably occurs due to the clogging of cohesive clay particles included in the stabilizing solution, transported via pore networks. On the other hand, such a micro-scale phenomenon has not been clear. This is because the previous studies have focused on whether the mud film is formed or not from macroscopic viewpoint. It is, therefore, that the mechanism of the mud film formation in soils has not been clear.

The objective of the present study is to clarify the mechanism of the mud film formation during infiltration of the stabilizing solution into soils from a microscopic viewpoint. The infiltration tests using bentonite stabilizing solution with different concentrations were conducted for the sand specimen. The internal microstructure of the specimen was visualized using an X-ray micro Computed Tomography (CT), and the location where the bentonite exists and the volume of the bentonite at pore spaces are clarified using image processing techniques. The influence of the concentration of the stabilizing solution on the bentonite distribution in pore spaces is investigated.

2. Methodologies

A sand specimen saturated with degassed water is infiltrated vertically downward with a stabilizing solution made by bentonite, and the cumulative flow rate drained from the bottom of the specimen is measured. In the actual construction site, the stabilizing solution infiltrates horizontally into the ground. On the other hand, in this test the infiltration of the stabilizing solution is set in the vertical direction for the convenience of CT imaging.

The sand material used in the present study is Silica sand No.3, whose D_{50} is 1.48 mm. The specimen was prepared by the water pluviation technique with a target relative density of 60%. The stabilizing solution was prepared by mixing bentonite (Kunigel V2) and CMC (Kunipolymer A) = 7.0%: 0.1% in 2 L of water for the 6% concentration case, considering the dissolving residue.

The stabilizing solution was infiltrated into the sand specimen by applying pressure of 50 kPa, and the cumulative flow of the stabilizing solution was measured using an electronic scale. The infiltration was kept until the cumulative flow was kept constant. If the cumulative flow was kept increased, the infiltration was suspended in 10 minutes or until the stabilizing solution was depleted. Figure 1 shows the state of the surface of the sand specimen after the infiltration of the stabilizing solution with different concentrations. It is found

that there is almost no bentonite for the stabilizing solution with 3% and 4% concentrations, while there clearly exists the bentonite for the stabilizing solution with 5% and 6% concentrations. X-ray CT imaging was performed before and after the infiltration of the stabilizing solution. A voxel size was $62^2 \times 68\ \mu m^3$.

3. Results

Figure 2 shows the three-dimensional view of the bentonite distribution inside the specimen, characterized by a morphology analysis [2]. The colors in the figure are IDs that identify the clusters; different colors mean that the clusters are not contiguous with each other. This figure confirms that a continuous bentonite cluster on the surface of the specimen for the stabilizing solution with 5% and 6% concentrations, respectively, which corresponds to the results shown in Figure 1. Some large bentonite clusters exist for the 4% concentration case on the surface of the specimen, while they are discontinuous with each other. There also exist a lot of bentonite clusters inside the specimen, and it is clear that the bentonite clusters with larger volume exists for the larger concentration of the stabilizing solution. Therefore, the large concentration of the stabilizing solution leads to easily mud film creation.

4. Conclusions

It is found that the larger the concentration of the stabilizing solution is, the larger the volume the bentonite tends to distribute in pore spaces, making it easier for the mud film to be created on the surface of the sand.

5. References

[1] Nagura, K. & Higuchi, Y. (1992). Stability of slurry trench in sandy ground, *Ground Engineering*, **10**,(1) :25-32. (in Japanese).

[2] Kido et al. (2020). Morphological transitions for pore water and pore air during drying and wetting processes in partially saturated sand, *Acta Geotechnica*, **15**:1745-1761.

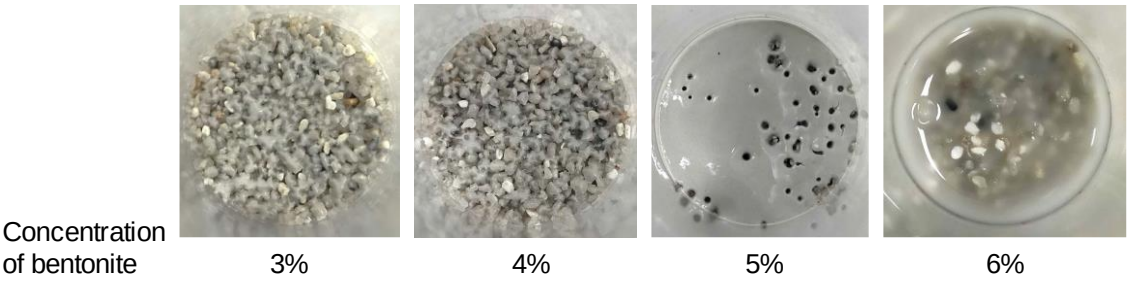

Figure 1. Surface of sand specimen after infiltration of bentonite stabilizing solution.

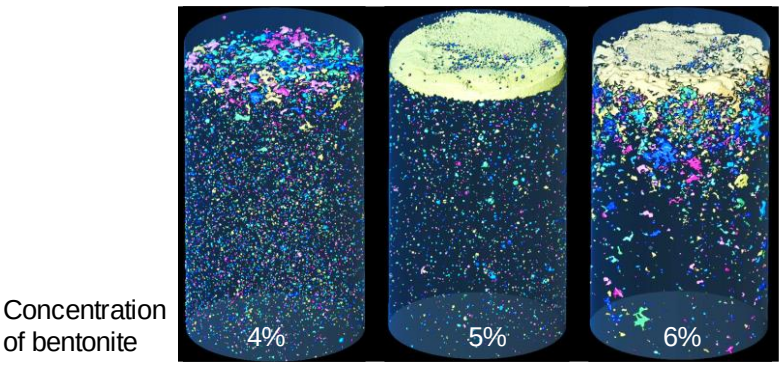

Figure 2. Three-dimensional view of bentonite distribution visualized by CT image processing.

MICRO-MECHANICS OF MULTIPHASE GEO-MATERIALS BASED ON MICRO-CT IMAGE ANALYSIS: UNSATURATED SOIL, VEGETATED SOIL AND BIO-CEMENTATION

J. Wang[1]*, J. Luan[1], M. Li[1], J. Sha[1], M. Qi[1], A. Dadda[1]
[1] Shandong University, School of Civil Engineering, Jinan, China

1. Introduction

Under the influence of climate change, extreme weather such as rainstorms may cause soil water content change above the groundwater level, which will lead to geological disasters, such as slope failure, embankment settlement, etc. [1, 2]. Green and low-carbon engineering measures such as vegetation reinforcement [3] and bio-cementation [4, 5] could be used to mitigate these hazards. However, the unclear micro-mechanism of multiphase geomaterials restricts the development of macro theory and engineering applications. X-ray computed tomography (CT) has become an increasingly popular experimental approach in geomaterials research [6-8]. In this study, the micro-mechanical properties of multi-phase geomaterials, including unsaturated soil, vegetation-reinforced sand and bio-cemented sand were studied based on CT scanning technology and related image analysis methods.

2. Experiments based on CT technology

For the experiment of unsaturated soil, triaxial tests on unsaturated sand were carried out under different suction conditions, and the loading was paused at different strain stages for CT scanning (see Figure 1).

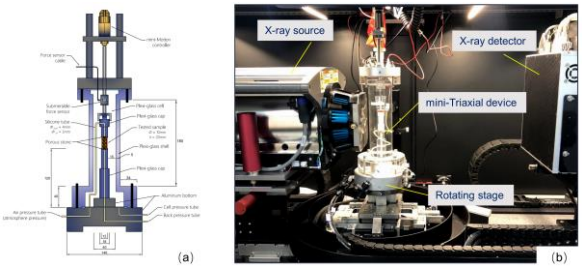

Figure 1. (a) The miniaturized triaxial device; (b) The X-ray scan set up

For the microscopic mechanism of vegetation and soil interaction, the in-situ time-domain CT scanning of the root-soil complex was carried out. A local CT scanning of the sample was performed to investigate the micromechanical properties of bio-cemented sand. The CT image processing results are shown in Figure 2.

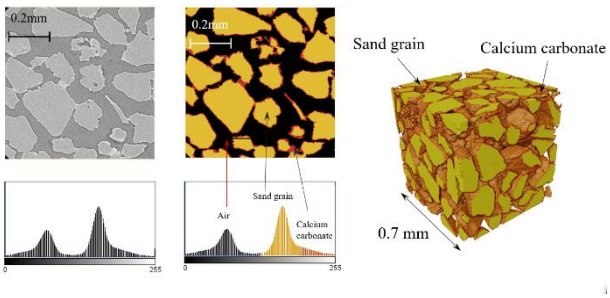

Figure 2. CT image processing results of bio-cemented sand

3. Main results

The main conclusions are as follows: (1) 4D investigation of macro and micro behaviours of unsaturated granular materials under the triaxial loading path was achieved through a self-designed in-situ CT scanning equipment. (2) The triaxial loading changes the distribution of the phase interfacial surfaces of unsaturated soil which influences the total strength. Triaxial loading expands the solid skeleton anisotropy and the suction stress anisotropy. (3) The global saturation (see Figure 3) of the root-soil complex decreases with root growth, and pore distribution predominantly impacts local saturation distribution. (4) In the unsaturated MICP process, low saturation conditions are more likely to provide effective cementation, but the saturation should not be as low as 20%. After calcification the particle contact coordination number would increase and the contact between soil particles keeps isotropy.

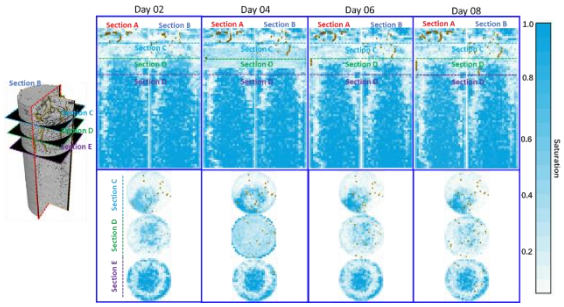

Figure 3. Saturation analysis based on RVE grid for root-soil interaction

4. References

[1] Griffiths, D. V. & Lu, N. (2005). Unsaturated slope stability analysis with steady infiltration or evaporation using elasto-plastic finite elements. *Int. J. Numer. Anal. Met.*, **29**:249-267

[2] Yao, Y. S., Ni, J. J. & Li, J. (2021). Stress-dependent water retention of granite residual soil and its implications for ground settlement. *Comput. Geotech.*, **129**

[3] Helliwell, J. R., Sturrock, C. J., Miller, A. J., Whalley, W. R. & Mooney, S. J. (2019) The role of plant species and soil condition in the structural development of the rhizosphere. *Plant Cell Environ.*, **42**:1974-1986

[4] Wang, Z. Y., Zhang, N., Jin, Y., Li, Q. & Xu, J. H. (2021) Application of microbially induced calcium carbonate precipitation (MICP) in sand embankments for scouring/erosion control. *Mar. Georesour. Geotec.*, **39**:1459-1471

[5] Xiao, Y., Ma, G. L., Wu, H. R., Lu, H. M. & Zaman, M. (2022) Rainfall-Induced erosion of biocemented graded slopes. *Int. J. Geomech.*, **22**

[6] Wang, J. P., Lambert, P., De Kock, T., Cnudde, V. & François, B. (2019) Investigation of the effect of specific interfacial area on strength of unsaturated granular materials by X-ray tomography. *Acta Geotech.*, **14**:1545-1559

[7] Ahmed, S., Klassen, T. N., Keyes, S., Daly, M., Jones, D. L., Mavrogordato, M., Sinclair, I. & Roose, T. (2016) Imaging the interaction of roots and phosphate fertiliser granules using 4D X-ray tomography. *Plant Soil*, **401**:125-134

[8] Dadda, A., Geindreau, C., Emeriault, F., du Roscoat, S. R., Garandet, A., Sapin, L. & Filet, A. E. (2017) Characterization of microstructural and physical properties changes in biocemented sand using 3D X-ray microtomography. *Acta Geotech.*, **12**:955-970

MICROMECHANICAL CHARACTERISATION OF A COMPLETELY DECOMPOSED GRANITE SOIL FROM HONG KONG

V. Nardelli[1] and M.R. Coop[2]

[1] University of Oxford, Department of Engineering Science, Oxford, United Kingdom

[2] University College London, Department of Civil, Environmental and Geomatic Engineering, London, United Kingdom

1. Abstract

Weathering is a process that leads to the physical and chemical decomposition of rocks, causing a decay of the mechanical properties of the original material and generation of a new material, which generally has different structure and composition. Weathering often occurs in tropical regions, where higher average temperatures and larger amount of precipitations accelerate this process [1]. Under the typical conditions encountered in tropical regions, chemical weathering prevails over physical weathering and the results of this process range from discolouration to a total loss of the original rock structure, giving origin to a residual soil. The territory of Hong Kong is underlain by rocks having volcanic origins (granite, granodiorite and tuff) and a significant amount of these materials is affected by weathering, even dozens of meters below the original ground level (Fig. 1).

Figure 1. CDG on a tunnel face in Hong Kong and Schmidt hammer test results (N≈0).

The weathering grade of rocks in Hong Kong, such as granite, has been studied and classified by GEO [2], which identified 6 different grades. Completely decomposed granite (CDG) is a residual soil that corresponds to Grade 5, for which the original rock texture is only partially preserved, micas are completely decomposed, feldspars are powdery to soft and zero N Schmidt rebound value are recorded. The material in its natural state can be easily crumbled by hand resulting in sand-sized particles, which typically are hard quartz grains surrounded by a soft coating [3, 4]. This material covering the surface of quartz grains is the resultant of the chemical decomposition of mica and feldspar, and the individual particles found on the coating have silt to clay size. CDG is often used as a fill material or for the construction of land reclamation for the expansion of urban areas.

CDG from Hong Kong has been previously studied by means of element tests. Typical angles of shearing resistance at critical state for this material are around 38° [3], whereas values between

32° and 38° were measured for both CDG and specimens characterised by different weathering degrees (e.g., highly decomposed granite) [5]. The inhomogeneous structure of CDG justifies approaches other than that of continuum mechanics and therefore the study presented hereby, for which CDG particle pairs have been tested at their contacts.

The experiments on CDG particles were performed using an inter-particle loading apparatus, which was custom-designed and built for the purpose of studying the micromechanical contact behaviour of grains [4]. The apparatus was equipped with linear actuators, high-resolution load cells and eddy-current displacement sensors installed along three orthogonal axes in order to apply different displacement and/or loading combinations at particle contacts (Fig. 2a). The micro-scale behaviour of CDG was studied by carrying out normal loading and tangential loading tests on natural particles. Also, a selected number of particles were "washed", in order to remove the soft coating covering the quartz particles and study the behaviour of the hard grains constituting the CDG solely. The particles of the washed material (WCDG) were characterised by surface roughnesses and regularity lower than those of the natural CDG (Fig. 2a and b).

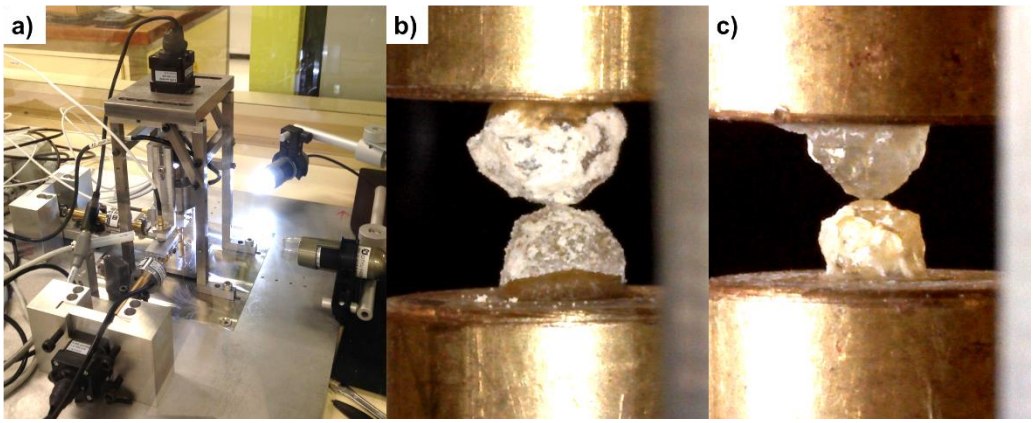

Figure 2. a) Inter-particle loading apparatus; b) CDG particles during a test; c) WCDG particles.

The results show that the CDG behaviour under normal loading is heavily affected by the soft coating, which affects the contact stiffness, when compared to WCDG. On the other hand, given the scatter of the data, a clear effect of the soft coating on the tangential loading response cannot be easily identified. The results obtained for CDG and WCDG were compared to those obtained for Leighton Buzzard quartz sand (LBS), which was extensively studied at the micro-scale [4] and can be considered a suitable reference material considering its shape, surface and mechanical properties.

2. References

[1] Mitchell, J.K. and Soga, K. (2005). Fundamentals of Soil Behavior. 3rd Edition, John Wiley & Sons, New York.

[2] Geotechnical Engineering Office (2017). Geoguide 3, Guide to rock and soil descriptions. Hong Kong.

[3] Madhusudhan, B. N. and Baudet, B. A. (2014). Influence of reconstitution method on the behaviour of completely decomposed granite. Géotechnique, **64**, No. 7, 540–550.

[4] Nardelli, V., and Coop, M.R. (2019). The experimental contact behaviour of natural sands: normal and tangential loading. Géotechnique, **69** No. 8, 672–686.

[5] Rocchi, I. and Coop, M.R. (2015). The effects of weathering on the physical and mechanical properties of a granitic saprolite. Géotechnique, **65**, No. 6, 482–493.

NUMERICAL INVESTIGATION OF PARTICLE CRUSHING EFFECT ON PORE STRUCTURE EVOLUTION AND UNSATURATED SOIL CHARACTERISTICS

M.S. Alam[1], S. Mufti[1] and A. Das[1]
Department of Civil Engineering, Indian Institute of Technology Kanpur, India

1. General

Investigating particle crushing in geomechanics is crucial for a comprehensive understanding and prediction of the hydro-mechanical behavior of soils. Recently, there has been a growing focus on particle crushing in soils, driven by mounting evidence highlighting its significant role in dam engineering, transportation infrastructure, and pile design. The implications of particle crushing extend beyond mere mechanical alterations, as they encompass changes in the void structure of soil, thereby influencing the hydraulic properties of soils [1]. This transformative process alters the water retention capacity of soils and induces changes in hydraulic conductivity, underscoring the multifaceted impact of particle crushing on the broader geotechnical landscape.

However, due to the time-consuming nature of experiments required to measure soil water retention curve (SWRC) and unsaturated hydraulic conductivity function (UHCF), studies addressing the impact of particle crushing on SWRC and UHCF are limited. Therefore, this work aims to investigate the effects of particle crushing on the void structure of granular soils, contributing to a more nuanced understanding of this complex soil-water interplay.

2. Methodology

This study employs pore network modeling (PNM) to predict the pore structure evolution under different stress intensities, reflecting varying degrees of particle crushing. Pore network modeling, a relatively recent simulation technique in geomechanics, conceptualizes the void structure of porous media as a network comprising interconnected pores and throats [2]. The methodology for investigating the impact of particle crushing on void structure and unsaturated characteristics comprises two distinct phases:

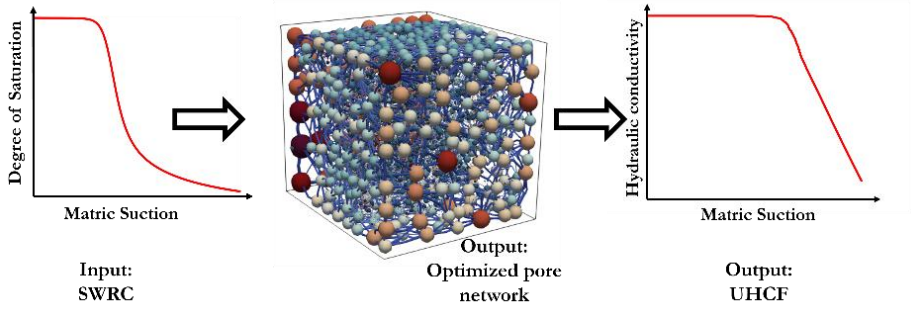

Figure 1 Workflow for predicting UHCF.

1. Generating Pore Network Models (PNM): This process involves establishing PNM parameters that represent the void structure of granular soils within a cubic domain, sized at 20

times the mean particle diameter. Subsequently, pores are randomly placed in the domain and interconnected via throats. The shapes of pores and throats are determined by the shape factor, defined as the ratio of the cross-sectional area to the square of its perimeter. Pore size distribution, aspect ratio distribution (influencing throat size), and coordination number distribution (influencing connectivity) are assumed to adhere to a truncated Weibull distribution. The shape and scale parameters of the Weibull probability density function for each property are optimized using genetic algorithm, with SWRC serving as input. These optimized pore network models accurately represent the void structure of soils and are instrumental in studying the evolution of void structure due to particle crushing.

2. Predicting UHCF: Once pore networks corresponding to varying degrees of particle crushing are obtained, the second phase involves simulating air-water flow within these networks to predict UHCF. Both drainage (air displacing water) and imbibition (water displacing air) are simulated in the pore network by incorporating relevant pore-scale processes. This includes piston-type advance and corner flow during drainage, as well as piston-type advance, snap-off, and I_n mechanisms during wetting [3]. Applying a pressure gradient across the water phase and assuming the two phases flow independently of each other allows for the determination of UHCF.

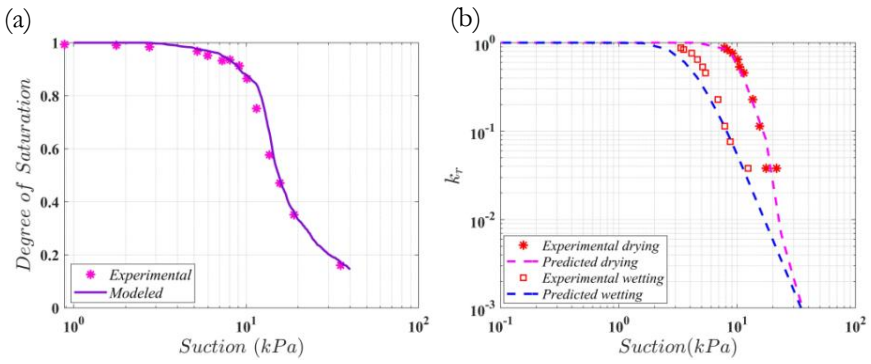

Figure 2 (a) Optimized SWRC. (b) Predicted UHCF.

3. Results

Figure 2 shows the predicted UHCF using the proposed. The experimental data [2] is availed for generating pore network models of soils which are used to investigate the alterations in the void structure of soils and the consequent impact on the UHCF caused by particle crushing.

4. References

[1] Gao, S., Zhang, Y., Sonta, A., & Buscarnera, G. (2016). Evolution of the Water Retention Characteristics of Granular Materials Subjected to Grain Crushing. *J. of Geotech. Geoenv. Engg.*, 142(9):1-8.

[2] Mufti, S. & Das, A. (2023). Multiscale pore network construction for two phase flow simulations in granular soils. *Adv. Water Res.*, **173**:1-16.

[3] Mufti, S. & Das, A. (2022). An advanced pore-scale model for simulating water retention characteristics in granular soils. *J. Hydrol.*, **615**(Part A):1-14.

On the role of porous aggregates in the fracture mechanisms of lightweight concrete using XCT and Machine Learning

***Z. Karatza*[1], *N. Gkikizas Lampropoulos*[2], *K. Tsivolas*[1], *I. Kumpová*[3], *K. Sotiriadis*[3], *P.P. Nomikos*[4] *and E. Badogiannis*[1]**

[1] *School of Civil Engineering, National Technical University of Athens, Greece*

[2] *Satalia, London, UK*

[3] *Institute of Theoretical and Applied Mechanics of the Czech Academy of Sciences, Czech Republic*

[4] *School of Mining & Metallurgical Engineering, National Technical University of Athens, Greece*

1. Introduction

The need to reduce CO_2 emissions, or make use of sustainable materials to increase the life cycle of urban construction has led to the development of alternative types of concrete with properties such as self-compaction, self-healing, or low density etc. Lightweight concrete (LWC) (i.e. density between 1120 and 1920kg/m^3) offers several advantages, including reduced construction costs, a high strength-to-weight ratio, low coefficient of thermal conductivity and improved durability [1], yet cracking at early ages poses a significant concern for its structural use [2]. In this work, we use X-ray computed tomography (XCT) to get full-field measurements of LWC before and after loading that will enhance our understanding of how pumice affects the development of tension cracks in the concrete matrix.

2. Materials and experimental campaign

Lightweight concrete specimens of 200mm height and 100mm diameter were cast using ordinary Pozzolanic cement, CEM IV/B (P-W) 32.5R (380kg/m^3) with 0.40 water-to-cement ratio, limestone sand and gravel (0-4mm and 4-8mm, respectively), pumice (8-16mm), and a commercially available silica fume (SikaFume HR-D; 20 kg/m^3) as an additive. The raw concrete contained 5.2% air and had a fresh concrete density of 1820kg/m^3, both measured according to the ASTM C138/138M-17a standards. After 28 days of curing, the compressive strength of the LWC was measured at 22.7MPa. 3D images were acquired before loading (LWC-i) and after failure (LWC-f) using a custom-developed patented Twinned Orthogonal Adjustable Tomograph [3], and were reconstructed with a voxel size of 72.725µm.

3. Image processing with Machine Learning

Machine Learning was used to create a model that can detect whether a new (unseen) image has pumice particles, as well as their exact position in the image, given a set of pairs (X,y) where X is a 2D greyscale image of concrete and y its binary image (1: pumice, 0: everything else). To implement this, a Deep Neural Network (DNN) is used. The exact architecture is a modification of the original U-NET [4] with 512 x 512 pixel, greyscale images as input. The training utilises a GPU-powered virtual machine in the cloud. The process resulted in a model with a testing accuracy of approximately 96%.

For the training, an image representing ground truth had to be defined. One of the greyscale images was originally binarised using the open-source software Fiji. This resulted in an image where both the pumice and pores were filtered out of the concrete specimen due to their similar range of grey values, after which the pumice was isolated taking advantage of its highly non-circular shape and much larger size compared to the pores. This required several iterations and user interventions, however, justifying the creation of the DNN model.

4. Results and Conclusions

Breakage is mainly located around areas of high concentration in pumice or large macroscopic pores (e.g. arrows in left images in Fig. 1), as expected due to the lower strength of pumice (Los Angeles coefficient, LA = 38) in comparison with the limestone aggregates (LA = 21). when fractures develop in the rest of the specimen, they tend to form along the boundaries of the limestone aggregates, as can be seen in the right images in Fig. 1.

The images of pumice indicate an anisotropy in their intra-porosity, evidenced by the rounder or more elongated pores shown in the orthogonal to the loading slices in the central images in Fig. 1. Therefore, the direction of the pumice particles, to that of loading, will dictate whether a particle will break or not. The use of the DNN model will provide a quantitative description of the orientation of the pores, and the shape and orientation of the particles, explaining the development of the fracture network.

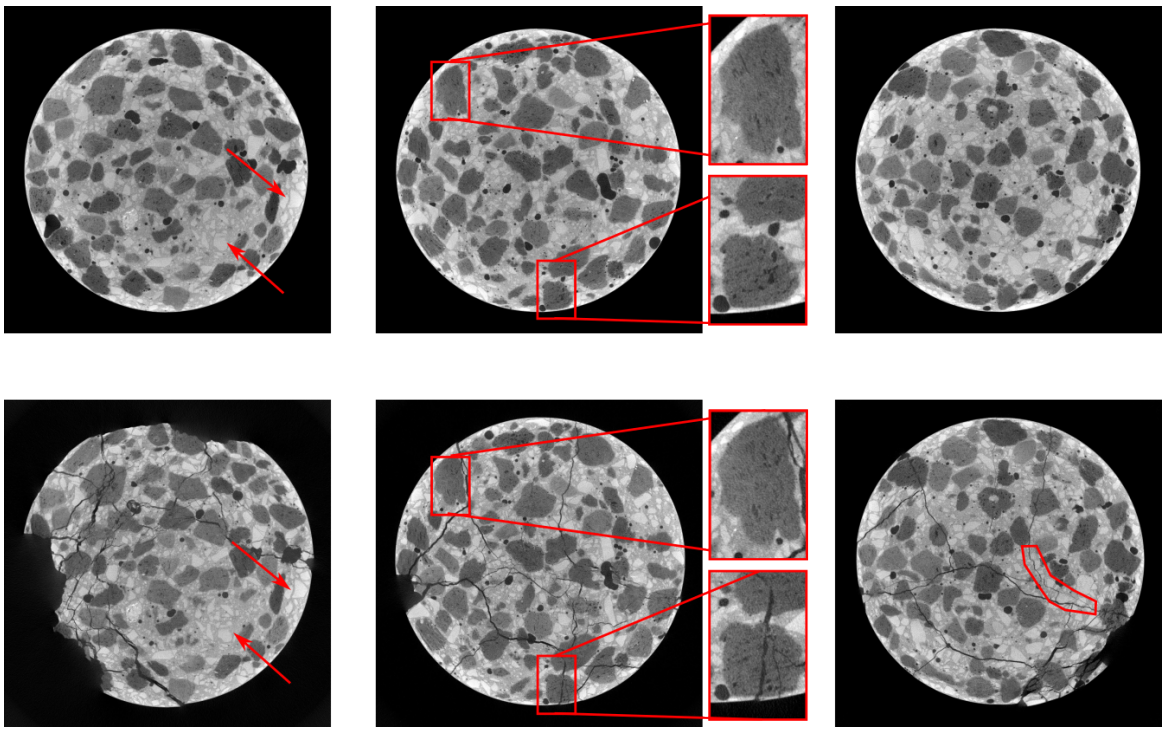

Figure 1. Examples of fracture mechanisms. Top row: LWC-i, bottom row: LWC-f.

References

[1] Anwar Hossain, K. M. (2004). Properties of volcanic pumice based cement and lightweight concrete. *Cement and Concrete Research*, **34**, 283–291.

[2] Badogiannis, E., Christidis, , and Tzanetatos, G. (2019). Evaluation of the mechanical behavior of pumice lightweight concrete reinforced with steel and polypropylene fibers. *Construction and Building Materials*, **196**, 443–456.

[3] Sotiriadis, K., Hlobil, M., Viani, A., Mácová, P., and Vopálenský, M. (2021). Physical-chemical-mechanical quantitative assessment of the microstructural evolution in portland-limestone cement pastes exposed to magnesium sulfate attack at low temperature. *Cement and Concrete Research*, **149**, 106566.

[4] Ronneberger, O., Fischer, P., and Brox, T. (2015)., U-net: Convolutional networks for biomedical image segmentation.

PARTICLE SHAPE CLASSIFICATION AS A TOOL TO INFORM THE GENERATION OF REPRESENTATIVE ELEMENT VOLUMES IN THE DISCRETE ELEMENT METHOD

***V. Angelidakis*[1,2], *S. Nadimi*[2] *and S. Utili*[2]**
[1] *Queen's University Belfast, School of Natural and Built Environment, Belfast, United Kingdom*
[2] *Newcastle University, School of Engineering, Newcastle upon Tyne, United Kingdom*

1. Motivation and significance

Natural granular materials, such as geomaterials, feature a wide variety of irregular particle shapes, which makes their behaviour challenging to predict. Discrete element simulations can shed light into the micromechanics of systems with irregular particles, but modelling realistic particles is not a straightforward process, mainly due to numerical challenges and lack of a systematic selection process of appropriate particle shapes to be simulated. This work introduces a method to generate Representative Element Volumes (REVs) of non-spherical particles, which represent the statistical distribution of particle size and shape. Railway ballast is selected here as the material of choice, as it consists of highly irregular particles which have the capacity to interlock due to their shape, while it bears tremendous importance for railway infrastructure worldwide.

2. Particle shape analysis

Imaging data of 100 real granite ballast particles derived via laser scanning [1] are analysed, with sizes varying from 16 mm to 63 mm (D_{50} = 41 mm). Particle shape is characterised in the `SHAPE` open-source code [2] in terms of elongation (el), flatness (fl) and compactness (co), using a recently proposed set of formulae (Equation 1), and their shape is classified into four categories, namely flat, compact, bladed and elongated, as shown in Figure 1. Classification is carried out using a newly developed classification system [3] based on the values of these indices, which improves on known shortcomings of the Zingg system.

$$el = \frac{a \cdot c}{a \cdot c + b^2} - \frac{c}{a + c} \qquad fl = \frac{b^2}{a \cdot c + b^2} - \frac{c}{a + c} \qquad co = \frac{2 \cdot c}{a + c} \tag{1}$$

These particle scans are employed to generate multi-sphere (clump) representations for each particle using the `CLUMP` open-source code [4] and a newly developed clump generation method based on the Euclidean distance transform of three-dimensional images.

3. Discrete element modelling of triaxial compression tests

Simulations of triaxial compression are then performed for granular packings of 5000 multi-sphere particles made of the 100 different particle shapes, i.e. following the real particle shape distribution of the sampled material. The shearing resistance of the material at the bulk scale is expressed via the macroscopic mobilised friction angle, calculated based on the maximum and minimum principal stresses σ_1 and σ_3, respectively:

$$\phi = \arcsin\left(\frac{\sigma_1 - \sigma_3}{\sigma_1 + \sigma_3}\right) \tag{2}$$

Models of simplified particle shape distributions of low polydispersity are also constructed, to test their efficacy in approximating the shearing resistance of the highly polydisperse sample. These simplified shape distributions are made of only four different particle shapes, taking one characteristic shape for each of the four distinct shape classes, as shown in Figure 1. It is found that REVs

with simplified representation of shape polydispersity can adequately model the shear strength of the railway ballast material, as long as the statistical distribution of flat, compact, bladed and elongated particles is in proportion to the that of the real material.

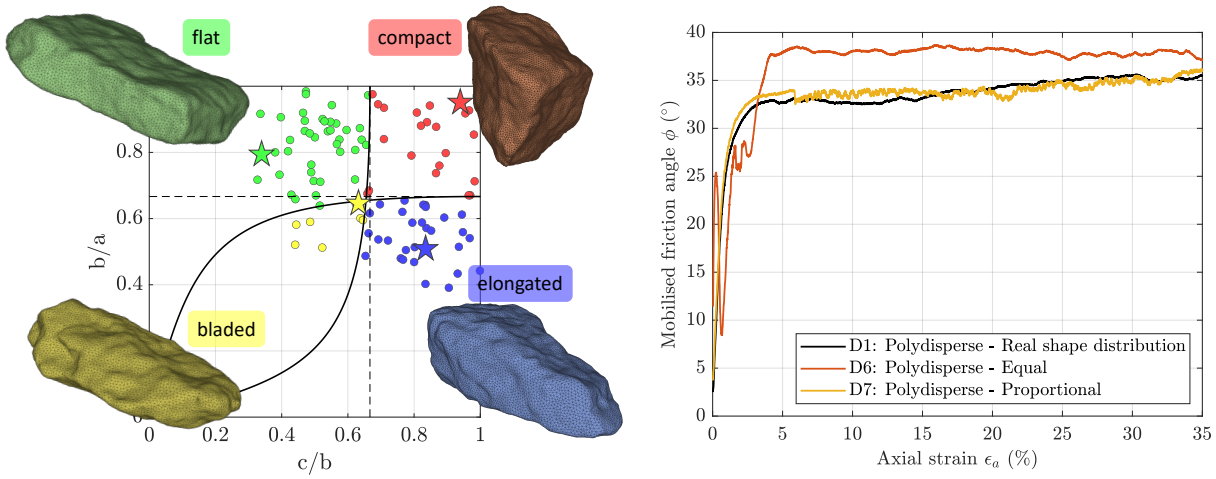

Figure 1. Particle shape classification and characteristic particles of each class (left); macroscopic friction angle considering the real shape distribution (D1) and simplified distributions where four particles are used in equal amounts (D6) and in proportion (D7) to the real shape distribution (right).

Table 1. Particle shape distributions.

Shape distribution	Different particle shapes	flat	compact	bladed	elongated
Real	100	37%	23 %	9%	31%
Equal	4	25%	25%	25%	25%
Proportional	4	37%	23%	9%	31%

References

[1] Xiao, J., Zhang, D., Wei, K., and Luo, Z. (2017). Shakedown behaviors of railway ballast under cyclic loading. *Construction and building materials*, **155**, 1206–1214.

[2] Angelidakis, V., Nadimi, S., and Utili, S. (2021). SHape Analyser for Particle Engineering (SHAPE): Seamless characterisation and simplification of particle morphology from imaging data. *Computer Physics Communications*, **265**, 107983.

[3] Angelidakis, V., Nadimi, S., and Utili, S. (2022). Elongation, flatness and compactness indices to characterise particle form. *Powder Technology*, **396**, 689–695.

[4] Angelidakis, V., Nadimi, S., Otsubo, M., and Utili, S. (2021). CLUMP: a code library to generate universal multi-sphere particles. *SoftwareX*, **15**, 100735.

PORE NETWORK 3D RECONSTRUCTION FOR CLAYS USING FIB-SEM IMAGES

Fares Bennai[1], Yanzheng Ding[1], Mohamad Jrad[1], Julien Guyon[1], Mahdia Hattab[1],
[1]Université de Lorraine, CNRS, Arts et Métiers ParisTech, LEM3, F-57000 Metz, France

Abstract

The study of the microstructure of clays could provide valuable information regarding the fabric of the clay and the pore space within the material. Under the influence of mechanical loading, local mechanisms can be activated at the microstructural scale, dependent on the loading path applied at the scale of the clay's Representative Elementary Volume (REV). Consequently, pores can undergo changes in size, shape, and orientation. Given that pores serve as conduits for water transfers in the soil, these changes can impact the macroscopic properties of clay, such as permeability. For instance, oedometric loading may induce an anisotropy in permeability between directions parallel and the perpendicular to the stress axis.

The aim of this study is to propose a new approach permitting the investigation of the 3D pore variation of kaolin K13 in relation to mechanical loading, with a specific focus on pore space identification and quantification. To achieve this, we developed a methodology using FIB-SEM imaging coupled with image processing techniques to generate a three-dimensional microstructure from an appropriate 3D reconstruction. This analysis can enhance our understanding of the clay microstructure state, as well as the evolution of local mechanisms in relation with the mechanical loading.

Kaolin K13, characterized by geotechnical parameters (liquid limit wL = 42%, plastic limit wp = 21%, and solid density ρs = 2.63 g/cm3), serves as the studied clay.

To prepare the sample, the clay was mixed with distilled water to obtain a slurry with a water content 1.5 times the liquid limit (i.e., $w_0 = 1.5w_L$). Subsequently, it was introduced into either a double drainage consolidometer for one-dimensional compression at 120 kPa or into an oedometer cell for loading at various stress levels. After each mechanical test, a small parallelepiped sample was cut from the loaded specimen and subjected to freeze-drying for post-mortem microscopic observations.

A protocol using scanning electron microscopy (SEM) coupled with Focused Ion Beam (FIB) was carried out to observe and then obtain a large number of slices of an extracted sub-volume from the small sample. Image analysis, using a new processing method, enabled the reconstruction of the observed and extracted sub-volume into a 3D structure. A protocol for pore identification was proposed consisting of three steps: alignment of images to rebuild the extracted sub-volume from the observed small sample, machine learning segmentation of pores and particles, and individualization using a watershed algorithm.

Pore network properties were studied through different parameters like size, orientation, and morphology, analyzing pore elongation and flatness. Results of Pore Size Distribution (PSD) were compared with those obtained by mercury intrusion porosimetry.

The results obtained and the method developed in this study highlight the significant potential of three-dimensional FIB-SEM observations in characterizing the microstructures of saturated remolded clays.

Keywords: clay, FIB - SEM observations, pore network, machine learning, microstructure

SEALING CAPACITY OF A PRE-FISSURED OPALINUS CLAY TO CO_2 INJECTION

E. Stavropoulou [1] and L. Laloui [1]
[1] École Polytechnique Fédérale de Lausanne (EPFL), Laboratory for Soil Mechanics (LMS), EPFL-ENAC-LMS, Station 18, 1015 Lausanne, Switzerland

1. Introduction

The integrity of low-permeability caprocks such as shales, is crucial for CO_2 containment, particularly at early times when the buoyancy of the injected CO_2 might drive upward migration, or in cases where the reservoir is overpressured during injection. In such situations, the transport behaviour of fractures, either naturally pre-existing or induced, in the sealing unit becomes crucial for evaluating the safety of injected CO_2. The sealing and transport properties of intact Opalinus Clay make it a good caprock candidate for geological CO_2 storage: CO_2 entry pressures between 2 and 6 MPa and water permeability in the order of 10^{-20} m^2 [1, 2]. Therefore, for lower CO_2 overpressures, leakage through low-permeability caprocks requires the presence of fractures. The long-term evolution of such potential conduits is highly uncertain and dependent on an intricate coupling between geomechanical and hydrogeological processes. For instance, the Opalinus Clay has been shown to induce self-sealing in conductivity due to clay swelling when in contact with water [3]. However, the impact of CO_2 flowing through micro-fractures in shaly caprocks is not yet well understood as different competing mechanisms take place (e.g. caprock desiccation, local effective stress modification) [4]. In this work, the processes associated with the role, initiation and propagation of fissures in caprocks are studied.

2. Methodology and tools

CO_2 injection is performed in a pre-fissured Opalinus Clay sample and the hydromechanical response of the material is analysed with quantitative image analysis of real-time x-ray tomographies. To study the sealing capacity of the caprock material, a new high pressure mini-cell has been designed that allows CO_2 injection during live x-ray tomography (XRCT). This original cell can reproduce conditions representative to the field including high loading stress (max. 30 MPa) and pore pressure (max. 16 MPa). The mini-cell is designed to host cylindrical samples of 5 mm diameter and 10 mm height. A pixel size of 6 μm is achieved during a scan duration of 1 h. The impact of CO_2 injection on the sealing capacity of the material is studied directly from the acquired tomographies and compared to previous results of CO_2 breakthrough.

3. CO_2 injection in pre-fissured Opalinus Clay

CO_2 injection is performed in a pre-fissured Opalinus Clay sample under isotropic confinement. An initial confining stress p = 3 MPa is applied (scan 00) that is increased to 10 MPa (scan 01). Water is then introduced in the downstream line of the sample in contact with the top side of the sample under atmospheric pressure during 2 days (scan 02). CO_2 is introduced from the bottom of the sample (upstream line) and injected under drained conditions at four different pressure levels: 1 MPa (scan 03), 2 MPa (scan 04), 3 MPa (scan 05) and 4 MPa (scan 06). A final scan (07) is performed after unloading the sample to zero pore pressure and confining stress. The middle horizontal and vertical slice of the sample at each scan are presented in Figure 1.

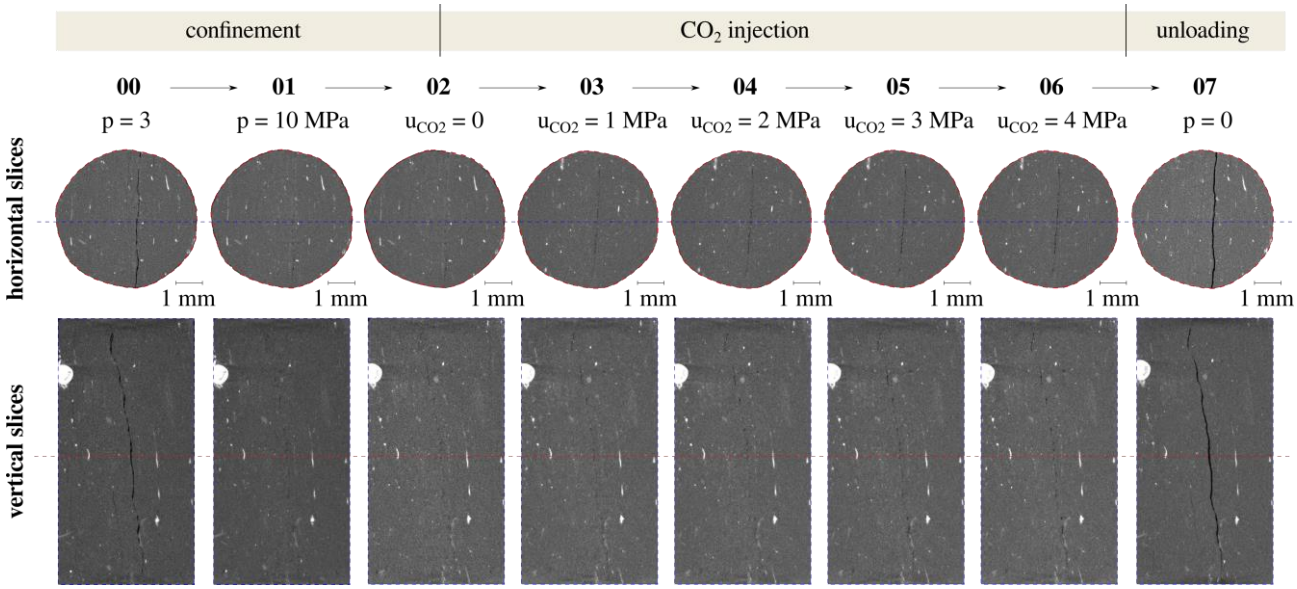

Figure 1. Horizontal and vertical slices of the x-ray tomographies during the different testing phases – the straight dashed lines indicate the location of the corresponding perpendicular slices.

CO_2 injection results in fissure opening already during the first pressure level (1 MPa) (reference scan 02). During the following two injection steps (2 and 3 MPa) the fissure opens further, while it remains stable during the last injection step (4 MPa). This response suggests that until uCO2 = 3 MPa (scan 04), the main pre-existing fissure serves as the principal CO_2 conduit. A pronounced swelling of the intact material at the bottom of the sample combined with the stabilisation of the fissure at u CO_2 = 4 MPa, indicates CO_2 entry in the material, i.e. breakthrough pressure from 3 to 4 MPa.

4. Conclusions

The exact CO_2 breakthrough pathway in the caprock is not easy to predict because of the extremely small pore size (nano-metric scale) and the high micro-structural heterogeneity of the material. In this work, 3D imaging of a pre-fissured caprock sample revealed that the main fissure drives the hydromechanical response of the material until a certain injection level. The fissure starts re-opening already at low CO_2 overpressure (1 MPa) until a certain level (3 MPa) where it does not seem to further evolve (4 MPa). The fissure kinematics combined with the overall volumetric response of the sample suggest that at the final injection step the contribution of the fissure to CO_2 migration is stable and CO_2 breakthrough in the matrix of the material takes place.

5. References

[1] Minardi, A., Stavropoulou, E., Kim, T., Ferrari, A., & Laloui, L. (2021). Experimental assessment of the hydro-mechanical behaviour of a shale caprock during CO2 injection. International Journal of Greenhouse Gas Control, 106, 103225.

[2] Stavropoulou, E., & Laloui, L. (2022a). Evaluating CO2 breakthrough in a shaly caprock material: a multi-scale experimental approach. Scientific Reports, 12(1), 10706.

[4] Voltolini, M., & Ajo-Franklin, J. B. (2020). The sealing mechanisms of a fracture in opalinus clay as revealed by in situ synchrotron x-ray micro-tomography. Frontiers in Earth Science, 8, 207.

[3] Stavropoulou, E., & Laloui, L. (2022b). Insights into the interaction of a shale with CO2. Solid Earth, 13(12), 1823-1841.

Sub-pore scale analysis of particle-fluid heat conduction in granular materials

T. Morimoto[1,2], C. O'Sullivan[2] and D. M. G. Taborda[2]
[1] The University of Tokyo, Department of Civil Engineering, Tokyo, Japan
[2] Imperial College London, Department of Civil and Environmental Engineering, London, UK

1. Introduction

Investigating heat transfer in granular materials is of great importance to a variety of engineering fields. In geotechnical engineering, there is increasing deployment of thermo-active structures, such as piles, retaining walls and tunnels, and this motivates studies into heat transfer phenomena in soils under substantial groundwater flow.

Particle-fluid heat conduction can be characterised using the Nusselt number (Nu), defined as:

$$Nu = \frac{h\mathcal{L}}{k_f} \tag{1}$$

where h is the convective heat transport coefficient [$W \cdot K^{-1} \cdot m^{-2}$], $\mathcal{L}$ is the characteristic length [m], and k_f is the thermal conductivity of the fluid [$W \cdot K^{-1} \cdot m^{-1}$]. Recently, Morimoto et al. [1] proposed the following expression for Nu for a single pore throat based on fully-resolved Computational Fluid Dynamics (CFD):

$$Nu = 1.453 Nu_{pipe} \tag{2}$$

where Nu_{pipe} is the Nu value for a pipe with a constant cross-section, which has the same $f \cdot Re$ as the pore throat (f being the friction factor and Re the Reynolds number), the same length and the same hydraulic radius as the pore throat (the ratio of the fluid volume to the wet solid surface area). This equation suggests that granular materials may more efficiently transport heat between solid to fluid than a pipe with a constant cross-section due to their complex geometry at a pore-scale. This expression can be implemented in a pore-network model, ultimately enabling coupled DEM-CFD simulations of heat transfer.

To improve understanding of particle-fluid heat conduction in granular materials, this paper describes sub-pore scale analysis using a fully-resolved CFD simulation approach.

2. Methods

Heat transfer simulations considering fully saturated regular (face-centred cubic) packings of uniformly-sized spheres were completed using OpenFOAM [2]. In these simulations the temperature of the particles was fixed at T_s. The results of these analyses were validated against data in Zick and Homsy [3] and Romkes et al. [4]. From the simulation data, a sub-domain comprising a single pore throat was identified to be a single fluid pipe within the pore space (see Figure 1). This fluid pipe, which corresponds to an edge in a pore network model, was discretized into 31 regions as schematically illustrated in Figure 2. Each region is characterised by its particle-fluid heat flux ($\boldsymbol{q}$), the velocities of the inlet and outlet faces ($\boldsymbol{u_{in}}$ and $\boldsymbol{u_{out}}$), and the temperature of the inlet and outlet faces (T_{in} and T_{out}), with which the sub-pore scale Nu can be calculated.

3. Results

The sub-pore scale Nu values for a single pore throat in FCC packings with a variety of solid fractions (ϕ) and the same Peclet (Pc) number of 15 are shown in Figure 3. As seen in Figure 3, the

Nu values are higher for the inlet and outlet of the pores. This may imply that converging-diverging shape of the fluid pipes in granular materials contribute to more efficient particle-fluid heat transfer.

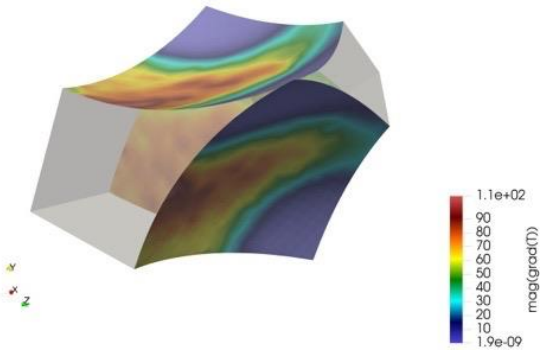

Figure 1. A unit fluid pipe of a face centred cubic (FCC) packing. Particle surfaces were coloured based on the magnitude of the particle-fluid heat flux.

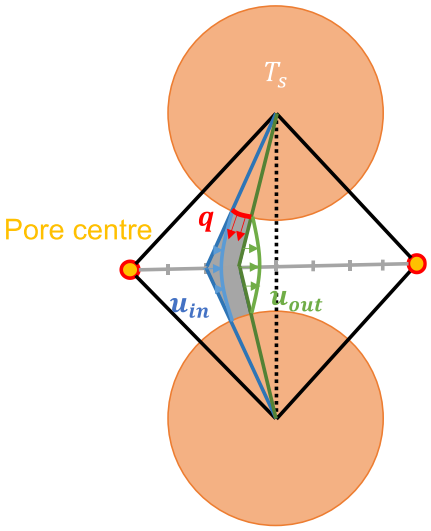

Figure 2. Schematic illustration of the sub-pore scale analysis.

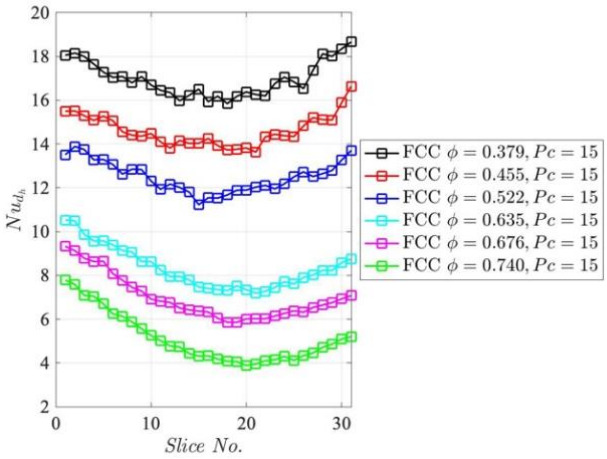

Figure 3. The Nusselt number distribution at a sub-pore scale.

5. References

[1] Morimoto, T., O'Sullivan, C., & Taborda, D. M. (2023). Capturing particle-fluid heat transfer in thermo-hydro-mechanical analyses using DEM coupled with a pore network model. *Powder Technology*, **429**, 118944.

[2] Weller, H. G., Tabor, G., Jasak, H. & Fureby, C. (1998) A tensorial approach to computational continuum mechanics using object-oriented techniques. *Computers in physics*. **12** (6), 620–631.

[3] Zick, A. & Homsy, G. (1982) Stokes flow through periodic arrays of spheres. *Journal of fluid mechanics*. **115**, 13–26.

[4] Romkes, S., Dautzenberg, F., Van den Bleek, C. & Calis, H. (2003) CFD modelling and experimental validation of particle-to-fluid mass and heat transfer in a packed bed at very low channel to particle diameter ratio. *Chemical Engineering Journal*. **96**, 3–13.

TENSILE BREAKAGE OF PARTICLES IN GRANULAR MEDIA

J. Sánchez[1], G. Auvinet[2] and B. Cambou[3]
[1] Univ. Nacional Autónoma de México, FES Aragón, CIMA., México, México
[2] Univ. Nacional Autónoma de México, Instituto de Ingeniería, México, México
[3] École Centrale de Lyon, LTDS, Lyon, France

1. Abstract

The experience in dam construction and laboratory tests has shown that grain breakage is present even at low stress levels [1]. Changes in grain size distribution, porosity and therefore the deformation characteristics of the granular material have been observed [1, 2]. Two main factors control the breakage of particles in a granular medium: the resistance of the rock particles and the contact forces acting on them.

This paper proposes a method to assess the probability of breakage by tension of particles in a granular medium subjected to a triaxial stress state. It is considered that the intragranular acting tensile stress (T) and the resistant stress (R_T) are random variables. The probability of breakage is calculated by comparing of the probability densities of the tensile strength and the acting tensile stress on the grains.

Several triaxial test resorting to Discrete Element Method (DEM) were simulated. Each granular sample consist of 30,000 friction spheres subjected to an initial isotropic confinement σ_3=1MPa. For the present study, granular samples of monosized spheres, binary (mixture of two particle sizes) and continuous grain size distributions are considered.

DEM numerical simulations allow to evaluate the acting forces at contact points of the particles for different stress levels. From these forces, the acting stress tensor is computed for each particle [3, 4], and the maximum tensile stress (T) is estimated. Then, the probability density $f_T(t)$ for many particles is obtained.

To evaluate the tensile strength of the particles (R_T), indirect tensile test data were collected. Probability densities of R_T were obtained by type rock (andesite, conglomerate, limestone and gneiss), and it was observed a truncated normal probability density (with $R_T \geq 0$) for the tensile strength.

The estimation of the probability of grain breakage (P_R) is carried out from the probability densities of R_T and T according to equation 1. As an example, figure 1 shows the R_T and T probability densities. The overlapping region between these densities is a quantitative indicator of the probability of failure.

$$P_R = P[R_T < T] = \int_{-\infty}^{\infty} F_{R_T}(t) f_T(t) dt \qquad (1)$$

Equation 1 was applied for different stress levels assuming that each granular sample is constituted by a single type of rock. This probability can be converted to the fraction of particles breakage relative to the solids volume (P_{RV}).

As in experimental results [1], the simulations show that there is a greater probability of grain breakage when a greater stress is applied (figure 2). It is also observed that in continuous grain size distribution, grain breakage decreases considerably.

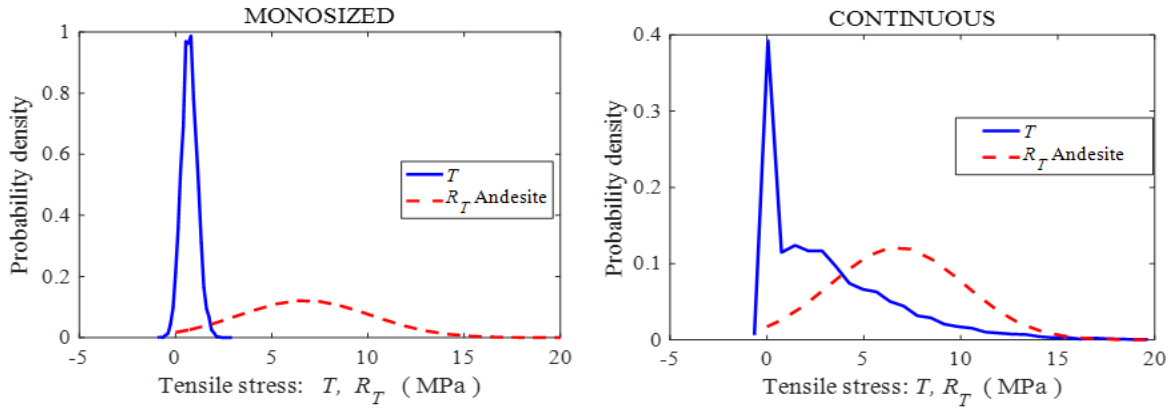

Figure 1. Examples of probability densities of T and R_T.

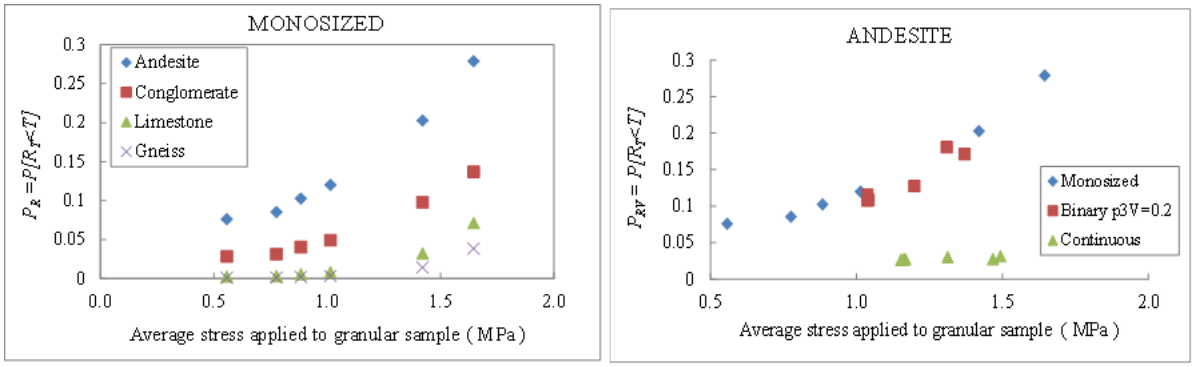

Figure 2. Examples of grain breakage by volume.

Except when the small particles are free between the pores of the large ones, these are the most prone to rupture. This result is consistent with X-ray experiments [5], where it has been observed that large particles do not break because they are protected by adjacent small grains.

Finally, accepting that both grains strength and acting stress are random variables, it can be concluded that it is possible to assess the tensile breakage of grains in granular media. As expected, the grains breakage increases when the rock is weaker and when the average applied stress is greater. Materials of monosized particles and binary mixtures present a higher volume proportion of broken particles than materials with continuous grain size distribution. Relevant practical implications can be obtained from this research.

2. References

[1] Marsal, R. (1973). *Mechanical Properties of Rockfill, Embankment-Dam Engineering. Casagrande Volume*. John Wiley and Sons, New York.

[2] Auvinet G. & Marsal R. (1975). Statistical Model of Grain Breakage. Proceedings, *Fifth Panamerican Conference on Soil Mechanics and Foundation Engineering*. V. 1, pp. 193 – 203.

[3] Weber J. (1966). *Recherches concernant les contraintes intergranulaires dans les milieux pulvérulents. Application à la rhéologie de ces milieux*. Cahiers du G.F.R. 3, 161-170.

[4] Cambou B. & Sidoroff F. (1985). Description de l'état d'un matériau granulaire par variables internes statiques à partir d'une approche discrète. *Journal de Mécanique Théorique et Appliquée*. V. 4, 223-242

[5] Yang W. Shi Y., Mukonoki T. & Otani J. Visualization of grain crushing using micro-focused X-ray CT scanning. *Geomechanics from Micro to Macro* – Soga *et al*. (eds). V. 2, 1131-1135.

THE COMPUTATION OF SOIL WATER RETENTION CURVES FROM PARTICLE SIZE DISTRIBUTIONS: IDENTIFICATION OF ALPHA FFROM SAND-GRAVEL DATA

E. Imre[1], D. Barreto[2], J. Leak[2], D. K. Mwinken[3] V. P. Singh[4]
[1] *Bánki Donát Faculty of Mechanical and Safety Engineering, Budapest, Hungary*
[2]*Edinburgh Napier University, School of Engineering and the Built Environment, , Edinburgh*
[3]*AIAM Doctoral School, Óbuda University, Budapest, Hungary*
[4] *Dept. of Bio. and Agric. Eng, & Dept. of Civil & Env. Eng, Texas A and M University, Texas, USA*

1. General

In the ongoing research the unsaturated soil functions of some gravel-sand-silt mixtures are studied in the context of grading entropy theory and the interpolation of soil properties in the function of the grading curve using grading entropy coordinates is planned [1 to 3].

In the first part of the research the retention curve was measured for 7 fractions and, 21 optimal (continuous) mixtures with relative base entropy of A=2/3, the related fractal distributions are similar to the Fuller curves [2 to 3].

The measurements were approximate since (i) the grading curves of the fractions were more or less differing from the ideal one, (ii) the load steps of the Soil Science Institute SWCC equipment were related to more plastic soils.

The measured data were corrected by a data mining procedure, based on the fact that the steep parts of the mixture retention curves were nearly linear and parallel for a given N and, the absolute value of the slope of the steep parts decreases with N.

In the second part of the research the model validation related to the SWCC computation from the grading curve has been started [4 to 8].

2. Model, model validation

The computation of the SWRC requires prior estimation of the pore-size distribution (POSD) which is computed from the PSD. The process described in detail by [4-6] entails first dividing the PSD into many (N) size fractions. Then the following assumptions are required:

1. In each size fraction N_i (with i = 1 , ..., N), particles have the same shape and size.
2. The specific gravity (G_s) of all particles for all N fractions is the same.
3. The volume of resulting pores corresponding to each size fraction are approximated as capillary tubes whose radii are closely related to the particle size in the fraction.
4. The total pore length is assumed in the form of $2n_i^{\alpha}Ri$,, where R_i is the particle radius of fraction i, α is a model parameter related to particle shape and orientation, and n_i is the number of (spherical) particles in a cubic packing of uniform-size. On the basis of empirical data, the work by [6] suggests α between 1.3 and 1.5, while [4, 5] used between 1.35 and 1.39 for a smaller number of soil types.

A model fitting study has been started for determining the alpha parameter of the pore size distribution. The van Genuchten solution was inverted, to have suction for your given water content. Then Least Squares fitting was made for the alpha parameter ([7-8]).

3. Results, discussion

According to the first results (Figure 1, Table 1), the α is 1.0 and 1.2, is not too sensitive on change in the void ratio (in the case of the gravel-sand fractions). The first results are tentatively explained by the fact that the measured SWCC curves of the gravel-sand-silt mixtures also deviate from the typical sand SWCC data (see eg., [1]).

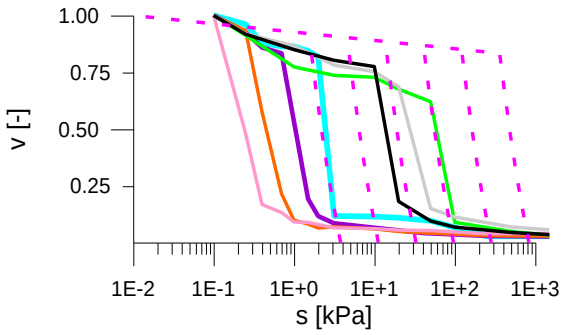

Figure 1 The fractions. The modelled data (dashed line) assuming alpha = 1,37, the measured data (solid lines)

Table 1 The fraction 1, model fitting data in the function of the void ratio

alpha	1,097548	1,087331	1,127492
e	1	0,6	1,1

4. References

[1] Imre,E; Mwinken, D K; Barreto, D; Leak, J., Datcheva, M; Baille, W (2024) Soil water-retention curves of sand mixtures with fractal distribution, submitted to Agrokémia és Talajtan.
[2] Lőrincz, J (1990). Relationship between grading entropy and dry bulk density of granular soils. Periodica Politechnica 34:3:255-265.
[3] Lőrincz, J (1993). On particle migration with the help of grading entropy. Filters in Geotechnical and Hydr.Eng. Brauns,Hheibaum, Schuler,BALKEMA,63-65.
[4] Wang, M., Kong, L. & Zang, M. (2015). Effect of sample dimensions and shapes on measuring soil-water characteristic curves using pressure plate. Journal of Rock Mechanics and Geotechnical Engineering, 7(5), 463–468.
[5] Wang, M., Pande, G.N., Kong, L. & Feng, Y.T. (2017). Comparison of pore-size distribution of soils obtained by different methods. International Journal of Geomechanics, 17(1):06016012
[6] Arya, L.M., Leij, F.J., Shouse, P.J. & van Genuchten, M.T. (1999). Relationship between the hydraulic conductitvity function and the particle-size distribution. *Soil Science Society of America Journal*, **63**(5), 1063–1070
[7] Imre, E ; Berzi, P; Hegedus, Cs; Kovacs, S; Kovacs, L (2021)
[2102.08210] Reducing numerical work in non-linear parameter identification (arxiv.org)
[8] Imre, E (2023) [2301.03427] A comment on the combination of the implicit function theorem and the Morse lemma (arxiv.org).

THREE-DIMENSIONAL GEOMETRIC MORPHOLOGY OF PEBBLES AND ROCK FRAGMENTS FOR EMBANKMENT DAMS

Z.-T. Zhang[1], H.-C. Liu[1], J. Hu[1], X.D. Zhang[1], Z. Zhang[1] and K. Li[1]

[1] State Key Laboratory of Simulation and Regulation of Water Cycle in River Basin, China Institute of Water Resources and Hydropower Research, Beijing 100038, China

1. Introduction

The geometric morphology of particles is an important factor of the mechanical properties of granular materials, e.g., sands, pebbles and rock fragments. Those mechanical properties include the limit void ratio [1-2], compression characteristics [1], shear strength [3,4] and dynamic characteristics [5]. However, as pointed out by Miskin et al. [6], more than 200 years after the publication of Coulomb's theory, a universal relationship between mechanical properties and particle geometric morphology has still not been established.

Accurate measurement of particle geometric morphology is a prerequisite for analyzing its morphological characteristics. There exist relatively abundant data on the morphology of 0.075~2mm sand particles, but the data for relatively large particles with a size larger than 2mm is limited. Those relatively large particles account for 70~90% of the materials, e.g., pebbles or rock fragments used to build embankment dams, hence, the morphology of those materials for embankment dams remain unclear. The measurement data for large particles above 100mm is extremely limited. In addition, regarding the basic law of size effect on particle geometric morphology, the data is inconsistent and no consensus has been reached. There is still controversy in the description of the three-dimensional geometric characteristics of particles for dam construction, mainly due to the lack of measurement of particles. It is vital to further expand the measurement data of particles of different sizes used in dam construction, especially for large particles with sizes above 100mm.

This study measured the three-dimensional geometric morphology of pebbles and rock fragments using a SfM-MVS approach. The research results will help deepen the understanding of the three-dimensional geometric morphology of large particles for embankment dams.

2. SfM-MVS approach

The hardware mainly consists of a camera and a support platform to place the particle to be measured on. This research uses a high-resolution, high-frame-rate GoPro camera (Model: HERO 9 Black; GoPro, USA), with a maximum resolution of 5120×2880 (5k) at a frame rate of 30fps; the maximum frame rate is 240fps, with a corresponding resolution of 1920×1080 (1080p). After selecting an appropriate resolution and frame rate, the camera is handheld and moved around the support platform to shoot the particle to be measured. To address the difficulty of photographing the contact surface between the particle and the support platform, the particle is photographed twice. After obtaining videos of both sides of the particle, frame images are extracted at fixed time intervals to acquire multi-perspective images of the particle. It is important to note that the extracted adjacent images should overlap, with an overlap rate of no less than 50%. To meet this requirement, the camera's frame rate, the image extraction time interval, and the shooting speed should be coordinated with one another. In this study, the selected resolution is 5120×2880 (5k) with a frame rate of 30fps, and the frame extraction time interval is 0.8s. The filming time for a single side of each particle is approximately 1 minute, yielding 90~130 images of the particle from different perspectives. Using the three-dimensional reconstruction software Agisoft Metashape, a digital hemi-model of the particle

is obtained from a sequence of single-sided images. A complete 3D point cloud model obtained by using the ICP (Iterative Closest Point) point cloud registration algorithm to merge the two hemi-models. Fig. 1 presents examples of the reconstructed digital models of rock fragments and pebbles. The measurement error in length is ±0.15mm, which meets the requirements for measuring the three-dimensional geometric morphology of large particles with sizes above 100mm.

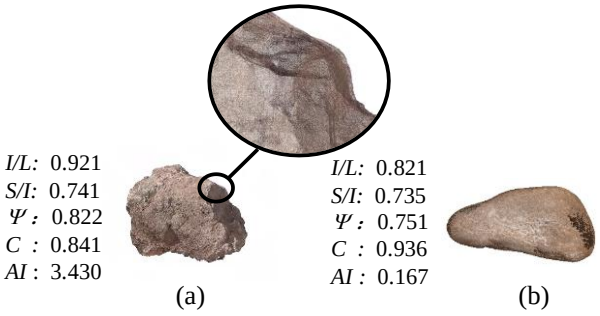

Figure 1. Examples of reconstructed digital models of (a) rock fragments and (b) pebbles for embankment dams.

3. Concluding remarks

This study proposed a SfM-MVS approach for measuring three-dimensional geometric morphology of pebbles and rock fragments for embankment dams. The total cost of hardware and software is only 1,200 USD. This cost is significantly lower than that of 3D laser scanning and computerized tomography (CT) scanning, which generally ranges from several hundred thousand to over a million USD. The number of points in the particle point cloud models in this study ranges from 294,000 to 14,118,000. Compared with 3D laser scanning and CT scanning, this method offers similar levels of digital model precision, point cloud density, and measurement efficiency, and is capable of capturing more three-dimensional morphological information, e.g, color, meanwhile reducing costs to 1/10 to 1/100, offering excellent cost-effectiveness.

5. References

[1] Cho, G.C., Dodds, J. & Santamarine J. (2006). Particle shape effects on packing density, stiffness, and strength: natural and crushed sands. Journal of Geotechnical and Geoenvironmental Engineering, 29(9): 1328-1340.

[2] Suh, H.S., Kim, K.Y. & Lee, J., et al. (2017). Quantification of bulk form and angularity of particle with correlation of shear strength and packing density in sands. Engineering Geology, 220: 256-265.

[3] Wu, M.M., Wang, J.F., Russel, A., et al. (2021). DEM modelling of mini-triaxial test based on one-to-one mapping of sand particles. Géotechnique, 71(8): 714-727.

[4] Yang, J. & Wei, L.M. (2012). Collapse of loose sand with the addition of fines: the role of particle shape. Géotechnique, 62(12): 1111-1125.

[5] Gao, G. & Meguid, M.A. (2018). On the role of sphericity of falling rock clusters—insights from experimental and numerical investigations. Landslides, 15(2): 219-232.

[6] Miskin, M.Z., Jager, H.M. (2013). Adapting granular materials through artificial evolution. Nature Materials, 12(4): 326-331.

UNIFORMITY ASSESSMENT OF MOIST TAMPED SILT TAILINGS SPECIMENS AFTER SIGNIFICANT SATURATION COLLAPSE

D. Reid[1], R. Fanni[2] and A. Fourie[1]
[1] The University of Western Australia, Perth, Australia
[2] WSP, Perth, Australia

1. Introduction

Sands and low plasticity silts, including mine tailings, are generally impossible to sample in an undisturbed manner. This emphasises the reconstitution procedures of such materials in the laboratory for element testing. In current tailings engineering practice, the moist tamping (MT) procedure is most used as it allows easy preparation of loose specimens which produce undrained strain softening responses consistent with field-scale performance of loose silts, enabling also the critical state line (CSL) to be inferred.

Despite the current prevalence of MT, it has been the subject of significant criticism. In particular, the initial non-uniform density distribution of MT sands has been demonstrated through X-ray [1] and computed tomography (CT) scanning [2] efforts. Although the initial non-uniformity of sands has been clearly demonstrated, much current laboratory testing using the MT approach is being carried out on tailings silts. A subtle difference in silts prepared very loose with the MT approach is the significant collapse that occurs on saturation, easily exceeding 10% volumetric strain. The potential effect of such significant collapse on resulting density profile within specimens does not appear to have been investigated. This is important, both to provide context as to the limitations of the MT approach in tailings silts, and to inform numerical modelling of "element" tests where the initial non-uniformities are included to assess their implications on results.

This paper investigates the density profile of a predominately silt tailings prepared using MT, after significant volumetric collapse. The density profile is investigated using the gamma density technique as part of a multi-sensor core logging system (MSCL) and CT scanning.

2. Methods and materials

Testing was carried out on a platinum tailing previously characterized by Ayala et al. [3], with 72%<75μm, a liquid limit of 24 and Plasticity Index of 6. The investigation outlined in the current paper has been carried out in the following stages:

1. Gamma density in MSCL, where 72mm diameter and 120mm high specimens were initially prepared in eight layers in plastic tubes using MT to produce samples similar in dimensions and preparation to previous triaxial testing of the platinum tailings. After tamping, a bedding load of 10 kPa was applied and the specimens were soaked in a water bath overnight, within an oven set to 50° C. The water was then decanted, and the specimens allowed to drain and dry in the oven. This process was developed to avoid moving the samples prior to drying as this could result in undesirable densification and/or disturbance.
2. Further gamma density profiling in the MSCL on duplicate samples prepared at a loose density and only 70mm height, to prevent side friction of the tube from affecting the collapse response.
3. CT scanning on 90mm diameter, 90mm high specimens prepared in custom-built columns, flushed, and then drained and dried in an oven similar to Stage 1 and 2 procedures. The drying process for these specimens is currently underway.

3. Preliminary results

The results of the Stage 1 and 2 MSCL gamma density profile are presented in Figure 1. For Stage 1 profiles examining the effect of different density, the densest specimen shows the classic irregular density profile previously seen in X-ray and CT scanning of MT sands [1,2]. However, the looser specimens, while still showing density variation, exhibit a different profile with a relatively consistent decrease in density with depth. Owing to concerns that this density decrease with depth could be partially a result of side friction in the 2V:1H specimens which were within a plastic tube (distinct from a triaxial specimen, without such side friction), the Stage 2 tests with shorter specimens were carried out.

The Stage 3 density profiles produced using CT scanning are currently underway and will be presented in the final paper.

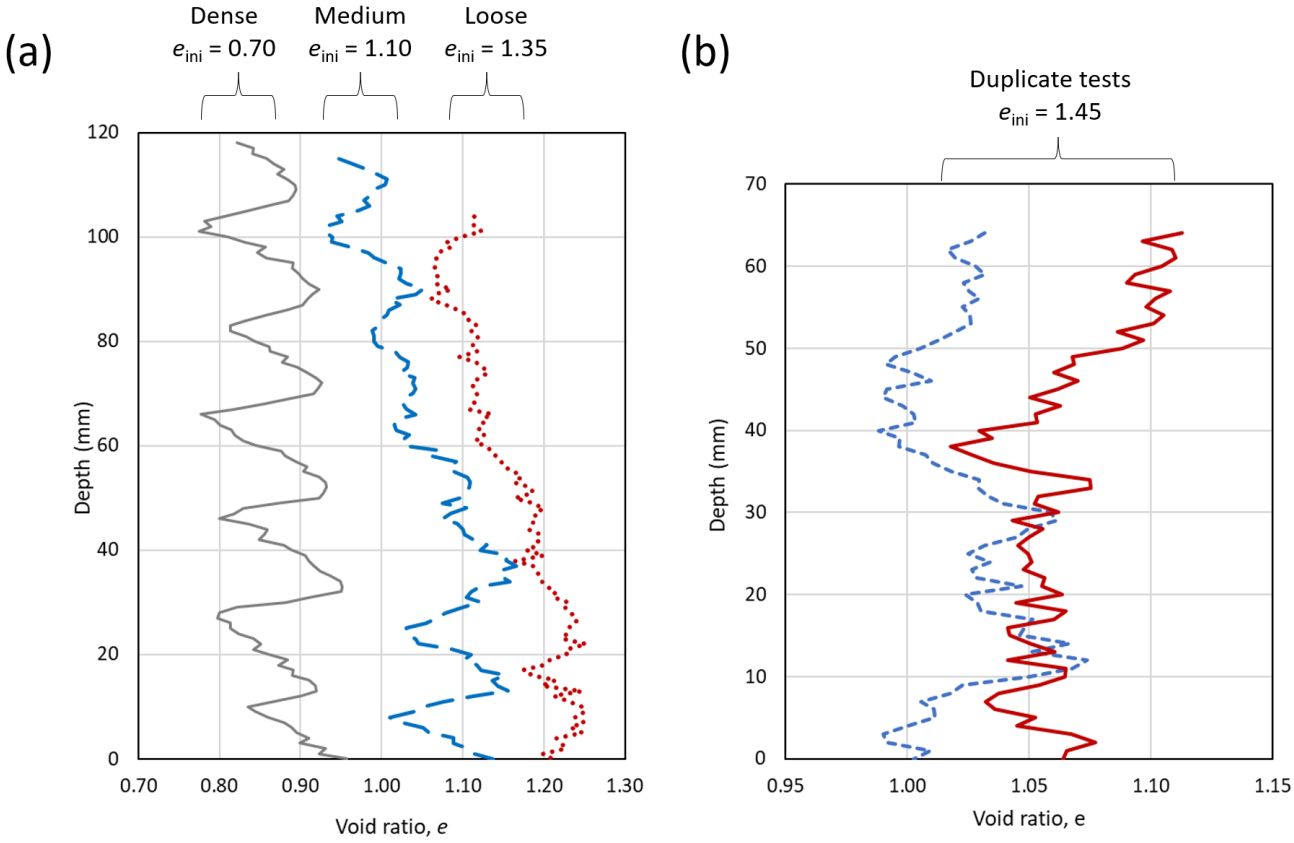

Figure 1. Post-saturation MSCL gamma density profiles: (a) Stage 1, with different initial densities (b) Stage 2, duplicate tests with identical initial density and 1V:1H initial sample height

4. References

[1] Frost, J.D. & Park, J.-Y. (2003). A critical assessment of the moist tamping technique. *Geotechnical Testing Journal*, **26**: 57-70.

[2] Thomson, P.R. & Wong, R.C.K. (2008). Specimen nonuniformities in water-pluviated and moist-tamped sands under undrained triaxial compression and extension. *Canadian Geotechnical Journal*, **45**: 939-956.

[3] Ayala, J., Fourie, A.B. & Reid, D. (2022). Improved cone penetration test predictions of the state parameter of loose mine tailings. *Canadian Geotechnical Journal*, **59**: 1969-1980.

VARIATION IN CRITICAL POROSITY FROM DIFFERENT PORE FLUID COMPOSITIONS EVALUATED THROUGH NUCLEAR MAGNETIC RESONANCE

***E. M. Kinslev*[1]**
[1] *Tech. Univ. Denmark, Kgs. Lyngby, Denmark*

1. Introduction

Recent focus on repurposing depleted oil reservoirs in the North Sea for carbon storage has brought focus to the problems with ensuring a lasting seal at the existing wells. A promising sealing technology involves using the existing cap rock formations as a barrier by inducing swelling in the clay rich shale formation resulting in closure of cracks and well annuli. However, since the swelling caused by stress release is already "utilised" in existing wells, additional swelling must be achieved by other means. Van Oort et al. [1] showed how flushing with sodium or lithium silicate successfully created a seal at the laboratory scale. Since the chemically induced swelling is related to the electrostatic repulsion between the soil particles, the effectiveness of a given brine in causing swelling could be assessed through the self-weight sedimentation porosity (critical porosity) in a similar way to that employed by Meireles et al. [2] to quantifying the electrostatic repulsion in pure minerals.

Although the effects of pore water chemistry on various clays is generally well studied (e.g. [3] and [4]), the focus is primarily on the effects of different cations and pH. Since the results by van Oort et al. [1] indicate a benefit from the silicate and in the light of other indications that the sorption equilibrium depends on the anionic background [5], there is due cause for investigating the anionic composition more thoroughly as well.

This research therefore aims at assessing the potential swelling caused by a large series of pore water compositions through measurement of the critical porosity. The investigation is carried out on cuttings from the Lark formation which acts as the cap rock formation in large parts of the North Sea.

2. Material and methods

The investigated soil originates from a depth interval of 5400-5500 feet below Kelly bushing in the TEB-09 well in the North Sea and has key descriptive measurements as shown in Table 1.

Fines fraction (<0.002 mm)	Grain density	Specific surface area	CEC	Quartz	Kaolinite/ Chlorite	Smectite/ Illite	Cristobalite	Pyrite
42%	2.62 g/cc	28.7 m2/g	30 mEq/100g	~22%	~9%	~57%	~9%	~3%

Table 1. Composition (mass fraction of mineralogy) and key properties of the studied soil.

The dry soil was grinded until passing a 250µm sieve and mixed with the relevant brine in ratios 8g soil to 20g brine in closed glass cylinders. After self-weight sedimentation for two weeks the porosity as well as the shape of the pore size distribution was measured through NMR T_2 relaxometry. To quantify the evolution of the pore space during self-weight sedimentation, continuous T_2 relaxometry measurements were conducted during the sedimentation for the sample with demineralised water.

In addition to demineralised water, the investigated brines vary the cations between H, Li, Na, Mg, K and Ca while the anion is constantly Cl and varies the anion between OH, SiO_3, SO_4, ClO_4

and I while the cation is constantly Na. All brines are tested at concentrations 0.01M, 0.1M and 1M and NaCl is additionally tested at 0.02M, 0.05M, 0.22M, 0.46M and 2.15M.

3. Results and discussion

The variation in measured critical porosity from the studied brines is illustrated in Figure 1.

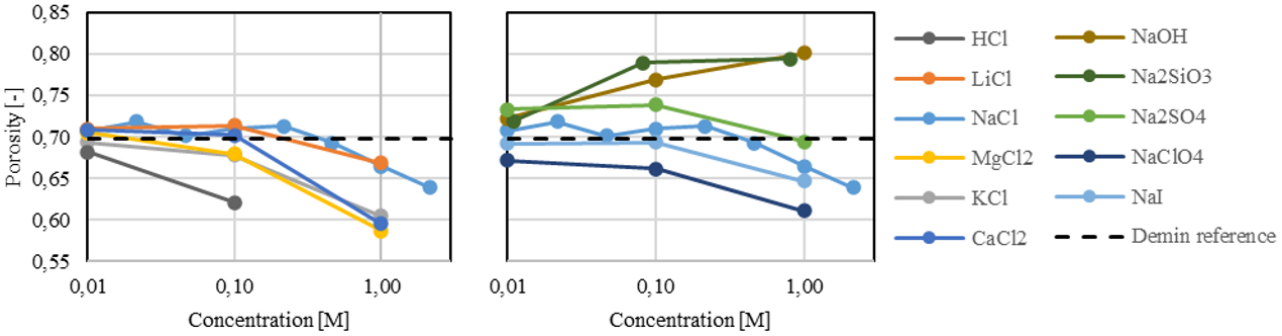

Figure 1. Variation in critical porosity for the investigated brines

From Figure 1 it may be seen, that the majority of the brines follow the same general pattern with concentration where the porosity is almost unaffected by increasing concentration until ~0.1M from where the porosity decreases as concentration increases. This is shown in more detail for the NaCl samples where better discretisation of the concentration axis was investigated. However, the Na_2SiO_3 and NaOH samples does not follow this pattern but rather shows a significant increase in porosity with increasing concentration. These two brines had a significantly increased pH which supports the concept of high pH causing swelling (as e.g. mentioned in [1]). For the cation series, a general pattern of critical porosity follows Li=Na>Ca>Mg=K>H which is comparable to (but not exactly a replication of) previous observations [3]. For the anion series, the same general pattern follows SiO_3>OH>SO_4>Cl>I>ClO_4.

In this extended abstract it was not feasible to present the results related to the variation in pore space between the different brines as well as the evolution of pore space during sedimentation. These results will be presented in the full paper.

4. References

[1] van Oort, E., Juenger, M., Aldin, M., Thombare, A., McDonald, M., Lucas, A. & Ditlevsen, F. (2022). Simplifying well abandonment using shale as a barrier. *Proc. of the Int. Drilling Conf. and Exhi., Galveston Texas, USA.*

[2] Meireles, L. T. P., Storebø, E. M. & Fabricius, I. L. (2020). Effect of electrostatic forces on the porosity of saturated mineral powder samples and implications for chalk strength. *Geophysics* **85**(1).

[3] Sridharan, A., Rao, S. M. & Murthy, N. S. (1986). Compressibility behaviour of homoionized bentonites. *Géotechnique* **36**(4):551-564

[4] Di Remigio, G. (2021). Multiscale assessment of swelling and compressibility of fine grained geomaterials. Ph.D. thesis at Technical University of Denmark.

[5] Tournassat, C., Gailhanou, H., Crouzet, C., Braibant, G., Gautier, A. & Gaucher, E. C. (2009). Cation exchange selectivity coefficient values on smectite and mixed-layer illite/smectite minerals. *Soil Chemistry* **73**(3):928-942.

VISUALIZATION OF THE FORCE NETWORK MICROSTRUCTURE IN 3D EXPERIMENTS

D. Leśniewska[1], B. Świtała[1], M.A. Kalwar[1,2] and J. Sławińska[1]
[1] Institute of Hydro-Engineering, PAS, Gdańsk, Poland
[2] Doctoral School at Gdańsk University of Technology, Poland

1. Motivation

Understanding the response of granular materials to various types of loading requires more experimental research on the mechanisms governing the formation, characteristics and evolution of the force chain network.

2. Experimental method and substitute granular material

More systematic knowledge on characteristics and structure of force chain networks can be gained by applying image analysis to photo-elastic tests on granular materials [1-4].

The PDMS elastomer, chosen as a substitute material, has the advantage over the previously used glass granules that it requires significantly less stress to produce the photo-elastic effect. On the other hand, in the appropriate load range, PDMS grains exhibit sufficient hardness to model common granular materials [5].

3. Test arrangement

Fig.1a shows the layout of a simple compression test on a cuboidal sample with a diameter of 4.0x3.0x3.7 cm and a view of a granular sample saturated with immersion liquid, thus transparent. Several such tests were performed in a wide range of grain diameters (from 1.6 to 8 mm) on mono- and polydisperse samples.

Recording the tests from four directions was possible by rotating the test box, thus obtaining an image of the force chain network in planes I - IV, marked in Fig.1b. The process of force chain formation and evolution at the micro-scale was studied, including the grain selection mechanism to initiate the effect.

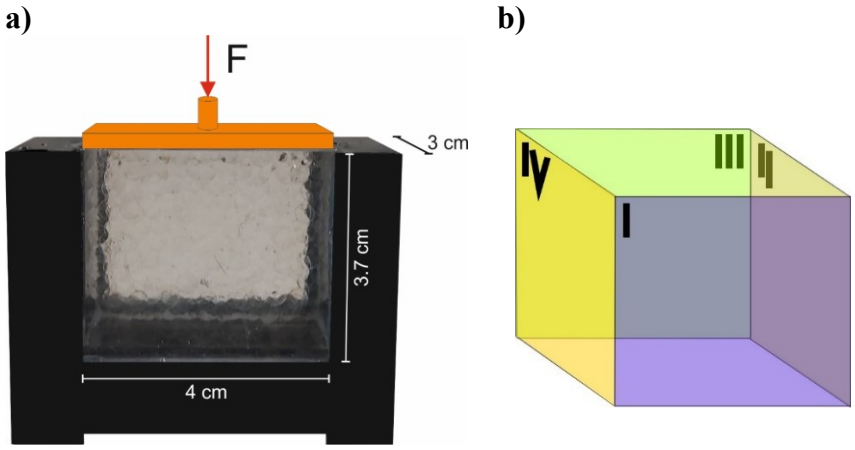

Figure 1. a) Layout of the compression test and view of a sample saturated with an immersion liquid, b) four planes of image registration.

a) force network microstructure for loading force 20N

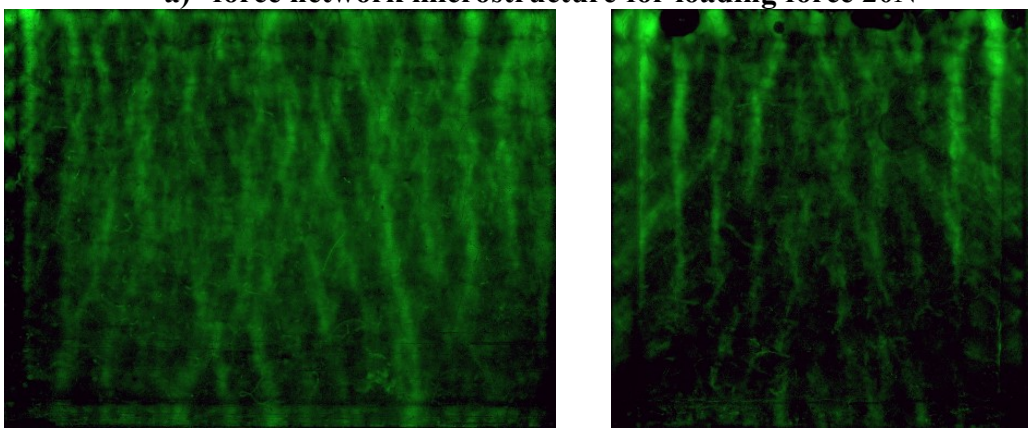

I –front view **II – side view**

b) macro-scale response – the average image brightness

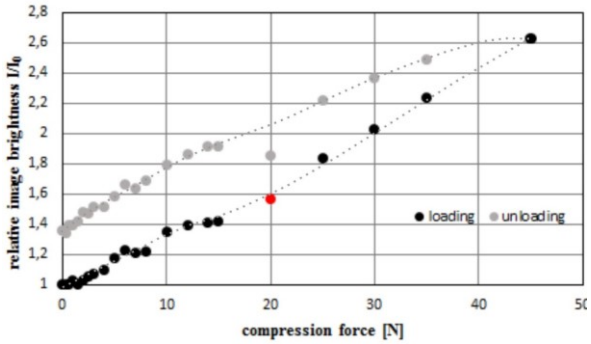

Figure 2. Visualization of force chain network in a 3D-box compression test (Fig.1) on monodisperse PDMS grains.

4. Results

A significant relationship exists between the formation of force chains and the occurrence of grain selection mechanisms at the microscale. A well-developed structure of the force network has been observed in most cases. Its geometrical arrangement depends most on the degree of grain diameter statistical dispersion, but a certain regularity is found in each investigated case. The force network mesh size for monodisperse samples of different grain diameters varies. However, some angular relationships are maintained, which can form the basis for more universal parameters, classifying the network.

5. References

[1] Aben H (1979) *Integrated photoelasticity*. McGraw-Hill International Book Company

[2] Leśniewska D, Muir Wood D (2009) Observations of stresses and strains in a granular material. *Journal of Engineering Mechanics* 135(9):1038–1054

[3] Leśniewska D, Nitka M, Tejchman J, et al (2020) Contact force network evolution in active earth pressure state of granular materials: photo-elastic tests and DEM. *Granular Matter* 22(71). https://doi.org/https://doi.org/10.1007//s10035-020-01033-x 795

[4] Muir Wood D, Leśniewska D (2011) Stresses in granular materials. *Granular Matter* 13:395–415

[5] Frank-Richter, S. (2014). *Disordered Binary Granular Packings in Three Dimensions*, doctoral dissertation, Düsseldorf, Heinrich-Heine-Universität.

VISUALIZATION OF 3D LOESS MICROSTRUCTURE USING μXCT AND FIB-SEM

B. Yu[1], W. Fan[1], T.A. Dijkstra[2]

[1] School of Geology Engineering and Geomatics, Chang' an University, Xi'an, China

[2] School of Architecture, Building and Civil Engineering, Loughborough University, LE11 3TU, UK

1. Introduction

Loess is a wind-blown quaternary deposit covering large areas across the world. The strength of loess is high under dry condition but reduces dramatically when submerged with water. This is responsible for disasters including landslide and subsidence in loess regions [1].

Loess microstructure is featured by silt-sized skeleton particles bonded by primarily clay-sized particles or clay aggregates. The inter-particle clay bonding controls the stability of the loess skeleton and thus the stiffness and strength of the material. The microstructure and microscale behaviour of loess have been studied using standard scanning electron microscope (SEM) and indirect method such as mercury intrusion porosimetry (MIP)[2, 3]. Recently, the evolution of loess microstructure at particle-scale (several to tens of microns) during wetted collapse has been non-destructively visualized and characterized using X-ray micro-computed tomography (μXCT)[4, 5]. However, the complex clay structures in loess has not been fully characterized as for skeleton particles and their role in loess collapse remains not well understood.

In this study, a correlative characterization of inter-particle clay structures in upper Pleistocene Malan loess using μXCT and focused ion beam scanning electron microscope (FIB-SEM) is performed, with special attention to the inter-particle clay structures.

2. Material and method

Undisturbed Malan loess samples were taken from an exposed cut, 2 m below the ground surface, at Yan'an, China. The material contained 14.95% in-situ moisture and had a void ratio of 0.83. A small blade-shaped fragment (about 1.5×0.5×0.3 mm^3) was sampled by gentle breakage of a bigger air-dried loess block. The mini sample was impregnated with epoxy resin to enhance the material integrity.

The mini loess sample was scanned non-destructively using a Zeiss Xradia Versa 610 X-ray microscope. Three-dimensional 16-bit greyscale tomographic images with a voxel size of 0.7×0.7×0.7 μm^3 for the entire mini sample were obtained, based on which an ideal region of interest (ROI) was selected for subsequent FIB-SEM test with a much higher resolution. The FIB-SEM test was performed for the targeted ROI using a Zeiss Crossbeam 350 Ga-sourced focused ion beam scanning electron microscope, resulting in a stack of equally-spaced 8-bit greyscale images which were then constructed into 3D nano-tomographic images having a dimension of 40×30×30 μm^3 and a voxel size of 10×10×10 nm^3.

3. Results

Based on segmentation of 3D microstructural features from the FIB-SEM images, various types of clay structures that connect silt-sized skeleton particles were seen with substantial details as exemplified in Figure 1. The two skeleton particles (Particles 1 and 2) are not in direct contact and the contact force between them is majorly transmitted through the bridging structure. The bridging structure is composed of several thin flaky particles, which are typically several microns long and

would not be classified as clay-sized, and fine clay particles that support the flakes. The mechanical properties (stiffness and strength) of such clay-supported bridges are likely to be anisotropic. Bridge structures formed by only fine clay particles (i.e., without micron-sized flakes) are also seen elsewhere. The formation of different types of clay bridges depends on local availability of fine clays/colloids as well as thin mineral flakes. If we look at the clay-supported bridge structure in the y-z plane, interestingly, we see that bending occurs to one of the flaky particles. This is an evidence of in-situ microstructure evolution as a result of a gradual increase in effective stress during deposition. More importantly, such minor deformation found in contact structures provides indications of the direction of force transmission between skeleton particles.

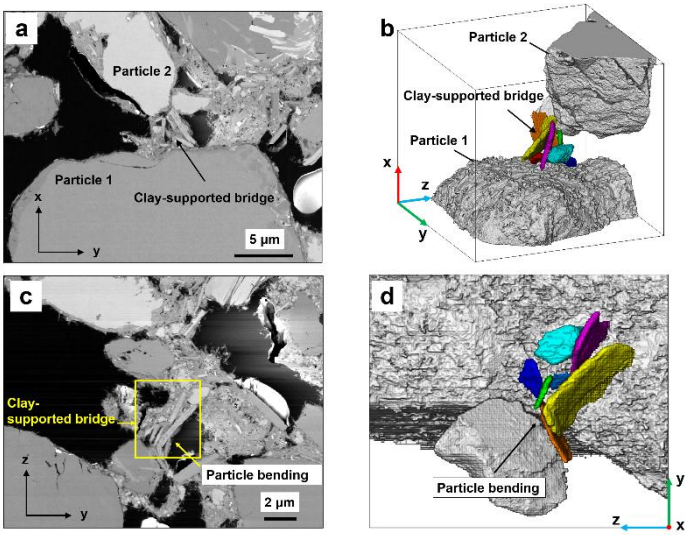

Figure 1. Observation of a clay-supported bridge structure: (a) and (b), FIB-SEM slice and 3D visualization showing the bridge structure; (c) and (d), FIB-SEM slice and 3D visualization showing a bent flaky particle within the bridge structure.

4. Conclusions

In this study, the details of inter-particle clay structures in loess, which play a key role in controlling mechanical behaviour at the macro-scale, are visualized and characterized using µXCT and FIB-SEM. The characterization of a clay-supported bridge structure connecting two silt-sized skeleton particle demonstrates the high potential of this approach to provide useful information on the complex interaction between skeleton particles. Our results, many not shown here, provide important insights into micro-mechanisms in loess behaviour and have potential applications in generating more realistic and accurate numerical models in the context of discrete element method.

5. References

[1] Juang, C.H., Dijkstra, T.A., Wasowski, J., Meng, X.M. (2019). Loess geohazards research in China: advances and challenges for mega engineering projects. *Eng. Geol.* **251**:1–10.

[2] Ng, C.W.W., Mu, Q.Y., Zhou, C. (2016). Effects of soil structure on the shear behaviour of an unsaturated loess at different suctions and temperatures. *Can. Geotech. J.* **54** (2):270–279.

[3] Wang, J.D., Li, P., Ma, Y., Vanapalli, S.K., Wang, X.G., (2019). Change in pore-size distribution of collapsible loess due to loading and inundating. *Acta Geotech.* **15**:1081–1094.

[4] Yu, B., Fan, W., Fan, J.H., Dijkstra, T.A., Wei, Y.N., Wei, T.T. (2020). X-ray microcomputed tomography (µ-CT) for 3D characterization of particle kinematics representing water-induced loess micro-fabric collapse. *Eng. Geol.* **279**: 105895.

Theoretical and analytical developments

Theoretical and analytical developments

Analytical developments

EVALUATION OF THE FILLING DIAGRAM METHOD FOR MEASURING SUFFUSION ON EARTH DAMS

M J. Chaparro-Lopez[1], B. Caicedo[1] and M. Cabrera[2]
[1] Universidad de Los Andes- Department of Civil Environmental Engineering - Bogotá, Colombia
[2] Delft University of Technology, Faculty of Civil Engineering and Geosciences, Delft, The Netherlands

1. Abstract.

The suffusion of earth dams due to internal erosion is one of the most significant causes of earth dam failures [1] [2]. Existing analytical methods evaluate the influence of the grain size distribution on the suffusion potential [3]; however, variables like the relative density also influence it, and it needs to be explored. Consequently, this research evaluates the filling diagram method to measure the suffusion potential in earth dams to prevent failure risk, considering the grain size distribution and the relative density.

The filling diagram is a method used to measure segregation in concrete mixtures. In this work, the functionality of this method for measuring the suffusion potential in earth dams is evaluated. For this purpose, first, a comparison is made employing statistical variables of two existing geometric methods in the literature with the new method studied. Subsequently, an experimental design was carried out to compare the results obtained in the laboratory with those obtained using the new method. Finally, a contribution was presented that supports, through experimental and statistical analysis, that the filling diagram effectively detects suffusion in dams, considering more variables than geometric methods, such as material density.

2. Methods description.

This study aims to assess the accuracy of the suffusion method in evaluating the suffusion on earth dams. The study is divided into two stages: theoretical and experimental. In the theoretical stage, the suffusion potential of 33 different grain size curves was assessed using existing theoretical methods such as Kenney and Law, which use a control size particle, and the tree segment method, which focuses on determining the slope of the grading curve's fine, intermediate, and coarse particle zones [3] [4] (see Figure 1 (a) and (b)). Also, the grain size curves were evaluated by the filling diagram method to assess the grain size curves' suffusion potential. The validity of the results was determined through a statistical analysis of sensitivity and specificity, comparing the theoretical methods and the filling diagram.

Referring to the filling diagram theory. François de Larrad [5] developed the method based on the "Linear Packing Model"; its approach consists of measuring the segregation potential of a granular mixture employing the "Filling diagram," which is constructed from the filling coefficient $\frac{\emptyset_i}{\emptyset_i{}^*}$ (see Figure 1 (c)). In this assessment, a polydisperse mix with diameters d_i is considered. An external seepage can transport the smaller particles d_{i2} through the soil matrix. This phenomenon can generate spaces in the matrix where there are no particles of class $d2_i$. Hence, the filling coefficient $\frac{\emptyset_i}{\emptyset_i{}^*}$ is the ratio of the volume occupied by a class d_{i2} particle in the total volume $\emptyset_i$, with the maximum volume

that class d_{i2} can occupy $\emptyset_i^*$. The segregation, in this case, suffusion potential, is derived by the gap of diameter d_{i2} (see Figure 1 (c)) [3].

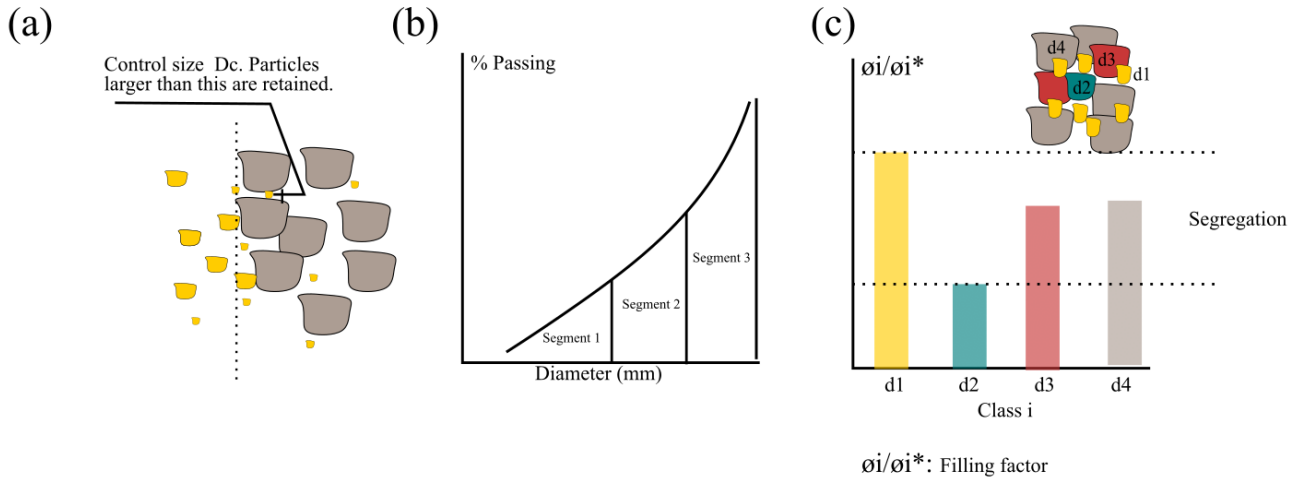

Figure 1. (a) Kenney and Lau method. (b) Three segment method. (c) Filling Diagram.

The current methods focused on the grain size distribution [1]. However, the filling diagram, in addition to this factor, also considers the density of the sample. Therefore, in the experimental phase, the influence of particle size and density on the internal erosion of the materials was evaluated, introducing these variables in the filling diagram method. For this purpose, samples with different grain size distributions, well-graded and poorly graded, were made with varying relative densities in the range of D_r=20 to 75%.

3. Main conclusion.

An experimental and statistical study is presented supporting the reliability of the filling diagram in detecting dam collapse. The filling diagram captures more information about soil conditions, such as density and grain size distribution, than the geometric methods reported in the literature. The study also found a linear relationship between the erosion rate per pore unit and the segregation average *S* parameter obtained in the filling diagram. Furthermore, there is evidence of a decrease in permeability as water passes through and segregates the soil.

5. References.

[1] F. Bendahmane y D. Marot, «Experimental Parametric Study of Suffusion and Backward Erosion,» ASCE, pp. 57-67, 2008.
[2] R. CORREIA DOS SANTOS y L. CALDEIRA, « Experimental study on crack filling by upstream fills in dams,» Geotechique , vol. 65, pp. 218-230, 2015.
[3] H. Rönnqvist y P. Viklander, «On the Kenney-Lau Approach to Internal Stability Evaluation of Soils,» Enviromental and Natural Resources Engineering, pp. 129-140, 2014.
[4] J. Lafleur y M. T treault, «Controlling constriction sizes of granular filters: discussion.,» Canadian Geotechnical Journa, Vols. %1 de %223(1),, pp. 97-98., 1986.
[5] B. Caicedo, Geotechnics of Roads, CRC Press, 2016.

INTERGRANULAR PRESSURE SOLUTION CREEP COUPLING WITH PHREEQC

***S. Erol*[1]**
[1]Izmir Inst. of Tech. (IZTECH), Depart. of Energy Systems Eng., İzmir, Turkey

1. Introduction

Assessment of intergranular pressure solution (IPS) creep has substantial safety and economic importance in reservoirs for hydrocarbon production, geothermal operations, underground CO_2 sequestration, and hydrogen storage processes [1, 2]. IPS creep is a temperature-dependent, stress-driven deformation mechanism that alters mineral grain shapes by dissolution, precipitation, and diffusion in a chemically closed system [3]. The mechanical compaction and chemical reactions of minerals lead to dissolution or precipitation related to alterations in porosity and permeability that impact the flow and, ultimately, the lifetime of the reservoir.

IPS creep can be examined with experiments and some thermodynamic analytical solutions [3, 4]. Spiers et al. [5] developed theoretical IPS creep equations for uniaxial compaction and assumed linear kinetic relations between chemical dissolution and precipitation rates. According to the theory, the mineral grains have spherical shapes arranged in a cubic-packed form.

Similar models also estimate the compaction occurred at slightly greater porosities. These models are typically a makeshift solution. They frequently overestimate compaction and strain rates by up to many orders of magnitude when the porosity is below 0.2. The reason is that the reaction rate parameters are estimated based on empirical equations in which the saturation indices of minerals are assumed constant. Moreover, the rate of change of grain diameters is set constant. Van den Ende et al. [6] proposed a modified thermodynamic IPS model by introducing an upscaled equation to capture the physics at lower porosity.

A better approximation can be achieved using the thermodynamic databases and iterative time-dependent chemical equilibrium mass balance calculations that can be carried out in a geochemical computation program PHREEQC [7]. The proposed simple algorithm combines the conventional IPS equation with PHREEQC, is helpful for better inspection purposes, and provides good agreement with experimental results.

2. Methodology

The typical IPS equation contains three strain rate equations constituting major mechanisms: dissolution, precipitation, and diffusion. The calculations are carried out with strain measurements obtained from a uniaxial compaction experiment for a wet sample and empirically determined chemical kinetic rates. The overall strain rate is obtained with the sum of these three equations. Instead, the total strain rate $\dot{\varepsilon}_T$ can be obtained from a single equation as given below:

$$\dot{\varepsilon}_T = R_{dp} \frac{\left[\exp\left(\frac{\beta \sigma_e \Phi}{RT}\right) - 1\right]}{d} \phi_t(t) \tag{1}$$

R_{dp} is the kinetic dissolution/precipitation velocity computed in Appello's Notepad++ interface to PHREEQC coupled with MATLAB. σ_e is the applied stress, Φ is the molar volume of the mineral, β is the strain-dependent parameter, $\phi_t(t)$ is the rate of change of porosity calculated based on the grain radius change iterative calculations.

3. Results

To compare the novel method with the previous evaluations, stain and strain rate measurements are obtained from Zhang et al. [4]. The system has 6 grams of calcite powder saturated in pure water.

As can be seen from Figure 1b, the conventional IPS overestimates the strain rate, whereas the novel method coupled with PHREEQC provides much better agreement. The reason is the dynamically computed saturation indices in a batch system via PHREEQC using LLNL thermodynamic database.

The algorithm can be modified and applied to more complex heterogeneous fluid-rock interaction systems that can be handled in the PHREEQC.

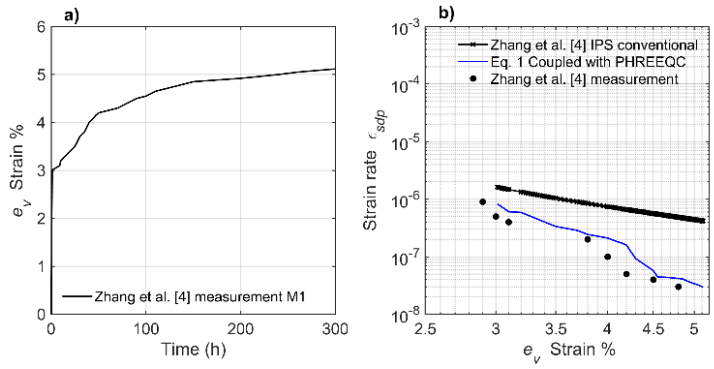

Figure 1. a) Strain measurements roughly obtained from Zhang et al. [4] for M1 calcite sample applied pressure σ_e = 30 MPa, grain diameter d = 37±8 μm. b) Strain rate comparison between the conventional IPS equation and Eq. 1 coupled with PHREEQC.

4. References

[1] Lehner F.K. (1995). A model for intergranular pressure solution in open systems. *Tectonophysics*, **245**(3-4): 153–170. https://10.1130/10.1016/0040-1951(94)00232-X

[2] van Noort, R., Spiers, C. J., & Pennock, G. M. (2008). Compaction of granular quartz under hydrothermal conditions: Controlling mechanisms and grain boundary processes. *Journal of Geophysical Research*, **113**: B12206. https://10.1130/10.1029/2008JB005815

[3] Croizé, D., Bjørlykke, K., Jahren, J., & Renard, F. (2010). Experimental mechanical and chemical compaction of carbonate sand. *Journal of Geophysical Research*, **115**: B11204. https://10.1130/10.1029/2010JB007697

[4] Zhang, X., Spiers, C. J., & Peach, C. J. (2010). Compaction creep of wet granular calcite by pressure solution at 28°C to 150°C. *Journal of Geophysical Research*, **115**: B09217. https://10.1130/10.1029/2008JB005853

[5] Spiers, C. J., de Meer, S., Niemeijer, A. R., & Zhang, X. (2004*). Kinetics of rock deformation by pressure solution and the role of thin aqueous films*. In S. Nakashima (Ed.), Physicochemistry of Thin Film Mater pp. 129–158). Tokyo: Universal Academy Press.

[6] Van den Ende, M. P. A., Niemeijer, A. R., & Spiers, C. J. (2019). Influence of grain boundary structural evolution on pressure solution creep rates. *Journal of Geophysical Research*: Solid Earth, **124**: 10,210–10,230. https://10.1130/10.1029/2019JB017500

[7] Parkhurst DL, Appelo CAJ (2013). Description of input and examples for PHREEQC version 3 a computer program for speciation, batch-reaction, one-dimensional transport, and inverse geochemical calculations. U.S. Geological Survey Techniques and Methods. Amsterdam, Netherlands. https://pubs.usgs.gov/tm/06/a43/.

SOME NOTES ON THE PACKINGS OF SPHERES

I. Talata[1,2], E. Imre[1], T. Goda[1], D. Barreto[3], J. Leak[3]

[1] Óbuda University, Bánki Donát Faculty of Mechanical and Safety Engineering, Budapest, Hungary;
[2] Budapest Business University, Faculty of International Management and Business, Budapest, Hungary;
[3] Edinburgh Napier University, School of Engineering and the Built Environment, Edinburgh, UK

The paper addresses the densest – loosest packing problem in two ways. (i) The equal sphere case (ii) General case, entropy approach.

1. The densest – loosest packing problem – equal sphere case

As far as the theoretical approach, we know very few about the relation of the densest – loosest packing of the grains and the grading curve. The densest and the loosest states are available for equal spheres only. Hales (2006 [2]) proved that the maximum density of packing of equal diameter spheres is $\pi/\sqrt{18} \approx 0.7404\ldots$, so the void volume has density at least $1-\pi/\sqrt{18} \approx 0.2595\ldots$.

The paper presents the content of a paper written b Lajos Filep on „Sets of equal spheres” (Publications in Hydrology) in 1937 [1]. He introduced the term „uniform sphere packing” for such sphere packings when the packing is connected and the configurations of touching spheres at every sphere are congruent in the packing. He determined the possible uniform sphere packings when the configurations of touching spheres at every sphere lie in at most 3 consecutive parallel layers of spheres in the sphere packing. He calculated the densities of those uniform sphere packings, determined their minimum density, and gave explanation when they may occur in nature. At first some particle configurations were explored to find the densest – loosest packing and it was found that if the

void volume is larger than about 66%, then there are possibly some adhesion type contact forces between the grains. If the void volume is less than about 26% then this can be attributed to the different particle size exclusively (e.g. Filep, 1937 [1]). Some recent computer simulations are made, and the results are compared with existing knowledge on uniform sphere packings.

2. The densest – loosest packing problem – entropy approach

In the ongoing research the properties of some granular mixtures are studied in the context of grading entropy theory and the interpolation of soil properties in the function of the grading curve [3]. Some earlier data made on three kinds of grading curve series, fractal, contimuous and gap-graded distributions with fixed fraction numbers (N=1, 2, 3 and 5) are analysed, searching the relation between the minimum dry density e_{max} and maximum dry density e_{min}. The minimum dry density e_{max} data are split into two components (weighted mean fraction density and the increment in the true mixture). It is shown that the first component is the linear function of the base entropy, the second one follows the shape of the entropy diagram. The density– along a given grading curve series for N>1 – is maximal around at the point where internal structure changes from unstable to stable, A=2/3. The ratio of the minimum and maximum dry density e_{max}/e_{min} is discussed.

3. References

[1] Hales, Th. C. (and Ferguson, S.) (2006). The Kepler conjecture. Discrete Comput. Geom., Special issue, Vol. 36 No1 2006, 5-267

[2] Filep, L. (1937): Set of equal diameter spheres. Hidrológiai Közlöny. Volume XIX. Number 1, p. 128-145.

[3] Imre, Emőke ; Lorincz, J ; Trang, P. Q. ; Csonka, I ; Kaczvinszki-Szabó, V ; Telekes, G ; Goudarzy, M ; Rahemi, N ; Baille, W ; Schanz, T et al. Preliminary study on the relationship between dry density of sands and the grading entropy parameters In: Haraldur, Sigursteinsson; Sigurdur, Erlingsson; Bjarni, Bessason (eds.) XVII European Conference on Soil Mechanics and Geotechnical Engineering - Reykjavík, Iceland : 1–6 of September 2019 : Geotechnical

Engineering, foundation of the future : Conference proceedings Reykjavík, Izland : Icelandic Geotechnical Society (IGS) (2019) pp. 996-1002.

Studies on the Spatial Distribution of Chambers in Ant Nests

M. Belachew[1], C. Arson[2] and J.D. Frost[1]

[1] Georgia Institute of Technology, School of Civil and Environmental Engineering, Atlanta, GA, USA

[2]Cornell University, School of Civil and Environmental Engineering, Ithaca, NY, USA

1. Background

Harvester ants are known for constructing intricate subsurface structures. The unique geometry and design of their nests inspired this study. To enable the study, ant nests are molded in-situ by aluminum casting [3], and following extraction, the molded structure is then scanned to create a digital twin for further analysis. The nest structure of Harvester ants has two distinct components known as shafts and chambers, as shown in Figure 1. A prior study by the authors [4] showed that the topology of the different segments of the helical shafts enhanced their stability. The focus of the current study is on the chambers, which serve as critical spaces for ant habitation and egg storage, to see if they also serve a structure stability function. The effect of spatial distribution on arching between chambers and nest stability is assessed analytically and numerically.

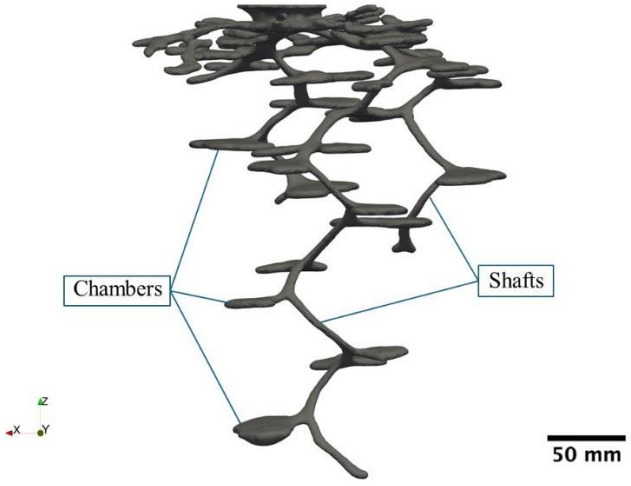

Figure 1 3D scan of an Ant Nest Casting and its components

2. Methodology

We first employ analytical elasticity solutions to examine the influence zone of individual ellipsoidal chambers. We extend the concept of the zone of influence used in 2D plane strain elasticity solutions of cavities [1] to the 3D problem we have at hand. Triaxial ellipsoids are fitted to the scanned chambers and the zones of influence of individual chambers in 3D are evaluated by means of analytical solutions developed specifically for a triaxial cavity in 3D [2]. Equations 1 and 2 (Figure 2), describe the concept of zone of influence in 2D plane strain elasticity. Because this plane strain solution cannot be applied to 3D directly, a similar zone of influence is generated for the triaxial ellipsoidal cavities in 3D using the appropriate elasticity solutions [2].

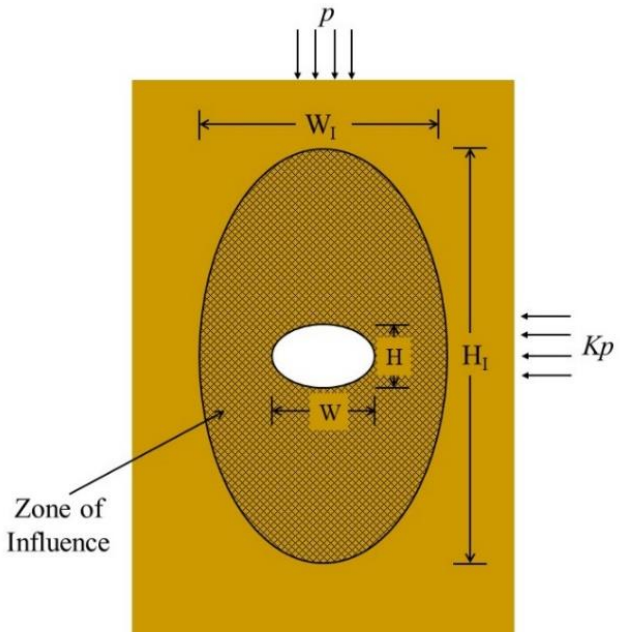

$$W_I = H[\alpha\{A(K+q^2)+Kq^2\}]^{\frac{1}{2}} \quad (1)$$

$$H_I = H[\alpha\{A(K+q^2)+1\}]^{\frac{1}{2}} \quad (2)$$

Where $q = W/H$;

$A = 100/2C$;

$$\alpha = \begin{cases} 1 \; if \; K < 1 \\ 1/K \; if \; K > 1 \end{cases}$$

Note: The Zone of Influence here is defined as the zone where there is more than c% departure of stresses from the far field. (c can generally be taken as 5%)

Figure 2 Zone of Influence for a cavity in 2D plane strain

We analyze the aspect ratio, orientation, and spatial distribution of the chambers and their zones of influence to understand their interactions. We then use the Finite Element Method (FEM) to model the natural complex geometry of the chambers and provide insight into their mechanical interactions. By conducting parallel analyses of both analytical and numerical solutions, we seek to uncover the underlying principles guiding the construction of these intricate structures.

3. Preliminary Results and Conclusions

Preliminary results indicate a pattern in chamber distribution that allows for the influence zones of individual chambers to interact optimally, suggesting a strategic placement that enhances the overall structure stability. It is also evident that the spatial layout is not solely optimized for mechanical stability. This suggests that the spatial distribution is designed to support a wider range of the nest's functionalities, including population distribution, ventilation, efficiency, and foraging, among others but ensures that the mechanical stability is also enhanced. Our findings can help improve the practice of underground construction by taking advantage of the beneficial interaction between different subsurface openings instead of analyzing and designing subsurface cavities individually.

4. References

[1] Bray, J.W. (1986). Some applications of the elastic theory. *Analytical and Computational Methods in Engineering Rock Mechanics* (ed. E. T. Brown), 32 – 94. Allen & Unwin: London

[2] Sadowsky M. A. and Sternberg, E. (1949), Stress Concentration Around a Triaxial Ellipsoidal Cavity, *J. Appl. Mech. Trans. ASME*, vol. 16, no. 2, pp. 149–157.

[3] Tschinkel, W. R. (2021), *Ant Architecture: The Wonder, Beauty, and Science of Underground Nests*. Princeton University Press, New Jersey, USA

[4] Belachew, M., Yamamoto, K., Nichols, E., Zhang, D., Frost, J.D., Arson, C. (2024). Ant Nest Geometry, Stability and Excavation – Inspiration for Tunneling; *Acta Geotechnica - Special Issue on Bio-Inspired Geotechnics* (Accepted)

Theoretical and analytical developments

Theoretical developments

A DISCRETE ELEMENT METHOD INVESTIGATION INTO THE STABLE REGION OF THE GRADING ENTROPY STABILITY CRITERIA

J. Leak[1], D. Barreto[1], E. Imre[2], V. Dimitriadi[1] and J. Bernal-Sanchez[1]

[1]Edinburgh Napier University, School of Engineering and the Built Environment, , Edinburgh

[2]Óbuda University, EKIK HBM Systems Research Center, Budapest, Hungary.

1. Introduction

The particle size distribution (PSD) is amongst the most important descriptors of granular materials. Moreover, tests to quantify the PSD are accessible to all soil mechanics laboratories. It is well recognised that granular behaviour is strongly affected by the PSD. Implementation of the PSD into models/methods is often done so via gradation descriptors such as the coefficient of uniformity (C_u), amongst others, that may correlate to other model input parameters. However, many of these descriptors do not account for the full range of grain sizes and are also non-unique. Crucially, fines and gravel content are also excluded by said descriptors entirely. This is important as the coarsest particles have been shown to be influential in creating strong fabric networks, whereas smaller particles are known to provide additional support to the strong fabric network by means of a weak force chain network. Hence the ability to quantify the entirety of the PSD has important implications in accessing a soils overall stability, and even resistance to unstable behaviours/geo-hazards.

Lőrincz (1986) established the grading entropy method to quantify the entirety of a soils PSD. This is achieved by accumulating the information entropy within each soil fraction to ascertain the total grading curve entropy, unique to each PSD. The total grading entropy is split into two components which form a coordinate pair:

$$S = \Delta S + S_0 \tag{1}$$

where S is the total grading entropy, ΔS is the entropy increment, typically on the y-axis, and S_0 is the base entropy typically on the x-axis. S_0) is a logarithmic mean of the average grain diameter, and ΔS is a measure of how much a PSD is influenced by all its fractions. ΔS and S_0 have normalised counterparts: A is the normalised base entropy and B is the normalised entropy increment, given by:

$$A = \frac{S_0 - S_{0min}}{S_{0max} - S_{0min}} \quad B = \frac{\Delta S}{\ln(N)} \tag{2}$$

Where N denotes the number of fractions within a PSD. A stability criterion was also proposed to compliment the method, which denotes different regions on an entropy diagram, characterised by observed geotechnical behaviours (see Figure 1).

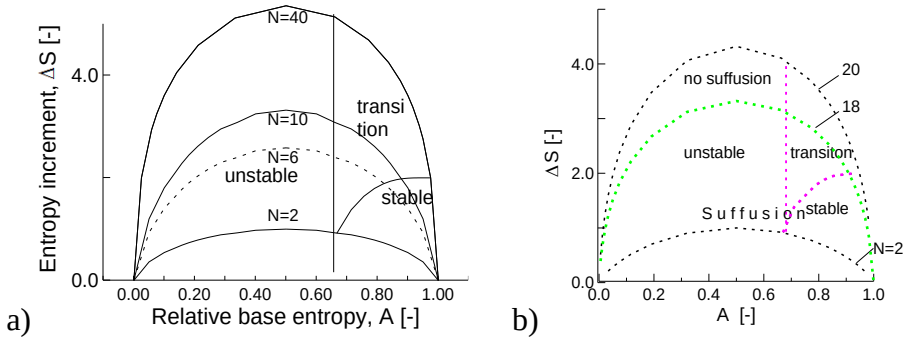

Figure 1. Internal or grain structure stability criterion in the partly normalised diagrams (modified after Lőrincz, 1986).

A defining feature of the stability criterion is the stability line, located at A = 2/3 (A= 0.667). Soils are suggested to be internally unstable if their A-coordinate is less than A= 2/3, whereas soils are seen to be internally stable provided their A-coordinate is greater than A=2/3. Whilst grading entropy and the stability criteria have been used in a number of studies (e.g., Nagy et al., 2014; Barreto et al., 2019, amongst others), the criteria has never been investigated from a micro-mechanical perspective. Up to now such a criteria has only been explained on the basis of physically meaningful hypotheses which are not necessarily supported by data. This study aims to address this knowledge gap.

2. Method & Results

Monotonic discrete element simulations (DEM) were performed on PSDs in the stable zone using the open-source software YADE to investigate the microscale behaviours suggested to take place in the stability criteria. With reference to both the macro and microscale behaviours, it is seen that the location of a PSD on an entropy diagram is indicative of the ability for stable fabric networks to form. The observed DEM behaviours in this work provide a micromechanical basis for the stable region set out in the stability criteria. In the stable zone, PSDs appear to be provided with ample amounts of both the major and minor principal fabric components; providing a micromechanical explanation for greater stability and stiffness behaviours seen in this region. With reference to the major and minor components of the 2nd order fabric tensor, it is suggested that greater stability is a result of a combination of high A-coordinates which indicate the strong force chain network, that are supported orthogonally by smaller grains comprising the weak network - associated with higher Δ*S*/B-coordinates.

3. References

Lőrincz, J. (1986) Grading entropy of soils. PhD thesis, Technical Univ. of Budapest (In Hungarian)

Barreto, D., Leak, J., Dimitriadi, V., McDougall, J. (2019). Grading Entropy Coordinates and Criteria for Evaluation of Liquefaction Potential -In Earthquake Geotechnical Engineering and Protection and Development of Environment and Constructions, (1346-1353).

Nagy, L. (2012) 'Characterization of sand boils with grading entropy', Zbornik Matice srpske za prirodne nauke, (122), pp. 73–88. Available at: https://doi.org/10.2298/zmspn1222073n

A SIMPLE ANISOTROPIC FAILURE SURFACE BY USING MICROMECHANICAL PARAMETERS FOR GRANULAR SOILS

***H. Shaverd*[1], *F. Kalantary*[2]**

[1] *Department of Civil Engineering, Ilam University, Iran*

[2] *Geotechnical Department, Khaje Nasir Toosi University of Technology, Tehran, Iran*

1. Extended Abstract

Granular soils deposited under gravitational loading usually result in anisotropic structure. Experimental tests showed that considering isotropic failure criteria for soils can be inaccurate. This paper presents a simple anisotropic strength criterion for sands. The shear mechanism of granular soils has been investigated from the microscopic point of view in order to find the macroscopic anisotropic shear strength of granular soils. For this reason, micromechanical transmission of shear and normal forces between the particles are considered for direct shear test. By introducing the concept of the frequency distribution of the contact normals proposed by Rothenberg and Bathurst (1991), the relationship between the shear to normal stress ratio, τ/σ , the interparticle friction angle, ϕ_μ , and the anisotropic parameters have been derived from microscopic analysis of the behavior of grains under shear.

Three types of anisotropy have been introduced by Oda et al. (1985). Two parameters are considered for the two types of anisotropies, one for the intensity of anisotropy, α and the other one for the orientation of the particles, θ_f with respect to the mobilized plane, θ_σ . If the samples are subjected to shear with different bedding angles, the shear resistance difference between soils with the same density can be attributed to the anisotropic shear resistance.

Rowe et al., (1962) and also, Guo and Su (2007) showed that the shear strength of soil it made up of three components: friction, dilatancy (or density) and interlocking due to the rearrangement of particles. The effect of friction is considered by using the interparticle friction angle, ϕ_μ . The dilatancy or density dependent of the shear strength is included by the state parameter in micro-level proposed by Chang and Hicher (2005). The anisotropy strength of granular soils is incorporated by the intensity of the anisotropy, α and the deviation between the bedding angle with respect to the maximum shear stress plane, $\theta_f - \theta_\sigma$.

Evolution of the intensity of anisotropy is included in this formulation. Shaverdi et al. (2014) developed an equation in which the intensity of anisotropy is attributed to the shear to normal stress ratio in the mobilized plane and the initial anisotropy. It will reach its critical value at large shear strain (critical state).

Normalization of the anisotropy by considering the specific volume of the soil $(1+e)$ developed by Li and Dafalias (2015) is also taken into account. All the important factors such as friction of the interparticle, initial density and fabric anisotropy are included in the new formulation for anisotropic shear strength of cohesionless soils under direct shear test.

Guo and Su (2007) and Guo (2008) conducted some direct shear tests on two types of sands, Ottawa sand (sand O) and crashed limestone sand (sand L) with different bedding angles and two normal stresses, i.e., $\sigma_n = 50KPa$ and $\sigma_n = 100KPa$. Verification of the proposed equation for modeling of granular soils shows that this model can predict the anisotropic shear strength of sands in direct shear tests with relative accuracy.

2. Basic References

[1] Matsuoka, H., (1974), .A microscopic study on shear mechanism of granular materials. *Soils and Foundations*, Vol. 14, No. 1, 29-43
[2] Rothenberg, L. and Bathurst, R.J. (1992), .Micromechanical Features of granular assemblies with planar elliptical particles. *Geotechnique*, Vol. 42, No. 1, 79-95
[3] Rowe, P.W., Barden, L., Lee, I.K., (1964) .Energy components during the triaxial cell and direct shear test. *Geotechnique*, Vol. 14, No. 3, 247-261
[4] Chang, C.S., Hicher, P.Y., (2005) .An elasto-plastic model for granular materials with microstructural consideration. *International journal of solids and structures*, 42, 4258-4277
[5] Guo, P., Su, X., (2007) .Shear strength, interparticle locking, and dilatancy in granular materials. *Canadian Geotechnics Journal*, 579-590
[6] Guo, P., (2008) .Modified direct shear test for anisotropic strength of sand. *Journal of Geotechnical and Geoenvironmental Engineering*, Vol. 134, No.9, 1311-1318
[7] Shaverdi, H., Taha M.R., Kalantary, F., (2014) .A flow rule incorporating fabric anisotropy and non-coaxiality in granular materials. *Granular Matter*, Vol. 16, 675-685
[8] Li, X., Dafalias, Y.F., (2015) .Dissipation consistent fabric tensor definition from DEM to continuum in granular media. *Journal of the Mechanics and Physics of Solids*, Vol. 78, 141-153

A novel perspective on clay modelling using hydrodynamic principles

M. Wiebicke[1]***, I. Einav***[1]

[1] *Sydney Centre in Geomechanics and Mining Materials, School of Civil Engineering, The University of Sydney*

Laboratory description of clay normally distinguishes the scale of atoms from the scale of clay particles and aggregates. By considering this scale separation, we introduce a robust physics-based constitutive model for clay adept at capturing key rheological and mechanical phenomena in clay. The model is derived using the rigorous hydrodynamic procedure from Landau and Lifshitz [1]. While some imagine that by considering rigour and physics, their models would get complicated, the resulting set of equations reveal a surprising degree of simplicity. The model's simplicity is showcased in Figure 1, which includes all equations necessary for the integration of the model in a triaxial invariant form.

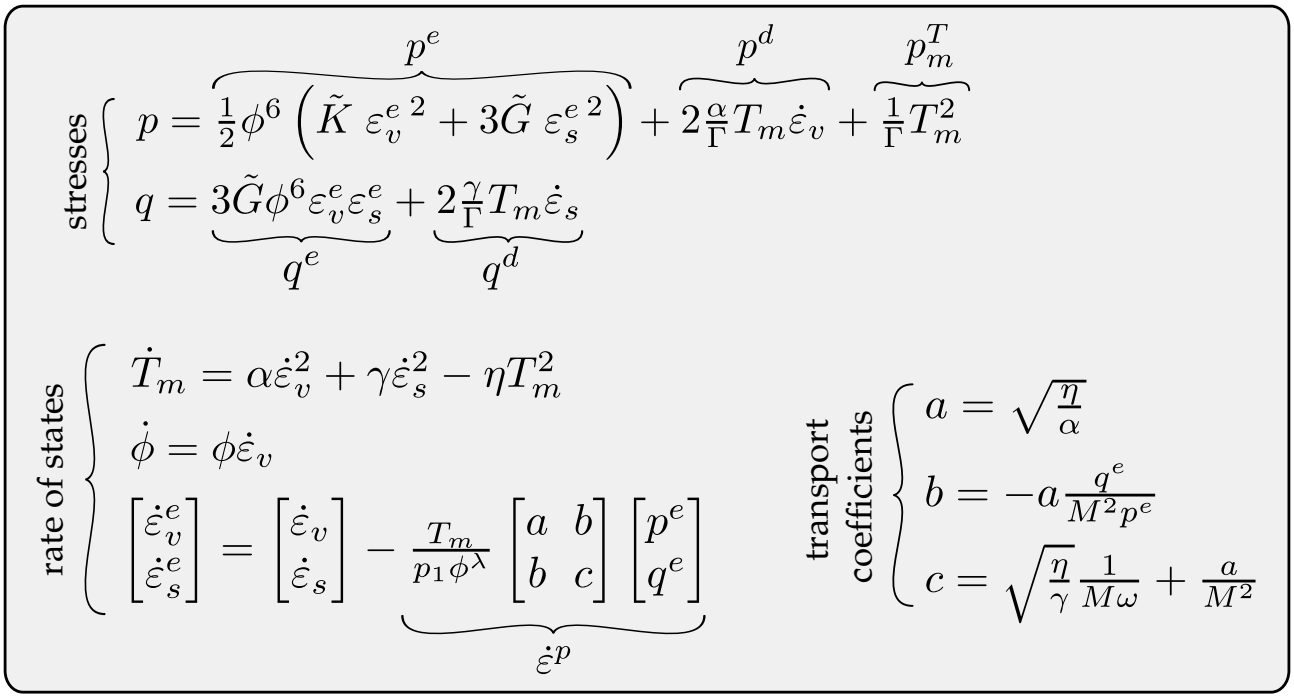

Figure 1. The 'Terracotta' model – all the required equations. In the above, p and q denote the volumetric and deviatoric stress invariants; ε_v and ε_v the volumetric and deviatoric strain invariants; ϕ the solid fraction; T_m the meso-related temperature; superscripts e, d, T, p refer to the elastic, dissipative (or viscous), thermodynamic and plastic contributions; $\tilde{K}, \tilde{G}, M, \omega, p_1, \lambda$ are material constants; α, γ, η are coefficients, chosen to be constant in this paper, while Γ is a fixed coefficient that sets the unit of the meso-related temperature.

To address the scale separation in clay, a second temperature is introduced as a non-equilibrium state variable: the meso-related temperature T_m. While the thermal temperature T captures the fluctuating motions of the atoms, the meso-related temperature accounts for the non-affine motion of meso-structures such as clay particles and aggregates. The energy flow within the material is described using the principle of two-stage irreversibility by Jiang and Liu [2]: it either flows directly to the micro-scale elevating T or first causes fluctuating motions at the meso-scale elevating T_m and

subsequently flows to the micro-scale. One standout feature of the model with respect to other hydrodynamic models is the consideration of a volumetric-deviatoric coupled plastic flow as given in the last row of Figure 1 by the fully populated matrix of coefficients a, b and c. To identify these coefficients, we have proposed a novel scheme using conventional steady-state observations. These choices, among other crucial physical concepts, lead to the simplicity of the model.

Despite this simplicity, the model robustly captures a plethora of clay behaviours. In particular, the model can readily explain the broad spectrum of rate-dependent phenomena during transient loading, along with creep and relaxation processes. To this point, Figure 2 shows a comprehensive oedometer test on a highly organic Gyttja reported by Niemunis and Krieg [3]. While the experiment encompassed a strain rate jump, it focused on the behaviour during different creep stages of the same time duration preceded by either unloading, primary loading or relaxation. The figure shows a remarkable performance of the simple model in capturing the volumetric response in this comprehensive test.

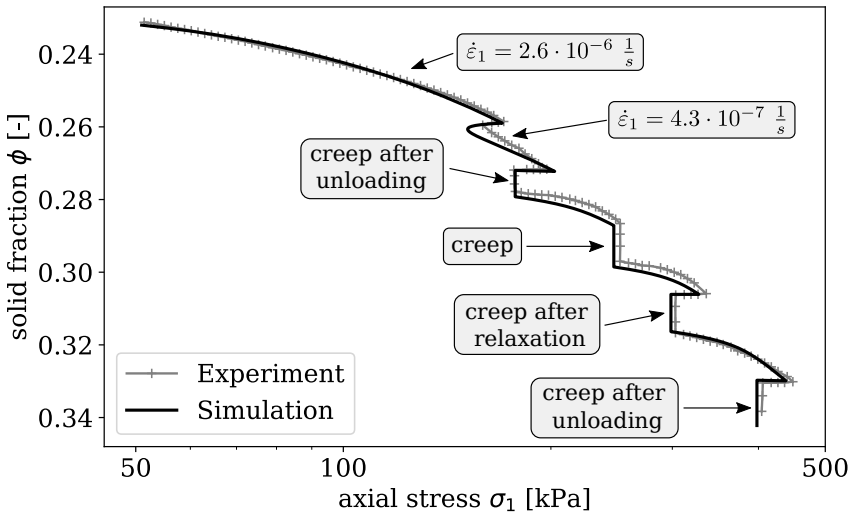

Figure 2. Comprehensive oedometer test with one change in loading rate and different stages of unloading, relaxation and creep reported in [3].

The primary goal of the proposed presentation is to elucidate some key physical concepts that allowed us to arrive at such a simple, yet predictive constitutive model. By shedding light on these and the thermodynamically rigorous hydrodynamic procedure, we hope to foster a deeper appreciation and understanding of physics-based modelling in the geotechnical community, traditionally inclined towards phenomenology and intricate mathematical approaches. We will conclude our presentation by demonstrating the model's robust performance through a comparison with a variety of experimental observations.

References

[1] Landau, L. D. and Lifshitz, E. M. (1987). *Fluid Mechanics*. Butterworth.
[2] Jiang, Y. and Liu, M. (2009). Granular solid hydrodynamics. *Granular Matter*, **11**, 139–156.
[3] Niemunis, A. and Krieg, S. (1996). Viscous behaviour of soil under oedometric conditions. *Canadian Geotechnical Journal*, **33**, 159–168.

Anisotropic elastic-plastic coupling model for sands considering fabric evolution

Yang Yu[1,2], Zhongxuan Yang[1], Tianhao Chen[1] and Angelo Amorosi[2]

[1] Department of Civil Engineering, Zhejiang University, Hangzhou, Zhejiang, 310058, China

[2] Department of Structural and Geotechnical Engineering, Sapienza University of Rome, Rome, Italy

Many solids exhibit a mechanical response in the reversible regime that is influenced by the previous stress-strain history experienced by the material. This phenomenon, also known as elasto-plastic coupling, has been recognized experimentally in different geomaterials as clayey or sandy soils and hard and soft rocks.

In recent decades, various constitutive models have been developed to replicate diverse forms of elasto-plastic coupling, drawing inspiration from the available experimental observations on soils and rocks. Essentially, within the classical elasto-plasticity framework, the incorporation of plastic strains or other internal variables, whose evolution is governed by irreversible processes, into the elastic formulation introduces a coupling mechanism, which leads to a dependence of the reversible response on the stress-strain history experienced by the material as accounted for by its internal variables. Noteworthy in this context are the pioneering works of Dafalias [1,2] and Maier & Hueckel [3], primarily focused on replicating elasto-plastic coupling as observed in rock samples under uniaxial compression. While grounded in different premises, these works were the first to deduce the implications of elasto-plastic coupling on the flow rule. Following this line of research, various constitutive models have been proposed, employing hypoelastic or hyperelastic formulations [4-8]. Additionally, Hueckel & Tutumluer [9] and more recently Amorosi et al. [10] introduced a form of anisotropic elasto-plastic coupling, linking two fabric tensors that characterize the elastic and plastic anisotropy of clays. It is worth remarking that any macroscopic fabric tensor is expected to be intimately linked to a microscale directional counterpart, as for example that related to the orientation of the contact forces or of the grains when elongated.

In this work we present a new macroscopic constitutive law for granular materials within the framework of Anisotropic Critical State Theory (ACST) [11], combining a hyperelastic formulation and a bounding surface plasticity model, including an anisotropic form of elasto-plastic coupling. In detail, a unique deviatoric tensor **F** is adopted to describe the fabric of soils, which affects both the reversible response of the material, via the elastic strain energy function, and the irreversible behaviour as described by a newly defined stress ratio and plastic strain-driven evolution equation. This leads the model is capable of reproducing the key aspects of the mechanical behaviour of sand-like materials, with the evolution of the fabric direction, which gradually aligns with the loading one, and the variation of the fabric norm, that attains different asymptotic values depending on the applied loading paths. The evolution of elastic anisotropy is naturally captured by the model due to its coupled formulation.

The developed macroscopic model is here adopted to reproduce the results of a series of discrete element method (DEM) analyses. The granular material is characterized by clump particles, whose basic particle is formed by two identical but overlapped spheres, and linear elastic contact law. They were subjected to different loading paths, either radial or deviatoric. Along those paths, a set of probing tests were carried out to detect different components of the reversible stiffness tensor for different states as expressed in terms of stress, porosity and contact fabric, aiming at validating the assumed elastic energy function and the proposed fabric evolution laws. Some laboratory test results are also adopted to validate the simulated macroscopical mechanical responses.

References

[1] Dafalias, Y. F. (1977a). Il'iushin's postulate and resulting thermodynamic conditions on elasto-plastic coupling. *Int. J. Solids Struct,* **13**(3), 239–251.

[2] Dafalias, Y. F. (1977b). Elasto-plastic coupling within a thermodynamic strain space formulation of plasticity. *Int. J. Non Linear Mech*, **12**(5), 327–337.

[3] Maier, G. & Hueckel, T. (1979). Nonassociated and coupled flow rules of elastoplasticity for rock-like materials. *Int. J. Rock Mech. Min. Sci. Geomech. Abstracts,* **16**(2), 77–92.

[4] Bigoni, D. & Hueckel, T. (1991). Uniqueness and localization—II. Coupled elastoplasticity. *Int. J. Solids Struct,* **28**(2), 215–224.

[5] Houlsby, G.T., Amorosi, A. & Rojas, E. (2005). Elastic moduli of soils dependent on pressure: a hyperelastic formulation. *Géotechnique,* **55**(5), 383–392.

[6] Gajo, A. & Bigoni, D. (2008). A model for stress and plastic strain induced nonlinear, hyperelastic anisotropy in soils. *Int. J. Numer. Anal. Meth. Geomech,* **32**(7), 833–861.

[7] Lashkari, A. & Golchin, A. (2014). On the influence of elastic–plastic coupling on sands response. *Comput. Geotech*, **55**, 352–364.

[8] Zhao, J. D. & Gao, Z. W. (2015). Unified anisotropic elastoplastic model for sand. *J Eng Mech*, 142(1), 04015056-1-12.

[9] Hueckel, T. & Tutumluer, E. (1994). Modeling of elastic anisotropy due to one-dimensional plastic consolidation of clays. *Comput. Geotech*, **16**(4), 311–349.

[10] Amorosi, A., Rollo, F. & Dafalias, Y.F. (2021). Relating elastic and plastic fabric anisotropy of clays. *Géotechnique,* **71**(7), 583–593.

[11] Li, X.S. & Dafalias, Y. F. (2012). Anisotropic critical state theory: role of fabric. *J. Eng. Mech*, **138**(3):263-275.

CONSTITUTIVE MODELING BASED ON MESO SCALE BEHAVIOUR

***G.D. Nguyen*[1], *H.H. Bui*[2]**
[1] *University of Adelaide, School of Architecture and Civil Engineering, Adelaide, Australia*
[2] *Monash University, Department of Civil Engineering, Clayton, Australia*

1. Introduction

The development of a constitutive model should involve not only key mechanisms behind macro-observable behaviour, but also experiments to determine and calibrate parameters of the model, along with the analysis of boundary value problems (BVPs). This is to assure consistency and good correlations between experiments and modelling for maximising the performance of the model.

This short communication addresses three important aspects: constitutive modelling based on meso scale behaviour, extraction of meso scale behaviour from experiments, and analysis of BVPs. Localisation of deformation and meso scale localisation band are used as the basis, given they are important characteristic of failure. All three mentioned aspects are based on a theoretical framework (Nguyen & Bui, 2020) that allows connecting meso and macro scales so that the behaviour at one scale can be determined from another. The embedded mechanisms of localised failure also acts as a localisation limiter in analysing BVPs without having to resort to ad hoc regularisation.

2. From meso to macro: constitutive modelling

Figure 1 illustrates the concept of a constructive structure based on meso scale behaviour. A localisation band with both geometrical properties and constitutive behaviour (in red colour) is assumed to mainly govern inelastic responses of the volume element containing it. The enrichment of kinematic field allows obtaining both macro stress and macro strain in volume-averaged forms. Different constitutive responses inside and outside the localisation band are connected through the traction continuity across the boundary of the band. Macro behaviour (black) can be determined if meso scale responses (red) are known, along with assumed elastic behaviour outside the localisation zone (blue). Details can be found in Nguyen & Bui (2020).

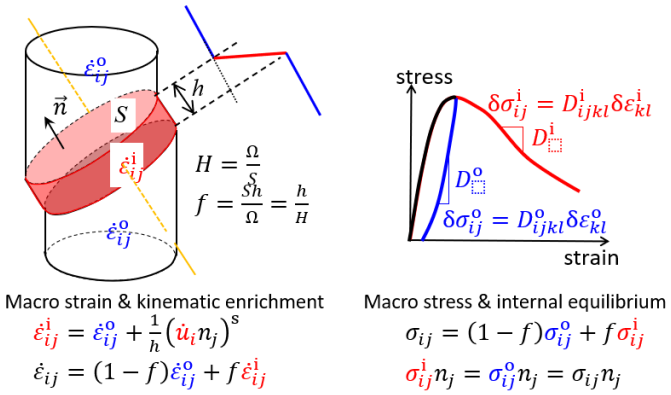

Figure 1. Macro-meso connections: from meso behaviour to macro response.

3. From macro to meso: analysing experimental data

On the other hand, if macro behaviour is known from standard tests of geomaterials involving localised failure, one should be able to obtain meso scale behaviour for the development of

constitutive models at the meso scale, using the inverse of the relationships presented in Figure 1. The key relationships and how to determine are illustrated in Figure 2, and details can be found in Le et al (2022).

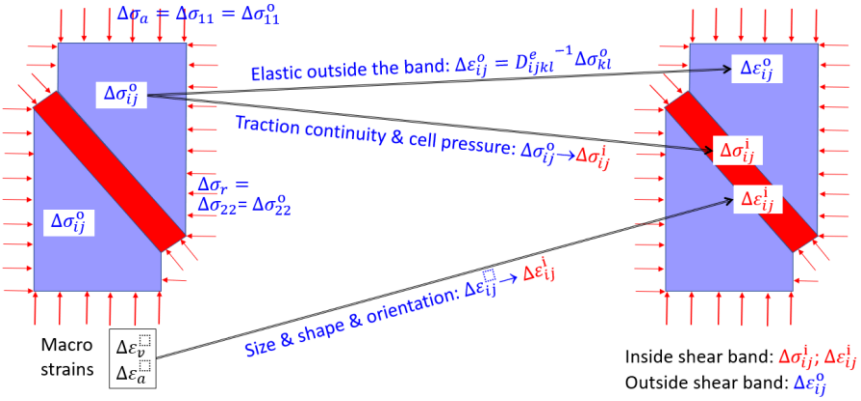

Figure 2. From macro test data to meso-scale behaviour.

4. In-built regularisation in analysis of BVPs

In the analysis of BVPs, an integration point (or particle) represents a volume element that can be much larger than the thickness of the localisation band. Under the same loading condition, embedded meso scale details in an integration point (thickness, orientation and behaviour of localisation band) are invariant with respect to the size of the volume element containing it. This naturally results in invariance of the dissipation with respect to changes of discretisation resolution, and hence convergence of the inelastic responses upon discretisation refinement (see Figure 3). Details can be found in Le et al (2018).

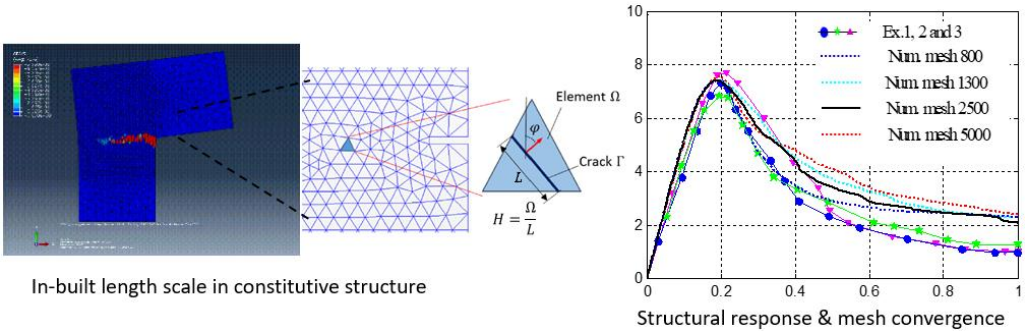

Figure 3. An example of BVP involving localised failure.

The choice of the meso scale as the basis is to keep a balance between complexity, predictive capability, computational efficiency, and ease of implementation. In principle lower scales can also be used as the basis for model developments, if explicit links between quantities at different scales involved (micro/grain, meso, macro) are available, along with experiments to determine them.

5. References

[1] Nguyen G.D., Bui H.H. (2020). A thermodynamics- & mechanism-based framework for constitutive models with evolving thickness of localisation band, *Int. J. Solids Struct.*, **187**:100-120.

[2] Le L.A., Nguyen G.D., Bui H.H., Andrade J.E. (2022). Localised failure of geomaterials: how to extract localisation band behaviour from macro test data, *Géotechnique* **72** (7):596-609.

[3] Le L.A., Nguyen G.D., Bui H.H., Sheikh A.H., Kotousov A. (2018). Localised failure mechanism as the basis for constitutive modelling of geomaterials, *Int. J. Eng. Sci*. **133**:284-310.

Elastic moduli of granular materials composed of polyhedral particles during triaxial compression

***Duc Chung Vu*[1,2], *Lhassan Amarsid*[1], *Jean-Yves Delenne*[3], *Vincent Richefeu*[4] *and Farhang Radjai*[2]**

[1] *CEA, DES, IRESNE, DEC, SESC, LDOP, Saint Paul les Durance, France*
[2] *LMGC, CNRS, University of Montpellier, Montpellier, France*
[3] *IATE, INRAE, Institut Agro, University of Montpellier, Montpellier, France*
[4] *3SR, CNRS, University of Grenoble Alpes, Grenoble, France*

The elastic moduli have been a subject of extensive experimental work with various soils and simple granular materials as well as particle dynamics simulations based on the Discrete Element Method (DEM). However, there is presently no general model capable of relating the elastic moduli of a granular material to particle properties and predicting their evolution with shear. A key issue is the nonaffine nature of the displacement field, leading to over-estimation of the moduli by the Effective Medium Theory (EMT) [1, 2]. Another important issue concerns facetted particles, which can have face-face or face-edge contacts with other particles. Such contacts involve geometrical constraints that differ from those of simple contacts and, what is more, they are not governed by Hertz-like elasticity.

By means of particle dynamics simulations, we investigate the orthotropic elastic moduli of dense packings of polyhedral particles with different number of faces. The samples are prepared by isotropic compaction under constant load and zero friction, leading to random close packed configuration of particles with highest density. Then, they were sheared under tri-periodic boundary conditions for four values of friction coefficient μ_s = 0.1, 0.2, 0.3, and 0.4 between particles. During shearing, 16 instances corresponding to a wide variety of contact orientation anisotropies were stored and relaxed a static state before applying two distinct strain probes to measure the five independent elastic moduli of the sample.

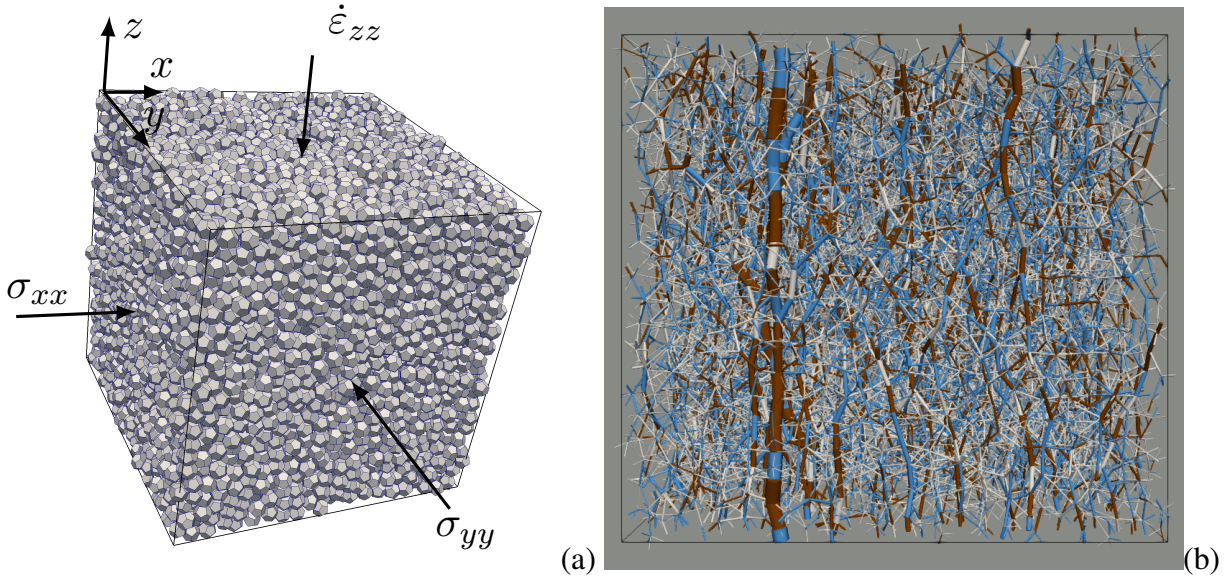

Figure 1. A snapshot of the sample of dodecahedral particles in the isotropic state (a), and the normal force network of a dodecahedral particle packing near stress peak with friction coefficient $\mu_s = 0.1$ (b). Line thickness is proportional to the normal force. Single contacts are in white, double contacts in blue, and triple contacts in brown.

By comparing the simulation data with effective medium theory (EMT), our results clearly show that the elastic moduli are functions of two microstructural parameters: 1) a constraint number that accounts for contact types (face-face and face-edge contacts between polyhedra), and 2) the contact orientation anisotropy. The proposed expression of elastic moduli isolates the direct effect of particle shape, related to the nonaffine particle displacement field from the indirect effect, related to the granular microstructure. The effect of particle shape appears at two levels: on the one hand, through four parameters in the proposed expression, which are independent of friction coefficient, and, on the other hand, through the microstructure reflected by the values of constraint number and fabric anisotropy, which depend on both particle shape and interparticle friction coefficient. Furthermore, the elastic moduli have been compared between polyhedral and spherical particle packings under similar conditions in order to fully highlight the particle shape effect [3].

To our best knowledge, this work provides the first simulations of the elastic behavior of polyhedral particles and the first general expression that can be applied to both polyhedral and spherical particle packings and accounts for the first-order microstructural parameters.

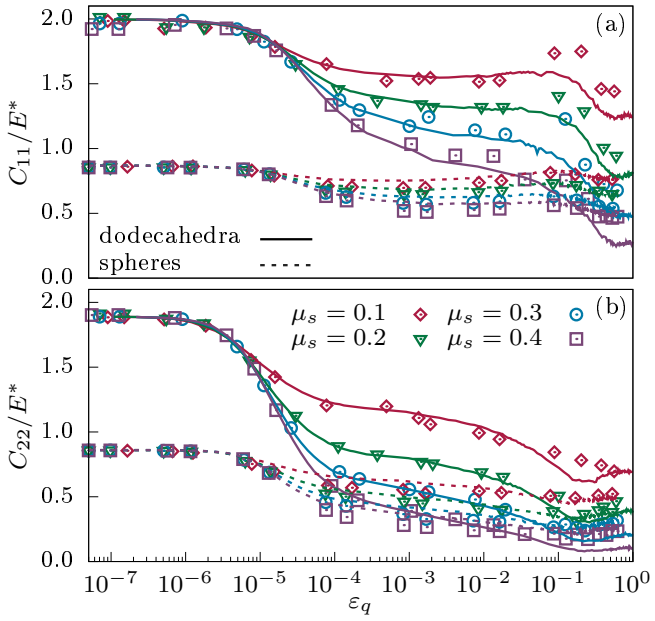

Figure 2. Normalized longitudinal elastic moduli (a) C_{11}/E^* and (b) C_{22}/E^*, as a function of shear strain ε_q for packings of spherical and dodecahedral particles with different values of friction coefficient μ_s. The dashed and solid lines are theoretical predictions for packings of spheres and dodecahedra, respectively.

References

[1] Makse, H. A., Gland, N., Johnson, D. L., and Schwartz, L. M. (1999). Why effective medium theory fails in granular materials. *Physical Review Letters*, **83**, 5070.

[2] Zaccone, A. and Scossa-Romano, E. (2011). Approximate analytical description of the nonaffine response of amorphous solids. *Physical Review B*, **83**, 184205.

[3] Vu, D. C., Amarsid, L., Delenne, J.-Y., Richefeu, V., and Radjai, F. (2023). Macro-elasticity of granular materials composed of polyhedral particles. *Granular Matter*, **26**, 6.

Granular matter is a two-phase composite for the purpose of stress transmission

Rafi Blumenfeld

University of Cambridge, UK

A basic problem in the science of realistic granular matter is the plethora of heuristic models of the stress field in the absence of a first-principles theory. Such a theory is formulated here, based on the idea that static granular assemblies can be regarded as two-phase composites. A thought experiment is described, demonstrating that the state of such materials can be varied continuously from marginal stability (aka the critical state), via a two-phase granular assembly, then porous structure, and finally be made perfectly elastic.

I review briefly the general solution for the stress equations in marginally rigid media in two dimensions, of which the Mohr-Coulomb solution, for example, is a special case and I argue that it is consistent with the two-phase idea. A method for identifying the phases of finite regions in larger systems is constructed, providing a stability parameter that quantifies the `proximity' to the marginally stable state. The difficulty involved in deriving stress fields in such composites is a unique constraint on the boundary between phases and, to highlight it, a simple case of a stack of plates of alternating phase is solved explicitly. I then describe a newly developed effective medium approximation for this problem, which satisfies this constraint, and analyse it in some detail. This approach forms a basis for the extension of the stress theory to general granular solids that are not at the yield threshold.

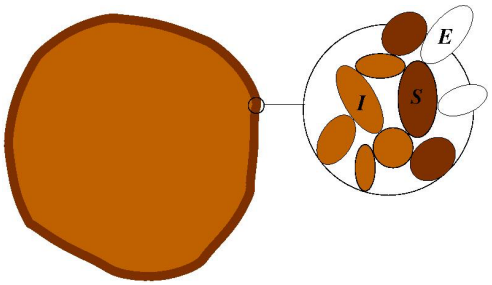

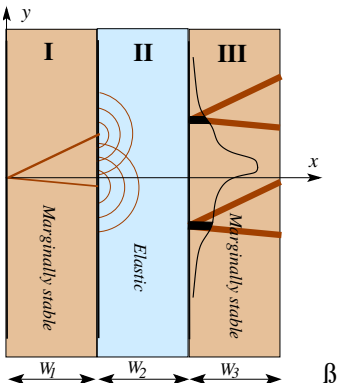

Indirect and Direct Consideration of Microstructure in a Constitutive Model

Tianchi Wu[1], Peter Cleall[1] and Snehasis Tripathy[1]
[1] Cardiff University, School of Engineering, Cardiff, Wales, UK

Abstract

It is important to describe and quantify microstructure when modelling microstructure-related behaviour of soils. There are indirect and direct methods to consider microstructure in modelling. Indirect methods only consider the impact of microstructure on soil behaviour. Whilst direct methods focus on geometric and structural features of microstructure such as pore size distribution (PSD). This paper presents an example of indirect and direct consideration of microstructure in a constitutive model. The indirect method considers the microstructural impact through effective degree of saturation and the direct method adopts the pore size distribution as microstructure index. The performance of each approach is evaluated based on experimental results and it is found that both have good potential in studying the hydro-mechanical behaviour of soils.

Keywords: microstructure; pore size distribution; constitutive model; hydro-mechanical model

1 Introduction

It is widely acknowledged that microstructure has a significant impact on the hydro-mechanical behaviour of soils [1–3]. To describe and quantify microstructure in a model, there are indirect methods and direct methods. Indirect methods focus on the effect of microstructure on soil behaviour but ignore the exact microstructural features. Direct methods attach more importance to the detailed microstructural features such as pore shape, pore size and pore size distribution (PSD).

One modelling example of both indirect and direct methods is presented in this paper and is compared with experimental results. For the indirect method, the effective degree of saturation is adopted as a microstructural index because it is defined to neglect the residual degree of saturation stored in intra-aggregate pores (micropores) [4–6]. For the direct method, PSD is selected to represent microstructure due to its direct description of pore sizes and their volumes which are highly related to volume change behaviour of soils. The other reason to choose PSD is that the water content can be directly obtained from PSD. This gives the model the potential in predicting hydraulic behaviour such as soil-water characteristic curve (SWCC). PSD and its interaction with stress-strain behaviour are considered in the model through a PSD-dependent effective stress [3]. The Glasgow Coupled Model (GCM) [7] is adopted as the hydro-mechanical framework for both methods.

Both methods have their own merits and deficiencies. The indirect method requires only one parameter to represent microstructure. However, this method fails to consider the evolution of microstructure because the residual degree of saturation is assumed to be constant and not impacted by changes to the microstructure. The direct method assumes soil pores are cylindrical and evolution of PSD is solely related to the change of void ratio. Direct methods will typically require more parameters to represent microstructure and can make the model much more complex. However, direct methods give the possibility of studying microstructural-hydro-mechanical coupled behaviour within a unified framework and can be applied to predicting the evolution of microstructure and SWCCs.

2 Main results and brief conclusions

The result of modelling by both indirect and direct method is presented in Fig.1(a), (b) and (c) for an isotropic loading path for Speswhite kaolin from net mean stress of 50kPa to 250kPa [5].

Compared with experimental results [8, 9], both methods can give a satisfactory result in reproducing the stress-strain behaviour of soils. It should be noted that PSD data has been assumed based on information available in the literature thereby limiting its fidelity. The direct method can also predict the evolution of PSD that it evolves with the compression of macropores and so gives the advantage of allowing the representation of microstructure evolution during loading and hydraulic behaviour such as SWCC.

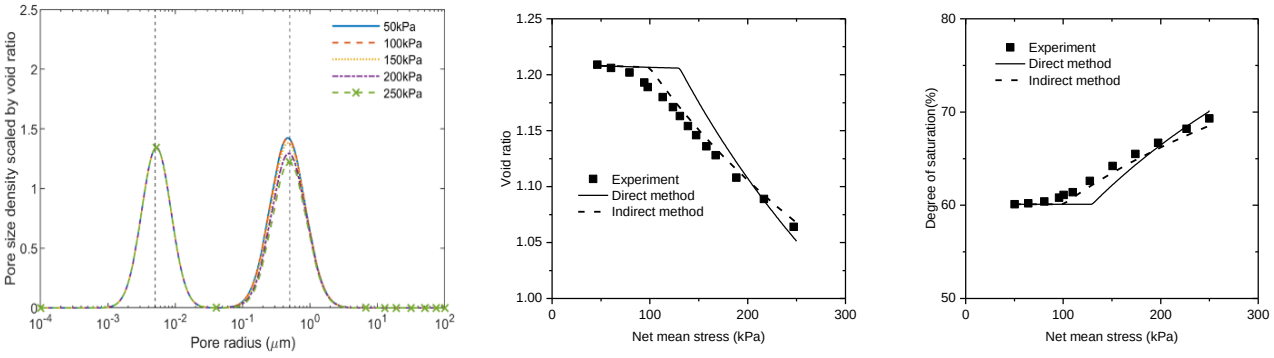

(a) PSD evolution from direct method (b) p_{net}-e (c) $p_{net} - S_r$

Fig.1 Comparison among indirect method, direct method and experimental results

References

[1] Romero, E., Gens, A. and Lloret, A. (1999). Water permeability, water retention and microstructure of unsaturated compacted Boom clay. *Eng. Geol.* **54** 117–27.

[2] Romero, E. and Simms, P. H. (2008). Microstructure investigation in unsaturated soils: a review with special attention to contribution of mercury intrusion porosimetry and environmental scanning electron microscopy. *Geotech. Geol. Eng.* **26** 705–27.

[3] Vaunat, J. and Casini, F. (2017). A procedure for the direct determination of Bishop's χ parameter from changes in pore size distribution. *Géotechnique* **67** 631–6.

[4] Alonso, E. E., Pereira, J.-M., Vaunat, J. and Olivella, S. (2010). A microstructurally based effective stress for unsaturated soils. *Géotechnique* **60** 913–25.

[5] Wu, T., Cai, G., Cleall, P. and Tripathy, S. (2022). Microstructurally related model for predicting behavior of unsaturated soils with double porosity in triaxial space. *Int. J. Geomech.* **22** 04022216.

[6] Wu, T., Cleall, P., Tripathy, S. and Cai, G. (2023). Consideration of microstructure in modelling the hydro-mechanical behaviour of unsaturated soils. *E3S Web Conf.* **382** 11005.

[7] Lloret-Cabot, M., Sánchez, M. and Wheeler, S. J. (2013). Formulation of a three-dimensional constitutive model for unsaturated soils incorporating mechanical-water retention couplings. *Int. J. Numer. Anal. Methods Geomech.* **37** 3008–35.

[8] Cui, Y. J. and Delage, P. (1996). Yielding and plastic behaviour of an unsaturated compacted silt. *Géotechnique* **46** 291–311.

[9] Sivakumar, V. (1993). *A critical state framework for unsaturated soil*. University of Sheffield, United Kingdom.

Mathematical formulation of Elastic Moduli of Granular Materials with Consideration of Structural Heterogeneity

***Zijun Shi*[1], *Xia Li*[1*]**
[1] *Southeast University, School of Civil Engineering, Nanjing, China*
[*] *Corresponding author*

Keywords: Granular materials; Elastic moduli; Structure heterogeneity; Mean field; DEM

Due to the heterogeneity and randomness in its internal structure, granular material exhibits complex stress-strain behavior. Extensive attempts have been made to derive the macroscopic material behavior from the particle-scale governing mechanisms and material properties via homogenization techniques [1-3]. Great successes have been achieved in a number of aspects, including establishing the mathematical expression of the elastic moduli of granular materials showing that the effective bulk modulus of random packing is proportional to the confining pressure in power of 1/3 based on the uniform strain assumption [4], and that the Poisson's ratio in dense systems is contingent upon the ratio of tangential to normal contact stiffness [5]. Later Kruyt and Rothenburg [6-7] derived the upper and lower bounds for the stiffness tensor of two-dimensional, isotropic assemblies comprising bonded, nonrotating disks. The derivations from the result provided by Discrete element simulations (DEM) are believed due to local fluctuations and consequently adjusted [8-10]. Nevertheless, the microscopic origin of the local fluctuations and the mechanics have never been quantified and clarified.

This study revisits the mathematical formulation of elastic moduli of granular materials. It is noted that with specified internal structure and contact model, a strictly uniform strain field may lead to local unbalanced forces, while a strictly uniform stress field may not satisfy local displacement compatibility. Both are determined by the local structure and contact model. Here, we quantify the structure heterogeneity in terms of the statistics of local geometrical information contributing to local unbalanced forces and in-compatible displacements, as exemplified in Fig. 1.

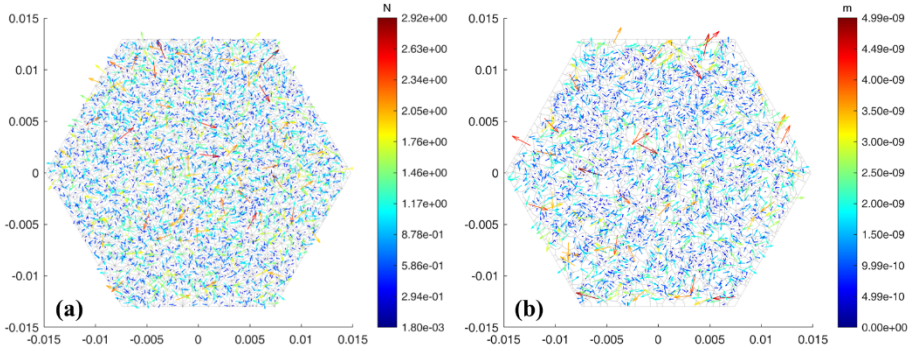

Figure 1. Local fluctuations when subjected to deviatoric shearing (a) Unbalanced forces with uniform strain and (b) non-compatible displacement with uniform stress.

Viewing the response of granular materials as that predicted from the uniform-field theory superimposed by the local relaxations. Numerical experiments have been carried out on 2D samples and provide detailed particle-scale data enabling the statistical quantification of the structural heterogeneity and the corresponding local relaxation. Attention has also been placed on the non-

affined displacement developed in the granular system shown in Fig. 2. The correlation between unbalanced forces and non-affine displacements has been carefully examined.

Leveraging these insights, we have proposed the mathematical formulation for elastic moduli of granular materials with consideration of structure heterogeneity. The mathematical formation has been used to evaluate the elastic moduli of granular materials at different sheared stages and gives satisfactory results based on the discrete element simulations.

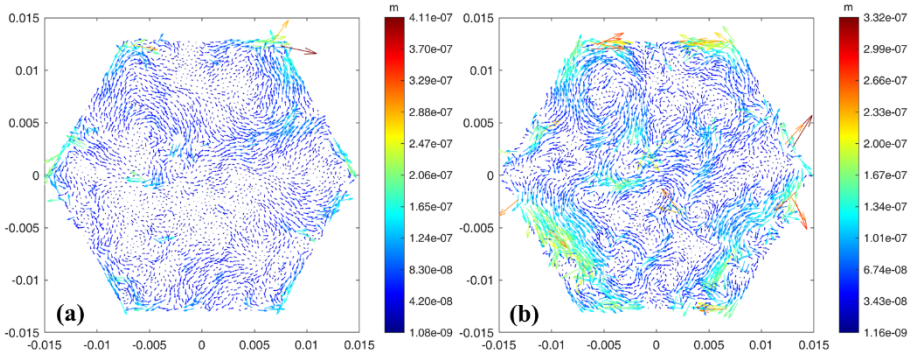

Figure 2. Non-affined particle displacements (a) isotropic compression and (b) deviatoric shearing.

References

[1] Nicot, F. and Darve, F. (2005). A multi-scale approach to granular materials. Mechanics of Materials, p. S016766360400167X.

[2] Cambou, B., Dubujet, P., Emeriault, F., and Sidoroff, F. (1995). Homogenization for granular materials. European Journal of Mechanics a-Solids, 14, 255–276.

[3] Li, X. and Li, X.-S. (2009). Micro-macro quantification of the internal structure of granular materials. Journal of Engineering Mechanics, 135, 641–656.

[4] Walton, K. (1987). The effective elastic moduli of a random packing of spheres. Journal of the Mechanics and Physics of Solids, 35, 213–226.

[5] Bathurst, R. J. and Rothenburg, L. (1988). Micromechanical Aspects of Isotropic Granular Assemblies With Linear Contact Interactions. Journal of Applied Mechanics, 55, 17–23.

[6] Kruyt, N. and Rothenburg, L. (1998). Statistical theories for the elastic moduli of two-dimensional assemblies of granular materials. International Journal of Engineering Science, 36, 1127–1142.

[7] Goldenberg, C., Tanguy, A., and Barrat, J.-L. (2007). Particle displacements in the elastic deformation of amorphous materials: Local fluctuations vs. non-affine field. Europhysics Letters, 80, 16003.

[8] Kruyt, N. and Rothenburg, L. (2004). Kinematic and static assumptions for homogenization in micromechanics of granular materials. Mechanics of Materials, 36, 1157–1173.

[9] Agnolin, I. and Kruyt, N. P. (2008). On the elastic moduli of two-dimensional assemblies of disks: Relevance and modeling of fluctuations in particle displacements and rotations. Computers & Mathematics with Applications, 55, 245–256.

[10] Kruyt, N. P., Agnolin, I., Luding, S., and Rothenburg, L. (2010). Micromechanical study of elastic moduli of loose granular materials. Journal of the Mechanics and Physics of Solids, 58, 1286–1301.

NUMERICAL INVESTIGATION OF A PERMEABILITY-MICROSTRUCTURE RELATIONSHIP IN THE CONTEXT OF INTERNAL EROSION

***M. EL SHAMIEH*[1], *N. NGUYEN*[1], *F. BIGNONNET*[1], *R. GELET*[1], *D. MAROT*[1]**
[1] *Nantes Université, École Centrale Nantes, CNRS, GeM, UMR 6183, F-44600, Saint-Nazaire, France*

Keywords: Permeability, suffusion, granular soils, Discrete element method, fast Fourier transformation, Delaunay triangulation, Kozeny-Carman.

Abstract

Earth made hydraulic structures have several essential functions for our society which include irrigation, hydropower, water supply and flood control. These structures are built with soil materials that can easily be reused and are in good harmony with the environment. Nevertheless, numerous earth structures display heterogeneities, large linear lengths, age and sometimes disorders leaving them susceptible to geotechnical instabilities. One of the major concerns affecting the integrity of these structures is internal erosion. This phenomenon is characterized by the migration of soil particles within hydraulic earth structures due to seepage. Among the four mechanisms of internal erosion, we focus on suffusion also called volumetric erosion. It involves the simultaneous detachment, transport and partial self-filtration of fine particles through interconnected pore spaces within the soil matrix. Suffusion is a strongly coupled mechanism that induces significant changes in permeability, porosity, flow velocity, microstructure and strength of granular soils. The modelling of suffusion requires a relationship that links permeability with the evolving microstructure. Recall that permeability strongly influences the flow evolution, favoring or preventing the kinetics of suffusion. We aim to investigate the link between the permeability and the microstructure of eroded granular soils. To achieve this micro-macro investigation, the following work methodology is proposed. Initially, numerical samples with different gradings of spherical particles (Figure 1) are generated with discrete element method DEM. Subsequently, each microstructure undergoes a characterization of its constriction size distribution CSD using the Delaunay triangulation method [3]. Afterwards, macroscopic permeability is numerically computed using a method based on Fast Fourier Transform [1].

In literature, several authors have tried to link permeability to different microstructure parameters. In this work, the first step is to apply and validate Kozeny-Carman model [2] for different homogeneous samples. The latter model, (equation 1), links the permeability K to the porosity Φ and a specific length called the hydraulic radius R_H. This radius is the ratio of the pore volume to the area of the solid-fluid interface. However, it is crucial to note that this empirical relationship has been developed for stable homogeneous microstructures only. This means that it may not be applicable to a suffusion context that involves a significant evolution of the pore size distribution and the CSD due to rearrangements of the grains at the pore scale. Our work, introduces a modified version of the Kozeny-Carman approach by incorporating a characteristic constriction diameter obtained from the CSD such as the controlling constriction size Dc* (equation 2).

$$K = \frac{R_H^2 \Phi}{k} \qquad (1) \qquad\qquad K = \frac{D_c^{*2} \Phi}{k_1} \qquad (2)$$

Figure 2 shows the dimensionless constants k and k_1 of the original and modified Kozeny-Carman models applied to homogeneous gap-graded samples. It is shown that the Kozeny-Carman

coefficient k is around 4.7 with a coefficient of variation of 6.5%, while the coefficient k_1 in the modified model shows a larger coefficient of variation but a clear decrease trend with porosity.

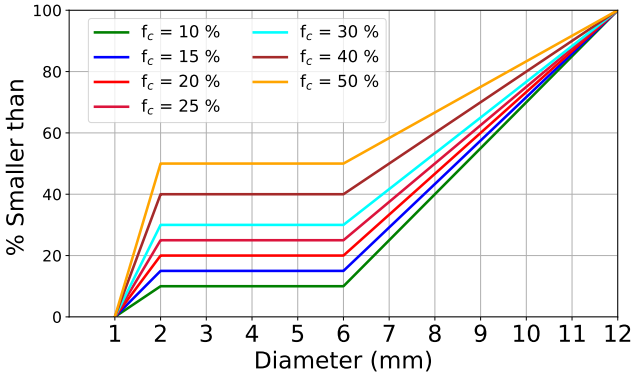

Figure 1. Grain size distribution for gap graded specimens having different fine contents.

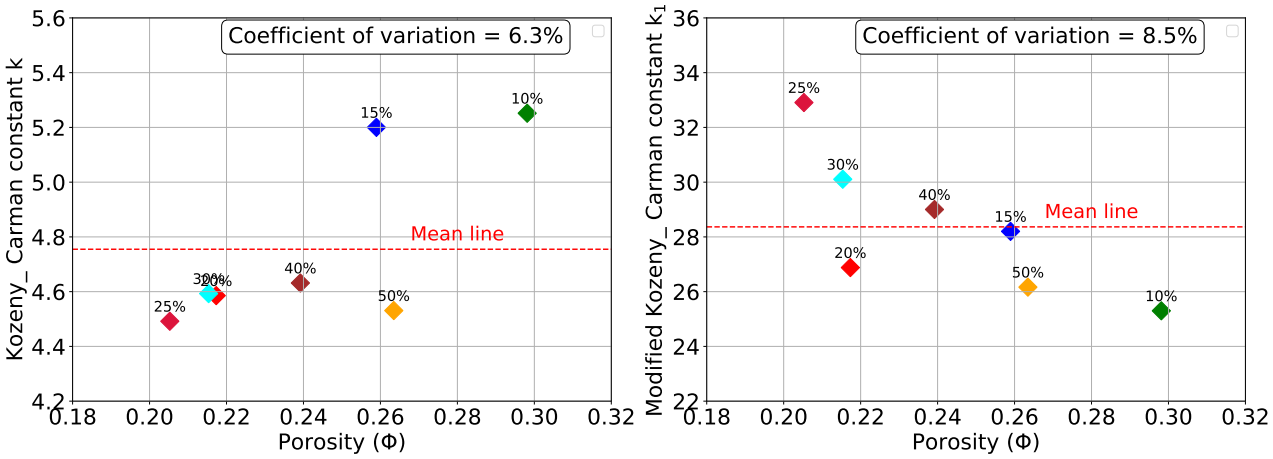

Figure 2. Kozeny-Carman constant k (left) and modified Kozeny-Carman constant k_1 (right) for seven gap-graded specimens. The dash lines represent the mean.

The above results show that the Kozeny-Carman model works quite well for homogeneous samples. However, an open question is whether or not it still works for heterogeneous samples. For such samples, the modified Kozeny-Carman model becomes of interest as the CSD would allow us to capture the heterogeneity. Hence, this work will be extended later to non-homogeneous specimens by applying drag forces to fine particles and thus simulating suffusion.

References

[1] François Bignonnet. Efficient fft-based upscaling of the permeability of porous media discretized on uniform grids with estimation of rve size. *Computer Methods in Applied Mechanics and Engineering*, 369:113237, 2020.

[2] Josef Kozeny. Uber kapillare leitung der wasser in boden. *Royal Academy of Science, Vienna, Proc. Class I*, 136:271–306, 1927.

[3] Ngoc-Son Nguyen, Habib Taha, and Didier Marot. A new delaunay triangulation-based approach to characterize the pore network in granular materials. *Acta Geotechnica*, 16(7):2111–2129, 2021.

Numerical Integration of HISS Model with Finite Element Method: Strain Localization Analysis in Sand

Pavan Yadav[1] and Amit Prashant[1]
[1] Indian Institute of Technology Gandhinagar, Gujarat, India

1. Abstract

Strain localization forming shear bands in the geomaterials has ensued significant damage to the structures. The present study is focused on the numerical simulation of strain localization using a finite element tool, namely ABAQUS. The hierarchical single surface model (HISS model) provides a suitable elastoplastic framework to predict the response of soils. The HISS model has been implemented in ABAQUS through the user-material subroutine (UMAT). A fully implicit radial return mapping algorithm is used for the model implementation, which includes the Newton-Raphson method for convergence of the solution. This is subsequently validated with hydrostatic and triaxial compression tests on cubical specimen results using single-element simulations. The results from drained experiments available in the literature were used for validation. Furthermore, the model is used to analyze strain localization in the saturated cylindrical specimens under triaxial loading conditions. Deviatoric strain corresponding to the onset of strain localization was used for the evaluation of mesh size dependency. Further, the effect of initial confining pressure on the onset of strain localization has been examined.

Keywords: HISS model; UMAT; strain localization; radial return mapping.

2. Methodology

Desai and co-workers have developed a hierarchical single surface (HISS) model to capture the response of material [1]. Various versions of HISS model have been proposed to include the material properties such as nonassociative (δ_1), anisotropy and kinematic hardening (δ_2), and viscoplastic (δ_{vp}). The HISS- model is adopted to predict the response for initially isotropic material, hardening isotropically with nonassociative plasticity. The yield (y) and plastic potential (g) function of the HISS- model is expressed as [2,3]

$$y = \frac{J_{2D}}{P_a^2} - \left[-\alpha\left(\frac{J_1}{P_a}\right)^n + \gamma\left(\frac{J_1}{P_a}\right)^2\right](1-\beta S_r)^m \tag{1}$$

And

$$g = \frac{J_{2D}}{P_a^2} - \left[-\alpha_Q\left(\frac{J_1}{P_a}\right)^n + \gamma\left(\frac{J_1}{P_a}\right)^2\right](1-\beta S_r)^m \tag{2}$$

Where $\alpha_Q = \alpha + k(\alpha_0 - \alpha)\left(1 - \frac{\xi_V}{\xi}\right)$ and α is hardening parameter which can be defined as $\alpha = \frac{a_1}{\xi\eta_1}$. k is nonassociative constant. J_{2D} and J_1 are the second invariant of the deviatoric stress tensor and the first invariant of the stress tensor. S_r is the stress ratio. n, γ, β, and m are the material constants. a_1 and η_1 are hardening constants. P_a is the atmospheric pressure.

3. Numerical model and material constants

In this study, the saturated sand specimen of a triaxial setup is modelled in a finite element tool, named ABAQUS [4], with 3-D cylindrical mesh. Figure 1(a) depicts the schematic of the numerical model with a small heterogeneity in the middle of the specimen with boundary and loading conditions. The height and diameter of the cylindrical sand specimen is considered as 100 mm and 50 mm. C3D8 type element (8-node linear brick element) is considered to represent soil sample. The numerical simulation is performed in two steps (geostatic and shear) on Munich sand [5] with an initial void ratio (e_0) and confining pressure (σ_0) of 0.65 and 200 kPa. The rate of shear deformation was 0.1 m/min and a total deformation of 10 mm was applied on the top surface of the specimen. The material parameters used in the simulation are presented in the table (1).

E/kPa	ν	γ	β	n	m	a_1	η_1	k_1	P_a/kPa
113685	0.3	0.1	0.747	3.2	-0.5	0.477	0.00224	0.35	101

Table 1. Material parameters for Munich sand [5]

4. Results

Figure 1 (b) and (c) illustrates the contour of plastic deviatoric strains and void ratios for isotropically consolidated drained tests performed on Munich sand. Strain localization forming persistent shear bands is observed in the saturated sand specimen. The shear bands propagate diagonally from the weaker zone (in the middle of the soil sample) of the soil specimen and form an X-shape band. The void ratio inside the shear band is higher as compared to the outside the shear band which indicates the dilative response of materials inside the band and contraction of materials outside the band during shearing. Further, it is observed that the onset of stain localization is delayed with the increase of initial effective confining pressures.

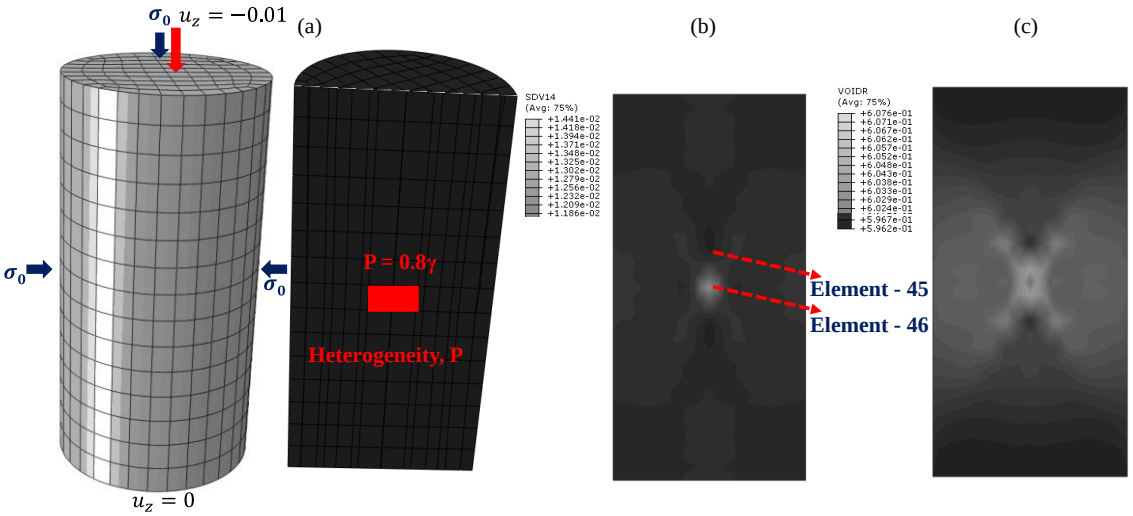

Figure 1. (a) Schematic of triaxial specimen with loads, and boundary conditions ; (b) contour of plastic deviatoric strains ; (c) contour of void ratio.

5. References

[1] Desai, C. S., Somasundaram, S., & Frantziskonis, G. (1986). A hierarchical approach for constitutive modelling of geologic materials. *International Journal for Numerical and Analytical Methods in Geomechanics*, *10*(3), 225-257.

[2] Desai, C. S. (2000). *Mechanics of materials and interfaces: The disturbed state concept*. CRC press.

[3] Desai, C. S., & Hashmi, Q. S. E. (1989). Analysis, evaluation, and implementation of a nonassociative model for geologic materials. *International journal of plasticity*, *5*(4), 397-420.

[4] Abaqus, S., Fallis, A. D. S., & Techniques, D. (2014). ABAQUS analysis user's guide (6.14). *Dassault Systemes Simulia Corp., Providence*.

[5] Hashmi, Q. S. E. (1987). *Nonassociative plasticity model for cohesionless materials and its implementation in soil-structure interaction*. The University of Arizona.

Packing and strength properties of agglomerates of platelet particles

***T. D. Tran*[1,2], *F. Radjai*[1], *J.-P. Bayle*[2], *L. Amarsid*[3] *and S. Nezamabadi*[1,4]**
[1] *LMGC, University of Montpellier, CNRS, Montpellier, France*
[2] *CEA, DES, ISEC, DMRC, University of Montpellier, Marcoule, France*
[3] *CEA, DES, IRESNE, DEC, Cadarache F-13108 Saint-Paul-lez-Durance, France*
[4] *IATE, CIRAD, INRAE, Montpellier SupAgro, University of Montpellier, F-34060, Montpellier, France*

1. Introduction

There is growing need for quantitative understanding of the influence of particle shape on the microstructure and mechanical behavior of granular materials [1]. We investigate the mechanical and microstructural characteristics of granular materials composed of platelets of pentagonal cross section by means of particle dynamics simulations [2]. Platy particles are encountered, for instance, in clayey soils, where the observed local ordering and clustering of the particles is often attributed to the cohesive interactions between particles. But, it is well known that platy particles in dry cohesionless particles tend also to form locally-ordered structures [3]. A general issue is therefore how the combined effects of particle shape and cohesive interactions between particles control the microstructure and the cohesive strength of a granular assembly.

By varying the platelet aspect ratio, the particle shape changes from sphere to thin platelets, as shown in Fig. 1. Using radial compaction, we construct frictionless spherical agglomerates for different values of aspect ratio. We characterize several features of the microstructure as a function of aspect ratio as shown in Fig. 2(a). We then add adhesion and friction forces to all contact points inside the agglomerate and we subject these cohesive agglomerates to diametral compression between two platens to measure their strength. The average stress obtained by dividing the force at failure by the sectional area of the agglomerate represents its overall compressive strength. Its value reflects the nucleation and propagation of cracks inside the agglomerate at locations where the shear stress or tensile stress reach a yield value.

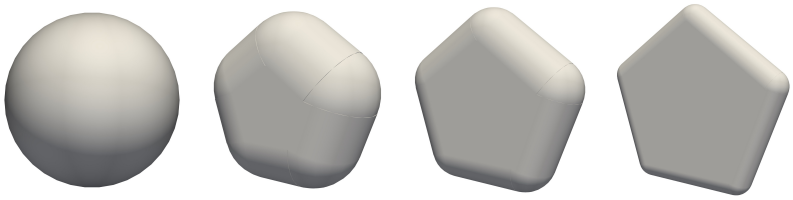

Figure 1. Platelets of increasing aspect ratio from left to the right.

2. Results

We find that the microstructure evolves considerably with the aspect ratio of platelets. As aspect ratio increases, the packing fraction first increases and then declines to lower values. The increase of aspect ratio also leads to higher number of face-face contacts and local nematic ordering. Additionally, we delve into platelet connectivity, probability density functions of forces, and bulk modulus as functions of aspect ratio. We show that the distributions of contact forces broaden with aspect ratio, reflecting stronger force chains often captured by face-face contacts. By means of a small strain prob

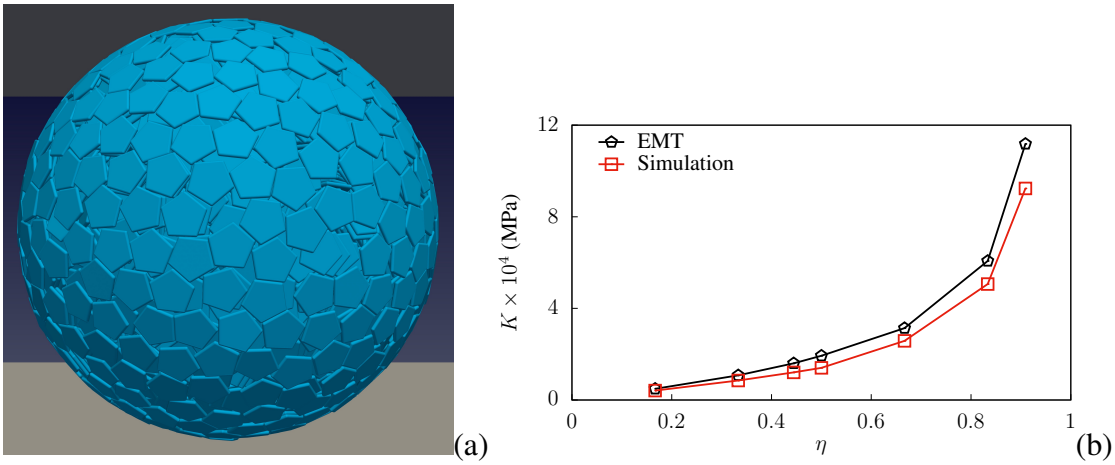

Figure 2. (a) Agglomerate composed of platelet particles constructed by isotropic compaction. (b) Bulk modulus K as a function of platyness η as measured from simulations (red continuous line) and as predicted by the Effective Medium Theory (black dashed line).

applied to the agglomerates, we also measure the bulk modulus as a function aspect ratio. We find that the bulk modulus is an increasing nonlinear function of the playness of particles; see Fig. 2(b).

Our results demonstrate that the cohesive strength of these agglomerates, measured at the peak stress, increases with aspect ratio, reflecting the concentration of force chains along face-face contacts. For a constant adhesion force acting between particles, the strength increases almost linearly with a platyness parameter, revealing the amplifying effect of particle shape on the cohesive strength of agglomerates.

3. References

References

[1] Tran, T.-D., Radjai, F., Bayle, J.-P., Amarsid, L., and Nezamabadi, S. (2024). Microstructure and cohesive strength of agglomerates composed of platelet-shaped particles. *Soft Matter*, p. Submitted.

[2] Radjai, F. and Dubois, F. (2011). *Discrete-element modeling of granular materials*. Wiley-Iste.

[3] Boton, M., Estrada, N., Azéma, E., and Radjaï, F. (2014). Particle alignment and clustering in sheared granular materials composed of platy particles. *The European Physical Journal E*, **37**, 1–8.

PHASE TRANSITION IN GRANULAR SYSTEMS

D. Vescovi[1] and D. Berzi[2]
[1] Politecnico di Milano, Dept. of Civil and Environmental Engineering, Milano, Italy

1. Introduction

Granular systems can behave like either fluids, meaning that they yield under shear stress, or like solids able to resist applied stresses without deforming. In the presence of force chains, the stress tensor has a rate-independent component, revealing a solid-like behavior of jammed and shear-jammed granular systems. In the absence of a stable contact network spanning the entire domain, the granular material is unjammed and behaves like a fluid, with a rate-dependent stress tensor. Furthermore, if the anisotropy of the contact network is such that the force chains span the domain only along one direction, buckling is more likely and the granular material is termed to be in a fragile state. Understanding the different states of granular materials and, in particular, the transitions from one state to another seems crucial in view of realistic mathematical models able to deal with engineering applications. Whereas several numerical results have been obtained in the literature concerning steady, shearing granular flows in both fluid- and solid-like conditions [1], unsteady flows have been less investigated.

The goal of this work is to investigate the phase transition in unsteady, homogeneous flows of a collection of spheres, by discrete element numerical simulations. Two different unsteady problems are analyzed: shearing and cooling. The two flow configurations are illustrated in Figure 1.

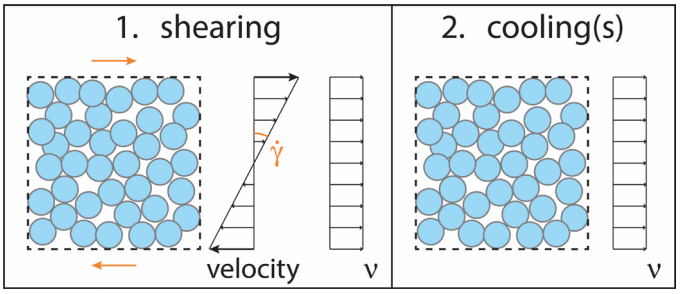

Figure 1. Sketch of the two flow configurations.

2. Numerical simulations

In a first set of simulations, constant-volume, homogeneous shear flows are considered, in which a constant shear rate $\dot{\gamma}$ is applied to static assemblies of 5000 identical spheres, previously compressed at given densities [2,3]. A freely available code, Mercury-DPM (www.mercurydpm .org) has been used, in which particles interact through linear springs and dashpots in both the normal and the tangential direction with respect to the line connecting the centers of the spheres in contact. Sliding occurs whenever the ratio of the normal to the tangential force at contact exceeds the friction coefficient. Depending on its density, the granular system is expected to reach the final steady state in fluid, solid, or near-to-critical conditions.

One question that we asked ourselves was whether the supposedly solid systems retain their rigidity once we remove the applied shear and let the system relax. Then, in the second set of simulations, after homogeneously shearing an initially marginally solid-like system, we stop shearing at different times and let the system relax and dissipate its fluctuation kinetic energy (cooling) [4].

We measure the average and the distributions of contacts per particle and the anisotropy of the contact network. We characterize the contact network through the fabric tensor, that gives a macroscopic measure of the contact orientation distribution. Moreover, the distribution of contacts is measured through the contact fraction, that is the ratio of the number of particles having c contacts (for c = 0 and 1) to the total number of particles.

3. Results and conclusions

In the homogeneous shearing configuration, we observed that, during the transient, fluid-like and solid-like behavior can be distinguished based on the fluctuations of the coordination number (average number of contacts between all particles) and the pressure: fluid-like systems are characterized by large fluctuations, due to the continuous destruction/re-building of multi-particles aggregations, whereas fluctuations are much smaller when a contact network spanning the entire domain develops in the granular material (solid-like behavior). The fluid-solid transition in unsteady, homogeneous shear flows is characterized by a critical value of the coordination number, independent of the imposed volume fraction and the shear rate. Such a critical coordination number coincides with that already defined in the past with reference to steady conditions.

In the second set of simulations, i.e. when the shear was suddenly removed and the granular material was free to progressively dissipated its kinetic energy, we observed that, depending on the initial fraction of mechanically stable particles, the granular material at the beginning of cooling can be shear-jammed, fragile or unjammed. The initial state determines the subsequent evolution of the dense assembly into either an anisotropic solid, an isotropic or an anisotropic fluid, respectively. While anisotropic solids and isotropic fluids rapidly reach an apparent final steady configuration, the microstructure continues to evolve for anisotropic fluids.

The present work reinforces the idea that the solid volume fraction is not enough to determine the state of granular materials and the microstructure of the contact network must be included in mathematical models, at least when dealing with unsteady problems.

4. References

[1] Vescovi D. & Luding S. (2016). Merging fluid and solid granular behavior. *Soft Matter*, **12**:8616-8628.

[2] Vescovi D., Berzi D. & di Prisco C. (2018). Fluid-solid transition in unsteady, homogeneous, granular shear flows. *Granular Matter*, **20**:27.

[3] Vescovi D., Redaelli I. & di Prisco C. (2020). Modelling phase transition in granular materials: From discontinuum to continuum. *Int. J. Solids Struct.*, **202**:4905-510.

[4] Berzi D. & Vescovi D. (2021). Cooling after shearing: three possible fates for dense granular materials. *Granular Matter*, **23**:47.

Rupture distances and capillary forces of liquid bridges in the pendular regime: Closed-form expressions and machine learning predictions

Albert Argilaga[1] ***and Chaofa Zhao***[1]
[1] *Zhejiang University, Department of Civil Engineering, Hangzhou, China*

Abstract

The validity of the predictions of existing expressions for the rupture distances and capillary forces of capillary bridges in wet granular materials has been limited to small volumes for a long time. Recently, new predictions attempted to enhance the validity range, resulting in expressions with more than twenty calibrated coefficients. In this work, two soft computing methods and a large database of Young-Laplace numerical solutions are used to find better predictions. First, machine learning allows us to obtain predictions with very good accuracy. Second, metaheuristics help to search for new closed-form expressions with less complexity. Combining solutions from the two soft computing approaches in complexity-accuracy plots, the tracing of Pareto-optimal fronts proves the superiority of the presented solutions compared to previous ones.

1. Introduction

In wet granular materials, capillary forces are the dominant cohesive force, and cohesion is derived from these capillary forces between the particles. The present study focuses on pendular capillary bridges with axisymmetric surfaces and assumes quasi-static equilibrium conditions, ignoring the effect of viscosity and gravity.

The key properties of the pendular capillary bridges between two spheres are the rupture distance and the capillary force. Those have been well studied for their dependence on the capillary bridge volume and separation distance (volume control) [1] and on the pressure difference between the liquid and surrounding gas of the capillary bridge and separation distance (suction control) [2]. The Young-Laplace equation states that the mean curvature of the surface of the capillary bridge is constant and proportional to the suction value; this geometry is responsible for the properties of the capillary bridge. The accuracy of the Young-Laplace equation in describing capillary bridge properties has been demonstrated experimentally.

The properties of capillary bridges under both volume and suction control have been explored through a combination of numerical, analytical and experimental approaches [3], each with its own limitations. Analytical theories for capillary bridges are typically based on the toroidal approximation, which represents the meridional profile as part of a circle. More recently, analytical theories using the ellipse approximation [4, 1] have been developed. In the latter, the profile is represented as part of an ellipse, and the mean curvature along the liquid bridge surfaces is constant, thus satisfying the requirement of the Young-Laplace equation. These theories provide expressions for the rupture distance and capillary force function of the capillary bridge volume or suction and separation distance, nevertheless their applicability is limited to equally-sized particles and small volumes.

Analytical theories based on the toroidal and ellipse approximation, that do not require any calibrated parameters, and closed-form expressions with coefficients determined by curve fitting to the large dataset of numerical solutions of the Young-Laplace equation have been developed [4, 1, 2]. However, these theories are limited in their applicability to small capillary bridge volumes, and the use of many calibrated parameters in the closed-form expressions makes their implementation cumbersome. Therefore, it is desirable to obtain simpler expressions to determine capillary forces and rupture distances of capillary bridges in a wide range of volume and suction control scenarios.

To achieve this goal, soft computing methods have been retained. More specifically, metaheuristics (PSO) will be used to obtain better closed-form expressions, and machine learning models will assist in obtaining more precise predictions.

Metaheuristics have experimented a revived interest in recent years. Their main appeal is the avoidance of local optima and not the need to compute the derivative of the problem like in the Newton method. On the other hand, they usually require numerous evaluations of the objective function.

In this study, the purpose of PSO is to provide the optimal calibration of proposed multivariate expressions, bypassing the calibration of each individual variable in recursive stages. Reciprocally, machine learning is used to predict rupture distances and capillary forces of liquid bridges by the use of Artificial Neural Networks (ANNs). Thanks to the characteristics of ANNs, predictions can achieve higher levels of accuracy compared to closed-form expressions, allowing us to provide a wider range of solutions in the trade-off complexity-accuracy.

The objective of this study is, by the use of the largest capillary bridge database obtained by numerically solving the Young-Laplace equation [1] and the use of metaheuristics and machine learning, to find better predictions for rupture distances and capillary forces [5].

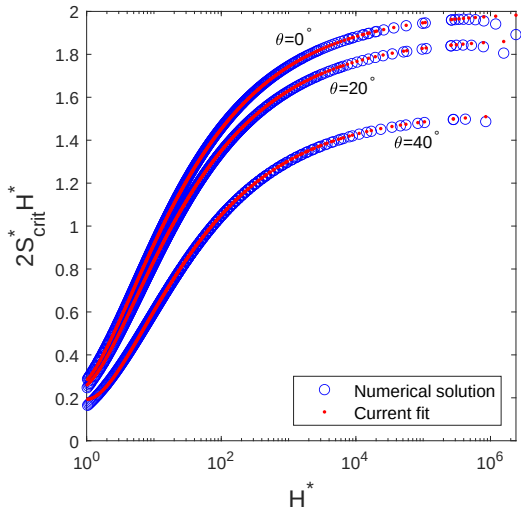

Figure 1. Rupture distances multiplied by dimensionless suction $2S^*_{crit}H^*$ from the numerical solution of the Young-Laplace equation and predicted by the closed-form expression for a range of dimensionless suctions.

References

[1] Zhao, C.-F., Kruyt, N. P., and Millet, O. (2019). Capillary bridges between unequal-sized spherical particles: Rupture distances and capillary forces. *Powder Technology*, **346**, 462–476.

[2] Zhao, C.-F., Kruyt, N. P., and Millet, O. (2020). Capillary bridges between spherical particles under suction control: Rupture distances and capillary forces. *Powder Technology*, **360**, 622–634.

[3] Scholtès, L., Hicher, P.-Y., Nicot, F., Chareyre, B., and Darve, F. (2009). On the capillary stress tensor in wet granular materials. *International Journal for Numerical and Analytical Methods in Geomechanics*, **33**, 1289–1313.

[4] Zhao, C.-F., Kruyt, N. P., and Millet, O. (2018). Capillary bridge force between non-perfectly wettable spherical particles: An analytical theory for the pendular regime. *Powder Technology*, **339**, 827–837.

[5] Argilaga, A. and Zhao, C. (2023). Rupture distances and capillary forces of liquid bridges: Closed-form expressions and ANNs-trained prediction models. *Powder Technology*, **427**, 118702.

SOME NOTES ON THE INTERNAL STABILITY AND SEGREGATION CRITERIA OF GRADING ENTROPY

E. Imre[1,2], I. Talata[1], T. Goda[1], D. Barreto[3], J. Leak[3], J. McDougall[3], V. P. Singh[4]

[1] *Bánki Donát Faculty of Mechanical and Safety Engineering, Budapest, Hungary* [2] *AIAM Doctoral School, Óbuda University, Budapest, Hungary* [3]*Edinburgh Napier University, School of Engineering and the Built Environment, , Edinburgh*[4] *Dept. of Bio. and Agric. Eng, & Dept. of Civil & Env. Eng, Texas A and M University, Texas, USA*

1. General

The grading entropy is the statistical entropy of the finite discrete grain size distribution with *N* uniform statistical cells in terms of a kind of log diameter, consisting of two terms, called entropy coordinates with normalised forms as well ([1-6]). The base entropy (the first coordinate) is a kind of mean, the entropy increment (the second coordinate) is similar to the variance, normalised base entropy, and is a kind of skew. On the other hand, the normalised entropy increment is a kind of kurtosis. The relative base entropy is also an internal stability measure. There is a unique grading curve called optimal grading curve among the grading curves with a given relative base entropy value, at the maximum normalised entropy increment. This is a mean grading curve for a fixed base entropy value, with finite fractal distributions, the fractal dimension is varying from minus to plus infinity ([5]).

2. Internal stability rule and segregation rule

The internal stability rule of Lőrincz (1986 [1]) is well-known and is used for several internal stability problems ([2 to 5]). It is formulated by the A=2/3 condition with the A entropy parameter. The geometrical probability is investigated on the basis of the simplex analogy of the space of the possible grading curves. The result is discussed and explained in the light of the grading entropy path during particle breakage and the formation of the fractal grading curves. The stable fractal dimensions - between 2 and 3 – are in agreement with the fractal dimension occurring in nature. The stable mixtures with fractal distribution are formed by degradation, with

directional entropy path ([5-6]).

The micromechanical condition of the internal stability is analyzed from Physics viewpoint as the larger particles are "wedged" by the small particles, they are not allowed to rotate. The micromechanical process of segregation during piping is started to be examined on the basis of the result of Lampl ([7-8]). He found that the grains are sized according to size radius in piping. Formed in nature during floods the differences between the sizes of the grains are than in the laboratory experiments.

References

[1] Lőrincz, J. Grading Entropy of Soils. Univ. Doct. Thesis, Technical University of Budapest, Budapest, Hungary, 1986. (In Hungarian).
[2] Lőrincz, J.; Imre, E.; Fityus, S.; Trang, P.Q.; Tarnai, T.; Talata, I.; Singh, V.P. The Grading Entropy-based Criteria for Structural Stability of Granular Materials and Filters. *Entropy* **2015**, *17*, 2781-2811.
[3] Imre, E.; Nagy, L.; Lőrincz, J.; Rahemi, N.; Schanz, T.; Singh, V.P.; Fityus, S. Some Comments on the Entropy-Based Criteria for Piping. *Entropy* **2015**, *17*, 2281-2303.
[4] Singh, Vijay P. *Entropy theory in hydraulic engineering: an introduction* (ASCEPress), 2014. ISBN978-0-7844-1272-5.
[5] Imre E, Talata I, Barreto D, Datcheva M, Baille W, Georgiev I, Fityus S, Singh VP, Casini F, Guida G, Trang P. Some notes on granular mixtures with finite, discrete fractal distribution. Periodica Polytechnica. Civil Engineering. 2022;66(1):179-92.
[6] Lőrincz J, Imre E, Gálos M, Trang QP, Rajkai K, Fityus S, Telekes G. Grading entropy variation due to soil crushing. International Journal of Geomechanics. 2005 Dec;5(4):311-9.
[7] H. Lampl, 'Buzgárképződés és talajtörés (Sand boil formation and soil failure)', *Vízügyi Közlemények*, vol. 41, no. 1, pp. 25–49, 1959.
[8] Imre, Emőke ; Koch, Edina ; Nagy, László ; Illés, Zsombor ; Hortobágyi, Zsolt ; Barreto, Daniel Several cases of backward erosion/liquefaction piping from Hungary ISC6 (2021) Paper: ISC2020-524.

Author Index